SAUPEC - 96
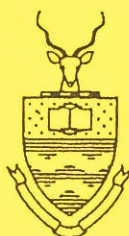
SAUKIK - 96

SOUTHERN AFRICAN UNIVERSITIES POWER ENGINEERING

UNIVERSITY OF THE WITWATERSRAND

RAND AFRIKAANS UNIVERSITY

TECHNIKON WITWATERSRAND

CONVENED BY

UNIVERSITY OF THE WITWATERSRAND
RAND AFRIKAANS UNIVERSITY
TECHNIKON WITWATERSRAND

Proceedings of the Sixth Conference

JOHANNESBURG

22 - 23 JANUARY 1996

S A U P E C - 96

S A U K I K - 96

SIXTH SOUTHERN AFRICAN UNIVERSITIES

POWER ENGINEERING CONFERENCE

22 - 23 JANUARY 1996

VENUE:

CHAMBER OF MINES BUILDING
UNIVERSITY OF THE WITWATERSRAND
WEST CAMPUS

SAUPEC NATIONAL COUNCIL

Prof JD van Wyk	Rand Afrikaans University - Convenor
Prof RG Harley	University of Natal - Treasurer
Prof JHR Enslin	University of Stellenbosch
Prof JA Ferreira	Rand Afrikaans University
Dr R Herman	University of Stellenbosch
Dr IR Jandrell	University of the Witwatersrand
Mr WC van der Merwe	Eskom

SAUPEC '96 LOCAL ORGANISING COMMITTEE

Dr IR Jandrell	In the chair & National Council Representative
Mrs JF Dockerty	Conference Liaison Secretary
Dr JM van Coller	Proceedings
Mr S Bhutt	Organisation
Mr SD Nielsen	Programme
Prof MJ Case	Rand Afrikaans University
Mr P Lazanas	Technikon Witwatersrand
Mr M Engelbrecht	University of the Witwatersrand
Mr R Kelly	University of the Witwatersrand
Dr AJ Phillips	University of the Witwatersrand
Mr DA Reynders	University of the Witwatersrand

I

ABSTRACTS REVIEW PANEL

Prof MJ Case   Rand Afrikaans University
Prof CF Landy   University of the Witwatersrand
Prof JP Reynders   University of the Witwatersrand
Dr JM van Coller   University of the Witwatersrand
Dr IR Jandrell   University of the Witwatersrand
Dr AJ Phillips   University of the Witwatersrand

* * * * * * * *

MONDAY/MAANDAG	8:30 - 9:45	FOYER

TEA AND REGISTRATION

MONDAY/MAANDAG	9:45 - 10:00	CM1

OPENING ADDRESS: PROFESSOR C.F. LANDY

MONDAY/MAANDAG	10:00 - 10:30	CM1

INVITED LECTURE 1: DR W.C. BEATTIE

The generation of electrical power from sea waves

MONDAY/MAANDAG	10:30 - 10:45	FOYER

TEA

| HIGH VOLTAGE 1 | CM1 | CHAIRMAN: PROFESSOR JP REYNDERS |

The basic physical processes in gas breakdown Zhou M., Reynders J.P. and Nielsen S.D. - University of the Witwatersrand	5
Corona stabilisation in SF6: current understanding Bhutt S., Jandrell I.R. and Reynders J.P. - University of the Witwatersrand	9
Corona stabilisation in SF6: modelling Bhutt S., Jandrell I.R. and Reynders J.P. - University of the Witwatersrand	13
Preliminary results in the development of a resonant parallel plate coupler for detection of partial discharges in GIS Nielsen S.D. and Reynders J.P. - University of the Witwatersrand	17
Effect of Perchlorethelene on physical and insulating properties of mineral oil Minhas M.S.A. and Reynders J.P. - University of the Witwatersrand	21
Capacitive bushing voltage dividers Vets L. - Eskom T-R-I	25

| POWER SYSTEMS 1 | CM2 | CHAIRMAN: MR RG KOCH |

High speed flicker and power factor compensation Beattie W.C. and Beattie S. - The Queen's University of Belfast	31

Voltage dips and their effects on industrial equipment
    Smit E. - University of Cape Town
    McAllister D.W. - SAPPI Ngodwana
    Dingley C.E. - University of Cape Town
	35

Power system harmonic field measurements and the application of standards including simulation
    Atkinson-Hope G. - Cape Technikon
    Petroianu A. - University of Cape Town
	39

'n 88kV analoog transmissielynmodel vir harmoniese ondersoeke Jordaan H.A. and Rens A.P.J. - PU vir CHO	43

An active and systematic approach to achieve electromagnetic compatibility (EMC) throughout a large electric power system
    Pretorius P.H. - Eskom T-R-I
    Britten A.C. - Eskom T-R-I
    Reynders J.P. - University of the Witwatersrand
	47

Interior magnetic fields associated with driving an electric vehicle: a case study Pretorius P.H., Baholo M.S. and Britten A.C. - Eskom T-R-I	51

LUNCH

TEA

| POWER ELECTRONICS 1 | CM1 | CHAIRMAN: PROFESSOR MJ CASE |

Single-to-three-phase converter for induction motors Cruise R.J. and Landy C.F. - University of the Witwatersrand	101
Development of a generic tension control system Van Blerk B.D. and Diana G. - University of Natal	105
The use and development of specialised software tools for parallel real-time controllers for power electronic systems Van der Westhuizen M.J., Harley R.G. and Levy D.C. - University of Natal	109
Transfer function for the partial series resonant converter Roos S.D. and Ferreira J.A. - Rand Afrikaans University	113
An improved control scheme for solid state series reactance compensation Rigby B.S. and Harley R.G. - University of Natal	117
A linear hysteretic pulse width modulator Botha L.J. and Bredenkamp G.L.	121

| POWER SYSTEMS 3 | CM2 | CHAIRMAN: MR P LAZANAS |

Energy, economy and environment: the impact of conventional fuels and industrial pollutants Davidson I.E. - University of Cape Town	125

Energy management issues in Nigeria: implications on manufacturing technology and national development
        Davidson I.E. - University of Cape Town
        Oni J.O. - Federal University of Technology, Nigeria
	129

Potential of renewable energy sources in rural electrification Ijumba N.M. and Wekesah C.W.	133
Potential for supplying remote communities by tapping from HV lines Holmes T. and Dingley C.E. - University of Cape Town	137
Solar water heating support systems from an electrical supply network viewpoint and new design goals Lemmer E.F. and Delport G.J. - University of Pretoria	141

BANQUET

| TUESDAY/DINSDAG | 7:30 - 8:00 | FOYER |

TEA

| TUESDAY/DINSDAG | 8:00 - 8:15 | CM1 |

OPENING ADDRESS: PROFESSOR JP REYNDERS

| TUESDAY/DINSDAG | 8:15 - 8:45 | CM1 |

INVITED LECTURE 2: PROFESSOR K.D. SRIVASTAVA

Some current challenges in high voltage engineering for electrical power systems

| TUESDAY/DINSDAG | 8:45 - 9:00 | FOYER |

TEA

TEA

MACHINES 1	CM1	CHAIRMAN: PROFESSOR CF LANDY

Detection of broken rotor bars by axial vibrations produced in squirrel cage induction motor having interbar currents Muller G.H. and Landy C.F. - University of the Witwatersrand	195
Universal brushless permanent magnet motor drive Gieras J.F. and Wing M. - University of Cape Town	199
Aandrywing van 'n driefasige induksie motor vanaf 'n enkelfasige toevoer Strydom J.J. and Parsley G.M.J. - University of Pretoria	203
Development of a cost efficient FEM system for the design of power apparatus Cronje W. - Rand Afrikaans University	207
The use of finite element analysis to optimise induction motor rotor profiles for synchronous reluctance operation Rohde M.A., Meyer A.S. Landy C.F. - University of the Witwatersrand	211

POWER SYSTEMS 5	CM2	CHAIRMAN: MR J RENS

Facility location optimisation in electrical distribution design Apostolellis J., Dwolatzky B. and Meyer A.S. - University of the Witwatersrand	215
Aerial photograph interpretation for electrical reticulation Levitt S.P., Dwolatzky B. and Meyer A.S. - University of the Witwatersrand	219
A technique for automating stands to junction allocation in electrification design using heuristics Tumazos S.C.J., Dwolatzky B. and Meyer A.S. - University of the Witwatersrand	223
Utilisation of a rule based expert system to aid in power reticulation design Patricios M.P., Dwolatzky B. and Meyer A.S. - University of the Witwatersrand	227

The sensitivity of calculated voltage drop to changes in load sample averaging interval
    Sellick R.L. - University of Cape Town
    Gaunt C.T. - HKS Law Gibb
    Herman R. - University of Stellenbosch
    Dingley C.E. - University of Cape Town
	231

Using the bootstrap method for evaluating variations due to sampling in voltage regulation calculations Herman R. - University of Stellenbosch	235

TUESDAY/DINSDAG	12:15 - 13:45	CANTEEN

LUNCH
(The SAUPEC council meeting will be held during this lunch)

MACHINES 2	CM1	CHAIRMAN: MR AS MEYER

POWER SYSTEMS 6	CM2	CHAIRMAN: MR S NIELSEN

TUESDAY/DINSDAG	*15:15 - 15:30*	*CM1*

CLOSING ADDRESS: PROFESSOR CF LANDY

INVITED PAPERS

The Generation of Electrical Power from Sea Waves

W C Beattie and T J Whittaker

The Queen's University of Belfast. UK

1 Introduction

1.1 Alternative energy

The attitude to energy in the world today has changed significantly from that of a few years ago. The concepts of global warming, acid rain and pollution of the environment have become major issues in the developed countries. In the UK, encouragement has been provided for alternative energy sources by the legal requirement on the supply authorities to accept a certain percentage of energy from alternative sources at the best possible bid price. This has encouraged the growth of technologies such as wind-power and biomes and the bid price for these has steadily fallen over the past six years from a factor of 10 over the price for fossil fuel generation until it has now reached 1.5. Wave power is at the very early stages of the development cycle and at present is relatively expensive. As with wind, the gains will come when the technology is fully understood, thus giving acceptable reliability, and the design has been optimised to provide the maximum power for the minimum investment. The number of operating plants using wave power is still in single figures and those connected to the supply system may be only 2 or 3.

1.2 The role of alternatives

Alternatives are never likely to entirely supplant the use of fossil fuels and must, certainly in the short term, be seen as being useful in displacing the consumption of fossil fuel. Thus to be of value they should be capable of supplying energy when it is most needed. In the UK the availability of wave energy matches almost exactly the peak demand curve of the supply system, maximum energy being available during the winter when the system load is at a maximum. It is also interesting to consider the power potential available in waves and again for the UK it can offer a significant contribution to the total energy demand if fully developed. In addition the nature of the structures is such that they do not have the same visibility as wind turbines and therefore will be more acceptable to the general public.

1.3 Energy costing

As with all alternative energy systems it is important to be able to envisage a system which is cost compatible with existing energy sources. If this is not possible in the near future it is not worth developing it further. Thus schemes which are proposed for the collection of energy from the waves must show that it is possible to become economic in the cost per unit of energy. Essentially this means that the structures must be designed to be made and installed as cheaply as possible and yet at the same time have the strength to withstand the exceptional forces which are experienced during storms. Thus it is useful to compare the costing of a wave power station with that for wind turbines which is showing promise for a break-even point in electricity cost in the near future.

2 The energy source

2.1 Collection of energy power

A key feature in using wave power is that a suitable site must be chosen. Thus in the North Atlantic the wave power climate on the West coast of Europe is many times better than that on the east coast of North America. This is a function of the prevailing winds which in general are blowing from the West. The passage of these winds over the surface of the water creates the waves and the process is an integral one in that it is a way of collecting wind energy into a much more intense form that that which is available from wind itself. Thus in the North Atlantic average power levels of 80 kW/m wave front can be achieved. This level would be related to deep water and therefore will be some distance off the coast. As the waves approach the shore and shallower water, average power levels of 20 kW/ m would be more typical[1]. However these figures give an energy density much higher than that for wind and therefore should relate to a smaller structure for the same power output.

2.2 Wave length and frequency

As with most waves there is a relationship between wavelength and frequency. For waves of a particular frequency, say having a period of 10 s, the frequency will be 0.1 Hz and the wavelength about 150 m. The phase velocity is given by:-

$$c = \sqrt{\frac{g\lambda}{2\pi}}$$

where c is the celerity in m/s, g = 9.81 and λ is the wavelength in metres

For an ideal wave the wavelength is given by :-

$$\lambda = c \cdot T$$

where T is the wave period in seconds.

Thus the wavelength is given by:-

$$\lambda = \frac{gT^2}{2\pi} \text{ metres}$$

Typical seas are not monochromatic and the effect is generally one which provides a modulated waveform in that the total energy rises and falls with each wave but the energy in each wave also rises and falls with a frequency of about one eighth of the individual wave frequency. This, as will be seen later, has implications for the energy capture devices.

It is also worth remembering that the motion of a wave is not the motion of the water as such.. The waves are caused by the motion of water particles in a roughly circular manner. This leads to the water particles at the surface moving in one direction at the peak of a wave and in the opposite direction in a trough. The motion of the particles will penetrate below the surface by an amount related to the wavelength but the majority of the energy is carried near the surface of the water.

2.3 The energy equation

The average power available from a wave is a strong function of the height of the waves and for deep water will be given approximately by:-

$$P_{av} = \frac{1}{32\pi} \rho \, g^2 H^2 T \quad \text{W/m}$$

The height of a wave is not without limit and after a certain stage the wave will break and the energy carried will be dissipated. Thus it is essential to capture waves which have not broken. This problem is exacerbated when the water depth is reduced as the shore is approached. The bed of the ocean will slow the motion at the bottom of the wave and this will accentuate the breaking of the waves giving the familiar pattern which exists around any coastline. Thus for a shore-line station, it is essential to have deep water close inshore if the wave resource is to be fully realised.

The equation shows that the power available is a function of wave length and the longer the wavelength the greater the energy which is carried. Thus the waves which are most damaging will be those with the longer wavelength and since these will penetrate further below the surface of the water they are more likely to break in shallow water and thus disperse their energy. This can be beneficial in that a wave-power station built on the coast will be protected from the worse excesses of the wave climate and thus may be built of lighter construction. However, the rise and fall of wave climate is much slower than that for wind and it is therefore much easier to predict the resource available over the next few hours or days.

2.4 Wave resource

In wave systems the energy can vary from almost calm conditions, which are very rare, to violent storms. The variation in power levels can range from a few kW per metre front to values 1000 times larger. Thus a wave-power device must not only cope with the variation in the power available during a wave but also with the hour to hour variation in the wave climate.

3 Wave capture devices

3.1 Shore line

A number of devices can be visualised for shore line operation. The most obvious might be considered to be the so-called 'tapchan' which consists of a tapered channel facing the wave fronts. As a wave enters the channel the decreasing width forces the wave height to increase and the water spills over the side walls of the channel into a reservoir. The water in the reservoir is then used to power a low head hydro plant. The major difficulty with such an arrangement is in finding suitable sites. Areas between islands, where a minimum of barrier must be built and which has a small tidal range, would be deemed the most suitable position.

The oscillating water column devices are more flexible and can be installed in natural gullies or built as a separate unit and floated into position. The principle is that the incoming energy from the waves is used to excite a resonant water column. As such it is primarily tuned to one frequency of waves and a major effort has been put into manufacturing devices with a wide frequency range. As with any resonant circuit the amplitude of the oscillation is a strong function of the damping or in this case the amount of energy extracted from the device. The design must therefore address the problem of frequency response to match the wave climate and the appropriate amount of damping to ensure maximum extraction of energy from the system[2].

3.2 Near shore

In this area the oscillating water column has been used with designs which can be floated into position, either of steel or concrete. Generally they will include some form of harbour or wings on each side of the device so as to improve the capture width.

There are a number of float pump systems which depend on the heave of the waves and, either by an attachment to the bottom of the sea or by reaction on an inertial element, are used to pump water or oil at a relatively low pressure. Generally this is conceived as being pumped to shore where the head is used to power a turbine. These devices will usually be of relatively small power and would be used in arrays where the combination would make a significant contribution to the power available.

3.3 Off shore

In deep water the potential for wave power is greatest but it is in this location that the greatest difficulties will arise. Thus the peak powers available will be very high and the difficulties of transmitting the energy to shore will present the greatest problem[3]. Design approaches to this problem have used the so-called 'duck' which by a nodding action will extract energy from the waves leaving calm water behind it. A similar possibility is to use an array of buoys which will again be able to extract the energy from the waves. It is clear that devices moored off-shore will have a considerable effect on the shore-line wave climate. In some instances this may be advantageous, such as in reducing the wave climate at harbour entrances, whereas in others the lack of vigorous wave action may lead to changes in the type of material deposited along the coastline.

4 Wave capture efficiency

4.1 Matching

In considering the extraction of energy from waves, it is clear that there can be two extreme types of behaviour. Firstly the waves can impact on a solid object and the majority of the energy be reflected out to sea. Secondly a buoy may be free to move with the waves so as to have little effect on the waves passing it. In both cases the energy extracted will be zero. Between these two extremes there must be a point of maximum power transfer when the movement of the device is constrained so as to maximise the energy extracted from the wave source. In the ideal case the reflected wave will be zero and the wave height behind the buoy would be zero.

4.2 Wave capture width and arrays

In many ways the capture of energy from sea waves is similar to that associated with the design of aerials for the electromagnetic spectrum. Thus the devices will capture energy from a wave front much wider than the device itself and as such will therefore have a 'gain' associated with it. Also by arranging an array of devices at a particular spacing it is possible to control the 'bandwidth' of the array. However, in practice this does not provide a significant advantage since unlike a transmitting station the energy does not always come from the same direction.

5 Energy conversion

5.1 Gear ratio

In all devices there is a need to convert the slow movement of the waves into high speed rotation. This can be achieved in the oscillating water column since the surface area of the water in the column can be large relative to the breathing tube. The result will be high air speed which can be used to drive a turbine which can rotate at several thousand rpm. In the case of the tapchan and water pump devices, the head of water can be used to power a low-speed turbine and the rotation geared up mechanically to drive a generator at a moderate speed, say 750 rpm. Using rams or vane pumps to produce high pressure oil would enable the oil to be used to power high-speed oil motors and again a high-speed electrical machine could be used.

6 Energy usage

The discussion thus far has centred on the conversion of wave power into electrical power. This does not have to be the case and there are a number of other opportunities to use wave energy which could be more appropriate in different locations. Thus it would be possible to use the variation in pressure or the motion of a buoy to power a desalination plant without conversion to an intermediate form of energy.

Another possible application is in the use of the air pressure to aerate lagoons used in fish farms or to circulate fresh water through enclosed areas.

6.1 Electricity

Electricity is a valuable form of energy due to the flexibility of use and it would therefore offer considerable advantages if wave energy could be easily converted into electrical energy. In general, electrical machines will operate best at high speed and therefore it is essential to be able to provide a high speed rotating shaft if the costs of electrical generation are to be minimised. For a given power output the cost and size of an electrical machine will be approximately inversely proportional to the speed of the shaft. Again this can be seen as a trade-off since it may cost more in capital and efficiency than is would cost for a low-speed electrical machine. There are therefore two broad options facing the designer of wave power stations.

6.1.1 Low-speed shafts

Most hydro power stations fall into this category where they will have shafts running at perhaps 100 rpm and huge electrical generators. As indicated earlier this type of arrangement is associated with those stations which are creating a head of water of a few metres. The technology of such devices is well proven and if the head is constant the design is simple. In many cases the head will vary and this will require some form of speed or vane control which will add to the cost and complexity of the machine.

6.1.2 High-speed shaft

There are no wave-power systems which are capable of producing high heads of water but the use of oil will allow rams and pumps to be used which can yield high pressures. The high-pressure oil in turn can be used to power turbines or pumps which can be designed for high-speed rotation.

Alternatively, the use of an air turbine can allow high speed rotation to be achieved and again this can easily be matched to electrical generation[4].

7 Energy quality

7.1 Voltage

Electrical energy will only be acceptable if it is of acceptable quality. A key feature in this will be voltage level since lighting is very sensitive to voltage variations and can create considerable annoyance to the user.

7.2 Frequency

For a wave power system connected into a major network the variation in power level during a wave will have little effect on the system frequency. However, in small system such as might be found on an island supplied by diesel generators it is possible for the variation in power to influence the frequency. Here the sensitivity will depend greatly on the type of load as to whether it is mostly lighting of contains a significant proportion of rotating machinery which will have the effect of adding inertia to the system. The result could be serious hunting on the governors on the diesels. For an independent system it would be necessary to provide smoothing of power flow in the form of a flywheel and also to provide some form of dump load for the excess power. This could be in the form of water heaters which could be used to store the energy if required.

7.3 Harmonics

Many suggested schemes for electrical generation involve semiconductor convertors and these can cause serious harmonic pollution on the supply system. Filtering of the supply will then prove to be necessary.

8 Control strategies

8.1 Reactive power

In schemes such as this it has proved efficient to use an induction generator. This type of machine will change in reactive power demand as the load varies during each wave. Reactive power has a significant effect on the voltage of the system and it may be necessary to provide some form of high-speed reactive compensator. This can be achieved by the use of thyristor switched capacitors which can easily hold the voltage at a constant level during each wave cycle at the same time as compensating for the reactive power drawn by the generator.

8.2 Real power

As indicated earlier real power may need to be smoothed and it is possible to use a flywheel on the turbine shaft and an induction machine with a soft characteristic. This can provide a simple form of smoothing but it can be more effective to either control the rotor resistance or to use a convertor to recycle the rotor power on to the supply. If this is done then a wider speed range can be achieved and the power flow smoothed more effectively.

9 Device costing

the cost of a wave power station is closely related to the design. An understanding of the forces involved and of the factors controlling the efficiency of the device can result in less material in the device and hence a lower cost. Anther salient point is the way in which the device is constructed. It is possible to design a device which can be made in a shipyard and towed into position or it could be made from prefabricated parts and assembled in situ. The form of construction chosen will have to address the over cost. Finally, the cost of a device will depend on the number of units which are made. Thus if a device is designed which can easily be replicated for numerous sites over the world then it would be expected that the costs will fall. All these issues must be addressed if wave power is to become economic.

10 Conclusion

Wave power has much to contribute to the energy scene. At present it is at an early stage in the development life cycle and therefore it will be some years before the technology is fully understood so that an acceptable level of reliability may be achieved over a specified life. In addition the design must be such that it will produce an acceptable quality of supply and that it can be constructed in a cost effective manner.

11 References

1. Generic Technical Evaluation Study, DGXII Joule Wave Energy Initiative, Preliminary Actions in Wave Energy R&D August 1993.

2. On the application of non-linear modelling and parameter estimation to a wave energy extraction device.. Linden, BM and Beattie, WC. 28th Universities Power Engineering Conference, 21-23 September 1993. Stafford.

3. Elements of large wave-power plants. Remmer, M, Nielsen, K, and Beattie, WC. European Wave Energy Symposium, 21-24 July 1993.

4. Electrical aspects of contra-rotating turbines in wave-power devices. 29th Universities Power Engineering Conference. 14-16 September 1994, Galway.

Address

- Dr. W C Beattie, Department of Electrical Engineering, Ashby Building, Stranmillis Road, BELFAST BT9 5AH.   e-mail w.beattie@ee.qub.ac.uk

THE BASIC PHYSICAL PROCESSES IN GAS BREAKDOWN

M Zhou, JP Reynders and SA Nielsen
Department of Electrical Engineering
University of the Witwatersrand

Abstract

The basic physical processes involved in gas break-
down are discussed. It is found that the breakdown
strength is largely controlled by the electron energy
distribution function and the electron-molecular in-
teractions at the molecular level, especially the elec-
tron capturing and the electron slowing-down pro-
cesses in the subexcitation energy range. Knowledge
of these processes allows a predication of the dielec-
tric properties of the gas and a choice of the appro-
priate gaseous mixtures for particular applications.

1 Introduction

A dielectric gas in its normal state is a perfect insu-
lator and is used widely for high-voltage equipments.
However, when an electrical field is applied to a gas-
insulated system, free electrons can gain energy and
cause ionization. If a sufficient fraction of electrons
cause ionization, gas breakdown occurs.

Although the gas breakdown strength depends on
many factors (such as the nature, number density,
and temperature of the gas, the electrode geometry as
well as surface condition), the transition of a gas from
an insulator to a conductor is crucially determined by
the behavior of electrons, ions, and photons, particu-
larly the electron producing and depleting processes.
The electron is the most important particle and plays
a crucial role in determining the dielectric strength.

A most effective way to prevent free electrons from
initiating breakdown is to remove them from the
dielectric. This can be achieved by attaching free
electrons to gas molecules to form negative ions.
Unattached free electrons must be slowed down and
be prevented from ionizing the gas and triggering
breakdown.

In this paper, after a brief introduction to the funda-
mental knowledge, we will discuss some of the basic
processes which influence gas dielectric strength and
enable us to understand and optimize the gas prop-
erties.

2 Electron Energy Distribution Function

Based on the research by Christophorou[5], we know
that in designing a gas dielectric the quantity

$$\int_0^\infty \sigma_a(\epsilon) f(\epsilon, E/P) d\epsilon \tag{1}$$

should be maximized and the quantity

$$\int_I^\infty \sigma_i(\epsilon) f(\epsilon, E/P) d\epsilon \tag{2}$$

should be minimized.

Where $\sigma_a(\epsilon), \sigma_i(\epsilon)$ are attachment cross section and
ionization cross section, respectively. $f(\epsilon, E/P)$ is the
electron energy distribution as a function of ϵ (elec-
tron energy) and the pressure-reduced electric field
E/P (E is the electric field strength and P is the gas
pressure). I is the ionization threshold.

To maximize (1), $\sigma_a(\epsilon)$ should be as large as possi-
ble over as wide an energy as possible, and since the
$\sigma_a(\epsilon)$ increases with decreasing ϵ, $f(\epsilon, E/P)$ should be
shifted to as low energy levels as possible. To min-
imize (2), $\sigma_i(\epsilon)$ must be as small as possible. For a
given $\sigma_i(\epsilon)$, $f(\epsilon, E/P)$ must also be shifted to low ϵ
to minimize (2).

From the above, it appears that the optimum gaseous
dielectric is not a single gas but rather a gas mixtures
in order to provide the best effective combination of
electron-attaching and electron-slowing down proper-
ties.

Though the role of the electron energy distribution
function in understanding gas dielectrics has been
recognized, there is still a general lack of knowledge
about $f(\epsilon, E/P)$ for practical situations. However,
we know that at least keeping $f(\epsilon, E/P)$ in a low
electron energy range will improve the gas breakdown
properties.

3 Basic Physical Processes

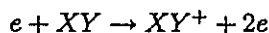### 3.1 Electron Ionization

3.1.1 Initiation Electrons

Where do the initiation ('seed') electrons come from?
The main source of such electrons in a gas-insulated
system is directly or indirectly connected with the

ionization of the gas by cosmic and terrestrial radiation. The estimated total ionization rate is about 4×10^{-5} electrons $s^{-1}cm^{-3}p_a^{-1}$[6]. In electron attaching gases, all the free electrons can be captured by the gas molecules to form negative ions, thus it seems the major source of breakdown-initiating free electrons is electron detachment from these negative ions in stressed electronegative gases[8]. So in a highly stressed electrical system, the highest probability of breakdown occurs at the vicinity of positive electrode.

3.1.2 Electron Impact Ionization

Basically, there are two electron-impact ionization processes:

- Ionization by electron impact:

$$e + XY \rightarrow XY^+ + 2e$$

- Dissociative ionization by electron impact:

$$e + XY \rightarrow X(X)^* + Y^+ + 2e$$
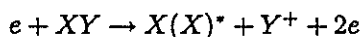
An electron can ionize a molecule only if its energy is at least in excess of the ionization potential of the target molecule. If the ionization potential of a gas molecule is low, the gas molecule is readily to be ionized. So adding gases with low ionization potential to an electronegative gases can improve the corona stabilization. However, the breakdown strength of the dielectric gas does not correlate with the ionization potential. Experimental results show that some gases have a high dielectric strength although their ionization potential is quite low. For example, c-C_4F_8 has a high dielectric strength (even better than SF_6) in spite of its ionization potential being quite low($\leq$12eV)[3].

The breakdown strength is associated with the ionization cross section of the molecule. Out of considering other factors, breakdown occurs at relatively low stress when the ionization cross section is large[4].

3.2 Electron Attachment

This is one of the most important microprocesses which determines the gas breakdown strength. With a strong attaching process, electrons can be effectively removed from the gas. The dielectric strength of a gas depends on the ability of gas molecules to attach free electrons over an wide energy range. In general, the strongly attaching gases have high breakdown strength, weakly attaching and non-attaching gases have low breakdown strength.

The attachment processes to form negative ion are:

- Directly attachment: XY+e $\rightarrow$XY$^-$+energy

- Dissociation attachment: XY+e $\rightarrow$X+Y$^-$

In the low electron energy range, direct attachment is the main process to form negative ions. The energy difference between the neutral molecule plus an

electron at rest at infinity and the molecular negative ion, when both neutral molecule and negative ion are in their ground states, is defined as the electron affinity (EA). If EA is positive, that means the excess internal energy is removed. As we know, the lower the energy state of the particle, the more stable the particle. Thus these negative ions are more stable than neutral molecules. The larger the EA, the more stable the negative ion.

In strongly attaching gases, the attachment cross section possesses a peak value at certain narrowly defined energy ranges. Although there is only a small fraction of electrons whose energies are expected to be below 1eV (especially below 0.5eV), this strong attachment processes can quickly remove all low energy electrons. Then the electron energy distribution will reshape its functional form at a very much short time ($\leq 10^{-12}$s) compared with the time ($\sim 10^{-8}$s) for breakdown development. So new low energy electrons can be generated and almost immediately removed. This electron generating and removal process continues ensuring constant attaching of free electrons.

3.3 Electron Detachment

For electron attachment processes to be most effective, the attached electron should not be easily detached from a negative ion. In addition, electron detachment is the mechanism responsible for the production of discharge initiating electrons in electronegative gases.

The detachment processes are:

1. Autodetachment:

$$X^{-*} \rightarrow X + e + energy$$
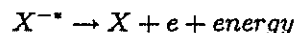
where the asterisk indicates excess internal energy. This process happens only if the negative ion can't be collisionally stabilized within a short time after the electron is captured. If the collision time is much short in the region where the electric field to gas number density ratio, E/N, lies below the critical value (E/N)c, then this process is not of any significance.

2. Field-induced detachment:

$$X^- \rightarrow X+e$$

It has already been shown that for negative ions with EA excess 1.0eV (EA for SF_6 is 1.05eV), this process is highly unlikely for electrical field below 10MV/cm. For most practical system, breakdown occurs at values of the field far below 10MV/cm.

3. Collisional detachment:

$$X^- + Y \begin{array}{l} \nearrow X+Y+e \\ \searrow XY+e \end{array}$$
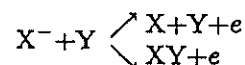
Both these processes seem to be the most promising mechanism for the detachment process, particularly for steep-fronted voltage

pulses. However, experimental results show that the probability of detachment increases abruptly at a threshold kinetic energy which is approximately twice the EA of the negative ions. So unless the ion can acquire an energy from the electric field between collisions which is in excess of this threshold, collisional detachment will not occur.

4. Photodetachment: $h\nu + X^- \rightarrow X + e$

The cross section is quite small for this process so it is not likely to be significant.

3.4 Electron scattering

3.4.1 Classification

There are two kinds of scattering processes, elastic and inelastic, both of which cause the electron to lose its energy. A large scattering cross section can strongly influence the $f(\varepsilon, E/P)$ and shifts it to low electron energy range where the strong attaching processes can remove free electrons efficiently.

The following processes are key processes in determining the electron energy distribution in the gas. The electron slowing-down capability of a gas depends on the cross-sections of those processes:

- Direct elastic scattering: $e + XY \rightarrow XY + e$

- Direct inelastic scattering: $e + XY \rightarrow XY^* + e$

- Ion pair formation: $e + XY \rightarrow X^+ + Y^- + e$

- Dissociative scattering:

$e + XY \rightarrow XY^{-*} \rightarrow X + Y(Y^*) + e$

- Indirect scattering:

$e + XY \rightarrow XY^{-*} \rightarrow XY(XY^*) + e$
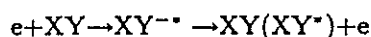
The last two processes are associated with the mechanism of negative ion resonance which is suggested to be the most effect way to slow electrons down[1].

3.4.2 Negative ion resonance

Negative ion resonance states are sates in which an electron is temporarily captured by a molecular system.

From the last two scattering reactions, we can see that there is a negative ion metastable state (XY^{-*}). Because the state of this negative ion lies above the ground state of the neutral molecule, this negative ion will decay by autodetachment (indirect scattering) or by dissociative detachment. So the lifetime τ of the resonance is longer than the time of the projectile traversing the target molecule. With these short lived negative ions, the scattering cross section can be enhanced significantly in certain defined energy ranges. Thus electrons can be effectively slowed by this indirect scattering process. In the low-energy range (0-20eV), which is the energy range of principal

significance to gaseous dielectrics, such indirect (resonant) processes constitute an efficient slowing down mechanism.

Molecular NIR states are abundant[1]. We are only interested in those which lie in the low energy range and possess peak values in a certain narrowly defined energy ranges. It has been found there are some low-lying NIR states in many gases such as H_2, O_2, CO, CO_2, N_2, perfluorocarbon etc..

4 Application

4.1 SF$_6$-N$_2$ Mixtures

It is well known that SF$_6$ has an excellent dielectric characteristic. However, its sensitivity to surface roughness and its relatively high cost limit its use. Over the past few decades, many investigations have been made to try to use gas mixtures containing SF$_6$ instead of pure SF$_6$.

At present SF$_6$ and N_2 mixtures appears very attractive. Experiments display that mixtures containing 50-60% of SF$_6$ have dielectric strengths of up to 85-90% that of pure SF$_6$ and in a certain range, the gas mixtures can even show a higher breakdown strength than that of pure SF$_6$[2]. Besides this, gas mixtures can reduce the sensitivity of gases to the surface roughness.

We know that the electron capturing cross-section of SF$_6$ is strongly peaked for nearly zero-energy electrons. The lifetime of SF_6^- formed by capturing a slow electron is longer than that of SF_6^- formed by capturing a fast electron. When N_2, which has a very strong negative ion state at ~ 2.3eV (Fig.1), is added
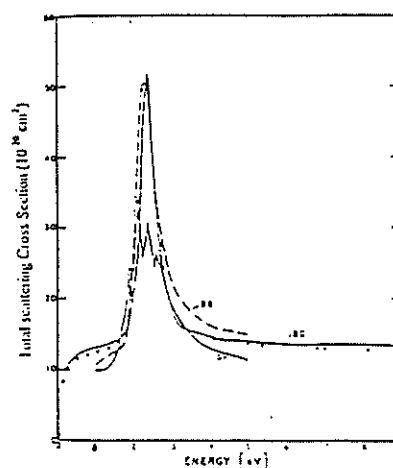
Figure 1: Energy dependence of electron scattering cross section for e-N_2

to SF$_6$, this narrow, but strong low-lying NIR state can scatter electrons into a low energy range very effectively. Researchers found that electrons scattered by N_2 have an angular distribution which has a strong backward component[7]. If these electrons are scattered in a direction opposite to the drift direction, they would have to almost come to rest before reversing direction, and then, they can be captured very

efficiently by SF_6 molecules at these extremely low energies. So even with a decreasing concentration of SF_6, the dielectric strength of gas mixtures does not decrease significantly.

4.2 SF₆ with other gas mixtures

Gas mixtures of SF_6 with other slowing down gases have also been investigated. Gas mixtures exhibit distinct synergism when each of the electron slowing down gases is mixed with the strongly electron attaching gas SF_6 (fig.2). The synergistic effects increase with increasing ability of each gases to scatter electrons via the low-lying NIR states.
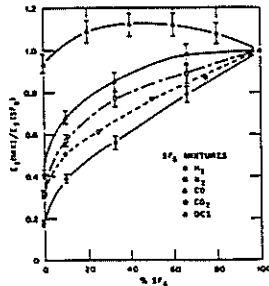
Figure 2: $E_{s(Mix)}/E_{s(SF_6)}$ for mixtures of SF_6 with: H_2, N_2, CO, CO_2, and OCS

5 Conclusion

From the above, it appears that the electron attaching process by which electrons can be removed from the gas, electron scattering process by which electrons can be slowed down and then can be attached easily, and electron-impact ionizing process by which electrons can be added into the dielectric gas play crucial roles in determining the gas breakdown strength. The effect of the large capturing and scattering cross section are suggested to be far more important than that of the magnitude of ionization cross section. A typical example is that the breakdown strength of A_r is in general superior to N_e in spite of the fact that the ionization cross section of A_r is much large than that of N_e and the ionization potential of A_r is less than that of N_e. It is attributed to the differences in scattering cross section between A_r and N_e $((\sigma_{A_r})_s \gg (\sigma_{N_e})_s$, so A_r is a much more efficient electron slowing-down gas than N_e).

Thus in designing a dielectric system, we prefer to use gas mixtures of strongly electron attaching gases with electron slow-down gases. An optimum gas mixtures should have

- Large attachment cross section

- Large electron affinity

- As many NIR states as possible over the entire subexcitation energy range

- Small ionization cross section

All those basic properties are highly desirable for a gas insulation system.

6 Planned Investigations

As we know, SF_6 has a large attachment cross section and a large EA. So it is an ideal electronegative gas and is chosen for our experiment. In addition, we choose electron slowing-down gases N_2, CO, and CO_2 as the additive gases. In these gas mixtures, there are at least three NIR states, which are ~ 2.3eV for N_2, ~ 1.75eV for CO, and ~ 3.85eV for CO_2, at the subexcitation level. So electrons can be kept in a low energy range via those NIR states to maximize the electron attachment and to minimize the electron ionization. The breakdown strength can thus be improved.

In order to get a good combination of the electron attaching gas with electron slowing-down gases, investigations will be carried with different combinations of four gases at pressures from 1bar to 4bar at room temperature. Experimental results will be compared with the predicated value.

References

[1] Bardsley JN and Mandl F, *Resonant scattering of electrons by molecules*, Rep. Prog. Phys. 31, 1968, pp472-531.

[2] Baumgartner RG, *Dielectric characteristics of mixtures of sulfurhexafluoride and nitrogen*, Third Inter. Conf. on Gas Discharge, 1974, pp366-369.

[3] Christodoulides AA, Christophorou LG, Pai RY and Tung CM, *Electron attachment to perfluorocarbon compounds. I*, J. Chem. Phys. 70, 1979, pp1156-1168.

[4] Christophorou LG, James DR and Mathis RA, On the role of the electron impact ionization and electron scattering cross-section in the breakdown strength of dielectric gases, J. Phys. D: Appl. Phys., Vol. 12, 1979, pp1223-1236.

[5] Christophorou LG, *Electronegative gases*, Electrical Breakdown and Discharges in gases, 1989, pp133-176.

[6] Christophorou LG and Pinnaduwage LA, *Basic physics of gaseous dielectrics*, IEEE Trans. Electr. Insul. Vol. 25 No.1, 1990, pp55-74.

[7] Lane NF, *The theory of electron-molecule collisions*, Rev.Mod. Phys., Vol 52, No. 1, 1980, pp29-119.

[8] Wiegart N, *A model for the production of initial electrons by detachment of SF_6 ions*, IEEE Trans. Electr. Insul. Vol. 20, 1985, pp587-594.

Corona Stabilisation In SF₆ : Current Understanding

S. Bhutt   I.R. Jandrell   J.P. Reynders

Department of Electrical Engineering
University of the Witwatersrand

Abstract

Corona stabilisation is a phenomenon that has been studied extensively by various researchers. Some of the significant work done to date with reference to this phenomenon in SF₆, with the exception of the effect of gas mixtures, is reviewed and coalesced in this paper. Corona stabilisation terminology is clarified. Finite element simulations are used to investigate the effect of various proposed ion-distributions around the point electrode. The results give some indication as to the feasibility of using each of the various conceptual models used to understand corona stabilisation.

1. Introduction

In SF₆ gas insulated equipment it is desirable to attain an operating pressure that is as high as possible since this reduces the size and cost of the equipment. However, it is difficult to manufacture and assemble such equipment with perfectly smooth surfaces and without some metallic particles being present. Surface roughness and particle contamination cause non-linearities and therefore locally enhanced fields. It is therefore of great practical significance to understand the physical processes behind discharges and breakdown under very non-linear fields. For all waveshapes, in inhomogeneous geometries, negative breakdown voltages are higher than the positive breakdown voltages (Sastry et al [1]). Therefore only positive applied stresses are concentrated on in this work.

2. Nomenclature Clarification

The term *corona stabilisation* is sometimes used synonymously with the terms *space charge effects* or *ion drift effects*. However, all these terms often refer to different phenomena (or to different *stages* of a discharge phenomenon) .

Space Charge
In the most general context, space charge refers to any or all of the three charged particle species that may exist in the interelectrode space in an SF₆ insulated vessel; and thereby modifying the applied Laplacian electric field in some way.

The term space-charge is also often used to describe the charge at the tip of a streamer filament which controls the growth of the filament - specifically, in theoretical modelling of corona (Morrow [3]), the effect of space charge production during the discharge growth and its effect on the Laplacian Electric field is taken into account by means of simultaneous solution of the continuity equations for electrons and ions and the Poisson equation for electric field strength [3].

Ion-drift
Within the context of the formation of a leader precursor (described in section 4 below) ion drift refers to the process whereby positive and negative ions formed at the end of a streamer filament drift apart and cause a local field enhancement which may cause a re-start of avalanche activity.

As described by Van Der Zel [2] , ion drift may also refer to the phenomenon when the voltage applied to the geometry is not high enough to result in a seed electron being detached from a negative ion and the negative ions are allowed to *drift* out of the high stress region near the point (the critical volume), a discharge might not occur due to the lack of the initiating electron. This is also sometimes referred to as the "sweep-field effect."

Corona Stabilisation
Corona stabilisation generally refers to the specific phenomenon whereby positive ions created by a partial discharge are allowed to accumulate around the point electrode due to a slowly rising applied voltage (positive polarity). This accumulated positive charge decreases the electric field strength at the point. The inception of a leader will consequently occur at a higher voltage. This is discussed in more detail in section 5 of this paper.

3. Significance Of Corona Stabilisation

Of great importance in determining the reliability of gas insulated equipment are diagnostic tools. Defects in the metal-enclosed equipment are difficult to locate and characterise, and yet this has to be done by external measurements. One of the most common types of defect in SF₆ GIS are metallic particles which occur despite meticulous manufacture and assembly of the equipment.

These particles cause a local field enhancement which leads to partial discharges and sometimes to breakdown and thus failure of the equipment and an expensive forced outage. Invariably, breakdown occurs on the positive half cycle of the a.c. voltage. The pressures at which the GIS operates is within the corona-stabilisation zone, and this is most likely the breakdown mechanism that operates in the case of such particle induced faults. It is thus important to understand the physical mechanism of corona stabilised breakdown.

Furthermore, in addition to in-service, on-line diagnostics, research is being done in diagnosing a GIS while off-line by means of applying impulse voltages to the system. The corona stabilised behaviour of certain defects under impulses of different risetimes will provide information on the defect characteristics.

4. Impulse Breakdown In Non-Uniform Field Gaps

In order to understand corona stabilised breakdown, it is essential to understand the stabilisation-free mechanism under fast rising impulses, since certain physical processes that occur in the latter case *must* take place under slow-rising voltages as well.

The most recent state of understanding of the mechanism of breakdown in electronegative gases in non-uniform fields and under fast-rising voltage waveforms is discussed here. This theory was mainly developed by Niemeyer [4] and Wiegart et al [5]. In SF₆, under the conditions just mentioned, breakdown will

occur via a mechanism called *leader breakdown* for pressures greater than about half an atmosphere.

Leader breakdown occurs via a sequence of physical processes. These will be discussed with the aid of Figure 1 below, where they are schematically represented :
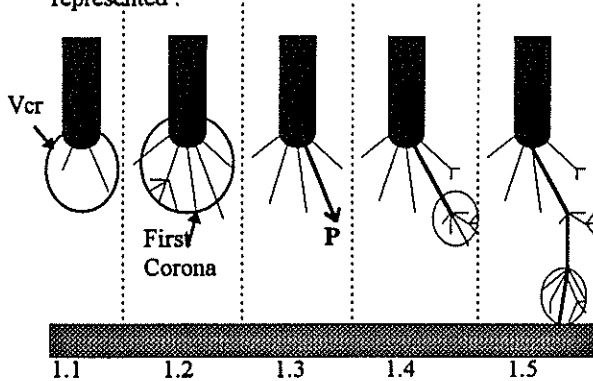
Figure 1 : Stepped Leader Breakdown [4]

The mechanism responsible for leader formation (under positive breakdown) is the *Leader Precursor* mechanism.

As the voltage applied to the point increases, a region develops around the electrode where the electric field strength within this region exceeds the Critical Electric Field strength for SF_6 , E_{cr} (which is about 89 kV/cm bar, the field strength where the ionisation coefficient equals to the attachment coefficient). This region is called the *Critical Volume* V_{cr} (Figure 1.1). Electrons are required for avalanches to begin - for positive polarity these primary electrons become available via *field-induced detachment from negative ions* present in the critical volume. For negative polarity, electrons are emitted from the metallic cathode via field emission. Electron avalanche ionisation takes place. Furthermore, once the streamer inception criterion is met , filamentary streamers form.
The streamer criterion is given by

$$\int_0^{x_{cr}} \overline{\alpha} \ dx > K \qquad \ldots(1)$$

where $\overline{\alpha}(E)$ is the field dependent net ionisation coefficient, x is the co-ordinate on the electric field line along which the streamer develops and K is an approximate constant determined by the critical avalanche size needed for streamer propagation - approximately 10.5 for SF_6 .

These streamers propagate into the gap and form the first corona (Figure 1.2). A streamer is a narrow channel of ionisation which propagates under control of the space charge in its tip and having a field in its trail equal to E_{cr} .

Photoionising quanta from the first avalanches cause streamers to develop at other locations in the critical volume, and in this manner a *complex pattern of filaments* is formed. One or two of the streamer filaments protrude out from the critical volume (Figure 1.2) because they carry more space charge in their tips which cause higher localised electric fields, these are then likely candidates to form leaders.

The streamers stop propagating at the boundary when the conditions for streamer propagation at the streamer tips are not fulfilled any longer. When this happens, the electrons in the streamer channels get rapidly attached . This leads to a number of positive and negative ions being left in the channels.

Now, the mechanism that creates the Leader is the Precursor (P in Figure 1.3) : The ions left behind in the

channel drift apart due to electrostatic forces - the negative ions towards the anode and the positive ions towards the cathode. The electric field near the corona periphery is close to E_{cr} , and the incremental potential developed between the opposite polarity ions drifting apart increases the electric field by ΔE. This means the critical field is exceeded and ionisation activity begins anew. The increase in current due to ionisation activity soon leads to field distortion making the process unstable and leading to further avalanches. The filament soon becomes conductive when the current reaches the point electrode and a leader is formed. The Precursor therefore starts at the corona boundary and propagates towards the electrode.

Once a leader section is formed , it serves as a virtual electrode which is a conductive channel from the periphery of the primary corona to the point electrode. A second corona is launched from the leader tip further into the gap (Figure 1.4 shows secondary corona formed). The second corona injects more current into the leader channel leading to increased ohmic heating and thermal expansion of the leader. Eventually the gas in the leader channel dissociates.

As a result of dissociation, the attachment ability of SF_6 is diminished and consequently the value of the critical electric field in the dissociated region becomes smaller. The critical field in the leader is strongly reduced and a plasma channel is thus formed. The leader now has strongly reduced further heating and a low voltage drop. The potential at the leader tip is therefore close to that of the electrode. The process is now repeated and the leader extends into the gap in jagged steps until in reaches the plane and thus bridges the gap completely (Figure 1.4 and Figure 1.5).

5. Corona Stabilisation Under Slow-Rising Waveforms

Figure 2 below shows schematically the difference between breakdowns from a point electrode to which fast rising and slowly rising positive voltages are applied.
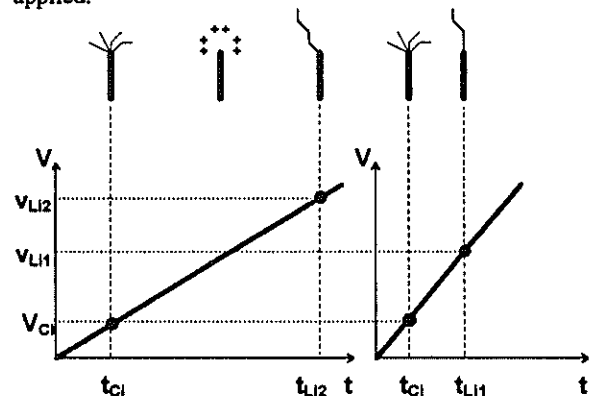
Figure 2: Schematic representation of breakdown from a point electrode under slow and fast rising applied voltage waveforms

In both cases, V_{ci} is that potential at which measurable corona (i.e. streamer corona as described in section 4 above) is formed at time t_{ci} . In the case of the waveform with the high dV/dt, the voltage at which there is a sufficiently high field to allow leader development (V_{Li1}) is reached in a short time t_{Li1}. The leader almost always follows a path along the central axis of the point - i.e. the leader follows a straight path. Breakdown then occurs when the final leader step arrives at the cathode.

In the case of a slowly rising waveform, once the streamer corona is formed, there is a time lag that is

long enough to allow the negative ions that remain in the streamer channels to drift back into the point anode. The only charged particle species remaining in the gap are positive ions which are drifting towards the cathode. It is believed that the presence of the positive ions decreases the field strength at the point sufficiently to prevent leader formation even though the applied voltage is at a high enough level that would cause leader inception in the absence of the positive charge. The positive ion distribution thus acts antagonistically to the applied voltage. As time elapses, the applied voltage increases further and the ions drift farther away from the point. A stage is thus reached when the applied voltage overcomes the opposing effect of the positive ions and a leader is allowed to form. The leader path is curved, indicating that the ions have not drifted far enough away not to have an influence on the field. There is a specific pressure above which the streamer inception voltage is equal to the breakdown voltage - that is, corona-free breakdown occurs. This pressure is called the critical pressure P_{cr} and is also dependent of the electrode geometry. Corona stabilised breakdown thus occurs at pressures smaller than P_{cr} and greater than the pressure at which streamer-breakdown can take place (this range is generally about 1bar to 5bar). Thus predicting the critical pressure is also a necessary part of a quantitative model. A detailed description of the dependence on pressure can be found in Pinnekamp et al [11].

6. Current Qualitative Models

To date there have been no successful attempts to quantify corona stabilisation. It has been shown as early as in 1980 by Parekh et al [12] that there is no simple quantifiable relationship that can correlate all the variables such as pressure, field non-linearity, applied waveform to corona stabilisation. The conceptual model used in [2] is that of a conducting sphere at anode potential placed at the tip of the electrode. This model was proposed in Niemeyer [4] and Wiegart et al [5] but not to describe ion-drift, but to determine the critical charge needed for leader formation. Another common concept used (in Pinnekamp [11] and elsewhere) is that of an "effective rod radius" which is based on the concept of a "cloud" of ions surrounding the point and states that modelling the point electrode with an increased radius equal to the cloud radius could explain some of the observations during stabilised breakdown.

7. Recent Experimental Investigations

Almost all experimental work done thus far has been investigating the external measurable effects of the stabilisation phenomenon. There have been few experiments done investigating the microscopic physical processes (such as the spatio-temporal distribution of charge), this is because of the difficulty and expense of designing such experiments. An example of an experiment that measures the distribution of space charge field distribution in *air* using a excimer-laser is given in Soulem et al [6]. Unfortunately, no such work has been done in SF_6, the experiments that have been done however, have improved our understanding of corona stabilisation considerably. Two of the most recent works published will be described here, namely the work by Rong et al [7] and Van Der Zel [2].

Rong et al [7] investigated the effect of positive waveforms of different risetimes on corona

stabilisation - this is the only work that investigates the *steepness* of applied waveforms rather than the actual waveshape (the voltage steepness is taken as the ratio of peak voltage to the front time of the impulse). Investigations into the effect of waveshapes have been done in earlier work by Chalmers et al [8] and by Sastry et al [1]. The key results of Rong et al are as follows : For small particle defects, under positive applied voltages and operating pressures above 1 bar, there is a 100% probability of corona stabilisation if the voltage waveform steepness is smaller than 5kV/μs ; there is almost a 0% probability if the waveform rises faster than 100kV/μs. The probability drops almost linearly (on a log scale) from the 5kV/μs limit to the 100kV/μs limit. Thus for off-line on site impulse tests, an impulse faster than about 50kV/μs must be used to ensure a high probability of a particle defect in the enclosure causing a breakdown and being detected.

Van Der Zel [2] measured the angle at which the leader is launched under applied impulses of different risetimes (including Very Fast Transients). The times to breakdown were statistically correlated with the leader launch angle. The findings of this study were that the current rule-of-thumb than an impulse with a risetime greater than 10μs always causes stabilisation is false. It was found that breakdown with and without corona stabilisation occurred both above and below the 10μs threshold. Also, it was found that when corona stabilisation occurred, the leader almost always followed a curved path.

8. Finite Elements Model

In order to understand the characteristics of the corona ion sheath or "cloud" and its influence on the electric field distribution it was thought that a finite elements model could prove useful. The finite elements model could also be used to test the "equivalent rod-radius" concept of corona stabilisation which uses a conducting sphere to model the situation. A commercial finite elements package, in particular a two-dimensional axi-symmetric electrostatic solver was used. The geometries modelled were the following, corresponding to the experimental setup used by Van Der Zel [2] :

3.1   3.2   3.3
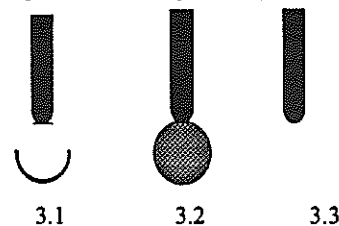
Figure 3: Models Used (Figures not to scale)

Figure 3.3 shows a space-charge free point, figure 3.2 a conducting sphere of radius 1mm at the point, and figure 3.1 shows a thin (about 10 microns) hemispherical shell in space around which charges are distributed. All the points were 0,5mm in radius and the plane 20mm away. The radius of the sphere in figure 3.2 and the radius of the arc in figure 3.1 is 1mm. The radius of the corona sphere\hemisphere used here was determined experimentally in [2] and theoretically in [4].A voltage of 100V was applied to the rod. The actual magnitude of voltage applied is not important since we are interested in comparing the results obtained for the three geometries, and the results will thus be normalised to the maximum value.

9. Results and Discussion

A plot of the electric field magnitude versus angle along an arc close to the tip of the rod is shown in figure 4, the central axis of the rod corresponds to 0 degrees and the arc spans 90 degrees in an anticlockwise direction. The results for the conducting sphere are not plotted, but will be described.

E-field magnitude versus Angle
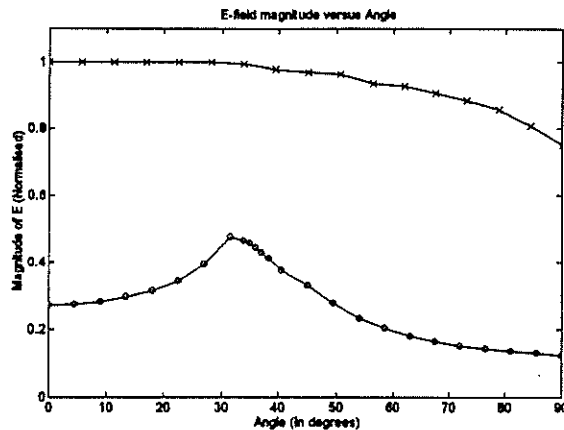
Figure 4 : E-Field magnitude versus angle along an arc in front of the tip (normalised to the maximum value) :
4.1 x = *without space charge*
4.2 o = *hemispherical shell distribution of space charge(Q=1pC)*

Modelling the space charge as a conducting sphere does not seem to be the best way to do so. The field strength in the region between the sphere and the rod is highly reduced - since the sphere is conducting, it is at the same potential as the rod, so the junction forms an equipotential surface. Thus in this case, the leader will not develop at an angle, since the maximum field is found to be at the *tip* of the sphere - i.e. along the central axis of the point.

It is clear from the plot in figure 4.1 (for the space charge free point) that the maximum stress occurs when the angle is zero - that is along the central axis. By placing positive charges in a hemispherical shell distribution with a radius the same as that of the conducting sphere the results allow tentative conclusions to be drawn about leader launch angles. It is clear from the graph in figure 4 (4.2 - with space charge), that the electric field magnitude is greater along paths that are at angles greater than 0 degrees - i.e. away from the central axis. Also, as the magnitude of charge was increased, the magnitude of the field dropped accordingly. Thus the larger the amount of charge injected by the discharge, the greater the degree of stabilisation. Also, the spread of angles of leader launches found experimentally by Van Der Zel [2] (i.e. most of the leaders leaving at angles greater than about 40 degrees) have been to an extent verified - the field strength reaches a maximum at about that angle and then drops off slowly - a leader will form more easily in a higher field region.

The charged conducting sphere method is clearly not a useful device for looking at corona stabilisation effects. This model was proposed by Wiegart et al [5], because it could model corona structure effectively when calculating the *critical charge* necessary for leader inception - it was not meant to model the ion cloud. The idea of conceptually using a

thicker "virtual point" of radius equal to the space-charge "cloud" to model stabilised breakdown will probably predict the higher breakdown voltage (since it accounts for a reduced field). It does not however describe the physical processes and will not predict the angular leader launch.

10. Conclusions

It is clear from the previous simulations that the distribution and magnitude of residual charge at the end of a discharge is the key factor controlling the field stress around the point electrode which controls the next discharge\leader formation. It is therefore important to understand how the first discharge develops in the virgin gap. From experimental evidence (Van Brunt [9], Niemeyer [10]), it has been shown that under dc and ac conditions (in a positive point-plane arrangement), discharges consist of a number of randomly spaced pulses with an initial large pulse and a trail of smaller pulses before breakdown occurs. Any attempted physical description must be able to explain these effects . The results presented here are used in modelling the phenomena [13].

References

[1] Sastry K.S.A. et al , *Breakdown Of SF₆ Gas Under Inhomogeneous Fields Under Impulse Voltage Of Different Waveshapes*, Sixth International Symposium On High Voltage Engineering, New Orleans, Paper 32.01, 1989

[2] Van Der Zel G.L. , *The Effect Of Corona Stabilisation On Positive Impulse Breakdown In SF₆* , Ph.D. Thesis, University Of The Witwatersrand, 1993

[3] Morrow R. , *Theory of Positive Corona in SF₆ Due To A Voltage Impulse*. IEEE Transactions On Plasma Science, vol. 19, no. 2, pp.86-94, 1991

[4] Niemeyer L. et al , *The Mechanism Of Leader Breakdown in Electronegative Gases*. IEEE Transactions on Electrical Insulation, Vol. 24, No.2 ,pp.309-324, 1989

[5] Wiegart, N. et al. *Research Report CEA No. 153 t 310 Corona stabilisation to testing of gas-insulating switchgear*, Canadian Electrical Association, 1985

[6] Soulem N. et al, *Laser Investigation Of Positive Point To Plane Corona Discharge In Ambient Air*, Tenth International Conference On Gas Discharges And Their Applications, Swansea, p.286, 1992.

[7] Rong X. et al, *Influence Of The Steepness Of Impulse Voltages On The Corona Stabilization In SF₆* , Tenth International Conference On Gas Discharges And Their Applications, Swansea, p.298, 1992.

[8] Chalmers I.D. et al, *The effect of impulse waveshape on point plane breakdown in SF₆* , Gaseous Dielectrics IV, Proceedings of the Fourth International Symposium on Gaseous Dielectrics, Knoxville, p.344, 1984.

[9] Van Brunt R.J. and Leep D., *Characterization of point-plane corona pulses in SF₆* ,J. Appl. Phys. , 52, p.6588, 1981

[10] Niemeyer L. et al, *Phase Resolved Partial Discharge Measurements In Particle Contaminated SF₆ Insulation*, Gaseous Dielectrics VI, Proceedings of the Eighth International Symposium on Gaseous Dielectrics, Knoxville, p.579, 1991

[11] Pinnekamp F. and Niemeyer L. , *Qualitative Model Of Breakdown In SF₆ In Inhomogeneous Gaps*, J. Phys. D: Appl. Phys., Vol 16, p.1293, 1983

[12] Parekh H., Srivastava K.D., *Some Computations And Observations On Corona Stabilised Breakdown In SF₆* , IEEE Trans. Elec. Ins., EI-15, p.87, 1980

[13] Bhutt S. et al, *Corona Stabilisation In SF₆ : Modelling*, These Proceedings

Address of main author
Mr. Sanjeev Bhutt, Electric Power Research Group, Department of Electrical Engineering, University of the Witwatersrand, Private Bag 3, WITS, 2050. E-mail : bhutt@odie.ee.wits.ac.za

Corona Stabilisation In SF$_6$: Modelling

S. Bhutt   I.R. Jandrell   J.P. Reynders

Department of Electrical Engineering
University of the Witwatersrand

Abstract
A qualitative description is proposed of the physical processes that occur during partial discharge and corona stabilised breakdown in non-linear geometries, under positive applied stresses in SF$_6$. A method is propounded to obtain an approximate quantitative model for corona stabilised breakdown. Only those processes leading up to leader formation are dealt with, that is, leader channel modelling and random leader propagation models are not included. This approach to modelling has not been validated since certain assumptions and dimensional scaling factors need to be empirically reinforced.

1. Introduction
The case of a conducting particle placed in a background electric field is technically more significant than a point to plane laboratory setup. One of the main factors limiting the operating stress of GIS equipment is particle contamination which can reduce the insulation level by as much as 90 percent (Dale et al [2]). Furthermore, one of the primary uses for a model would be identification of the particle in the context of GIS diagnostics. Thus a model relating the particle characteristics to measurable discharge parameters would be very useful. The approach to modelling the discharge processes presented here is based on a generalised model for partial discharge proposed by Niemeyer [3]. A simplified treatment is presented of most of the concepts and references are given to the appropriate publications where a more thorough treatment may be found.

2. Qualitative Description Of Physical Processes
Experimental findings show that partial discharges from point electrodes (i.e. very non-uniform fields) under positive applied stresses consist of a sequence or burst of pulses with an initial pulse of large amplitude followed by much smaller pulses (Van Brunt [4] and Niemeyer [5]).

The first large magnitude pulse probably corresponds to the initial streamer corona as described in [1]. The initial streamer propagates a considerable distance into the virgin gap. The corona structure has a roughly spherical envelope with a well defined boundary (Niemeyer [6]). The corona consists of a complex pattern of streamer filaments which have a mainly radial spatial extension.

At the tips of each streamer filament, when the corona stops growing, electrons get rapidly attached thus forming negative ions. If, at this stage the applied voltage is not high enough to cause leader precursor development (as described in [1]), the highly mobile electrons in the streamer trails drift back into the anode.

The negative ions in the streamer also begin to drift back towards the anode, whereas the positive ions in the streamer tips drift towards the cathode. Since the corona boundary is roughly spherical, the positive ion distribution is assumed to be roughly hemispherical in the finite elements model used in [1].

The positive ion distribution acts to lower the electric field magnitude around the point. However, the negative ions that are still in the region between the positive ions and the point act to *increase* the field at the point. Conceptually, this may be thought of as a new

critical volume which is smaller in size than that in a space charge free gap. Besides causing the field enhancement, these negative ions also serve the purpose of supplying seed electrons for new avalanches. The negative ions produce electrons via detachment and these electrons cause avalanches - these avalanches are therefore the secondary events in the measured burst of pulses. Also, the temporal distribution of the secondary pulses are found to be random, and this randomness can be explained by the probabilistic nature of field detachment from the negative ions.

These secondary avalanches or streamers which develop in the wake of the first streamer will not propagate as far into the gap due to the shielding effect of the residual positive ion space-charge, and thus will be of lower magnitude than the primary pulse. The secondary streamers clearly leave behind more positive ions, the negative ions that are also formed have a short distance to travel to be absorbed into the anode. The number of negative ions in the gap diminish with time after the initial streamer, thus steadily reducing the probability for initiating electron formation time [4].

In the case of a dc applied voltage, once a critical amount of positive charge builds up , thereby ensuring that the field in front of the anode is sub-critical everywhere, all ionisation activity stops and the measured burst of pulses also stops. After a time has elapsed that is sufficient for the positive ions to have drifted far enough away from the anode to allow a critical field to exist again, ionisation activity will restart once a first electron becomes available in this critical volume. Another pulse burst will then be measured.

For the dc case, the Laplacian background field stays constant and there are thus only two factors controlling the change in the field distribution around the point - that is, the positive and negative ion distributions. For the case of a slowly rising applied impulse, the Laplacian field is also increasing slowly. The initial discharge stages will be almost the same as in the dc case. However, once the initial corona burst occurs, the rising voltage ensures that there is always a finite increasing critical volume surrounding the point electrode. Therefore, once the initial large corona has formed, and the positive ions form the hemispherical sheath at the corona boundary, the negative ions drifting to the anode provide the seed electrons which lead to the formation of a new streamer corona. This secondary corona will be larger than in the dc case because the increasing applied voltage will ensure a larger critical volume. It is clear from the modelling done in [1] that if a secondary streamer "brush" develops between the anode and the positive ion sheath, those filaments of the streamer that develop at angles greater than 0 degrees from the central rod axis are subjected to a larger background field. These filaments are therefore likely candidates for leader precursor formation. This explains the predominantly curved nature of leader paths. The applied voltage will have to increase to a large enough magnitude to allow the secondary streamer to produce a precursor. This explains the larger breakdown voltages under the slow impulses.

The rate of formation of the positive ion cloud from the primary event is a key factor controlling the

following discharge events. The rate of ion accumulation is dependent on the drift velocity (and thus the mobility) of positive ions in SF_6 . Positive ion mobility is dependent on pressure according to an approximate inverse relationship (Wiegart et al [7]), i.e. $\mu_+ \propto \frac{1}{P}$

Therefore, at higher pressures the mobility of the ions is reduced and a faster build-up of ions could be expected to occur and therefore a corresponding increase in stabilisation.

Implications for modelling

We are interested in a model for breakdown under slowly rising voltages - that is, ac as well as slow switching impulses. Clearly, in the case of the ac waveform, there are discharge events that occur during the negative half cycle, the memory effects of which may affect events on the next positive half cycle. There has not been any work done to date that quantifies these effects, so we will treat the ac case as just a slowly rising positive waveform. Furthermore, the formation of the "brush" type streamer pattern has been questioned by Farish [8], who has found that under dc corona, there is only *one* streamer filament, which is measured as the initial pulse, and the subsequent measure pulse burst is due to the re-striking of the same filament and Farish states that this is the mechanism more likely to occur for slowly rising ac waveforms. It has been suggested by Niemeyer [5] that the restrike mechanism operates at low voltages, and that the size and complexity of the streamer corona increases with voltage. Also it has been found that at high pressures, the bursts are very narrow and often only the single pulse appears(Van Brunt [4]). It is therefore deemed acceptable to base a model on the concept of a single initial "brush" streamer corona.

3. Approach To Quantitative Modelling

It is apparent from the foregoing discussion that the breakdown process comprises of complex and interwoven physical processes dependent on a large number of parameters. An approach is presented whereby approximate relationships between defect characteristics and discharge events are used to provide an order of magnitude estimate model. Note that only the partial discharge and the inception of the leader is considered. A complete breakdown model will have to model the leader channel growth and propagation. Once the first leader step is formed, it launches a new corona which gives rise to the next leader step and so on until the leader channel either extinguishes or the final leader step reaches the cathode and breakdown occurs.

Modelling the leader stepping process is in itself highly complex and will not be looked at in this work. Detailed treatment of the physics of leader propagation may be found in Niemeyer et al [6] and Wiegart et al [7]. The actual path followed by a leader is a random process and is of great importance in some practical situations such as in disconnector flashover where a leader model should predict whether the flashover will occur from the moving contact to the opposite electrode or to the grounded enclosure. The random aspects of leader branching is dealt with by Niemeyer et al in [6], [9] and [10].

4. Geometry Used

The geometry used is that of a fixed conducting particle defect in a uniform background field. The particle is characterised by its length and radius as shown in figure 1, where L_p is the particle length, r_p the particle radius and E_0 the applied background field.
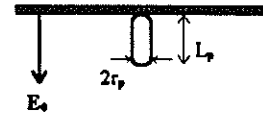
Figure 1: Particle In Uniform Field

5. Method Of Modelling

The modelling process is as follows :
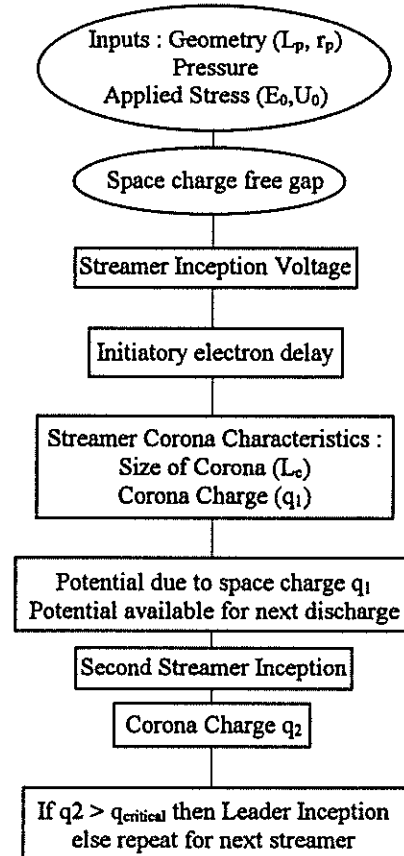
Figure 2: Simplified Flow Diagram For Leader Inception Calculation

Applied Stress

The applied waveform may be taken as ac, in which case the peak charge contained in the discharge at the peak of the voltage waveform may be calculated as in [3],[5]. Or the model may be adapted so that the values of U_0 (and thus E_0) may increase in time according to some slowly-rising applied waveform. For example, according to Rong et al [13], there is a 100% probability of stabilisation if the steepness of the applied impulse is smaller than 5kV/µs, therefore using time steps of 1µs and increasing U_0 by 5kV each time step could be a method used.

Electrode Geometry

If a point-plane geometry is used, it is necessary to use some numerical calculation method to determine the electric field magnitude at the point. In the case of a particle in a background electric field, it is possible to derive an analytical expression for the field intensification caused by the particle. Cooke [11] has derived an expression to calculate the electric field at the tip of a particle of length L_p and a hemispherical tip of radius r_p. Equation (1) gives the electric field magnitude, E, at a radius x from the centre of the hemispherical tip of the particle with the applied background field E_0.

$$E = E_0\left[1+\left(\frac{L_p}{2r_p}\right)\frac{4r_p^2}{4x^2}+\frac{\left(2r_p\right)^3}{4x^3}\right] \qquad \ldots (1)$$

Streamer Inception

To calculate the voltage at which streamer inception occurs, the well known Nitta-Shibuya [14] formula (equation (2)) may be used.

$$U_{si}=\left(\frac{E}{p}\right)_{cr} p\frac{\left(1+\frac{a}{\sqrt{pR}}\right)^2}{\left(\frac{E}{U}\right)_{max}} \quad , a\approx 2{,}783\ Pa^{1/2}m^{1/2} \qquad \ldots (2)$$

(R is the rod-radius)

This equation was however conceived for point to plane geometries. A method of determining inception in the case of a particle defect is derived by Niemeyer [3] :

$$U_{si}=\frac{\left(\frac{E}{p}\right)_{cr} pF\left[\left(pL_p\right)\left(\frac{L_p}{r_p}\right)\right]}{\frac{E_0}{U_0}} \qquad \ldots (3)$$

The ratio E_0/U_0 is the reduced background field at the defect location (in the absence of the defect). F is a dimensionless streamer inception function. For a given defect (i.e. defined by aspect ratio L_p/r_p), F is dependent on the product pL_p. Curves plotting the function F in dependence of pL_p for various L_p/r_p ratios are given in [3]. From equation (3) it can be seen that the measured inception voltage provides information (at a known pressure) about the particle's physical characteristics, length and aspect ratio, as well as the reduced background field at the particle location. This could be useful for GIS diagnostics.

First-Electron Delay

The measured streamer inception voltage for increasing waveforms of positive polarity is invariably larger than that predicted by the streamer criteria. This is mainly due to first electron delay. The initial electron needed to start an avalanche is, in SF_6, believed to be provided by field-induced detachment from negative ions created in the ambient gas by cosmic radiation [7]. The probability of the "first" electron being made available for an avalanche and of the avalanche surviving to reach streamer size has a significant effect on the streamer inception and breakdown voltages. There have been a few attempts to describe this probability mathematically, detailed accounts of which may be found in [7] and [12]. Wiegart et al [7] have produced an approximation for the first electron delay which takes into consideration factors such as the equilibrium ion concentration in the virgin gas, the influence of the electric field and electrode geometry on the ion concentration as well as the field dependent detachment process. The approximate time lag may be calculated using a modified volume-time law [7]:

$$P(t)=1-e^{\{-\int_0^t\int_{Vcr}\frac{dn_e}{dt}\left(1-\frac{\eta}{\alpha}\right)dVdt\}} \qquad \ldots (4)$$

The integration in space in (4) is done over the critical volume (Vcr). dn_e/dt is the electron production rate, the calculation of which is not a trivial problem, but simplifications are given in [7].

Corona Length

We will assume a hemispherical distribution of charge in space around the defect. The radius of this distribution will be necessary to calculate the potential difference due to the space charge. Once the first streamer corona has formed and reached its maximal length, the positive ions are distributed at the boundary

of the corona. We need to calculate the distance drifted by these ions towards the opposite electrode in order to work out the radius of the space charge distribution. The approximate radius will thus be given by the sum of the radius of the first corona boundary and the distance drifted by the ions in a given time.

The mobility of positive ions is given by equation (5) below [7] :

$$\mu_+ = \mu_+^0\left(\frac{p_0}{p}\right)\left(\frac{T}{T_0}\right) \qquad \ldots (5)$$

$$\approx 6x10^{-5}\frac{m^2}{Vs}\cdot\frac{760x1{,}33x10^2 Pa}{p}\cdot\frac{T}{273{,}16K}$$

assuming an ambient T of about 300K,

$$\mu_+ \approx 6\frac{m^2}{Vs}\cdot\frac{1}{p} \qquad \ldots (6)$$

The drift velocity is therefore :

$$v_{d+} \approx \mu_+.E \approx 6\frac{m^2}{Vs}\cdot\frac{E}{p} \qquad \ldots (7)$$

The distance covered by the ions in time t is thus :

$$L_{drift} = v_{d+}.t \qquad \ldots (8)$$

As an approximation, the corona length may be taken as the length of the longest streamer which is given in [6] :

$$L \approx C_1\left(\frac{U}{E_{cr}}\right) \qquad \ldots (9)$$

where C_1 is approximately $= 0.5$

The radius of the positive ion distribution is therefore approximately equal to $L_{drift} + L$, i.e.

$$L_{total} = L_{drift} + L \qquad \ldots (10)$$

Corona Charge

The charge in the initial corona structure can be calculated using the method described in [3], where the true charge deployed by the initial discharge has been derived to be approximately given by :

$$q_1 \approx \frac{\pi\left(L_p.E_0\right)^2}{\left(\frac{E}{p}\right)_{cr}.P} \qquad \ldots (11)$$

This equation for charge arises from a more complicated expression derived in [3] by taking the space charge distribution to be in the shape of an ellipsoid by taking the positive space charge deployed ahead of the protrusion to induce a mirror negative charge in the electrode. The approximate assignment of ellipsoidal axes is shown below :
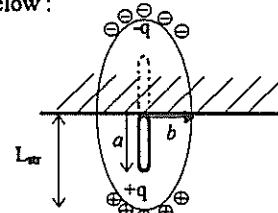
Figure 3: Equivalent ellipsoidal axes a and b

The charge deployed in a partial discharge is given by a dimensional relationship between the defect length, the potential difference due to the discharge and a dimensionless proportionality factor which accounts for the charge distribution. The details of deriving this form of charge calculation are given in [3], only the equations are reproduced here :

The equation for the true charge deployed is

$$q = \pm g.\pi.\varepsilon_0.L.\Delta U \qquad \ldots (12)$$

and the dimensionless proportionality factor g is given by

$$g=\frac{1}{2}\frac{a/L}{\left(a/b\right)^2}\left[1+\varepsilon_r\left(K\left(a/b\right)-1\right)\right] \qquad \ldots (13)$$

where a and b are the approximate axes of the ellipsoid and K is a dimensionless function of a and b. K is approximately 3 for a spherical ellipsoid and is about equal to $4a/b$ for prolate ellipsoids [3].

The potential due to the space charge is then

$$\Delta U_{qs} = \frac{q_s}{g\varepsilon_0 L} \qquad \qquad ...(14)$$

g can be calculated from (13) where a is approximately equal to the defect length, and b equal to the streamer length [3]. We can replace the b by the streamer length plus the distance drifted by the ions as calculated by equation (10). q_s is the true charge injected by the first corona, q_1.

Second Corona Charge

According to Niemeyer [3], there are two contributions to the enhanced field (driving the partial discharge) at the defect. The applied voltage which is the enhancement of the background field E_0 by the defect, as well as the effect of space charge. These two contributions can be integrally expressed by the potential differences they cause over the gap. This is expressed in equation (15):

$$\Delta U = \Delta U_a + \Delta U_q \qquad \qquad ...(15)$$

ΔU is the potential difference available across the gap to drive the discharge. ΔU_a is due to the enhanced applied field. ΔU_q is given by equation (14) above. Whereas in the calculation of the first streamer corona (space charge free) the contribution of ΔU_q is neglected, the calculation is repeated for the second corona with the potential due to the space charge from the previous discharge included. A new value for injected charge, q_2, can now be calculated by using the same method as for the space-charge free case but with a new value of potential difference (and electric field) corrected for the space charge potential difference.

Critical Charge

Wiegart et al [7] have determined a leader-inception criterion based on the amount of charge injected by an impulsive streamer corona. Once a critical value of charge is exceeded, there is sufficient energy to allow leader formation. This criterion is simplified into an equation suitable for use in a model

$$Q_{cr} = 45nC\left(\frac{p}{100kPa}\right)^{-2,2} \qquad ...(16)$$

If the second corona charge q_2 is greater than Q_c, then the leader inception criterion has been met. If this condition is not met, the calculation method should be repeated with the new space charge q_2.

6. Limitations

It is important to note that the work presented here applies to *fixed* particle defects. That is, the effect of the particle's motion is not taken into consideration. This would be the next step once a verified model is constructed. Work done on investigating the effects of particle motion on breakdown and partial discharge has been done by Anis et al [15] and Mosch et al [16].

The modelling method presented here represents an amalgamation of models presented by various sources for different aspects of the total breakdown process. Each stage therefore needs to be experimentally verified so that the various dimensional factors can be "tweaked" so that they are more accurate and practically applicable.

7. Conclusions

A detailed qualitative description of corona stabilised breakdown was presented. This qualitative model accounts for the angular leader launch, pre-discharge pulse bursts, as well as for the higher breakdown magnitudes. Also presented was an approach to obtaining order-of-magnitude quantitative models for discharge and leader formation in the case of a fixed conducting particle defect. Due to the complexity of the various processes that occur during corona stabilised breakdown, the approach of using order-of-magnitude dimensional scaling factors and semi-empirical criteria is the only way to obtain some sort of quantitative model. It is believed that further work in implementing this model and experimentally enhancing the model by verifying the dimensional scaling factors will lead to a useful reasonably accurate model.

References

[1] Bhutt S. et al, *Corona Stabilisation In SF_6 : Current Understanding*, These Proceedings

[2] Dale S.J. and Wooton R.E., *Effect of fixed particle protrusions on 60Hz and Impulse Breakdown Voltage-Pressure Characteristics In SF_6* , paper 32.10, Third International Symposium On High Voltage Engineering, Milan, 1979

[3] Niemeyer L. , *A Generalized Approach To Partial Discharge Modeling* , IEEE Trans. Dielec. and Elec. Ins., vol.2, no.4, p.510, 1995

[4] Van Brunt R.J. and Leep D., *Characterization Of Point-Plane Corona Pulses in SF_6* ,J. Appl. Phys. , 52, p.6588, 1981

[5] Niemeyer L. et al, *Phase Resolved Partial Discharge Measurements In Particle Contaminated SF6 Insulation*, Gaseous Dielectrics VI, Proceedings of the Eighth International Symposium on Gaseous Dielectrics, Knoxville, p.579, 1991

[6] Niemeyer L. et al , *The Mechanism Of Leader Breakdown in Electronegative Gases*. IEEE Transactions on Electrical Insulation, Vol. 24, No.2 ,pp.309-324, 1989

[7] Wiegart, N. et al. *Research Report CEA No. 153 t 310 Corona stabilisation to testing of gas-insulating switchgear*, Canadian Electrical Association, 1985

[8] Farish O. et. al. , *Prebreakdown Corna Processes In SF6 And SF6 Mixtures*, paper 31.15, 3'rd International Symposium on High Voltage Engineering, Milan , 1979

[9] Niemeyer L. , *A Stepped Leader Random Walk Model*. Journal of Physics D: Applied Physics. Vol. 20 , pp.897-906, 1987

[10] Niemeyer et. al. , *Fractal Dimension Of Dielectric Breakdown*, Physical Review Letters , vol. 32, no. 12, pp.1033-1036, 1984

[11] Cooke C.M., *Surface Flashover Of Gas/Solid Interfaces*, IIIrd International Symposium on Gaseous Dielectrics, Knoxville, p.337, 1982

[12] Wiegart N. , *A Model for the production of initial electrons by detachment of SF_6 ions*, IEEE Trans. , vol 20, p.587, 1985

[13] Rong X. et al, *Influence Of The Steepness Of Impulse Voltages On The Corona Stabilization In SF_6* , Tenth International Conference On Gas Discharges And Their Applications, Swansea, p.298, 1992

[14] Nitta T. and Shibuya Y., *Electrical Breakdown of Long Gaps In Sulphur Hexafluoride*, IEEE Trans. PAS-90, p.1065, 1971

[15] Anis H. et al, *Corona Stabilized Breakdown In Particle Contaminated Compressed SF_6 Systems*, Gaseous Dielectrics IV, Proceedings of the Fourth International Symposium on Gaseous Dielectrics, Knoxville, p.387, 1984

[16] Mosch W. et al, *Phenomena In SF_6 Insulations With Particles And Their Technical Valuation*, Third International Symposium On High Voltage Engineering, paper 32.01, Milan, 1979

Address of main author
Mr. Sanjeev Bhutt, Electric Power Research Group, Department of Electrical Engineering, University of the Witwatersrand, Private Bag 3, WITS, 2050, E-mail : bhutt@odie.ee.wits.ac.za

PRELIMINARY RESULTS IN THE DEVELOPMENT OF A RESONANT PARALLEL PLATE COUPLER FOR DETECTION OF PARTIAL DISCHARGES IN GIS.

S.D. Nielsen and J.P. Reynders
Department of Electrical Engineering
University of the Witwatersrand
Johannesburg.

Abstract:

This paper presents the preliminary results in the development of a parallel plate resonant PD coupler. The coupler has a calculated dominant resonant TM mode at 1.953GHz. It has been shown that for the greatest sensitivity at the dominant resonant mode, the pick off point should not be in the centre of the plate, but at the edge of the plate. In order to eliminate the excitation voltage signal, it is proposed that the coupler should be shorted out in the middle of the plate. In order to reduce the dominant resonant frequency of the coupler down to one that can be accommodated by the equipment at hand, a capacitively tuned coaxial resonant cavity was constructed. This resonator has a resonant frequency of 172 MHz.

1) Introduction:

The detection of PD's (Partial Discharges) in GIS has become widely used as an important diagnostic technique for GIS /1/. This paper will describe the preliminary results in the development of a resonant parallel plate coupler to be used as part of a research project on the detection of PD's in GIS under both power frequency conditions and under LI (Lightning Impulse) conditions.

Parallel plate PD couplers in the TEM mode can be viewed as a high frequency capacitve voltage divider with a high pass characteristic. The "divider" should have as low a division ratio as possible for best sensitivity. Commercial couplers are generally terminated into 50Ω /1/. The combination of the termination resistance and the capacitance of the coupler result in a high pass characteristic. This high pass characteristic is used to filter out the excitation

voltage signal. For the coupler constructed this high pass filter would have a corner frequency of 238MHz if the coupler was terminated into 50Ω. This 50Ω termination also prevents reflections of the PD signal along the co-axial cable. Removal of the terminating resistance on an energised system will result in the appearance of a potentially lethal voltage at the output of the coupler.

The aim of this work was to construct a coupler that could be used to detect PD's under both power frequency conditions and Lightning Impulse (LI) excitation. The resulting high pass filter using a 50Ω termination would not be effective against LI excitation and the noise produced by the impulse generator. Some other method must therefore be found to reject noise and the exciting voltage signal.

2) Resonant frequency of a disc coupler:

This section will present the theory of the resonant modes of a UHF disc coupler. *Figure 1* shows the basic construction of the parallel plate coupler. Provided that the disc is relatively close to the ground plane in comparison with its radius, only two-dimensional resonances need to be considered. Fringing fields at the edge of the disk are not included in the analysis. Because of the small height of the dielectric compered to the radius of the plate, all fields in the coupler are of TM mode with respect to the z axis. The angular resonant frequencies ω_{nm} are given by /1, 2, 3/:

$$\omega_{nm} = \frac{x_{mn}}{a\sqrt{(\mu\varepsilon)}} \qquad (1)$$

Where:

ω_{nm} = angular resonant frequency.

x_{nm} = the mth non-zero root of

$J_n(x)$, the Bessel function of the first kind of order n.

$J'_n(x) = 0$ is the derivative with respect to x of

ϵ = permittivity of the insulating dielectric layer

μ = permeability of the insulating dielectric layer.

a = Radius of plate (m).
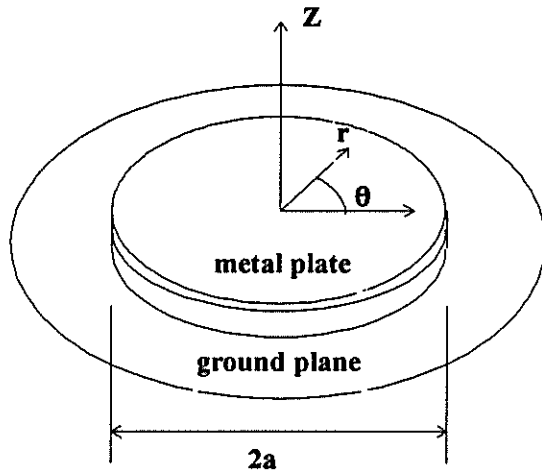
Figure 1 Configuration of the disc coupler

The non-resonant solution $x_{00} = 0$, for which the field is uniform below the disc, corresponds to the static case of a parallel plate capacitor. **Table 1** shows the first 10 higher order resonant mode frequencies and the capacitance of the plates using air as an insulating layer. The diameter of the plates is 98mm and their separation 5mm. The x_{11} mode is the dominant resonant mode because it has the lowest resonant frequency. The electric-field E_Z under the disc at resonance is described by /1/:

$$E_Z = E_0 \sin(\omega_{nm}t)J_n\left(\frac{r}{a}x_{nm}\right)\cos(n\theta) \qquad (2)$$

$$(r=0 \rightarrow a, \ \theta = 0 \rightarrow 2\pi)$$

Where:

E_0 = Constant.

Jn = nth Bessel function for all $n \neq 0$

ω_{nm} = Resonant frequency (rad/s).

t = Time (s).

Table 1 Calculated 10 higher order TM resonant modes.

n	m	x_{nm}	C_n (pF)	ω_{nm} x 10^9 (rad/s)	f_{nm} (GHz)
0	0	0	13.4		
1	1	1.841		12.27	1.953
2	1	3.054		18.69	2.975
0	1	3.832		23.46	3.734
3	1	4.201		25.70	4.090
4	1	5.318		32.54	5.179
1	2	5.331		32.62	5.192
5	1	6.416		39.26	6.248
2	2	6.706		41.04	6.532
0	2	7.016		42.94	6.834
6	1	7.501		45.90	7.305

Figure 2 shows the electric field E_Z in the dielectric layer at resonance for x_{00}, x_{11}, x_{21} and x_{01}, the first three resonant modes (Equation 2).
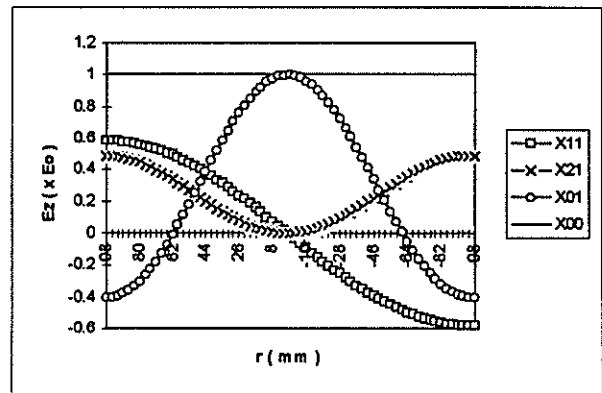
Figure 2 Electric field E_Z under the plate with $\theta=0$ and r going from 98mm to -98 mm. The electric field is plotted for x_{00}, x_{11}, x_{21} and x_{01}.

Due to the small size of the coupler (diameter 98mm), the higher order resonant frequencies of the coupler are $f_0 > 1GHZ$. Due to limitations in the measurement equipment the lowest resonant frequency possible must be used. This lowest resonant frequency is the dominant resonant mode of the parallel plate coupler corresponding to x_{11}. From Equation 1, the resonant mode of the coupler can be lowered by inserting a dielectric with a relative permittivity or permeability greater than that of air. However it was found that readily available dielectric when used at the frequency range of interest had large losses. Therefore air or SF_6 was used as a dielectric in the

prototype coupler. This gave the coupler a dominant resonant mode at approximately 1.9 GHz

3) Pick up point and short circuiting of the coupler:

Figure 2 shows E_Z for x_{11} and x_{21}. There is a maximum of the field at the two opposite edges of the plate and $E_Z = 0$ at the centre of the plate. From this it was proposed that the pickup from the top plate should be on or near to one of the edge of the plate for maximum sensitivity.

In order to reject the exciting voltage signal and any noise, it was decided to short out the coupler in the centre of the plates. This would effectively ensure that when the coupler was in the TEM mode, there would be no signal out of the coupler. This condition is met when the coupler is excited with power frequency signals and a LI signals. Shorting the coupler will modify the x_{01} electric field distribution below the plate.

4) VSWR measurements on the coupler:

VSWR (Voltage standing wave ratio) measurements were performed on the coupler. These measurements were done with a Hewlett Packard 8753C Network Analyser. The results are shown in **Table 2**. These measurements were made into 50Ω. A low VSWR points to a point of maximum power transfer. The measurements were done with the coupler shorted at the centre and at the edge of the plate opposite the pick off point.

Table 2 VSWR measurements on the coupler.

Frequency	VSWR
Coupler with no shorting points	
1705 MHz	1 : 1.88
2397 MHz	1 : 1.28
2752 MHz	1 : 2.09
Coupler shorted at the centre	
1717 MHz	1 : 1.96
2403 MHz	1 : 1.37
2767 MHz	1 : 1.88
Coupler shorted at end	
1838 MHz	1 : 5.09
2516 MHz	1 : 1.32
2950 MHz	1 : 3.26

From these measurements it is shown that the best power transfer is obtained at approximately 2.4GHz.

This does not coincide with any calculated resonant frequency of the coupler. From these measurements it is clear that two things must be done, namely:
a) Determine the true resonant points of the coupler.
b) Improve the VSWR at these true resonant points.

5) Coaxial resonant cavity:

In order to reduce the dominant resonant frequency of the coupler down to one that can be accommodated by the equipment at hand, a capacitively tuned coaxial resonant cavity was constructed. This resonator was to have a resonant frequency of 200MHz.

The type of resonator used was a short gap cavity. This is a coaxial resonator with one end shorted and the other end terminated in a capacitor to earth. For very small values of capacitance, the resonator is in the lowest resonance mode (this is nearly a quarter wave length), but for larger values of capacitance, the resonant frequency is much smaller than the frequency at which the physical parameters of the resonator give a quarter wavelength. This is due to the large capacitive loading of the coaxial line which diminishes the resonant frequency of the resonator. The resonant frequency of the resonator can be calculated using /4/:

$$\tan\left(\frac{\omega l}{c}\right) = \frac{1}{Z_o \omega C_g} \tag{3}$$

where:

ω = Resonant frequency in radians per second.
l = Length of the centre conductor of the coaxial line in m.
c = speed of light 300×10^6 m/s.
Z_o = TEM characteristic impedance of the line.
C_g = The capacitive loading of the line.

The constructed resonator has a characteristic impedance Z_0 of 48.16Ω and a length l of 220mm. *Figure 3* shows the calculated resonant frequency of the resonator verses the capacitive loading.

The resonator was designed to have a resonant frequency of approximately 200MHz. The resonant frequency could be changed by chancing the loading capacitance. The load capacitance is adjusted by changing the gap between the end of the line and earth. This is performed by means of a brass screw.

Figure 4 shows the response of the resonator to a step with a fast rising edge. The resonant frequency of the

resonator is 172Mhz. This resonator when used in conjunction with the parallel plate coupler will result in an output that is within the capability of our instruments.
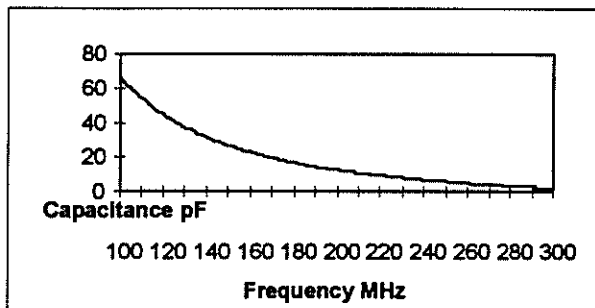
Figure 3 Shows the calculated resonant frequency of the resonator verses the capacitive loading of the resonator.
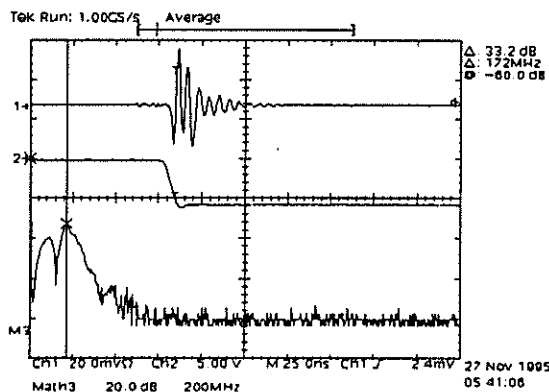
Figure 4 Response of the resonator set to resonate at 172MHz. The top trace is the response of the resonator (vertical scale 20mV/div horizontal scale 25ns/div) to a step input. The step input is shown in the middle trace (vertical scale 5V/div horizontal scale 25ns/div). The FFT of the response is shown in the bottom trace (vertical scale 20dB/div horizontal scale 200MHZ/div).

6) Conclusions and recommendations:

The preliminary results are presented in this paper regarding the development of a parallel plate resonant PD coupler. Due to the size limitations of the port in which the coupler is to fit, the diameter of the coupler is 98mm. This gives the coupler a calculated dominant resonant mode at 1.953GHz. The resonant modes are in the TM mode.

It has been shown that for the greatest sensitivity at the dominant resonant mode, the pick off point should

not be in the centre of the plate, but at the edge of the plate.

In order to eliminate the excitation voltage signal, it is proposed that the coupler should be shorted out in the middle of the plate. This corresponds to a zero during the dominant resonant mode.

In order to reduce the dominant resonant frequency of the coupler down to one that can be accommodated by the equipment at hand, a capacitively tuned coaxial resonant cavity was constructed. This resonator has a resonant frequency of 172 MHz.

From the VSWR measurements performed on the coupler it is clear that two things must be done in order to improve the design of the coupler namely:
a) Determine the true resonant points of the coupler.
b) Improve the VSWR at these true resonant points.

References:

/1/   Judd M.D., Farish O. and Hampton B.F., "Broadband couplers for UHF detection of partial discharges in gas-insulated substations", IEE Proc. Sci, Meas, Technol, Vol. 142, No. 3, May 1995, pp 237 - 243.

/2/   Wolf I., Knoppik N., "Rectangular and circular microstrip disk capacitors and resonators", IEEE Transactions on microwave theory and applications, Vol. MTT-22, No. 10, October 1974, pp 857 - 864.

/3/   Shen L.C., Long S.A., Allerding M.R. and Walton M.D., "Resonant frequency of a circular disc, printed-circuit antenna", IEEE Transactions on antennas and prorogation,, July 1977, pp 595 - 596.

/4/   Gandhi O.P., Microwave engineering and applications, Pergamon Press, 1981, pp 261 - 265.

Address of author

Shawn D Nielsen
Department of Electrical Engineering
University of the Witwatersrand
Private Bag 3
Wits
2050
South Africa.

Effect of Perchlorethylene on Physical and Insulating Properties of Mineral oil

M S A Minhas   J P Reynders

Electric Power Research Group
University of the Witwatersrand
Johannesburg

Abstract

The overall performance of the transformer oil improves with the addition of perchlorethylene (C_2Cl_4). Enhanced heat transfer, improved breakdown strength, partial discharge reduction (in frequency and magnitude) and classification as a non-flammable liquid can all be demonstrated. However, an increasing trend of Loss Tangent ($Tan\delta$) with increase of C_2Cl_4 concentration was observed. The compatability of C_2Cl_4 with respect to Ozone layer is also discussed.

1   Introduction

The ageing of the insulation in oil-paper insulated systems is primarily dependent on temperature and partial discharge activity. If the working limits of the temperature are exceeded by 8°C the degradation of the insulation is approximately doubled, called "The 8°C Rule"[1]. Improved heat transfer is a means of controlling temperature ageing. The heat can be effectively removed from the winding of an oil filled transformer if the liquid has a low viscosity. The addition of perchlorethylene (C_2Cl_4) lowers the viscosity of mineral oil and enhances the heat transfer [2, 3, 4].

Partial discharge (PD) activity which degrades the insulation can be minimised by introducing electronegative components in the liquids of insulating systems [5]. The electronegative molecules capture the free electrons, enhance the breakdown strength and reduce the partial discharge activity considerably [4, 6, 7, 8]. In recent years, an extensive study on perchlorethylene-oil mixtures has proved that the addition of C_2Cl_4 increases the breakdown strength [8, 7] and extinguishes PDs [2, 3, 4, 8, 7]. A 35% C_2Cl_4 mixture with 65% oil shows a 30% higher breakdown strength than the pure mineral oil [9]. It has been found that the mobility of the charges is extremely low in a 35% perchlorethylene-oil mixture compared with pure oil [9]. In this work,

the 35% mixture have been used due to its superior electrical qualities of higher breakdown strength and PD behaviour.

The study is a comparison of PD activity of an oil-paper insulated systems with the same system impregnated with 35% perchlorethylene-oil mixture. $Tan\delta$ changes with the variation of electric stress and temperature are also presented.

2   PD Test on 22 kV CT

A 22 kV HV oil-paper insulated current transformer (CT) which had been out of service for some time, was used for this particular test. The straight detection method was employed [10]. The output of the discharge detector with power frequency waveform was fed to a 50 MHz storage oscilloscope. This arrangement made possible to view the position of the PDs on power frequency waveform.

To test the PD activity in the mixture, the CT was drained and flushed with pure perchlorethylene to remove the oil, sludge and other contaminations from the winding by circulating it in a closed system. After draining, it was filled with 35% perchlorethylene-oil mixture. This mixture was circulated for 6 hours, and the CT was left un-attended for 4 days before the partial discharge test was carried out.

3   PD Test on Coaxially Taped Paper Samples

The Common mode rejection method [10] of partial discharge detection was employed. Coaxially taped paper samples shown in the Figure 1 were used as the test objects. The inner copper tube served as HV electrode while the ground electrode was the layer of tin coated copper wire on the outer side of wound paper tape. This geometry is the same as

that used to insulate the hair pin of the CT (HV winding). The output of the discharge detector was fed to a 500 MHz 1500M samples/sec storage oscilloscope and to a PC for subsequent data processing to evaluate the total charge dissipation (Σq) in 50 cycles.
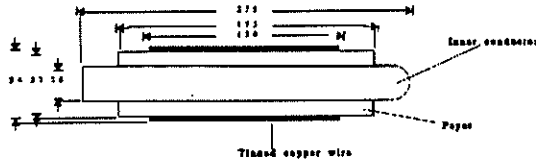
Figure 1: Coaxially taped paper sample. (Dimensions in mm)

4 Loss Tangent ($Tan\delta$) Measurement

The $Tan\delta$ measurement was done according to an IEC standard [11] on oil and different compositions of mixtures. A three terminal cell was used. The variation in $Tan\delta$ with temperature and with applied electric stress was observed.

5 Observations

5.1 PD Test on 22kV CT
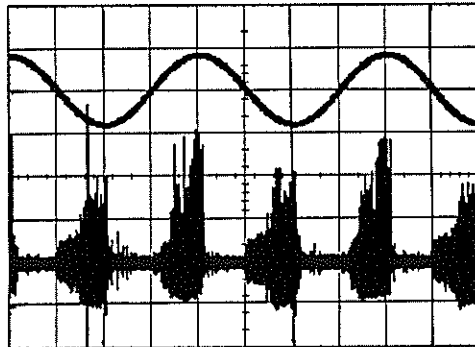
Figure 2: Partial discharge pattern for the CT at 27kV in oil. (PD waveform 6pC per vertical division)
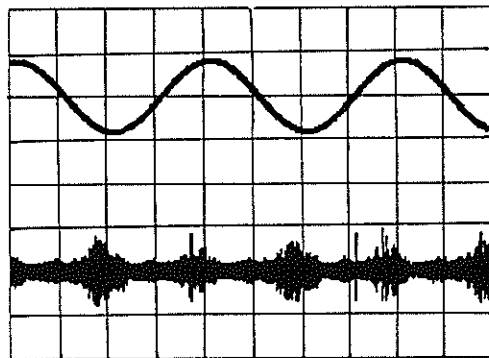
Figure 3: Partial discharge pattern for the CT at 27kV in 35% mixture. (PD waveform 6pC per vertical division)

Smp. N°	Ave. No. of Discharges	Peak Mag. (pC) in oil	Peak Mag. (pC) in mix.	Ave. (pC) in oil	Ave. (pC) in mix
1	781	450	0	11672	0
2	904	746	0	188621	0
3	1640	952	904	845575	19036

Table 1: PD activity in taped paper samples over a period of 1 sec.(50 cycles)

An increase of 25% in partial discharge inception voltage (PDIV) and 21% in extinction voltage was observed. The peak discharge magnitude dropped from 24 pC to 5pC. The Fig 2 shows typical PD activity in oil and Fig 3 represents the 35% perchlorethylene-oil mixture.

5.2 Coaxially Taped Paper Samples

The partial discharge magnitude and the discharge pulses frequency decreased considerably in the mixture when compared to oil. The results are tabulated in Table 1 and the visual plots are shown in Figures 4 to 6 for Sample 3.
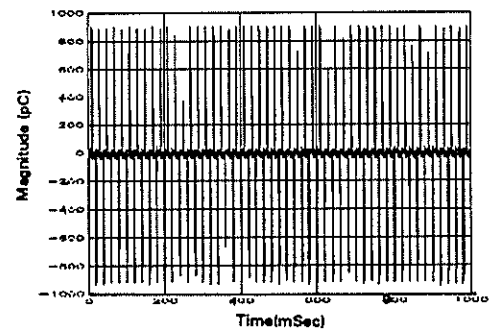
Figure 4: Typical PD activity in oil observed in the taped paper samples at 5kV.
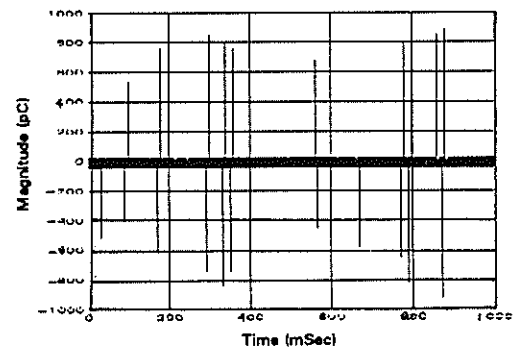
Figure 5: Maximum PD activity in 35% perchlorethylene-oil mixture for mixture impregnated taped paper samples out of 10 randomly selected waveforms at 5kV.

5.3 Tanδ Measurement

The results of Tanδ measurements are shown if Figures 8, 9, 10 and 11.
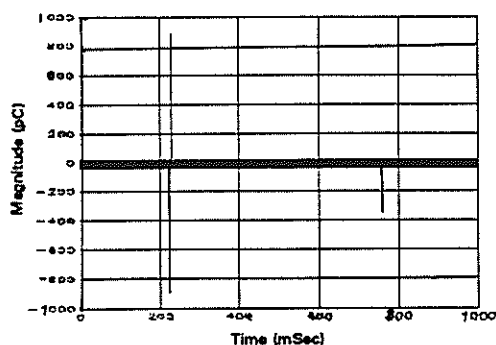
Figure 6: Minimum PD activity in perchlorethylene-oil mixture for the taped paper samples out of 10 randomly selected waveforms at 5kV.
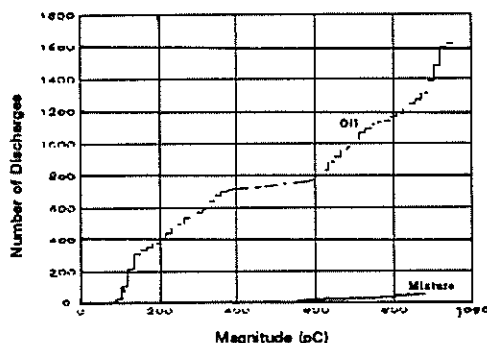
Figure 7: Comparison of the number of discharges in oil and 35% perchlorethylene-oil mixture impregnated paper taped samples at 5kV.
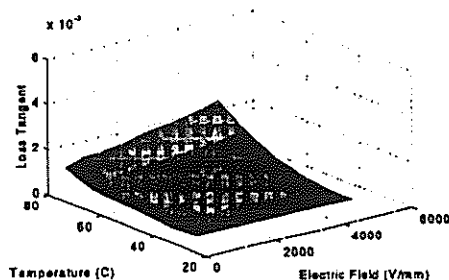
Figure 8: Variation of Tanδ with temperature and electric stress in mineral oil.
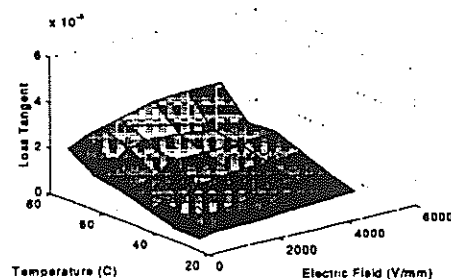
Figure 9: Variation of Tanδ with applied electric stress and temperature in 35% C_2Cl_4-oil mixture.
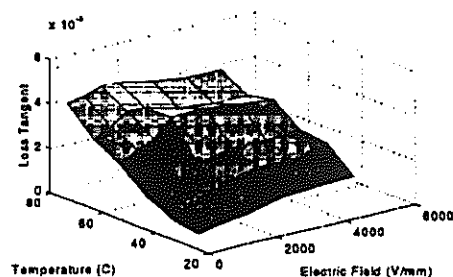
Figure 10: Variation of Tanδ with applied electric stress and temperature in 50% C_2Cl_4-oil mixture.
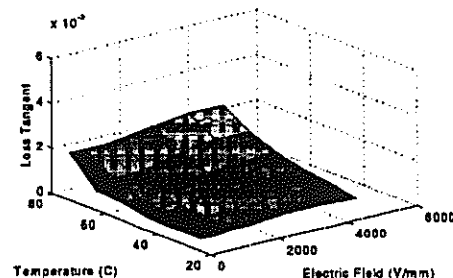
Figure 11: Variation of Tanδ with applied electric stress and temperature in pure C_2Cl_4.

6 Discussion

It has been established that introduction of perchlorethylene lowers the viscosity of the mixture compared with pure oil and improves the heat transfer by ensuring faster thermal currents in the liquid which is also reflected in the higher top liquid temperature and lower temperature gradients (winding to top liquid) [2, 3]. The higher surface tension [12] of the C_2Cl_4 aids the penetration of the liquid into the winding and facilitates heat transfer.

The electronegative components in oil decrease the PD activity [6, 5]. The perchlorethylene molecules are highly electronegative and have an electron attachment cross-section of 0.02×10^{-15} cm^2 at an energy level of 1.0 eV which is higher than that of the other haloethanes [13]. This gives a significant electron attaching capability to the C_2Cl_4 molecule, which leads to the reduction in the charge carrier mobility of 0.22×10^{-9} m^2/Vs in 35% mixture as compared to oil of mobility 70×10^{-9} m^2/Vs [9]. This give the mixture the superior qualities of breakdown strength and partial discharge extinction.

When an electron collides with a molecule, several different phenomena can take place. Scattering, excitation, dissociation, electron capture and a combination of these processes can all occur [14]. For the C_2Cl_4 molecule, the electron attachment at energy levels below 2eV is significant [13]. At this energy level C_2Cl_4 molecule can generate three attachment

carriers (Cl^{-1}). This is the reason for the discharge suppression.

The high values of the Tanδ observed in the mixtures may be due to the dissociation of C_2Cl_4 molecules, which give rise to a leakage current. This is still under investigation.

Solvents which are not fully halogenated have no or very little effect on the Ozone layer. Perchlorethylene is not a fully halogenated compound, which makes it Ozone friendly. C_2Cl_4 is a commercial liquid which is widely used in the cleaning machines as a non-flammable solvent. It is also recommended in the precision metal cleaning and in high quality electronic component cleaning [12]. The Ozone depletion potential (ODP) of C_2Cl_4 vapours is 0 as compared to carbon tetrachloride of 1.1 [12]. However conservation and recovery is advised in industrial processes.

7   Conclusions

1. The addition of perchlorethylene to the mineral oil makes it non-flammable, lowers the viscosity and improves the heat transfer.

2. The improved heat transfer results in lower winding temperatures and increased top liquid temperature thereby enhancing the heat rejection.

3. The improved heat transfer properties can improve the performance of the transformers in an overloaded condition and longer overloads can be applied without reducing the life of the equipment.

4. Low viscosity perchlorethylene-oil mixtures improve the impregnation of the paper insulation.

5. The electron attaching capability of the electronegative C_2Cl_4 molecules improves the breakdown strength and suppresses partial discharge activity.

6. The higher Tanδ values of the mixtures compared to that of the basic constituents need further investigation.

7. The ODP of C_2Cl_4 is 0, which makes it Ozone friendly.

References

[1] F.N. Clark, *Insulating Materials for design and Engineering Practice.* John Wiley an Sons, Inc., 1962.

[2] M.S.A. Minhas, D.A. Hoch and J.P. Reynders, "Enhancing the flame, thermal and partial discharge performance of mineral oil.," *Proceedings of 4th International Conference on Properties and Application of Dielectric Materials*, Paper 4231, July 3-8 1994.

[3] M.S.A. Minhas, D.A. Hoch and J.P. Reynders, "The use of perchlorethylene to enhance the thermal and insulating properties of mineral oil.," in *Southern African Universities Power Engineering Conference-95*, 1995.

[4] M.S.A. Minhas and J.P. Reynders, "Perchlorethylene as an Additive with a view to control Thermal ageing and Partial Discharge ageing.," *9th International Symposium on High Voltage Engineering.*, Paper: 1078, 1995.

[5] A. Ruffini, D.A. Hoch, J.P. Reynders "Discharge behaviour of halogenated liquids.," in *Sixth International Symposium on High Voltage Engineering.*, Paper: 319, 1989.

[6] D.A. Hoch and J.P. Reynders, "The effect of increasing concentration of perchlorethylene on the electrical performance of mineral oil.," in *7th International Symposium on High Voltage Engineering*, 1991.

[7] D.A. Hoch and J.P. Reynders, "Partial discharge behaviour of mineral oil/perchlorethylene mixtures.," in *8th Interantional High Voltage Symposium, Yokohama, Japan*, no. Paper 24-04, August 23-27 1993.

[8] D.A. Hoch and J.P Reynders, "The effect of perchlorethylene concentration on partial discharge and pre-breakdown phenomena in insulating liquids.," in *South African Universities Electrical Power Engineering Conference*, 1992.

[9] D.A. Hoch, *Perchlorethylene / Mineral oil blends : Experimental and Theoratical Investigation of Electrical Insulating Properties.* PhD thesis, University of the Witwatersrand, Johannesburg, 1993.

[10] F.H. Keruger, *Partial Discharge Detection in High-Voltage Equipment.* Butterworths, 1989.

[11] *IEC: 257*, 1978. Measurement of relative permitivity, dielectric dissipation factor and dc resistivity of insulating liquids.

[12] "Solvent coatings and adhesives," Industry and Enviroment Program Activity Centre, 1992. Protecting the Ozone Layer.

[13] D.L. McCorkle, A.A. Christodoulides and L.G. Christophorou, "Electron attachment of halocarbons of interest in gaseous dielectrics.," in *Fourth International Symposium on Gaseous Dielectrics, Knoxville, Tennesse, USA.*, April 29-May 3 1984.

[14] S. Trajman, "Cross-section for electron-molecule collision processs," in *Proceedings of the 4th International Symposium on Gaseous Dielectrics, Knoxville, Tennessee, USA*, April 29- May 3 1984.

Address of Author :
M S A Minhas
Electric Power Research Group
Department of Electrical Engineering
University of the Witwatersrand
Private Bag 3
WITS 2050
South Africa
email : minhas@odie.ee.wits.ac.za

CAPACITIVE BUSHING VOLTAGE DIVIDERS

L VETS

DEPARTMENT OF ELECTRICAL ENGINEERING , PORT ELIZABETH TECHNIKON, SOUTH AFRICA

Quality of supply and related investigations require accurate instrumentation to be coupled to the measurement points via readily available voltage and current interfaces with high frequency characteristics.

1. INTRODUCTION

The study of high frequency phenomena in medium to high voltage transmission systems generally requires the application of portable broad bandwidth dividers which are expensive, bulky, often unavailable and time consuming to install. Standard substation equipment like transformer bushings and current transformers can be adapted as an alternative means of stepping down voltage levels for monitoring harmonic and transient voltages.

A recent study of reactor switching transients provided the ideal opportunity to evaluate the particularly useful technique of using power equipment bushings as a capacitive voltage divider.

The voltage interfaces of Eskom Technology Research & Investigations (T-R-I) transient measurement team presently consists of a three phase set of resistor - capacitor dividers. Although accurate and capable of measuring voltages up to 765 kV, in a frequency range from dc to several megahertz, these dividers are expensive, bulky and time consuming to install. For this reason transient measurements and various supply quality assessments involving harmonic measurements are often either limited in scope or even avoided at the expense of damage to plant and a more reliable supply to consumers.

A recent investigation at Proteus substation, for example, required that switching voltage be measured at the terminals of the 200MVA 400kV reactor. The excessive costs involved in transporting and erecting the measurements facility's high voltage dividers was not justified within the scope of the investigation.

The Proteus investigation provided the ideal opportunity to demonstrate one of a number of potential applications for the capacitive bushing voltage divider technique.

2. BUSHING DIVIDER MEASURING TECHNIQUES

The application of transformer, reactor or current transformer bushings as capacitive dividers for measuring and testing purposes is not a new concept. Two methods of acquiring measurable waveforms from a bushing were identified.

2.1   MEASURING THE EARTH RETURN CURRENT

This technique has resulted in the development of a measuring system patented by Dr Malewski of Hydro Quebec in Canada [1]. It involves measuring the earth return current of the bushing via a wide bandwidth current transformer (CT) and converting the signal via an integrator.

This system is however very expensive and a price of R100 000 per phase was quoted by Dr Malewski.

2.2   CAPACITIVE TAP-OFF MEASUREMENT

Connecting an external impedance in series with the capacitive tap and down to earth as shown in Figure 1, converts the selected bushing into a capacitive divider providing a less complex and cheaper measuring technique than that described in section 2.1 above.

Capacitance C_2 makes up the secondary impedance of the divider with C_1 being the actual bushing capacitance or the primary impedance of the divider. The secondary unit has been designed using low loss capacitors and has built in protection components to prevent failures.

This technique originally met with the disapproval of plant owners due to the need to break into the solid earth connection of the capacitive tap. It was widely believed that insertion of the required circuitry would endanger the plant during normal operation.

A prototype secondary unit, known as the dividers low voltage arm, was developed to convert bushings into capacitive dividers, while providing a secure, protected path from the capacitive tap down to earth.

Laboratory tests verified the reliability of the LV arm in terms of plant safety, and delivered promising results with respect to bandwidth. Various applications of the LV arm have since proved to be successful in the Eskom network.

3.   LOW VOLTAGE ARM LAYOUTS

By arranging the low Tan δ capacitors in different configurations, the bandwidth of the low voltage arm can differ significantly.

Figure 2 indicates low inductance rectangular capacitors in a circular form. The one side of the capacitor is connected to a plate and the other end of the capacitors are connected together on the copper rod. The inductance in this design is quite high and tests revealed a bandwidth of the unit of 150kHz without any resonance.

Figure 3 indicates an improved design for the low voltage arm. A low self inductance of the unit is obtained by assembling the capacitors in concentric and symmetric layers as shown in Figure 3. The capacitors are soldered between two copper plates. This reduces the lead length of the capacitors as well as the self-inductance of the low voltage arm. Tests revealed a bandwidth of 2MHz.

4.   BANDWIDTH OF CAPACITIVE BUSHING DIVIDER

The bandwidth of the capacitive bushing divider was tested on a 400kV, F & G type 1425/42 bushing. The test was conducted by impulsing the entire divider using a Haefely lightning impulse generator, a 1000/1 probe as well as a digital oscilloscope.

The bushing was impulsed and both the input and output were recorded simultaneously on the digital scope. An FFT (Fast Fourier Transform) was conducted on both signals and the output was divided by the input.

The frequency response of the divider is shown in Figure 4. The divider is linear from 1Hz to better than 100KHz and a step down ratio 2670/1 was calculated.

5.   PROTEUS REACTOR SWITCHING INVESTIGATION

The Proteus 400kV reactor switching investigation was part of an Eskom Transmission quality of supply project involving the commissioning of a point-on-wave switching relay installed onto the reactor's circuit breaker control system. The high speed monitoring of reactor current and voltages was necessary to evaluate the performance of the relay.

Reactor inrush currents contain harmonic components which under certain conditions can interfere with the operation of sensitive electrical plant on consumer networks. Reducing the magnitude of the inrush currents can be achieved by controlling the closing of the reactor's circuit breaker. The point-on-wave relay provides this control.

Installation of the measuring facility's voltage dividers was neither practical nor cost effective, and without an alternative voltage interface it would not have been feasible to acquire reliable voltage quality parameters during the various switching modes. Such recordings, were desirable to determine, conclusively, the benefit of the relay in terms of voltage quality to the consumer.

Figure 5 indicates the reactor terminal voltages recorded using capacitive bushing dividers during a breaker trip operation.

6.   CONCLUSION

The capacitive bushing voltage divider proved itself in the Eskom Transmission network for various applications. The bandwidth of the device is sufficiently broad for transient measurements. It provides a cost effective and straight forward means of conducting circuit breaker switching tests, short or long term voltage transient and harmonic surveys and on line tan δ monitoring of bushings. It has the potential to be developed for a variety of other applications in commissioning and investigative projects.

Measurements at numerous different points in the network can be performed simultaneously by simply installing the LV arms onto available reactor, transformer bushings. The measurement technique can be used in conjunction with high voltage dividers to further increase the measurement scope.

7.   FIGURES

Line Voltage

C1 — High voltage arm

— Bushing

— Connection between bushing and low voltage arm

Resistor

R1

To measurement
equipment

Coaxial
cable

C2

Low voltage arm

Capacitor

Protection components
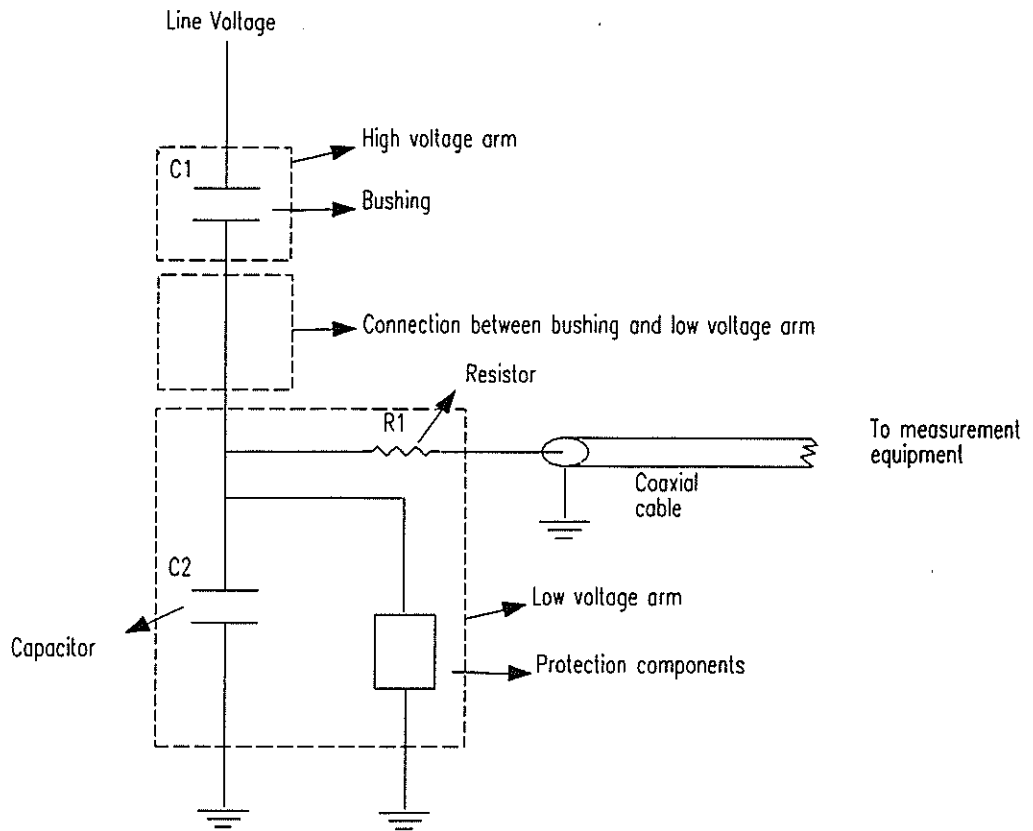
Figure 1 : Schematical diagram of capacitive bushing voltage divider
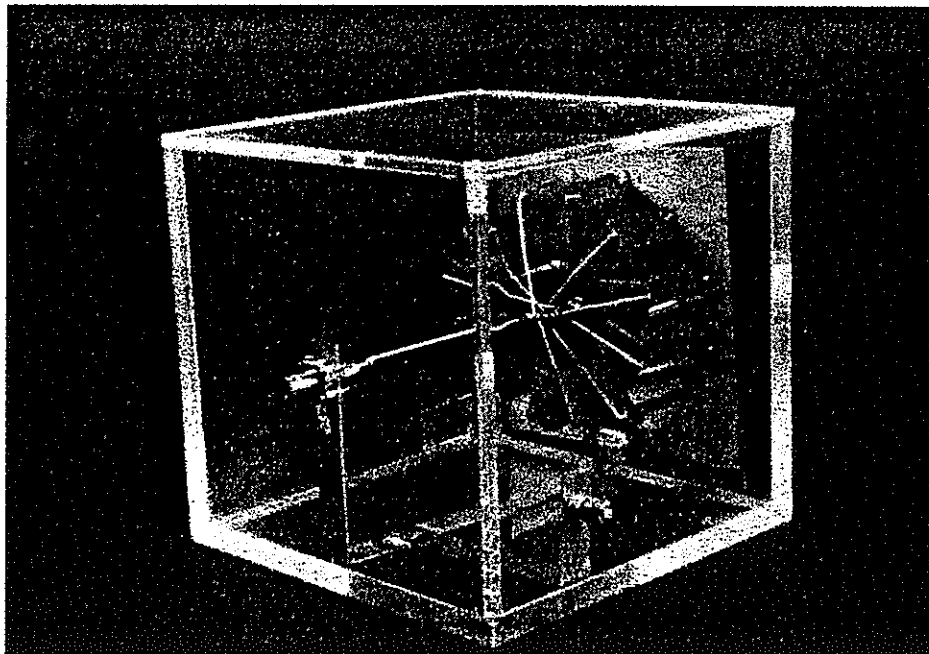
Figure 2 : Bad low voltage arm design
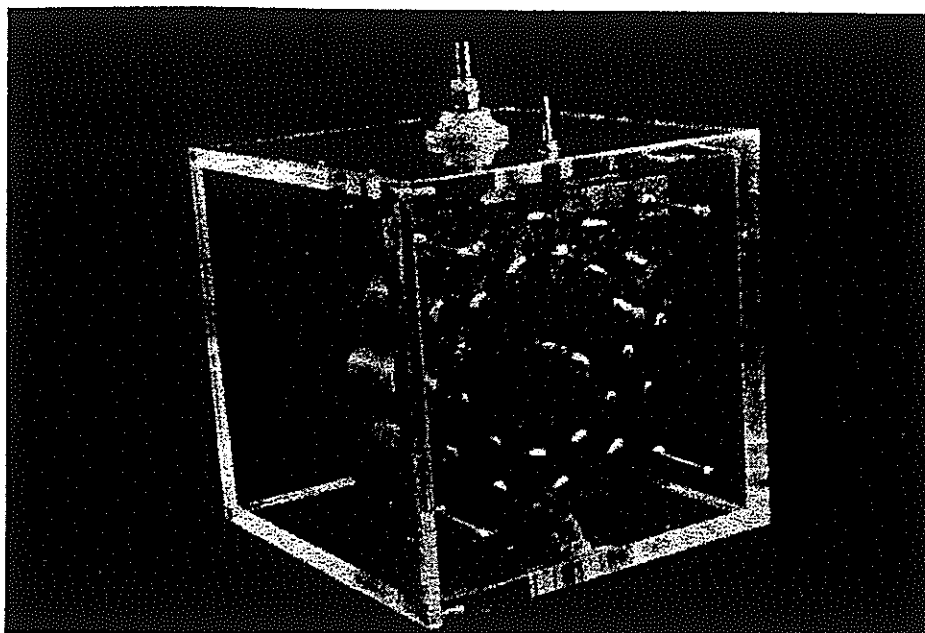
Figure 3 : Improved low voltage arm design
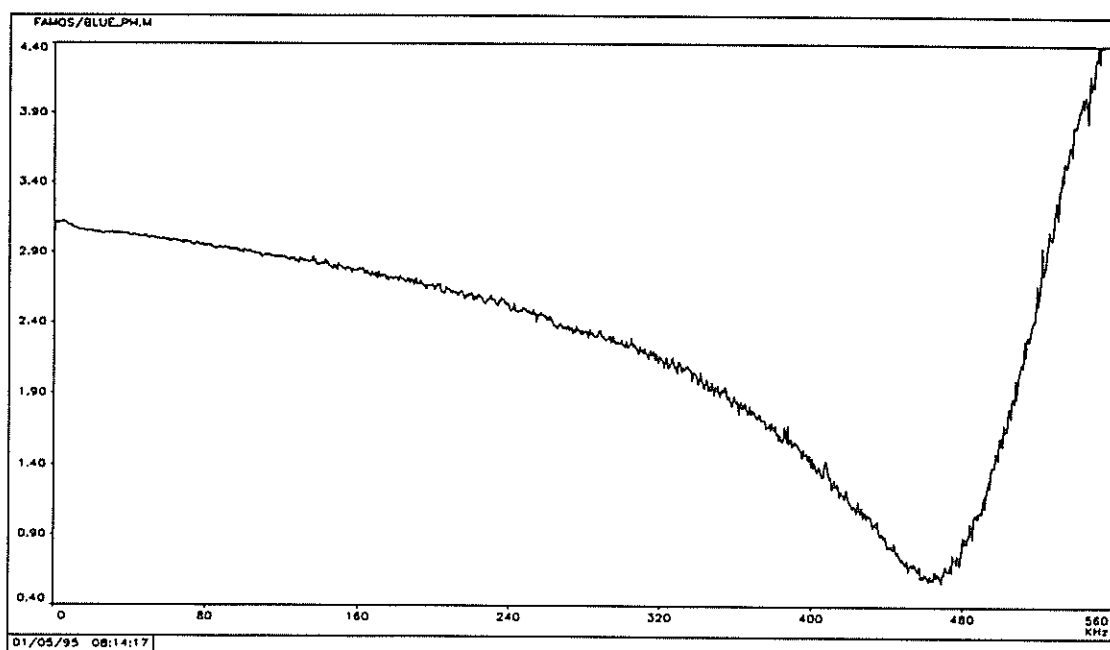
**Figure 4. : Frequency Response of Proteus Reactor Bushing Voltage Divider
With Prototype LV Arm Connected.**
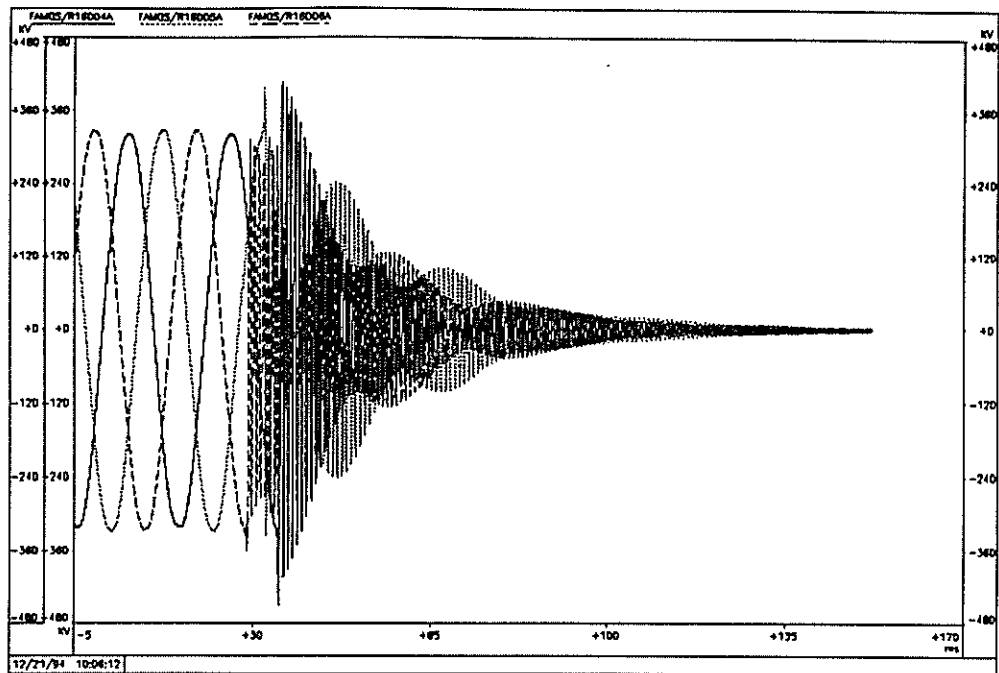
Figure 5 : Reactor terminal voltages recorded during a breaker trip operation.

7.   REFERENCES

[1]   Malewski R, Douville J, Lavallee L, "Measurement of Switching Transients in 735kV Substations and Assessment of their Severity for Transformer Insulation." IEEE Transactions on Power Delivery, Vol 3, No 4, October 1988.

8.   Address of author

Luc Vets, Eskom T-R-I, Electrical section, Private Bag 40175, Cleveland, 2022, South - Africa. E-Mail LUC@TRI.ESKOM.CO.ZA

High-speed Flicker and Power-factor Compensation

W C Beattie and S Beattie
The Queen's University of Belfast. UK and Kelman, Lisburn. UK

1.   Introduction

1.1.   Quality of supply

The quality of electrical supplies has steadily become a more important issue with the continuing development of electronic control systems. These have created two problems. Firstly they are sensitive to EMC and if the supply system carries a significant harmonic content then the behaviour of the equipment may not be as expected. Secondly, the electronic equipment may itself give rise to interference which may influence the performance or other pieces of equipment. These may be on the system itself or indeed may be entirely separate such as telecoms apparatus. Attempts have been made to resolve this issue and various standards are now available for specifying the immunity which a piece of equipment must be able to withstand if it is to be acceptable.   Similarly, the emissions from a piece of equipment can be defined and specified.   The combination of these two should ensure that equipment operates as designed.   However, equipment may operate satisfactorily when tested but may not behave as expected in the field. This can be due to the supply impedance which can influence the magnitude of the harmonics which are experienced by other consumers. A simple example can be in the starting of a large machine where the voltage drop on starting may influence other customers at the point of common coupling or even inside the plant itself. Specifications for harmonic emissions must therefore be associated with supply impedance if it is prove effective. The present paper addresses the problems caused by loading of a supply system which can give rise to repetitive variations in the voltage known as 'flicker'. This can prove annoying in creating variations in the lighting level but can also influence the quality of the work produced.

2.   Flicker

2.1.   Sources

Sources of flicker are usually due to large loads relative to the supply of the distribution network and can be associated with rapid changes in the loading. Thus electric hoists in mines, arc furnaces in smelting plants or spot welding in a car factory would be typical of the loads which can give rise to flicker. In many cases the loading is not significant from a power aspect but it is the reactive loading which gives rise to the majority of the problem. Typical of this are the use of thyristor drives at low speed, spot welders and arc furnaces which will all have a very low power-factor.

2.2.   Problems

Apart from complaints from neighbouring plant due to lighting flicker or interference being experienced in the behaviour of the machinery, difficulties can arise internally in a plant. This can be due to the transient drop in voltage causing unsatisfactory performance. Thus the starting of a large induction machine will cause a voltage drop throughout the factory which can cause other pieces of equipment to shut down. The voltage drop due to several welders striking simultaneously can give rise to faulty welding due to the reduced voltage. It is thus essential that the problems be addressed at source as the difficulties which arise can impinge directly on the performance of the plant where the flicker originates.

3.   Solutions

3.1.   Grid reinforcement

The most obvious approach to the problem is to provide a stronger supply network. This will inevitably mean an increase in the voltage levels of the feeder and this can prove very effective. This reduces the supply impedance and also moves the point of common coupling to a stronger point in the grid system. However the cost of such a scheme may prove exorbitant and this is particularly the case when the plant is in a remote location.

3.2.   Energy storage

A further approach to the problem is to use energy storage. Frequently this is carried out by using a flywheel powered by an induction machine with a soft characteristic   On the same shaft will be a synchronous generator. When the load is applied to the system the speed of the machine set falls and energy is drawn from the flywheel thus reducing the energy flow from the supply. This will give rise to a transient drop in frequency with load which may not have serious effects on the plant. The cost of such a machine set is high and the no-load losses of two machines and a flywheel can prove significant as the machines must be rated for the full load power of the equipment causing the flicker. Furthermore this approach does not address the real problem

which is that the majority of the voltage drop is caused by the reactive loading on the supply and not by the real power transmitted.

3.3.   High-speed compensation

A much better approach is to address the problem directly and to provide reactive control within the plant. The diagrams shown in Figure 1 show how it is possible for a poor power-factor to have a serious effect on the terminal voltage and that by reactive compensation it would be possible to control the voltage. Here the difficulty is that the more normal forms of reactive compensators do not respond rapidly enough for the majority of applications which would give rise to problems. Some form of semi-conductor type of compensator would therefore be necessary to provide a rapid enough response to be effective. In general there are three types of compensation which might be considered.
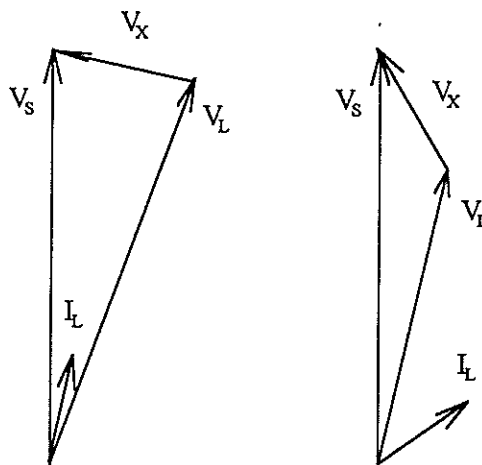
Figure 1. (a) Voltage drop under conditions close to unity power factor and (b) at poor power factor

4.   Switch-mode compensators

4.1.   Compensator design

Switch-mode compensators are now available which are based on the use of IGBT's in a bridge configuration. The concept is to have a relatively small capacitor in the place of the d.c. link. The a.c. lines of the bridge are connected through small inductors to the supply. Switching of the transistors will take place at a frequency of about 7 kHz for systems operating at a reasonable power level and the on/off periods are arranged so that a leading or lagging current is drawn from the supply. This seems to be an admirable solution but in practice it will be found that the costs of the unit will be of the order of £200 per kVA and that the interference generated on weak lines may not be acceptable. Such a system in proximity to measuring equipment has been found to create serious problems. On the positive side, the speed of response can be very rapid and the unit can be used to either buck or boost fixed capacitance on the network.

4.2.   System balance

In weak networks the system is frequently unbalanced due to the large number of single-phase loads on the line caused by farms and other domestic loads. The effect of unbalance on such a compensator is to require a larger d.c. link capacitance. In general the reactive VA is associated with the swing of energy in and out of each phase. Thus in the typical induction machine the stored energy in the air-gap will be constant but the flux linkage with an individual phase will vary with time. With an unbalanced system the stored energy will not be constant and the d.c. link capacitor must be large enough to allow for the variations in voltage caused by this total energy swing.

5.   Switched inductors

A further possibility for high-speed reactive compensation is to install a bank of capacitors and use a parallel inductor with thyristor phase control to offset the reactive VA of the capacitor bank. This can present a number of problems. Firstly the use of thyristors in phase delay mode will give rise to harmonics which can create problems on the system. Secondly the design is such that the stored energy in the system will be twice what is required since the stored energy in the capacitors must equal the stored energy in the inductor if full range compensation is needed. Thirdly, there will be a delay while the inductor current rises to the new value and the response will not be as rapid as that for a switched-mode compensator. Nevertheless, such devices have been used, especially at high voltages where the high currents and voltage rating of thyristors have enabled a viable system to be built.

6. . Switched capacitors

6.1. Thyristor switches

As indicated earlier the cause of flicker is usually associated with high current fluctuating loads and therefore the devices used for compensation must be capable of handling such voltages and currents. Thus the use of capacitors switched by thyristors would prove a feasible solution for the reactive powers involved. For an a.c. system the thyristor switches will comprise a pair of anti-parallel devices. Such an arrangement must be capable of supporting at least twice the peak supply voltage due to the turn-off action of the capacitor.

6.2. Switching point

With capacitors the point of switching is critical and it is essential that it is chosen to ensure that minimum transient current is generated. Switching a capacitor at the wrong instant can lead to huge currents and the destruction of the switching devices. The optimum turn-on point is close to that of zero voltage across the switch. If indeed there were no inductance in the supply system this would be exactly correct but for the systems envisaged where the supply inductance is resulting in excessive voltage drop this is clearly not the case. In fact, the point of zero transient would be at the same conditions where the capacitor had switched off. This is clearly not possible to attain and therefore the point of minimum transient must be used. Practical tests have shown that this minimum transient is entirely acceptable.

6.3. Control

If a compensator is to respond rapidly the control must be based on a measurement which will also be available as quickly as possible. A measurement of peak voltage will only be available every half cycle but if the measurement is based on reactive VA then it can be available almost immediately. In installing plants with sizes up to 2.2 MVA it has been found that some form of learning algorithm can provide a superior response to that based entirely on measurement systems. This is the case even though the correction can only be switched into circuit once every cycle. The equipment has utilised a binary pattern of capacitor banks with the option of switching any bank on at one point in the cycle and off at two points. A scheme such as this can provide compensation with an acceptable speed of response and will need only the capacitive rating which the system requires, i.e. no inductors. In addition, it depends on thyristors for switching which have been shown to be robust and reliable.

7. Practical results

7.1. Flicker control

Shown in Figure 2 are results gained during the commissioning of thyristor switched capacitor banks on a welder producing steel grids for reinforcing concrete. Initially the flicker measurement, carried out by the local supply authority, shows the excessive levels of flicker pertaining to the site. Flicker measurement is based on both short and long terms measurements and the flicker levels can be seen to fall steadily. At this stage the unit was tuned which resulted in a further drop in flicker levels. Following this the compensator was switched off and the flicker level was seen to rise to its initial value and again fall to acceptable levels when the compensator was again switched on.
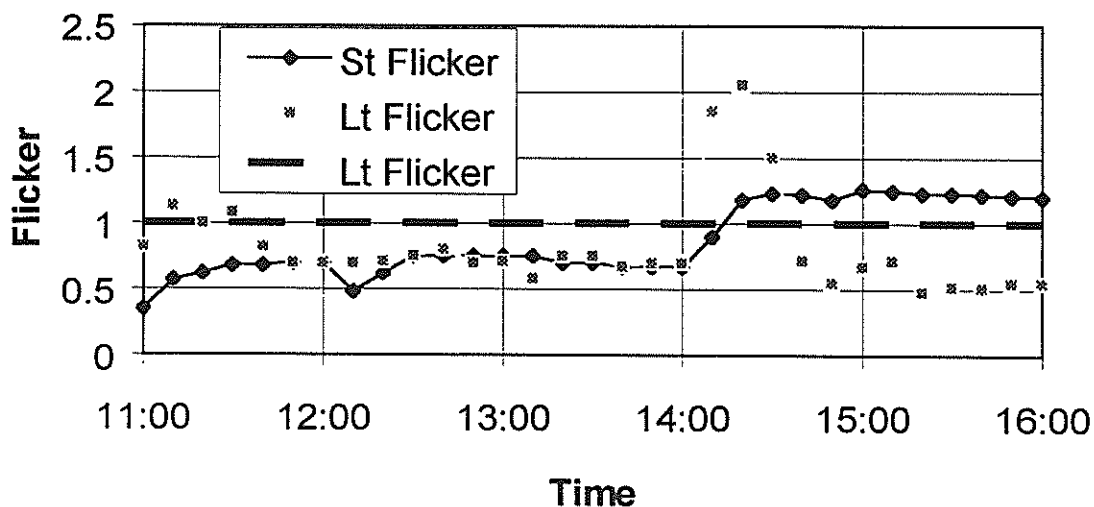
Figure 2. Flicker measurements with high-speed compensation.

7.2.   Harmonic control

The figure shown illustrates the influence of high-speed compensation with correction for harmonics. This unit is based on switching filters into circuit. One of the difficulties with filters is that the better they are as a filter the longer they take to reach steady-state. It is thus essential that if they are to be effective in the high-speed scenario that the point of switching is such as to allow the steady-state condition to be achieved as quickly as possible. The case shown iin Figures 3 - 6 is for a welder which has a three-phase diode bridge rectifier on the output. The harmonics are therefore mostly the 5th and the 7th. An assessment of the voltage and current waveforms shows that the harmonic content is greatly reduced and that voltage compensation is also achieved. Again this was welding reinforcing bars for concrete.
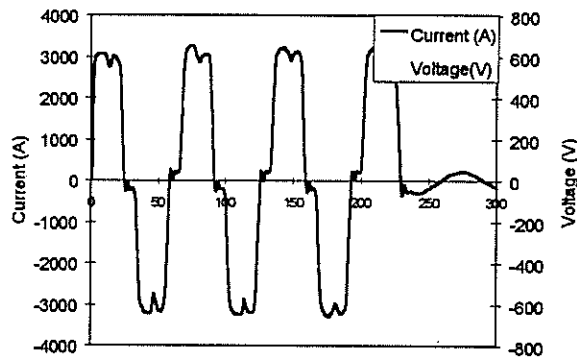
Figure 3. Uncompensated welder currents
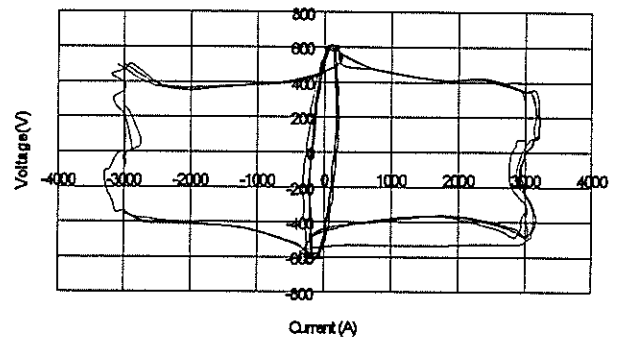
Figure 1 Uncompensated phase angle plot
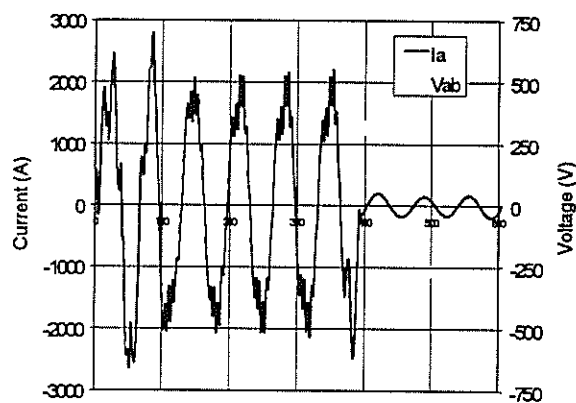
Figure 5. Compensated welder currents
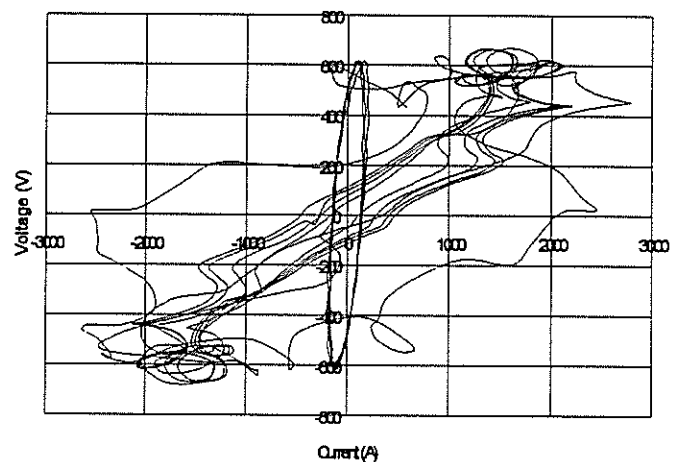
Figure 6. Compensated phase angle plot

8.   Conclusion

1. High-speed reactive compensation has a significant role to play in the correction of flicker and voltage drop in a.c. systems. the majority of the drop will be due to the reactive component of the current and thus compensation can often solve the problem simply be removing the quadrature component of current. However if the lines are largely resistive it is possible to restore the voltage to normal by overcompensating during the load periods. To achieve high-speed compensation only thyristors can offer the reliability and power levels which will provide an acceptable level of performance and with the direct switching of capacitor banks without transients an economic solution to the problem is possible. Practical results have been shown which illustrate thyristor switched capacitors is two different modes of operation giving virtually transient free operation and providing the compensation required for the pulsating loads.

9.   References

1. Power-factor correction and harmonic control by high-speed switching of semiconductor devices. Beasant, RR, Beattie WC and Refsum, A. 25th Universities Power Engineering Conference Aberdeen, 1990, UK.
2. Maintaining power quality with phase-controlled welders using current pulse compensation. Matthews, SR and Beattie, WC. 30th Universities Power Engineering Conference 1995, Greenwich, UK.
Address Dr. W C Beattie, Department of Electrical Engineering, Ashby Building, Stranmillis Road, BELFAST BT9 5AH.   e-mail w.beattie@ee.qub.ac.uk

Voltage Dips and their Effects on Industrial Equipment

E. Smit[1], D.W. McAllister[2], C.E. Dingley[1]

Department of Electrical Engineering, University of Cape Town

ABSTRACT

Flashovers, caused by lightning and sugar cane fires, result in voltage dips on the high voltage network. Many industrial processes, but particularly continuous ones, are sensitive to such voltage dips. The estimated cost of the downtime associated with voltage dips in South Africa is R1 billion per year. This paper considers, in broad terms, the voltage dip problem and available mitigation strategies. The paper further describes action taken at a paper mill to improve the mill's ride-through capability. It was found that the most financially attractive solutions develop from an understanding of the principle of operation of equipment.

1. INTRODUCTION

Flashovers, caused by lightning and sugar cane fires, result in voltage dips on the high voltage (HV) network. Many industrial processes, but particularly continuous ones are sensitive to such voltage dips. The estimated cost of the downtime associated with voltage dips in South Africa is R1 billion per year.

This paper is based on an undergraduate thesis [1] detailing two investigations. The first investigation involved an extensive literature review that provided information describing the voltage dip problem and a variety of experiences and solutions. The second investigation covered the voltage dip problems experienced at the SAPPI Kraft Ngodwana paper mill. The actions already taken to address the voltage dip problem were considered before further investigation of the problem was undertaken. Particular attention was given to the paper machines' sensitive DC drive systems. This attention required an in-depth analysis of the drive systems' operation and interaction with their loads.

This paper has two main objectives. The first objective is to present a broad-based understanding and approach to the voltage dip problem. The second objective is to present the specific voltage dip problems at SAPPI Kraft Ngodwana and to present recommendations that developed from the investigation into these problems.

2. OVERVIEW OF VOLTAGE DIPS, THEIR EFFECTS AND MITIGATION ACTION

A voltage dip is a brief reduction in rms voltage caused by an emphasised voltage drop resulting from the flow of a fault current. Voltage dips are typically caused by flashovers that result from lightning or insulation breakdown caused by pollution such as from sugar cane fires. The severity of a voltage dip depends mainly on two characteristics, namely its depth and its

Figure 1: A Typical Voltage Dip

duration. Factors such as the associated phase shift and the number of phases affected are however often critical when considering a dip's impact on equipment.

---

[1] Department of Electrical Engineering, University of Cape Town
[2] SAPPI Kraft Ngodwana

The most popular method of recording voltage dip information is through the scatter plot. A number of different variations are used. These variations include the Eskom ABCDE chart and the IEEE/ANSI voltage withstand tolerance standard curve (IEEE Standard 446-1987).
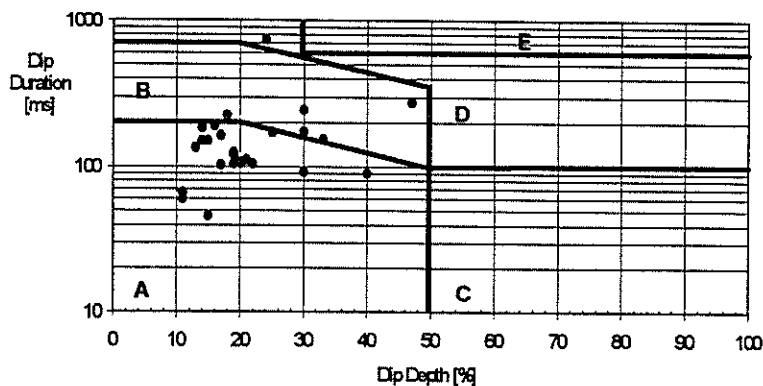
Figure 2: Eskom ABCDE Chart

The impact of the voltage dips on equipment depends on two factors, namely the severity of the dip and the sensitivity of the equipment. Different types of equipment have different levels of sensitivity. In addition, equipment is often sensitive to particular dip characteristics, such as phase shifts or voltage unbalance. The three types of equipment dealt with are electronic equipment, semiconductive devices and rotating machinery.

Electronic based equipment such as computers, PLCs (programmable logic controllers), DCSs (distributed control systems) and operator stations are particularly sensitive to voltage dips. Their sensitivity can be ascribed to there being no or little energy stored in their power supplies. Typical results of malfunction are loss of computer data, because of volatile memory, and unpredictable responses of control systems, because of lost system integrity. In an industrial context, where automation is becoming increasingly popular, electronic equipment is playing a vital role in controlling and monitoring processes. The malfunction of such equipment often leads to significant production losses.

Semiconductive devices such as line frequency converters make use of firing pulse circuitry for thyristor switching. This switching needs synchronising with the supply voltage wave forms. Depending on the dip characteristics and the operation principle of the firing circuitry, the dip could have a number of effects. Phase shifts experienced during dips can cause misfiring of thyristors. According to Coney and Smit [2] popular, but slow acting, phase lock loops used to reference firing angles are unable to respond to such fast changes. The typical result is ruptured fuses and even blown thyristors. Another scenario is that during voltage dips firing angles of rectifying converters open to compensate for the reduced voltage. On the voltage's recovery, the overcurrent drawn may cause trips or damage to equipment. With improved modern control strategies, equipment design should include the detection of dips and enable ride-through co-ordination.

In the past *rotating machinery* was not affected by dips as significantly as today. This is as a result of a trend to decrease rotor inertia hence saving material and improving dynamic response. Reduction in voltage during a dip inhibits the transfer of energy to the motor for the dip's duration. The decrease in voltage causes a varied number of responses in different machines.

A *DC motor* will always be connected to the supply through a rectification circuit that converts AC into DC. Transients impact on a DC motor through its armature circuit since the field circuit has significant inductance that is able to absorb transients. Rectification circuits can either provide a constant or a variable voltage. If the motor is supplied with a constant voltage through a diode bridge, an AC supply dip will be translated directly into a DC voltage dip. An unbalanced dip condition will result in some harmless DC pulsations that pass with the dip before any damage can be done to the motor or diodes. During the dip the motor's EMF will be larger than the applied voltage and hence reverse bias the bridge until the speed reduces to such an extent that the EMF is less than the applied voltage. No regeneration will however take place into the supply system. The speed reduction will be dictated by the mechanical time constant of the motor. If however the motor is controlled by a variable voltage applied to the armature, such as in an ASD (Adjustable Speed Drive), the situation is rather different. In this case a line frequency converter, consisting of a thyristor stack, is normally used. The

vulnerable areas of the converter equipment are discussed in the previous section. The motor will respond in a similar fashion to a motor being connected to a diode rectifier. DC Motors and converter equipment could be sized to enable proactive control strategies making the equipment insensitive to instantaneous phase shifts and voltage reductions. This management of dip ride-through co-ordination requires the control equipment to detect voltage dips, and maintain the DC voltage at the required level, thus eliminating mechanical responses to the dip.

Induction motors form a significant percentage of the electrical load in industry and have in recent years become more popular than DC drives in ASD applications. The induction motors that are connected directly on-line regenerate directly into a voltage dip when there is an initial reduction in voltage. Regenerating into a voltage dip supports the voltage level. When the voltage recovers, large currents are drawn to reaccelerate induction motors. These currents can sustain the dip duration if adequate fault levels are not available. A number of strategies are proposed by Mulukutla and Gulachenski [3] for safely ensuring process continuity. These methods are based on tripping the motor and then re-accelerating the motor by resynchronising the supply with the rotating field when the voltage has recovered. Alternatives such as automatically transferring the motor onto a healthy bus are also feasible. Some manufacturers already have resynchronising capabilities, allowing motors to spin through voltage dips, using their inertia.

Synchronous machines such as generators and synchronous condensers and even synchronous motors have an inherent ability to support voltage because of their rotational inertia. Further dynamic support can be obtained by automatic voltage regulation through the exciter system. The excitation however can only assist mitigating long duration voltage dips as the inductance in the excitation system does not allow immediate response.

Having considered equipment responses, action to deal with dips is considered here. Even though significant improvement in frequency of occurrence of voltage dips can be obtained by action such as reducing earthing and static wire resistance, voltage dips propagating through the utility supply system will never be entirely eliminated. Depending on the sensitivity of equipment, looking at these problems at a plant level may be crucial. A number of different power conditioning devices are available to mitigate dips. These include UPSs (uninterruptible power supplies), SMES (superconducting magnetic energy storage) devices, MG (motor generator) sets, Written-Pole™ machines, CVTs (constant voltage transformers) and magnetic synthesisers. For larger loads however this type of solution is often too costly and the problem requires more attention.

The best approach to dealing with voltage dips that affect industrial equipment is through *design*. Considering voltage dips in equipment design can improve the equipment's ride-though capability. Plant design considerations can keep sensitive equipment out of the plant through procurement specification. Plant design considerations can also protect sensitive equipment through strategic location of the equipment in the network. Utility design considerations can reduce the number of dip occurrences and the dip severity.

3. VOLTAGE DIP EXPERIENCES AT SAPPI KRAFT NGODWANA

SAPPI Kraft Ngodwana has come along way with its voltage dip problems. Some significant improvements have been made over the past years, yet the situation is still not acceptable with significant downtime resulting from voltage dips. It is estimated that voltage dips have the potential to cause annual production losses of about R6 million if dip avoidance strategies are not used.

Some unique mitigating strategies have been implemented at SAPPI Ngodwana. These include an islanding strategy where the mill is cut off from the HV network when lightning activity is close to either the mill or critical transmission lines. Further action involves installing a series reactor that places an increased impedance between the mill and the HV network. This allows the mill's 117 MW generating capacity to support the mill's voltage without attempting to support the entire network.

For lower powered applications, such as the DCS and PLC systems, the greatest success has been achieved by installing UPSs on these systems. Besides the use of UPSs, improved ride-through in the boiler complex was achieved by making use of delayed undervoltage trips. The paper plant auxiliary systems was recently put on UPSs and great improvement was experienced during subsequent dip events with only six drive panel trips. These trips all occurred on a minor protection function that will shortly be reviewed to rectify the problem.

The investigation into the DC drive system installed on the paper machines revealed that the ability of the control supply voltage to ride through dips was questionable. Losing the integrity of the control system results in the drive resetting without indication. The option of installing battery backup to improve DC support of the control supply voltage is under investigation. The drive system is also known to trip on instantaneous armature overcurrent and supply undervoltage conditions. The investigation further revealed that the settings of these trips were not optimally configured. The aim of the undervoltage trip is to shut the drive down if there is total power failure and to guarantee correct operation. It was recommended that all the undervoltage trips be removed, since another mechanism will shut the system down if there is an entire power loss. In addition, if the drive's operation veers slightly from acceptable limits without tripping and continuity of the process is retained, significant downtime is avoided. The instantaneous armature overcurrent tripping level was set conservatively at about 120% of rated motor current on some drives. This is much lower than even the maximum current of 200% allowed by the overload tripping for short duration. This caused a significant number of nuisance trips resulting from voltage recovery after dips. The instantaneous overcurrent tripping levels were set to 150% and 200% of the motor rated current on various drives and a recommendation to set these levels to 230% is under investigation. The system should be able to cope with this setting for short durations such as those experienced after voltage dips. Because of the reduced extinction angle in drives that operate in a normal regenerative mode, phase shifts during dips make these drives particularly prone to commutation failure. It was recommended that automatic restart cards be installed on all drives operating under these conditions. These cards inhibit the drive firing pulses when a supply undervoltage condition is detected. The cards reapply the pulses when the voltage recovers, thereby allowing the motor to spin through a voltage dip.

4. CONCLUSION

Considering the findings of the investigations undertaken a number of conclusions were drawn. It was found that the best approach to dealing with voltage dips that affect industrial equipment is through design. Existing electricity users are worst affected by the voltage dip problem as installed equipment and existing design configurations take inadequate consideration of dips. A popular, but expensive solution is power conditioning. Process specific action requiring the analysis of equipment operation is often a less expensive than power conditioning. SAPPI Kraft Ngodwana's continuous DC drive system is a prime example of where process specific action is expected to yield significant improvements.

REFERENCES

[1]   Smit, E.: "An Investigation into Voltage Dips and their Effects on Industrial Equipment", UCT undergraduate thesis, 1995
[2]   Coney, R. and Smit, I.: "Voltage Depressions- (DIPS)", *Elektron*, April 1995, pp 15-17
[3]   Mulukutla, S. and Gulachenski, E.: "A Critical Survey of Considerations in Maintaining Process Continuity During Voltage Dips while Protecting Motors with Reclosing and Bus Transfer Practices", *IEEE Power Engineering Society Transmission and Distribution Conference Proceedings*, 1991, Dallas Texas, pp 266-272

POWER SYSTEM HARMONIC FIELD MEASUREMENTS AND THE APPLICATION OF STANDARDS INCLUDING SIMULATION

G Atkinson-Hope, Cape Technikon
A Petroianu, University of Cape Town

ABSTRACT

In this paper international and local power system harmonic standards are compared and applied to field measurements taken at a 11 kV manufacturing plant and in a 33 kV traction substation. The 11 kV plant was simulated using two industrial grade harmonic software packages and their results compared to the actual values measured.

1   INTRODUCTION

With the increase of non-linear loads in power systems, the voltage and current waveforms are becoming more distorted and the power quality is deteriorating. Because of this development it has become essential to assess any adverse effects which harmonics may produce in a system. These effects are best ascertained by carrying out field measurements. Computer simulations can be used to check field measurements and are particularly useful for newly designed installations or where installations are to be upgraded to include non-linear loads. Any adverse effects can be pre-determined and remedial steps taken.

These measurements need to be compared to a standard to evaluate whether or not they are harmful.

Certain international and local standards governing permitted levels are in place. In the USA an American Standard (IEEE) applies whereas in Europe a different standard (IEC) applies. South Africa (ESKOM) tends to follow the European standard but has slightly different limits for distortion levels. Measured harmonics significantly higher than the recommended levels would be considered unacceptable.

These standards are applied to a South African 11 kV manufacuring plant and to a 33 kV traction substation to demonstrate their differences.

The 11 kV plant is also simulated using two leading international industrial grade software analysis packages to ascertain the harmonic penetration being caused by a 6 pulse dc drive. The results of the simulation being compared to the actual field measurements taken.

2   HARMONIC STANDARDS

Three standards are compared, namely:

a.   IEEE519 Recommended Practice and Requirements for Harmonic Control in Electrical Power Systems [1].

b.   IEC1000 series standard [2].

c.   ESKOM - ESKASAA18 standard [3].

These standards all make use of the total harmonic distortion (THD) voltage or current, defined as:

$$\text{THD} = \frac{100 \sqrt{\sum_{n=2}^{k} U_n^2}}{U_1} \quad \ldots\ldots (1)$$

where: U_1, is the fundamental component, U_2 to U_n are the harmonic components.

IEEE STANDARD

This standard sets limits for percentage "individual harmonic component distortion" and "THD". It limits both utility voltage and end user current distortions at the point of common coupling (PCC).

Voltage
Tabel 1 lists the limits to ensure quality of voltage and decrease with PCC voltage increase.

NEW IEEE STD 519 VOLTAGE DISTORTION LIMITS		
Bus voltage at PCC	Individual voltage distortion (%)	Total harmonic distortion (%)
Below 69 kV	3.0	5.0
69 kV to 138 kV	1.5	2.5
138 kV and above	1.0	1.5

Table 1

Current

This standard also limits PCC current. Table 2 lists the limits for systems below 69 kV and increase as the ratio of the short circuit current to load current (I_{SC}/I_L) increases. The standard provides similar tables for PCC's above 69kV.

NEW IEEE STD 519 CURRENT DISTORTION LIMITS FOR NONLINEAR LOADS						
Maximum Harmonic Current Distortion in % of fundamental						
Harmonic Order (Odd Harmonics)						
I_{sc}/I_L	h<11	11≤h<7	17≤h<23	23≤h<35	35≤h	THD
<20	4.0	2.0	1.5	0.6	0.3	5.0
20-50	7.0	2.5	2.5	1.0	0.5	8.0
100-1000	10.0	4.0	4.0	1.5	0.7	12.0
≥1000	12.0	5.0	5.0	2.0	1.0	15.0
	15.0	6.0	6.0	2.5	1.4	20.0

Table 2

Table 2 applies to 6 pulse convertors, but can be adapted for higher pulse numbers. See application examples in the standard.

IEC STANDARD

The following is a brief outline of the IEC standards:

a.   IEC555-I (1982) Definitions of disturbances caused by household appliances.

b.   IEC1000-1-1 (1992) Definitions used in IEC1000.

c.   IEC1000-2-1 (1990) Disturbances in public power supply systems.

d.   IEC1000-2-2 (1990) Defines the compatibility levels for individual harmonic voltages in public low voltage power supply systems.

e.   IEC1000-2-4 (1994) Prescribes the compatibility levels for industrial and non-public networks. It applies to low and medium voltage supplies. It distinguishes between the *"Point of common coupling (PCC)"* and the *"In Plant point of coupling (IPC)"*. This standard defines 3 classes:

CLASS 1: Relates to equipment very sensitive to disturbances. (e.g. equipment using UPS, filters etc.)

CLASS 2: Applies to PCC's and IPC's in industrial environments. The compatibility levels are identical to those of public networks. (see 1000-2-2). Therefore components designed for application in public networks may be used in this class.

CLASS 3: Applies only to IPC's in industrial environments. It has higher compatibility levels than Class 2. This class should be considered when loads are fed through convertors.

Compatibility levels (THD %) for these classes are:

Compatibility levels for harmonics			
	Class 1	Class 2	Class 3
Total harmonic distortion (THD)	5%	8%	10%

Table 3

They are for harmonic voltage components only. No limits are specified for currents. They apply to line voltages, class 1 to LV, classes 2 and 3 to LV and MV. Standards for HV and higher are not yet in place. See application examples in the standard.

f.   IEC1000-3-2 (1995) This standard replaces IEC555-2 (1982). It refers to equipment having input currents ≤16A/phase connected to public low voltage distribution systems. (e.g. lighting).

ESKOM STANDARD

This standard sets limits for percentage "individual harmonic distortion" and "THD" at PCC's for Transmission, Distribution and Reticulation voltage ranges. It is based on IEC standards and on experience in South African Systems.

Table 4 lists the limits for the 1,1 to 44 kV PCC voltage range. The standard also provides limits for PCC ranges below and above 44 kV.

Limits for steady state voltage harmonics		
Nominal voltage at PCC		Recommended limits (% of nominal supply frequency component)
Above 1 100V, up to and including 44 kV	THD odd even <14th inter 14th – 25th >25th	5,0 4,0 ⎤ limits on 2,0 ⎥ individual 1,0 ⎦ harmonics 0,5 x <14th 0,25 x <14th ⎦

Table 4

3.   COMPARISON OF STANDARDS

In brief the IEEE standard limits both voltage and current distortion at a PCC. The voltage limits are sub-divided into three voltage ranges (Table 1). The current limits are categorized in accordance with typical I_{sc}/I_L ratio found in power systems. (Table 2.) In contrast the IEC and Eskom limits are for harmonic voltages only. No limits are specified for currents.

The IEC limits do not vary in accordance with voltage ranges but apply singularly to the LV and MV range. They however are grouped in classes (Table 3). Unlike the IEEE and Eskom standards, the IEC standard caters for both PCC's and IPC's. The Eskom standard differs from the IEC standard in that its limits vary like the IEEE in voltage ranges. The IEEE has 3 ranges (Table 2) whereas Eskom has 5 voltage ranges. (Table 5).

In terms of voltage "THD" the 3 standards can be compared as follows.

IEEE		IEC		ESKOM	
PCC	THD %	PCC/IPC	THD%	PCC	THD%
		LV/MV		<1,1kV	8%
<69kV	5%	CLASS 1	5%	1,1 to 44kV	5%
69 to 132 kv	2,5%	CLASS 2	8%	44 to 132kV	3%
>138kV	1,0%	CLASS 3	10%	132 to 275kV	2,5%
				275kV	2,0%

Table 5

4. FIELD MEASUREMENTS AND THE APPLICATION OF STANDARDS

Figure 1 shows the one-line diagram for the 11 kV plant in which harmonic field measurements were taken:
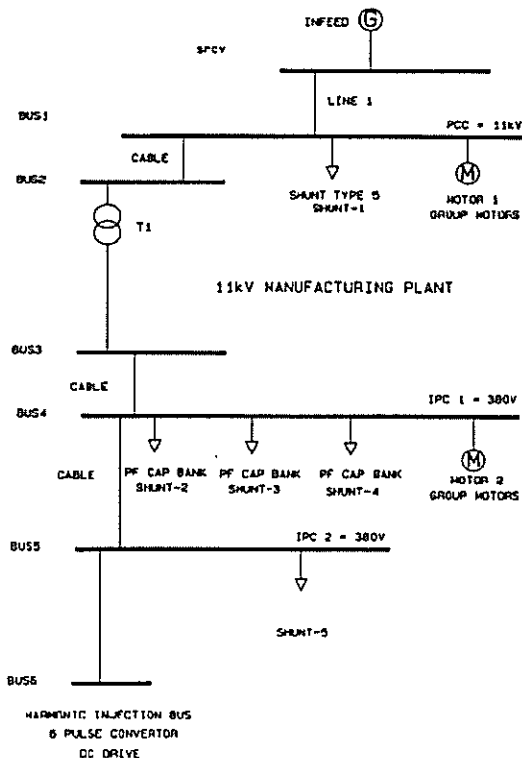
Figure 1

Measurements were taken at inputs to buses 1(PCC), 2,4(IPC1), 5(IPC2) and 6. The following results *inter alia*, were measured at the PCC and IPC1.

FIELD MEASUREMENTS				
NO	FREQ	PCC = BUS 1(HV)		IPC1 = BUS 4 (LV)	
	HZ	V(v)	C(A)	V(v)	C(A)
1	50	11 410	99.2	380	888.0
5	250	60.0	0.4	3.0	36.0
7	350		0.4	1.0	6.0
11	550				6.0
THD %		0,7	1.1	1.4	5.2

Table 6

11 kV MANUFACTURING PLANT

IEEE (PCC ONLY)

The full load current at PCC = 105 A, I_s = 13 kA, I_{SC}/I_L = 125, ∴ From Table 2 the THD% = 15%. The 1,1% (Table 6) is well within the current standard. The voltage "THD" measured is 0,7% and is also well within the 5% standard (Table 1).

IEC (PCC and IPC1)

In terms of Table 3 Class 2 (PCC's) voltage "THD" must not exceed 8%. Class 3(IPC's) is 10%. The measured THD's of 0,7% (PCC) and 1,4% (IPC1) are both well within these standards.

ESKOM (PCC ONLY)

The 11 kV PCC falls within the 1.1 to 44 kV, 5% THD range (Table 4). The measured "THD" of 0,7% is well within this standard.

Measurements were taken under two different switching configurations:

SWITCHING CONFIGURATION	THD%			
	PCC		RECTIFIER"A"	
	VOLTS	CURRENT	VOLTS	CURRENT
Bus coupler closed Eskom 2 open	2.2	9.9		
Bus coupler open Eskom 2 closed	1.9	15.8	4.5	94.8

Table 7

33 kV TRACTION SUBSTATION

Figure 2 shows one-line diagram of a 33 kV Switchroom for a traction substation.
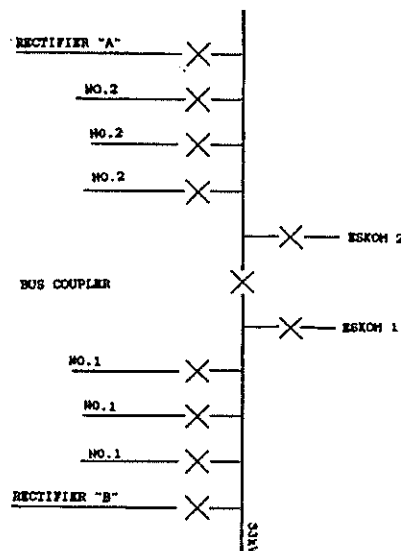
Figure 2

IEEE (PCC ONLY)

I_{sc}/I_L = 25000/1250 = 20, from Table 2 THD% = 5%. The measured THD's of 9,9% and 15,8% exceed the standard limits. The limit for the voltage (Table 1) is 5%. The 2,2% and 1,9% are within the limits.

IEC (PCC ONLY)

Class 3 (Table 3) prescribes 10% as the limit. The 2,2% and 1,9% are within standard.

IEC (IPC - RECTIFIER A)

Class 3 prescribes 10%. The 4,5% is within the range.

ESKOM STANDARD (PCC ONLY)

The 33 kV voltage standard is 5% THD (Table 4). The 2.2% and 1,9% are within the standard.

5. FIELD MEASUREMENT RESULTS COMPARED TO SIMULATION RESULTS

The 11 kV plant has been simulated using the ERACS [4] and the SUPERHARM [5] industrial grade harmonic analysis packages. The following results have been obtained and are listed in Table 8.

COMPARISON OF HARMONIC FIELD MEASUREMENTS TO SIMULATION RESULTS										
No	1	5	7	11	13	17	19	23	25	THD
Freq	50	250	350	550	650	850	950	1150	1250	
PCC = Bus 1 (HV)										
V	11410	60.0								0.7
V1	10923	2.71		54.2	2.47	2.0	0.62	0.78	0.35	0.51
V2	10960	5.0	1.0	5.0	3.0	6.0	1.0	1.0	1.0	0.2
C	99.2	0.4	0.4							1.1
C1	92.6	0.56	0.11	1.42						1.67
C2	97.0	0.3	0.1	0.1	0.1	0.1				2.1
IPC1 = Bus 4 (LV)										
V	380	3.0	1.0							1.4
V1	377	1.22	0.35	6.77	0.31	0.24	0.06	0.08	0.05	1.85
V2	376	1.0		1.0		1.0				0.5
C	888.0	36.0	6.0	6.0						5.2
C1	819.6	17.9	3.56	45.2	1.75	1.07	0.31	0.31	0.12	5.95
C2	917.0	11.8	2.0	4.9	2.2	4.0	0.8	0.6	0.2	8.3
FIELD MEASUREMENTS V = VOLTAGE, C = CURRENT					SIMULATION PACKAGE V1 and C1 = SUPERHARM V2 and C2 = ERAC PACKAGE					

Table 8

6. CONCLUSION

From the results obtained it can be concluded that all three voltage standards are adequate. They may be different in their approaches but their applications lead to similar findings.

The simulation results are encouraging and it is considered that if measurements are taken under defined conditions and under conditions where simultaneous measurements are taken at different points in a network, then a closer correlation should be obtained. The packages indicate the presence of the same harmonics as were measured.

7. REFERENCES

[1] "IEEE Recommended Practices and Requirements for Harmonic Control in Electrical Power Systems", IEEE-519, 1992.

[2] "IEC 1000 Electromagnetic Compatibility standard", 1990-1995.

[3] "Eskom Handbook Power Quality", March 1994.

[4] ERACS Power System Analysis Package, ERA Technology Ltd, England, 1988-1992.

[5] SUPERHARM Harmonic Analysis Package, Electrotek Concepts, Inc., USA, 1995.

8. ADDRESS OF AUTHOR

G Atkinson-Hope, School of Electrical Engineering, Cape Technikon, P O Box 652, Cape Town, 8000. E-mail: garyah@norton.ctech.ac.za

'n 88 kV analoog transmissielynmodel vir harmoniese ondersoeke.

H.A. Jordaan   A.P.J. Rens

PU vir CHO

Uittreksel: Hierdie artikel gee 'n oorsig oor die ontwikkeling van 'n analoog kragstelsel se transmissielynmodel. Dit word gebruik in die ondersoek van harmoniese penetrasie in 'n kragnet. Die ontwikkeling van 'n driefase analoog transmissielyn model geskik vir hoër frekwensies word bespreek. Hierdie model se ontwerp en digitale verifiëring word aangetoon.

1. Inleiding

Transmisielyn teorie is lank reeds gevestig, reeds in 1959 en 1963 is van digitale maniere gebruik gemaak om transmissielyn konstantes te bereken [5], [6]. Daar bestaan hoofsaaklik twee modelle vir kragstelsel transmissie lyne, die nominale-pi model (vir medium lengte transmissielyne) en die ekwivalente π model (vir lang transmissie lyne). Medium transmissielyne word gereken as tussen 50 en 200 km lank op grond van die fundamentele 50 Hz komponent.

Met harmoniese versteurings in die toevoer aanwesig, word die lynlengte wat akkuraat deur die nominale π model gebruik word aansienlik beïnvloed. Hoër frekwensie komponente veroorsaak dat transmissielyn modules in hierdie geval as 10 km lynlengtes voorgestel moet word (met die nominale π model) ten einde akkuraatheid tot by die 25ste harmoniek te behou.

Slegs die nominale π model is analoog fisies modelleerbaar, die ontwikkeling hiervan word analities beskryf en gemotiveer.

2. Ekwivalente π model

Vir langer transmissielyne moet die ekwivalente π model gebruik word vir digitale hoër frekwensie analise. Die ekwivalente π model is die enigste model wat bevredigende akkuraatheid bied vir "langer" afstande [8]. Hierdie model lyk as volg [8], [2], [3]:
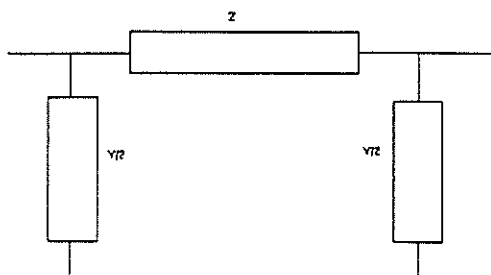
Figuur 1. Ekwivalente- pi model

Die impedansies en admitansies word gedefinieer as:

$$Z = Z_0 \sinh(\gamma . l)$$

$$\frac{Y}{2} = \frac{1}{Z_0} \tanh(\frac{\gamma . l}{2})$$

waar

$$\gamma = \sqrt{zy}$$

$$Z_0 = \sqrt{z/y}$$

z = serie impedansie per kilometer
y = sjunt admitansie per kilometer

Elke frekwensiekomponent in die versteurde golf veroorsaak dat ander elektrodinamiese en -statiese eienskappe in die model moet bestaan om daardie frekwensie se gedrag reg te modelleer. Die frekwensie afhanklikheid van die lynparameters word bevestig deur die eienskappe van die parameters in bostaande uitdrukking.

Analoogmodellering met ekwivalente π bane beteken dat 'n ander model vir elke frekwensie moet bestaan en dit is nie prakties uitvoerbaar nie. Die akkuraatheid van die ekwivalente π model maak dat kontrole van die akkuraatheid van enige kombinasie van nominale π bane maklik digitaal gedoen kan word.

As finale kontrole van die akkuraatheid van die analoog nominale π modelle sal metings op werklike installasies vergelyk word met die geskaleerde laboratoriummodel se gedrag.

3. Nominale-pi model

Die nominale-pi model gebruik sien as volg daaruit:

Figuur 2. Nominale pi-model

88kV- Lyn
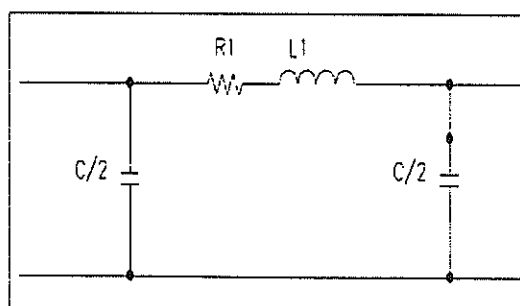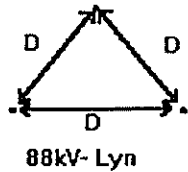
Figuur 3a. Tipiese geleierspasiëring vir 88kV transmissie lyn.

Tipiese 88kV struktuur
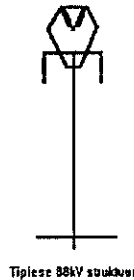
Figuur 3b. Tipiese 88kV toring struktuur

Vir 'n transmissielyn waar die geleiers gerangskik is op die wyse aangetoon in figuur 3 word die onderskeie komponente vir die nominale π model as volg bereken [1]:

$$L_a = 2x10^{-7} \ln\frac{D}{r}(Henry / meter)$$

$$C_n = \frac{2\pi.k}{\ln(D_{eq} / r)}(Farad / meter)$$

met:
C_n = fase na grond kapasitansie van n-de fase
L_a = selfinduktansie van a fase
r = radius van geleier deursnit
k = permitiwiteit van materiaal
D = geometries gemiddelde afstand tussen fasegeleiers

$$D_{eq} = \sqrt{(D_{12}D_{23}D_{31}}$$

$D_{i,j}$ = Onderskeie afstande tussen fasegeleiers se middelpunte

Eienskappe van 'n 88 kV enkelbaan "kite" struktuur is as volg:

GMR: 3613 mm

* Afstand tussen grond en onderste
  twee geleiers: 9120 mm
* Afstand tussen grond en
  boonste geleier: 12 500 mm

Deurhang tussen strukture:
* 7500 mm vir onderste twee geleiers.
* 10 880 mm vir boonste geleier.

Geleiertipe: 70 mm Cu

Die weerstand van 'n transmissielyngeleier bestaan uit twee komponente:
* Die voorwaartse gelykstroom weerstand.
* Die weerstand wat die gevolg is van die skileffek.

Die gelykstroom weerstand is slegs 'n funksie van die materiaal tipe en geleierkonstruksie [1], [8] en word beskryf deur:

$$R_0 = \frac{\rho.L}{A}$$

met:
R_0 = gelykstroom weerstand
ρ = spesifieke weerstand van die geleiermateriaal
L = Lengte van die geleier
A = Deursnit oppervlakte van die geleier

Soos wat die frekwensie toeneem begin die skil effek belangrik raak. Stevenson [1] gee 'n metode waar die wisselspannings weerstand van 'n ronde geleier as 'n verhouding van die gelykstroom weerstand uitgedruk word.

$$\frac{R}{R_0} = \frac{mr}{2} \frac{ber(mr)bei'(mr) - bei(mr)ber'(mr)}{(ber'(mr))^2 + (bei'(mr))^2}$$

met

$$mr = 0.0636\sqrt{f / R_0}$$

R_0 = Gelykstroom weerstand
ber = reële bessel funksie
bei = imaginêre bessel funksie
ber' = afgeleide van reële bessel funksie
bei' = afgeleide van imaginêre bessel funksie

Dit is duidelik dat uit die bostaande vergelykings die onderskeie komponente van die nominale π model frekwensie afhanklik is. Die impedansie matriks van 'n driefase stelsel word gekompliseer deur die harmoniese frekwensies. Die wedersydse induktansies en kapasitansies moet ook in berekening gebring word.

Bostaande probleem kan word hanteer deur 'n aantal drie fase nominale π bane in kaskade te koppel [2]. Transmissielyne (50 Hz) word deur die ekwivalente π model voorgestel as dit langer as 300 km is, dit is 5 persent van die 50 Hz golflengte. Vir hoër frekwensies kan die afstand wat 5 persent van die golflengte voorstel, benader word met [2]

L = 300/h (km)

waar h die orde van die harmoniek is. Dit beteken in hierdie geval (hoogste frekwensie = 1250 Hz) dat daar van nominale seksies van hoogstens 12 km gebruik gemaak moet word om aan bogenoemde vereiste te voldoen. Vir praktiese doeleindes is daar besluit om 'n lynlengte te kies van 10km. Dit vereenvoudig die probleem om verskillende lyne

voor te stel, 'n 90km transmissielyn kan nou met behulp van nege 10km seksies gemodelleer word. Die kombinasie van modules om 'n lyn voor te stel mag ook bestaan uit verskillende toringstrukture se onderskeie analoogmodelmodules. Die kaskade beginsel is geimplementeer, die verifikasie word met EMTP gedoen.

'n Ekwivalente 90 km kringbaan is ondersoek vir frekwensies van 50-1250Hz. Daar is vir elke frekwensie 'n nuwe impedansie matriks bepaal uit die lynparameters. Nege nominale π seksies van 10km elk is in kaskade gekoppel en die frekwensie gedrag (50-1250 Hz) is bepaal. Dieselfde is gedoen vir twee 45km nominale-pi kaskade seksies om aan te toon watter mate van onakkuraatheid reeds op hierdie afstand bestaan.

4. Kaskade gekoppelde nominale-pi modelle

Die kaskade beginsel is geimplementeer deur die 88kV transmissielyn in figuur 3 te modelleer as nominale π seksies. Die ontwerp en simulasies is gedoen vir die frekwensieband 50-1250Hz.

Om vas te stel hoe die lynimpedansie vir verskillende frekwensiekomponente lyk, is die lyn in elke geval getermineer deur dieselfde vaste lineêre weerstand met 'n 88 kV bronspanning en nulfase. Die figure gee die verloop van die stroomgrootte as funksie van frekwensie wat in wese ook die modulus van die impedansie van die lyn teen verskillende frekwensies is. Alhoewel die akkuraatheid ook op ander maniere bevestig kan word, is hierdie die enigste wat hier weergegee word.

Hierdie ontwerp en resultate wat hier weergegee word is vir 'n werklike 88 kV installasie van 90 km tussen Lichtenburg-Slurrey en Ventersdorp. Dit word getoon in figure 4 tot 6. Hierdie is 'n lyn wat juis versteurde golwe gelei en uit slegs een toringstruktuur bestaan. Metings op hierdie lyn bied derhalwe 'n geskikte kontrole vir die EMTP en die laboratoriummodel.
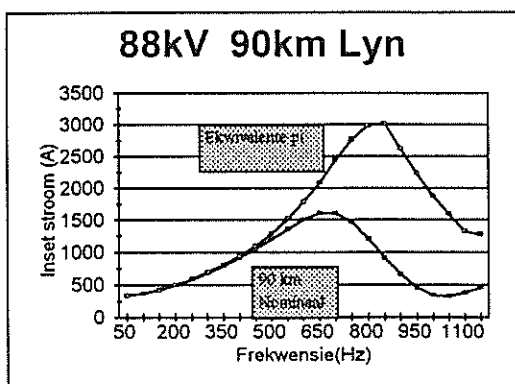
Figuur 4. Vergelyking tussen die ekwivalente π model vir 90 km en 'n enkele 90 km nominale π seksie. (EMTP resultate)
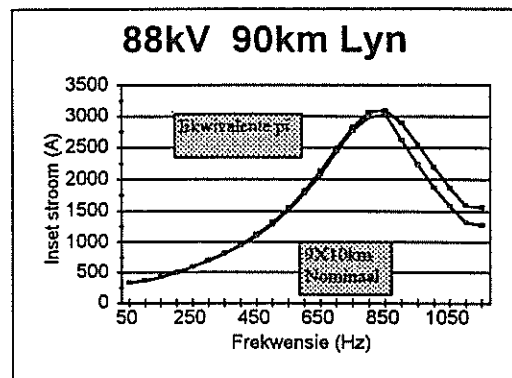
Figuur 5. Vergelyking tussen die ekwivalente π model vir 90 km en nege 10 km nominale π kaskades.
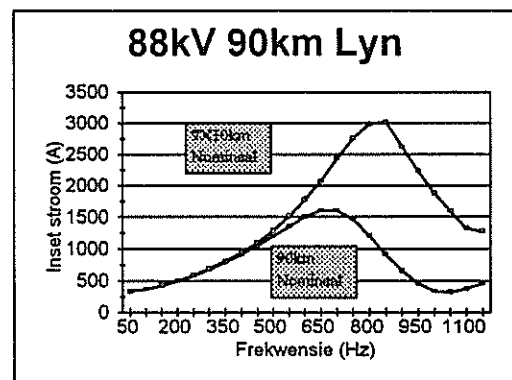
Figuur 6. Vergelyking tussen 'n enkele 90 km nominale π seksie en nege 10 km seksies.

Die resultate wat verkry is in figure 4 tot 6 bevestig dan ook die verwagte resultate wat Arrillaga [4] beskryf met simulasies van die tipiese verloop van impedansie van 'n transmissielyn teen frekwensie.

Die impedansie matriks wat bereken is vir 'n 10km nominale π baan lyk as volg:

1.0005+j7.3+ 1/j24.3e-6	0.4797+j2.8- 1/j1.920e0	0.4740+j3.799- 1/j7.796
0.4797+j2.83 -1/j1.92e0	1.0116+j7.3+ 1/j24.5e-6	0.479+j283- 1/j1.9204
0.4740+j3.79 9-1/j7.796	0.479+j283- 1/j1.9204	1.0005+j7.3+ 1/j24.3e-6

Hierdie impedansie matriks is 'n matriks wat bereken is vir die 88kV toring struktuur getoon in figuur 3 en 4, die berekeningprosedure is dieselfde vir ander toring strukture.

Bogenoemde proses herhaal vir elke tipe transmissielyn. Deur die onderskeie resultate vir die verskillende 88kV transmissielyne te gebruik, kan 'n fisiese analoog transmissielyn model ontwerp en gebou word soortgelyk aan die tegniek beskryf deur Shoults [9]. Die module word getoon in figuur 7. Deur gebruik te maak van die basiswaardes van die laboratoriumstelsel van 5 KVA en 380 V, word die skalering van die berekende lynparameters na die basisvlak gedoen. Die implementering van hierdie

ontwerp is omslagtig aangesien wedersydse induktansie en kapasitansie nie elementêr voorgestel kan word nie. Die bou van hierdie module is tans nog nie afgehandel nie.

Die ontwerpprosedure sal geverifieër word deur metings op 'n werklike lyn te vergelyk met beide die EMTP en laboratoriumresultate.
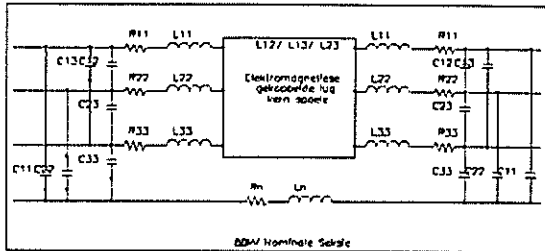
Figuur 7. Analoog nominale π seksie Shoults[9].

5. Samevatting

Die resultate toon duidelik dat 'n nominale π model se hoë frekwensie gedrag ernstig deur die lynlengte beinvloed word soos bevestig deur die ekwivalente π baan se frekwensie gedrag. Derhalwe moet 10 km seksies in kaskade gekoppel as die nominale π baan gebruik word om 'n aanvaarbare akkuraatheid vir die verlangde frekwensies te verkry. Dit bevestig ook die norm [2] wat die afstand as 12 km voorgestel het. Die betrokke 10 km seksie word dan elektrodinamies en elektrostaties voorgestel word met 'n enkele geskaleerde module. Die kaskade koppeling van modules kan gebruik word om 'n 88 kV lyn korrek analoog te modelleer.

Verwysings

[1]   Stevenson, W.D., **Elements of Power System Analysis**, Second Edition, New York, MGraw-Hill, Inc., 1962.

[2]   Shultz, R.D., Smith, R.A., Hickey, G.L., "Calculation of maximum harmonic currents and voltages on transmission lines", IEEE Transactions on Power Apparatus and Systems, Vol. PAS-102, No.4, April 1983.

[3]   Gross, C.A., **Power System Analysis**, New York, John Wiley & Sons, 1979.

[4]   Arrillaga, J., Bradley, J.A., Bodger, P.S., **Power System Harmonics.** New York: John Wiley & Sons. 1985.

[5]   Coleman, D., Watts, F., Shipley, R.B., "Digital Calculations of Overhead Transmission Line Constants", IEEE Transactions, pt. III (Power Apparatus and Systems), vol. 77, 1958 (Feb. 1959 section). pp. 1266-70.

[6]   Hesse, M.H., "Electrostatic Transmission-Line Parameters by Digital Computer." 1963

[7]   Mahmoud, A.A., Shultz, R.D., "A Method for Analyzing Harmonic Distribution in A.C. Power Systems.", IEEE Transactions on Power Apparatus and Systems, Vol. PAS-101, No. 6 June 1982, p.1815-1824.

[8]   Glover, D.J., Sarma, M., **Power System Analysis and Design**. Second Edition. Boston: PWS Publishing Company. 1994.

[9]   Shoults, R.R., Chen, M.S., Domijan, J., "The Energy Systems Research Center Electric Power System Simulation Laboratory and Energy Management System Control Center.", IEEE Trans. on Power Systems, Vol. 2, No. 1, Februarie 1987, p239-246.

Adres van skrywer

H.A. Jordaan, Departement Elektroniese en Elektriese Ingenieurswese, PU vir CHO, Privaatsak X6001, Potchefstroom, 2520. Tel: 27-148-299 1978 eeihaj@puknet.puk.ac.za

AN ACTIVE AND SYSTEMATIC APPROACH TO ACHIEVE ELECTROMAGNETIC COMPATIBILITY (EMC) THROUGHOUT A LARGE ELECTRIC POWER SYSTEM

P H Pretorius   A C Britten   J P Reynders*

Eskom Technology Research and Investigations
*University of the Witwatersrand

1. Introduction

The legal obligation of Member States of the European Community (EC) to comply with the Electromagnetic Compatibility (EMC) Directive 89/336/EEC as from 1 January 1996, not only re-vitalised thinking about the EMC concept, but also heightened awareness among the uninitiated in South Africa [1, 2]. The Directive essentially means that any electrical or electronic equipment manufacturer placing products or systems on the European market must prove firstly, that the product or system does not emit, and secondly, that it is immune to the effects of unwanted electromagnetic energy. This applies to both new and existing designs and embraces conducted and radiated emissions, conducted and radiated immunity, mains disturbances, electrostatic discharge and lightning induced surges [3].

Unlike local manufacturers and exporters of electrical and electronic equipment, implementation of the European EMC Directive will have no direct and immediate effect on electric utilities in South Africa. This does not mean that a utility, such as Eskom, adopts a position ignorant to EMC, but rather that its interest in the topic does not result from the initiation and implementation of the European EMC Directive.

Despite the fact that an electric utility, such as Eskom, is not affected by the Directive, it must guard against becoming a "drop zone" for inferior electrical and electronic equipment from a EMC standards point of view. On the other hand, paying exorbitant prices for products marketed under the "CE mark", purely as a sales initiative, must also be guarded against.

An active and systematic approach to ensure electromagnetic compatibility (EMC) in a large power utility, such as Eskom, its relevance and particular aspects that are presently being focused on are discussed in this paper. In addition, this paper builds on earlier statements on EMC by Eskom [5,6].

Quality of supply, a subject studied and managed in its own right by Eskom is not treated in this discussion.

2. Relevance of EMC in a Utility Context

Any electric current carrying conductor can act as a radiator of electromagnetic energy. Correspondingly, any conductor in the vicinity of an electromagnetic field can act as a receiving antenna [4]. It is therefor clear that a large electrical network (consisting of power lines, power and substations) with supporting electronic networks (auxiliary, protection and control systems, etc) may in many cases not only be susceptible to electromagnetic interference (EMI) but can also contribute to it. Figure 1 illustrates the aspects related to electromagnetic interference (EMI) in the

Eskom context as viewed by its Technology Focus Group on EMC. These aspects cover natural and manmade sources of EMI and are considered both from an intrasystem and an intersystem point of view. Intrasystem interference relates to interference and effects within the Eskom system whilst intersystem interference relates to interference and effects involving the Eskom system and systems other than the Eskom system. Examples are respectively, interference impinging on telecommunication equipment due to switching activities in substations and lightning impinging on power equipment.

In addition, interference related problems are considered in the categories of radiated emissions (RE), conducted emissions (CE), radiated susceptibility (RS) and conducted susceptibility (CS). Subdividing problems into these categories assists greatly in the understanding and solving of EMI problems.
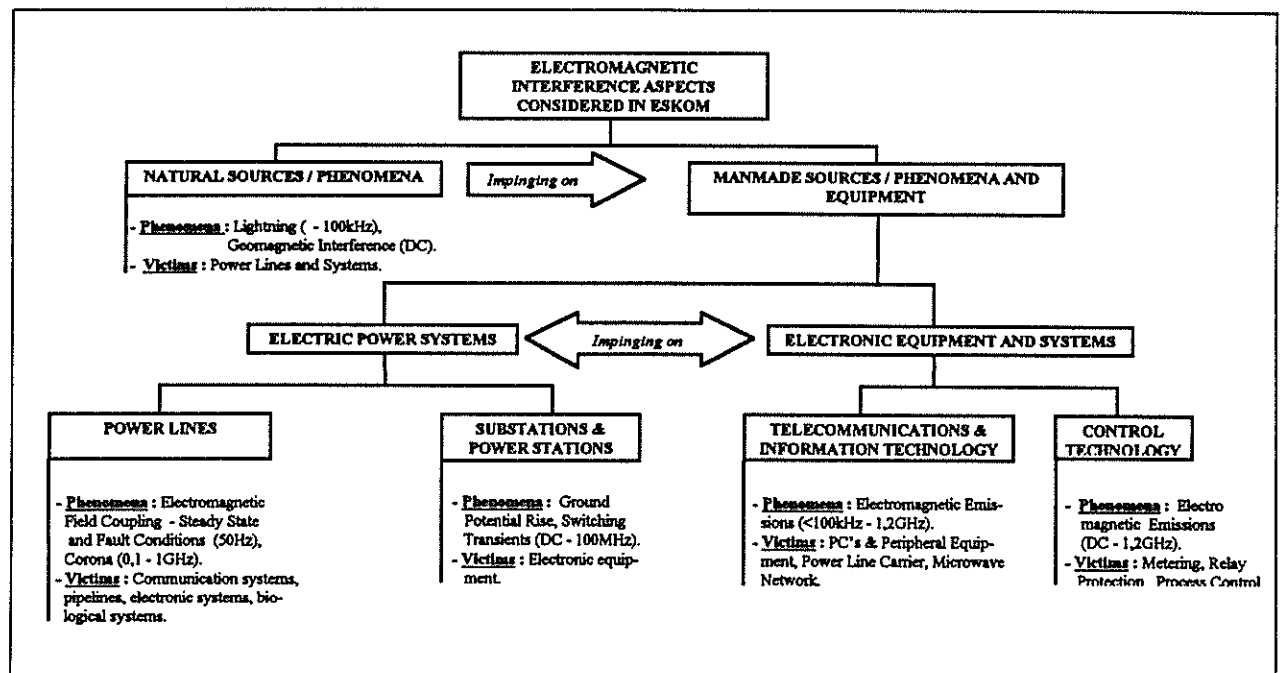
Figure 1. Electromagnetic Interference (EMI) Aspects Considered in the Eskom Context.

Utility involvement in EMC, as in the case of Eskom, is thus motivated and based on the following:

i)   To ensure that the electric power system does not cause any unwanted interference or is not electromagnetically interfered with,

ii)   To assure both product and human safety and

iii)   To achieve enhanced plant reliability.

EMC is not a new concept in the power industry and points i) and ii) have largely been addressed for existing plant. The third point, namely, to achieve enhanced plant reliability, is of a strategic nature as far as Eskom's electrification programme and its vision 'to supply the lowest cost electricity in the world' are concerned. Figure 2 illustrates the cost curves associated with EMI prevention and EMC improvement.
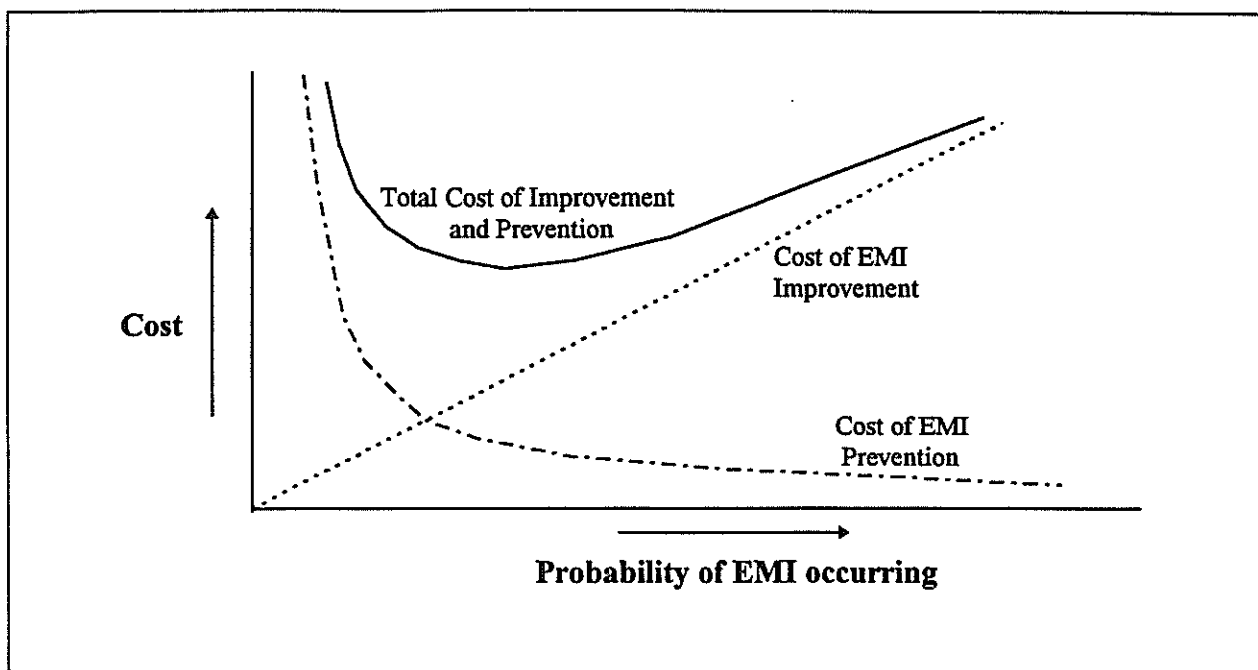
Figure 2. Cost Curves Associated with EMI Prevention and EMC Improvement [7].

3. Proposed Approach to Achieve EMC

Figure 3 illustrates the proposed approach to be adopted in order to achieve EMC throughout a large electric power system such as Eskom's.
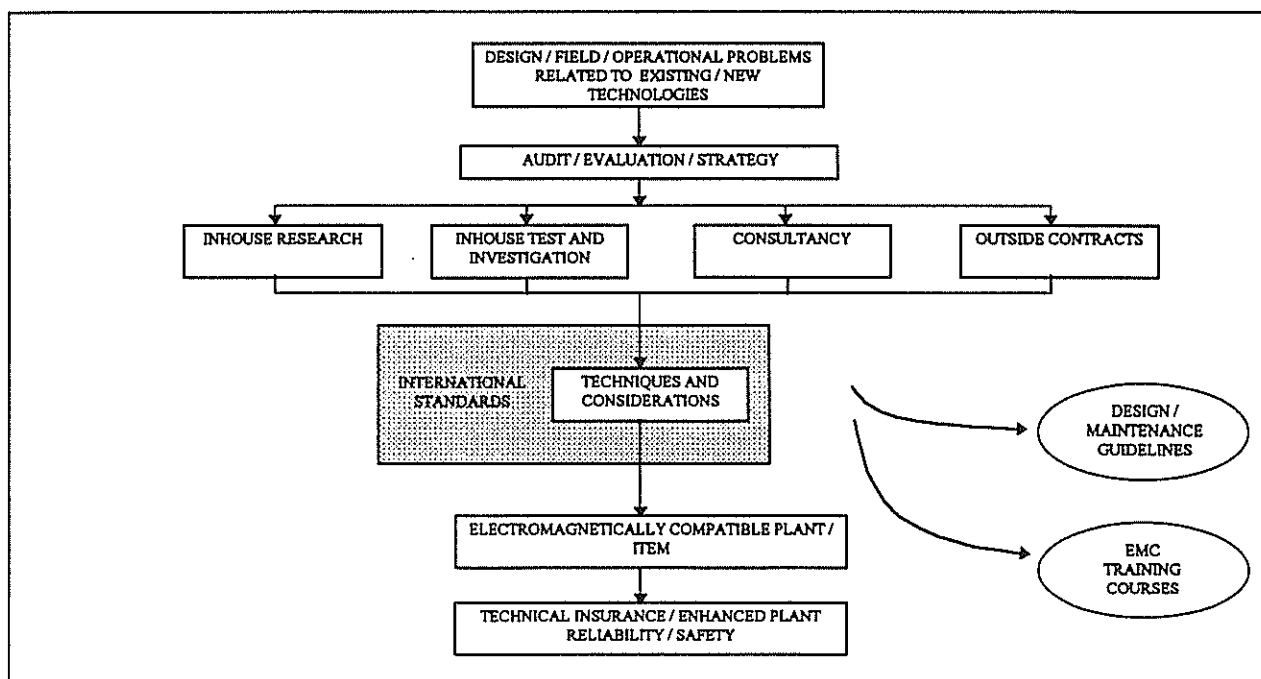
Figure 3. Proposed Approach to Achieve EMC Throughout a Large Electric Power System.

The approach used to achieve EMC throughout Eskom's electrical network should cater for "interference problems" associated with both existing and new technologies. This approach will find application during the design stage through to the maintenance stages of any technology.

Evaluation of the particular EMI problem should be allowed through technical investigative processes, test and research. In addition, avenues for outside contracts must exist if evaluation is called for that cannot be treated within Eskom.

The approach must further allow the existing or new technology to be evaluated against the backdrop of existing / new international standards, such as, those prepared by IEC, CISPR, CENELEC, etc.

It is anticipated that this approach will naturally lead to the development of guidelines on EMC that can be applied in the design and maintenance of electrical plant, and the experience gained can be ploughed back into the organisation through training courses, for example.

4. Specific Research

Specific research that will be concentrated on by Eskom's Technology Research and Investigations (T-R-I) during 1996 will be the following : The assessment of EMI levels in protection bay kiosks, interference immunity and surge protection in power stations, radiated fast transients resulting from switching activities in substations, EMI from Flexible AC Transmission (FACTS) devices, EMI from mobile phones and effects on electronic equipment, quantification of the risk associated with magnetic field exposure, characterisation of magnetic fields in residential and occupational environments and conductor corona generated noise.

5. Concluding Remarks

The objective with the proposed approach is : Through EMC, to introduce technical insurance against EMI, assuring enhanced plant reliability and safety.

The proposed approach supports Eskom's EMC research programme and policy on EMC. Implementation can be achieved without major expenses. An increase in EMC related activities will however require additional manpower and equipment. Detail of these resources should be addressed separately and is not treated in this document. In addition, it allows involvement of EMC expertise in the process, not only locally but also from abroad.

References

[1]   59th IEC General Meeting (TC 77 / 77A / 77B / 77C), 16 to 28 October 1995, Durban, South Africa.

[2]   Vrolijk M, "CE Marking and CE Directive", Half-Day International EMC Seminar on Development and Implementation of EMC Standards, Organised by the IEC, SABS and University of Natal, 21 October 1995.

[3]   Marshman C, "The Guide to the EMC Directive 89 / 336 / EEC", IEEE Press, ISBN 0-7803-0445-4, 1992.

[4]   Keiser BE, "Principles of Electromagnetic Compatibility", Artech House Inc, ISBN 0-89006-065-7, 1983.

[5]   Britten, AC, Johnson, PA, Lings, RJ, "The Scope of EMC in Eskom", Elektron, April 1995.

[6]   "Eskom Electromagnetic Compatibility Policy Document", ESK PB AA1 (Rev 0), March 1994.

[7]   Borm, C, "Electromagnetic Compatibility in Open Air Substations", Eskom report TRR/E/94/EL 142, December 1994.

Address of Main Author : Pieter H Pretorius, Eskom Technology Research and Investigations, Private Bag 40175, Cleveland, 2022. E-mail : PHPEMF@TRI.ESKOM.CO.ZA

INTERIOR MAGNETIC FIELDS ASSOCIATED WITH DRIVING AN ELECTRIC VEHICLE : A CASE STUDY

P H Pretorius   M S Baholo   A C Britten

Eskom Technology Research and Investigations

1. INTRODUCTION

Concern has been expressed for a number of years about the possible adverse health effects that may result from exposure to Extremely Low Frequency (ELF) magnetic fields [1,2]. Eskom has conducted surveys in a variety of environments containing magnetic field sources to determine the levels of these. A survey conducted on the magnetic field levels associated with driving an electric vehicle is discussed in this paper. The objective of this survey was to determine the magnetic field levels inside one of Eskom's Electric Vehicles, fitted with the latest technology, and to compare these with the magnetic field exposure limits set by the International Radiation Protection Association (IRPA) / International Commission for Non-Ionising Radiation (ICNIRP) and the European Committee for Electrotechnical Standardisation (CENELEC).

2. APPROACH

2.1 Vehicle

Arrangements were made to use Eskom's Honda, Civic VX, for the survey. The vehicle was driven on the N1 South, between the South Gate Mall and the Grassmere Toll Plaza, clear from any overhead power lines and other magnetic field sources. The electric vehicle is driven by a 100kW, 4 pole, 3 phase induction motor. Speed control is achieved through variation of the frequency of the voltage fed to the motor. A frequency of 400Hz yields 12 000 rpm.

2.2 Measurements

Magnetic field measurements (resultant, rms) were made during the following operational conditions:

i)   Moderate acceleration up to 60km/h,
ii)   Constant travelling at 60km/h,
iii)   Moderate acceleration up to 120km/h,
iv)   Constant travelling at 120km/h and
v)   Deceleration from 120km/h to standstill.

The terrain on which the vehicle travelled on during the conditions mentioned in i) to v), included flat ground and stretches with both up and downhills.

Further measurements were made during:

vi)   Accelerating from standstill to 20km/h, from 20km/h to 40km/h, to 60km/h, to 80km/h, to 100km/h and from 100km/h to 120km/h. These were all done whilst driving uphill.

Measurements were also conducted during:

vii) Rapid acceleration uphill and
viii) Rapid deceleration downhill.

Rapid acceleration was achieved by prompt stepping on the accelerator from a state of standstill until the vehicle speed reached 120km/h. Rapid deceleration was achieved by prompt removal of all force from the accelerator (to allow complete re-generation), without any mechanical breaking assistance, bringing the vehicle from 120km/h to a state of standstill.

Magnetic field measurements were conducted at the following locations inside the vehicle :

i) At chest level of the Driver ,
ii) At chest level of the passenger sitting next to the driver (Passenger #1) and
iii) At chest level of the passenger sitting behind the driver (Passenger #2).

2.3 Instrumentation (MultiWave II System)

The Multiwave II System waveform capture unit has the capability to measure and record three dimensional steady state and AC magnetic fields. One auxiliary channel for optional current, electric field or high frequency magnetic field RMS sensors is available. The system has the ability to store waveforms from a variety of sensors in memory and floppy disk. Data recorded with the system is processed into ASCII files. System II plotting programmes or commercially available spreadsheet or plotting packages can then be used to analyse and plot the recorded data. This system also has software programmes which provide system configuration options, data acquisition control and sensor calibration files. Detailed descriptions of these programmes can be found in the System II Users Manual.

2.4 Magnetic Field Limits

Tables 1 and 2 indicate the safe levels recommended by IRPA/ICNIRP and CENELEC respectively for continuous magnetic field exposure of the public.

Table 1. Safe 50Hz Magnetic Field Exposure Levels for Public Exposure Recommended by IRPA/ICNIRP [3].

Magnetic Field (μT)	Descriptor
100	Continuous exposure
1 000	Short-term (2h per day) exposure

Table 2. Safe Magnetic Field Exposure Levels Recommended by CENELEC [4].

Frequency (Hz)	Reference Level (mT, rms)
1,15 - 1 500	$32/f*$ (0,64 @ 50Hz)

$*f$ - frequency in Hz.

3. Results

Figures 1 to 3 indicate the results of the magnetic fields (in the frequency range 10Hz to 400Hz) measured with the Multiwave II System at the positions of the Driver, Passenger #1 (next to the driver) and Passenger #2 (behind the driver) for conditions i) to v) respectively.

Figures 4 to 6 indicate the results of the magnetic fields measured with the Multiwave II System at the positions of the Driver, Passenger #1 and Passenger #2 for condition vi) respectively.

Figures 7 to 9 indicate the results of the magnetic fields measured with the Multiwave System II at the positions of the Driver, Passenger #1 and Passenger #2 respectively for condition vii) and viii).

Table 3 indicates the Power Consumption of the vehicle during the acceleration processes indicated in Figures 4 to 9.

Table 3. Typical Power Consumption of the Electric Vehicle.

Condition	Battery Voltage (V)	Battery Current (A)	Power (kW)
Accelerating to 20km/h	350	10	3,5
Accelerating to 40km/h	345	20	6,9
Accelerating to 60km/h	340	50	17
Accelerating to 80km/h	<340	90	<30,6
Accelerating to 100km/h	325	120	39
Accelerating to 120km/h	320	160	51,2
Rapid Acceleration	290	370	107
Rapid Deceleration	380	~200	~76

4. Concluding Remarks

The magnetic field levels generated in the interior of the electric vehicle (Honda Civic VX) are well within the allowable magnetic field levels set by IRPA/ICNIRP and CENELEC for continuous public exposure. Maximum magnetic field levels of approximately $1\mu T$ was measured during typical driving conditions. These included normal driving conditions, rapid acceleration and rapid deceleration.

It may be a good idea for future work to include magnetic field dosage measurements over daily and weekly periods.

References

[1] Wertheimer, N, Leeper, E, Electrical Wiring Configurations and Childhood Cancer, Am J Epidemiol, 109 (3) : 273 - 284, 1979.

[2] Electromagnetic Fields and the Risk of Cancer, Supplementary Report by the Advisory Group, National Radiation Protection Board (UK), Vol 5, No 2, 1994.

[3] South African Forum for Radiation Protection, Publication 7 : Comments on the 1991 IRPA Guidelines on Protection Against Non-Ionising Radiation.

[4] EMF Health & Safety Digest, Vol 13, No 2, 6, Feb 1995.

[5] Eskom and Electric Vehicles on the Move, 1994.

Address of Main Author : Pieter H Pretorius, Eskom Technology Research and Investigations, Private Bag 40175, Cleveland, 2022. E-mail : PHPEMF@ESKOM.TRI.CO.ZA
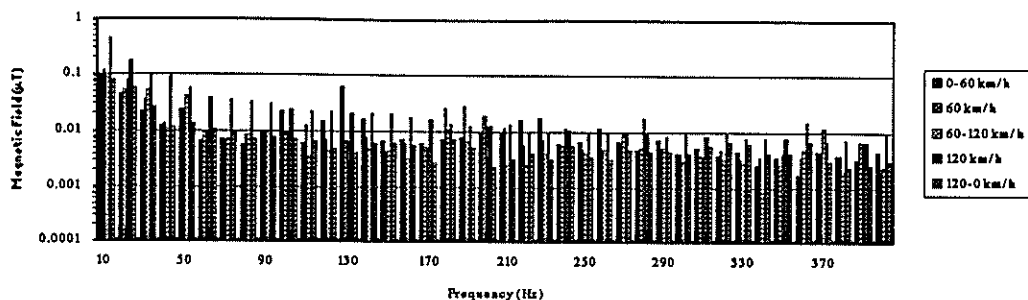
Figure 1. Magnetic Field Levels Associated with Acceleration to 60km/h, Constant Driving at 60km/h, Moderate Acceleration to 120km/h, Constant Driving at 120km/h and Deceleration to Standstill at the Position of the Driver.
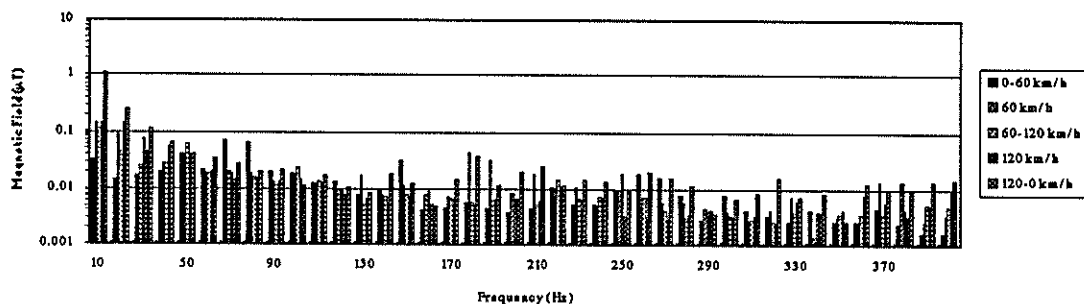
Figure 2. Magnetic Field Levels Associated with Moderate Acceleration to 60km/h, Constant Driving at 60km/h, Moderate Acceleration to 120km/h, Constant Driving at 120km/h and Deceleration to Standstill at the Position of Passenger #1.
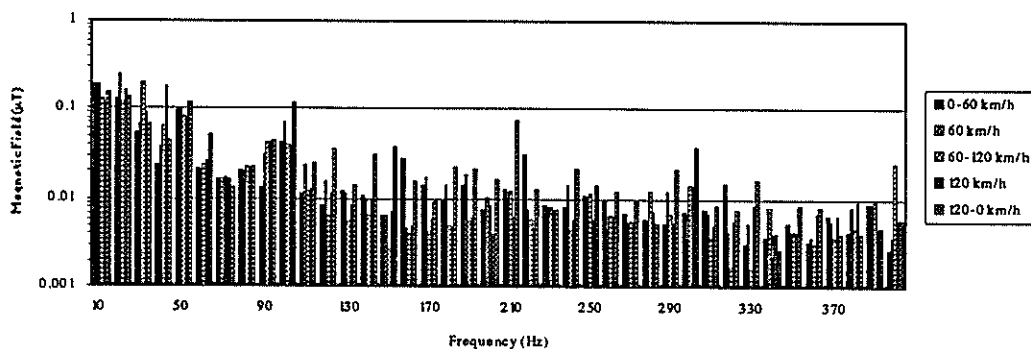
Figure 3. Magnetic Field Levels Associated with Moderate Acceleration to 60km/h, Constant Driving at 60km/h, Moderate Acceleration to 120km/h, Constant Driving at 120km/h and Deceleration to Standstill at the Position of Passenger #2.
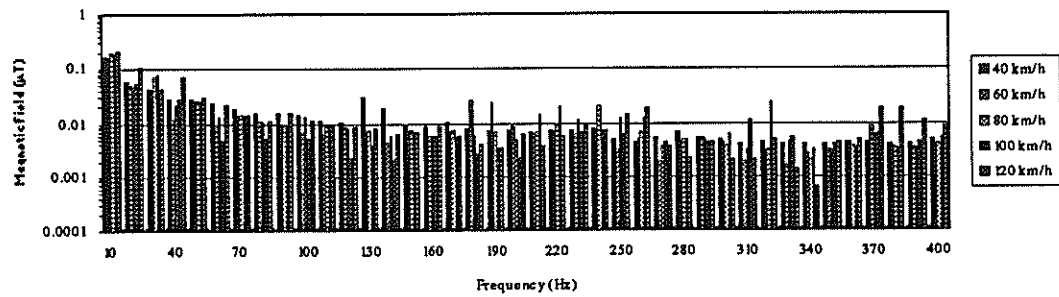
Figure 4. Magnetic Field Levels Associated with Accelerating to 40km/h, 60km/h, 80km/h, 100km/h and 120km/h (All Uphill) Measured at the Position of the Driver.
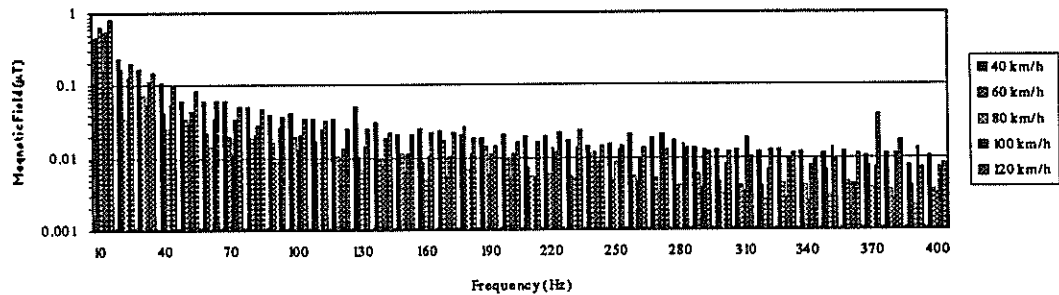
Figure 5. Magnetic Field Levels Associated with Accelerating to 40km/h, 60km/h, 80km/h, 100km/h, and 120km/h (All Uphill) Measured at Passenger #1.
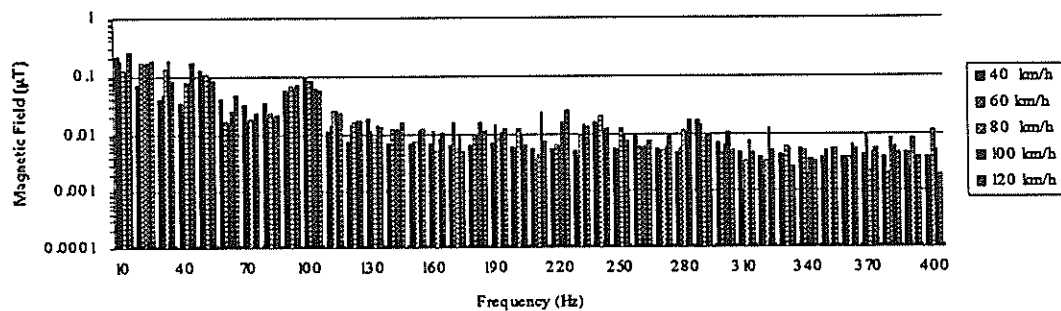
Figure 6. Magnetic Field Levels Associated with Accelerating to 40km/h, 60km/h, 80km/h, 100km/h and 120km/h (All Uphill) Measured at Passenger #2.
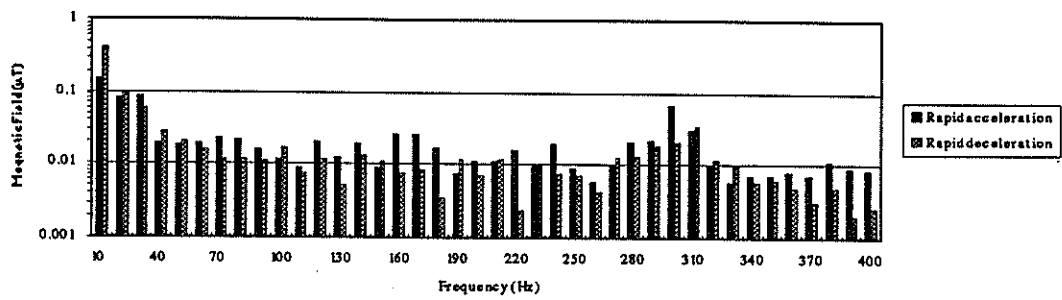
Figure 7. Magnetic Field Levels Associated with Rapid Acceleration and Rapid Deceleration Measured at the Driver.
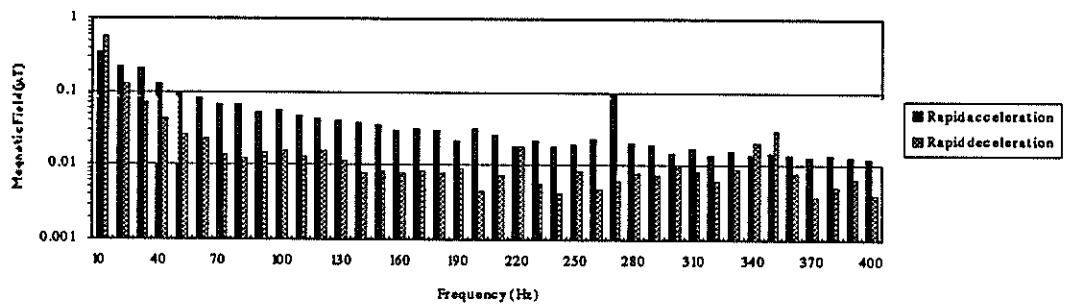
Figure 8. Magnetic Field Levels Associated with Rapid Acceleration and Rapid Deceleration Measured at Passenger #1.
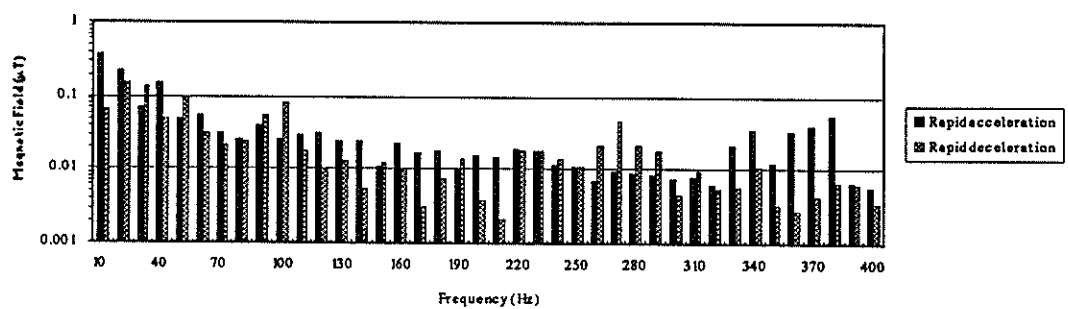
Figure 9. Magnetic Field Levels Associated with Rapid Acceleration and Rapid Deceleration Measured at Passenger #2.

LABORATORY CALIBRATION and PRELIMINARY FIELD RESULTS of an INSULATOR POLLUTION MONITORING APPARATUS (IPMA)

L. van Wyk   J.P. Holtzhausen   W.L. Vosloo*

Department of Electrical Engineering, University of Stellenbosch
*ESKOM, TRI

1. ABSTRACT:

The pollution phenomenon is one of the most severe problems facing the operation of transmission lines in areas near the coast and industrial areas. An Insulator Pollution Monitoring Apparatus (IPMA) was therefore developed to quantify the severity of pollution in a particular area. The area severity is determined by measuring the surface conductivity of the wetted pollution layer on the test insulator. The measured conductivity is then converted into an equivalent salt deposit density (ESDD). IPMA had to be calibrated in the laboratory prior to installation. Insulators used for calibration were artificially polluted and then artificially wetted with steam to enable the flow of leakage currents. This procedure was repeated for increasing pollution levels to obtain the regression of conductivity versus ESDD. The calibration curve shows that all data points lie within a band of values. Insulators, taken from both industrial and marine environments, were tested on IPMA and the results superimposed on the calibration curve. It was found that a correlation exists between the laboratory tested insulators and field insulators. IPMA has been installed at a marine test station at the west coast of South Africa and is currently used to predict the severity of pollution on the field insulators.

2. INTRODUCTION:

Outdoor insulators in various areas are subjected to ever changing environmental conditions and pollution levels. The insulator surface is exposed to industrial pollution or saline coastal pollution. These pollution deposits may lead to electrical discharges and even flashover on contaminated high voltage insulators. Flashovers may result in the unwanted disruption of electrical supply. A reliable assessment of the pollution severity would assist to determine the probability of flashover due to pollution.

An Insulator Pollution Monitoring Apparatus, better known as IPMA, was therefore developed by the University of Stellenbosch, in conjunction with ESKOM, to be able to quantify the severity of pollution in a particular geographic area [1]. CESI in Italy [2] developed

a Pollution Monitoring Equipment (PME) and showed that this approach is effective for the measurement of site severity.

IPMA is a transportable, self-contained test apparatus that can be installed at any substation to perform real-time pollution measurements. It houses a high pressure steam generator, shell raise/lower motor, 220/3 kV transformer, dryers, the test insulators and a control and data logging system. The electrical and mechanical operation is discussed in detail by Davel [3], [4].

The test procedure is based on the principle of a surface conductance measurement on site polluted insulators while artificial wetting is applied. Surface conductance is calculated by measuring the leakage current flowing over the insulator surface when a voltage of 3 kV is applied. The conductivity value is then found by multiplying the conductance value with the form factor of the insulator. The voltage duration is limited to five 50 Hz cycles (100 ms) to prevent the effect of dry band formation [5].

Ionic salts present in the pollution layer become conductive when wetted. Greater amounts of salt will therefore result in the measuring of a higher surface conductance. The amount of salt is expressed as an equivalent salt deposit density (ESDD) in mg/cm^2 and is a method often used to determine the pollution severity. The ESDD is the equivalent deposit of NaCl on the surface of the insulator that will have the same electrical conductance than that of the actual deposit dissolved in the same amount of water [6]. The conducting substances often consist of salts other than NaCl, e.g. $CaSO_4$, KCl, SiO_2, etc. [7]. The ESDD is, however, expressed in terms of an equivalent amount of NaCl.

IPMA, therefore, had to be calibrated in the laboratory to establish the relation between surface conductance and ESDD. IPMA was also used to investigate whether there exists a correlation in this above-mentioned relationship between artificially and naturally polluted insulators.

3. LABORATORY CALIBRATION:

The laboratory work was done at the University of Stellenbosch. The calibration consisted of measuring the surface conductivity of artificially polluted insulators with IPMA. The ESDD of the same tested insulator was then determined. The calibration process was also aimed at establishing suitable operating cycles for IPMA.

3.1 Artificial Pollution Process:

Glass cap and pin insulators (U120BS) were polluted in accordance with the solid layer method prescribed by the IEC 507 [8]. A suspension was prepared using 40g of kaolin per litre water. Different pollution levels were simulated by adding different amounts of NaCl to the suspension. Kaolin is a non-dissolving inert material used as a bonding agent for the salt on the insulator surface. It simulates typical non-dissolving materials found in the field, e.g. cement, lime, dust, etc., which perform the same bonding function. The conductance of kaolin is found to be very low and does not, therefore, contribute to the conductance of the pollution layer due to the salt present.

The insulator was artificially polluted by dipping it in the suspension. Care was taken that the insulator was fully immersed to ensure a homogeneous distribution of pollution on both the top and bottom surfaces. The insulators were then left to dry prior to testing.

3.2 Wetting process:

The surface resistance of a dry pollution layer is usually very high. With the addition of a solvent, e.g. water, the electrical withstand capabilities are reduced and leakage currents can flow. When all free salt is dissolved by wetting, maximum leakage current flows. However, if overwetting occurs, washing will take place and reduce the amount of free salt, thus lowering the of leakage current. The wetting rate is therefore of particular importance. An approach is followed to ensure that the point of critical wetting is reached. The point of critical wetting is defined as the wetting level just before particles are washed from the pollution layer.

An IPMA test is performed as follows:

- The shell is raised to enclose the insulators from the surrounding environment.
- Hot air is blown into the chamber (drying cycle).
- Steam is injected and reacts with the pollution to form an electrolytic solution (wetting cycle).

After the drying cycle the thermal inertia of the insulator glass causes the surface temperature to remain higher than the temperature inside the chamber. This temperature gradient inhibits the process of condensation of the steam on the warmer insulator glass. The steam wet the layer and dissolve the free ions. The dissolved NaCl creates a

difference in the solution concentration between the surface and ambient air. The diffusion due to the concentration difference drives water to the surface and causes further wetting to occur. The water dilutes the concentration and decreases the rate of accumulation [9]. Another wetting process is due to the hygroscopic properties of kaolin which leads to absorption. The vapour pressure adjacent to the hygroscopic material is lower than that of the steam-filled air. This is due to the salt having a lower saturation vapour pressure than that of air with a high relative humidity. This also leads to a driving force of water to the surface. The main wetting mechanism is therefore absorption and not condensation. The process of absorption causes less washing to occur than that of condensation. Collision of water droplets with the surface is another main wetting process on both top and bottom surfaces. It has been found by Karady that smaller droplets wet the bottom and larger drops the top [10].

3.3 Calibration Curve:

The calibration procedure consisted of the measurement of surface conductivity and ESDD values. This procedure was repeated for increased pollution levels to obtain the regression of conductivity versus ESDD. The calibration curve is given in figure 1.

CALIBRATION CURVE for U120BS
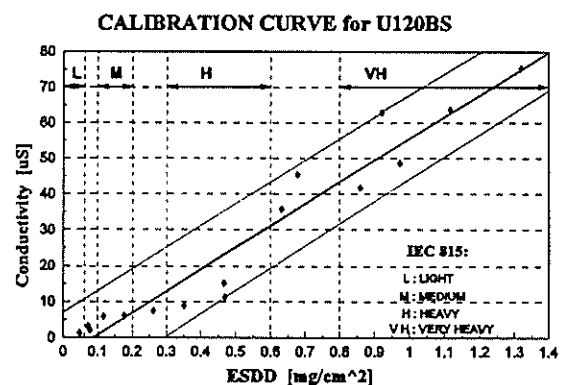
Figure 1   Surface Conductivity vs ESDD

Given in figure 1 is the IEC 815 ESDD classification levels. It is seen that the data for lower ESDD values (light to medium) have a flatter distribution than those for higher values of ESDD (heavy to very heavy). A possible explanation can be attributed to the uneven distribution of the few salt particles in the pollution layer for lower ESDD levels. This prevents conductive salt chains to form in contrast with highly polluted disks, where the dense salt layer creates a continuous path for higher leakage currents to flow. This phenomenon may be the cause for the scattering of data between an upper and a lower tolerance band of approximately 10 µS. The effect of scattering was also observed by CESI [2].

4. FIELD RESULTS:

Investigations were carried out in the Western Cape on several field insulators installed in different industrial areas with varying pollution levels. Following the calibration procedure, IPMA was installed at Koeberg Insulator Pollution Test Station (KIPTS). Insulators under test at KIPTS, one of the most severe pollution sites in South Africa and representing a marine environment, were monitored in IPMA as well.

4.1 Industrially Polluted Insulators:

Two of the transmission lines were in the vicinity of cement plants and the third line near a lime factory. The test insulators (U120BS) had been exposed to the natural contamination process and were removed from the 66 kV lines for testing purposes. The strings were taken down carefully to prevent the loss of pollution and were then transported to the laboratory. Visual inspection of the insulators showed a predominant deposit of non soluble type of pollutant. This made the measurement of the non soluble deposit density, (NSDD), an essential parameter to measure. The NSDD is also an indication of the amount of bonding material on the insulator surface.

Measurements of the following parameters were made:

- NSDD (mg/cm^2) for the top and bottom surfaces and their average.
- ESDD (mg/cm^2) for the top and bottom surfaces and their average.
- Surface conductivity (μS) using IPMA.

Results obtained are given in Table 1:

TABLE 1 :   **Measured Parameters for Industrial Polluted Insulators:**

	DISK1	DISK2	DISK3	DISK4	DISK5
SITE	Lime	Cement	Cement	Cement	Cement
NSDD TOP	-	0.2989	-	0.0231	0.252
NSDD BTM	0.472	0.0966	-	2.461	0.9234
NSDD AVG	0.472	0.1978	-	1.242	0.5877
ESDD TOP	0.221	0.0326	0.0324	0.045	0.0655
ESDD BTM	0.153	0.0734	0.0789	0.601	0.122
ESDD AVG	0.187	0.0529	0.0557	0.323	0.0936
Conduct	2.678	1.457	3.156	4.170	3.514

It is evident from the table 1 that the higher the overall ESDD and NSDD values the higher its conductivity value, e.g. disk 4. The comparison of disk 1 with disk 5 shows that disk 1 has a higher overall ESDD rating yet disk 5 shows a higher surface conductivity. This can be attributed to disk 5 having a higher NSDD value than that of disk 1. The tested industrially polluted insulators all prove to fall in the light to medium severity range of the IEC 815.

4.2 Marine Polluted Insulators:

A disk installed on a 22 kV busbar and an unenergized disk were tested. These insulators were tested on site soon after IPMA was installed at KIPTS. ESDD (top and bottom) and surface conductivity for the U120BS insulators are given in Table 2:

TABLE 2 :   **Measured Parameters for Marine Polluted Insulators:**

	DISK1 UNENERGIZED	DISK2 22 kV
ESDD Top mg/cm^2	0.281	0.103
ESDD Btm mg/cm^2	0.385	0.318
Conductivity μS	31.528	38.549
NSDD Top μg/cm^2	1.1167	1.1321
NSDD Btm μg/cm^2	0.9965	7.4240

From table 2 it is seen that the bottom ESDD value is greater than the top ESDD. This effect is due to natural washing and the aerodynamics around the pin. The top surface of disk 1 (bottom disk on string of six) has better protection from the weather conditions, e.g. mist, wind, rain, natural washing, than disk 2 (bottom disk on string of two). This results in less pollution being lost and thus a higher ESDD. This occurrence illustrates the importance of the aerodynamic properties of field insulators.

The NSDDs show that disk 2 contains more non soluble deposits than disk 1. Ramos found that the conductivities of these low soluble contaminants vary with the amount of wetting [11]. In IPMA, the entire pollution layer is completely wetted without the occurrence of washing, i.e. the point of critical wetting is achieved. The conductivity of the inert material, therefore, has a definite contribution to the total conductivity of the insulator. This explains the higher surface conductivity of disk 2 irrespective of its lower ESDD values.

In figure 2 the field data is given for the industrial and marine polluted insulators superimposed on the calibration curve. The marine data points relate to higher values of ESDD than the industrially polluted disks. It is also seen that insulators from the marine environment yield higher conductivities than the industrially exposed insulators.
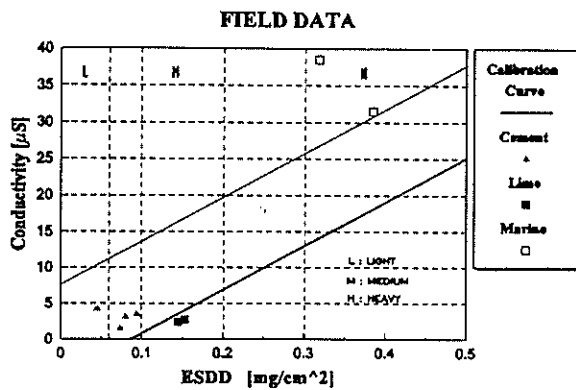
FIELD DATA

Figure 2   Field Data Superimposed on Calibration Curve

5. DISCUSSION:

The industrially polluted insulators relate to the lower ESDD and conductivity range though with higher levels of NSDD. The marine insulators prove to be in the higher conductivity band of the laboratory calibrated curve although the non soluble particles tend to be less.

A deviation of field results from that of the laboratory can be attributed to the following effects:

- A variation of salts and elements is found at KIPTS (high levels of Si, Cl, Na, Ca) compared to NaCl being the only salt present in the artificial pollution layer.

- Kaolin has a low conductivity where non soluble materials, e.g. lime, cement, sulphur, have much higher conductive properties.

- The pollution distributions on the field insulators are non homogeneous. This has the effect of high resistive band formations on the surface compared with the even pollution distribution on artificially polluted insulators.

- Each test area is exposed to different environmental and electrical conditions. The calibration curve for each site is therefore unique.

- Different levels of NSDD and ESDD are found in relation to the environment where the insulators are installed. Both parameters have a major effect on the surface conductance of the pollution layer.

An insulator pollution monitoring apparatus has been commisioned, calibrated and installed at a coastal test station. Surface conductivity measurements are done and correlated with equivalent salt and non soluble deposit densities.

On-line leakage current monitoring is done at KIPTS and these leakage current data will be combined with ESDD, NSDD and IPMA conductivity values to obtain a global definition of the pollution severity on different field insulators.

6. REFERENCES:

[1] Holtzhausen J.P., Smith J.M., Potgieter O.C.T., "Insulator Pollution Monitoring of Leakage Currents During Artificial and Site Test Conditions", SAUPEC, Jan. 1990, Paper 3.4.

[2] Bertazzi A., Perego G., Sampaoli G., Vachiratarapadorn Y., Eamsa-ad V., "A Device for the Automatic Measurement of Surface Conductivity of Insulators", 6th Intern. Symp. on HV. Eng., New Orleans, USA, Aug/Sept. 1989.

[3] Davel P, Holtzhausen J.P., Vosloo W.L., "Low Voltage Measurement of the Pollution on High Voltage Insulators", UPEC, 1994, p. 798 - 801.

[4] Davel P., Holtzhausen J.P., Vosloo W.L., "The Commissioning and Performance of a New Insulator Pollution Monitoring Apparatus", SAUPEC, Jan. 1994, p. 211 - 214.

[5] IEC Report, Publication 507, "Artificial Pollution Tests on HV Insulators to be used on A.C. Systems", Geneve, 1975.

[6] Schneider K.H., "The Measurement of Site Pollution Severity and its Application to Insulator Dimensioning for A.C. Systems", Electra, May 1979, p. 101 - 116.

[7] Gouda O.E., "Factors Affecting the Conductivities of Pollution Layers of HVTL Insulators", 7th Intern. Symp. on HV. Eng., Dresden, Aug. 1991, Paper 44.08.

[8] IEC Publication, "Revision of IEC Public. 507: Artificial Pollution Tests on HV Insulators to be used on A.C. Systems", Technical Committee No. 36: Insulators, Jan. 1987.

[9] Leclerc M.., Bouchard R.P., Gervais Y., Mukhedkar D., "Wetting Processes on a Contaminated Insulator Surface", IEEE Transactions on Power Apparatus and Systems, Vol. PAS-101, No. 5, May 1982.

[10] Karady G., "The Effect of Fog Parameters on the Testing of Artificially Contaminated Insulators in a Fog Chamber", IEEE Transactions on Power Apparatus and Systems, Vol. PAS-94, No.2, March/Apr. 1975.

[11] Ramos G.N. , Campillo R.M.T., Naito K., "A Study on the Characteristics of Various Conductive Contaminants Accumulated on HV Insulators", IEEE Transactions on Power Delivery, Vol. 8, No.4, Oct. 1993.

7. Address of main author:

L. van Wyk, Department of Electrical and Electronic Engineering, University of Stellenbosch, Private Bag X1, Stellenbosch, 7601.
E-mail: lvanwyk@firga.sun.ac.za

POLLUTION FLASHOVER PERFORMANCE OF CERAMIC HIGH-VOLTAGE INSULATORS: A CRITIQUE OF USING SOLELY SPECIFIC LEAKAGE DISTANCE FOR DIMENSIONING PURPOSES

by

D A Swift

University of Natal

ABSTRACT

Essentially this paper is a progress report covering one aspect of a major review that is being made by CIGRE into the flashover performance of outdoor insulators. Using data from extensive research testing of 124 types of insulator, it is concluded that leakage path per unit system voltage is not sufficiently adequate for dimensioning purposes. Also, there is no obvious simple modification that can be made and mathematical models are insufficiently developed - as yet - to provide a solution. A proposal is briefly mentioned to cope with this difficulty.

1. INTRODUCTION

CIGRE Working Group 33.04 (Polluted Insulators) is currently conducting a comprehensive review of knowledge on the flashover of high-voltage insulators. Part of this exercise involves assessing the accuracy of the IEC Guide [1] for dimensioning the length of ceramic insulators for operating at AC voltage in a location of given pollution severity. Apart from some restrictions on profile and corrections for diameter, this Guide implies that only the length over the insulator surface per unit operating voltage (called "specific leakage distance") need be used to determine the correct design.

This CIGRE exercise has analysed the pollution flashover performance of 58 insulator types under AC energization and 66 insulator types under DC energization. Such insulators vary in overall diameter from 200 mm to 1200 mm and in length up to nearly 4 m. Although this analysis is much too extensive to report herein, the main findings and the references for the data are provided (a full account will probably follow in two IEE papers.)

Because these findings clearly show that specific leakage distance alone is a poor method for correctly dimensioning insulators for outdoor use, alternative approaches are speculated upon - for which a much simplified theoretical explanation of the pollution flashover process is given as a necessary precursor.

2. INSULATOR PROFILE, DEVELOPED SURFACE AND FORM FACTOR

An example of a line insulator (cap and pin type) is provided in Figure 1; the parameters referred to in this analysis are shown in this figure.
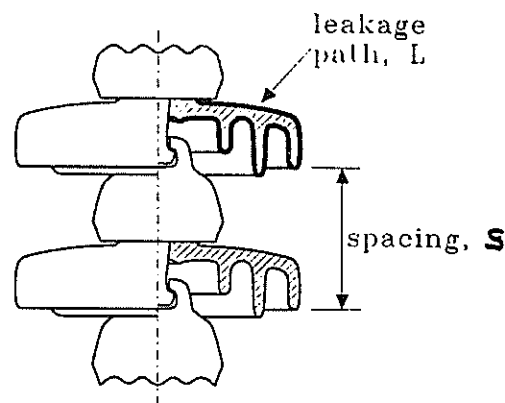
(a) string arrangement
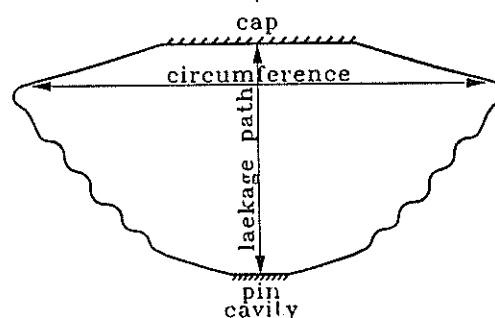
(b) developed surface

Figure 1: Profile and leakage surface of an antifog cap and pin insulator (OD 394mm).

To obtain the resistance of the surface for a uniform layer of pollution, the form factor (FF) is calculated from the developed surface by using the simple relationship:

$$FF = \frac{1}{\pi} \int_0^L \frac{dl}{D(l)} \qquad ...(1)$$

where D(l) is the diameter of the insulator at leakage position l from the reference point and L is the total leakage path of the unit of insulation.

3. SUMMARY OF FINDINGS

The flashover performance of each set of insulator types at the same severe pollution conditions - some artificial, others natural - are presented in Tables 1 and 2 for AC energization and DC energization respectively; the range and average values are provided and the standard deviation is typically 30%. Generally, the test voltage was representative of that of transmission systems (ie. 100 kV to 500 kV).

Table 1. AC data for vertically mounted insulators

Pollution *	No. of Types **	Parameter ***	Range of Values	Average Value	References
A	34	kV/m	9-29	19	2,3,4,5,7,9,10
N(E)	4	LR	0.9-1.3	1.0	8
N(S)	20	kV/m	30-55	41	5

* A is artificial salt-fog of 80 kgm⁻³ or ESDD = 0.6 mgcm⁻², N is natural marine, (E) is in England and (S) is in Sweden
** Different insulator shapes and sizes.
*** kV/m is rms stress along insulator surface, LR is leakage path of test insulator divided by that of a reference insulator (see Figure 1).

Table 2. DC data for vertically mounted insulators

Pollution *	No. of Types	Parameter **	Range of Values	Average Value	References
N(J)	5	RL	1-1.5	1.3	11
A(T)	12	kV/m	15-34	23	11
A(C)	19	kV/m	41-63	49	12
A(K)	25	kV/m	15-26	20	13
A	6	kV/m	17-32	24	14

* N(J) is natural marine pollution in Japan
A(T) is artificial pollution, Tonoko/NaCl of ESDD = 0.05 mg cm⁻².
A(C) is artificial pollution, cement slurry
A(K) is artificial pollution, kaolin/NaCl of ESDD = 0.05 mgcm⁻².
A is artificial saltfog of 28 kgm⁻³.
** RL is ratio of leakage path of test insulator to that of a reference insulator (standard cap and pin).

The artificial tests were conducted as the standard methods for producing salt fog or a solid layer of pollution plus clean fog for AC stressing [15], or the equivalent thereof for the DC case. The performance is expressed as the average stress along the insulator surface (ie. applied voltage divided by leakage path) to cause flashover.

Marine pollution was present in the natural tests and the results were determined as the critical length of leakage path at which flashover occurred for the same voltage and pollution severity. In the Swedish case, the surface stress has been calculated for the same number of flashovers during the test period whilst the English and Japanese data are expressed as the ratio of leakage path of the test insulator to that of a standard insulator (in both cases, a cap and pin type) to have the same pollution flashover performance. Although only four insulator types were used in the English tests, the number of insulators totalled 36.

4. DISCUSSION

4.1 Analysis of Data

A measure of the accuracy of using solely specific leakage distance for dimensioning purposes is to consider the ratio of the best insulator performance to the worst one for the same conditions of pollution and energization. Using the data presented in Tables 1 and 2, this ratio is shown in Table 3.

Table 3. Ratio of best to worst insulator performance

Energization	AC			DC				
Pollution	N(E)	N(S)	A	N(J)	A(T)	A(C)	A(K)	A
Performance ratio	1.4	1.8	3.2	1.5	2.3	1.5	1.7	1.9

It is useful to consider this information from the viewpoints of: (a) natural pollution and (b) artificial pollution, since the former is the closest to operational conditions whilst the latter covers a much wider range of insulator types. The average values of this performance ratio are, therefore, 1.45 for natural pollution and 2.1 for artificial pollution; the corresponding average for all conditions is 1.9.

These values are put into perspective by considering the range of specific leakage distance given in the IEC Guide [1]; ie 16 mm/kV for light pollution to 31 mm/kV for very heavy pollution thereby yielding a ratio of 2.4 for the values at the extremes.

Such facts can hardly give much comfort to the practising design engineer when it is seen that the performance variation between the insulator types at a given value of pollution is nearly as great as that specified for the complete range of pollution severity.

A particularly disturbing fact is revealed by comparing the flashover stress of a large diameter cap and pin insulator (typical value 15 kV/m in a salt fog of 80 kg/m³) with that of a small diameter one (typical value 50 kV/m at same pollution severity). The practical importance of having identified this difference can be appreciated by noting that the pollution flashover performance of an existing small power line (eg 132 kV) is sometimes used to estimate that of a new large one (eg 400 kV) to be erected in the same area.

The consequence of using the wrong length of insulation can be quantified by considering the flashover frequency, F (ie number per year) and the normalised axial stress, E(a)(kV/m), across the insulator. The data determined at Brighton [8] showed that such a relationship can be specified as:

$$F = k\left[\frac{E(a) - E(o)}{E(o)}\right]^m \qquad ...(2)$$

where E(o), k and m are constants having average values at Brighton of 99 kV/m, 16.1 and 2.1 respectively.

For a particular type of insulator of known figure of merit (FOM) - based on its pollution flashover performance relative to that of a string of reference insulators (type shown in Figure 1), E(a) is given as:

$$E(a) = \frac{V(s)}{L(a) \times FOM} \qquad ...(3)$$

where V(s) is the system voltage in kilovolts and L(a) the axial length in metres of the test insulator.

From this simple viewpoint, the correct design would be to make E(a) = E(o); ie F = 0. When E(a) is substantially less than E(o), then money is wasted by

having the insulator longer than it need be whilst when E(a) is substantially greater than E(o) frequent flashovers occur, which may be even more costly to rectify. Taking as an example the IEC Guide for severe pollution of 31 mm/kV system voltage, the corresponding surface stress is 18.5 kV/m (ie. $1000/31\sqrt{3}$). As this is about the average value (ie. 19 kV/m) found from doing the artificial salt fog tests at 80 kg m^{-3} and AC stressing, it is therefore instructive to use the range of values found in that test (ie A data in Table 1). Then at the upper extreme with E(o) of 29 kV/m, an insulator designed on 18.5 kV/m would be 50% larger than necessary; whilst at the lower extreme with E_o of 9 kV/m, the flashover frequency - for conditions equal to those at Brighton - would be 16 per year.

4.2   Flashover Process

To understand why specific leakage path is not the only factor that substantially affects pollution flashover performance, it is useful to consider briefly the flashover process as follows.

The flow of leakage current I due to an average stress E across a uniformly polluted surface of resistivity ρ, length L and form factor FF is,

$$I = EL/\rho FF \qquad ...(4)$$

Note: the main variation of ρ occurs with ion type and concentration, water thickness and temperature.

Such a current causes Joule heating of the electrolyte due to power dissipation, p, per unit area expressed as,

$$p = j^2\rho \qquad ...(5)$$

where j is the surface current density. Therefore, as j = $I/\pi D$, moisture evaporation is a maximum when D is a minimum (eg. near a pin cavity, Fig. 1). When this evaporation rate is greater than the moisture deposition (eg. condensation) rate, dry bands form.

Discharges occur across these dry bands in order to complete the current path. Many such discharges can occur in parallel and the effective width, w, of a length, L(e), of electrolyte can be shown [16] to be,

$$w = 3L(e)/2 \qquad ...(6)$$

Therefore on the insulator's surface, many such discharges often occur in a parallel/series array. It is valid, however, to consider a line along the length of the unit of insulation involving a discharge of length x. Then the voltage, V, and current, I(d), relationship can be expressed as,

$$V \approx I(d) R + V(e) + I(d) \rho f(x) \qquad ...(7)$$

where R is the resistance of the discharge, V(e) is the sum of the voltage drop at the junctions between the discharge and electrolyte (ie. anode and cathode phenomena) and f(x) is a function of x, L(e) and the effective radius r of the discharge root on the electrolyte's surface; obviously, r can have two values - one for the anode and the other for to the cathode.

The resistance R of the discharge can be considered from the viewpoints of: (a) the spark, for very short times and (b) the arc, for longer times.

From Toepler's spark equation [17]

$$R = Kx/Q \qquad ...(8)$$

where Q is the charge conducted up to the time t and K is a constant, which for air at atmospheric density (sea level) is $\approx 5 \times 10^{-6}$ Vs mm^{-1}.

From Suits's arc equation [18]

$$R = I(d)^{-(1+n)} \int_0^X A(x)dx \qquad ...(9)$$

where n is a constant (~ 0.5) and A(x) has a value (possible range 6 to 14 V mm^{-1}) that depends upon the proximity of the arc to the surface, the amount of water on the surface [19] and the extent to which thermalisation has taken place [20].

As the resistance of both the arc and the spark decreases as its current increases, the discharge extends when in so doing its current increases. That is,

$$\frac{dI(d)}{dx} > 0 \qquad ...(10)$$

The function f(x) can be considered from various viewpoints. For a rectangular strip of electrolyte of width W and length L(s), the simplified expressions for (i) a narrow strip and (ii) a wide one are [21]:

(i)   Narrow strip (ie W < L(s)

$$f(x) = (2\pi)^{-1}[\ln W/2\pi r + \pi (L(s) - x)/W] \qquad ...(11)$$

(ii)   Wide strip (ie W > 3 L(s))

$$f(x) = (2\pi)^{-1} [\ln 2 L(s)/\pi r - \ln \tan \pi x/2 L(s)] \qquad ...(12)$$

With respect to equation 6, the corresponding value of f(x) for an effective width on an actual insulator can be approximated to the average of that for a narrow strip and that for a wide strip.

For actual insulator shapes, a finite element approach has been used to good effect [22].

(a) surface arc   (b) gap
    shortening   breakdown

arc produced   water droplets
on surface

arc moved off   air discharge
surface
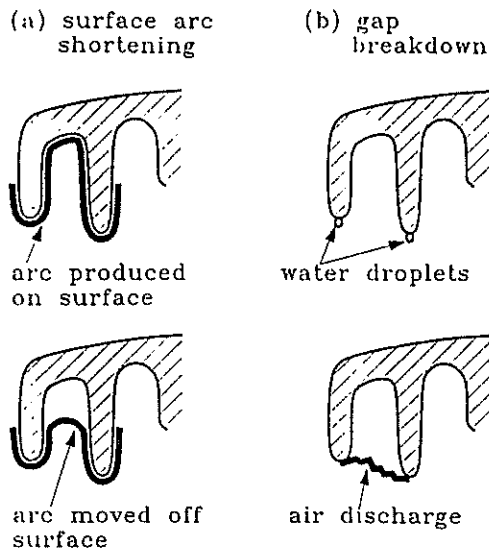
Figure 2:   Formation of gap discharges.

The AC case is further complicated because of reignition following current zero.

Various mathematical models have been employed to determine the flashover voltage [23]; they all assume that only breakdown along the insulator surface needs to be considered. However, air gap discharges between the ribs of a shed and between sheds may also be playing an important part, especially for complex profiles (as illustrated in Figure 1). Such air-gap discharges can arise from two causes; in one, a discharge moves off the surface (Fig 2a) whilst, in the other, breakdown of the air occurs (Fig 2b).

In the former case, the voltage-drop decreases because: (a) the electric field of a free-burning arc is lower than that of one bounded by a wet surface - due to heat transfer processes and (b) the arc length is less. However, buoyancy forces may counter this movement off the surface.

Breakdown of the air gap occurs when the voltage across it exceeds a certain value; this voltage is a function of the surface resistance and the leakage current flow between such point. Pendant water drops also may play their part as stress enhancers [24].

By either the shortening of the discharge or the shorting-out of some of the leakage path, more of the voltage is impressed across the remainder of the insulator - thereby increasing the current, and so the likelihood of completing the flashover process.

4.3   Examination of Various Factors

For the very simple case of a long rectangular strip of uniform electrolyte (ie ρ constant) of width W, DC energization and one uniform arc under constant

cooling conditions (ie A and n constants), the solution of the preceding equations yields the critical current, I(c), to cause flashover to be:

$$I(c) = (AW/\rho)^{1/1+n} \qquad ...(13)$$

As the average field, E, on the surface of the electrolyte is $I\rho/W$, its corresponding critical value, E(c), is:

$$E(c) = A^{1/1+n}(\rho/W)^{n/1+n} \qquad ...(14)$$

Therefore, for a given value of surface resistivity, the flashover field decreases only slightly as the width of strip increases (ie $E(c) \propto W^{-0.2}$ when n = 0.5). Further, the effective width can be appreciably less than the actual width (equation 6). This simple reasoning thereby implies that the specification of solely leakage path is indeed adequate for insulators of simple shape, which to a large extent has been found to be the case for the porcelain long rod [5]. On the other hand, by considering a large number of insulator types the effective value of n/(1 + n) covers the range 0.1 to 0.6 [25] thereby indicating the complexity of the flashover process on practical shapes.

As seen from the above simple analysis the flashover process of polluted insulation is essentially a critical surface current phenomenon. Equation 4 shows that this current varies as L/FF for given values of E and ρ. From the published data used to arrive at the information shown in Table 1 for an artificial salt fog of a given salinity (ie constant ρ), the experimental relationship between E and L/FF is shown in Figure 3a. In addition to the influence of L, inspection of equation 1 shows that FF increases as D reduces. Again using the salt fog data, the relationships between E and minimum and maximum diameter are shown in Figures 3b and 3c plus 3d respectively; note a brief description of the insulators is provided in the Appendix.

The influence of air gap discharges - be they due to arc shortening or air breakdown events - is likely to be related to the ratio of spacing, S, of the unit of insulation to the corresponding length L of the leakage path and/or to subunits of such a ratio. Again, for the salt-fog data, the relationship between E and L/S is shown in Figure 4 - in order to investigate if it is simple.

As Figures 3 and 4 clearly show that there are no simple trends that can be used to modify the leakage-path approach for arriving at the correct dimensions for insulators to operate under severely polluted conditions. Therefore, a more sophisticated analysis must be undertaken to arrive at more relevant design rules.
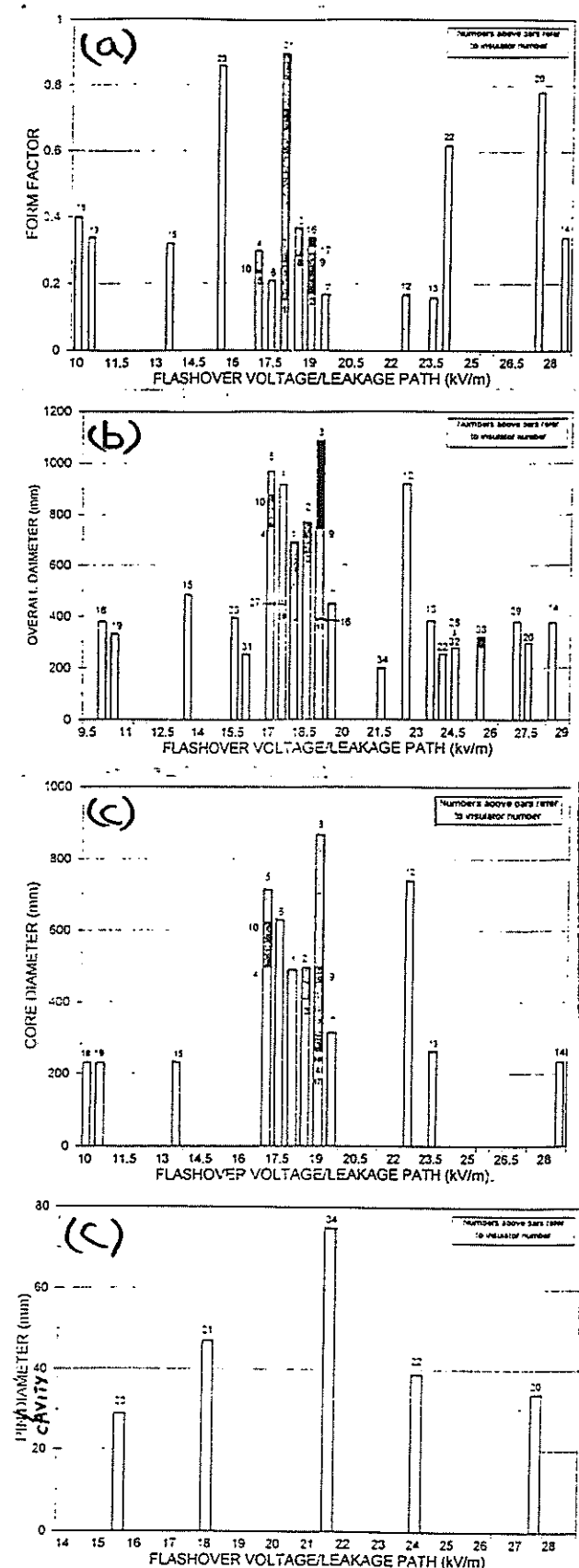
Figure 3: Correlation of average surface stress at flashover in salt fog with (a) form factor (b) overall diameter and (c) minimum diameter for many insulator types (see appendix).
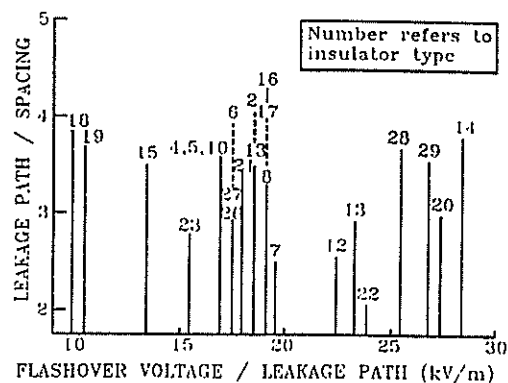
Figure 4: Correlation of average surface stress at flashover in salt fog with ratio of leakage path to spacing for same insulator types referred to in Figure 3.

4.4 Proposal

In correctly dimensioning high-voltage insulators, the aim is usually to minimise the spacing between the live and earthed components. Therefore, it seems more logical to use specific axial length as the design parameter rather than specific leakage path.

Starting from this viewpoint, the insulators can be ranked in terms of flashover voltage per unit axial length and a corresponding catalogue of the insulators' details of profile and size can be built into a computer data base. Then a programme can be developed to analyse these data. This approach has both practical and theoretical advantages.

Should the pollution flashover performance of any other relevant type of insulator need to be known, then its details can be inserted into this computer programme to arrive at an informed estimation. This approach will never, however, preclude the need for further experimental work but it could be employed to develop a more structured testing programme.

The next generation of flashover models need to take air-gap discharges into account and so such a computer programme could aid the development of more sophisticated mathematical models - albeit containing empirical factors based on many practical measurements.

5. CONCLUSIONS

1. Data obtained from many major research programmes indicate that there is a large spread in performance - as assessed by flashover voltage divided by leakage path - of high-voltage insulators subjected to the same pollution environment. As this spread at one pollution level is very nearly as great as that

specified in the current IEC Guide - in terms of specific leakage path (ie leakage path divided by system voltage) - to embrace all pollution levels, it is obvious that leakage path alone is inadequate for dimensioning outdoor insulation. The IEC are, therefore, wise in reviewing their guide - which is to be put in hand shortly.

2.   The analysis of the data from the viewpoints of AC or DC stressing, form factor, maximum diameter, minimum diameter and leakage path to spacing ratio has failed to find a simple method by which the IEC Guide can be readily modified.

3.   Employing solely specific leakage path, it is not sensible to use service experience for a small insulator (eg 132 kV cap and pin type) to design a system using a much larger insulator (eg 400 kV cap and pin type) for the same location. Where this has been done successfully, it seems probable that the lower-voltage system is over insulated.

4.   As the flashover process is very complex, mathematical models are not yet sufficiently developed to enable the pollution performance to be calculated to an acceptable accuracy.

5.   A way out of the difficulty may be to have a "shape and size recognition" system by incorporating all known information into a data base and develop a computer programme that will enable the flashover performance under the same type of pollution of any other insulator type - made of the same material and similarly mounted - to be reasonably well estimated.

6.   ACKNOWLEDGEMENTS

Miss S Rodgerson is greatly thanked for analysing the data presented in Figures 3 and 4.

7.   REFERENCES

[1]   IEC Publication 815, 1986.
[2]   Ely C H A et al, Proc. IEE, Vol. 118, No 1, 1971.
[3]   Swift D A, 8th ISH, paper 47.15, 1993.
[4]   Houlgate R G and Swift D A, IEE paper submitted.
[5]   Verma M P, IEEE Trans. Vol. EL-16, No 3, 1981.
[6]   Naito K, EHV/UHV Transmission, New Delhi, 1993.
[7]   Lambeth P J et al, CIGRE paper 33-02, 1970.
[8]   Houlgate R G et al, CIGRE paper 47-15, 1982.
[9]   NGK Tech. Guide, Cat. No. 91R.
[10]   Houlgate R G and Swift D A, IEEE Power Delivery, Vol. 5, No 4, 1990.
[11]   Kawamura T et al, CIGRE paper 33-10, 1984.
[12]   EPRI, Transmission Line Reference Book, HVDC ± 600 kV.
[13]   EPRI TR-102764, HVDC Transmission Line Reference Book, 1993.
[14]   Pargamin L et al, CIGRE paper 33-11, 1984.
[15]   IEE Publication 507, 1987.
[16]   Erler F, Elektrie, Vol 3, 1969.
[17]   Toepler M, Arch. f Elektotechn. Vol 1, 1926.
[18]   Suits C G, Phys. Rev. Vol 55, 1939.
[19]   Swift D A, 6th ISH, paper 30.10, 1989.
[20]   Rizk F A M, IEEE paper CP135-PWR, 1970.
[21]   Wilkins R, Proc IEE, Vol 116, No 3, 1969.
[22]   Holtzhausen J P and Toit L P, Trans. SAIEE, March 1991.
[23]   Rizk F A M, Electra No 78, 1981.
[24]   Swift D A, 4th ISH, paper 44.07, 1983.
[25]   Lambeth P J, Proc IEE, Vol 118, No 9R, 1971.
[26]   Swift D A, Unpublished information.
[27]   Houlgate R G and Swift D A, 6th ISH paper 47.30, 1980.

APPENDIX

Insulator Details with respect to Figures 3 and 4

No	Type	Ref
	Tapered Barrel/Post	
1.	Plain Shed	2
2.	3-skirt antifog-shed a.b.c.b. support	2
3.	3-skirt antifog-shed sealing end	2
4.	2-skirt antifog-shed a.b.c.b. support	2
5.	2-skirt antifog-shed oil-filled c.t.i.	2
	Parallel Barrel/Post	
6.	'Easy-grease'-shed a.b.c.b. support	2
7.	2-unit plain shed	2
8.	2-skirt antifog-shed SF6-filled c.t.i.	2
9.	2-skirt antifog-shed a.b.c.b. support	2
10.	2-skirt antifog-shed a.b.c.b. support	2
11.	Italian 3-skirt antifog-shed	2
12.	Italian 2-unit plain shed	2
13.	V1 Int. Head, NG	4
14.	P1 Post, NG	4
15.	Reference, NG	3
16.	70/60 Profile	3
17.	70/50 Profile	3
18.	NCBP1	3
19.	NCBP2	3
	Cap and Pin	
20.	Bullers 10509	2
21.	Doulton Type 6672	26
22.	IEEE	27
23.	Reference A (CERL)	27
24.	F16	5
25.	NGK Insulator 210kN	6
26.	NGK Insulator 680kN	6
27.	NGK Insulator 820kN	6
28.	Glass 120 kN(ENEL)	7
29	Glass 374 kN(CEGB)	7
30.	254mm normal	9
31.	254mm fog	9
32.	280mm normal	9
33.	320mm fog	9
	Long Rod	
34.	L75/24sn/1360	5

THE SURFACE CHEMICAL COMPOSITION OF CORONA CONDITIONED SILICONE RUBBER INSULATORS

A E Dickson and J P Reynders
University of the Witwatersrand
Johannesburg

ABSTRACT

It has been found that streamer corona and to a lesser extent glow corona cause a temporary loss of hydrophobicity in room and high temperature vulcanised silicone rubber insulators. Chemical analysis on the surface of samples has indicated that silicone compound is removed from the surface by corona but returns to the surface by diffusion once the corona activity has ceased. Should this removal and subsequent replenishment of silicone compound by corona continue for an extended period of time, the silicone rubber insulator will permanently lose its hydrophobic properties.

1 INTRODUCTION

In recent years silicone rubber (SR) insulators have provided supply utilities with a more attractive alternative to traditional glass and porcelain insulators. The increased tensile strength and improved insulator performance that composite insulators exhibit are particularly advantageous in the quest for more compact transmission line design /1,2/. However, there is a lack of information on the surface chemical structure of SR insulators.

In an effort to provide data that will illustrate the effects that corona has on the surface of the insulator and provide possible answers to the loss and recovery processes, chemical analysis has been completed on samples conditioned by corona. This analysis has been completed on High Temperature Vulcanised (HTV) silicone rubber (typically used for weathersheds), and Room Temperature Vulcanising (RTV) silicone rubber (mainly used for coatings on ceramic insulators).

The chemical analysis has highlighted the transient surface chemical composition that occurs immediately after the completion of corona conditioning.

2 EXPERIMENTAL PROCEDURES

Commercially available RTV silicone coating and HTV silicone insulator samples were conditioned by separate exposure to streamer and glow corona. The RTV coating was applied to a metal sphere with a diameter of 108mm prior to conditioning. 30mm x 20mm x 2mm samples were removed from the shed of an HTV insulator. All samples were exposed to the corona conditioning for 48 hours.

The experimental methods used for the creation of streamer and glow corona as well as the contact angle measurement method used for the calculation of hydrophobicity have been fully described elsewhere /3/.

The chemical analysis method used for the results described in this paper was X-Ray Spectroscopy (XPS). The chemical changes that occurred at the surface of the SR samples once the corona conditioning had been completed were monitored. A VG ESCALAB MkII spectrometer irradiates the sample surface with Mg Kα X-rays at a voltage of 15kV and an incident angle of 45°. This experimental set-up allowed the outermost 30 to 50Å of the SR samples to be analysed.

XPS irradiates the surface of the sample with monoenergetic soft x-rays. The photons penetrate the sample to a depth of between 1- 10μm where they interact with atoms in the surface region. This interaction causes electrons to be emitted by the photoelectric effect. The emitted electrons have a kinetic energy governed by /4/:

$$KE = h\nu - BE - \phi_S$$

where $h\nu$ is the energy of the photon, BE is the binding energy of the orbital from which the electron has been emitted, and ϕ_S is the work function of the spectrometer.

Each element has a unique set of binding energies which allow XPS to identify elements and their concentrations on the surface of the sample.

To monitor the transient chemical composition of the corona conditioned SR samples they were monitored at 30 minute intervals until the chemical changes had stabilised.

3 EXPERIMENTAL RESULTS

The analysis of the silicone spectrum after corona conditioning showed that two silicone peaks, equating to two different silicone compounds, were present. This enabled a direct comparison between these two compounds to be made, and presented an accurate method of monitoring the changes in silicone concentration and compound structure at the surface of the sample.

3.1 RTV Sample

The surface chemical structure of a reference virgin sample was determined. *Figure 1* shows the binding energy spectrum for this sample. Peak curve fitting applied to the spectrum identified two silicone compounds at the surface of the sample. The two peak binding energies are 103,40ev and 102,10eV which correspond to the compounds SiO_2 and $H_{22}C_{16}OSi_2$ respectively.
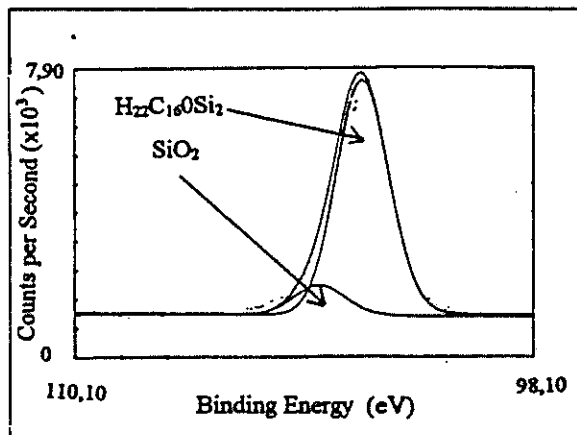
Figure 1: Binding Energy Spectrum of a Virgin RTV Sample

Table 1 shows the results of the chemical surface analysis on a virgin RTV sample.

Table 1: Chemical Analysis of RTV Virgin Sample

Binding Energy (eV)	Chemical Composition	Concentration (Counts)
102,30	$H_{22}C_{16}OSi_2$	3008
103,50	SiO_2	768

Exposure to 48 hours of streamer corona resulted in a decrease in the concentration of $H_{22}C_{16}OSi_2$ at the surface of the sample and an increase in the SiO_2 concentration. Once the conditioning of the SR sample with streamer corona was completed the concentration of $H_{22}C_{16}OSi_2$ became larger while that of the SiO_2 decreased. This trend of surface chemical composition continued as time elapsed.

Figure 2 shows the comparative peak binding energy spectra of a RTV sample shortly after the completion of streamer corona conditioning and after a 2 hour rest period.
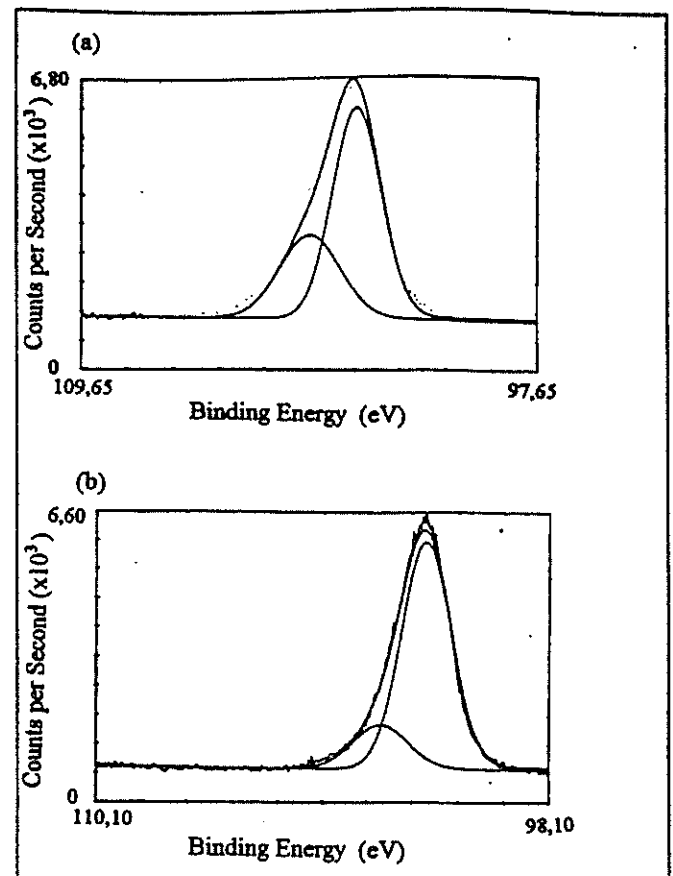
Figure 2: Changes in Surface Chemical Composition of a RTV Sample. (a) Immediately after Streamer Corona Conditioning and (b) after a 2 hour rest period

The relative concentrations of the silicone compounds as time progressed is tabulated in *Table 2*.

Table 2: Chemical Concentrations of Silicone Compounds on RTV Surface after Streamer Corona Conditioning

Time (Minutes)	Concentration (Counts)	
	$H_{22}C_{16}OSi_2$	SiO_2
30	2432	1248
60	2848	1152
90	2880	1184

Glow corona produced a similar trend to that of the streamer corona for both silicone compounds over the measurement period. The change in surface silicone concentrations over time is tabulated in *Table 3*.

Table 3: Chemical Concentration of Silicone Compounds on RTV Surface after 48 Hours of Glow Corona

Time (Minutes)	Concentration (Counts)	
	$H_{22}C_{16}OSi_2$	SiO_2
30	2546	1158
60	2885	1032
90	2960	985

3.2 HTV Sample

The surface chemical structure of a reference HTV SR virgin sample was determined. *Figure 3* shows the binding energy spectrum of this virgin sample. The peak has a narrow window and it was determined that a single peak of $H_{22}C_{16}OSi_2$ with a centre binding energy of 102,15eV was present at the surface of the sample. The concentration of $H_{22}C_{16}OSi_2$ on the HTV virgin sample surface was measured to be 1392 counts.
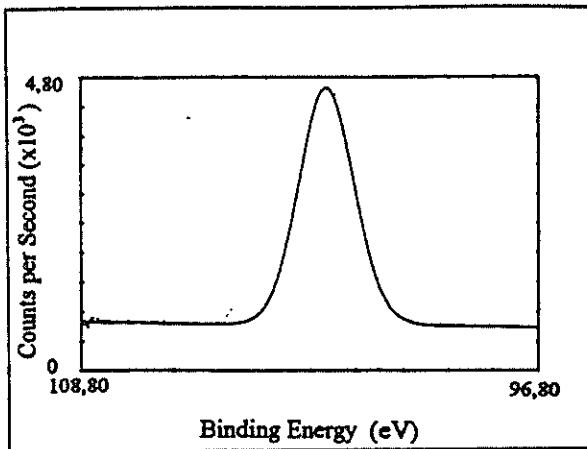
Figure 3: Binding Energy Spectrum of a Virgin HTV Sample

The HTV sample conditioned by streamer corona for 48 hours resulted in a pronounced decrease in the $H_{22}C_{16}OSi_2$ concentration and a corresponding increase in the SiO_2 concentration at the surface of the sample. *Figure 4* illustrates the changes in chemical composition that occur between the time the streamer corona conditioning is first removed and after a 2 hour rest period.

The concentrations of the silicone chemical compounds derived from the spectra are tabulated in *Table 4*.

Table 4: Chemical Concentrations of HTV Surface Silicone Compounds after Streamer Corona Conditioning.

Time (Minutes)	Concentration (Counts)	
	$H_{22}C_{16}OSi_2$	SiO_2
30	944	832
60	1128	720
90	1312	656
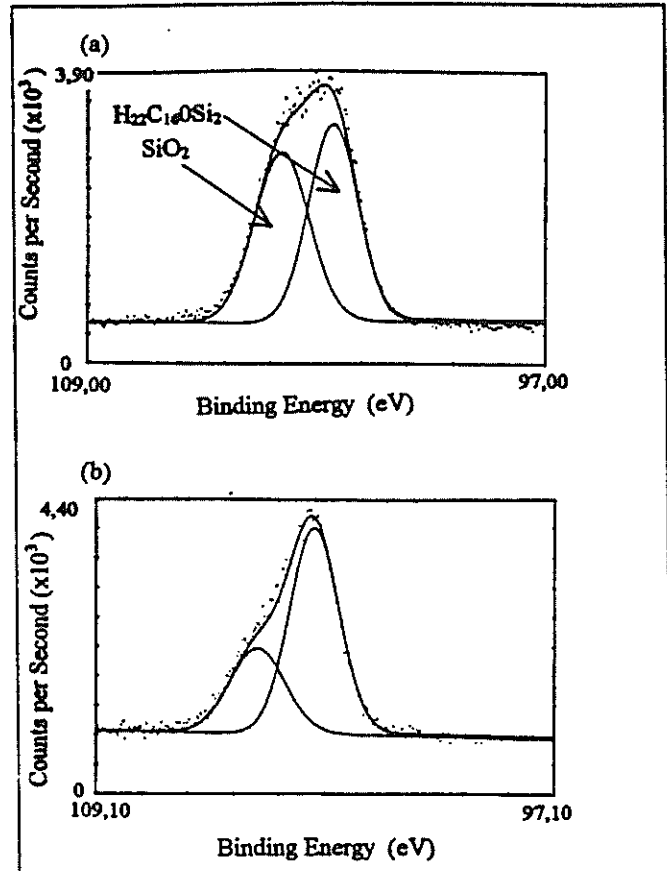
Figure 4: Chemical Composition Changes that occur on the Surface of an HTV Sample. (a) Immediately after Streamer Corona Conditioning and (b) after a 2 hour rest period.

The surface chemical composition changes that occurred after glow corona conditioning were not as pronounced as the streamer corona case. They do, however, continue to indicate the trend that has been noted in the previous analysis and the results are summarised in *Table 5*.

Table 5: Chemical Concentrations of RTV Silicone Compounds after Glow Corona Conditioning

Time (Minutes)	Concentration (Counts)	
	$H_{22}C_{16}OSi_2$	SiO_2
30	1096	360
60	1192	320
90	1136	296

4 DISCUSSION

The exposure of both RTV and HTV SR samples to extended periods of either streamer or glow corona result in a temporary loss of their hydrophobic properties. It would appear that the processes that result in the loss and recovery of hydrophobicity are the same for both HTV and RTV SR insulators.

The two surface chemical compounds observed by the XPS analysis, $H_{22}C_{16}OSi_2$ and SiO_2, are identified as being the LMW molecules and the filler respectively /5/.

The loss of hydrophobicity in SR insulators is attributed to the removal of low molecular weight (LMW) silicone molecules from the surface of the insulator during corona conditioning. This theory is supported by the chemical surface analysis completed by XPS. The virgin sample surface concentrations of $H_{22}C_{16}OSi_2$ are very much larger than the comparative count after the completion of the corona conditioning. This indicates that there is a removal of LMW molecules from the surface during exposure to corona.

The diffusion of LMW chains from the bulk to the surface, in order to restore hydrophobicity, is supported by the XPS results that illustrate the increase in surface concentrations of $H_{22}C_{16}OSi_2$ once the exposure to corona is removed.

As the LMW chains are removed by electrical discharges such as corona or dry band arcing for example the filler embedded in the SR bulk is exposed and it is this hydrophilic filler that causes the loss of hydrophobicity. This is illustrated by the high concentrations of SiO_2 monitored at the sample surface by the XPS analysis.

Both the RTV and HTV samples exhibited a lower LMW oil concentration on the surface after streamer corona when compared to glow corona. This fact corroborates the physical evidence /3/ that indicates that streamer corona causes a larger decrease in hydrophobicity than the glow corona.

The diffusion process, that leads to the recovery of hydrophobicity, is removing LMW molecules from the insulator bulk and replenishing the sample surface. This implies that there is a general erosion of the insulator bulk. It can be concluded that a continuation of this process will result in SR insulators having a finite operating life.

5 CONCLUSIONS

- The exposure of RTV or HTV SR insulators to either glow or streamer corona results in a temporary loss of their hydrophobic properties.

- Chemical analysis of the surface of RTV and HTV samples indicates that silicone compound is being removed from the surface. This removal of silicone and the subsequent exposure of the filler in the silicone polymer is the cause of the loss of hydrophobic properties.

- Chemical analysis highlighted the fact that a diffusion process exists once the corona is removed. The silicone count on the surface of the insulator increases and results in the recovery of hydrophobicity.

Exposure of RTV and HTV SR insulators to corona and the resulting removal and replenishment of silicone from the surface indicates that SR insulators will have a finite operating life. Thereafter the hydrophobic properties of SR insulators will no longer be evident.

6 REFERENCES

\1\ S M Gubanski, "Properties of Silicone Rubber Housings and Coatings", IEEE Transactions on Electrical Insulation, Vol. 27 No. 2, April 1992, pp 374 - 382.

\2\ J W Chang and R S Gorur, "Hydrophobicity of Silicone Rubber used for Outdoor Insulation", Proceedings of the 4th ICPADM, Brisbane, Austrailia, Paper No. 5201, Vol. 1, pp266 - 269, July 1994.

\3\ A E Dickson and J P Reynders, " The Effects of Corona on the Surface Properties and Chemical Composition of Silicone Rubber Insulators", 9th International Symposium of High voltage Engineering, Graz, Austria, Paper 3231, Vol. 3, September 1995.

\4\ Briggs and M P Seah, "Practical Surface Analysis - Auger and X-Ray Photoelectron Spectroscopy", Vol. 1, John Wiley and Sons, New York, 1990.

\5\ Winter H.J, Wacker-Chemie GmbH, Burghausen, Germany, Personal Communication.

7 ADDRESS OF AUTHOR

A E Dickson
Electric Power Research Group
University of the Witwatersrand
Private Bag 3
2050
Johannesburg

e-mail dickson@odie.ee.wits.ac.za

THE EFFECT OF CORONA ON THE SURFACE HYDROPHOBICITY
OF POLLUTED SILICONE RUBBER INSULATORS

A E Dickson, M A Moeiz, I R Jandrell, J P Reynders and Z Adam
University of the Witwatersrand
Johannesburg

ABSTRACT

This paper discusses the effects that glow and streamer corona have on the surface hydrophobicity of polluted Silicone Rubber (SR) coatings. The effect, on surface hydrophobicity, of polluting the SR samples using the fog withstand method was noted. The application of pollution, fog and the two types of corona all resulted in the reduction of the surface hydrophobicity of the SR coating. The SR did, however, recover its hydrophobic properties after a rest period. Possible mechanisms for the loss and recovery of hydrophobicity are introduced.

1 INTRODUCTION

For the past few years, SR has become popular as a High Voltage outdoor insulating material. It has been used for insulator strings on transmission lines, bushings, surge arrestors and other HV equipment in the form of high temperature vulcanised SR insulators and as room temperature vulcanised SR coatings. The main reason for its usefulness is its hydrophobicity - which prevents the formation of contamination and moisture on the surface of the insulator as a uniform film /1/. Rather, contamination and moisture form as discrete droplets on the surface. If both moisture and contamination are allowed to form a uniform film, surface leakage currents start to form, which create dry bands on the surface of the insulator. These dry bands result in dry band arching, which accelerates the ageing process of the insulator and can lead to flashover at operating voltages.

While research has bean completed on non-polluted SR insulators /1/, a need exists to study the performance of a hydrophobic material under polluted conditions. In particular, the processes involved in the transition between hydrophilic and hydrophobic Room Temperature Vulcanised (RTV) insulators is studied.

2 BACKGROUND THEORY

The hydrophobic properties of SR can be attributed to the formation of a layer of LMW polymer chains on the surface of the SR insulator. These molecules are formed during the production of the SR coating, and as they have a smaller chemical structure are able to diffuse to the surface of the insulator.

Research has shown that exposure to glow corona, streamer corona and electrical discharges result in the

loss of surface hydrophobicity /1,2,5/. This loss is followed by the subsequent recovery of the hydrophobicity. In the case of exposure to the coronas, the recovery can be modelled as a first order exponential with an associated rise time. The loss in hydrophobicity has been also noted /3,4/ under wet and polluted conditions along with a recovery of the hydrophobicity during a dry period. Also noted after wetting has been an increase in weight of the SR test object /3/, suggesting that the SR may have absorbed the moisture through a process of diffusion.

3 EXPERIMENTAL SET-UP

The SR coating was sprayed onto the surface of a metallic ball with a diameter 108 mm.

The pollution method used is the Fog Withstand method /6/, and it is designed to simulate marine and industrial pollution. It involved the spraying of the surface of SR insulator with a mixture of 20 g of salt and 20 g of kaolin (the binding agent) per litre of water. After the drying of the pollution mixture, the sample is then exposed to cold fog in a fog chamber for one hour. The fog chamber used is plastic covered cubicle of sides 1,5m × 1,5m × 1,5m. The fog is generated by air atomising nozzles. The experimental set-up is shown in *Figure 1*.
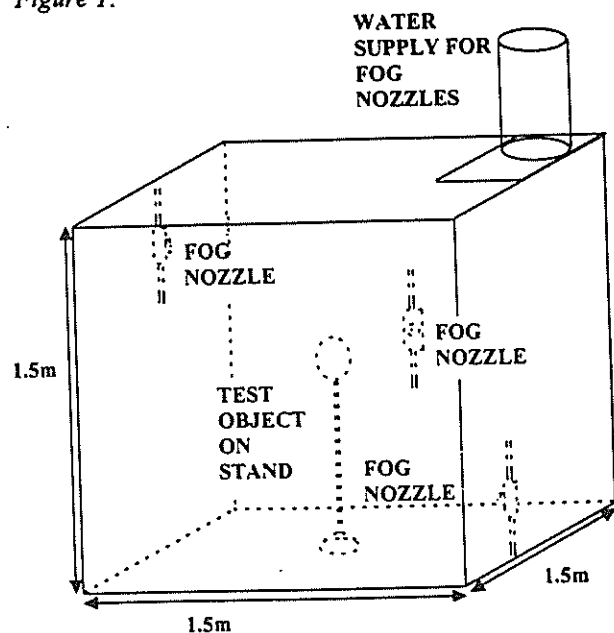
Figure 1: The Fog Chamber used for the Polluting of SR Insulators

The experimental set-ups used to create glow and streamer corona and the contact angle measurement used for the measurement of surface hydrophobicity have been fully described elsewhere /1/. The initial static contact angle on all the samples was > 95°.

4   RESULTS OBTAINED

4.1 Application of Pollution

The loss of surface hydrophobicity during the application of pollution is roughly linear and results in a final surface contact angle of 40°. The recovery of hydrophobicity can be modelled as a first order exponential with a corresponding rise time of 108 minutes. The loss and subsequent recovery of surface hydrophobicity is shown in *Figure 2*.
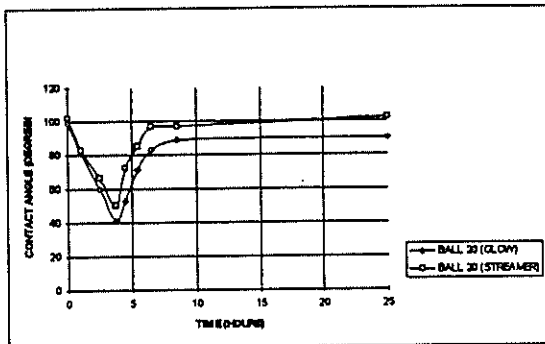
Figure 2: Loss and Recovery of Surface Hydrophobicity of a SR Insulator under Polluted Conditions. Note that the initial decrease in contact angle is due to the application of the pollution. Rise times are only calculated after the completion of the application of pollution.

4.2 Application of Fog

Fog was applied for an hour during which the surface contact angle was reduced to 56°. Once again, the recovery of hydrophobicity follows a first order exponential path, with a rise time of 211 minutes. The wetting and subsequent recovery period is shown in *Figure 3* below.
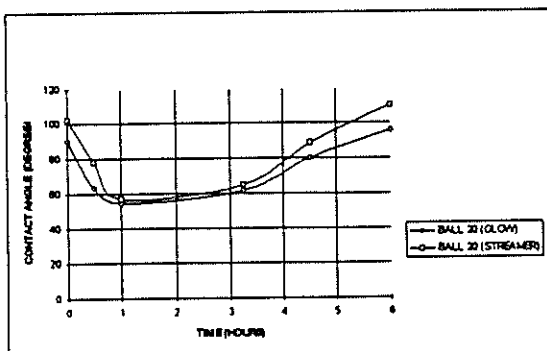
Figure 3: Loss and Recovery of Hydrophobicity due to the Application of Cold Fog. The rise times are only calculated after the completion wetting period.

4.3 Streamer Corona

The effect of conditioning the SR sample with streamer corona for 48 hours was to reduce the contact angle to 29°. The recovery of the SR followed a 1st order exponential with a corresponding rise time of 83 minutes. These results are shown in *Figure 4*. The results are compared to the data of an unpolluted SR insulator exposed to streamer corona, as described by Dickson /1/.
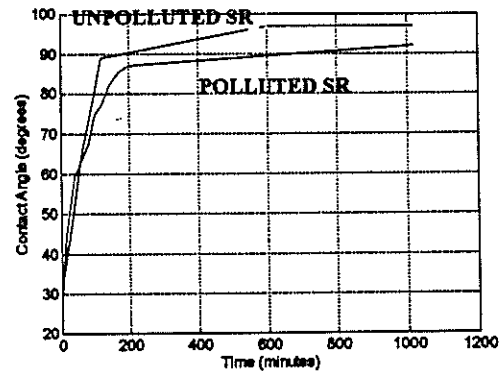
Figure 4: Recovery of Hydrophobicity of Polluted and Unpolluted SR Insulators after Streamer Corona Conditioning.

4.4 Glow Corona

After 48 hours of exposure to glow corona the contact angle was reduced to 51°. The recovery of the surface hydrophobicity mirrored that of the streamer corona case and had a rise time of 58 minutes. Figure 5 is the plot of the recovery of surface hydrophobicity and is shown along with that of unpolluted SR exposed to glow corona /1/.
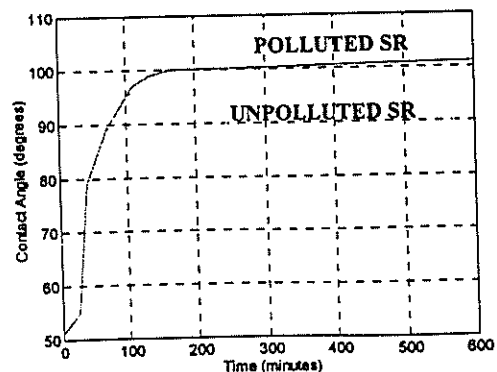
Figure 5: Recovery of Hydrophobicity of Polluted and Unpolluted SR Insulator after 48 Hours of Glow Corona Exposure

5   DISCUSSION

Applying the pollution mixture to the SR sample reduced the surface contact angle to below 50°. This is due to the formation of a porous hydrophilic pollution

layer on the surface of the SR coating. The recovery of surface hydrophobicity can be explained by the diffusion of LMW chains from the bulk, through the pollution layer, to the sample surface.

The effect of fog on surface hydrophobicity appears to have been the most severe. From *Figure 3* it can be seen that after the initial reduction in the contact angle the surface hydrophobicity remains constant between the first and third hour, and thereafter the recovery process begins. This can be explained by the fact that the LMW chains may have absorbed some of the moisture, and this moisture had to evaporate before the recovery of hydrophobicity could occur. This theory is supported by the findings of Mizuno *et al* /3/, who showed that a hydrophobic material that is submerged, absorbs moisture. Although there is no total immersion in this experiment, the trend noted by Mizuno is followed.

Streamer corona caused a greater loss in contact angle, 29°, when compared to glow corona, 51°. The corresponding rise times for streamer corona were also longer, 83 minutes, than for glow corona, 58 minutes. These results are supported by the findings in /1/ where similar results were obtained when comparing the effects of the two coronas on unpolluted SR samples.

The fact that the hydrophobic recovery rise times for both the polluted and unpolluted SR samples were very similar was surprising. It was felt that the pollution layer would greatly hinder the diffusion of the LMW molecules from the bulk to the sample surface. This has not occurred and the comparative recovery times may be attributed to the fact that the LMW chains are considerably smaller than the pollution layer. There would therefore be no change between the diffusion of LMW chains through the bulk or a pollution layer.

6 FURTHER WORK

The experiment conducted provided useful insight into the properties of polluted SR insulators under corona conditions. However, the author would like to recommend the following research be undertaken at a later stage to gain further information about the behaviour of SR under polluted conditions and when exposed to corona:

•   The SR sample should be polluted even further. A recommended level of pollution would be 60 g salt and 60 g kaolin per litre of water. This may provide information relating the level of pollution to the rate of hydrophobic recovery.

•   Research should be completed to determine if the loss of LMW chains from the surface of the SR insulator reaches a "saturation level". Are the LMW molecules removed to a level whereafter the

application of corona causes no further loss of hydrophobicity?

7 CONCLUSIONS

•   Exposure to pollution, fog, streamer corona and glow corona results in a decrease in the surface hydrophobicity of the SR sample. The recovery of the hydrophobicity is due to a process of diffusion of the LMW polymer chains resident in the bulk of the SR. This recovery process displays a rising first order exponential form with an associated rise time.

•   The application of pollution and the subsequent loss of hydrophobicity of the SR coatings was due to the fact that hydrophilic pollution particles were exposed to the water droplets being used in the measurement of the contact angle. The recovery of the SR was due to the migration of the LMW chains from the bulk to the top of the pollution layer via pores in the pollution layer. The rise time for this phase of the experiment was 108 minutes.

•   The application of fog to the polluted SR sample caused a reduction in the level of surface hydrophobicity. This may have been caused by the dilution of the LMW polymer chains on the surface due to the moisture present, and the absorption of the moisture by the pollution layer on top of the SR coating. Hence, during the recovery process, the moisture first had to be evaporated before the hydrophobic recovery process could occur. This factor would explain the longer rise times (211 minutes) experienced during the fog phase.

•   Streamer corona was seen to be the more severe of the two types of corona, with the contact angle being reduced to 29° as compared to 51° for glow corona. This is because streamer corona is known to produce higher energy photons and UV radiation than glow corona, which would then bombard the surface of the SR coating and erode it. This same phenomena would explain the longer rise time associated with streamer corona (83 minutes as compared to 58 minutes for the glow corona case).

•   The rise times of both the polluted and unpolluted samples are of the same order. This may be due to the fact that in both cases the LMW chains are considerably smaller than the surrounding material, SR bulk or pollution. The ability of the LMW chains to diffuse to the surface is not limited in either case.

8 REFERENCES

/1/ Dickson A E, Reynders J P, "The Effect of Corona
Activity on the Hydrophobic Properties of Silicone
Rubber Insulators", Ninth International Symposium on
High Voltage Engineering, Graz, Austria, August 28 -
September 1 1995, pp 3231-1 to 3231-4.

/2/ Bhana D K, Swift D A, "An Investigation into the
Temporary Loss of Hydrophobicity of Some Polymeric
Insulators and Coatings", Proceedings of the 4th
International Conference on Properties and Applications
off Dielectric Materials, July 3-8 1994, Brisbane
Australia, pp 294-297.

/3/ Mizuno Y, Naito K, Ishii K, Matsuoka R, Nakajima
I, Kondo K, "Time Variation of Hydrophobicity and
Weight of Silicone Rubber material", Ninth
International Symposium on High Voltage Engineering,
Graz, Austria, August 28 - September 1 1995, pp 3050-
1 to 3050-4.

/4/ Naito K, Nishiwaki S, Matsuoka R, Shinokubo H,
"Investigation Results of Silicone Rubber Insulators
Under Wet and Contaminated Conditions", Proceedings
of the 4th International Conference on Properties and
Applications off Dielectric Materials, July 3-8 1994,
Brisbane Australia, pp 294-297.

/5/ Chang J W, Gorur R S, "Surface Recovery of
Silicone Rubber Used for HV Outdoor Insulation", IEEE
Transactions on Dielectric and Electrical Insulation,
Volume 1, No. 6, December 1994, pp 1039-1046.

/6/ Working Group 04 of Study Committee No.33
(Overvoltages and Insulation Co-ordination), "A
Critical Comparison of Artificial Pollution Test
Methods for HV Insulators", International Conference
on Large High Voltage Electric Systems (CIGRE),
ELECTRA No. 64, May 1979, pp 117-136.

/7/ Comber M G, Deeno D W, Zafanella, "Corona
Phenomena on AC Transmission Lines", Transmission
Line Reference Book: 345kV and Above, Electric
Research Institute, Palo Alto, California, 1982.

/8/ Loeb L B, "Electrical Coronas: Their basic Physical
Mechanisms", University of California Press, Berkeley
and Los Angeles, 1965.

9 ADDRESS OF AUTHOR

A E Dickson
Electric Power Research Group
Department of Electrical Engineering
University of the Witwatersrand
Private Bag 3
2050
Johannesburg

e-mail: dickson@odie.ee.wits.ac.za

SIMULATION OF LIGHTNING SURGES ON ESKOM'S MV/LV DISTRIBUTION NETWORKS

R. A. Kelly   J. M. Van Coller   A.C. Britten*

Department of Electrical Engineering, University of the Witwatersrand

*Corporate Consultant - HV Engineering, Eskom TRI

1 Abstract

Lightning surge phenomena on Eskom's MV/LV (Medium/Low Voltage) distribution networks are simulated using EMTP. The aim of the work is to examine the surge stresses appearing on LV aerial bundled conductor (abc) circuits, which includes the surges transferred from the MV to the LV side of the distribution transformer, the resulting surges imposed on LV abc cable insulation and the electricity dispensers (EDs). An EMTP computer model has been designed in order to simulate the propagation of a variable shaped lightning surge waveform entering the MV side of the Eskom standard distribution transformer. This includes an accurate simulation of the transfer of surges from MV to LV and subsequently the propagation of the modified waveform along the LV distribution network. Suitable models for the distribution transformer, LV abc cables, and the various associated circuit components (surge arrestors, earth electrodes, down conductors, service connections and customer loads) have been developed in order for them to be simulated in EMTP. The results will be compared with actual test line measurements in order to verify the models derived.

2 Introduction

MV/LV overhead reticulation is prone to lightning surges resulting from both direct and indirect strikes [2]. To date, several questions remain unanswered regarding the effects that various components and configurations of Eskom's LV networks have on the attenuation of lightning surges and related transient overvoltages. It is therefore essential to have an understanding of lightning surge phenomena in MV/LV networks.

This study forms part of a larger study of the lightning performance of MV/LV distribution systems. A research programme now being set-up between the University of the Witwatersrand and Eskom TRI has the following major areas of investigation.

- Quantifying and qualifying the waveshape and frequency of occurrence of lightning generated surges appearing in LV abc circuits, and thus the surges impinging on EDs.
- Quantifying and qualifying the waveshape and frequency of occurrence of lightning generated stresses on LV abc cable as a function of the earthing of the LV neutral. The effect of a bare and covered neutral will also be examined.
- Transfer of lightning surges from the MV to LV side of the transformer to answer the question: are surge arrestors at the LV terminals of the transformer necessary?

The objective of this paper is to discuss some of the important modelling techniques and tools used to simulate the distribution transformer and LV reticulation.

In order to simulate transients in the distribution network, the software package EMTP (Electromagnetic Transients Program) has been selected [1] as it provides tools for modelling power system components which may accommodate non-linear characteristics. It allows for each phase to be treated separately. Modelling a power system is achieved by identifying significant nodes in the power system and defining the electrical behaviour of the interconnecting branches.

3 Background on High Frequency Transformer Modelling

In order to accurately simulate the propagation of lightning overvoltages through a distribution transformer (MV to LV), a suitable model must be derived for use in the EMTP. For the simulation of network transients, the basic transformer representation used in the EMTP does not take into account the high frequency behaviour of the transformer [3], hence a wide frequency range model is required (referred to as a high frequency

transformer model). The model must be able to simulate a multi-phase (three phase), multi-winding transformer.

A power transformer is a complex arrangement of coils around an iron core. With the close spacing of the coils, transformers have significant stray capacitances (inter-winding and winding to ground) as well as inductances. These stray capacitances come into effect at high frequencies. Thus, transformers exhibit a number of resonances at various frequencies. Surges, as a result of lightning strokes, excite these resonances and cause voltage amplification inside the windings. Morched et al. [3] state that modelling the distributed stray capacitances along the windings with lumped capacitances connected across the terminals of the transformer cannot reproduce the behaviour of the transformer beyond the first resonance frequencies. The distribution transformer possesses certain non-linearities, the degree of which varies for different frequency ranges. If, under certain conditions, the non-linearities could be neglected, these resonances could be modelled using a linear RLC network and the transformer model would accurately predict the output waveform for any shaped input waveform (transient).

Soysal [4] motivates a procedure for the wide frequency range modelling of power transformers based on external terminal impedance measurements. At lower frequencies, up to some tens of kHz, terminal connections (i.e. loading effects) of transformers affect the performance. The linearity assumption is acceptable provided not all the windings are open circuited. However, at high frequencies (above 100 kHz), the characteristics tend to be linear due to the reduced flux penetration into the iron core. In the discussion by Seitlinger following the paper on a method for modelling non-linear core characteristics [6], the investigation of lightning impulses needs a model with a bandwidth of at least 100 kHz, and the effect of saturation does not (or not very much) influence the behaviour of these transients. The assumption is that resonant frequencies are determined mostly by the short circuit impedances between windings and winding parts, therefore a change in the reluctance of the core (due to saturation) does not change the resonance frequencies significantly. Woivre et al. [5] shows that the transformer winding behaves as a linear system without saturation effects for the duration of a lightning-speed transient, provided the state of the core magnetisation at the beginning of the transient is considered. Vaessen, Hanique [7] and Malewski [9] experimentally show that for higher frequencies (> 1 kHz) the transformer behaves linearly and the iron does not play a significant role. Swift[8] discusses the non linearities introduced into the transformer behaviour during transient conditions as a result of the iron core (namely saturation, hysteresis and eddy

currents). He shows that a linear model of the eddy-current effect is very accurate for commercial power transformers. The hysteresis phenomenon is less easy to simulate but also less important since it contributes less loss. The magnetic effects of hysteresis, except for the initial condition due to remanence, can be neglected altogether since the hysteresis loop is very narrow for power transformers [6]. Neglecting the losses due to hysteresis seems to be reasonable for most transients with a few exceptions where the losses may have a significant effect in the damping of the transient.

A standard lightning wavform (i.e. 1.2/50 µs) has significant signal energy up to at least 500 kHz, whereas the signal energy of a chopped waveform (due to flashover) extends up to a few MHz (1-4 Mhz) [5]. Thus the transformer behaviour should be modelled up to about 4 MHz.

4 High Frequency Transformer Model for the EMTP

The high frequency transformer (HFT) model used belongs to the class of models where the frequency dependent response at the terminals of the transformer is reproduced by means of equivalent networks. The frequency characteristics are determined from measurements made at the terminals of the transformer. This is done by using the concept of the short circuit admittance function [11]. The transformer to be modelled is one of the Eskom standard distribution transformers with the following relevant specifications: 100 kVA, 22 kV/416 V, delta-star (D yn 11) completely self protected (CSP). However, the model described below can be applied to any transformer, should a different size, design or manufacture be used in future.

The model [3] is applicable to multi-winding, multi-phase transformers and is based on the frequency characteristics of the transformer admittance matrix between its terminals over the frequency range of interest. The transformer admittance characteristics can be obtained from measurements taken according to the method used by Vaessen [10] which is based on low voltage impulse techniques. It is not possible to describe the measurement techniques in this paper due to space limitations. The elements of the nodal admittance matrix, shown in equations 1 and 2, are approximated with rational functions consisting of real as well as complex conjugate poles and zeroes. The fitting techniques used to approximate the admittance functions of the transformer produce approximations of exceptional quality using a least squares curve fitting process. These approximations are realised in the form of an RLC network in a format suitable for direct use with EMTP.

$$\begin{bmatrix} Y_{11} & Y_{12} & \cdots & Y_{1m} \\ Y_{21} & Y_{22} & \cdots & Y_{2m} \\ \vdots & \vdots & & \vdots \\ Y_{m1} & Y_{m2} & \cdots & Y_{mm} \end{bmatrix} \begin{bmatrix} V_1 \\ V_2 \\ \vdots \\ V_m \end{bmatrix} = \begin{bmatrix} I_1 \\ I_2 \\ \vdots \\ I_m \end{bmatrix} \qquad (1)$$

$$[Y_{ij}] = \begin{bmatrix} y_{ij,aa} & y_{ij,ab} & y_{ij,ac} \\ y_{ij,ba} & y_{ij,bb} & y_{ij,bc} \\ y_{ij,ca} & y_{ij,cb} & y_{ij,cc} \end{bmatrix} \qquad (2)$$

where [Yij] is a 3x3 sub-matrix and m is the number of groups of three-phase terminals under consideration.

Software was written in MATLAB® to evaluate the R, L and C components from the digitally recorded measurements. The model developed is valid up to 5 MHz in order to accommodate chopped lightning waves which may possess significant frequency components up to a few MHz. The LV neutral is modelled as a third separate terminal which is not earthed to the transformer tank so that the model can be used to simulate the resultant differential voltages arising between the neutral and tank as shown in figure 1. Note that it is possible to allow for the inclusion of the MV earth (which would be connected to the transformer tank) in the EMTP simulations.
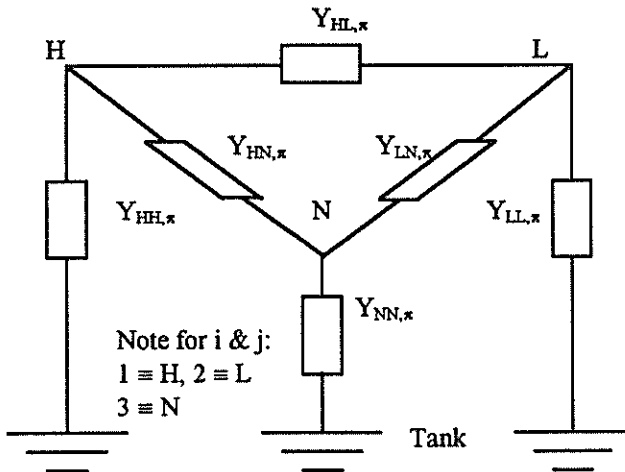
Figure 1. Single-line diagram of the multi-terminal π-equivalent

The parameters of this π-equivalent network are calculated from its nodal admittance matrix (equation 1) using the well known relationships shown in equations 3 and 4.

$$[Y_{ii,\pi}] = \sum_{j=1}^{m} [Y_{ij}] \qquad (3)$$

$$[Y_{ij,\pi}] = -[Y_{ij}] \qquad (4)$$

The HFT model is used as an add on module of a more comprehensive low frequency EMTP model where iron core nonlinearities are represented in detail. The HFT model matches the difference between the measured data and the frequency response of the linear portions of the low frequency model. Combining non-linear and frequency dependant effects always introduces a certain degree of approximation. In the case where a high frequency transient excites a transformer which is unsaturated, the transformer is generally not driven into saturation. This is because, according to Faraday's Law, the flux produced by a voltage transient is proportional to its integral [12]. If a transient of sufficient magnitude is impressed on a transformer which is already saturated or near saturation, then superposition is strictly not valid. In the latter case, superposition would yield less accurate results due to the fact that the high frequency currents would be affected by a decreasing (non-linear) permeability, μ. The low frequency currents would be correctly taken care of by the non-linear EMTP low frequency model onto which the HFT model is superimposed.

5 Modelling of Low Voltage (LV) Reticulation Networks in the EMTP

The cable constants support program included in the EMTP was used to model the overhead LV abc cable (three phase with neutral) and service connections (single phase with separate neutral and earth (SNE)). The abc cable consists of stranded compacted aluminium conductors of equal cross section and insulated with carbon loaded XLPE. Both bare and covered neutral conductors were considered. The service connection is by split concentric cable. The low current footing resistance of ground electrodes is modelled in terms of the electrode length and surface area [13]. The surge response of the earth electrodes due to the effects of soil ionisation are modelled according to a method originated by Korsuncev [13]. Down conductors and customer loads are modelled using lumped resistances and inductances. The self inductance of a down conductor introduces significant voltages due to the high di/dts inherent in lightning transients. Due to the comparatively short length of the down conductors, it is unnecessary to model them as short single phase transmission lines as the travel time is extremely short ($\approx$ height/300 μs). The non linear metal oxide surge arrestors are modelled as non linear resistors using the EMTP support program ARRDAT which fits exponential curves to a set of v-i data points [1].

6 Simulation Considerations

If a transient is impressed on the transformer when the 50 Hz voltage wave is at its peak, then the 50 Hz flux wave, which lags the voltage wave by

approximately 90°, is near a zero crossing irrespective of the magnitude of the voltage. This represents an instant when the transformer is clearly not in saturation. Such a situation would be accurately modelled by the combined low frequency and HFT model, resulting in a true simulation of a "worst case" scenario. Should the transient occur when the power frequency voltage wave is passing through zero (representing the extreme opposite case), then the flux wave is near its maximum magnitude. The combined model would still be accurate provided the power voltage magnitude is not large enough to drive the transformer into saturation and the transient voltage wave magnitude is also not of sufficient magnitude to drive the transformer into saturation. If any of the above conditions are not met, the model would produce results which underestimate the true magnitudes of current and overestimate the true magnitudes of voltage, but only in the high frequency range. This is because in the non linear saturation region, the ratio between voltage and current decreases since the permeability, μ, decreases.

It has been shown that transformers of the same design and manufacture show essentially the same frequency behaviour [3] and therefore the results obtained from this work are not only applicable to the particular transformer measured in this case.

7 Conclusions

In order to examine lightning surge phenomena in MV/LV distribution networks, the accuracy of the EMTP models derived must be validated using measurements carried out on an actual test line. The configuration of this line will thus be used for the EMTP simulations. At the time that this paper was submitted, the measurements from the test line were not yet available. The LV abc line to be used for this purpose has been set up on a mine dump at Eskom's Rosherville site. A step by step approach will be taken in order to validate and assess the influence of the individual components on the overall system. At the same time, the results from these tests will yield important findings which can be used to quantify the effect that the LV network configuration has on the attenuation (or amplification) of lightning transients.

8 References

1) Van Coller, J. M. "An Introduction to EMTP (Electromagnetic Transients Program), Revision 3.0" University of the Witwatersrand, Department of Electrical Engineering, 1993.

2) Van Coller, J. M. "Insulation Co-ordination in Distribution Systems" CEE Winter School: The Design of Low Voltage Reticulation Systems, 1993, ppC1-C34.

3) Morched, A., Marti, L., Ottevangers, J. "A High Frequency Transformer Model for the EMTP" IEEE Transactions on Power Delivery, Vol. 8, No. 3, 1993, pp1615-1621.

4) Soysal, A.O. "A Method for Wide Frequency Range Modelling of Power Transformers and Rotating Machines", IEEE Transactions on Power Delivery, Vol. 8, No. 4, 1993, pp 1802-1808.

5) Woivre, V., Arthaud, J.P., Ahmad, A., Burais, N. "Transient Overvoltage Study and Model for Shell-Type Power Transformers." IEEE Transactions on Power Delivery, Vol. 8,No. 1, 1993, pp212-220.

6) Valilian, M., Degeneff, R.C. "A Method for Modelling Non-Linear Core Characteristics of Transformers During Transients." IEEE Transactions on Power Delivery, Vol. 9, No. 4, 1994, pp1916-1925.

7) Vaessen, P.T.M., Hanique E. "A New Frequency Response Analysis Method for Power Transformers" IEEE Transactions on Power Delivery, Vol. 7, No. 1, 1992, pp384-390.

8) Swift, G.W. "Power Transformer Core Behaviour under Transient Conditions", IEEE Transactions on Power Apparatus and Systems, Vol PAS 90, No 5, 1971, pp2206-2210.

9) Malewski, R. Poulin, B. "Impulse Testing of Power Transformers using the Transfer Function Method" IEEE Transactions on Power Delivery, Vol. 1, No. 2, 1988, pp476-482.

10) Vaessen, P.T.M. "Transformer Model for High Frequencies" IEEE Transactions on Power Delivery, Vol. 3, No. 4, 1988, pp1761-1767.

11) Bobrow, L. S. "Elementary Linear Circuit Analysis.", 2nd Edition, Saunders College Publishing, 1987, pp571-578.

12) Sen, P.C. "Principles of Electric Machines and Power Electronics, Chapters 1 and 2", John Wiley & Sons, 1989, pp1-94.

13) Chisholm, W. A., Janischewskyj, W. "Lightning Surge Response of Ground Electrodes", IEEE Transactions on Power Delivery, Vol. 4, No. 2, April 1989.

9 Address of Main Author

R. A. Kelly, Department of Electrical Engineering, University of the Witwatersrand, 1 Jan Smuts Avenue, P.O. Box 2050, Johannesburg, Gauteng, South Africa. E_mail: kelly@odie.ee.wits.ac.za

Automation of a Current Impulse Generator

G Kwasnik and AJ Phillips*
Tecknikon Witwatersrand
* University of the Witwatersrand
Johannesburg, South Africa

1 Abstract

This paper discusses the development and automation of a current impulse test facility at the University of the Witwatersrand. The current impulse generator which is being developed will be capable of generating a number of standard test impulses. These include the 8/20μs, 10/350μs and the 1,2/50μs - 8/20μs combination waveforms. The unit consists of two major components, the first is the current impulse generator itself and the second is the generator control unit. The generator has been designed as a standalone mobile unit which has the charging circuitry, discharge capacitator, measurement devices and tuning circuitry in enclosed unit unit. The operator therefore has no access to potentially lethal areas of the generator. The control unit is a PC based system which has control over the charging and triggering functions of the generator. The emphasis of this paper is placed on the automation of the system and the construction of the generator.

2 Introduction

During the last five years a number of international standards relating to the management of the direct and indirect effect of lightning activity has been published [1, 2]. These standards include suitable evaluation techniques for surge protection devices (SPDs). The prescribed tests involve the application of either current or voltage impulses or a combination of voltage and current impulses onto SPDs.

Since the number of SPDs that need to be tested is increasing, the application of both current or voltage tests on SPDs needs to be carried out in a reliable and repeatable manner with the safety of the operator and measuring equipment being of upmost importance. To date, in most test facilites, this has required the operator to remain close to the impulse generator and the device under test (DUT) in order to trigger and monitor the impulse, as well as record the required impulse currents and residual voltages.

This paper describes the development of an impulse test facility which will require the operator only to select and attach the required waveshape tuning circuit and DUT and then via a menu driven user interface on the personal computer conduct the test according to the required specification which has been preprogrammed into the software. The test routine will then be automatically performed by the computer and the test waveforms recorded. A report will then be automatically generated. A number of safety checks, both using the hardware and software, will be built into the system and the operator will be able to abort the test and earth the system at any time.

At this stage the hardware has all been constructed and assembled while the software and control circuitry is under development.

The following section describes the physical construction of the generator.

3 Construction

The impulse generator consists of a frame into which the discrete components are fitted. The frame is constructed from angled steel sections and is mounted on castors. The sides of the generator are enclosed by mild steel plates which provide a level of electromagnetic shielding.

Internally the generator consists of three sections separated from each other by means of steel divider plates. The divider plates electrically and magnetically shield the various sections from one another preventing the coupling of unwanted noise onto the control circuitry. This is an implementation of the zoning concept described in the latest IEC specification on Lightning Electromagnetic Impulses (LEMP) [3].

The three sections (A,B and C) of the generator are shown in *figures 1, 2* and *3*.

3.1   Section A of the Generator

Section A of the generator consists of the high voltage transformer, the charging diode and resistor, the motorised variable autotransformer (variac) and the mains circut breaker.
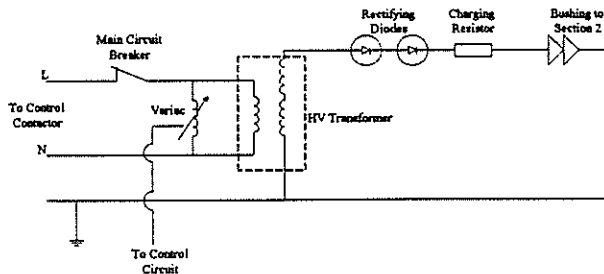
Figure 1: Components in Section 1.

These are configured in circuit as shown in *figure 1*.

The 220V/15A circuit breaker is supplied from a contactor controlled by the computer. If a fault occurs in the charging circuitry, the circuit breaker will clear the fault and the operator will have to manually reset the breaker realising that a fault has occured.

The breaker supplies the motorised variac which is also controlled by the PC. The variac supplies the primary winding of the HV transformer. Hence the computer has control over the output voltage of the HV transformer and therefore the charging rate and level of the capacitor. The voltage on the primary windings of the HV transformer is measured by the computer.

The transformer is rated at 15VA and has a 220V/20000V ratio.

The transformer supplies two HV diodes in series which in turn supplies the discharge capacitor via a current limiting resistor. The PIV of each of the diodes is 14kV and the current limiting resistor is a 60kΩ with a continuous power rating of 500W.

The connection from the current limiting resistor, in section 1, to the discharge capacitor, in section B, is done via a PVC bushing in the section divider plate.

3.2   Section B of the Generator

This section contains the discharge capacitors and the high voltage and high current measurement equipment as shown in *figure 2*

At present only one 10 kV / 34μF capacitor is mounted in position, but construction capacity allows for an additional four, for a total of five capacitors which can be configured in a number of ways to give a range of capacitance and charging voltage values.

The discharge capacitor DC charge voltage is recorded by the PC and A/D card using a resitive voltage divider circuit as indicated in *figure 2*. Since the voltage
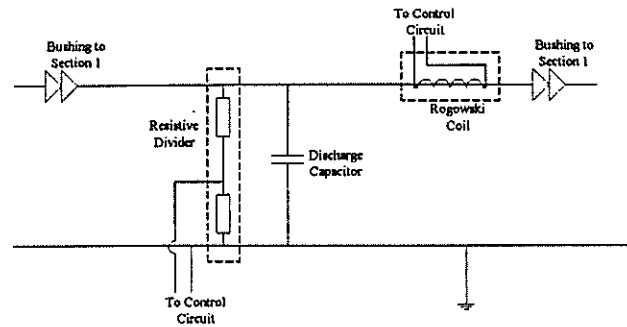
Figure 2: Components in Section 2.

at the input to the A/D card could not exceed 10 volts, a voltage divider was constructed. At 10 kV, the divider draws a current of 100μA dissapating 1 watt the divider consists of 47 off 2,2 MΩ half watt resistors connected in series and two sets of 100kΩ resistors connected in parallel to produce a 2000:1 or a 4000:1 ratio. The output signal from the divider is passed through a lowpass filter in order to remove any unwanted noise.

The Rogowski coil which measured the impulse current was designed at the University of the Witwatersrand [4] and has a 3dB bandwidth of 10Hz to 1MHz and a gain of 1V/kA. The coil is positioned before the DUT and not in the earth path as suggested in certain specifications [5]. This has been done since a HV probe is often placed across the DUT in order to measure the residual voltage during testing. The earth lead of the HV probe can provide an alternative path for the discharge current and a coil placed after this path to earth may not record the full impulse current passing through the device. The insulation of the Rogowski had to be increased in order to allow the placement of the coil on the high voltage side of the DUT.

The output of the capacitor is connected through the Rogowski coil to the spark gap in section C via a PVC bushing.

By keeping the both the DC voltage and current impulse measurement transducers in section B the level of interference that will be coupled onto the measurements will be kept at a minimum. This is due to the fact that there are more interference sources in sections A and B, eg. spark gap, "dump" gap and contactors.

3.3   Section C

This section consists of the earthing circuitry for the discharge capacitor (often called the "dump"circuitry) and the triggering spark gap as well as the power supplies for both the "dump" and triggering spark gaps. On top of section C is the working area where the DUT is placed and connected, as well as the terminals for the different waveshape tuning circuits.

The "dump" resistor and "dump" contactor are both installed onto the base of the frame. The "dump" con-
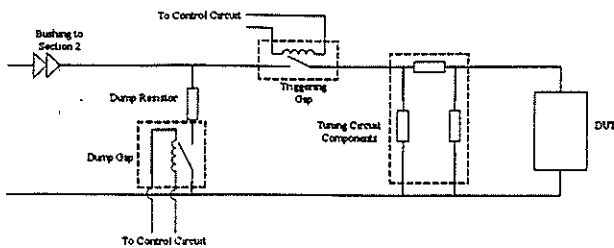
Figure 3: Components in Section 3.

Figure 4: Interconnections between the PC and the transducers and actuators.

tactor is a normally closed contact ensuring that the discharge capacitors are earthed via the 200kΩ "dump" resistor if testing is not in progress or the power to the gap is removed. The "dump" contactor was an inhouse design consisting of brass sphere gaps, a long travel solenoid and the required insulation.

The position of the triggering spark gap was carefully chosen in order to keep the inductance of the tuning circuit as low as possible. This decision invloved keeping minimising the loop and the length of the conductors. The inductance needs to kept as low as possible since the tuning circuits for certain of the test waveforms require exceptionally low tuning circuit inductance values to remain within specification.

Two PVC tubes are placed though the working area so that the tuning circuits can easily be mounted and exchanged. Tuning circuits for the 8/20µs, 10/350µs and the 1,2/50µs - 8/20µs combination waveforms have aready been individually contructed and the required waveforms are within specification [4]. The tuning circuits have been placed in PVC housings and enlosed in resin. By using these discrete waveshaping components the operator will be able to easily and quickly change the impulse form.

The working area is enclosed by a earthed hinged metal cage which protects the operator if the DUT malfunctions. A normally closed microswitch relays the position of the cage to the hardwired safety interlock system preventing the operator from charging the discharge capacitor if the working area is exposed.

4   Earthing and LEMP Protection of Control Circuitry

The basic circuit layout indicating both transducer and conrol line connections is shown in *figure 4*. The computer is positioned five meters from the generator in an earthed mild steel housing to ensure shielding. The control cables are run from the generator to the housing in a steel conduit to prevent both magnetic and capacitative coupling onto the control cables.

The zone concept outlined in the IEC 1312-1 series of specifications will be adehered to in order to minimise disturbances on the system due to the large transient
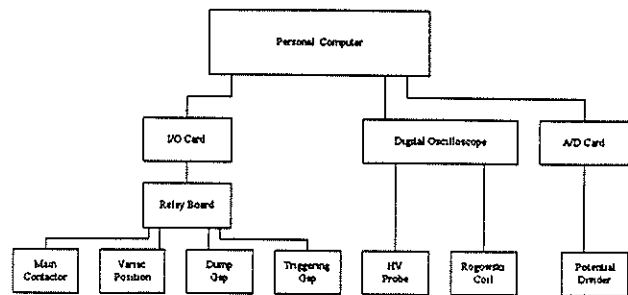
and steady state currents and voltages as well as the effects of the exceptionally "noisy" spark gaps [6]. The positioning of the SPDs and the method in which the SPDs, control circuitry, control cables and shielding screens are earthed will also be performed in accordance with the relevant IEC specifications.

5   Safety Interlocks

A number of saftey interlocks which are hardwired rather than software controlled have been included into the design.

The safety interlock system consists of a remotely activated breaker, which supplies both the HV transformer and the "dump" gap power supply with 220V and a number of either nomally open or normally closed microswitches.

If the remotely activated breaker is tripped, either using the remote connection or the breaker handle, the power to the HV transformer and the power supply of the "dump"gap is immediately cut. Since the "dump" gap is a normally closed contact the discharge capacitor is automatically earthed as the power is removed from the "dump" gap solenoid.

There are three hard wired saftey interlocks:

- A STOP button which is controlled by the operator.

- A microswitch on the cage which covers the working area.

- A microswitch on the side panel of the generator.

The safety interlocks and basic circuit are illustrated in *figure 5*.

6   Control Software

The computer together with the A/D card and digital oscillocope measures the status and output from the generator using the transducers shown in *figure 4*. The
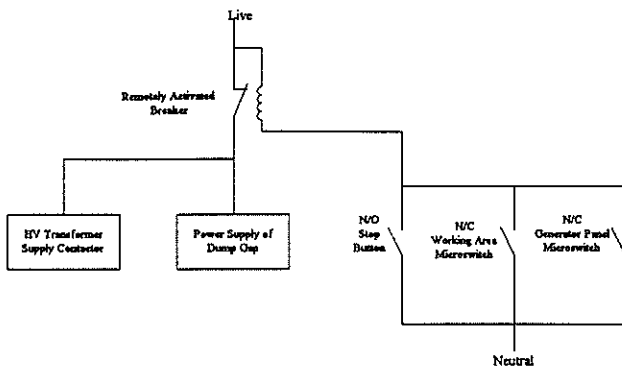
Figure 5: The hardwired safety interlock system.

PC can then using this information control, via the I/O card and relay board, the output current and voltage magnitudes as well as the impulse repitition rate.

Using the I/O card, control relays and contactors the computer has control over the following:

- The supply voltage to the primary of the Variac.

- The Variac Potision and hence the Voltage on the Primary of the HV transformer.

- The position of the "dump" gap.

- The position of the triggering gap.

The A/D card together with input ports and oscillocope supplies the following information:

- The voltage on the primary of the HV transformer.

- The voltage to which the discharge capacitor is charged.

- The impulse current waveform.

- The residual voltage waveform.

Using the above controls and inputs the charging and triggering cycle of the generator will be controlled by the PC and the impulse current and voltage waveforms downloaded from the oscillocope.

The software is still in the design phase but once the basic control features have been implemeted the next stage will be to preprogram the relevant standard's test procedures and test criterion making the results of standard's testing more reliable and less dependant on the operator.

7   Conclusion

The automated generator is being designed and developed in order to improve the safety and repeatability with which current impulse tests can be performed.

Due to the hazardous environment the generator will use the zone concept in improving the LEMP perfomance of the associated control circuitry. The generator may therefore be used in future as a test rig to measure and show improvements that can be attained by using the zone concept.

References

[1] International Electrotechnical Commission, "Protection against LEMP, Part 2: Electromagnetic fields inside structures in case of direct and nearby lightning strikes," *IEC*, 1995.

[2] International Electrotecnical Commission, "Protection against LEMP, Part 3: Requirements of Surge Protective Devices," *(IEC - ciculated for comment)*, November 1994.

[3] International Electrotechnical Commissison, "Protection against LEMP. Part 4: Application guide for protection against LEMP for structures," *IEC - Circulated for Comment*, November 1994.

[4] R. Melaia, I. Jandrell, J. Van Coller, and A. Phillips, "Development of a combination generator for lightning simulation," in *4th Southern African Universities Conference, Cape Town*, 1993.

[5] South African Bureau of Standards, "Uninterruptible power supplies," *SABS*, 1988.

[6] International Electrotechnical Commission, "Protection against LEMP. Part 1: General Principles," *IEC*, 1995.

8   Author:

Mr Glen Kwasnik
BFBA Consulting Inc.
PO Box 1339
Johannesburg
2000

DEVELOPMENTS IN RURAL PROTECTION SYSTEMS
Fuse policy, Protection settings and Co-ordination

Phillip Verster

Senior Engineer, Eskom, PO Box 222, Brackenfell, 7560

Synopsis

Two forces (or external pressures) are evident in the Eskom engineering environment: cost and quality of supply. With regard to the application of protection equipment these forces may be of opposite polarity, i.e. lower cost may imply lower quality equipment, lower reliability and accordingly extended outages. This paper states the protection requirements for rural distribution systems and reflects on how a clearer specification, given current technology and device functionality, enables both cost savings and improved quality of supply.

1   INTRODUCTION

The discussion is initiated from a fuse device application perspective. Any discussion on protection device settings can only be sensible after consideration of the fuse characteristics. A few suggestions are made with regard to the autoreclose cycles to be adopted.

2   FUSE APPLICATION

Fuse Element Rating   Protection devices are always set and applied in such a manner as to be able to reliably detect a bona-fide fault condition as well as to limit the damage due to that fault condition by facilitating rapid disconnection of the faulted plant from the power system. In the application of drop-out fuse assemblies to distribution power transformers (11kV or 22kV, 25kVA to 350kVA) this has amounted to pairing small fuse elements to lower rating transformers. Has the percentage lower rating transformers makes up about 85% of a typical feeder, the result is a system of transformers protected by small fuses. The problems experienced due to this practice has been a lack of *transient surge insensitivity*, i.e. with surge arresting device placed in-

zone to the fuse, fuse operation occurred as a result of surge arrester operation. This sensitivity to transient surges has resulted in the unnecessary loss of large segments of rural networks during adverse weather conditions.

Paradigm Shift   On review the ability of the fuse to limit fault damage was re-assessed and found to be insignificant: a faulted distribution transformer is not recoverable whether the fault duration was short or long. Thus the fuse need not be applied to protect the transformer in question, but should rather be applied to protect the power system against faulted plant. The criterion of fuse element selection now becomes one of *ensuring that the applied fuse will operate* for an in-zone fault as opposed to sensitive and fast operation. The sensitivity is now not dependent on the transformer the fuse is applied to, but to the power system source impedance and the typical impedance of the fault path. This appreciation has led to the adoption of two fuse element ratings which is intended to be the Eskom standard (20K and 30K). The 10K element was retained for special applications where sensitivity is at issue. The savings in terms of operating costs (less outages), simplified stock holding requirements, ease of fuse replacement, etc. are regarded as substantial.

Fuse-Fuse Co-ordination   The traditional concept of section fusing or fuse-fuse co-ordination was also revisited. A very important pre-requisite for fuse-fuse co-ordination is that the fault current up to which such co-ordination is attainable is that level of current where the "maximum operating time" of the lower rating fuse does not exceed 75% of the "minimum melting time" of the higher rating fuse. Both these time curves are uniquely defined in terms of pre-loading, energy, time, etc. considerations and define the parameters of any fuse's time-current characteristic. The constraint is a simple one: Fuse-fuse co-ordination is successful only for defined (low) fault current ranges (e.g. 30K-20K up to ±500A only). This makes a mockery of indiscriminate section fusing and demands that a single fuse level reticulation planning approach is essential. Field experience is that 85% of section fuse operations are non-damage in nature, i.e. on replacement of the fuse element the fuse stays in - the initial operation was not due to a solid system fault. This would be typical of an element that has deteriorated over time due to one or more through faults at previous occasions.

Group Fusing   A further cost optimisation possibility results from the above paradigm shift in the fuse element selection. As the standardised elements are now fairly large relative to the installed capacity, the fuse has an excessive *transient inrush stability* margin. This margin defines the capability of the fuse element to withstand the energy conveyed by the excitation current occurring due to magnetising inrush (i.e. fuse curve must be at least above 100ms at 12.5x I_{rated} and above 10ms at 25x I_{rated}). This implies that with the larger fuse elements (in order to get *transient surge insensitivity*) more than one transformer can be connected of a single fuse (in order to utilise the improved *transient inrush stability* margin). This implies

that the total number of fuse installations on the network can be decreased dramatically, again reflecting positively on operating and management costs.

3   EARTH FAULT PROTECTION

Fault Levels   Considering the predominance of earth faults on rural networks (80%) and the fact that reasonably inexpensive current limiting practices can be adopted due to the unique earth fault path (relative to the phase fault path), the use of Neutral Earthing Resistors (NERs) either individually or in combination with Neutral Electromagnetic Couplers (NEC/NERs) has found wide spread acceptance. An approximate resistance value of a 11kV NER is 20Ω, i.e. ±315 (6350/20) Ampere earth fault current for a solid close-in fault. Considering the fact that the rural line structures are predominantly unearthed in order to attain the preferred BIL and the fact that the distribution transformer earthing resistance may be up to 30Ω, it is reasonable to expect the probability distribution of close-in earth fault currents to be around a median of ±220A (single transformer source with NER). As the fault is moved deeper into the system, the expected fault levels decline even further. The fault current level of earth faults are thus severely influenced by the resistance components in the earth fault path, this giving a rate-of-change of fault level relative to distance that is not as severe as that of phase faults (where the line impedance size determines the drop-off rate).

Definite Time Preference   Given the fact that the expected range of fault currents fall in a very narrow spectrum of the log-log time-current co-ordination plane, and given the fact that the inherent IDMTL benefit of fast operation at high currents in order to minimise damage does not apply (due to the damage already being limited by current limiting), there seems to be no clear reason for adopting IDMTL relaying for earth faults. There is of course the view that IDMTL-type delayed tripping may facilitate co-ordination with fuse characteristics. I am of the opinion that low earth fault currents (due to current limiting) that are not cleared speedily may cause fault point ionisation that leads to phase-phase faults of high current level - which defeats the earth fault current limiting practice in the first place! Thus trying to *fully* co-ordinate earth fault characteristics and fuse characteristics at low current levels may be defeatist and detrimental to the power system (upstream power transformers being thermally and mechanically stressed for high current through-faults). I am a proponent of setting an upper time limit on delayed earth fault operations (e.g. 2 seconds) and then to regard any incidental co-ordination with fuse characteristics as a bonus. Where composite curves (or function overlays) are available, an IDMTL characteristic may be applied to further limit the operating time for currents higher than the DTL-fuse characteristic intersection.

Faster Sensitive Earth Fault   Accepting that the SEF function is not an ideal high resistance fault detector in either its sensitivity or time settings, the same argumentation as followed above applies. The traditional 6 second SEF delay implies that with a delayed earth fault pick-up of 40 Ampere (typical), an earth fault of 35 Ampere will only be cleared in 6 seconds! The

origin of this time delay seems to be to accommodate harmonic and power system effects, both accounted for with an appropriate harmonic insensitivity specification. It is recommended that a 6 Ampere/3 second SEF approach be adopted.

Reclose Philosophy   Each fast trip operation is associated with clearance of a transient fault, while a combination of two delayed operations are regarded as suitable relaying for a semi-permanent fault (e.g. wind borne debris on the line to burn free). Due to the low earth fault current levels and the fast relaying times proposed it is suggested that the maximum number of fast trip operations be executed, i.e. 2 or 3, with at least one delayed trip operation. A further refinement is to allow for reclosing on SEF operations, seeing that a small percentage of SEF operations are due to "conductor-down" conditions.

4   PHASE FAULT PROTECTION

Rapid Fault Clearance   One of the benefits of resistance earthing is that the distortion in the voltage triangle is minimal under earth fault conditions, i.e. the healthy phase voltages increase to approximately line voltage value. As Eskom distributes distribution power on a three-wire system, the fact that the voltage triangle is maintained implies that an earth fault on the distribution system is not transferred to the customer at the LV system side. As the voltage triangle is severely distorted for phase faults, a high priority is placed on rapid phase fault clearance - and the closer to a node (e.g. busbar), the higher the priority on rapid relaying!

Zone Sequence Co-ordination   With a downstream protection device and traditional relaying techniques fast phase fault operation at the substation is not possible due to the inevitable co-ordination loss for the first delayed operation of the downstream device. Zone Sequence Co-ordination (ZSC) is that feature that allows a distribution protection device to proceed in its sequence of fast operations whenever it sense the presence and removal of a fault condition. The ZSC feature enables fast curve settings on upstream devices. It allows for great flexibility in application - consider the case of a "stubby" network (i.e. high fault levels all round) and several important feeders of the substation busbar. The fact that the fault levels are high implies that all phase faults will have a dramatic effect on the busbar voltage and will thus cause all the feeders to experience the quality of supply deterioration, i.e. all the motors will drop out in about 40 - 100 milliseconds when a phase fault cause the voltage profile to collapse. With two protection devices in series on any feeder (e.g. substation protection and recloser downstream), one can now activate the ZSC on both protections and set *the substation protection to be instantaneous, i.e. faster than the recloser for the first fault.* With the recloser on 2F-2D and the substation on 1F-2D the substation busbar disruption and quality of supply distortions are optimally minimised (a price is paid in terms of customer disruption on the faulted feeder between the substation and the recloser). For a fault downstream of the recloser the substation protection will immediately disconnect the faulted

feeder thus preserving the node, the ZSC feature will move the recloser to its second shot in the sequence, and on reclosure of the substation breaker the recloser will retain a fast operation for further faults occurring during the reset time.

Cold Load Pick-up   The only constraint that *necessitates* the placement of a downstream protection device (e.g. recloser) is that of overcurrent sensitivity (not considering the gains due to selectivity in network sectionalising, etc.) - when your upstream protection cannot sense a feeder-end fault an intermediate protection stage must be introduced. The sensitivity setting of the overcurrent elements is thus directly relevant. As I have introduced fast tripping upstream, it is clear that the pick-up value must either be set high enough so that it does not operate under load pick-up (motor inrush, thermostatically controlled loads, etc.) or a feature must be introduced that recognise the cold-load condition. A two staged cold-load pick-up activated from a manual/supervisory close instruction desensitises the pick-up setting from 120% to 250% (of the line 90°C thermal current limit) while introducing a 3 - 6 cycle time delay. The desensitised pick-up accounts for sustained cold-load pick-up (households, thermostatically controlled loads) that may last for minutes, while the short time delay allows the modified function to restrain for the motor inrush currents which are typically of short duration on rural systems. The original function is blocked for a pre-set period after which the device reverts to the original, sensitive settings.

The One-and-Only Section Fuse   This brings the discussion to the one and only application of fuse-fuse co-ordination that *is* acceptable. Consider that I have suggested a single fuse level approach - anything else have a severely negative impact on quality of supply and supply continuity due to fuses co-ordinating only at low current levels. Also keep in mind that the sensitivity of the upstream device is dependent on the load in order not to give spurious operation. Now one may have the scenario where the upstream device is suitably insensitive to load, but that its "reach" in terms of fault detection does not overlap with the protection zone of the single fuse level - a blind zone exists between the end of the overcurrent element reach and the single fuse level. This is the only acceptable fuse-fuse application as the fault currents will typically fall within the range of acceptable co-ordination. It was for this reason that more than one element rating was retained and the K-type element selected as standard - D-type elements may give transient insensitivity but cannot be co-ordinated (same characteristic from about 100 Ampere upwards).

5   CONCLUSION

The ideas forwarded in this paper highlight the fact that an integrated approach towards the power system is essential in order to optimise the application of protection devices. Further investigation may be directed at how earth fault conditions evolve if kept on the power system for a long duration.

Medium Voltage Rural Distribution Line Protection

Kevin Miller   Charles Dingley

Department of Electrical Engineering, University of Cape Town

ABSTRACT

At present, Eskom have no national standard or guideline for the equipping of protection equipment on medium voltage rural distribution lines. Such a standard is necessary if depot staff are to move away from an "ad hoc" approach, to a more uniform national approach. The main conclusion reached, is that a national standard is not the best solution given the vastly differing conditions in different areas. A better approach is to implement a national guideline that staff can follow, while applying experience pertinent to their specific area.

1. INTRODUCTION

There are no national standards or guidelines for the selection and equipping of switchgear on rural lines and on the appropriate expenditure thereon. The paper investigates this, based on the findings of a final year thesis project[6]. The paper is based on the following research: a literature survey, visits to various equipment manufacturers, visits to four different distributors in South Africa, contact with four overseas distributors and an analysis of a rural line in the Western Cape.

The paper goes on to examine the following: protection equipment (with special emphasis on auto-reclosers), overseas practice, South African practice and cost and necessity of protection.

2. PROTECTION EQUIPMENT

When considering rural line protection equipment, there are five main types to choose from. They are: Automatic- reclosers, Sectionalisers, Fuses, Circuit breakers & associated relays and Surge arrestors.

An automatic-recloser (AR) is a circuit breaker that can sense overcurrent, time and interrupt overcurrent and re-energise the line. It is capable of tripping and reclosing a line a number of times to give a transient fault a chance to clear. If it doesn't, the AR locks out (remains open).

A sectionaliser is a device that automatically isolates faulty sections of a line from the rest of the system. They are used in place of fuses, and like reclosers can attempt a number of recloses before lockout. The difference is that they cannot interrupt fault current (as AR's can).

Fuses are the oldest protection device available in any application. A fuse contains a piece of wire which melts from the passage of overcurrent, and so isolates the system.

The circuit breaker is similar to the AR, but must have external relays connected to it, for example - comprehensive feeder protection and auto-reclose.

Surge-Arrestors protect the system from overvoltages caused mainly by lightning strikes or switching surges.

3. SURVEY OF PRACTICE IN FOUR OTHER COUNTRIES

The four countries examined in the project are : France, Northern-England, New-Zealand and Australia.

Northern Electric in England have extensive 20 and 11kV networks. Reclosers protect important spurs (for example dairy farmers), and fuses have traditionally been used as sectionalising devices. On the 20kV system mixed solid and fused policies have been implemented, while on the 11kV system a variable fuse size is the standard. Group fusing has been disregarded due to transient lightning. Northern Electric want to make the move to sectionalisers but are constrained by co-ordination problems. Overall experience at Northern Electric suggests[1] that a uniform policy may not be the most effective solution to rural protection. Rather, a mixed solid -fused system should be used constrained by geography, line performance, weather and load demand.

Electricite de France cover the needs of some 5.5 million rural people. According to Tellier[2], some 75% of faults are transient while 10% are semi-permanent. Because of these high figures, reclosers are extensively used. Sectionalisers are installed on a number of line branches, those identified as being most at risk to permanent faults. All overhead lines are protected by spark-gaps, especially at substations and pole mounted reclosers or sectionalisers.

Mercury Energy is a utility on New Zealand's North Island[3]. Substations are protected by circuit breakers and auto-reclosing relays, with multiple-shot reclosing. Reclosers are installed at main break points or points to which bulk groups of consumers are attached. Sectionalisers are installed at a few remote load points that have "important" customers attached to them, for example sheep and dairy farmers. Fuses are only used to protect the high voltage side of distribution transformers and nowhere else. As an example, on Waiheke Island, approximately 2000 customers are connected per substation breaker, 700 per recloser and 300 per sectionaliser.

South West Power is a utility that services South West Queensland[4]. Reclosers protect distribution lines, while circuit breakers and relays protect the substation. Single phase reclosers protect SWER lines. Sectionalisers are used, but their use is constrained by cost.

As can be seen, all of the four utilities have similar standards and practices, but are constrained by factors such as climate and "importance of customer". Importance of customer is not an easy concept to quantify and it is used loosely here.

4. SURVEY OF PRACTICE IN FOUR SOUTH AFRICAN REGIONS

The four regions examined in the project are : Western Cape, Eastern Cape, Natal and Northern Province.

In the Western Cape[Boland], reclosers and sectionalisers are positioned very much on an "ad hoc" basis. Depot staff use their operating experience and place equipment, for example, on feeders having the worst performance records. Section fuses and transformer fuses are used extensively, and are chosen using a derating factor of 1.6. Given that the Western Cape has the lowest lightning strike rate[5](0-1 flashes per km^2 per year) in the country, and with minimal fuse blowing due to weather and other causes[6], Eskom are keen to convert to a solid system.

In the Eastern Cape, reclosers protect no fewer than 100 customers to justify cost in terms of load usage. Other criterion include quality of supply, climatic conditions and "importance of customer". Sectionalisers are installed for no less than 50 customers, with the same secondary criteria as above. Fusing policy is similar to the Western Cape with Eskom in favour of a solid system, but this must be weighed against larger blocks of customers having outages during permanent faults.

Natal have some of the lowest fault levels in the country - some 80% are lower than 800A[6]. This has led to a relatively high usage of reclosers in the past as co-ordination problems arise. They have however been used where sectionalisers would have sufficed. This must be moved away from given that a sectionaliser costs one third of a recloser. AR's are installed at the head of the backbone with a second or third one in line as the fault level drops off. Other criteria, as in other provinces include environment, line length, climate, and operating history. An interesting statistic is that some 76% of faults are cleared after 1 reclose attempt[6]. This shows the acceptable quality of supply that a recloser can deliver. Sectionalisers are installed towards the end of secondary lines and there are no fuses on the Natal system due mainly to the high lightning strike rate[5] (12-14 flashes per km^2 per year).

The Northern Province, has the highest fault levels in the country - some 80% higher than 4000A. Reclosers and sectionalisers are placed according to the same criteria as in the other three provinces. The only difference is that certain makes of recloser and sectionaliser don't have the capacity to interrupt faults in excess of 9kA.

5. COST AND NECESSITY OF PROTECTION

The main questions being asked with rural protection are with regard to reclosers, sectionalisers and fuses.

The cost of a recloser is about R 90 000 while the cost of a sectionaliser is about R 50 000, both with radio control. A fuse cut-out costs R 230 while the link costs R 6.

Is it really necessary to protect rural lines with fuses and reclosers or sectionalisers and reclosers? Can't we in fact do away with all protection except for the substation breaker (which could be a recloser)? This is especially true since 80% of faults are transient in nature.[7] In theory yes, if the line is short enough and is not prone to too many permanent faults per year. A good example[6] is a feeder in the Western Cape where only one lockout (and hence permanent fault) occurred in a two and a half year period. For transient faults, the recloser at the substation recloses in milliseconds so an acceptable quality of supply would be maintained. The obvious downside to this is that for the one permanent fault, the whole of the feeder with be down while repairs take place. But since this happens so rarely, it's justified in terms of what would have been spent in protecting the line downstream with sectionalisers or fuses - R 50000 per sectionaliser and R 500 to replace every fuse that blows.

This approach would not suffice in Natal, where the lightning strike rate is high and the lines are up to 200km in length. The fault impedance becomes so large towards the end of the line that the substation protection has difficulty distinguishing between fault current there and load current at the substation. So the use of a second or third in-line recloser is necessary (for long lines). The second recloser would be placed halfway down the line, so that for the 50% of faults occurring downstream from it the customers upstream will still have supply.

6. CONCLUSIONS

Protecting rural lines in a country with such diverse conditions as South Africa is no easy task. Given the widely varying conditions, it is felt that a rural protection standard or policy would not work. A far better approach is to set a national guideline that would allow depot staff to follow a central theme while using their invaluable operating experience in their particular area.

The most relevant factors that depot staff have to weigh up and that may not easily be standardised are as follows : climatic conditions, fault level, fauna and flora, "importance of customer, line length, operating history, personal preferences and safety.

REFERENCES

1. Gardiner, M. 'The protection of the overhead system in Northern Electric'. *Power Engineering Journal*, JAN 1992, page 16.

2. Tellier, R. 'French distribution systems : basic features and practices'. *IEE Proceedings*, Vol 133, part C, No 7, NOV 1986, page 379.

3. Gibbons, R. 'Mercury Energy system protection practice'. General manager network, Mercury Electric, *Personal correspondence*, 28 AUG 1995.

4. Brennan, P. 'Distribution line protection'. Manager development & engineering services, SWQEB, *Personal correspondence*, 24 AUG 1995.

5. SAIEE. 'Lightning ground flash density : 1975-1986'. *Insulation co-ordination of unshielded distribution lines from 1kV to 36kV.*

6. Miller, K. 'An investigation into medium voltage rural distribution line protection : 11 or 22kV'. *Final year thesis project in the department of Electrical Engineering at the university of Cape Town, 1995.*

7. Money, S, Harris,J. 'Autoreclosing switchgear in distribution practice'. *IEE Proceedings*, Vol 115, No2, FEB 1968.

PROTECTING TWO OR MORE TRANSFORMERS BY AN HV BANK BREAKER ARRANGEMENT UTILISING MOTORISED ISOLATORS - THE COST EFFECTIVE OPTION

Johan Mostert, Senior Design Technician   Izak van der Merwe, Engineer

Eskom, Cape Distributor

SYNOPSIS

With the trend of electrification towards supplying as many customers as possible, in urban and rural areas, the emphasis has been placed on reducing the cost per connection while still maintaining an acceptable level of availability of supply to the customer. The design requirements for cost savings in automatic transformer fault clearance and remote control was identified. These design requirements are particularly relevant to remote farming communities where the substation is situated in an area which is difficult to reach at night time and during storms, which is when most non-permanent faults occur. This paper considers all aspects of protection and control for such a substation.

1.   INTRODUCTION

The main objective of the scheme described below is to utilise motorised isolators (MI) and an HV breaker for isolating one or more transformers under normal and fault conditions. No protection functionality is sacrificed whilst remote control is maintained. Cost savings are achieved.

2.   APPLICATION

This supply arrangement may be applied where a firm supply is deemed non-essential, i.e. in urban electrification, rural reticulation feeders, small towns and existing single transformer substations where a second transformer is needed. (The definition of non-firm supply, in the context of this paper, is where the customer might have a short supply interrruption during fault conditions after which supply is restored). Therefore it becomes acceptable to clear a fault on one transformer by tripping all transformers in the bank, disconnecting the faulty one and then restoring supply. It is proposed that this type of scheme be used with transformers with a rating of up to 10 MVA. However, in theory it may be

applied to any size transformer provided that it is not a firm supply.

Under certain conditions, the MI's may be used to do on-load switching during maintenance without loss of supply to the customer. This is dependent on the physical dimensions of the isolators (distance between phases when isolator is open) and the arc length during opening of the isolator. The arc length is dependent on the current (load or magnetising) that must be interrupted as well as the voltage at which this occurs.[1]

3.   PROTECTION

Standard transformer protection philosophies may be applied and should be determined by the size and importance of the transformer. In all cases it is preferable to use bushing CT's. The scheme as presented is preferably for a star-delta connected transformer with NEC. It consists of HV restricted earth fault (REF), HV IDMTL and high set overcurrent (O/C), LV IDMTL earth fault (E/F) and all transformer/NEC/NER/AUX protection (e.g. Buchholz, temperature, pressure etc.). However, this could be expanded to the following:

- for a star-star transformer with HV solidly earthed and LV earthed with/without NER it is proposed to use HV REF, LV REF, HV IDMTL and high set O/C, LV IDMTL E/F and all transformer associated protection;
- for a star-star transformer with HV unearthed and LV earthed with/without NER it is proposed to use HV balanced E/F (still using a REF relay without the neutral CT connection), LV REF, HV IDMTL and high set O/C, LV IDMTL E/F and all transformer associated protection;
- for a delta-star transformer and LV earthed with/without NER it is proposed to use HV balanced E/F

(still using a REF relay without the neutral CT connection), LV REF, HV IDMTL and high set O/C, LV IDMTL E/F and all transformer associated protection.

A transformer fault is defined to be such a fault that causes one or more of the following protection functions to operate:

- transformer protection such as Buchholz, oil temperature, pressure etc.
- HV or LV REF
- HV high set O/C

All other protection functions such as HV IDMTL O/C and LV IDMTL E/F act as back-up protection for the MV feeder protection. Winding temperature acts as overload protection for the transformer.

4.   SCHEME LOGIC

As shown in Figure 1 all the substation transformers are to be supplied through one HV circuit breaker and have no MV circuit breaker(s). Each transformer has its own HV and MV MI's.

For a transformer fault, the HV bank breaker will be tripped, the HV and MV MI's of the faulty transformer will be opened and the bank breaker reclosed automatically. If there is a possibility of infeed from the MV feeders during a transformer fault, the HV bank breaker and all MV feeder breakers will be tripped, the HV and MV MI's of the faulty transformer will be opened and the bank breaker as well as the MV feeder breakers reclosed. The process will be fully automatic and the delay in restoration of supply to the customers will be determined by the dead time of the scheme.

The dead time of the scheme is the total time determined by the opening time of the MI's plus a safety margin of the same

---

duration. Manufacturers specify that a MI will open in ±15 seconds, therefore the dead time of the scheme is 30 seconds

which is also the time of the supply disruption.
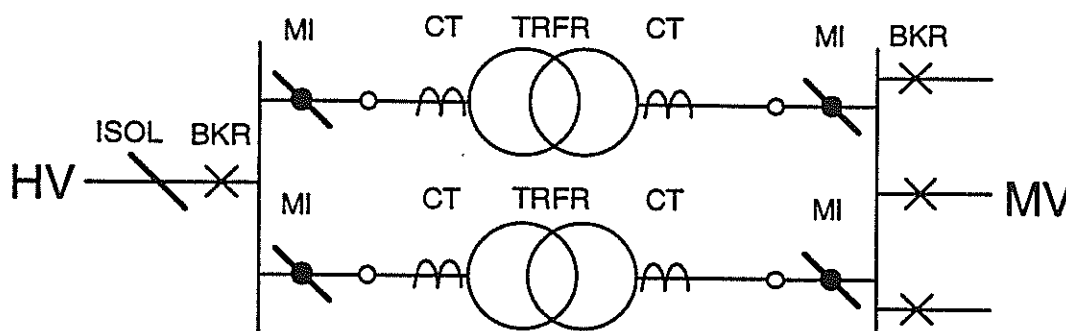
Figure 1   Single line diagram of a two transformer substation with an HV bank breaker

An MV fault would result in an almost equal sharing of fault current by the transformers. Due to the sharing being not quite equal, CT ratio errors, relay timing errors and breaker trip times not being equal, it is probable that one of the transformer's IDMTL O/C or E/F protection would operate before the other and temporarily remove the fault by tripping the HV bank breaker and the relevant MV MI. On reclosing, the fault would be fed by the remaining transformer(s) requiring a further trip and reclose of the bank breaker. To avoid multiple closing onto a fault it is deemed preferable to open all MV MI's for any single IDMTL O/C or E/F protection operation.

If an IDMTL O/C or E/F trip occurs on a transformer, the HV bank breaker will be tripped and the MV MI's of both transformers will be opened. The HV bank breaker will be reclosed after the dead time of the scheme restoring auxiliary supply to the substation. If the fault is a permanent one between the MV CT's and the MV MI of the transformer, the bank breaker will again be tripped,

the HV MI of the faulty transformer circuit will be opened and the bank breaker reclosed, restoring auxiliary supply.

In the case of a winding temperature trip affecting only one transformer, the bank breaker will be tripped, the MV MI of the affected transformer will be opened and the bank breaker reclosed. Supply to the customers will be restored via the healthy transformer(s).

Remote supervisory control on all isolators and circuit breakers (HV and MV feeders) is provided. All transformer trips and alarms are flagged locally as well as remotely via the Telecommunication system.

Interlocks are included in the scheme to prevent the MI from interrupting fault current. Breaker interlocks to prevent manual or remote opening/closing of the isolators are optional depending on whether on-load switching is permissible . In the event of a MI not opening on issuing of an open command to that MI, restoration of supply will not be initiated and the bank breaker will remain open.

---

96   SOUTH AFRICAN UNIVERSITIES POWER ENGINEERING CONFERENCE '96

The closing interlocks of the different transformer modules are connected such that conditions at each transformer must be suitable to allow automatic closing of the bank breaker.

Standard circulating current or master/follower on-load tap changing schemes may be applied to provide a degree of voltage regulation.

5.   MODULARITY

The scheme is fully modular in that any number of transformer protection schemes may be added without any loss of functionality.   The scheme typically consists of two basic modules. The first module comprises protection and MI controls for a transformer and the controls for the bank breaker. Local and remote alarms are also provided. The second (or more) module(s) consists of the second (or more) transformer's protection, its MI controls and local/remote alarms.   Each transformer has its own module but trips the same bank breaker.

6.   CONCLUSIONS

Disadvantages
- this is a non-firm supply arrangement;
- for a transformer fault the supply will be disrupted for the scheme dead time;
- the bank breaker must be tripped for manual isolation of one transformer where it is not possible to operate the MI's to interrupt the transformer magnetising or load current.   The supply will be interrupted for the time it takes to manually isolate the transformer and to restore supply to the remaining transformer;
- four isolators must be motorised.

Advantages
- cost savings are obtained because only one HV and no MV circuit breakers are used with this arrangement;
- the percentage cost saving increases dramatically for every transformer added to the scheme;
- less primary equipment to maintain;
- very little protection functionality is lost;
- future planning/design of a substation may be done using this arrangement with only one transformer. Expansion of the substation may easily be realised by adding the protection/control module of the new transformer;
- all interlocks are obtained with bank breaker and MI auxilliary contacts which are available, no other hardware is needed.

References

[1]   Alan Ware, "Recommended Limits of Current Levels for Permitting Interruption by Disconnectors", Technology Report, Cape Distributor, (report available on request).

Izak van der Merwe, PTM & C, Eskom, P.O. Box 222, Brackenfell, 7560
Tel. no: (021) 980-3187
Fax no: (021) 981-8957
E_mail:
IZAKVDM@BKLNFS01.ESKOM.CO.ZA

Johan Mostert, Izak van der Merwe   4 of 4

CURRENT TRANSFORMER DYNAMIC PERFORMANCES
UNDER FAULT CONDITIONS

N. Chuthi   S. Darie

University Of Cape Town, Department of Electrical Engineering

ABSTRACT

Over the past years, many papers have been written on steady state performance of current transformers and therefore their steady state behaviour is a well-known phenomenon. However very little has been written on transient performance or when tackled, the subject is not covered fully.

This paper present results of simulations carried out on a current transformer. The CT was modelled by using electromagnetic transient program (EMTP). EMTP has grown to be the most widely used program in power system transient studies over the years. A detailed EMTP current transformer (CT) model has been presented. Pure resistive, inductive and capacitive burdens were used in the simulations.

Keywords: Current Transformer, CT Transient Response, EMTP

INTRODUCTION

Dynamic performance of CTs become rather complicated when core saturation is taken into consideration. Non-symmetrical waves due to faults in a power system worsen CT performance during transient periods.[1,2] This is due to the presence of an exponentially decreasing direct current in the first few cycles after fault occurrence. EMTP has in built tools like saturable transformer, non-linear inductors (type 96 and 98) which were used to model saturation effects. Type 98 element does not account for hysteresis effects while type 96 does.

MODEL DESCRIPTION

Figure 1 shows the single phase power transformer model available in EMTP. This model comprises of an equivalent circuit built around an ideal transformer.

The magnetisation branch is represented internally as a non linear inductor whose flux linkage to current (λ - I) characteristics is specified by the user. Since λ - I characteristics are not readily available, EMTP provides an auxiliary routine CONVERT which convert the more commonly

V_{rms} - I_{rms} characteristics which are usually provided by manufacturers.
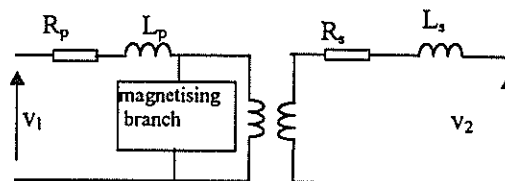
ideal tx

Figure 1
single phase saturable transformer
model in EMTP

In the model used in this paper, all parameters are transferred to the secondary side of CT. An equivalent way of modelling the CT with parameters referred to the secondary side was achieved by explicitly using Type 96 or 98 non-linear elements together with the above described saturable transformer model. In this case, the magnetisation branch was purposely made dormant in the saturable transformer model. Values of primary and secondary resistance and leakage inductance were made very small (1.0E-5) in the saturable transformer model to avoid singularity in program matrix.[3,4]

Pure resistance, inductance and capacitance were used as burdens (Z_b). This was done in order to model the worst possible scenarios as discussed by Arthur Wright.[5]

Modelling of magnetisation flux was achieved by placing an RC integrator across magnetisation branch and measuring voltage across the capacitor (flux linked = $1/(1 + RCs)$. In this case, $RC \geq 1$ to achieve results reasonably close to an ideal integration. To provide correct scaling for V_c and obtain correct value of flux linkage, a value of R = 100 kΩ and C = 10 μF were successfully used for RC = 1. In this case V_c equals the flux linked and therefore no scaling was required.

Figure 2 shows the diagram of the model described above
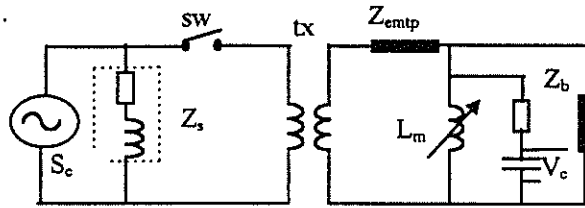
Figure 2
current transformer EMTP model

where:

S_c =   fault current
Z_s =   system impedance
Sw =   switch required by EMTP to
          model offset at time of fault.
tx =   saturable transformer
Z_{emtp} = impedance required by EMTP
L_m =   non-linear magnetisation branch
V_c =   voltage across capacitor. (measuring
          of magnetising flux)
V_b =   impedance burden

CT DATA

Ratio:	2000/5
Class:	C800
Burden (VA)	200
Insulation	138 kV

MODEL LIMITATIONS

- In this model no capacitances (stray and inter-turn) are included.
- The hysteresis loop employed in the model is valid only for ARMCO M4 oriental steel with no air gap.
- Power system harmonics have been neglected in the current source.
- Since pure burdens have been used, effects of transformer resistance and leakage reactance have been neglected in some simulations.

RESULTS

A fully offset fault current of 100 kA was used. A rated burden of 8 Ω was used. Other multiples of the burden i.e. (1, 0.5, 0.4, 0.2 and 0.1) were used.

Figures 3 to 5 show output currents   at rated burden.

The value of fault current used for capacitive burden model was reduced to 1000 A.

Figures 6 to 8 show excitation currents in the different cases considered in figures 3 to 5.

Figures 9 to 11 show output current, excitation current and magnetisation flux respectively for a capacitive burden of 4 Ω.
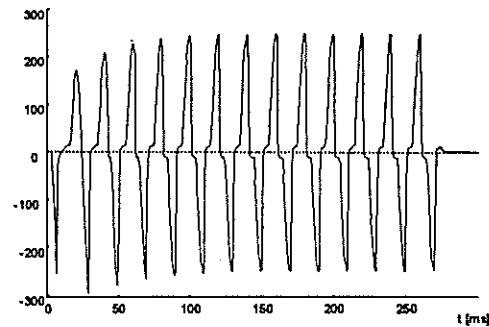
Figure 3
Current output in resistive burden
of 8 Ohms.
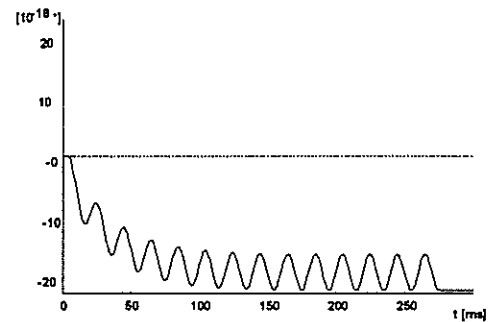
Figure 4
Current output in an inductive burden
of 8 Ohms.
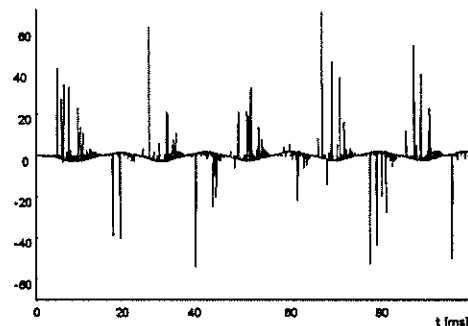
Figure 5
Current output in a capacitive burden of
8 Ohms. Fault current 1000 A.
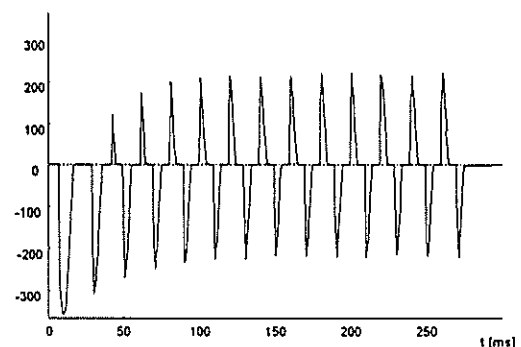
Figure 6
Excitation current for resistive burden
of 8 Ohms.
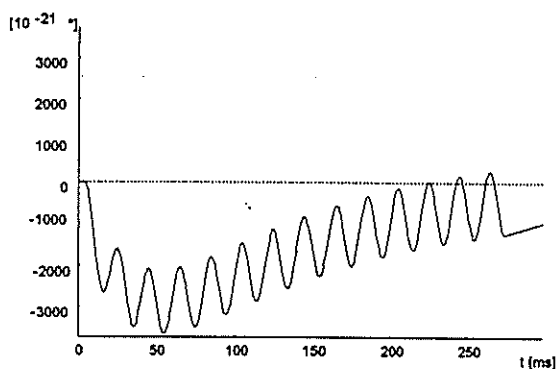
Figure 7
Excitation current for inductive burden
of 8 Ohms.
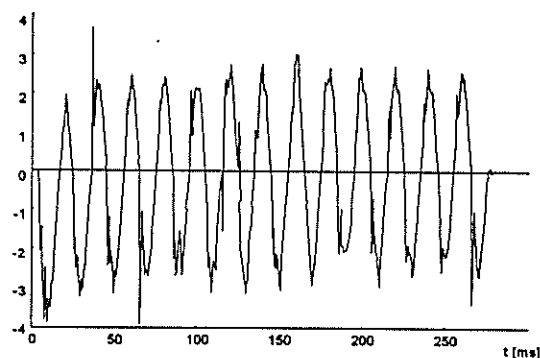
Figure 10
Excitation current for capacitive burden
of 4 Ohms. Fault current 1000 A
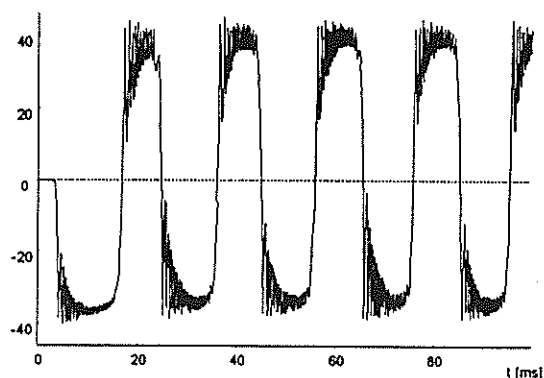
Figure 8
Magnetisation flux for capacitive burden of 8
Ohms. Fault current 1000 A.
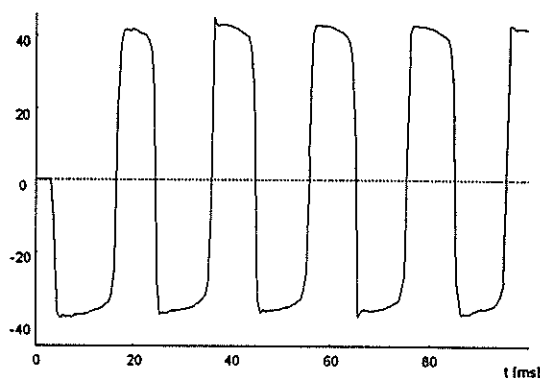
Figure 11
Magnetisation flux for capacitive burden
of 4 Ohms.
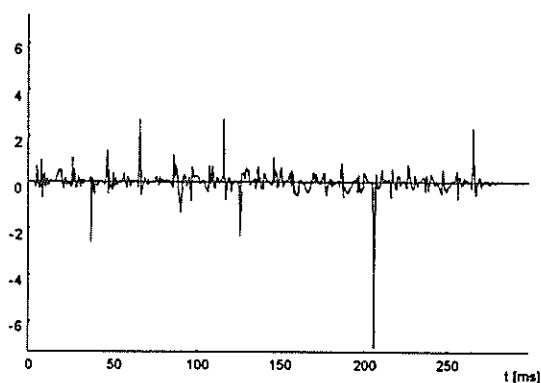
Figure 9
Current output in capacitive burden
of 4 Ohms
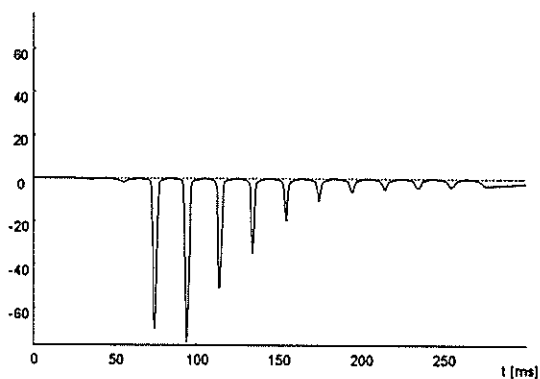
Figure 12
Excitation current for resistive burden
of 0.8 Ohms

DISCUSSION

In resistive burden, decreasing the resistor value while keeping fault current constant decrease saturation effects. Magnetising flux curves become more sinusoidal as resistance values reduce. Figure 6 and 12 show that reducing the resistance value increased time taken for by CT to reach saturation.[6

In inductive burden, as the burden value was reduced , output current in the burden does not change in shape. What changes is it's offset magnitude only. The shape of burden current wave and that of magnetisation flux were similar at full and half burden. This can be due to the fact that current divides proportionally as both branches are inductive. Saturation reduced quickest with inductive burden. This might not be true when harmonics are considered, however harmonics discussion is beyond the scope of this paper.

For capacitive burden, the value of fault current had to be reduced drastically to 1000 A as EMTP could not handle simulations with 100 kA since results became abnormally big. Even with a fault current of 1000 A which was smaller than the rated primary current of CT, the output current had a lot of harmonic content as seen in figure 5. Reducing the capacitive impedance changed the output current's shape. The shape of current wave were different therefore it can be concluded that the shape can not be predetermined in capacitive loads. However, as the impedance was reduced the outputs became less distorted i.e. saturation effects reduced. The shapes of magnetisation flux were similar to those of resistive load, the only difference being presence of a lot of harmonic pollution in capacitive loads. The pollution reduced as the values of burden were reduced. The excitation current was almost identical to the output current in the burden. The only difference was that they were 180 degrees out of phase. This was only true for 8 ohm burden. The shape of excitation current became more identical to those in inductive burden as the capacitive burden was reduced.

CONCLUSIONS

EMTP CT model was successfully used in transient dynamic performance modelling. It has been observed that output current from a capacitive burden is not easily predetermined. Capacitance values should be very high if they are to be used to avoid premature saturation. DC component in the transient period worsen performance of current transformers.[7,8]

REFERENCES

1. Working Group of Relay Input Sources Subcommittee, Transient Response of Current Transformers, IEEE Transactions on Power Apparatus and Systems, Vol. PAS-96 No. 2 November/December 1977 pp 1809-1814

2. J Linders, C.W. Barnett, Relay performance consideration with low ratio CT's and high fault currents, IEEE Transaction on industry applications Vol. 31 No. 2 March/April 1995 pp 392-404

3. H.W. Dommel , Electromagnetic Transient Program Reference Manual (EMTP Theory Book), 1986.

4. EMTP - ATP rule book, 1987.

5. A. Wright, Current Transformer , their transient and steady state performance. Chapman and Hall, 1968.

6. A. Chaudhary, Protection system presentation in the electromagnetic transient program, IEEE Transactions on Power Delivery, Vol. 9, No. 2, April 1994 pp 700 -708

7. Kezunovic, C.W. Fromen and F. Phillips, Experimental evaluation of EMTP based current Transformer models for protective relay transient study. IEEE Transaction on Power delivery, Vol. 9 No, 1, November 1994 pp 405- 413

8. E.C. Wentz and W.K. Sonnemenn, Current transformers and relays for high speed Differential Protection, with Particular Reference to Offset Transient currents, AIEE Transactions , August 1940, Vol. 59 pp 481 - 488.

Address: Noel Chuthi, Department of Electrical Engineering, University of Cape Town, Private Bag, Rondebosch, 7700.
Email: Nchuthi@eleceng.uct.za.ac

Single- to Three-phase Converter for Induction Motors

R.J. Cruise and C.F. Landy

The University of the Witwatersrand, Johannesburg.

Abstract: *The rapid extension of the electricity grid and the supply of fresh drinking water is crucial for the welfare and development of the Southern African region. Supplying three-phase power to rural communities is not always an economically viable option and consequently many rural areas are and will be supplied from single-phase lines. Single-phase supply is adequate for many domestic applications, however there are many water pumping, agricultural and light industry applications that require the use of three-phase motors. A comparison between the various types of phase converters is made and each one's suitability to rural applications is discussed. Phase converters are used to convert a single-phase supply to a fully balanced three-phase supply, however, the high material and manufacturing costs of these phase converters have rendered them impractical for rural applications. To overcome this problem, a component minimised phase converter has been proposed as one solution for operating three-phase motors off a single-phase supply. Due to the reduced number of power electronic components, the phase converter is considerably cheaper than other phase conversion schemes and is therefore ideally suited for many rural applications.*

1. INTRODUCTION

Rural communities do not have many of the facilities enjoyed by their urban counter-parts. This is due to the fact that the provision of amenities to a wide, sparsely populated area is not always an economically viable option. However, these communities need to have access to clean water and electricity in order to improve their primary health care and to conserve the natural environment.

The South African Government of National Unity has fully committed itself to *the Reconstruction and Development Program (RDP)*. The RDP essentially aims at improving the living conditions and primary health care facilities of the under-privileged of South Africa. The provision of electricity and fresh drinking water is essential for the welfare and development of these underdeveloped communities. Consequently, there has been a rapid extension of the electricity grid and many rural areas are now supplied by single-

phase lines. Unfortunately, up till now the supply of fresh drinking water has been a more difficult task to achieve.

If a three-phase motor could be run off a single-phase line, many of the problems experienced with supplying fresh drinking water could be eradicated. Also many farming and light industrial applications could be mechanised. Thus the need arises for a cost effective single- to three-phase power converter.

2. REVIEW OF PHASE CONVERTERS

2.1 History and Background Theory

The advantages of using the combination of a three-phase motor and a phase converter rather than a single-phase motor was first presented by Habermann[1] back in 1954. Since then there has been a great deal of research into the finding the most economical and efficient phase conversion scheme to run three-phase motors off single-phase supplies. Three-phase motors are generally more efficient, less expensive, more reliable and more readily available than their single-phase counter-parts[2]. Single-phase motors also have inferior starting characteristics and consequently less demand is placed on the supply when a phase converter is used in conjunction with a three-phase motor than when a single-phase motor is used on its own. Thus the combined phase-converter three-phase motor outperforms it's single-phase counter-part, but the question remains which phase-conversion scheme is the cheapest and most efficient?

2.2 Capacitor Phase-shift Converters

Habermann[3] and Brown et al[4] proposed a rather simple but effective scheme of running a three phase motor off a single phase supply by simply connecting a capacitor within the third line (*Figure 1*).
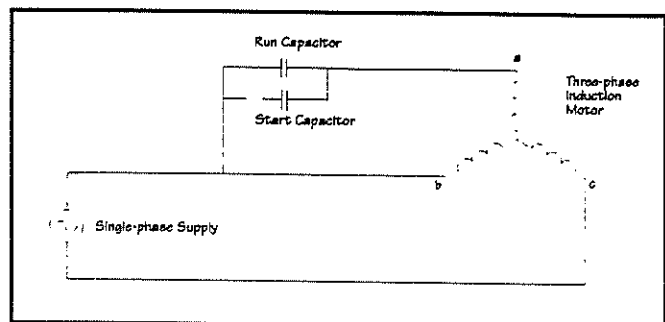
Figure 1: Capacitor phase-shift static converter

The capacitor, being a static element, has no way of controlling the phase angle or output voltage and thus cannot achieve perfect balanced operation particularly when the power factor angle is less than 60°. Unfortunately, this usually occurs within the normal operating range of an induction motor. The motor hence must be substantially de-rated[2]. Some designs[5] have tried to overcome this problem by including more static elements and switches, but the addition of more elements increases the cost of the device and the performance, although greatly improved, is still not satisfactory. Another approach is to include an autotransformer[6] (*Figure 2*). This configuration is a far better converter for maintaining voltage and current balance, but the addition of the autotransformer increases the material cost of the device.
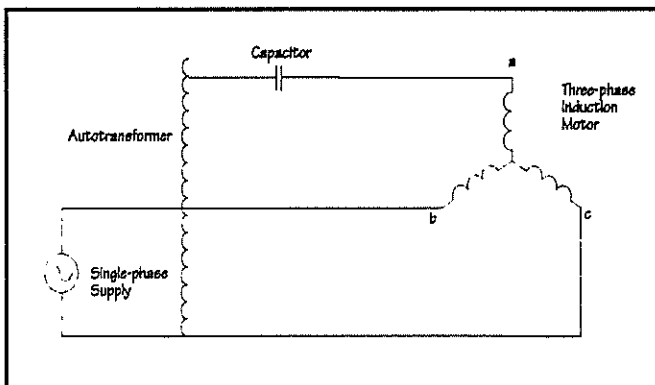
Figure 2: Auto-adjust static phase-shift converter

2.3 Specially Wound Motors

Goodarzi et al[7] proposes a new two phase inverter-fed induction motor with two pairs of bifilar wound stator windings. The problem with this type of arrangement is that special windings and hence specially designed motors need to be used. The employment of non-standard motors greatly increases the cost of the system.

2.4 Forced Commutated Cycloconverters
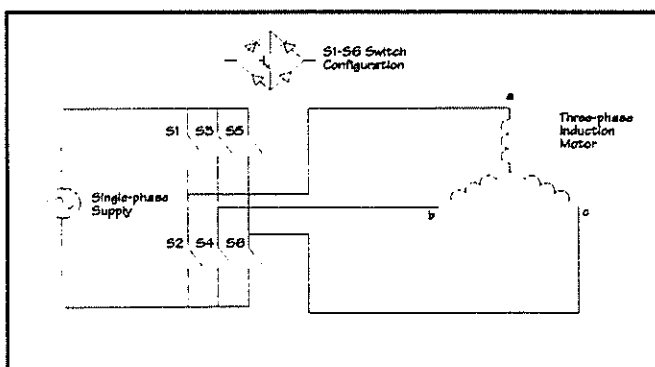
Figure 3: Cycloconverter Phase Converter

This approach utilises the direct cycloconversion principles and its implementation requires the use of

solid state switches only[8] (*Figure 3*). The cycloconverter can provide constant V/Hz speed control, however the output voltages contain a large third harmonic component and the maximum output voltage that can be generated is only 55 percent of the input voltage. A step-up transformer can be used to overcome this problem, however, the transformer and the large number of power electronic devices makes the system very expensive to implement.

2.5 Conventional DC Link Converters

Similar to the cycloconverter, these converters can generate any voltage and frequency on the output using *pulse width modulation* (PWM) techniques and with vector control methods they can provide adequate performance of the three-phase induction motor over a wide range of speeds and different load conditions. The topology of a conventional voltage-source inverter with an input current shaping feature is shown in *Figure 4*. The use of seven active power electronic devices and five diodes has an adverse impact on the cost effectiveness of the converter[9].
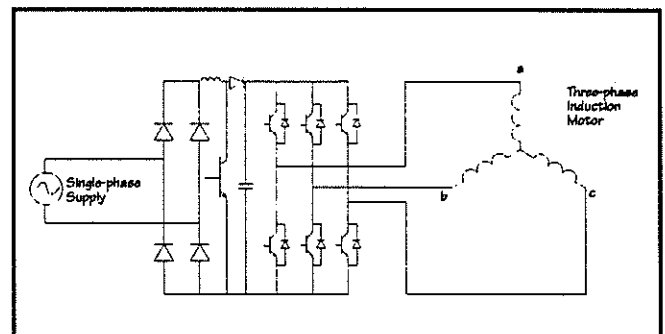
Figure 4: Voltage-fed PWM Inverter with input current shaping

2.6 Two-phase to Three-phase Transformer

This conversion scheme utilises a three phase transformer in conjunction with a reduced sized inverter[10]. The transformer performs two functions - stepping down the voltage; converting the single-phase supply to a balanced three phase supply. The single-phase supply is connected to the two outer limbs of the three-phase transformer in such a way that the current in the outer primary windings do not contribute to the flux linkage of the middle leg. The reduced size (50% smaller) inverter is connected to the winding on the middle leg and is used to create a separate phase. The two separate primary windings are de-coupled and in space quadrature to each other. With this set-up, balanced three-phase voltages can be generated in the secondary winding. The main advantage of the two-phase to three-phase transformer is that it utilises the distribution transformer. However, the disadvantage is that many rural applications still only require a

single-phase and therefore a large portion of the conversion process is unnecessary and/or redundant. Also, the overall rating of the inverter is higher than that of an inverter connected to a single motor and the large material costs of the three-phase transformer must be taken into account.

2.7 Written Pole Motor

The newest and perhaps the most innovative idea for operating machines off a single-phase has been developed by the Precise Power Corporation (Florida, USA)[11]. The *Written Pole Motor* is a special type of synchronous machine, where instead of using permanent magnets, the magnetic poles are continuously and instantaneously 'written' onto a magnetic layer on the rotor by an excitor coil in the stator. The magnetic layer is made from a non-conducting Strontium-Ferrite permanent magnet material. The magnetic poles are written to a different spot (whenever the rotor speed changes) on the rotor during each revolution, keeping the pole pattern at a constant poles per second. A complete sweep of poles from infinity to two is made as the motor runs from standstill to synchronous speed. To add induction torque to starting, a squirrel cage winding is included in the rotor. The written pole motor provides a smooth starting torque and current curve; has a very high inertial capability and a very low starting current. However, the low air-gap flux density (0.35 - 0.4 T) indicates that the written pole motors are relatively large machines (size ratio 2:1 when compared to three-phase induction motor). The high cost of the magnetic layer and the large amount of material needed place the written pole motor into the same price-category as a full-bridge PWM inverter, and therefore the written pole motor, although a novel approach, is by no means suited to rural applications.

3. PROPOSED PHASE CONVERTER TOPOLOGY
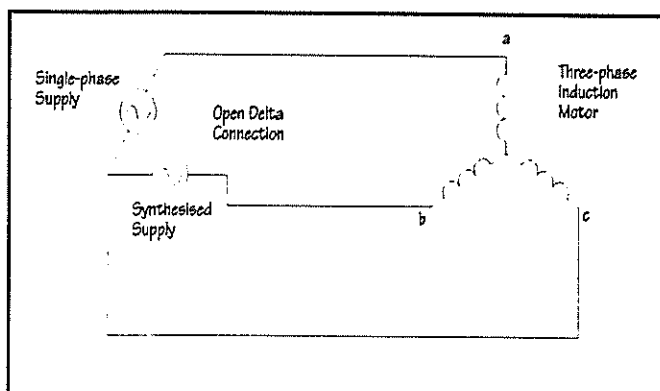
Figure 5: Principle of New Reduced Topology Phase Converter

A new type of static phase converter that uses the single-phase supply directly in conjunction with a

synthesised supply has been proposed[12]. The synthesised supply is displaced by 60° from the single-phase supply and both supplies are connected in an open delta configuration to supply the three-phase load (*Figure 5*). This situation results in an implicit third phase of the supply which can be used to operate three phase loads (*Figure 6*).
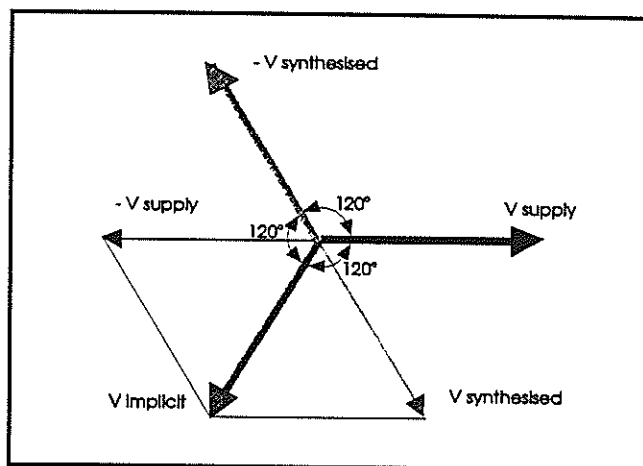
Figure 6: Phasor Diagram of Open-delta Connected Supplies

Using the above principle, a component minimised single-phase to three-phase converter can be built that can generate high-quality output voltages as well as shape the input current[13]. Comparing this reduced topology to the conventional VSI (*Figure 4* and *Figure 7*), it is clear that the number of power electronic elements has been reduced from 7 active and 5 passive devices to 6 active switches. This reduced topology brings down the cost of the converter considerably, making it ideal for rural applications.
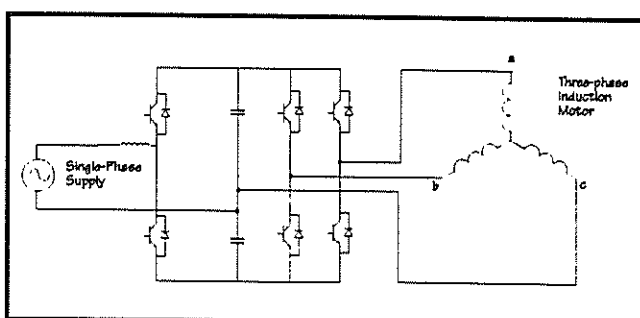
Figure 7: Proposed Component Minimised Phase Converter

4. CONTROL STRATEGY

Careful consideration must be given to the selection of the control strategy as any unbalance between the two phases will show up in the third phase[14], thus the control strategy has to be very accurate. Rotor-flux orientated vector control was selected for this reason. The same vector control techniques used for a six switch three-phase inverter can be employed for the

four switch inverter, the only significant difference being the generation of the reference voltages needed for the PWM switching strategy of the power transistors[15]. The output reference voltages of a vector controller are of the form

$$v_1^* = V_m \cos(\omega t) + \Delta v$$

$$v_2^* = V_m \cos(\omega t - 2\pi/3) + \Delta v$$

$$v_3^* = V_m \cos(\omega t + 2\pi/3) + \Delta v$$

As Δv does not affect the voltage vector in the $\alpha\beta$-plane, subtracting v_3^* from the above equations yields

$$v_1 = v_1^* - v_3^* = V_m \cos(\omega t - \pi/6)$$

$$v_2 = v_2^* - v_3^* = V_m \cos(\omega t - \pi/2)$$

$$v_3 = v_3^* - v_3^* = 0$$

The new reference voltages now have a sinusoidal waveform with the same amplitude but with a phase shift of $\pi/6$. These reference voltages are used to generate the switching waveforms for the four switches on the motor side of the phase converter.

The two switches on the single-phase supply side are also controlled using a PWM switching strategy, where the incoming mains voltage is used as the reference in order to shape the input current to be sinusoidal and to maintain a close to unity power factor[14].

5. COMPUTER SIMULATION

In order to test the effectiveness of the proposed reduced topology phase converter, a program called CASED is being used. CASED stands for Computed Aided Simulation of Electric Drives and is a powerful software tool developed at the University of the Witwatersrand to analyse ac variable speed drive systems. Particular care was taken to develop accurate models of the motor and converter and complete freedom of choice is given as to the converter configuration, firing policy and load characteristics.

Thus the complete system, that is the electrical supply, the phase converter, the induction machine and the motor load can be simulated and its transient response accurately determined. CASED has the facility to implement user defined control models and will therefore be used to simulate the proposed rotor-flux orientated control strategy.

6. FUTURE DEVELOPMENTS

Once an adequate control algorithm has been developed, a prototype model will be constructed to test the overall effectiveness of the system.

However, as the price of power electronic devices gradually drop with increased advancements in manufacturing technology, the use of reduced topology phase converters in conjunction with three-phase motors is becoming an ever increasing option for areas where only a single-phase supply is available. Adequate performance and the relatively low cost of the system indicate that these component minimised phase converters are well-suited to many rural applications. In the Southern African context, phase converters are an important development in providing disadvantaged and rural communities with an economic means of obtaining fresh, running water.

REFERENCES

[1]Habermann, M. Single-phase operation of a 3-phase motor with a simple static phase converter, *AIEE Transactions*, August 1954, pp. 833-837.

[2]Malengret, M. Review and proposed single phase to three phase converter, *Southern African Universities Power Engineering Conference*, Stellenbosch January 1994.

[3]Habermann, M. Single-phase operation of a 3-phase motor with a simple static phase converter, *AIEE Transactions*, August 1954, pp. 833-837.

[4]Brown, J. E. and Jha, C. S. The starting of a 3-phase induction motor connected to a single-phase supply system, *Proceedings of the IEE*, 106 A, April 1959, pp. 183-190.

[5]Tindall, C.E. and Monteith, W. Balanced operation of 3-phase induction motors connected to single-phase supplies, *Proceedings of the IEE*, vol. 123, No. 6, June 1976, pp. 517-522.

[6]Soderholm, L.H. and Hertz, C.M. Automatic balance of three-phase motor currents for variable motor loading using a static phase converter, *IEEE Transactions on IAS*, vol. 26, no. 4, July/August 1990, pp. 679-682.

[7]Goodarzi, G.A., Yang, G., Kawamura, A. and Hoft, R.G. Low cost two phase inverter-induction motor drive and simulation, *IEEE IAS Conference Recordings*, 1985.

[8]Kahn, S.I., Ziogas, P.D. and Rashid, M.H. A novel single to three-phase converter, *IEEE Transactions on IAS*, vol. 25, no. 1, January/February 1989, pp. 142-152.

[9]Nesbitt, J., Chen, C., Divan, D.M. and Novotny, D.W. A novel single phase to three phase converter, *IEEE IAS Conference Recordings*, 1991.

[10]Malengret, M., Naldrett, G. and Enslin, J.H.R Low cost three-phase rural electrification by single-phase to three-phase conversion, *Southern African Universities Power Engineering Conference*, Pretoria January 1995.

[11]Precise Power Corporation, 715 - 60th Street, Court East, Bradenton, FL USA, 34208.

[12]Biswas, S.K. A new static converter for the operation of three-phase motors on single-phase supply, *IEEE IAS Conference Recordings*, 1986.

[13]Enjeti, P.N., Rahman, A. and Jakkli, R. A new single-phase to three-phase converter with active input current shaping for low cost ac motor drives, *IEEE Transactions on Industry Applications*, vol. 29, no. 4, July 1993/1994, pp. 806-813.

[14]van der Broeck, H.W. and van Wyk, J.D. A comparative investigation of a three-phase induction machine drive with a component minimised voltage-fed inverter under different control options, *IEEE Transactions on Industry Applications*, vol. 20, no. 2, March/April 1984.

[15]Jacobina, C.B., da Silva, E.R.C., Lima, A.M.N. and Ribeiro, R.L.A. Vector and scalar control of a four switch three phase inverter, *IEEE IAS Conference Recordings*, 1995.

DEVELOPMENT OF A GENERIC TENSION CONTROL SYSTEM

B D Van Blerk and G Diana

Department of Electrical Engineering, University of Natal, King George V Ave, Durban, 4001, South Africa

ABSTRACT

This paper describes the development of a Generic Tension Control System (GTCS) test bed that is to be used to train people and demonstrate the principles of tension control. In order to correctly size the motors, the associated power electronics and sensors required by the GTCS a system model has to be developed in order to assess the performance and requirements via simulation in SIMULINK. The simulation results are presented and it is shown how the system components were sized.

1. INTRODUCTION

In the rolling industries, such as the paper, steel, aluminium, etc, it is important to maintain the correct tension in the material to achieve both high product quality and production output. Most tension control systems employed in this country are imported and there is very little understanding of the underlying principles. DC drives are employed in most industrial rolling applications as they allow both torque and speed control that are essential to achieve tension control.

In all tension control applications the underlying principles are similar although the manner in which they manifest themselves in specific applications may differ quite markedly. In the steel rolling industry for example the material is changed in shape by rolling it in a manner in which the cross-sectional area is reduced. By the conservation of the volume of the material elongation of the material must occur. Here tension control is used to maintain inter-stand tension so that each stand may roll independently of the stands on either side of it.

As it was not possible to build a steel rolling mill or a hot aluminium mill with the resources available to the project, a paper unwind, rewinder was chosen as it is relatively simple to build and can clearly demonstrate the principles of tension control and how this can be achieved with the use of AC motors.

2. SYSTEM DESCRIPTION

In most paper rolling applications the paper is wound off the unwinder and passes into a process at the line (paper) speed and tension required by the process. The same criterion generally apply to winders where the processed paper is rewound onto a reel. The objective of the control is to maintain tension at a specified line speed. In order to start the simulation process a system description is required with the relevant models for the system.

The paper rewinder being considered for the GTCS test bed system is shown in Fig. 1. The paper is initially on the unwinder and is wound onto the winder. Two three phase vector controlled AC induction motor drives are used to make the AC motors appear as DC motors [1]. The master controller is used to control the speed of the paper and the paper tension using the AC drives as torque controllers. The paper passes under two guide rolls and over a roller that is supported on force transducing bearings to provide the tension feedback required for closed loop tension control.
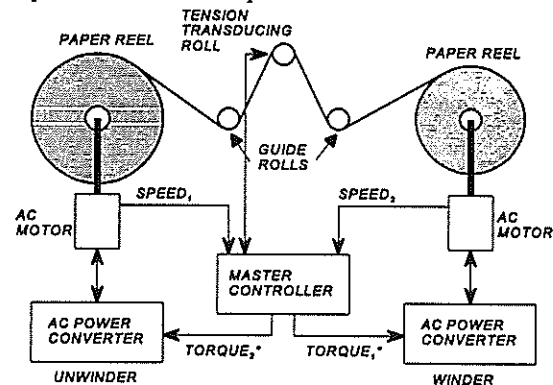
Fig. 1. Generic Tension Control System Test Bed

3. MECHANICAL SYSTEM MODELLING

The standard electrical torque equation for the AC motors appears in eq. 1. The electrical torque consists of an inertia torque, a frictional torque and paper tension torque. As the motor and load are to be directly coupled with a torsionally stiff coupling the motor inertia is lumped together with load inertia as is the frictional resistance of the motor and load. The corresponding differential equation for both the winder and unwinder is therefore:

$$T_e = J_{(R)} * \frac{d^2\theta}{dt^2} + B * \frac{d\theta}{dt} + PT * R \qquad (1)$$

$J_{(R)} = J_{reel} + J_{motor}$ kgm^2 PT = Paper Tension N
$B = B_{reel} + B_{motor}$ Nms^{-1} R = Reel Radius   m
T_e = Electrical Torque Nm θ = Reel Angle   rad

4. PAPER MODEL

Fig. 1 shows that the two reels are connected to one another by the paper . A model of the paper is required to give the desired paper tension as the paper stretched. To achieve this a model of an undamped spring was used for the paper with a fairly large spring constant K as paper is quite stiff. The paper model used is shown in Fig. 2
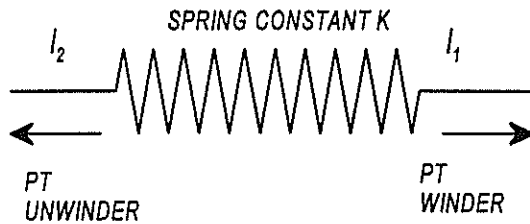
Fig. 2. Paper Spring Model

The equation for the paper model shown in Fig. 2 is thus:

$$PT = K *(l_1 - l_2)   \qquad (2)$$

l_1 = Length of paper wound off winder   m
l_2 = Length of paper wound off unwinder   m
K = Spring constant Nm^{-1}

But since it can be shown that: $l = \theta * R$

$$PT = K *(R_1 * \theta_1 - R_2 * \theta_2)   \qquad (3)$$

R_1 = Radius of paper on winder   m
R_2 = Radius of paper on unwinder   m
θ_1 = Angular displacement of winder   radians
θ_2 = Angular displacement of unwinder   radians

Tension in the paper is thus a function of the difference in the angular displacement of the reels with respect to one another. It could thus be seen as being analogous to the load angle in the synchronous machine.

5. SIMULINK SIMULATION MODEL

The system shown in Fig. 1 comprises four basic elements, namely the winder, unwinder, paper and master controller. In order to arrive at this model, certain underlying assumptions had to be made. The first was that electrical dynamics of the AC motors were assumed to be much faster than the mechanical system so that they could be neglected and a reduced order model of the AC machine used. Reel friction was assumed to be constant for all reel radii; this is justified as the co-effiecent of friction for ball bearings does not change appreciably over the load range that the bearings are subjected to.

Under these assumptions and using eq. 1 a combined motor and reel model was derived as shown by the block

diagram in Fig. 3. This model is first order and contains a pole which is dependant on the reel inertia; the reel inertia is in turn a function of the radius of the reel and may be described as follows:

$$J_{reel} = D *(Ro^4 - Ri^4)   \qquad (4)$$

Ro = Reel Outer Radius   m
Ri = Reel Inner Radius   m
D = Inertia Constant kgm^{-2}

For the simulation the following SIMULINK model of the motor was used.
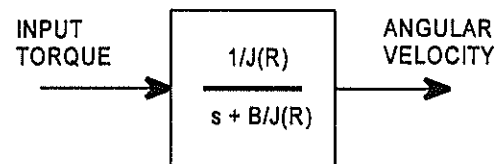
Fig. 3. SIMULINK Reel and Motor Model

The paper model shown in Fig. 2 and described by eq. 3 can be represented by the SIMULINK model shown in Fig. 4.
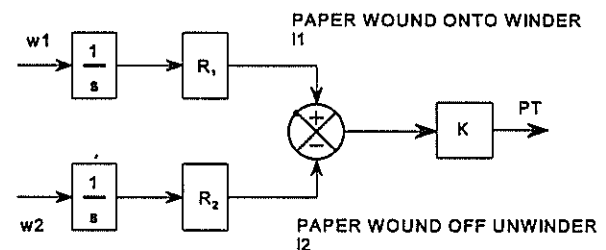
Fig. 4. SIMULINK Paper Model

The reel and motor model plus the paper model can now be used to derive the complete SIMULINK system model which is shown in Fig. 5.
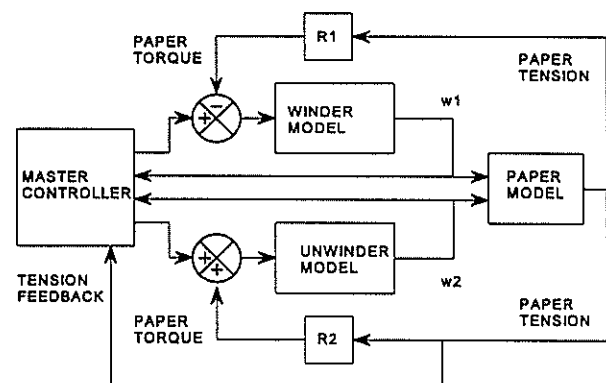
Fig. 5. Complete SIMULINK System Model

Eq. 4 and Fig. 3 show that the unwinder and winder

motor and reel models are time variant and whose dynamics are a function of reel radius. The master controller which comprises both the speed controllers for the winder and unwinder plus the tension controller must therefore be designed to compensate for this. In particular the speed controllers must be provided with "inertial compensation". This is now discussed in more detail.

6. DEVELOPMENT OF MASTER CONTROLLER

Due to the change in the inertias of the reels, inertial compensation is necessary, the extent of which variation had to be ascertained before the compensation could be applied to the motor speed controllers. In order to do this a suitable roll of paper for the system was sized at .4 m in diameter and .3 m in width. The inertia of the roll and motor thus varies from .0057 kgm^2 with no paper on the reel to 8.7 kgm^2 when the reel is fully wound; the co-efficient of friction is assumed to be constant (Section 5). Fig. 6 gives a plot of the variation of the motor pole (B/J(R)) as a function of the reel radius.
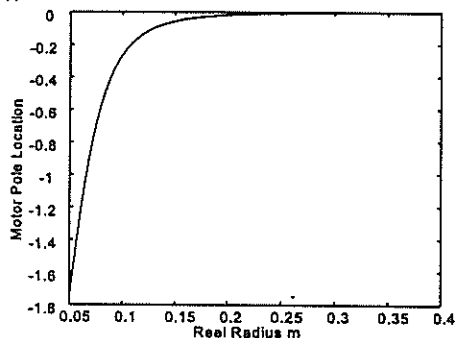
Fig. 6. Motor and Reel Pole Location as a Function of Reel Radius

A speed PI controller was implemented in the master controller for each motor and reel. The proportional and integral gains for these controllers were inertia compensated as a function of radius. This allowed the closed loop poles of the motors and reels to be independent of radius and the line speed and tension control could now be implemented.

To maintain the correct tension a speed difference is introduced by the tension controller into each motors line speed reference and this allows tension to be
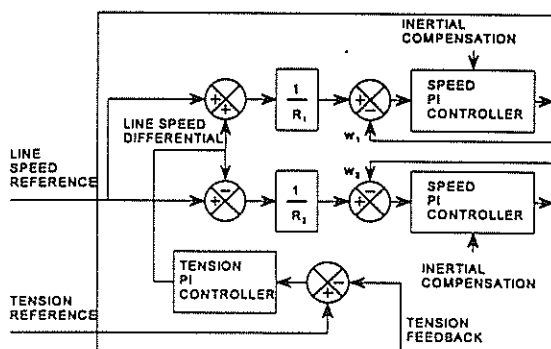
Fig. 7. Master Controller Block Diagram.

produced via a differential angular displacement of the reels. Tension and line speed control were thus achieved in the master controller as shown in Fig. 7.

7. SYSTEM EVALUATION

In order to size the motors, etc. suitable test responses were required to assess the system performance. Paper machines in industry are typically run at 1000 m/min with a line speed ramp time of 30 seconds. The paper is usually processed at a tension of 80 N per metre of web width; this corresponds to a tension of 24 N in our system. These are the criterion that were applied in the evaluation of the system.

Initial conditions for the system were determined as follows. A line speed reference of 1000m/min was chosen. At the minimum reel radius of .05m an angular velocity of 334 rads^{-1} would be required. This corresponds to 53 Hz for a 2 pole three phase induction motor. As variable speed drives are to be used this frequency may be achieved. The motor speed specification was thus obtained.

The initial torque required to accelerate a full roll to 1000 mmin^{-1} in 30 seconds requires 5 Nm from the motor; as the paper at this time will be coming off the roll the paper tension torque must be subtracted from this requirement. At a reel radius of .4 m and a paper tension of 80 Nm^{-1} the torque required is 9.6 Nm. If these torques were added together a sum of 14.6 Nm would result. From a variable speed drive it is often possible to extract more than rated torque from an induction motor for limited periods. It would thus be possible to achieve this requirement with a motor that produces a rated torque of 13.7 Nm. Thus a 2 pole 4kw three phase induction motor would satisfy our initial condition requirements. [2]

A simulation of the system was therefore conducted using two 4 kW 2 pole 3 phase induction motors. The speed was ramped up to 16.7ms^{-1}(1000 mmin^{-1}) in 30 seconds and a tension requirement of 24 N applied to the system. The results were as follows:
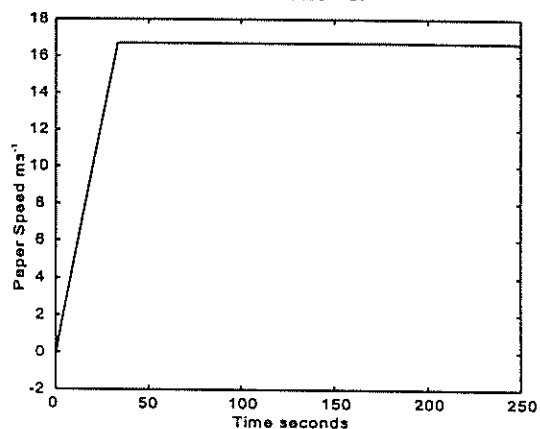
Fig. 8. Line Speed versus time.

The line speed tracked the line speed reference to within 0.04 ms^{-1} and had a maximum steady state error of 1%.
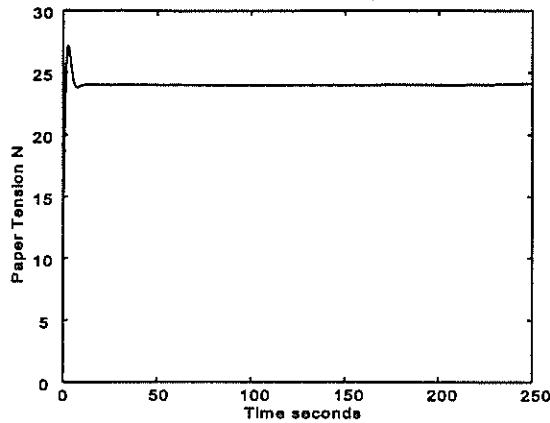
Fig. 9. Paper Tension versus Time

As may be seen from the plot of the tension this was achieved within 10 seconds and the steady state error was a maximum of 1%.
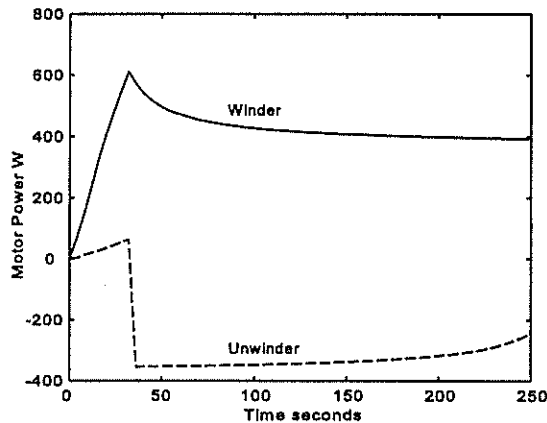
Fig. 10. Motor Power versus Time.

The motor power is never greater than 0.8 kW but this is due to high torque being required at low motor speeds as may be seen from the following two plots.
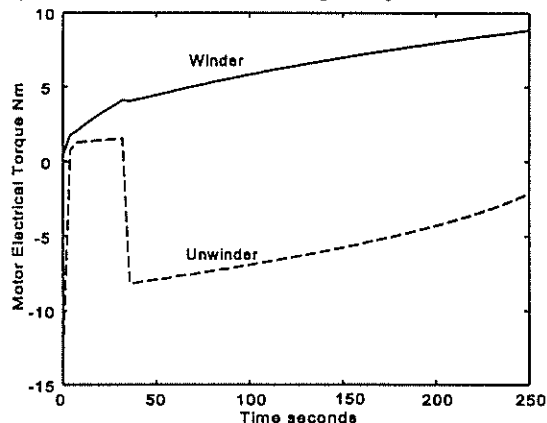
Fig. 11. Motor Torques versus Time.

Rated torque for the selected machines was 13.7 Nm. This was not exceeded and some torque is still available to deal with system disturbances.

The motors spend most of the simulation period at low speeds and thus the power of the motor appears to be far
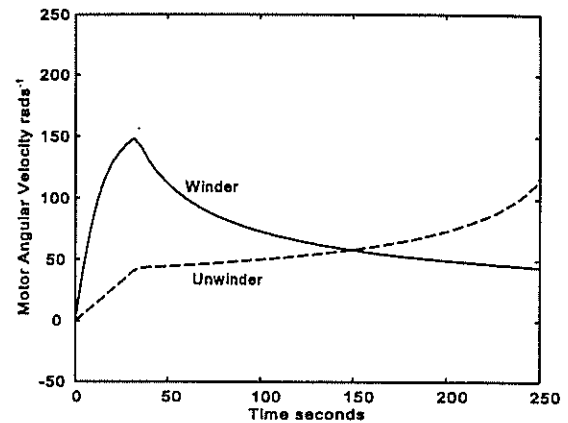
Fig. 12. Motor Angular Velocity versus Time.

over-rated. The size is however required to supply the necessary torque. From these simulation results the motor size chosen will supply the resources to successfully perform the required tests.

8. MISCELLANEOUS COMPONENT SIZING.

The tension transducing roll is mounted on load cells. To prevent damage to the cells the capacity of the cells would have to be greater than the maximum load that could be applied to the roller. This load would be applied via the paper tension. The maximum tension will occur when the reel diameter is a minimum. Rated torque and a minimum reel radius of .05m gives a maximum paper tension of 274N. Thus a weight of 27.4 kg would have to be supported by the load cells. 50 kg load cells were chosen as they were the next standard size up from the required value.

Ball bearings are to be used to support the rollers. With all the rollers having a radius of 50 mm the bearings would have to be capable of turning at 3200 rpm. If the guide rollers and tension transducing rollers were to have a radius of 25 mm, the bearings would have to be able to rotate at 6400 rpm. The choice of bearing would depend on the radius of the roller. These were the main components that had to be sized for the project.

9. CONCLUSION.

A mathematical model and SIMULINK simulation model was developed in this paper in order to size the components of a GTCS test bed. Further work on this project will be the building of the test bed.

10. REFERENCES.

[1] Diana G, Harley RG, "An aid for teaching Field Orientated Control applied to Induction Machines", *IEEE Trans. On Power Systems*, Vol. 4, No. 3, Aug., 1989, pp 1258-1262

[2] GEC ALSTHOM, "Cast Iron Frame 3 PH 50 Hz Squirrel Cage Motors Totally Enclosed Fan Cooled IP 55 (Sizes 90S to 132M",*GEC ALSTHOM*, 1995

The Use and Development of Specialised Software Tools for Parallel Real-time Controllers for Power Electronic Systems

MJ van der Westhuizen, RG Harley, DC Levy

Department of Electrical Engineering, University of Natal, Durban.
Phone: +27-31-2602725; Fax +27-31-2601300; e-mail: mwesth@elaine.ee.un.ac.za

Abstract: *This paper highlights some of the issues involved with using parallel processing and CASE technology for power electronic applications such as the Field Oriented Control (FOC) of AC motors. It also describes the use and development of a software scheduling tool for real-time embedded control.*

Key words: *Microprocessors for power electronics, real-time computing, parallelism, CASE.*

1 Introduction

Power Electronic (PE) systems often embody state-of-the-art control technology since the problems involved are usually non-linear, time-varying and with Multiple Inputs and Multiple Outputs (MIMO). Novel control methods such as fuzzy logic, neural networks and on-line spectral analysis applied to PE systems are computationally intensive. In addition, modern PE systems have advanced to the point where multitasking and multirate computing systems are commonly employed. In order to use the novel algorithms in the context of the high sample rates of several tens of kilohertz typically required for on-line PE systems, the latest and most powerful DSP microprocessors can be required. When the most powerful microprocessor is not fast enough, the PE systems designer can contemplate *parallelism*, ie the use of a number of fast microprocessors in tandem so as to improve performance. Most of the latest high-end DSP microprocessors have facilities for parallel operation and typical examples are the T9000 transputer, the TMS320C40 and the ADSP21060 (SHARC) processors.

2 Background

In order to achieve the tight and complex timing requirements of PE systems, the designer of the real-time software for PE systems using multiple DSPs as the controlling element has to solve a combinatorial optimisation puzzle. The combinatorial puzzle involves finding the best static schedule for the partitioning of tasks and the timing of multirate and multitasking software [1][2]. Whereas uniprocessor multitasking solutions can be found with known methods such as rate monotonic and deadline driven scheduling, solutions with guaranteed analytical results to parallel multirate applications are still not known [3][4].
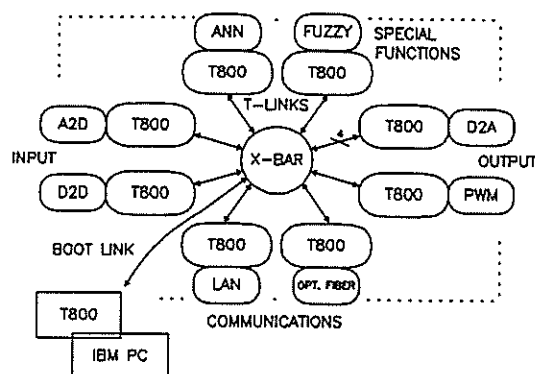
Fig.1 A T800-based rapid prototyping control platform for power electronic systems.

Our department built a transputer-based controller on the premise that complex IO and number-crunching could be obtained by building up the required prototype controller by using the ready-made transputer modules which incorporate A/D, PWM and other peripheral hardware (Fig.1). However, experience with programming such built-up controllers quickly proved to be excessively time-consuming and difficult. Subsequent theoretical analysis from a Computer Science point of view revealed that the problem of finding the best software configuration is NP-Hard. The NP-Hardness implies that the problem increases in difficulty in an exponential or factorial law with respect to the number of processors, tasks, control loops and peripherals. Finding the most optimal solution of programming even small networks consisting of say, twenty tasks on four processors will theoretically take millions of years unless a major breakthrough in theoretical computer science is made.
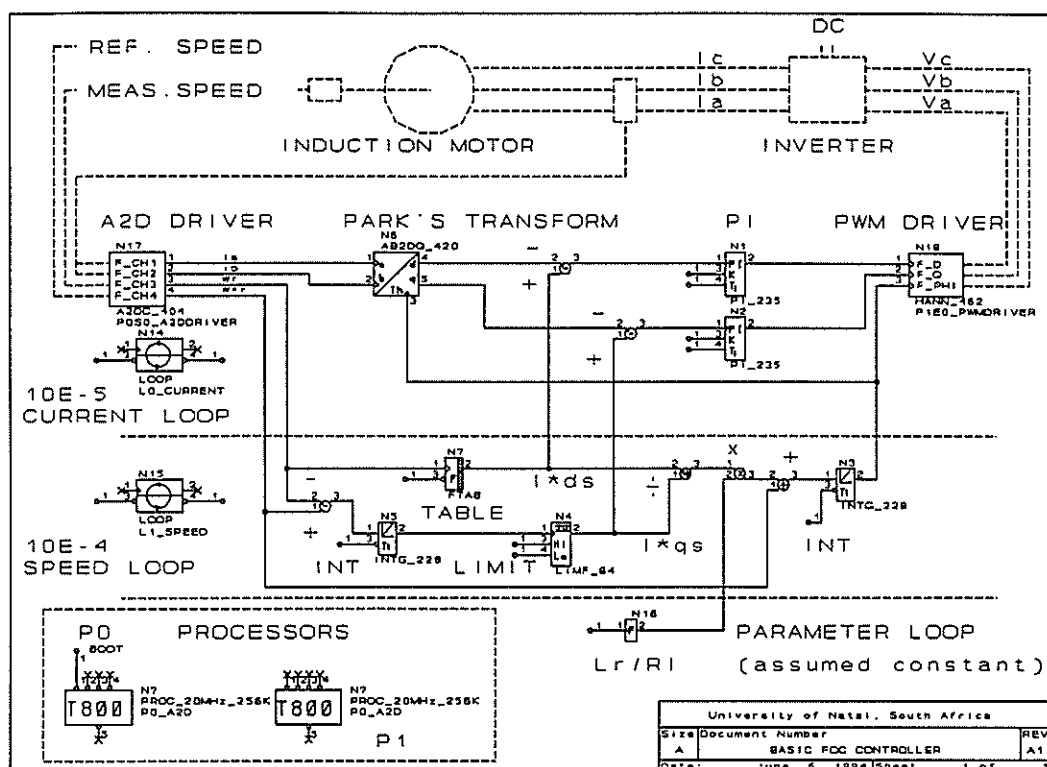
Fig.2 Example of real-time software designed with standard CAD software.

From the PE system designer's point of view, an ideal tool would permit him or her to design the system in a block diagram which would not only represent the control algorithm, but also the complex timing and switching matrix together with the hardware network. Such a tool would then provide automatic or interactive facilities for system optimisation. However, a market and research literature search revealed that such software tools are scarce or non-existent. Packages such as MatLab permits the design and generation of code for the control part of the software but do not help with parallelising the software in order to meet the sampling deadlines. By using Real-Time (RT) operating systems or kernels, the designer can enforce the program to react to external stimuli at predefined times. However, experience showed that this approach does not guarantee that buffering (z^{-1} delays) is not introduced in critical applications where it cannot be tolerated.

3 Serial-Parallel Load Allocation and Timing

The Serial-Parallel Load Allocation and Timing (SPLAT) tool developed in our department permits the power electronic engineer to develop the software for fast controllers by merely drawing on a PC screen the required control algorithm, the timing requirements and the processor topology with CAD software such as

OrCad. The SPLAT tool then produces optimised C programs for the processor network as well as Gantt (timing) charts for effective visualisation of the complex hardware and software interactions. The tool can also be used as a convenient and cost-effective simulation system. By generating the simulation code for the DSP in C, a twenty to fifty-fold increase in speed with relation to the fastest PC is achievable when DSPs such as the SHARC are used. The development of software such as the SPLAT tool requires both a knowledge of theoretical computer science (compiler technology) and motion control theory and practice.

The SPLAT tool has the structure of a compiler and includes parsers, lexical analysis (in a control systems context) and optimisation modules. The tool thus has front-end modules which parse netlists representing the block diagram information. Currently, only the netlist format of schematic diagram software such as OrCad and our own schematic capturer are supported. However, future research will examen the possibility of parsing the output of simulation packages such as MathCad which provide symbolic computing facilities as well as languages such as Lisp. The parsing modules are followed by the optimisation modules. The optimisation of the block diagrams on processor networks in the required time frames imposed by the sampling and switching requirements is an NP-hard optimisation problem which is closely related to Job-

Shop scheduling with the Critical Path as the cost function. The NP-Hard problem is effectively solved by heuristical methods such as Simulated Annealing (SA) and Genetic Algorithms (GA) which provide near-optimal solutions [5]. Apart from finding a suitable partitioning and ordering amongst processors, the optimisation routines also find an optimal solution to the time-slicing of slower loops into faster loops (static multitasking). After optimisation, a Gantt chart and the corresponding C code is generated automatically. The resulting C code executes multirate programs without the need for multitasking operating systems.

4 Example Applications

The direct (non-linear) control of inverters for the speed and torque control of ac motors at several kilohertz is an example of state-of-the-art closed-loop control. In Fig.2 part of the schematic of a vector controller of which the software is automatically generated and optimised by the SPLAT tool is illustrated. In Fig.3 the timing and partitioning of the neural net across several microprocessors is illustrated as a differential Gantt chart (event list) which shows time events in chronological order from the top downwards in equal spacings. The software generated corresponds to the Gantt charts and this permits the real-time software engineer to rearrange his software so as to meet the strict timing requirements.

5 Conclusions

Advances in technology can imply that previously unrelated engineering disciplines become dependent on each other. Whereas computer programming was only within the realm of mainframes a generation ago, embedded microprocessors programmed in C are quite common in PE systems nowadays. Advanced computer topics such as parallelism and multitasking were previously only studied by operating system designers but are now also being used in embedded computers for PE systems. In designing advanced PE systems, specialised software tools are required. Although the design of these specialised software tools requires advanced computer engineering, the specialized knowledge of PE and power systems engineers is also required since they are the end-users. The Department of Electrical Engineering at the University of Natal recognized this new field and is currently a leader in the development of specialized real-time software tools used for research in power electronic systems.

References

[1]   El-Rewini, H., Lewis, T.G. and Ali, H.H.,"Task scheduling in parallel and distributed systems",Prentice-Hall, Englewood Cliffs,NewJersey, 1994,ISBN 0-13-099235-6.

[2]   Ferrari,A.D., "Real-time scheduling algorithms". Dr.Dobbs Magazine, No.224, December 1994, pg.62.

[3]   Laplante, P.A.,"Real-time systems design and analysis: an engineer's handbook", IEEE Computer Society Press, New York, 1993.

[4]   Garey, M.R. and Johnson,D.S., "Computers and intractability", W.H. Freeman and Company, 1979.

[5]   Van der Westhuizen, M.J.,"Static scheduling of multirate motion control algorithms on transputer networks", MScEng Thesis, University of Natal, 1993.

```
read left to right -> time
    P|ͱͱͱͱͱͱͱͱͱͱͱ|ͱͱͱͱͱͱͱͱͱͱͱ|ͱͱͱͱͱͱͱͱͱ|ͱͱͱͱͱͱͱͱͱͱͱ|ͱͱͱͱͱͱͱͱͱͱͱ|ͱͱͱͱͱͱͱͱͱͱͱ
    1|
    0|▓▓▓▓▓▓▓▓▓▓▓▓▓▓▓▓▓▓▓▓▓▓▓▓▓▓▓▓▓▓▓▓▓▓▓▓▓▓▓▓▓▓▓
    Scale: 118 increments of 16 time units
```

read
top
down
|
V

Proc MHz/KB Links	P0 T800 20/256 b???	P1 T800 20/256 ????
0	A2DDRIV	▓▓▓▓
404	AB2DQ	▓▓▓▓
824	sL1P1v0	rLOPOv0
1124	SUB	SUB
1174	PI	PI
1409	sL1P1v1	rLOPOv1
1709	sL1P1v1	rLOPOv1
1359	sL1P1^2	rLOPO^2
2059	SPEED	PWMDRIV
2337	▓▓▓▓		
2521	▓▓▓▓	▓▓▓▓

Links	b1**	0***
Mem.	2165	370
Comm.	350	350
Comp.	1387	747
Total	2337	1697
Ratio	68%	127%
Busy	93%	67%

< exept from boot link on LOPO,
  other links are free
LEGEND:
x|XXX   func XXX starting at time x
 |▓XXX   hard-placed activity
  dlxPyvzy comm. on link x, to proc. y
  dlxPy^zz comm. used to update buffers
  ▓▓▓▓   wait state
  ▓|▓▓▓   state same as previous

< end time (in 50 μsec cycles)
          (2521 / 20 = 126 μsec)
< chosen link configuration
< memory used

```
    loop1slice[6] = loop1slice6;
    loop1slice[7] = loop1slice7;
    while(1){
    do_loop1slice = ++do_loop1slice%8;
0-404 A2DC(&A2DC_17);   /*A2DDRIVER*/
    FORK_25.IN = BUFFER_30.OUT1;
    AB2DQ_6.A = A2DC_17.CH1;
    AB2DQ_6.B = A2DC_17.CH2;
    AB2DQ_6.THETA = FORK_25.OUT1;
824   AB2DQ(&AB2DQ_6);
    SUB_10.POS = BUFFER_34.OUT1;
    SUB_10.NEG = AB2DQ_6.Q;
    packet_0_arr[(packet_0_dex=0)++] = AB2DQ_6.D;          /*    .... to proc 1 */
    ChanOut(chan_OT1, packet_0_arr, packet_0_size);
    SUB(&SUB_10);
    PI_2.IN1 = SUB_10.OUT;
    PI(&PI_2);
    packet_1_arr[(packet_1_dex=0)++] = PI_2.OUT;           /*    .... to proc 1 */
    packet_1_arr[packet_1_dex++] = FORK_25.OUT2;
    ChanOut(chan_OT1, packet_1_arr, packet_1_size);
    BUFFER_30.OUT2 = BUFFER_31.IN2;                        /*.... updating buffer 66*/
    BUFFER_29.IN1 = A2DC_17.CH4;
    BUFFER_28.OUT2 = BUFFER_29.IN2;                        /*.... updating buffer 68*/
    packet_2_arr[(packet_2_dex=0)++] = BUFFER_33.OUT2;     /*    .... to proc 0 */
    ChanOut(chan_OT1, packet_2_arr, packet_2_size);
    BUFFER_27.IN1 = A2DC_17.CH3;
    BUFFER_26.OUT2 = BUFFER_27.IN2;                        /*.... updating buffer 72*/
    BUFFER_34.OUT2 = BUFFER_35.IN2;                        /*.... updating buffer 74*/
1459  (*loop1slice[do_loop1slice])();
    }}
    void loop1slice0(){SUB(&SUB_8);}
    void loop1slice1(){INTG(&INTG_5);}
```

Fig.3 Gantt chart and C code for Fig.2

Transfer function for the partial series resonant converter.

S.D. Roos. and J.A. Ferreira

Research Group: Industrial Electronic Technology Rand Afrikaans University, PO Box 524
Aucklandpark 2006.

Abstract: **The partial series resonant converter (PSRC) is a variation of the well-known series resonant converter, it has proved itself in battery charging and welding applications. Optimising its dynamic performance in accurate voltage control loops has proven to be difficult due to its unique discontinuous mode of operation. In this paper a large signal analysis of the transfer function is described. Experimental results is presented on a 250-W 12 V converter using MOSFET's and switching at 12-280 KHz.**

1. Introduction

This paper will discuss the large signal transfer function of a PSRC. The PSRC a new clamped voltage DC to DC converter was proposed by [1] as a medium to high power, medium frequency converter. Topologically it is similar to a series resonant converter (SRC) in the half bridge configuration [2], with the only additions the clamping diodes in parallel with the resonant capacitors, the parallel inductance and the freewheeling diodes and the capacitors in parallel with each semiconductor switch as shown in figure 1.

The circuit is resonant for only a part of each half cycle, resulting in a substantial difference in operational behaviour when compared with the SRC of [2].
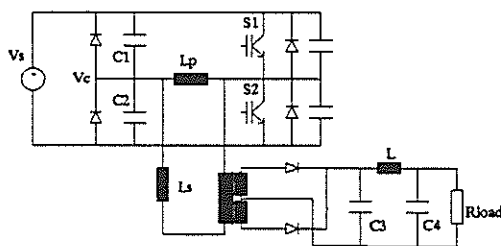
Figure 1 Partial series resonant converter without feedback

The voltage stresses on S_1 and S_2 is 1 p.u. because it is a clamped voltage topology, rendering a minimum over dimentioning of voltage. Furthermore the addition of the clamping diodes clamps the voltage over the two resonant capacitors to a maximum of the supply voltage V_s. Therefore, capacitors with lower

voltage specifications may be used.

The PSRC can operate as a ZCS or a ZVS converter depending on the ratio of the parallel and series inductors. A small enough parallel inductance will assure ZVS, ZCS is beyond the scope of this paper. Using of this, parallel inductance benefits the operation of this circuit. Among the benefits is, that ZVS is obtained for the entire load range, rendering lower EMI and switching losses. This is the case with all ZVS converters, additional conduction losses are generated, but are extremely low in the PSRC. The additional parallel inductance is the magnetising inductance of the transformer, and the correct inductance value is simply obtained by introducing an air gap in the transformer core, or by using a core with the correct relative permeability.

The PSRC with ZVS can operate in 2 modes: The first mode is if the output voltage is lower than half the supply voltage, if the transformer secondary is referred to the primary (on unity turns ratio) then the voltage V_c will drop to zero before the current i_s drop to zero as shown in figure 2.
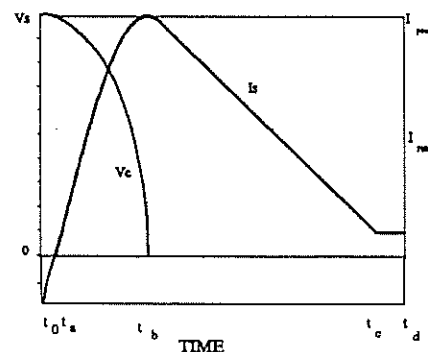
Figure 2 Mode 1 operation of the PSRC with ZVS

The second mode of operation is when the output voltage is bigger than half the supply voltage, then the current i_s will drop to zero before the voltage V_s will drop to zero. Only mode 1 operation is considered.

2 Circuit operation.

Mode 1 operation consists of a different sequence of operational intervals, which are subsequently described. These intervals can differ

in sequence for other modes of operation but this is beyond the scope of this paper. The duration of the intervals differs for different output voltages. The longer the intervals the more energy will be transferred to the load.

2.1 Regenerative interval (t_a - t_s)

During the regenerative interval, energy stored in L_p gets partly transferred to the supply V_s and partly to the combination of the load and L_s, with the ratio depending on V_{load}. The time this interval lasts is given by:

$$t_a - t_s = \frac{L_s(\alpha\sqrt{V_s} + \pi\ V_{load}L_p - \cos^{-1}(\beta)\ V_{load}L_p)}{\omega_0} \quad (1)$$

2.2 High frequency resonance (t_a - t_b)

During the high frequency resonance interval, one of the switches is conducting. Using Kirchhoff's laws the following equation is derived:

$$i_s(t) = \frac{1}{L_s\omega_0}(V_s(t_s) - \frac{V_{load}L_p}{L_s+L_p})\sin(\omega_0(t-t_s))$$

$$-7\frac{(i_s(t_s)+i_p(t_s))L_p}{L_s+L_p}(1-\cos(\omega_0(t-t_s)))\quad(2)$$

$$+i_s(t_s) - \frac{V_{load}}{L_s+L_p}(t-t_s)$$

The time this interval will last is given by:

$$t_b - t_a = \frac{\cos^{-1}(\delta)}{\omega_0} \quad (3)$$

2.3. Discharging interval.(t_b - t_c)

During this interval the energy stored in the series inductance is transferred to the load. The voltage V_c is zero throughout this interval. The discharging current is given by:

$$i_s(t) = i_s(t_b) - \frac{V_{load}}{L_s}(t-t_b) \quad (4)$$

The time the discharging interval will lasts is:

$$t_c - t_b = \frac{L_s V_{load}\cos^{-1}(\delta)L_p - 2L_p\sqrt{V_s}\phi - L_s\cos^{-1}(\delta)\ V_s L_p - L_s^2\cos^{-1}(\delta)\ V_s}{\omega_0\gamma}$$

$$- \frac{L_s\sqrt{V_s}\phi - 4\ V_s^{\frac{3}{2}}\frac{\phi}{V_{load}}L_s}{\omega_0\gamma} \quad (5)$$

In the above equations:

$$\alpha = \sqrt{L_p^2\ V_s - 2L_pL_s\ V_s - 2L_p^2\ V_{load} - L_s^2\ V_s - 2L_sL_p\ V_{load}} \quad (6)$$

$$\beta = \frac{L_p\ V_{load}}{V_sL_p + v_sL_s - V_{load}L_p} \quad (7)$$

$$\gamma = 2L_p^2\ V_s + 3L_pL_s\ V_s - 2L_p^2\ V_{load} + L_s^2\ V_s - 2L_pL_s\ V_{load} \quad (8)$$

$$\delta = \frac{L_p\ V_{las}}{V_{las}L_p - V_sL_p - V_sL_s} \quad (9)$$

$$\phi = \sqrt{L_p + L_s}\ \sqrt{V_sL_s + V_sL_p - 2\ V_{load}L_p} \quad (10)$$

2.4 Commutation interval (t_d)

The time interval t_c - t_d (see figure 2) depends on the switching frequency and can therefore not be expressed mathematically, but rather chosen. This interval causes the transfer to be discontinuous because no energy is transferred to the load during this interval. The commutation interval is the interval which is initiated by the turn off of one of the semiconductor switches. During this interval the only voltage or current that is not zero is the magnetising current. This time will only be as long as the dead time between the switches.

3. Modelling of the dynamic behaviour.

State space averaging as used by [6] cannot be applied due to the discontinuous current flow of the PSRC. Figure 3 shows a block diagram of the proposed feedback loop. Each block in this diagram will be discussed in the next sections.
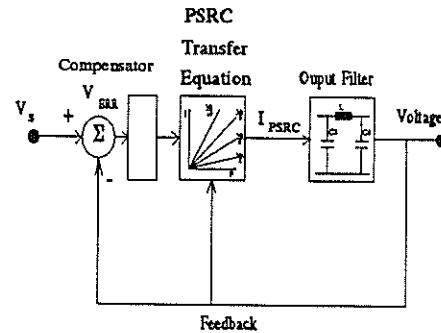
Figure 3 Block diagram of the converter and the feedback loop

The output voltage effects the transfer function of the PSRC and effectively influences the forward gain.

3.1 Output filter.

Figure 4 shows the output filter. The cutoff frequency is chosen so that it is much lower than the switching frequency. The transfer function of

this filter is given by the following equation:

$$\frac{V_{out}}{I_{psrc}} = \frac{R}{s^3 RLC_3 C_4 + s^2 LC_3 + sR(C_3 + C_4) + 1} \quad (11)$$
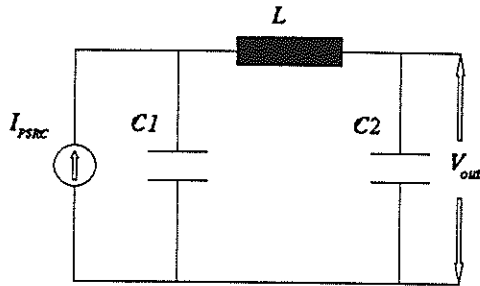
Figure 4 The output filter

3.2 Transfer equation.

The transfer equation is derived from simulations of the PSRC for all possible output voltages. The limitations of this simulation are that:
- the converter is only operated in mode 1 (the output voltage is smaller than half the supply voltage for a unity transformer).
- No losses in the transformer, MOSFET's or diodes are included in the simulation.
- The bus voltage and the load voltage are taken to be constant during one switching interval.
- The output is considered to be a voltage source.
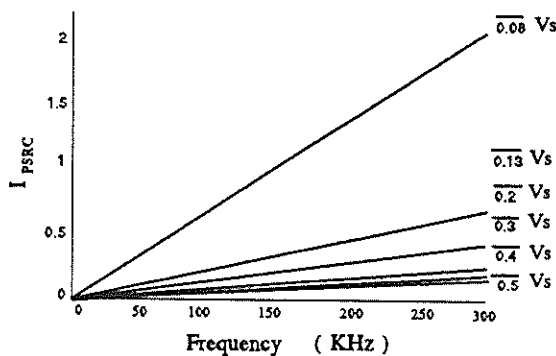
Figure 5 Transfer function of the PSRC.

Equations 1 to 10 are used in the model to simulate the converter for all possible constant output voltages. The pulsed current for each switching cycle can then be calculated for aconstant output voltage, from this it is possible to calculate the average current (I_{psrc}) by integrating the current i, for every interval. The time that each interval last is used in the integration and interval $t_c - t_d$ is varied to attain

the full range of switching frequencies. Figure 5 shows the output current for a set of constant normalized output voltage for all the switching frequencies. The voltages and currents on this graph are the average output values for a unity turn ratio transformer and the voltage and currents are normalized to the average input voltages and currents. The gradients of the average output current (I_{psrc}) for the different output voltage differ. Since these gradients differ, it is not possible to use a normal P controller. Clearly a transfer equation, which gives the relationship between the output current, output voltage and the switching frequency is needed to control this converter. The gradients of the lines of figure 5 are determined and found to be exponential. By using curve fittings a curve is fitted to the different gradients for the different output voltages and switching frequencies to give the required average current. The transfer equation for this simulation is given by the following equation:

$$I_{psrc} = I_{maxn} \exp(0.4487 - 0.633 V_{out} + 0.0337 V_{out}^2) \quad (12)$$

The on state voltage of the output diodes was not included in the simulation model at first, but was included in the equation by deducting the on-state diode voltage drop to the simulation output voltage, since the output voltage in the model is the total output voltage as seen by the transformer. The voltage measured on the output is not the voltage seen by the transformer but the modelled voltage, minus all the loses, in particular the on-state losses of the diodes. The on-state voltage drop of the diodes was measured and shown in figure 6.
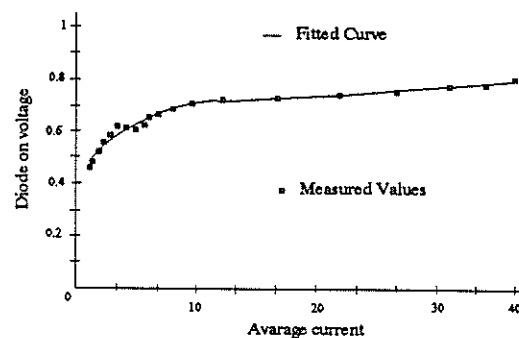
Figure 6 The measured values and curve fit for the on state diode voltage drop

The curve fitted to this data of the output diodes voltage drop for the different currents is:

$$V_{on} = -5.2 \cdot 10^{-7} I^4 + 6.17 \cdot 10^{-5} I^3 - 2.255 \cdot 10^{-3} I^2 + 4.51 \cdot 10^{-2} I + .455 \quad (13)$$

4 Experimental results.

The experimental measurements, done on a 250-W, 12V converter were tested to equation 12 and the results are shown in figures 7 to 10. It is clear from these figures that the measured and the values produced by the transfer equation with the varying diode on voltage are comparable. Thus, by measuring the output current and the voltage the switching frequency can with a 4% margin of error be calculated. By making use of a microcontroller this equation can be used to control the output voltage.

Figure 9 The simulation and measured values for a constant 8V output
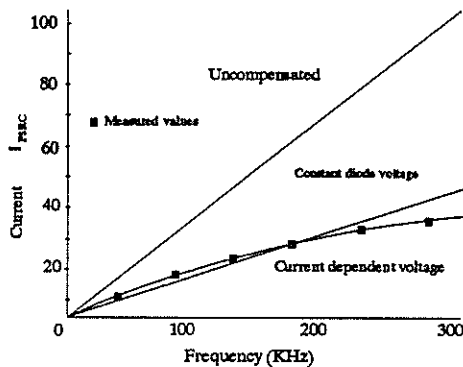
Figure 7 The simulation and measured values for a constant 3 V output

Figure 8 The simulation and measured values for a constant 10V output

6. References.

[1] P.C. Theron and J.A. Ferreira.:"The partial series resonant converter: A new zero voltage switching DC to DC converter." : The transactions of the SA institute of electrical engineers, March 1994, p18 - p23.

[2] F.C. Tsai and F.C. Lee. : "A complete characterisation of a constant frequency, clamped mode, series resonant converter." IEEE-PESC Conference Record, April 1988, p987 - p996.

[3] H.L.N.Wiegman, D.M.Divan, D.W.Novotny, R.Mohan. " A ZVS dual resonant converter for battery charging applications." IEEE-IAS Annual Meeting, 1991, p202-p208.

[4] R.L.Steigerwald. : "A comparison of the half bridge resonant topologies.", IEEE Transactions on power electronics, Vol.3 no.2 p174-182, April 1988.

[5] J.P. Agrawal, S.H.Kim, C.Q.Lee.:"Capacitor voltage clamped series resonant power with improved cross regulation." IEEE-IAS Annual meeting, p1141-p1146, 1989.

[6] N.Mohan, T.M. Underland,W.P. Robbins "Power Electronics: Converters, Applications, and design" John Wiley & sons, 1989.

Figure 8 The simulation and measured values for a constant 5 V output

5. Conclusions.

Optimizing the dynamic performance of the PSRC in accurate voltage control loop hasproven to be difficult due to the discontinuous mode of operation. The simulation for the large signal analysis of the converter is presented on a 250-W 12V converter, using MOSFET's and switching at 12-280 KHz. The uncompensated simulation values were not good enough to be used for accurate voltage feedback. The values from the transfer equation with compensation proven to be accurate to 4% of the measured values and can be used for accurate voltage feedback.

AN IMPROVED CONTROL SCHEME FOR SOLID STATE SERIES REACTANCE COMPENSATION

B. S. Rigby and R. G. Harley

Department of Electrical Engineering, University of Natal, Durban.

Abstract

This paper presents theoretical analysis and simulation results to highlight the shortcomings of a control scheme initially proposed for a solid state series reactance compensator. A modified control scheme is then proposed to address these shortcomings. Simulation results of this modified scheme indicate that it is in fact sufficiently robust for further investigation as a laboratory prototype.

Introduction

The pressure on power utilities worldwide to transmit increasing amounts of power conflicting with growing public opinion against constructing more transmission lines has lead to considerable research into Flexible AC Transmission Systems (FACTS). FACTS aims, through the integration of a new generation of high speed power electronic devices, to make existing transmission lines more efficient by providing high speed control of the factors influencing power flow. One of the most significant areas of FACTS research has been into controllable series compensation. In fact the first major FACTS initiative to be developed as a commercial product has been the Thyristor Controlled Series Compensator or TCSC [1,2].

However a further FACTS initiative receiving much attention is the proposed use of two back to back high power voltage source inverters in a transmission line to achieve control of one or more of the factors influencing power flow, the so called Unified Power Flow Controller (UPFC) concept [3]. The UPFC makes use of the two inverters to synthesize power frequency voltage sources, both in series and in parallel with the transmission line; these controllable voltage sources may then be used to provide rapid continuous-time control of the power flow in the line. One of the key advantages of the UPFC concept is its modularity - either of the two inverters (series and parallel) which make up the UPFC may be used on its own to provide a single function of the UPFC.

The series compensation function in the UPFC is achieved by using the inverter to inject a voltage at power frequency in series with the line through the injection transformer as shown in the scheme of Fig. 1. The UPFC control ensures that the phase of the injected voltage vector lags that of the line current by 90 degrees, and that its magnitude is proportional to that of the line current. The injected voltage source then appears to the transmission line to be a capacitive reactive volt drop; by controlling the proportionality between the magnitude of the injec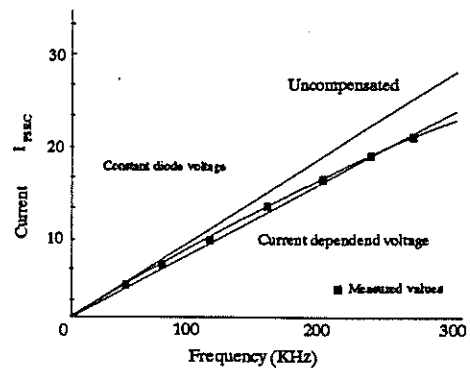ted voltage and that of the line current, the degree of compensation can be controlled. In the particular case shown in Fig. 1, when only the series compensation function of the UPFC is provided by a single stand alone inverter (the so called Advanced Series Compensator), the power required to support the dc voltage of the inverter must also be drawn from the line itself. Thus the overall control scheme for an Advanced Series Compensator (ASC) must combine the control requirements for synthesizing the desired reactive voltages in the transmission line with the regulation of the inverter's dc voltage. Previous papers [4,5] have introduced such a control scheme and shown that, under certain system conditions, it is in fact possible to design this controller to achieve suitable

dynamic performance of the ASC. This paper describes some of the limitations associated with this original control scheme and the reasons for these limitations. The paper shows how the addition of an inner loop to the original control scheme, together with a non-linear compensating block, enables the controller to be designed for suitable performance over a wide range of operating conditions.
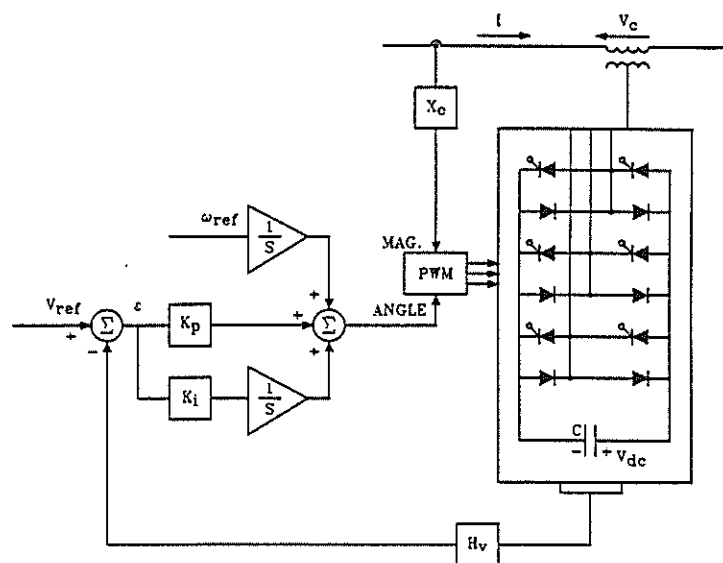
Fig. 1 Initial ASC Control Scheme
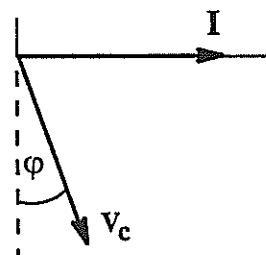
Fig. 2 Injected voltage vector V_c with error φ in phase

Initial Control Scheme

The initial control scheme investigated is based on the work of Ooi et al [6] and a detailed treatment of its operation can be found in earlier papers published by the authors on this work [4,5]. The control method is shown conceptually in Fig. 1, where the outputs of the controller are the instantaneous magnitude and angle of the desired voltage vector V_c at the power frequency, and these are passed directly to the inverter's PWM logic. The frequency of the injected voltage vector is determined by the fixed input ω_{ref} and its phase is determined by the output of a PI controller driven directly by the voltage regulator error ε. The controller adjusts the phase of the injected voltage vector relative to the phase of the transmission line current to ensure that at steady state, when the voltage regulator error ε is zero, no real power is

transferred in or out of the inverter at its ac terminals. Thus the null point of the controller ($\varepsilon = 0$) establishes both the desired voltage V_{dc} on the storage capacitor, and the required quadrature relationship between V_c and I. The magnitude of the injected voltage vector is determined by calculating the magnitude of the transmission line current vector and multiplying by the desired series compensating reactance value X_c.

Although it has been shown that the scheme in Fig. 1 is capable of controlling the injected voltage V_c to reproduce the effect of a desired value of compensating reactance X_c in the line, the practical implementation of such a scheme has been found to be unfeasible. The reason for this problem can be understood by considering the equation which describes the dynamic behaviour of the voltage regulator error ε in Fig. 1. A voltage regulator error ε develops as a result of the time integral of any non-zero real power P_i which may appear at the ac terminals of the inverter. Fig. 2 shows the injected voltage vector V_c and the line current vector I when there is some error φ in the quadrature relationship between these vectors. The real power P_i which appears at the ac terminals of the inverter as a result of this error is given by

$$P_i = V_c I \sin \varphi \approx V_c I \varphi$$

such that

$$\varepsilon \approx \frac{1}{C V_{dco}} \int V_c I \varphi$$

The above equation shows that the error ε in the voltage regulator is related to the error φ in the phase of vector V_c, and therefore explains why ε can be used to indirectly control φ. However the equation also highlights the deficiencies of the control scheme of Fig. 1:

Fig. 3 Admittance of ASC compensated line with initial control scheme at two different values of transmitted power.
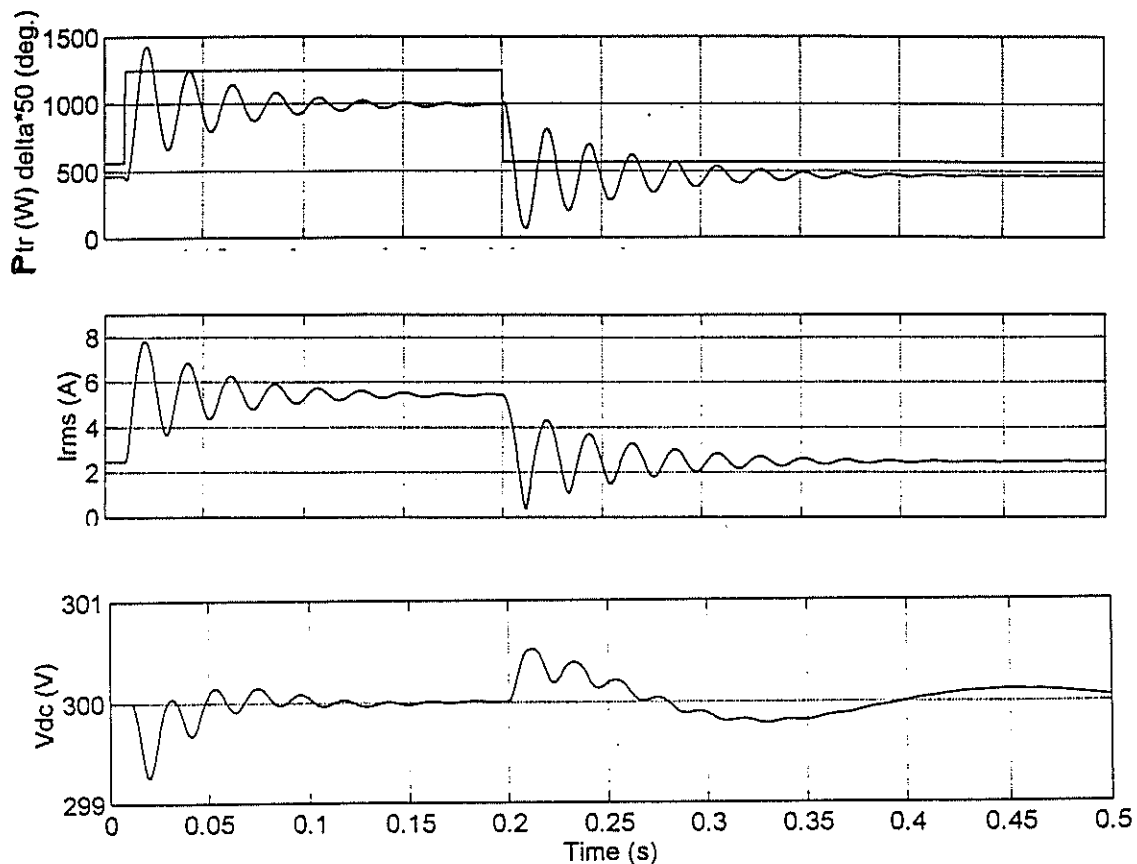
Fig. 4 Transient response of initial ASC controller scheme to changes in transmission angle
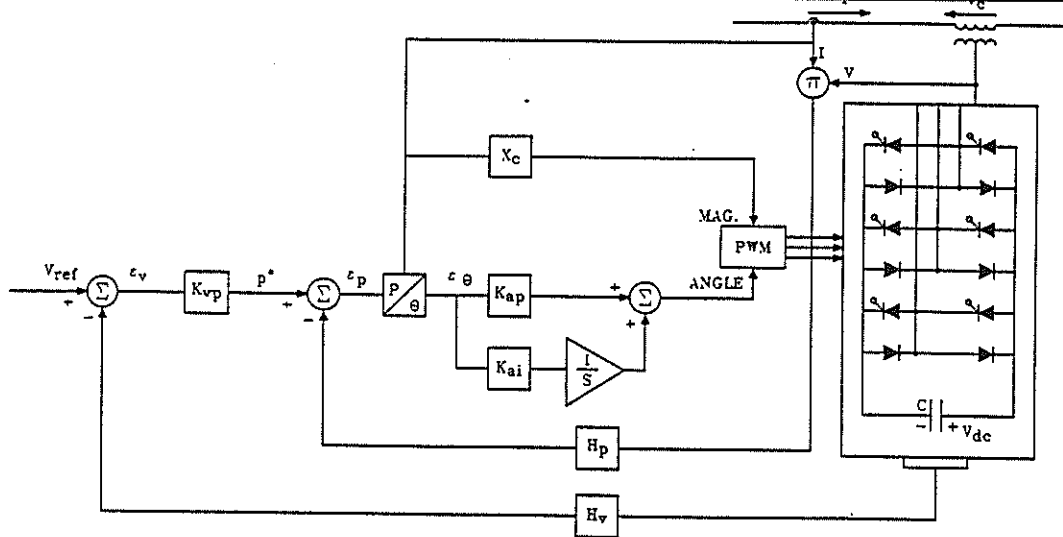
Fig. 5 Modified ASC Control Scheme

(i) the voltage regulator error ε depends on the *integral* of the error φ

(ii) the term $V_c I$ in the dynamic equation changes as the power transmitted by the line varies

The consequence of point (ii) above is that the dynamics of the voltage regulator loop change considerably as the power transmitted by the line varies, as is demonstrated below.

The two transfer functions shown in Fig. 3 represent the admittance as a function of frequency of a transmission line, with the same degree of compensation X_c provided by the ASC scheme of Fig. 1, but at two different values of transmitted power. In Fig. 3 the magnitude and phase of the transfer functions at dc (0 Hz) are the same, showing that the ASC does in fact provide the same compensated admittance value at *steady state*, irrespective of the power transferred by the line. However the fact that the transfer functions in Fig. 3 show different magnitude and phase characteristics over the rest of the frequency range, indicates that the *transient* behaviour of the ASC and transmission line is different at the two values of power.

Fig. 4 shows the simulated response of a laboratory model of a transmission line compensated with the ASC scheme of Fig. 1 to illustrate how the transient behaviour depends upon the amount of power transmitted by the line. The compensation value X_c in Fig. 4 remains fixed, but the transmission angle δ between the sending and receiving ends is first increased and then decreased back to its original value in order to change the power transferred by the line at steady state. The difference in the dynamic response of the system to these two changes in transmission line operating point is particularly evident in the transient of the dc capacitor voltage V_{dc}. Fig. 4 shows that t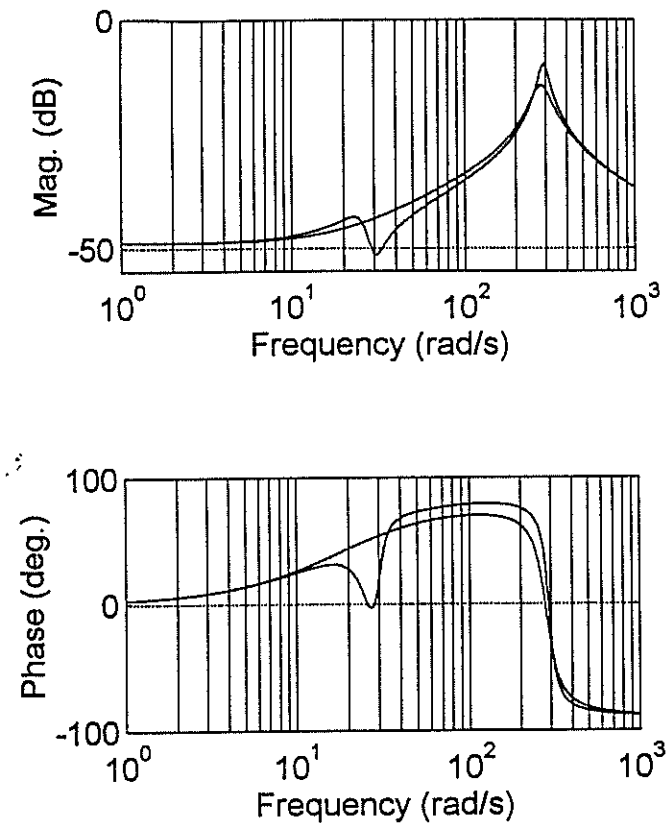he voltage regulator quickly restores the dc capacitor voltage V_{dc} to the desired steady state operating point at the higher value of transmitted power. However at the lower value of transmitted power the response of the voltage regulator is slow and poorly damped. In a realistic transmission line application, where the power transmitted by the line can swing dynamically over a wide range, such a control scheme is clearly not suitable.

Modified Control Scheme

In order to address the shortcomings of the system in Fig. 1, certain modifications have been made to the control scheme in order to remove the dependence of the regulator dynamics on the transmission line operating point. It was shown that although the error ε in the dc capacitor voltage depends on the integral of the error φ in the phase of V_c, in the initial
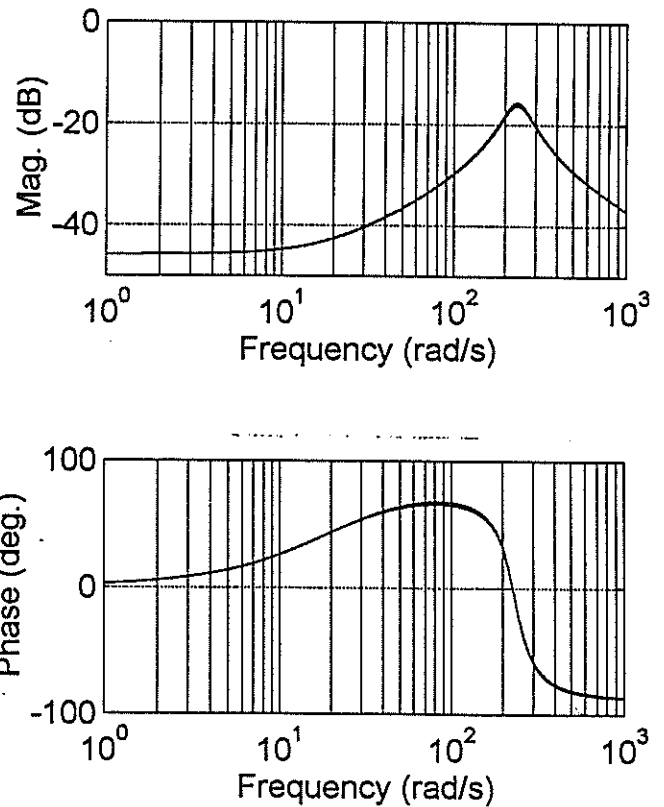
Fig. 6 Admittance of ASC compensated line with modified control scheme at two different values of transmitted power.

control scheme the error ε acts on φ directly. In the modified control scheme shown in Fig. 5 the error $ε_v$ in the dc capacitor voltage determines the desired power P^* at the inverter ac terminals; this desired power P^* is compared to the actual power at the inverter terminals to form a *power error* $ε_p$. Since the relationship between the power error $ε_p$ and the actual error in the phase of V_c depends on the magnitude of the product $V_c I$, the scheme of Fig. 5 includes a compensating block which determines the *phase error* from the power error $ε_p$ and the ac terminal variables of the inverter. The inner loop added to the controller in the modified scheme of Fig. 5 thus ensures that both the voltage V_{dc} and the phase φ are under direct control, as well as removing the dependence of the controller dynamics on the power transmitted by the line.

The transfer functions shown in Fig. 6 show the admittance of
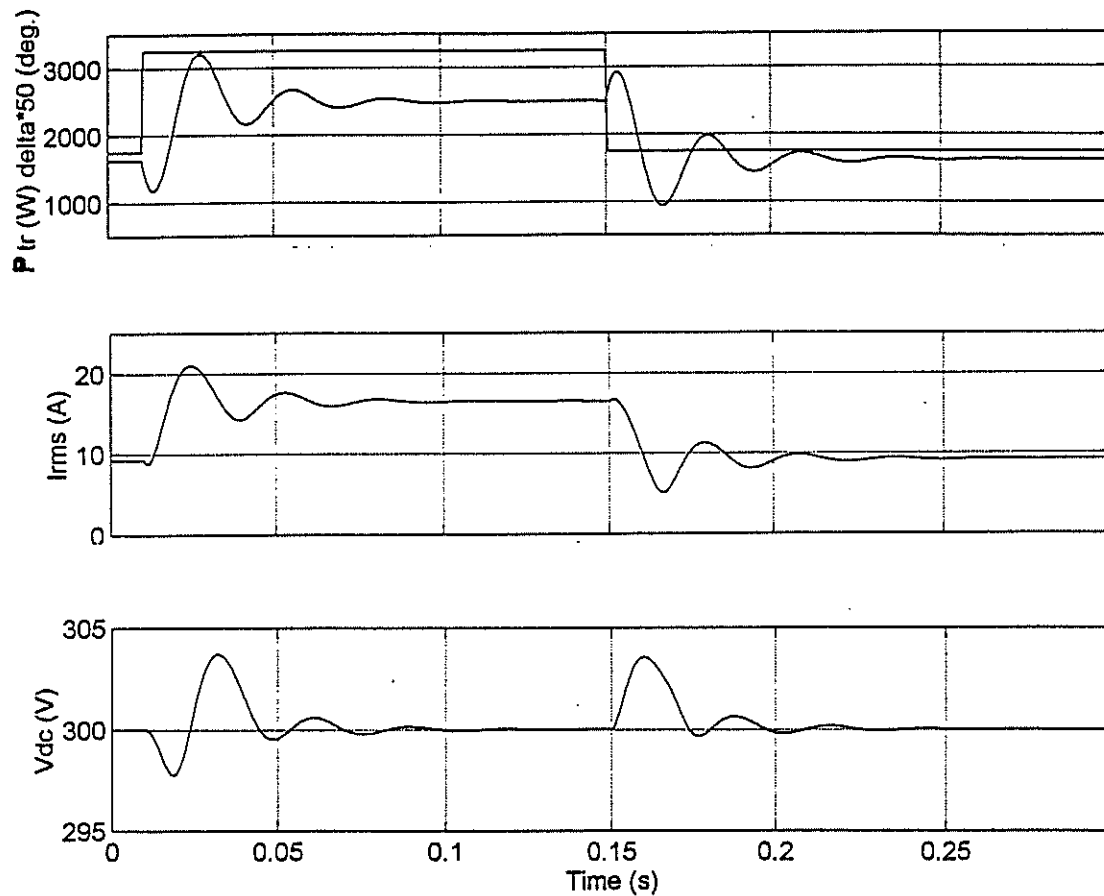
Fig. 7 Transient response of modified ASC controller scheme to changes in transmission angle

the transmission line as a function of frequency for the modified ASC scheme of Fig. 5 at two different values of transmitted power. In contrast to the results shown for the initial scheme (cf Fig. 3), the two transfer functions in Fig. 6 are almost identical, showing that the admittance is now independent of the power transmitted by the line. Fig. 7 shows the simulated response of a transmission line compensated with the modified ASC scheme of Fig. 5 to changes in the transmission angle. The transient response of the voltage V_{dc} is now similar at both operating points, indicating that the modified voltage regulator is in fact independent of the power transmitted by the line.

Conclusion

It has already been demonstrated that the ASC control concept proposed in earlier work, and shown here in Fig. 1, can operate successfully at steady state, and that it is possible to design this controller to have a suitable dynamic response at high levels of transmission line power. The results shown in this paper however, clearly demonstrate that the dynamic response of this controller depends on the level of transmitted power, so that the controller gains would need to be re-tuned for every conceivable operating point. Clearly this scheme is not suitable for realistic applications, where the transmission line power swings dynamically over a wide range following a disturbance to the system.

An analysis of the equations governing the voltage regulator dynamics has been presented to illustrate the reason for the shortcomings of the initial control scheme of Fig. 1, and a modified scheme has been described which overcomes these shortcomings. The results shown indicate that the dynamics of this modified controller are in fact independent of transmission line operating point, so that the controller response does not deteriorate at low levels of transmitted power. The results of these and other simulation studies

indicate that the modified control system of Fig. 5 is suitably robust to changes in operating point for the scheme to be implemented as a practical laboratory prototype ASC in the University's Micro-Machine Laboratory Facility.

References

[1] Larsen E V, Bowler C E J, Damsky B L and Nilsson S L: "Benefits of Thyristor-Controlled Series Compensation", CIGRE SC 14, Paris, 1992.

[2] Urbanek J, Piwko R J, Larsen E V, Damsky B L, Furumasu B C and Mittlestadt W: "Thyristor Controlled Series Compensation Prototype Installation at the Slatt 500 kV Substation", IEEE PES Summer Meeting, Seattle, 1992.

[3] Gyugyi L: "A Unified Power Flow Control Concept for Flexible AC Transmission Systems", IEE Proceedings - C, Vol. 139, No. 4, July 1992.

[4] Harley R G, Rigby B S and Jennings G D, "Design of a Controlled Converter which Emulates a Series Capacitive Compensator for Long Power Lines", Proceedings of the International Conference on Power Electronics and Motion Control PEMC'94, pp. 213-218, Warsaw, Poland, September 1994.

[5] Rigby B S, Harley R G, "Transient Analysis and Performance of a Solid State Series Reactance Compensator", Proceedings of the Fifth Southern African Universities Power Engineering Conference SAUPEC, pp. 85-88, Pretoria, South Africa, January 1995.

[6] Ooi B T, Dai S-Z and Wang X, "Solid-State Series Capacitive Reactance Compensators" IEEE Transactions on Power Delivery, Vol 7, No. 2, April 1990.

A Linear Hysteretic Pulse Width Modulator

Botha, L. J;   Bredenkamp, G. L.
Department of Electric an Electronic Engineering,
University of Pretoria,
Pretoria.

1. Abstract:

Classical PWM modulation method makes use of a ramp generator and comparator to generate the PWM signal. In applications where precision control of the output is desired the modulator is usually put inside a high gain feedback loop. This article describes a PWM modulation scheme with feedback inherent in the modulation method. This type of modulator is not unknown and is usually referred to as a hysteretic modulator because hysteresis is used in the generation of the PWM signal.

The hysteretic modulator described in this article has the additional feature of having a completely linear transfer characteristic. A further feature of this technique is that the slope of the transfer function is only dependent on the ratio of two resistors. The linear transfer characteristic makes this modulator ideally suited for the construction of a precision (high resolution and accuracy) digital-to-analogue-power converter (DAPCO). The modulator will accept voltage or current inputs, and can therefore also be used in conjunction with the popular current output digital-to-analogue converter integrated circuits. With a current input the gain is dependent on the value of one resistor only.

2. Introduction:

There are two standard PWM modulation methods: 1. PWM with uniform sampling and 2. PWM with natural sampling. Both types can be generated by the modulator shown in Fig. 1.
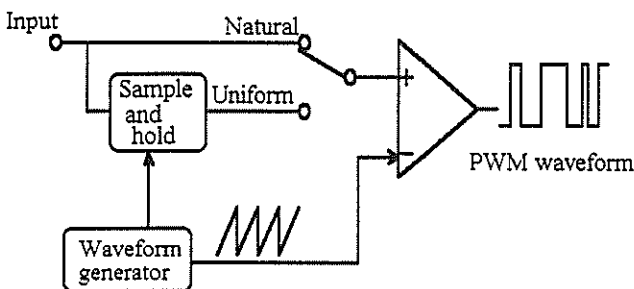
Fig. 1 PWM modulator for natural or uniform sampling.

If the input signal is fed directly to the comparator it is called natural sampling (NPWM), and if it first goes through a sample-and-hold circuit then it is called uniform sampling (UPWM). The two techniques generate different

PWM wave forms and therefore also differ in output spectrum. When the side bands of the switching frequency appear inside the modulation signal pass band it is referred to as "foldback" distortion. UPWM generates less foldback distortion but more harmonic distortion, while NPWM generates more foldback distortion and no harmonic distortion.[1,2]

With digital (discrete time) signals it is easier to construct a UPWM modulator because it is not necessary to interpolate between samples. However, regardless of which modulation technique is used there is still the problem of non-zero switching times in the power switches. Even if the pulse widths of the PWM signal can be generated to an accuracy commensurate with the resolution of the modulating signal (≈ 0.35 ns for 16 bit resolution and 44 kHz sample rate), the switching times of the switches (typically MOSFET's) could still vary with 50 ns or more, depending on the load.

The modulation method should therefore preferably include some kind of feedback, so that variations in switching times and output voltages can be compensated for. At the same time the chosen modulation method should generate as little as possible foldback and, if possible, no harmonic distortion.

3. Hysteretic modulator:
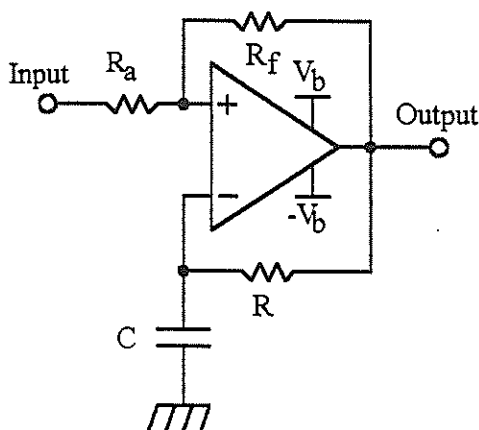
Fig. 2 Hysteretic Modulator

The well known RC hysteretic modulator is shown in Fig. 2.

This circuit is well known for it's use as an oscillator, with the input terminal simply grounded. With an input signal the duty cycle varies almost linearly with input voltage, as shown in Fig. 3, for the case where V_b = 10V.

The function relating average output voltage V_{out} to input voltage V_{in} (assuming V_{in} remains essentially constant over one switching cycle) is :

$$V_{OUT} = -(1-2D)V_b \dotfill (1)$$

where the duty cycle

$$D = \frac{\ln\left(\dfrac{V_{in}-V_b}{V_{in}-V_b(1+2\frac{R_a}{R_f})}\right)}{\ln\left(\dfrac{V_{in}^2-V_b^2}{V_{in}^2-V_b^2(1+2\frac{R_a}{R_f})^2}\right)} \dotfill (2)$$

If D were a linear function of V_{in} then there would have been no harmonic distortion in the output for low frequency inputs. For small input voltages (small output modulation) D approaches a linear function, as can be seen in Fig. 3. The harmonic distortion of this modulator therefore depends on the depth of modulation.
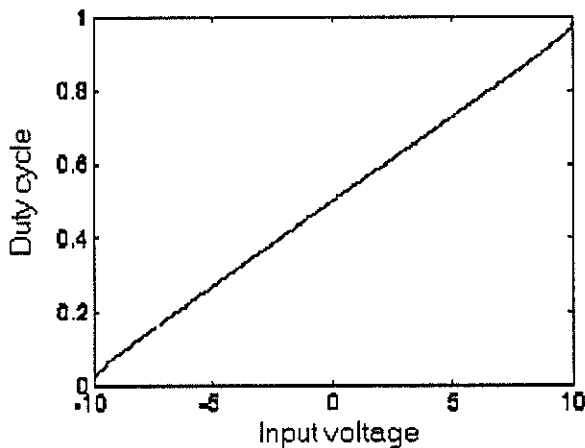
Fig. 3 Output duty cycle D as a function of input voltage for the circuit shown in Fig. 2.

4. Linear hysteretic modulator:

While the performance of the hysteretic modulator described in the previous paragraph is quite good for low modulation depth, a completely linear transfer function is still the ideal. A circuit which realises this ideal is shown in Fig. 4. The output is a pulse width modulated square wave which oscillates nominally between V1 and V2.

Operational amplifier IC1 integrates the difference of the weighted input and output voltages by the relationship

$$V_3 = \frac{1}{C}\int\left(\frac{V_{in}}{R_{in}} - \frac{\overline{V}_{out}}{R_1}\right)dt \dotfill (3)$$

IC2 is a comparator with hysteresis set by the ratio $\dfrac{R_2}{R_3}$.

The transfer function G from input voltage to average output voltage for this circuit is :

$$G = \frac{\overline{V}_{out}}{V_{in}} = -\frac{R_1}{R_{in}} \dotfill (4)$$
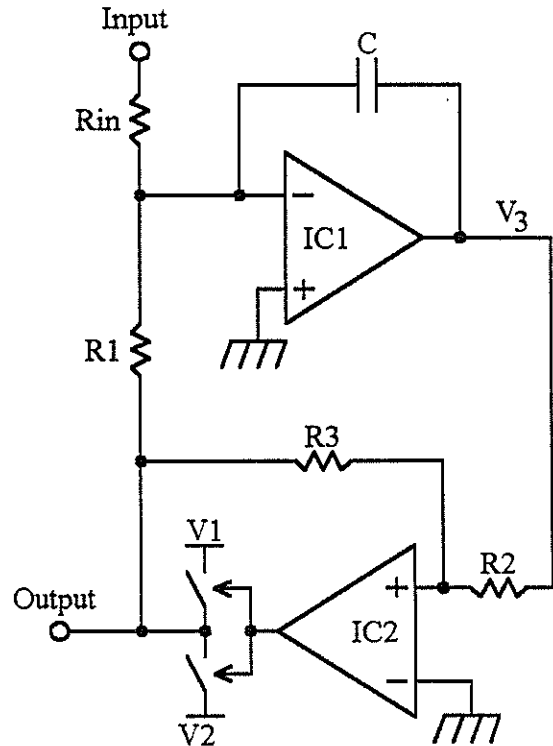
Fig. 4 Linear hysteretic power modulator.

This transfer function is completely linear and not dependent on any of the supply voltages. Normally V_1 = - V_2 = V_{cc}, but even if this condition does not hold, the transfer function remains as shown. This is important because in power applications the voltage drop across the switches will vary as the load current varies.

The only condition that must be satisfied is that Vin/Rin < Vcc/R1. The input can also come from a current source, in which case :

$$\overline{V}_{out} = -I_{in}R_1 \dotfill (5)$$

where I_{in} is taken as positive into the summing node of the op-amp.

The frequency of the resultant PWM wave form is not constant, nor is it a linear function of the input voltage. With the input grounded ($V_{in}=0$), the output is a 50% duty cycle square wave with frequency

$$f_o = \frac{V_1 V_2}{-R_1 C \frac{R_2}{R_3}(V_1 - V_2)^2} \quad\dots\dots\dots\dots\dots(6)$$

With $V_1 = -V_2 = V_{cc}$ the output frequency f_n, normalized to f_o, as a function of input voltage, is:

$$f_n = 1 - (\frac{V_{in} R_1}{V_{cc} R_{in}})^2 = 1 - (\frac{\overline{V_{out}}}{V_{cc}})^2 \quad\dots\dots\dots\dots\dots(7)$$

The output frequency therefore decreases proportionally to the square of the modulation depth. The effects of this frequency modulation are discussed in the following paragraphs.

5. Frequency spectrum:

Even though the transfer function is linear at DC, there is some distortion in the output signal at signal frequencies. Fig. 5 shows a typical spectrum of a simulation at 20% modulation depth. The authors developed a novel simulation technique adapted to this type of circuit. For a more general approach refer to reference 3.
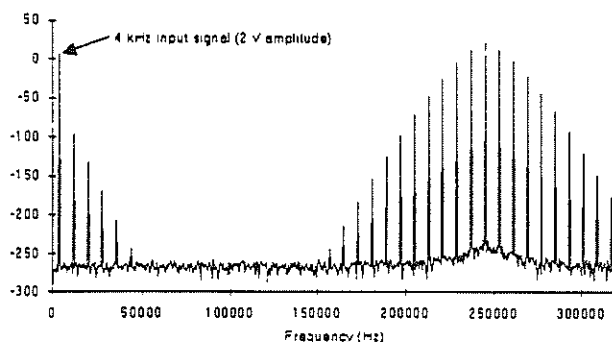
Fig. 5 Output spectrum (in dB re 1 volt) for a 4 kHz input signal.

This distortion increases as the frequency and/or modulation depth increases. The output spectrum contains only odd harmonics of the input frequency, as well as foldback distortion. In order to award a figure of merit to the modulator, it's performance as an audio amplifier was evaluated. A good audio amplifier has a total harmonic distortion (THD) and total intermodulation distortion (TIM) of less than 0.01% (-80 dB).

Fig. 6 and Fig. 7 display the relationship between harmonic distortion and modulation depth at different input frequencies. Fig. 8 and Fig. 9 display the relationship between intermodulation distortion and modulation depth at different input frequencies. The graphs display the amplitude of the largest distortion term below 20 kHz, in relationship to the input amplitude. This distortion is expressed in dB below the input amplitude. All these measurements were made with a zero modulation frequency (f_0 in eq. 6) of 250 kHz.

Because the distortion increases with frequency, the worst-case third harmonic distortion term below 20 kHz occurs at an input frequency of 6666 Hz. As can be seen from Fig. 5, the modulation depth should be kept below 50% to keep the THD below 0.01%.
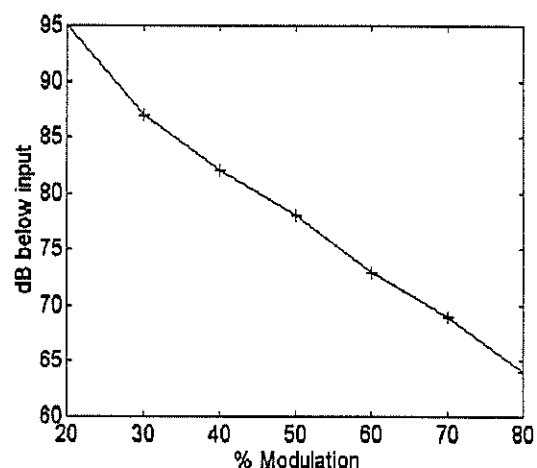
Fig. 6 Harmonic distortion vs. modulation depth at 6666 Hz.

If the effect of the 5th harmonic is also taken into account the distortion shown in Fig. 7 results. At 4 kHz the modulation depth should be below 60% to keep the THD below 0.01%.

The TIM (total intermodulation distortion) of the modulator also increases with input frequency and modulation depth. Fig. 8 displays the TIM with an 1 kHz and 2 kHz (1:1) input signal. At these frequencies and lower the TIM is less than 0.006%. The worst TIM distortion terms below 20 kHz also occur roughly at the third harmonic, and Fig. 9 displays the TIM vs. modulation depth with an 5 kHz and 6 kHz (1:1) input signal.

Fig. 9 shows that the modulation depth should be kept below 55% to keep the TIM below 0.01%.

6. Conclusions:

As mentioned earlier the PWM output frequency decreases as the modulation depth increases. This implies that the output cannot follow high frequency variations in the input signal accurately, because the switching frequency approaches the input frequency - see eq. 7. The THD and TIM therefore increases with modulation depth and input frequency. In order to reduce the distortion for precision applications the designer can take one of two routes : decrease the modulation depth, or increase the switching frequency.
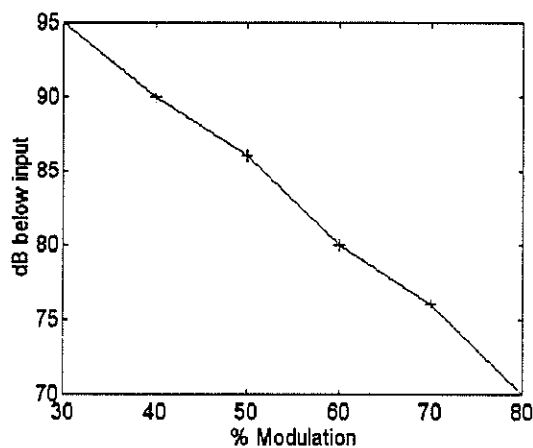
Fig. 7 Harmonic distortion vs. modulation depth at 4000 Hz.
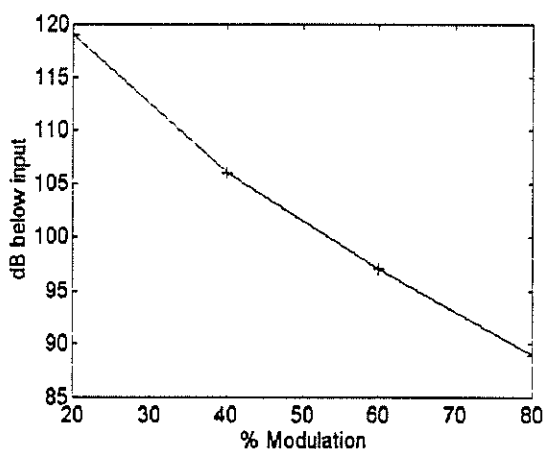
Fig. 8 Intermodulation distortion vs. modulation depth at 1000/2000 Hz.

At 250 kHz the modulation depths should be less than 50% to achieve less than 0.01% THD and TIM in the DC to 20 kHz band. At 350 kHz switching frequency the same distortion figures can be attained with 60% modulation.

If the input signal bandwidth is less than 20 kHz this modulator fares very well. At 1 kHz and 80% modulation the THD is 98 dB (0.001%) and the TIM is 89 dB (0.004%).

7. Applications:

This modulator is very well suited for low to medium frequency (audio) amplifiers, or any other application where a cost-effective accurate PWM modulator is required. The high DC accuracy and low distortion figures makes it an ideal base for a digital-to-analogue-power converter (DAPCO). The voltage gain is dependent on the ratio of two resistors which makes it inherently temperature stable. The modulator can also accept current inputs and can therefore be used in conjunction with the popular current output digital-to-analogue converters IC's. With a current input the gain is dependant on the value of one resistor. For high precision applications this should be a precision resistor.
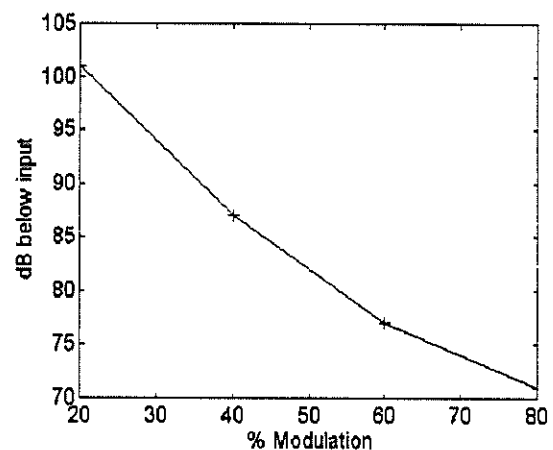
Fig. 9 Intermodulation distortion vs. modulation depth at 5000/6000 Hz.

8. References:

1.Goldberg J.M, and Sandler M.B, "New high accuracy pulse width modulation based digital-to-analogue convertor/power amplifier", IEE Proc.-Circuits Devices Syst., Vol 141, No.4, August 1994, p 315-324.

2. Halasz S, Comparison of Sinusoidal Pulse Width Modulation Methods. Periodica Politechnica, Electrical Engineering. V 37 n 4. 1993. p 273 - 290.

3. Mirkazemi-Moud M, Williams B.W, Green T.C, Novel Simulation Technique for the Analysis of Digital Asynchronous Pulse Width Modulation. IEEE Trans. on Industry Applications. V 30 n 5. Sept. - Oct. 1994. P 1284 - 1289.

9. Address of Main Author:

Prof. G. L. Bredenkamp, Dept. of Electrical and Electronic Engineering, University of Pretoria, Pretoria. 0002. E_mail: gordon.bredenkamp@ee.up.ac.za

Energy, Economy and Environment: The Impact of Conventional-Fuels and Industrial Pollutants

I E Davidson

Department of Electrical Engineering

University of CapeTown

Rondebosch, 7700

Republic of South Africa

Tel: (021) 650 4093

Fax: (021) 650 3565

Email: innocent@emf1.ee.uct.ac.za

Abstract

The industrial progress, national security and financial stability of a nation highly depend on the availability of energy supplies. But the production of most forms of energy from conventional fuels causes pollution which is hazardous to human health and animal life. Imperatively, research and development should focus on conserving natural resources and protecting the environment by reducing polluting emissions through the utilization of more energy-efficient systems to supply industrial, commercial and residential loads. This paper highlights the ecological dangers and consequences of excessive consumption of fossil-fuels; available alternatives from emerging technologies and how these will affect current and future trends in the electrical/chemical process industry.

1 Introduction

The course of human history reveals that the discovery, processing and application of new energy sources have had a profound effect on the quality of human life, organisation of society and economic development[1]. The possibilities afforded by modern technology can only be exploited with the availability of energy supplies especially electricity, due to it's flexibility, transmissibility and wide range of control.

Energy is required in various forms to do useful work and for the continual improvement in the living standards of people. Energy sources therefore have to be explored and developed to enhance industrial progress, national security and financial stability of a nation[2].

In the last century, wood was replaced as the primary fuel by coal in bulk-energy production. However, wood has not ceased to be a major source of cheap energy for domestic purposes in Africa. The historic Industrial Revolution which began with coal has since progressed through the use of petroleum, natural gas and uranium[3]. In this 20th century, oil replaced coal as the leading fuel. The versatility of oil has made it an invaluable commodity, but oil is depletable.

Harsh climatic conditions and distorted weather patterns have in recent times drawn global attention to the political and ecological consequences of excessive consumption of fossil fuels. Awareness is also growing about other dangers of long-term fossil-fuel consumption such as air pollution and global warming. The emission of nitrogen oxides and sulfur oxides (NO_x and SO_2) in tons by utilities, and chlorofluorocarbons from chemical and related industries will have damaging consequences on our environment, such as acid rain, soil degradation and subsequent destruction of vegetation.

With the recognition of the fact that domestic inflation and related economic factors, adjustments in lifestyle and national security are highly dependent on the availability of energy supplies, the pursuit of new, alternative sources of energy, it's conservation and protection of our environment, is a task for energy research and development.

2 Energy Sources and Emerging Technologies

There are two categories of energy sources, namely:

(a) conventional energy

(b) renewable energy.

2.1 Conventional Energy

This is the energy already existing in the earth and includes fossil-fuels, geothermal and atomic energy sources. Biomass and wood are other sources of energy in use.

2.2 Renewable Energy

This is energy reaching the earth from outer space and they include solar and lunar energy. In addition, energy from stars, planets and the moon as well as the potential energy from meteorites entering the earth's atmosphere. The only useful renewable energy sources are the direct solar energy of the sun and the gravitational energy of the moon.

2.3 Energy Demand, Conservation and Forecast

The utilization of renewable energy and it's emerging technologies is very attractive because they are non-depletable and relatively free of pollution in supplying society's energy needs. Other indirect forms of income energy include wind, ocean currents, hydro-power and tidal flows.

Experts predict that world energy needs will continue to grow long after the close of this millenium - not because man will persist in ignoring all dangers to the earth's delicate ecology, but because the world's population will continue to explode[4].

The fact remains that fossil and nuclear fuels are depletable energy sources. We are faced with a world in which oil and gas are running out, nuclear power has turned out to be problematic and the use of coal is constrained by the adverse environmental impacts of its extraction and burning[5].

This equally applies to other carbon-based energy sources. Research and development must focus on conserving natural resources; protecting the environment by producing energy more efficiently for use in transportation, agriculture, and to supply industrial, commercial and residential loads; and drastically reducing polluting emissions.

Energy policies have to be made in determining the types of energy we use, responsibility of research into those we need for the future and the way in which they are to be exploited; taking into account their feasibility, safety, and financial cost as well as the social and environmental effects.

According to Kwuale and Olufeagba[6], some factors affecting energy requirements, demands, consumptions, growth and forecasts are:

(a) the long time trend in energy consumption

(b) population and population growth

(c) climatic conditions and related variations

(d) levels and quality of life of the people

(e) necessary technological know-how, engineering skills and practices

(f) the will of the people to develop on their own (sometimes against both apparent positive, and serious negative international odds[7], and

(g) the correctness of political decisions.

3 Restrictions to the Extensive Utilization of Fuel Sources

Production of most forms of energy from conventional fuels causes pollution, which is hazardous to human health and animal life. For example[2];

(a) Oil Industry - Wells 'blow out'.
   - Pipelines burst (oil spilleage).
   - Oil tankers sink (endangering acquatic life)

(b) Engines - The internal combustion engine is not only noisy and inefficient, but the gases it produces are potentially lethal due to toxic proportions of lead and nickel in fumes. This poses a health hazard.

(c) Coal - This is a major source of air pollution. Burning coal emits sulphur oxides, heavy metals (such as lead, mercury and cadmium), radioactive elements (radium, and uranium); hydrocarbons and large quantities of carbon dioxide leading to acid rain, soil degradation and destruction of vegetation.

(d) Deforestation - This demages the ecology.

(e) Greenhouse Effect - Industrial and utility pollutants such as carbon dioxide and chlorofluorocarbons limit the amount of heat that escapes from earth to the outer atmosphere. This may lead to global warming and a rise in sea levels.

4 Proposed Strategies for Energy Conservation - Environmental Protection

The following contributions and strategies are proposed for energy conservation and environmental protection;

1. Power Plants: - Build new plants around emerging clean-coal technologies, such as fluidized-bed and coal-gasification systems.

- Installation of smokestack "scrubbers" to re-
duce sulfur dioxide emissions.

- Diversion to use of fuels with low sulfur content
and burning fuels in such a way as to produce
low emissions, and additional energy recovery
from heat exhaust gases.

2. Education: Adequate compaigns should be
launched by government to educate our peo-
ple on energy conservation and measures to be
taken to minimise waste.

3. Environmental Policy Act: It should be required
of every government agency that is planning
a project to file an assessment of the impact
on environment. Such an Act should charge
all planners with a responsibility to contribute
to the preservation and enhancement of the
environment.

4. Adequate Funding and Research on Renew-
able Energy: This must be a prerogative of
government - solar energy, wind power, and
implementation of emerging technologies for low
energy industrial applications.

5. Electricity Storage Facilities: Development of
bulk energy storage devices to boost power
supplies in the industry - high energy battery
installations, wind power exploitation and other
renewable energy sources.

6. Cooking Fuel Alternative: To minimise de-
forestation due to dependence on fuelwood,
'treated' gas is a suitable alternative for cooking.
This can be implemented effectively by a reduc-
tion in the prices of cooking gas, gas cookers and
gas storage cylinders[2].

7. Low Grade Uses of Electricity: Elimination of
low grade uses of electricity that can equally
or even better be than any other means- solar
heating, solar-powered fans

8. Deforestation Policy: This policy must be en-
forced with stringent penalties, to preserve our
forests and wildlife for ecological reasons, and to
check unauthorised exploitation of forest wood,
wildlife hunting and extensive bush burning.
Tree planting programmes should be promoted
from time to time to replace the forest, and to
check soil erosion and desert encroachment.

9. Energy Storage Facilities: Use of hybrid electro
mechanical storage facilities (e.g compressed air
or liquefied gas released under presssure)[1] to
serve particular indutrial energy needs.

10. Recycling: Use of biomass to produce artificial
fuel. An example is biogas from specially
designed soakaway pits for cooking purposes.

11. Atomic Energy Fusion: Using hydrogen fusion
by the passage of electricity and burning to
liberate heat to boil water, produce steam and
generate power. This form of energy is expected
to thrive since it has the added advantage of
having no adverse effect on our environment[8].

12. Factory Buildings: Design of factories that use
electricity, gas and oil more efficiently in their
manufacturing processes.

13. Low Energy Consuming Equipment: Promote
the use of LEC equipment - flourescent than
tungsten lamps, more efficient motors than large
inefficient motors, etc.

14. Power-Factor Improvement Facilities: These
should be employed in industries to improve on
power factor, and thus reduce energy consump-
tion of machines.

5 Conclusion

Energy, economy and environment are all interre-
lated. Environmental concerns relate to air pollution,
water pollution, thermal waste heat, and climatic
changes of the earth. The implementation and en-
forcement of the strategies and policies mentioned
will encourage interest and turn our attention more
towards renewable energy sources.

Society will have to change to accomondate new
forms of energy, while we at the same time adapt our
traditional sources to also cater for future needs. Such
a trend will exploit non-depletable energy sources
and reduce our ever-increasing trend towards a high
energy-intensive economy.

Our growing population is dependent upon large
inputs of energy to biological systems in other to
provide enough food, since natural systems are no
longer providing enough edible yield. Between one-
half and three-quaters of all the energy used in Nigeria
comes from crop wastes, firewood, charcoal and animal
dung.

The situation inwhich a large percentage of the
populace depend on traditional sources of energy and
little investment in research to develop appropriate
technology to meet future challenges must change.
Industry and government must invest more in techno-
logical research, education and enforcement of viable
energy policies to meet the challenge of the energy
needs of society.

This will improve on the living standards of our
people and reduce soil erosion, loss of much-needed
fertile land and the threatened disruption of the
delicate ecological balance of our society.

References

[1] I. E. Davidson. "New Horizons in Energy Explo-
    ration and Conservation". In *Proceedings of the
    32nd Annual SAN Conference*, volume 17(2), pages
    182–186, 1991.

[2] I. E. Davidson and J. O. Oni. "Energy Conser-
    vation Strategies and Alternative Resources for
    Africa". *Nigerian Journal for Renewable Energy*,
    NJRE-2(1):85–88, 1991.

[3] G. F. C. Roger and Y. R. Mayhew. *Engineer-
    ing Thermodynamics Work and Heat Transfer*.
    Longman Group Ltd, Essex, 1967.

[4] Siemens AG. "The Company Innovation and
    Quality for the World". A19100-F-A170-X-7600,
    Munich, Germany, 1991.

[5] M. Gibson. *The Energy Crisis*. Wayland Publishers
    Ltd, East Sussex, 1987.

[6] P. A. Kwuale and B. J. Olufeagba. "A Study
    for Energy Demand and Growth". *The Nigerian
    Engineer*, Jan-March 1980.

[7] B. Epstein and K. R. U. Mirow. "Transnational
    Corporations Accused of Restrictive Business Prac-
    tices in Brazil". *Electrical Review International*,
    202(9), March 1978.

[8] R. C. Dorf. *Energy, Resources and Policy*. Addison-
    Wesley, Massachussetts, 1978.

Energy Management Isues in Nigeria:
Implications on Manufacturing
Technology and National Development

DAVIDSON, Innocent E
Department of Electrical and Electronic Engineering,
University of CapeTown,
Rondebosch 7700, SOUTH AFRICA
Phone: 27 (21) 650 4093, Fax.: 27 (21) 650 3465
E-Mail: innocent@emf1.ee.uct.ac.za
and
ONI, Joe O
Department of Electrical and Electronic Engineering
Federal University of Technology
P.M.B. 704, Akure
Federal Republic of Nigeria

Abstract

The discovery, processing and application of new energy sources have had a profound effect on the quality of human life, organisation of society and economic development. Electrical energy has become the bedrock upon which the vast possibilities afforded by modern technology can be exploited, due to it's flexibility, transmissibility and wide range of control. This further enhances industrial progress, national security and financial stability of a nation. Nigeria is endowed with vast primary energy sources, but the high cost of utility installation and management has resulted in tremendous increases in electricity tariffs and cost of petroleum products. This paper evaluates the nation's energy managements issues, the impact of recent government policies on the manufacturing industry as well as economy, and proposes strategies for energy conservation, resource management and national development.
Key words: Energy, Management, Strategies.

1 Introduction

Nigeria is endowed with vast primary sources of energy such as fossil-fuels and hydro power. These huge potential resources make the country potentially rich but the country is yet to establish itself in the path of national excellence. Energy is a phenomenon, and to be quite useful, it is often converted from one form to another through various conversion processes, which are accompanied with losses.

The management of the conversion processes as well as the products from these processes has resulted in several consequences such as the energy crises, environmental pollution, greenhouse effect and a host of economic and social problems. There is a strong correlation between the standard of living as measured by the per capital gross national product and the per capital energy consumption[1], beside related social, cultural and geographical factors, all of which certainly influence energy utilisation and technological development.

2 Energy and Economic Development

It has been well established and accepted that for any nation to be empowered to thrive in 21st century trade realities and environment issues, she has to possess the following;

- Highly skilled and educated manpower
- Vast mineral wealth and resources
- A rich and well established Agro-Allied Industry
- Vast Energy resources, and
- Developed Modern Technology

According to [2], technology may be defined as the economic utilization of exploitable energy resources, men, money and materials (through the application of scientific knowledge and the practice of industrial arts) for the benefit of mankind. Very few nations certainly have all five requirements. In Africa, the focus in on a few key nations to make a breakthrough in this regard, which would require a thorough plan, great sacrifices and the national will to attain.

Nigeria as an oil-exporting developing country did not face the devastating impact of the energy crisis. Unlike most oil importing developing countries, the oil price shocks of 1973-74 and 1979-80 had the direct impact of increasing cost of imported oil, indirect impacts of global inflation, high interest rates and the collapse of many commodity prices. Increased earnings on exported oil, created a comfortable electric planning environment temporarily.

But this industry under the present negative climate induced by an inept national leadership and gross mismanagement faces numerous challenges such as load-growth assumptions, integrating the emerging and evolutionary renewable energy technologies, and many political and financial pressures as well as the enormous cost of infrastructural requirement of underdeveloped (rural) areas[3].

3 Energy Management

In 1990, Nigeria produced a total of 1003.9 billion cubic feet of gas, of which 791.5 billion cubic feet or 78.8% percent was flared[4]. Approximately 112.7 billion cubic feet was sold and 28.9 billion cubic feet was used as fuel in the production facilities This accounts for over tenfold rise in the price of gas in the past two years.

With this waste and environmental hazard, gas invaluably has become a scarce and expensive fule, hence the heavy demand on the use of kerosine as domestic fuel. Kerosine is a convenient alternative to cooking gas. However, with porous national borders and heavy demand precipitated by international bunkering, local consumers have to make their purchaces from illegal markets at excessive prices.

Production of most forms of energy causes pollution. For example in the oil industry[5];

• Wells 'blow out'
• Pipelines burst (oil spilleage)
• Oil tankers sink (endangering acquatic life)

The internal combustion engine is not only noisy and inefficient, but the gases it produces are potentially lethal due to toxic proportions of lead and nickel in fumes. This poses a health hazard.

Coal is a major source of air pollution. Burning coal emits sulphur oxides, heavy metals (such as lead, mercury and cadmium), radioactive elements (radium, and uranium); hydrocarbons and large quantities of carbon dioxide leading to acid rain. Furthermore these have a demaging ecological consequences.

3.1 Agriculture and Transportation

Large-scale application of solar energy in Nigeria is in the agricultural sector - drying operations. Diesel and petrol fuels are used extensively to drive agricultural machinery but this is confined to major mechanised schemes only. The low-scale technological activities in agricultural mechanization clearly reflects this.

Although there is no reliable statistics to cite, transportation consumes much more energy than any other sector, considering energy utilised in rail transport,

automobile, airplane and freight involving railroad, trucks (trailers), inland waterway, oil pipelines. In the United States, transportation accounts for 25% of total energy consumption.

3.2 Industry

Energy utilised in industries is predicated on economic consideration. Therefore the distinction between gross energy demand and useful energy is better weighed in terms of energy consumed to produce a certain worth of goods. Generally, energy utilised in industries include,

• Primary metal production - tin processing in Jos, steel processing in Ajaokuta
• Cement Industry
• Petroleum and coal production
• Stone, clay and glass proceesing
• Paper and pulp industry
• Chemical industry
• Food processing

3.3 Waste Energy Management

A lot of energy is lost or wasted during industrial and manufacturing processes. This could occur in the form of affluent and heat discharge into cooling medium, in addition to inefficient heat exchangers and converters. In a conventional operation method, rejected heat is considered a waste product, which is a significant percentage of the nation's annual fuel requirement. This offers opportunity for energy savings when properly managed as in cooperative generation schemes[4].

4 Government Policies

The governments unprecedented 700% increase in basic price of domestic fuel, kerosine, petrol and diesel is a price shock that has had the indirect impacts on national inflation, high interest rates and the collapse of many commodity prices. Increased earnings on petroleum products by government has consequently resulted in people using less of these fuels and in both domestic and commercial sectors, while the industrial sector has taken a further increase in production costs in general.

This trend has had a negative effect on the national prerogative for electrification, created imbalances in load-growth assumptions fro power planning, disrupted the program of integrating the emerging and evolutionary renewable energy technologies, and produced diverse political and financial pressures, as well as the enormous cost of infrastructural requirement of underdeveloped (rural) areas.

Nigeria envisages to boost her production of petroleum to capacity of 2.5 million barrels per day by 1995 [6]. Reserves capacity are estimated to,last for another 40 years given the present production capacity. With new oil wells being discovered prospecting activities continue, and reservoir management, Nigeria will remain in the oil production and exporting business for a long time given no drastic changes on modern energy utilisation systems and significant breakthroughs in alternative energy sources and systems.

5   Conservation Strategies

The following contributions and strategies are proposed for energy conservation and alternative resources;

1. **Hydropower** - Develop fully the hydroelectric potentials in Africa since it is a cheap energy source; giving adequate attention to irrigation needs and environmental effects.

2. **Manpower** - Training of scientists in developed countries as a means of technological manpower development and engineering skill acquisition.

3. **Natural Gas** - Exploitation of this potential in Nigeria rather than flaring away the gas while prospecting for oil. The Liquefied Natural Gas Project of Nigeria is a positive step in this direction[7].

4. **Cooking Fuel Alternative** - To minimise deforestation due to dependence on fuelwood, gas is a suitable alternative for cooking. This can be implemented effectively by a reduction in the prices of cooking gas, gas cookers and gas storage cylinders.

5. **Low Grade Uses of Electricity** - Elimination of low grade uses of electricity that can equally or even better be served by other means, e.g solar home heating, solar-powered fans, etc.

6. **Deforestation Policy** - This is a vital policy to preserve our forests and wildlife for ecological reasons, and to check unauthorised exploitation of forest wood, wildlife hunting and extensive bush burning. Tree planting programmes should be carried out from time to time to replace the forest, and to check soil erosion and desert encroachment.

7. **Factories** - Design of factories that use electricity, gas and oil more efficiently in their manufacturing processes.

8. **Houses** - Building homes that are well aerated (as well as insulated) to cut down on energy consumption on space heating and air conditioning during weather extremes.

9. **Low Energy Consuming Equipment** - Promote the use of the above, e.g. flourescent than tungsten bulbs; more efficient small motors than large inefficient motors in factories, etc.

10. **Use of Pumped Storage Scheme** - To take off excess generation as a means of energy storage.

6   Conclusion

The Nigerian National Petroleum Cooperation (NNPC) which is charged with a commitment to supply the Nigerian market with it's full requirement of petroleum products safely, reliably and at affordable cost must rise up to it's stated objective. With proper management, good storage and equitable distribution system by NNPC, this goal would be realised.

References

[1] R. C. Dorf. *Energy, Resources and Policy*. Addison-Wesley, Massachussetts, 1978.

[2] P. A. Kwuale and B. J. Olufeagba. "A Study for Energy Demand and Growth". *The Nigerian Engineer*, Jan-March 1980.

[3] I. E. Davidson. "Planning for Electric Power in Nigeria in the Face of Change". In *Proceedings of the International Conference on the Implementation of Renewable & Alternative Energy Technologies*, volume CRAET-92, 1992.

[4] J. O. Oni. "Improvement of the Economics of Energy Conversion Process through Cooperative Generation of Process Steam and Electricity". In *Proceedings of the International Conference on the Implementation of Renewable & Alternative Energy Technologies*, volume CRAET-92, 1992.

[5] I. E. Davidson and J. O. Oni. "Energy Conservation Strategies and Alternative Resources for Africa". *Nigerian Journal for Renewable Energy*, NJRE-2(1):85–88, 1991.

[6] J. Aminu. "National Press Briefing on Activities of the Ministry of Petroleum Resources for the year 1990". *The Daily Times*, May-4 1990.

[7] E. E. Agbah. "Liquefied Natural Gas(LNG) for Nigeria- The Journey So Far". *The Nigerian Observer*, pages 5-6, 11-12, Jun-30 1989.

POTENTIAL OF RENEWABLE ENERGY SOURCES IN RURAL ELECTRIFICATION

N.M. Ijumba
Department of Electrical Engineering
University of Durban-Westville
Durban - South Africa

C.W. Wekesah
Department of Electrical Engineering
JK University of Agriculture & Technology
Nairobi - Kenya

ABSTRACT

Rural electrification is increasingly being seen as an integral component of programmes designed to improve the environment and quality of life in the rural areas, where the majority of the population is. Rural load centres are normally remote and scattered, with low demand and poor load factor. It is not always cost-effective to supply them via grid extensions or stand-alone diesel stations. Renewable energy sources, such as PV solar and small hydro schemes, can be practical alternatives in areas where traditional sources are not viable. Their main disadvantages are the initially high capital investment costs(PV systems), and being site specific(hydro schemes).

1. INTRODUCTION

Rising costs and unsustainability of conventional energy sources , as well as, the need for environmentally friendly energy supplies, are considered to be the main factors that have stimulated interest into studies for practical applications of renewable energy sources.

Renewable energy supplies are considered to be partly or wholly generated in the course of an annual solar cycle. They are extremely variable in time and space, and are generally more difficult to store, compared to conventional energy supplies. Examples of renewable energy sources are biomass, wind, hydro and direct solar radiation. Such sources are usually site specific(e.g. hydro), appear in low concentrations(e.g. wind and solar), and hence require capital intensive equipment to convert into more useable forms of energy(e.g. electricity). However, renewable energy sources have relatively low maintenance costs, and are well suited for meeting energy requirements of sparsely populated, isolated and remote consumers, such as rural communities.

The impetus for rural electrification has mainly been due to the growing realisation of the importance of providing reliable and clean energy supplies to such areas, for their socio-economic development and environmental protection. In many developing countries, over 80% of the population is rural based. The major household energy requirements in rural areas are for cooking, lighting and heating. Wood-fuel supplies 80% of the cooking energy needs. Kerosene fuel is mainly used for lighting(1).

Utilisation of these resources places pressure on tree forests and subjects individuals to pollution due to inhalation of smoke and fumes in households. Provision of electricity to the rural areas would give people an alternative cleaner energy source. It will also stimulate socio-economic development, contributing to an improvement in the quality of life in the rural areas.

Electricity consumption in rural areas is generally very low, compared to the urban settlements. In Kenya, for example, less than 2% of the total electricity revenue is from rural areas, comprising mainly of domestic and small scale consumers, with peak demands of less than 25kW (1). In South Africa, the number of people in rural areas with access to electricity, is estimated to be much less than 15% (2). In both countries, comprehensive rural electrification programmes have been developed, to ensure a rapid growth in the number of communities with access to affordable electricity.

Electricity supply to rural areas is mainly by grid extensions or stand-alone diesel power stations, owned by the national utility companies. Normally, such companies consider rural electrification schemes uneconomical because the demand is low with poor load

factors, and the loads are so scattered that it makes it difficult to design and operate cost-effective supply systems. In many countries rural electrification schemes are initially subsidised to stimulate demand. The low demand can be attributed to factors such as poverty and lack of awareness among the potential consumers.

Renewable energy (RE) sources offer an attractive alternative to the traditional rural supply sources because: they are available in abundance in the rural areas, their implementation utilises local human and material resources, and they are environmentally friendly. RE based supplies can also be configured to meet demands of scattered, remote and isolated loads, giving consumers complete ownership and control over the supplies.

2. SOURCE AND LOAD CHARACTERISTICS

2.1 PV Solar Energy

Solar energy is low density sun's radiation, which is converted to electrical energy, using photovoltaic(PV) cells. Commercial PV cells have a conversion efficiency of between 10% and 12%. The most commonly used PV system is the stand-alone type, which is more suitable for meeting small rural electrical energy needs, ranging between 1W and 1 kW. Stand-alone PV systems are inevitably applied with storage batteries, because of the intermittent and variable nature of sun's radiation. A typical daily solar power output characteristic, obtained during this study , assuming a 12% conversion efficiency, is shown in Figure 1.
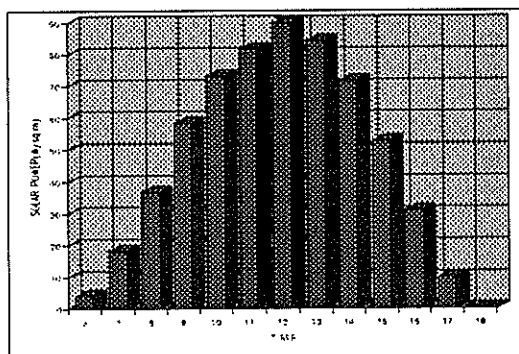
Figure 1: Mean daily solar power output

In rural areas PV systems are mostly used by: Domestic consumers for lighting, radio and TV supplies; small commercial centres and rural businesses to supply lights, refrigerators, cash

Widespread practical application of renewable energy sources will depend on their cost-effectiveness, compared to grid extensions and stand-alone sources.

This paper is based on the findings of a study conducted in Kenya, to assess the viability of PV and mini-hydro sources, to supply rural loads. An economic comparison of the alternative sources was made on the basis of energy unit cost(i.e. cts/kWhr), using the present worth method, assuming a 20 year equipment life-cycle. The unit cost was evaluated using energy consumption data of a rural community, as well as equipment and construction costs of PV and mini-hydro systems.

registers, computers, typewriters and security systems; social community facilities such as schools and health centres, for supplying audio-visual equipment, vaccine refrigerators, sterilisers and water pumps, telephone exchanges and telecommunication links. PV systems are normally considered for application where, either electricity is the only form of required energy, or reliability of supply is the main criteria. The main advantages of such systems are that they: Require less maintenance compared to conventional generators; can be tailored to meet individual requirements; and can easily be expanded by adding solar modules and batteries. However, their initial costs are high, they use batteries and, in some cases inverters, which require maintenance or replacement, and can be complex technologies for some of the consumers. Moreover they cannot meet the heavier energy requirements, such as for cooking.

2.2 Small Scale Hydro-Power

Small hydro power plants are hydraulic works which use water to generate electricity. They are further classified into the following categories, on the basis of power output: Micro-hydro(up to 100kW), mini-hydro(100kW-500kW) and small- hydro(500kW-2500kW). Small scale hydro schemes normally require low investments, have short construction periods and low operating costs. Their technology is relatively simple, reliable and well proven for application in developing countries. Local materials can be used in the construction and manufacture of generation equipment. The range of power outputs for the different schemes is quite sufficient to meet energy requirements

of domestic, commercial and industrial consumers in a rural community.

Hydro-power output depends on the rate of discharge and head, which are virtually constant throughout a given day. However, it has seasonal variations, which depend on the rate of precipitation in an area. The main disadvantage of an hydro-power source is that it is site specific. Normally, it is impracticable to develop a site, if the available head is less than 3m(1). Also, regulation of output power to match demand, can be a problem in small hydro schemes.

2.3 Rural Loads

The demand in rural areas is for domestic, commercial and agro-based industrial activities. Typical maximum demand values for a rural community can range between 30kW and 300kW, depending on the size of the community, level of sophistication of the consumers and facilities available in the community(3). Domestic consumption is mainly for lighting and entertainment(i.e. radio and TV), which requires about 10W to 50W .For the more well to do consumers, it might include ironing, refrigeration and cocking loads. The daily load profile depends on the social habits of the consumer. Generally, peak loads occur in the mornings and evenings, when lighting and cooking loads are required. There might be an additional peak around mid-day during weekends. The average weekday and weekend consumption patterns obtained for the rural load in this study, are shown in Figure 2.
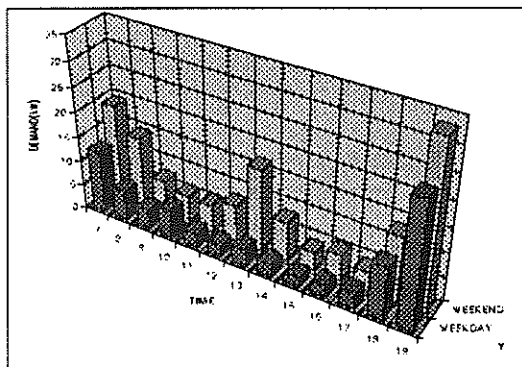
Figure 2: Mean weekday and weekend load demand

The majority of the consumers were domestic, and the average load factor was about 30%. The peak demand was about 35kW. Data obtained

during this study, also showed that about 70% of the rural load was domestic and small commercial consumers with individual maximum demands of less than 25kW. Commercial consumers included shops, small restaurants and bars, craftsmen and artisans, who are more likely to be located at community centres. Commercial activities tend to take place mostly during the middle part of the day, and this helps in improving the daily load factor.

3. ECONOMIC CONSIDERATIONS

Since system cost depends on a number of parameters, then conclusions drawn from an economic analysis of different systems, must be based on specified conditions. The alternative sources considered had different initial capital investment levels, and future annual costs. It was, therefore, decided to compare them on the basis of energy unit cost, as a common figure of merit. The energy costs were evaluated using the discounted cash flow method of analysis, assuming a 20 year life period of the equipment.
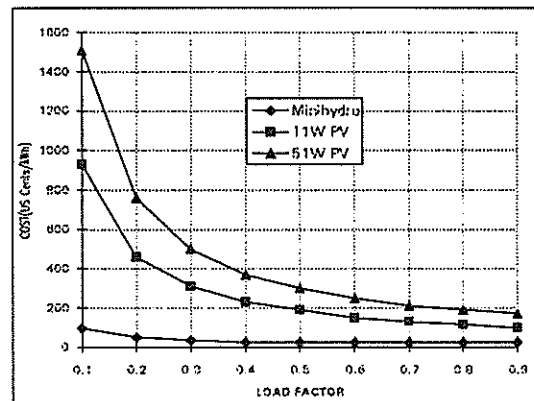
Figure 3: Variation of energy unit cost with load factor

The energy unit cost for the PV system was calculated on the basis of average market prices of equipment used(i.e. 11W and 51W solar panels, 100Ah and 75Ah batteries, 12V fluorescent bulbs and accessories). The battery replacement interval is normally difficult to determine, because it depends on the type, usage and maintenance procedure. It was reported in an earlier study that the cost of replacing a battery can be as high as 25%-40% of the total life cycle of a PV system(4). In this study, a 4 year replacement cycle was assumed. The unit

cost was found to depend on system capacity and load factor(Figure 3).

The unit cost of a small hydro scheme was dependent on the load factor and distance to the site. The cost becomes significant with increasing distance because of considerable losses along the low voltage transmission lines(Figure 4). The unit cost for supply from a grid extension depends on the tariff structure of the utility company. Tariffs for the rural consumers are usually lower because of the subsidies, and this makes it difficult to have a valid comparison with alternative systems. In Kenya, for example, rural consumers with demand of less than 25kW, pay about US cents 5/kWhr, regardless of the load factor.
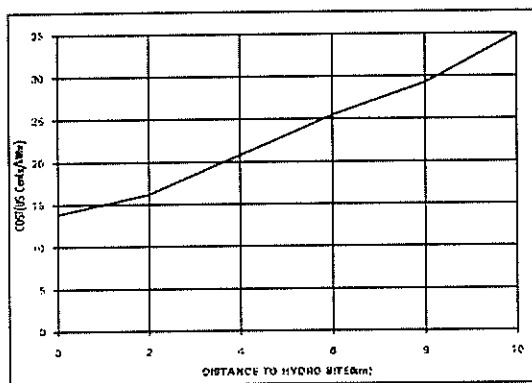
Figure 4: Variation of energy unit cost with distance for a micro hydro scheme

4. CONCLUSION

Based on cost considerations alone, grid extension is the most cost-effective system of supply for rural electrification. However, in cases where grid extension is not viable due to long distances or low returns, then small hydro schemes or PV systems can be practical alternatives. Communities living close to suitable sites can be supplied from hydro schemes. The available power is even sufficient to support small scale industrial activities, and the domestic or commercial consumers can connect more appliances.

PV systems are practical alternatives for supplying light loads in individual households, and community centres(e.g. schools and dispensaries), in remote areas with no suitable hydro sites. They have the advantages of low maintenance costs, and the consumer has total

control of the supply. However, the required capital investment is too high for the majority of rural consumers. It is estimated to be about US$6.2/W$_P$, and expected to fall to US$2.5/W$_P$, at the turn of the century(5).

5. REFERENCES

1. Wekesah, C.W., 'Assessment of renewable sources potential for rural electrification', M.Sc. Thesis, University of Nairobi, 1995.

2. Dutkiewicz, R.K., 'The ANC National Meeting on Electrification', Journal of Energy R&D in South Africa, Vol.3, No.1, 1992, p19-22.

3. Shanker, A and Krause, G.G, 'Decentralised small scale power systems', Rural Electrification Guidebook for Asia and the Pacific, Institute for Energy Research, Bangkok, 1992.

4. Cowan, D., 'PV power for rural areas of Southern Africa...', Journal of Energy R&D in Southern Africa, Vol.3, No.1, 1992, p7-18.

5. Mwanza, P.N. and Pashkov, Y.V., 'Renewable sources of energy in Africa:...', Journal of Energy in Southern Africa, Vol.6, No.3, 1995, p143-150.

ADDRESS
Professor N.M. Ijumba
Department of Electrical Engineering
University of Durban-Westville
P/Bag X54001, DURBAN 4000
SOUTH AFRICA

POTENTIAL FOR SUPPLYING REMOTE COMMUNITIES BY TAPPING FROM HV LINES

Trevor E Holmes, Charles E Dingley

Department of Electrical Engineering, University of Cape Town

ABSTRACT

Rural electrification is a problem in South Africa. Vast distances must be covered to reach remote communities, while population densities of the open regions are very low. These factors make electrification both difficult and costly.

Research is therefore done to find alternative methods for rural electrification that will make it both easier and cost effective. Five methods of tapping small quantities of power from HV lines are covered. These schemes are:

> *Fuse Protected Substations*
> *Shield Wire Insulation and Energisation*
> *Captap*
> *Power Voltage Transformers*
> *Magnetic Coupling*

It is concluded that each of the electrification methods studied display a certain amount of applicability to rural electrification needs. The system of magnetic coupling, however, seems fairly impractical. Fuse protection is adequate for 66/22kV and 132/22kV substations, while the other three methods are suitable depending on demand.

1. INTRODUCTION

A large proportion of South Africa's rural communities are as yet unelectrified. High voltage power lines often pass through these areas, connecting larger settlements to the national grid. Electrification of these communities is difficult due to both technical and economic constraints, though the inhabitants of these areas fail to understand these implications and wonder why they are without access to electricity. It is therefore necessary to research new alternative methods of power distribution, allowing small quantities of power to be tapped from the available HV lines. This power can then be distributed to the rural customers.

The research of this paper is based on numerous articles concerning tapping methods, together with information gathered from a 6 week period of residency within Eskom's System Planning Department, East London. An initial literature survey provided little information specific to this field of study.

Section 2 covers the 5 methods of HV line tapping studied, briefly discussing their function and considerations specific to each. Conclusions regarding these methods of power tapping are then made.

2. REVIEW OF POSSIBLE TAPPING TECHNIQUES

Fuse Protected Substation

This system of power distribution greatly decreases the cost of substation construction. The primary side circuit breakers are replaced with high quality fuses, while the transformer itself is designed without an on load tap changer. This is a more standardised method of distribution, however, it is only applied to 66kV and 132kV lines. The power capacity of these substations can vary from 0.5MVA to 5MVA. Figure 1 shows the general layout of the so-called "Flachberger" type substation [1].

The fuses offer both transformer protection and upstream system protection. Fuse rating is dependent on substation power rating. A 15A fuse would prove suitable for a 1MVA substation.

The length of the reticulation system and the load size are factors influencing whether fuses should be used on the MV feeder. NER's can reduce fault currents to adversely affect fuse operation. This implies that in general, if fault currents are low, fuses cannot be used.

Other factors influencing the use of fuses are the importance of the HV line on which the tee-off will occur; the fuse operation time, and the cost of a complete fuse assembly versus that of a circuit breaker. The cost of a 2.5MVA fuse protected substation is approximately R592,000.
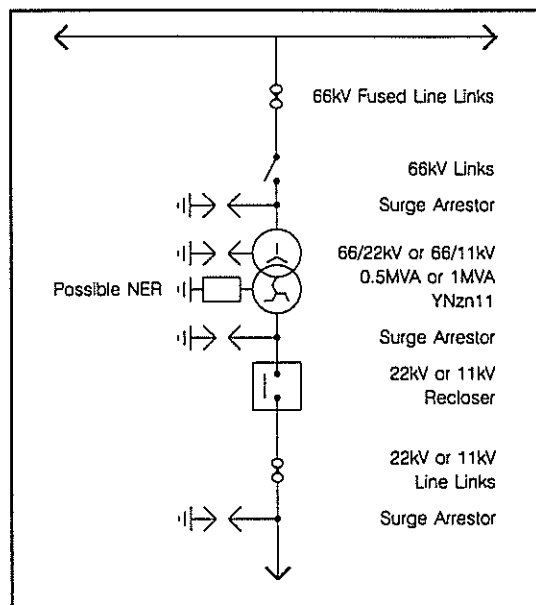
Figure 1: Flachberger Substation

Shield Wire Insulation

This method of power distribution involves the insulation and energisation of the protective shield wires above HV lines. The wires can be connected to an MV source to either supply single or three phase power. In the case of the three phase scheme, the 2 shield wires each carry a phase, while the earth acts as the third phase of the system. Unfortunately, a specially designed source transformer is required [2]. From then on, standard reticulation can be performed, with standard protection. Compensation resistors and inductors are necessary for the earthing of the third phase, and good earthing is required by the entire system.

The power transfer capability of the scheme is dependent on line lengths and line type. In some cases the shield wires would need replacing in order to make the system efficient, though this immediately increases production costs.

The fault level of the HV lines and possible effect on these lines must be considered before installation of the shield wire scheme. In some cases, correct insulation distances cannot be maintained. The importance of structural support offered by shield wires should also be considered, while a high rate of lightning strikes warrants the scheme impractical.

Possible advantages of shield wire insulation include the optimum use made of existing structures and land, and the possibility of supplying up to 2MW in single or three phase configuration, for distances as far as 80km. A case study performed by Eskom set the price

of this scheme at R680,000 for a three phase supply, while the single phase system would cost around R540,000. The scheme was designed to supply 15 potential customers [3].

Captap

Captap is similar to the system of shield wire insulation. In this scheme, however, energisation is obtained not by direct coupling, but by allowing capacitive coupling to energise the shield wires. This implies a large series inductance necessary to create an "ideal" source of power that does not suffer from voltage dips as load size is increased. A 10km length of line can create an 11kV voltage source capable of supplying 30kW of power [4].

It is only suitable to supply small domestic loads, which are largely resistive. A filter is necessary to overcome problems created by system energisation, load rejection, and loads generating harmonics. An earthing switch is available for system protection, while the standard shield wire performance of the lines is retained by the inclusion of spark gaps on the insulators and surge arrestors. The cost of a captap prototype was around R137,000 [4].
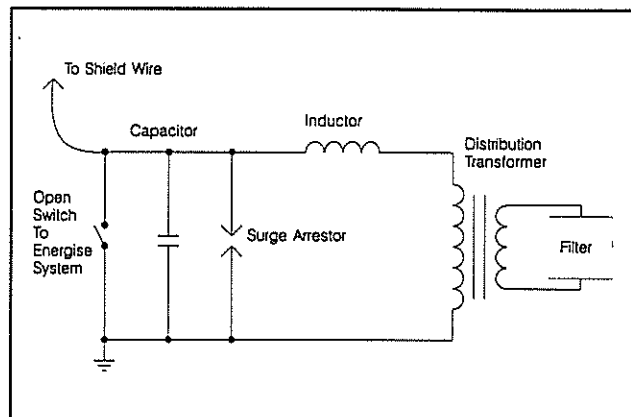
Figure 2: Captap System

Power Voltage Transformers

Power voltage transformers (PVT's) are an adaptation of the standard VT used as a measurement instrument. The German company Ritz has developed PVT's as a method of obtaining low voltage power from HV lines.

PVT's can be connected to supply single phase or three phase power, of up to 300kVA. The output voltage can be a supply voltage of 220V, or 3.6kV to 7.2kV if a small reticulation distance is to be covered before consumption [5]. The units are simply connected directly to the HV lines, with a small LV cabinet necessary for a circuit breaker, metering, and fused protection of the outgoing feeders. A tap changing device could also be included for voltage regulation. The cost of PVT's varies from approximately R49,000 to R172,000 per unit.

Magnetic Coupling

Magnetic coupling makes use of the induced power through the magnetic field radiated from the HV lines, where captap uses the electric field.

Due to the low voltage obtainable, the output is only suitable for charging batteries. Assuming simplistic conditions, a line length of 5.43km was calculated necessary to obtain 15V. This method of induced power requires a looped conductor, implying a total line length of around 11km. The light cable necessary makes cable costs of this system relatively low, though structural costs are comparatively high. The stored battery power is then available for use by a small household. It is intended for light loads such as room lighting and radio operation.

3. CONCLUSIONS

The fuse protected substation is a very economic way of supplying comparatively large amounts of power through more standardised methods of distribution. Correct fuse selection, dependent on fault levels and power rating, should make fused protection adequate for the safe protection of the system. Excluding the on load tap changer reduces cost appreciably, yet correct voltage regulation is no longer possible.

Shield wire insulation utilises existing structures to make medium voltage accessible to remote communities within close range of HV lines. The system is, however, not always applicable. Factors such as physical tower construction and lightning frequency decrease feasibility. The cost of the system as indicated by the case study can also make its application impractical.

The system of captap is acceptable for small loads, again making better use of existing structures. Far less standard equipment is necessary, making the cost of installation far less than that of shield wire insulation and standard energisation. The drawbacks of captap are the limitations imposed by load size and type, and the lack of three phase availability.

Power voltage transformers are easily installed and maintained to offer a reasonably large amount of power. In comparison to the cost of the fuse protected substation system, PVT's are fairly expensive. The three phase system would make the cost of a PVT scheme far more than that of a fuse protected substation transformer for 0.3MVA of power.

Magnetic coupling is impractical, as induced power by the captap system is far easier to obtain due to the single-line nature. The line length needed is therefore unnecessary if the same power is available through the captap method. The system also has the disadvantage that consumed power is only available from a storage scheme, making prolonged usage infeasible.

Although some schemes are more effective than others, all could find application in combatting the problem of rural electrification in South Africa.

REFERENCES

[1] Matthee, P & Mostert, J: *Low Cost Substations For Rural Supplies - Power Transformers Protected By Fuses.* Eskom Central Design, 1994.
[2] Hennessy, T D J: *An Insulated Earth Wire Distribution System - Shield Wire Scheme.* Journal Of Energy In South Africa, May 1994, pp41-45.
[3] Scott, R: *Landplaas Farmers' Scheme - Use Of 132kV Juno/Brandbaai Line Shieldwires.* Eskom Memorandum, 8 Nov. 1993.
[4] Stubbs, L: *A Novel Rural Electricity Supply.* Elektron, June 1993, pp14-15.
[5] Ritz Messwandler: *A Novel Source Of Electrical Energy To Remote Areas Situated Close To HV Transmission Lines.* Elektron, March 1992, pp17-19.

ACKNOWLEDGEMENTS

Solar water heating support system from an electrical supply network
viewpoint and new design goals.

E.F. Lemmer   Dr. G.J. Delport

Centre for New Electricity Studies,
Department of Electrical and Electronic Engineering, University of Pretoria.

Abstract
This article proposes new ideas in the design of solar water heating system. The effects of hot water systems on the electrical load profile have to be studied. Solar energy provides a means whereby the effect on the load profile can be limited.

i. Introduction
The usage of hot water is an important part of people's daily existence. Hot water is not only used for cleaning and purifying purposes but it is a well-known fact that various viruses and bacteria are destroyed when in contact with hot water with a temperature of above 55 °C. The usage of hot water undoubtedly leads to a healthy environment and a better living standard of the community.

ii. Method of heating water
The method with which water is heated varies. Coal, wood and gas are generally use for heating water in the rural areas of South Africa. However a more effective way to heat water is with electricity.

The electrical system that is mostly used is the electric geyser with a tank capacity of 150 liters and a 3 kW heating element. The usage of this system has a disadvantage in the sense that the usage pattern of hot water causes a load profile that is undesirable from an electrical supply network viewpoint.

iii. Load curve of hot water usage
The data required to compile Figure 1 was obtained by monitoring the energy used by 25 000 houses in Randburg [1]. The problem with the specific load profile is that the electricity network must be capable to handle the peak at 07:00 and at 20:00. The ideal flat load profile is also shown in Figure 1.

The load profile between the measured and ideal load profile can be achieve by utilizing solar energy. The energy of the sun can be utilized, during the day when the sun is shining, to heat the water that is required during the evening peak load period. Electricity should however still be used to preheat water before the early morning peak load period.

iv. Solar heating
South Africa is ideally suited for the usage of solar energy for the heating of water. Figure 2 illustrates the sun radiation of a day in the summer and in the winter as well as the average radiation [2].
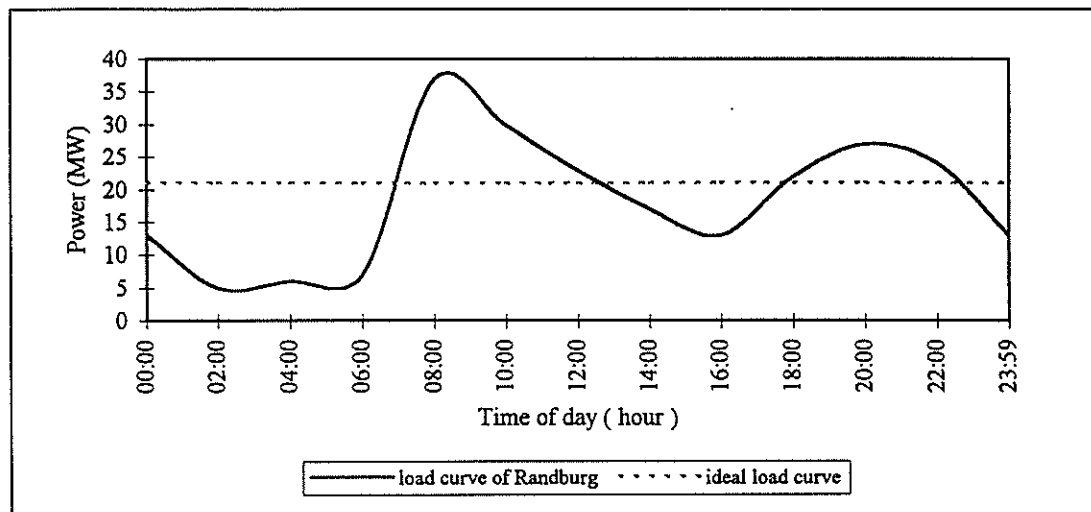
Figure 1   Load curve of Randburg
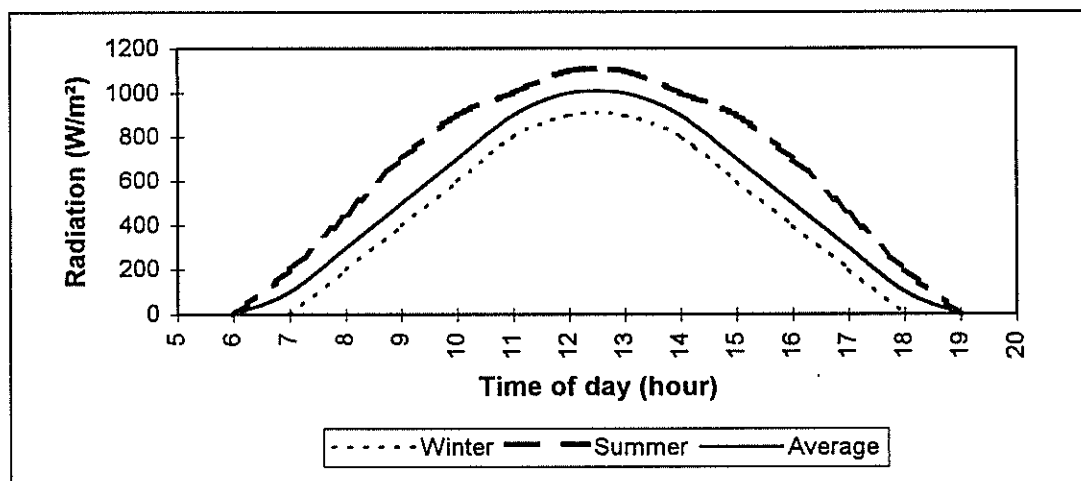
Figure 2   The average sun radiation of a year

In general a solar heating system consist of a solar panel, thermal storage tank, support heating, distribution and control systems. The solar panel is mainly used to heat the liquid. The heated liquid is stored in the thermal tank for later use. The support heating serves as a standby to prevent that the user is without hot water. The support heating can be generated by an electric element, gas, wood or coal.

Heat transfer occurs in two ways: direct and indirect. With the direct system the liquid that is heated in the solar panel is water and is in contact with the water in the storage tank. With the indirect system the liquid in the solar panel is separated from the water in the storage tank. The liquid in the solar panel is usually alcohol. Alcohol has a lower freezing point than water. It is essential where the night temperature drops below freezing point.

Studies have shown the need for the development of a better storage tank that will improve the efficiency of a solar electrical heating system [2].

v. Storage tank
The following equation is valid for a thermal storage tank [3]:

$$Q = V \cdot \rho \cdot c \cdot \Delta T \tag{1.1}$$

Q - The energy stored or required in the liquid [J]
V - The volume liquid [m^3]
ρ - The density of the liquid [$kg \cdot m^{-3}$]
c - Specific heat capacity of the
       liquid [$J \cdot kg^{-1} \cdot °C^{-1}$]
ΔT - Temperature change [°C]

$\rho \cdot c$ is a constant that is only dependent on the type of liquid being used. Therefore Q is direct proportional to $V \cdot \Delta T$. This makes the system controllable. The volume of water stored and the temperature of the stored water can therefore be control. In the present systems the volume of the water is keep constant. The pressure tank is either full or empty. The temperature is thus the only controllable variable.

The need arises therefore to develop a storage tank of which the water level can be control. The advantages of such a system will be enlighten in the following scenario's:

Scenario 1: A sunny day.
The temperature change can be regard as a constant in view of the fact that a specific quantity of solar energy is available. Thus is Q direct proportional to V. For maximum utilization of the solar energy the volume must be keep at a maximum. This will ensure that the least amount of electrical energy will be use to heat the water during the evening load peak.

Scenario 2: Take the period after the evening peak up to the beginning of the morning peak.
Electricity usage must be avoid during the peak periods. By using electricity during the above mentioned period to heat water the influence of the morning load peak will reduce. The efficiency is however a function of the quantity hot water that is stored beforehand. Therefore must V be a maximum.

Scenario 3: Suppose during the peak period the volume hot water stored is too little.
The system is then compel to use electricity to prevent the user having to received cold water. If V is kept at a minimum the amount of energy being used to heat the water will be less than in the cause of a full tank.

A. Construction of storage tank
As describe in the above scenarios the need has arises to build a storage tank in which the water level or quantity of water being stored can vary. The tank is constructed by using an ordinary 150 liter pressure tank of an existing water heater system. Figure 3 demonstrates how the pressure tank will be build.

An elastic pipe is fitted to the outlet and to a float. The hottest water in the tank will always be under the water level, because of stratification of warm water. By fitting the elastic pipe the hottest water in the tank will be let out first.
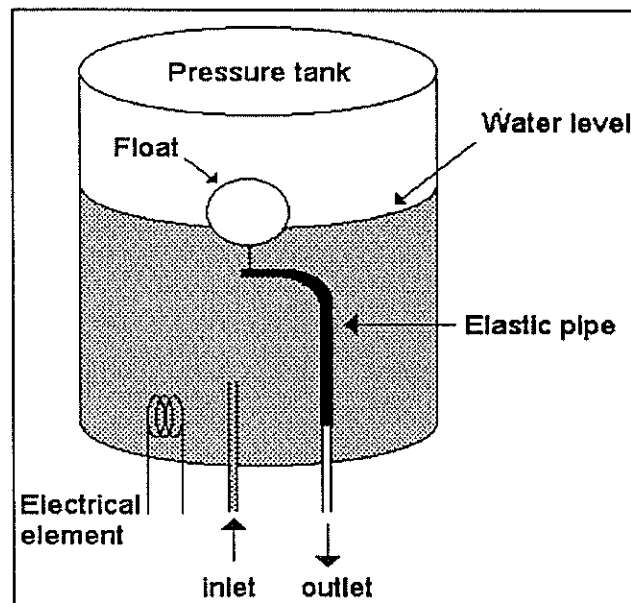
Figure 3   Construction of tank

B. Experimental results

Tests on the system have soon that the water level can be control efficiently (70 %), if the tank is operating under atmospheric pressure. The only set back is the rate of the outlet water. The rate can be improve by mounting the tank as high as possible. If the tank is operating under pressure the rate of the outlet water dramatically increased. The problem with operating the tank under pressure is that the quantity of water being controlled decrease. Only 10 % of the water in the tank is controllable.

vi. Conclusion

Consequently there is a need to develop an affordable solar heating system of which the volume water stored is controllable. The efficiency of the system must be taken into consideration when such a system is provided. The primary function of the system is to deliver hot water. The secondary function that must be taken into account is the effect that the system can have on the load profile. The ultimate goal is to achieve an ideal load profile.

References

[1] A. Janse van Rensburg, "Die invloed van Son-elektriese waterverhitters op die warmwaterlas", Finale jaar projek verslag, Departement Elektriese en Elektroniese Ingenierswese UP, 1993.

[2] L. von Maltitz, "Die invloed van son-elektriese waterverhitters op die stelsellasprofiel", Finale jaar projek verslag, Departement Elektriese en Elektroniese Ingenierswese UP, 1994.

[3] F. W. Sears, M. W. Zemansky and H. D. Young, "University Physics seventh edition", 1987.

E.F. Lemmer, Department of Electrical and Electronic Engineering, University of Pretoria, Kunenelaan 293, Sinoville, Pretoria, 0182. E_mail: Johan.delport@ee.up.ac.za

Integration of Power Electronics - A New Manufacturing and Packaging technology

I.W. Hofsajer, J.A. Ferreira, J.D. van Wyk

Research Group: Industrial Electronic Technology Rand Afrikaans University

Abstract- In this paper a new manufacturing and packaging technology for power electronics is described and evaluated. This technology is required to fulfil the need for cost effective, mass market, power electronics products. The packaging is based on a new planar technology, that is well suited to mass production. One of the features of the packaging is the incorporation of the entire converter inside the magnetic structures of the converter. This leads to very good magnetic shielding, as well as other benefits, but also gives rise to some problems. The technology is illustrated with the integration of an experimental dual active bridge DC-DC converter.

1. Introduction

Electronic energy technology has not made the same impact as information technology. This is especially noticeable in the commercial, residential and automotive fields. These fields of application are characterised by high production volumes and strong levels of competition. Cost is therefore of primary importance and greatly influences the application of any type of technology. The current high cost of power electronics can partly be attributed to a manufacturing technology that is difficult to automate. The successful mass production manufacturing technology for signal electronics is inherently two dimensional in nature, and could not yet be adapted successfully to the inherently three dimensional magnetic structures essential in higher power electronics.

In the reported case studies on design for manufacturing where products with a large electrical content (other than printed circuit boards) are designed and assembled [3] the fundamental electrical design has almost always been omitted from the manufacturing design. The emphasis is on the optimal placement and minimisation of component count from a mechanical point of view rather than an electrical one. If significant cost reductions are to be achieved, the fundamental electrical design must be developed along with the mechanical design, packaging and manufacturing processes.

The manufacturing technology described in this paper departs somewhat from conventional technology, and is based on planar electromagnetic integration [1-2]

2. Packaging overview

Any packaging technology for power electronics must take all the aspects of converter realization shown in fig. 1 into account. Each of the main component groups necessary for each function shown in fig. 1 have their own manufacturing processes and constraints. These processes should be as compatible as possible in order to simplify the total converter production process. The different components must also be electromagnetically compatible in order to ensure correct operation. In order to obtain a packaging technology suited to mass production, each of the component groups in fig. 1 is evaluated from both a manufacturing as well as an electromagnetic point of view.
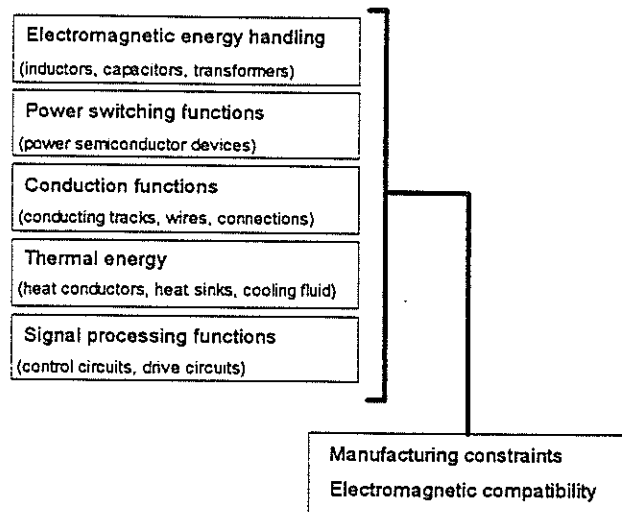
Figure 1 Power electronics converter subfunctions

A Electromagnetic energy handling

(i) Electric

Due to the planar nature of the interconnection structure, the capacitance between the conductors, if correctly designed can be used for snubber capacitance, and to a lesser extent filtering and resonance. As the capacitive structures are planar in nature, it is not possible to obtain large capacitance values by barrel winding conductors and dielectrics. It is also not feasible to manufacture capacitors with hundreds of layers. If large capacitance values are sought, use is made of ferro-electric ceramic dielectrics, which with their very high permittivities, can produce the required capacitance in a few layers.

(ii) Magnetic

As magnetic structures are fundamentally three dimensional in nature, these structures determine the overall form and shape of the total converter structure. Recently planar magnetics have received much attention, especially in high frequency applications [4-5]. Advantages often cited are low leakage effects and losses and high repeatability of device parameters, as well as higher power densities. In the new packaging technology discussed in this paper, the shape of the magnetic material of the main magnetic component of the converter (e.g. transformer), is adapted to allow for the inclusion of other components in, or very close to the conventional winding window [2]. This is best illustrated in fig. 2, where a cut-away view of a core is shown. A further requirement is that all the magnetic components share the same core. This is also one of the constraints on the use of this technology, as it is not possible to implement all converter topologies in this manner. The enclosing core gives very good magnetic shielding, and improves the EMI of the converter.
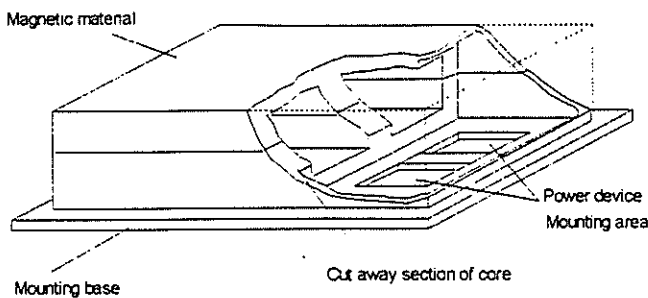
Figure 2. Packaging concept

B Power switching functions

Power semiconductors in their current discrete packaging can be used in the new technology, but due to the fixed nature of their pin-out connections, lead to restrictions on the optimal geometric layout of high current conductor paths. In a mass production environment, it is feasible to mount the semiconductor dies, directly into the converter, without an intermediate packaging step.

C Conduction functions

An important aspect of power electronic packaging is that of the interconnections between the different energy handling structures (semiconductors, transformers, capacitors etc.) These interconnections lead to high production costs, reduced reliability, and introduce additional losses into the system.

In the proposed technology the interconnections and conductors are constructed from a number of planar layers, stacked on top of one another [2]. A planar approach is beneficial from a production point of view, where multiple layers are stacked on top of one another, similar to conventional multi-layer printed circuit boards.

D Thermal energy handling

As heat is both produced in, and conducted through each section of the structure, a thermal analysis is necessary in order to ensure that the operating temperature of all the materials is not exceeded. If the conceptual converter structure of fig. 2 is mounted on a heat sink, thermal energy will generally be conducted vertically. The large flat nature of the structure aids in the thermal design, as in most cases it can be considered to be a one dimensional problem.

E Signal processing functions

The small signal control and drive circuits of the converter, need to be in close proximity to the high power sections, but should not be influenced by the electromagnetic fields of the power sections. The signal electronics functions will still be accomplished by conventional surface mount technology printed circuit boards, that can be mounted inside the converter in field free regions created by the magnetic core.

3. Converter topology and structure constraints

Due to the various constraints on the packaging technology, not all power converter topologies or designs can be integrated with equal ease. There are currently no fixed rules as to what constitutes an easily manufacturable converter topology or design, but the following guidelines can be used to obtain a general figure of merit.

A Minimisation of nodes in the circuit

The number of nodes in the circuit diagram of the converter indicates the number of independent conductors needed. Therefore the number of nodes in the circuit diagram should

be minimised. The exception to this rule is that of the two nodes on either side of an inductor (transformer winding). If an inductor as well as its two connections may be manufactured from a single conductor then for manufacturing purposes it can be considered as a single node, as only a single conductive structure is necessary to produce it.

B Minimisation of crossing conductors

The physical placement of the separate components with relation to each other, can create situations where conductors must cross one another. With the use of planar conductors, this will necessitate the inclusion of an additional layer of isolation material. The number of conductor crosses should therefore be minimised. The exception to this rule is when there is a need for capacitance between the two crossing conductors. Then the insertion of a dielectric between the conductors serves the purpose of both energy storage and isolation.

C Magnetic structures

The magnetic structures dominate the overall shape and layout of the converter. It is therefore necessary that independent magnetic components be compatible with each other, so that a single core (custom if necessary) can be used. This is easily achieved in the case of a series inductor and transformer, as the series inductor is incorporated into the leakage inductance of the transformer. It is more difficult to incorporate large output filter inductors together with a transformer.

D Minimisation of the number of electromagnetic functions

The number of separate energy storage and processing components should be minimised. This minimises the number of separate material parts that need to be handled during production. Use should also be made of integrated electromagnetic components such as LC filter structures, where one piece of material can fulfil more than one function.
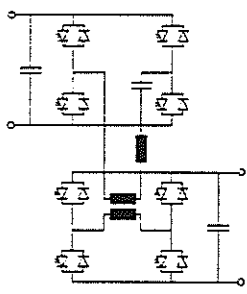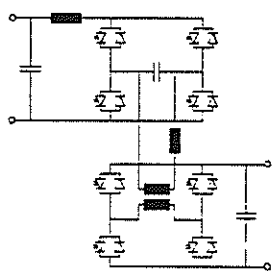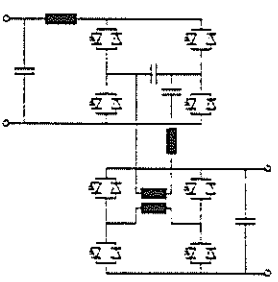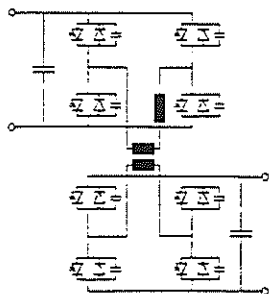
4. Manufacturing analysis example

A common power processing function, with potential high volume application is that of DC-DC conversion, particularly where battery energy storage is used, and where there is more than one DC bus voltage. Examples of this are:

a) Small (1-2kW) uninterruptable power supplies where low battery voltages are stepped up to a higher bus voltage for PWM sine-wave shaping.

b) Dual voltage systems for use in automotive and aerospace applications, where two or more distribution voltages may exist.

c) Power factor compensation, load levelling and impedance matching. As an example, a converter is sought for the interconnection of a 12V and 48V distribution bus, with galvanic isolation and bi-directional power flow. The latter two requirements greatly increase the topology complexity of which would otherwise be a relatively simple circuit. A power level of 360W is required, with higher power levels being achieved by multiple converters in parallel.

Using the guidelines described in the previous section, four possible resonant topologies are evaluated. The results are summarized in table 1. The number of nodes listed in this table is the total number minus a single node on each side of a magnetic structure. The number of crosses listed is the number of times two conductors must cross without there being any capacitance between them. The figure of merit

Table 1 Comparison of topologies from a manufacturing point of view.

Converter topology	No. of nodes	No. of crosses	Independent magnetic structures	Electro-magnetic functions	Figure of merit
Series Resonant	7	0	1	4	12
Resonant LC tank and transformer can be easily integrated Difficult to control for bi-directional power flow					
Parallel Resonant	7	1	2	5	15
Parallel LC tank difficult to integrate and input inductor is needed Difficult control					
Series / Parallel Resonant	7	1	2	6	16
Resonant tank is very difficult to integrate Difficult control					
Dual Active Bridge	6	0	1	3	10
Few reactive components Easy control					

listed is the sum of all the figures, with a lower figure of merit indicating better manufacturability.

The topologies listed in table 1, have certain characteristics in common with each other:

a) Switching frequencies in the order of 200kHz
b) Similar number of semiconductor devices
c) Similar number of windings on the transformers
d) Similar number and order of magnitude size of input and output filter capacitors.

The dual active bridge is well suited to integration, as amongst others the main energy transfer component (inductor in series with the transformer) can easily be integrated into the transformer as leakage inductance. An additional advantage is that there is only one main reactive component other than the DC filter capacitors.

5. Experimental converter

The converter that is used to illustrate this packaging technology is a dual active bridge [6], switching at 180kHz, and using MOSFET switches. The low voltage (12V) bridge is configured as a push-pull rather than a full bridge, due to the higher current. The use of a push-pull configuration instead of a full bridge configuration, on the low voltage side, introduces an extra node into the manufacturing design, but this is offset by reduced semiconductor losses. This additional node would have been introduced in all the evaluated topologies and therefore the relative figures of merit are not altered.

The construction of the converter can best be described by the exploded view shown in fig 3. A photograph of the experimental converter with the outer secondary cores removed is shown in figure 4. (the mounting plate measures 90mm x 110mm).
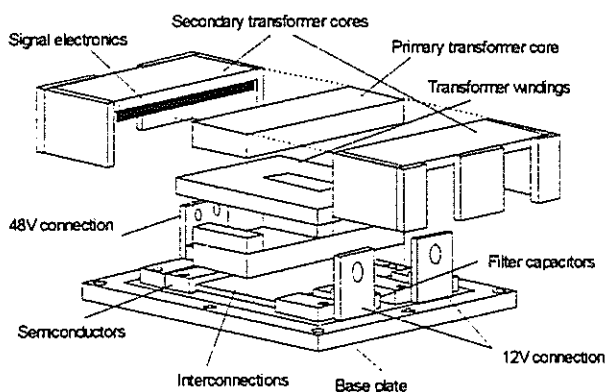
Figure 3 Exploded view of converter

6. Conclusions

A new manufacturing and packaging technology that could produce significant cost savings in the mass production market is described. This technology is not equally suitable to all converter topologies, and a critical evaluation has to be carried out in order to determine the manufacturability for each case considered.

Benefits that can be derived from this technology other than cost are power electronics systems that are more reliable due to a greater repeatability at the manufacturing level, and smaller and lighter systems due to integration.
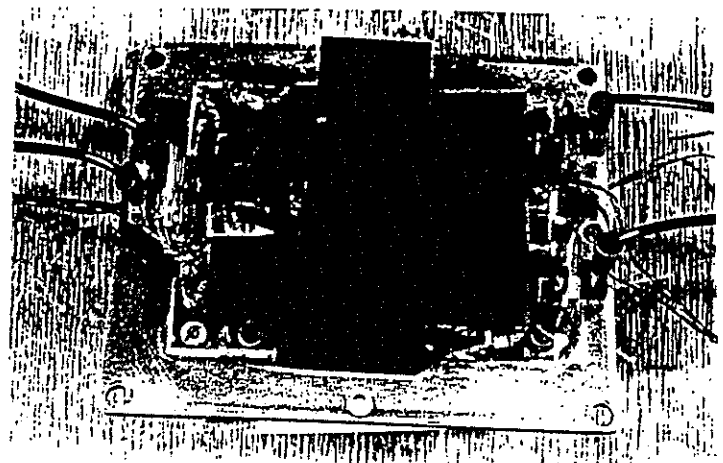
Figure 4 Experimental converter with secondary cores removed

7. References

[1] Van Wyk JD, Ferreira JA, "Some Present and Future Trends in Power Electronic Converters." Proceedings, IEEE IECON 1992, Vol.1 pp 9-18

[2] Hofsajer IW, Ferreira JA, Van Wyk JD, Smit MC, "Integrated Technology and Performance for Multi-kilowatt Power Electronic Converters- An Evaluation" Proceedings, IEEE IECON 1993, pp 779-785.

[3] Wesley Allen C, Simultaneous engineering: integrating manufacturing and design. Society of Manufacturing Engineers, Dearborn, Mi, 1990.

[4] Chew MW,Evans PD, Heffernan WJ, "High frequency inductor design concepts", Conf. Record IEEE PESC June 1991, pp 637-678.

[5] Sasada I, Yamaguchi T, Harada K, Notohara Y,"Planar inductors using NiZn ferrite thin plate and the application to high frequency DC-DC converters", IEEE Transactions on Magnetics, Vol 29, No. 6, November 1993, pp 3231-3233.

[6] Kheraluwala MH, Gascoigne RW, Divan DM, Baumann ED, "Performance Characterization of a High Power Dual Active Bridge DC-DC Converter", IEEE Transactions on Industry Applications. Vol 28, No. 6, Nov/Dec 1992 pp 1294-1301.

EVALUATION OF CONVERTER TOPOLOGIES FOR IMPROVED POWER QUALITY IN DC TRACTION SUBSTATIONS

Abram Horn   Richardt H. Wilkinson   Prof. Johan H.R. Enslin*

Department of Electrical and Electronic Engineering
University of Stellenbosch, Stellenbosch, RSA

Abstract - A high power converter is developed for improved power quality in DC traction substations. The proposed converter can be used as both an inverter and an Active Power Filter (APF). As an inverter, it can recycle regenerative energy caused by decelerating trains and as an APF, it can compensate for harmonic distortion produced by the rectifier substations.

1. INTRODUCTION

With the advent of industrial technology, the number of harmonic producing loads have increased. This caused the introduction of more stringent limits and standards. In South Africa, the electric utility company ESKOM has also introduced a "Standard for Maximum Voltage Distortion in Electrical Networks" [6]. Spoornet's DC Traction substations are a major cause of harmonic distortion in the AC supply. The railways could be seriously affected if these standards were to be enforced [1].

In the past, the excessive regenerative energy caused by decelerating trains, was simply dissipated in resistor banks. Through the use of modern technology, it is possible to recycle this energy. In future it will be all the more important to save energy. Through the use of an inverter in anti-parallel with the traction rectifiers, it is possible to redirect the recycled energy into the AC-supply. The proposed setup is shown in Figure 1.
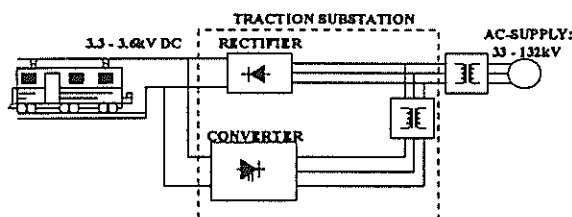
Figure 1 - Proposed DC Traction Substation

2. SOLVING THE AC SIDE HARMONIC PROBLEM

The harmonic problem can also be eliminated by this switching inverter. In this configuration, the inverter can also function as an Active Power Filter (APF) to compensate for the harmonic distortion on the AC side [1]. By dividing the total current drawn from the supply into an active- and a fictitious component using Ensign's correlation techniques [7, 8], the inverter can be used to supply these fictitious power components. This ensures that the current drawn from the utility will be purely sinusoidal. Therefore the harmonic currents circulate between the rectifier and the APF and do not affect the currents supplied by the AC supply. Although an APF is not a cost-effective solution to harmonic filtering, the fact that regeneration is incorporated into the system, makes this converter system an economical option.
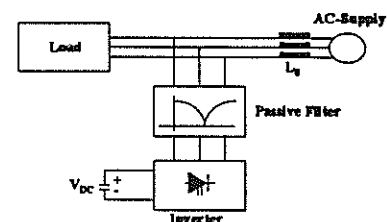
Figure 2 - Harmonic Isolator

An alternative solution is harmonic isolation as shown in Figure 2. Harmonic isolation involves the insertion of an active impedance in series with the line impedance. The active impedance exhibits zero impedance to fundamental frequency components and a high impedance to harmonic components. This ensures that the fundamental voltage drop across the line impedance is not too large. It also ensures a low-impedance path for harmonic currents, as the impedance of the passive filter is lower than the line impedance at harmonic frequencies.

---

* Corresponding Author

Currently, several theories for the determination of the harmonic content exist. The Instantaneous Reactive Power Theory (IRPT) introduced by Akagi [12] or the Synchronous Reference Frame of Divan [13] can be used. The IRPT still has to be evaluated for harmonic isolation and regeneration [4].

3. SOLVING OF THE DC SIDE HARMONICS

Standard 6 and 12 pulse rectifiers produce pn DC side harmonics, with p the pulse number and n an integer. These harmonics interfere with signalling of large traction networks and can be fatal under certain conditions. It is proposed that the anti-parallel converter, shown in figure 1, can also compensate for these DC side harmonics by using the converter as an APF or harmonic isolator on the DC side. For this reason, the DC-to-DC chopper is bi-directional and will have to have a high dynamic response.

4. INVERTER TOPOLOGIES

An IGBT-based switching inverter is proposed because it is expected of the inverter to work as an APF with a high dynamic bandwidth. The use of IGBT-devices leads to a higher switching frequency, resulting in smaller line-side filters. A disadvantage of the IGBT is its low power rating. The low blocking voltage (approximately 2500V) [2] of the IGBT, results in a multi-level converter topology in this high power application.

The multi-level converter can be a multi-level inverter or a combination of a multi-level chopper [3] and a lower voltage inverter. In terms of ease of control, the multi-level chopper and lower voltage inverter combination is the better option. When it comes to harmonic properties, this combination is the better option. The use of constant phase-shifted control signals cause a higher output switching frequency, hence lower harmonics. Using this combination it is also possible to filter the line side DC bus. The chosen topology is more cost effective, as it employs fewer components.

5. PROTOTYPE SYSTEM FOR EVALUATION PURPOSES

A 100 kVA prototype model for evaluation purposes of the DC traction substation is shown in Figure 3. A multi-level chopper with an inverter is proposed. The locomotive drive is represented by a DC machine and multi-level chopper. The modelling of the rest of the train, i.e. the load, is obtained with an AC machine and synchronous rectifier under space vector control. The space vector controller is implemented on a 80C196-based microcontroller [14].
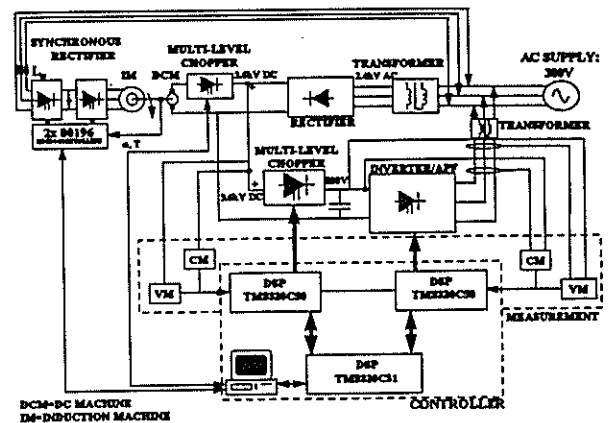
Figure 3 - Prototype Model of proposed DC Traction Substation

Digital signal processors (DSP) are used in the controller of the inverter and chopper. Two TMS320C50's are used for inner-loop control. A TMS320C31 floating-point processor is used for the outer-loop algorithms. In future different algorithms to solve the harmonic problem will be tested in the control system. The interface with the user is through a personal computer.

The measurement system uses optical isolation for voltage measurement and LEM modules for current measurements (VM and CM). A DC dumping system protects the inverter against over-voltage.

5.1 THE INVERTER

The inverter supplies the regenerative energy back to the AC supply and work as an active power filter (APF) under normal operating conditions [1]. When the inverter works as an APF, the power rating to compensate for the higher harmonics is not very large. The power rating of the inverter is determined by the regenerative power of the train's DC machine.

According to Suzuki [15], the relationship between the power capability of the inverter to the power capability of the rectifier will vary between 1:13 and 1:8.3 on a flat-track system. A typical traction substation rating is 4.5MVA. A prototype scale model of 100kVA is chosen for a 1:2.25 relationship between the substation and prototype. This prototype's power capability is more realistic and it is still practically possible to build and operate it in a laboratory.

Two prototypes have already been built in the laboratory: a 15kVA proof-of-concept prototype and a 100kVA prototype. The block diagram of the 100kVA prototype is shown in Figure 4.
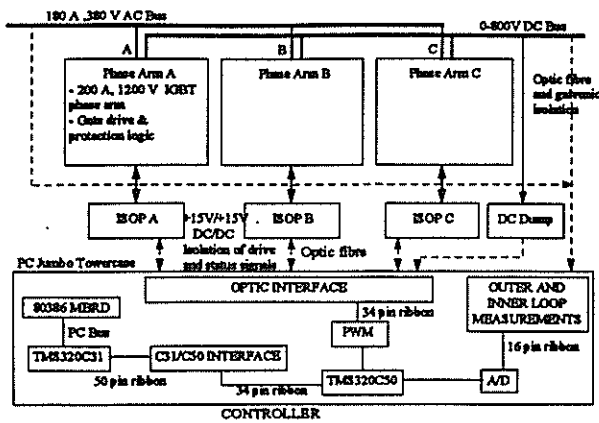
Figure 4 - Block Diagram of Inverter with Control System

Experimental results of the 100kVA inverter used as an APF is shown in Figure 5 and Figure 6. The first trace is that of the current (i_{s1}) drawn by the rectifier from the AC supply. The second trace shows the current (i_s) drawn from the AC supply before (Figure 5) and after (Figure 6) compensation. This trace is only a prediction based on experimental results. The injected current (i_{ax}) supplied by the APF to compensate for the harmonic distortion, is shown in trace three. This current was injected into a star-connected inductor and not into the network.
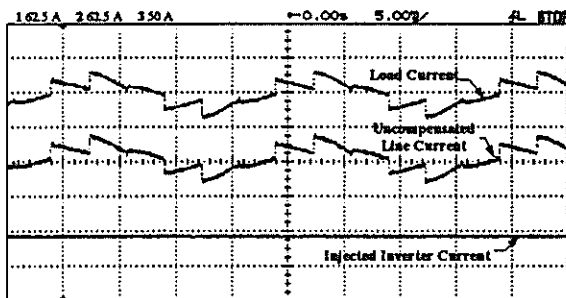
Figure 5 - Uncompensated Currents
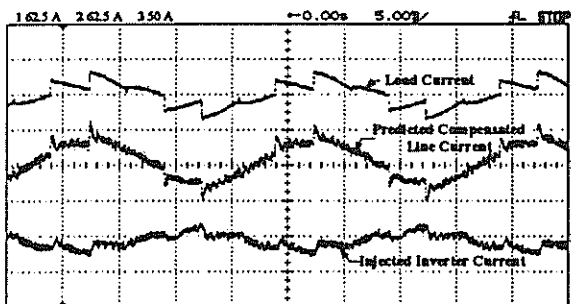
Figure 6 - Compensated Currents

5.2 THE MULTI-LEVEL CHOPPER

The chopper circuit is used to convert the regenerative energy on the DC side from 3-4kV, down to a DC bus voltage of 800V. Furthermore, the chopper is used as a modulator, to form a low impedance path for the DC side harmonics.

Currently, a prototype bi-directional multi-level chopper is evaluated for the design of a high power multi-level chopper. A switching method devised by [5], where phase-shifted control signals are used to switch the series connected devices has been tested. Usage of typical "step" switching, characteristic of multi-level choppers, is also investigated. The schematic diagram of the prototype multi-level chopper, is shown in Figure 7.
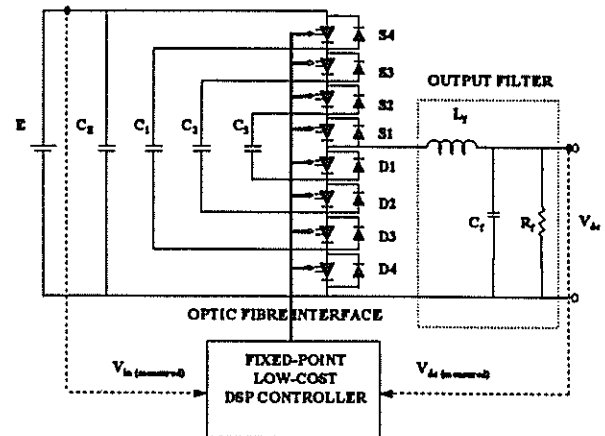
Figure 7 - Schematic Diagram of the Prototype Multi-Level Chopper

An experimental setup, using four series connected IGBT switches has been tested. It has been tested up to 400V DC. An example of the output waveform is shown in Figure 8.
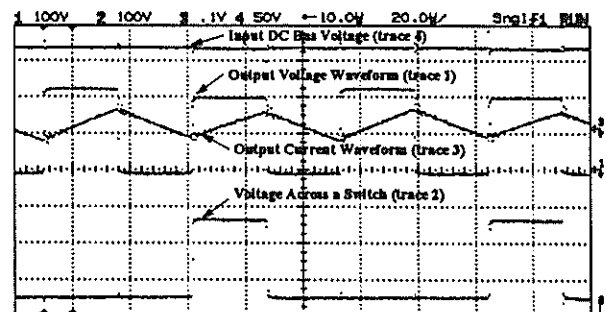
Figure 8 - Voltage and Current waveforms as shown. The current scale is 200mA/div (100mV/div) and the voltage scales are shown.

The input DC bus voltage is shown as 407.8V. The output voltage switches between 218.2V, 199.1V and 0V, i.e. the voltage across the switches are almost balanced. Improvement of voltage balancing is possible. The 15mH output inductor ripple current is 168.75mA and the DC current component is 6A. The maximum voltage stress across a single switch is shown as 218.2V.

6. CONCLUSION

To conclude, it was shown that the combination of a multi-level chopper and an inverter can be utilised more efficiently than a multi-level inverter in this application. The best topology for harmonic compensation and the best algorithm for harmonic determination is still being investigated.

In future, viability studies must be conducted to determine the cost effectiveness of upgrading the existing South African traction substations to the proposed substation before a full-scale prototype can be build. Final studies must also be conducted to determine the precise relationship between the inverter and the rectifier. The possibility to implement soft switching on the converter is also under investigation [16].

7. REFERENCES

[1] P-J. Randewijk, J.H.R. Enslin, "Inverting DC Traction Substation with Active Power Filtering Incorporated", *IEEE PESC'95*, Atlanta, USA, pp. 360-366, 1995.

[2] M. Hiyoshi, S. Yanagisawa, H. Matsuda, K. Nishitani, K. Kotake, S. Teramae, "A 1000A 2500V Pressure Mount RC-IGBT", *EPE'95*, Sevilla, Spain.

[3] T.A. Meynard, H. Foch, "Multi-level Conversion: High Voltage Choppers and Voltage-Source Inverters", *IEEE PESC'92*, Toledo, Spain, pp. 397-403, 1992.

[4] A. van Zyl, J.H.R. Enslin, W.H. Steyn, R. Spée, "A New Unified Approach to Power Quality Management", *IEEE PESC'95*, Atlanta, USA, pp. 183-188, 1995.

[5] F. Hamma, T.A. Meynard, F. Tourkhani, P. Viarouge, "Characteristics and Design of Multilevel Choppers", *IEEE PESC'95*, Atlanta, USA, pp. 1208-1214, 1995.

[6] D.A. Marshall, C.W.A. Lewis and H.W. Du Toit, "Standard for maximum Voltage Distortion in Electrical Networks", *ESKOM Standard*, ESKASAA18, March 1994.

[7] S. Fryze, "Wirk-, Blind-, und Scheinleistung in elektrisch Stromkeisen mit nichtsinusförmigen Verlauf von Strom und Spanning", *ETZ*, vol. 5.3, no. 25, pp. 596-599, 625-627, 700-702, 1932

[8] J.H.R. Enslin and J.D Van Wyk, "A new control philosophy for power electronic converters as fictitious power compensators", *IEEE Trans. on Power Electr.*, vol. 5, pp. 87 - 97, January 1990.

[9] H. Fujita and H. Akagi, "A practical approach to harmonic compensation in power systems - series connection of passive and active filters", *IEEE Trans. Ind. Appl.*, vol. 27, no. 6, pp. 1020 - 1025, November/December 1991.

[10] J. Arrilaga, D.A. Bradley and P.S. Bodger, *Power System Harmonics*, New York: John Wiley and Sons Inc., 1985.

[11] G.C. Choi, G.H. Jung, N.S. Choi and G.H. Cho, "Control of Static VAR Compensator (SVC) with DC Voltage Regulation and Fast Dynamics by Feedforward and Feedback Loop", *PESC '95*, Atlanta, USA, June 1995.

[12] H.Akagi, Y. Kanazawa and A. Nabae, "Instantaneous reactive power compensators comprising switching devices without energy storage components", *IEEE Trans. Appl.*, vol. IA - 20, no. 3, pp. 625 - 630, May/June 1984.

[13] Bhattacharya, D.M. Divan and B. Banerjee, "Synchronous Frame harmonic isolator using active series filter", *EPE 1991*, vol. 3, pp. 30 - 35, Firenze, Italy, September 1991.

[14] S.Bhowmik, R. Spée, G.C. Alexander and J.H.R. Enslin, "New Simplified Control Algorithm for Synchronous Rectifiers", *IECON '95*, Orlando, USA, pp. 494-499, November 1995.

[15] T. Suzuki, "Traction substations in an energy-saving regenerative braking system", *Mitsubishi Electrical ADVANCE*, pp. 1 - 4, June 1979.

[16] H.J. Beukes, J.H.R. Enslin and R. Spée, "Experimental Evaluation of AC/AC Converter Topologies in Utility Applications", *PESC '95*, Atlanta, USA, June 1995.

7. ADDRESS OF AUTHORS

Prof J.H.R. Enslin
Department of Electrical and Electronic Engineering
University of Stellenbosch
Private Bag X1
Matieland
7602
E-mail: jhenslin@firga.sun.ac.za

THE APPLICATION OF *CASED* AS A RESEARCH, DESIGN AND EDUCATIONAL TOOLBOX FOR DRIVES

C E Kleinhans, R G Harley, G Diana, M D McCulloch**, Landy CF*

Department of Electrical Engineering, University of Natal, Durban, South Africa
*Department of Electrical Engineering, University of the Witwatersrand, South Africa
**Department of Engineering Science, Oxford University, UK

ABSTRACT

CASED (*Computer Analysis and Simulation of Electrical Drives*) is a software toolbox tailored specifically for the analysis of drive systems. This paper gives a *brief* description of *CASED* and an overview of the application of *CASED* to the simulation and investigation of a diversity of *research* projects within the Motion Control Group at the University of Natal, Durban (UND). The paper also discusses the application of *CASED* in *industry* to the investigation of problems occurring in existing industrial installations. The power of *CASED* as an *educational tool* for teaching power electronics and drives technology is discussed. Finally some ideas on the *future* of *CASED* from a user perspective are presented.

1. INTRODUCTION

The increasing complexity and integration of drive systems into industrial process control has led to the emergence of software toolboxes to analyse and study new and existing drive systems, and assist in accelerated learning of drives technology through computer simulation. *CASED* (*Computer Analysis and Simulation of Electrical Drives*) is such a software toolbox, developed by the Machines Research Group, Department of Electrical Engineering, University of the Witwatersrand (WITS). It has subsequently been identified as suited to the work being done in the Motion Control Group of the University of Natal, Durban (UND). This paper summarises, from a users perspective, the progress made to date within the UND Motion Control Group in the application of *CASED* as a drives analysis and simulation tool. A *brief* description is given of *CASED* highlighting those features tailored specifically to simulation of drives in general. An overview is given of the application of *CASED* to the simulation and investigation of a diversity of projects as part of ongoing *research* within the Motion Control Group, UND. Also discussed is the application of *CASED* in *industry* to the investigation of problems occurring in existing industrial installations. The power of *CASED* as an *educational tool* for teaching power

electronics and drives technology is presented. Finally insight to some possible directions of *future* development for *CASED* are given to provide feedback from the users of *CASED* at UND.

2. CASED: A SOFTWARE TOOLBOX FOR ANALYSIS OF DRIVE SYSTEMS

CASED is a C based software toolbox which provides a simulation environment suited to the design and analysis of a wide variety of complete drive systems [1]. Features which are tailored specifically to motion control system simulation include:

(i) *Modularity*: Any drive system consists of sub-systems or *modules* each of which may be identified as an independent entity by virtue of its operation. *CASED* allows models for each *module* to be developed independently and then linked to form the complete drive system model. Both standard library *modules* and user defined *modules* may be used.

(ii) *A Piecewise linear state space model of a general converter*: The converter topology is generated through a graphical interface which then automatically configures the respective differential equations.

(iii) *A module linker and powerful simulator "brain"*: The linking up of system *modules* is achieved with a special *module linker*. Once the modules have been linked a central mixed-mode *simulator* or *"intelligent workhorse"* coordinates the continuous time simulation with discrete time events typically associated with changing converter switch states and discrete controllers.

(iv) *Analysis tools*: A graph routine allows viewing and manipulation of simulation data and a linearisation option within the simulator automatically generates the A-matrix for the converter and machine system.

3. CASED AS A RESEARCH TOOL

CASED has been used extensively in the UND Motion Control Group to investigate various drive topologies. These investigations have included both simulation and

practical implementation. *CASED* has proved to be a valuable tool to not only identify and solve problems at the simulation stage but to also reduce the time spent on hardware implementation. An overview of some of the research work in which *CASED* has been used in the Motion Control Group UND follows:

(i) *Field Oriented Control (FOC) of a Current Source Inverter(CSI)-fed Induction Motor (IM)*: [2]. *CASED* was used to develop a dynamic model of the CSI-fed IM which included the rectifier switching operation, link inductor dynamics, inverter commutation dynamics (auto-sequentially commutated CSI), IM stator and rotor electrical dynamics (dq-model) and mechanical load dynamics. This *CASED* model was then used to implement, investigate and improve a FOC based closed loop speed control strategy for the CSI-fed IM. The digital controller code was written in such a way as to be easily portable as real time· code for practical implementation on the transputer based Embedded Programmable High Speed Controller (EPHSC).

(ii) *Sensorless FOC of a CSI-fed IM*: [3]. The work of (i) above was extended to include speed sensorless control. The rotor speed was estimated from stator voltage and current measurements. The speed estimator was fast enough to be used on-line as the actual feedback signal for the speed controller. Simulation in *CASED* allowed problems associated with switching 'transients' and delays introduced by inverter commutation to be addressed at the simulation stage. Practical measurements on the EPHSC showed good correlation. Digital controller code from *CASED* was also used as real time code.

(iii) *FOC of a Voltage Source Inverter(VSI)-fed IM*: [4]. Closed loop speed control of the VSI-fed IM was simulated in *CASED*. The model included the IM electrical dynamics, the mechanical dynamics, the inverter switching and an ideal DC voltage supply. The system was practically implemented using the EPHSC but the controller code was re-programmed in OCCAM. This required two stages of debugging unlike in the preceding two projects (see (i) and (ii) above).

(iv) *Unity power factor low harmonic distortion rectifier*: [5]. A new force-commutated rectifier topology was investigated, capable of achieving unity power factor, near sinusoidal line currents and bidirectional power flow. *CASED* allowed the concept to be proven feasible in simulation first and then implemented on the EPHSC in floating point. Later, problems associated with integer implementation (using a commercial microcontroller) and quantisation effects were also investigated using the *CASED* model.

(v) *A Motion Control Development System*: [6], [7]. The EPHSC was developed to implement controller algorithm code and provide high speed I/O structures typically required for motion control applications.

CASED has been used as a complementary software toolbox aimed specifically at simulation of drive systems. Digital controller code was written in *CASED* in such a way·as to be easily portable as real time code to the EPHSC. In the practical system hardware the power electronics device drivers and sensors form an interface to the EPHSC digital controller which becomes transparent when looking at the simulated and practical hardware [6]. In [7] the *CASED* digital controller code was also used as real time code but the configuration and scheduling of such code was done automatically.

4. CASED AS AN DESIGN AND ANALYSIS TOOL IN INDUSTRIAL PLANTS

Although at UND *CASED* has been used primarily as a research tool, certain industrial case studies have been conducted at WITS. These include:

(i) *The interaction between two loosely coupled synchronous motors for a dragline system*: [8]. This study investigated whether different synchronous motors could be run in parallel on a dragline. The synchronous motors drive DC generators which were connected in a Ward-Leonard configuration to DC motors which performed the swing, drag, and hoist operations. Transient operation of the synchronous motors in the complete drive system was shown to remain stable without a significant degradation in dynamic performance.

(ii) *Drive systems for interparticle crushers*: [9]. A study was made prior to and during the implementation phases of an upgrade in a crushing process. The plant consisted of existing CSI drives to which were added additional VSI drives. The simulations investigated whether the new drives would trip under extreme loading conditions and how the speed dropped for different supply variations and load disturbances. Also investigated was the compatibility of low reactance motors with the proposed PWM system.

(iii) *Reswitching transients in induction motors*: [10]. The transient response of IM under conditions of re-switching were investigated and discussed.

5. CASED AS AN EDUCATIONAL TOOL FOR POWER ELECTRONICS

The modular structure of *CASED* is ideal for teaching drives and power electronics. Standard predefined library modules are available and user defined models can be developed and archived as user defined library modules. These standard and user defined modules may then be used to easily configure standard drive configurations. In this way *CASED* provides a useful platform for accelerated learning of existing drive topologies by means of simulation. The generalised converter model is particularly useful for teaching power electronics since the graphical user interface allows the

user to set up the converter schematic graphically and then automatically generate the differential equations describing that system. The user defined models include nonlinear models and digital controller models so that *CASED* can actually simulate not only drives but any complete control system in which drives are integrated into a complete control hierarchy. Although other simulation packages are available, e.g. SIMULINK, they are more generic and not directly suited to modelling drive systems which have time varying topologies.

6. *CASED*: FUTURE DEVELOPMENTS?

CASED has steadily grown, to being used in research and industrial case studies and serving as a useful tool in teaching power electronics. So what is the next step in the development of *CASED*? Although by no means certain, the following are possible future developments:

(i) Promotion and support for *CASED* in both the academic/research and industrial environment. This will include continued improvements to the user manual and offering courses on *CASED* to new users. The idea here is to make people aware of *CASED*, get them involved to provide *feedback* and users groups.

(ii) The growth of standard and specialised models in *CASED*. The specialised models may include toolboxes for analysis and/or teaching of drive specific subjects such as Pulse Width Modulation (PWM), volts/hertz drives, FOC drives, and drive/supply interaction.

(iii) Further development of analysis specific features, such as harmonic analysis and improved versatility of user defined models. User *feedback* is important here.

(iv) The upgrade of the menu driven system to a windows NT operating environment, allowing improved graphical user interfacing (GUI). This may entail a more graphical/windows approach to the connection and definition of system models.

(v) Choose some high performance hardware platform (computing and power electronics) to allow *CASED* controller C code to be automatically configured and down loaded for real-time implementation. Many issues are involved here such as what computing hardware platform should be used (a fast changing field) and how should controller code scheduling and profiling be done. A decision must be taken to maintain versatility balanced against hardware standardisation. Also important here is to keep the cost down so that users can afford the system!

7. CONCLUSION

This paper has presented an overview of *CASED* (*C*omputer *A*nalysis and *S*imulation of *E*lectrical *D*rives) and its application to research work done in the Motion Control Group at the University of Natal, Durban.

CASED has also been used to conduct case studies in industry and some of these studies have been briefly mentioned. The suitability of *CASED* to teaching power electronics and drives has been discussed and some ideas on possible future developments in *CASED* proposed.

8. ACKNOWLEDGMENT

9. REFERENCES

[1] McCulloch MD, Landy CF, Levy W, MacLeod I, "CASED: A simulation package designed for variable speed drives", *Technical article, Simulation 57:4*, Oct. 1991, Simulation Councils, Inc., ISSN 0037-5497/91, USA, pp 216-226.

[2] Kleinhans CE, Diana G, Harley RG, McCulloch MD, Randelhoff M, Woodward DR, "Analysing a CSI-Fed Field Oriented Controlled Induction Motor Using a New Simulation Package *CASED*", *Conference Proceedings of the IEEE Industrial Electronics Society, IECON*, 1994, Bologne, Italy, pp 192-197, paper no. EP237P102.

[3] Talbot KJ , Kleinhans CE, Harley RG, Diana G, "Simulation and Implementation of Sensorless Speed Control applied to a CSI-Fed Field Oriented Controlled Induction Motor", *Proceedings SAUPEC'95*, January 1995, Pretoria, pp 210-213.

[4] Hao B, Diana G, Harley RG, Woodward DR, Levy DC, "A Comparison between Simulated and Experimental results for a Field Oriented Controlled Induction Motor", *Proceedings SAUPEC'94*, January 1994, Cape Town, pp 51-56.

[5] Chathury AS, Diana G, Harley RG, "AC to DC Converter with unity power factor and minimal harmonic distortion",*Proceedings SAUPEC'94*, January 1994, Cape Town, pp 22-26.

[6] Kleinhans CE, Harley RG, Diana G, McCulloch MD, Randelhoff MD, "A drive Development Platform for Direct Portation of Control Algorithm Code Between Simulation and Hardware Environment", *Proceedings SAUPEC'95*, January 1995, Pretoria, pp 77-80.

[7] Randelhoff MC, Kleinhans CE, Harley RG, Levy DC, "A Development System for Automated Generation of Hard Real-Time Control Code for Motion Control Systems", *Proceedings SAUPEC'95*, January 1995, Pretoria, pp 89-92.

[8] McCulloch MD, Landy CF, Frank C, "Interaction between two loosely coupled synchronous motors for dragline system", *Proceedings SAUPEC'94*, January 1994, Cape Town, pp 64-66.

[9] Cassim A (Siemens Ltd), "Drive Crushers for interparticle crushers", *Elektron*, July '95, pp 31-33.

[10] Dusterwald R, Edwards W, "Reswitching transients -how do motors respond?", *Elektron*, July'95, pp 59-60.

UNIT CONNECTED HVDC SCHEMES

T A Rae   R G Harley   G D Jennings   M T Wishart*

Department of Electrical Engineering, University of Natal, South Africa
*Electrical Technology; ESKOM Technology, Research and Investigations, South Africa

ABSTRACT

Conventional High Voltage Direct Current (HVDC) has advantages in long distance transmission, and of decreased stability problems which limit High Voltage Alternating Current (HVAC) transmission, but in turn introduces other complexities. *Unit Connection* is a refined HVDC scheme which rectifies the power of each turbo-generator individually before connecting it to the DC line. Some simulated results of the Unit Connected scheme, some harmonic results and the effective converter transfer functions are presented. These results follow the paper titled 'Unit Connected back-to-back Pump Storage Schemes' presented at SAUPEC-95.

1 INTRODUCTION

Historically electrical power was generated and distributed in DC, and therefore utilized in this form. The advent of AC and the transformer allowed AC power to be transmitted over long distances at a higher voltage, but brought with it the concepts of synchronism between the sending and receiving ends, and thus the problems of maximum power transfer. The use of a HVDC line eliminates the synchronism problems and to a large extent the transmission distance limitations.

The conventional HVDC connection utilizes a common AC bus to which the AC filters and the converters, via transformers, are connected. The generators are connected to this common bus thus requiring that the generators all remain in synchronism with each other. The AC filters filter out all converter generated harmonics such that the waveforms on the common bus are sinusoidal (forming the commutating voltages). The converters may be connected in series or in parallel on the DC side to satisfy system requirements.

The conventional configuration may be altered such that each generator is connected to a single rectifier which is connected in series or parallel on the DC side to other such units. Such a scheme is referred to as a *Unit Connected Scheme* as each generator is matched to a single rectifier, thus creating a module or individual *unit*.

2 UNIT CONNECTION

The Unit Connection scheme is displayed as Fig.1 showing the converters in a series DC connection, as opposed to the parallel or group DC connection [1].
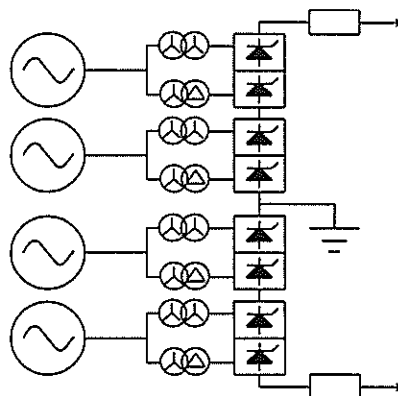
Fig.1. Unit Connected Scheme

The Unit Connected scheme eliminates one voltage transformation step, the AC filters, and most of the AC switchgear and busbars at the rectifier station, by directly connecting each generator to its' two converter transformers (for twelve pulse operation). The elimination of the common AC bus eliminates the need for the generators to run in synchronism. The on-load tap-change transformers can also be eliminated due to the rectifier converter voltage control being exercised by the generator excitation control. The reduction in AC equipment leads to significantly reduced capital cost as well as reduced operating costs due to lower station losses [2]. The avoidance of low order harmonic resonances, due to the absence of AC filters, results in a significantly improvement in reliability.

The disadvantages of such a Unit Connection is that the converter created current harmonics are injected into the generator stator winding creating ripple torques, generator voltage distortion and heating effects.

Traditionally synchronous generators are run at constant synchronous speed, however in the Unit Connection scheme the speed of the generator is not necessarily fixed due to the only electrical connection occurring on the DC side. In the case of a hydro scheme the deviation from synchronous speed allows the generator and turbine set to be run at the maximum possible efficiency as a function of water head and electrical load requirements [1].

The investigation into the Unit Connection principles is lead by the creation of a DC line model in the *Electro-Magnetic Transients Program* (EMTP) to observe the

Unit Connected characteristics.

3 SIMULATIONS
3.1 Model Description
The developed model shown as Fig.2 consists of a single synchronous generator connected to two transformers connected in a star-star and star-delta configuration. Each secondary of these transformers is connected directly to a six pulse converter, which is connected in series on the DC side thus creating a twelve pulse converter. The DC line is simulated as a low resistance (0.5 Ω) and a series inductance (100 mH) representing a back-to-back HVDC scheme. The inverter consists of two six pulse converters in series connected to a transformer each, which are in a similar star-star and star-delta connection. These transformers are connected to an infinite bus modelled as voltage sources via a finite impedance representing network impedance changes.

Transformers   Transformers

Synchronous
Generator   Infinite
                                   Bus
            Bridges
        Rectifier - Inverter
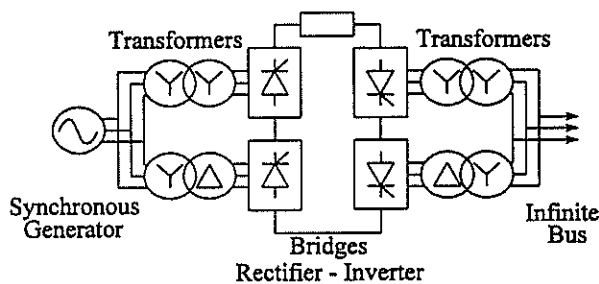
Fig.2. EMTP model

The transformers are modelled as having a leakage impedance of 0.13 p.u. and the synchronous generator is modelled with the parameters found in appendix.A.

3.2 DC Power Control
Under normal operating conditions the rectifier pole controls the DC current and the inverter pole controls the DC voltage. In steady-state conditions the DC voltage is held at a maximum value (by the inverter) for two reasons: firstly to keep the DC transmission efficiency at a maximum value and secondly to limit the reactive power consumed by the inverter.

Fig.3 displays the DC controller characteristics, where the horizontal lines (AB and FE) indicate the uncontrolled operation of the converter bridges; as the voltage output is at the maximum possible value (diode operation). The vertical lines (BD and FG) display the operation of the converters at some finite values of delay angle, as the DC voltage is being varied at a constant current, indicating a constant current controller. The DC feedback current for the inverter is decreased by a current margin (ΔI_d). At a specific DC current (under rectifier control) the inverter controller attempts to increase the DC current as the difference between the desired current and the feedback current (minus ΔI_d) is not zero. To increase the DC current the inverter controller attempts to increase the inverter DC voltage resulting in the largest firing delay permissible and thus

the largest inverter DC voltage.
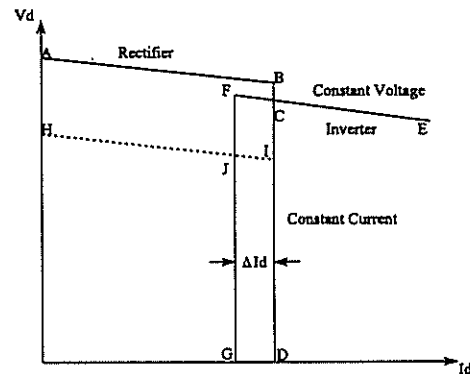
Fig.3. DC Controller Characteristics

The equilibrium point is at point C where it can be seen that the inverter voltage is at its maximum value and the rectifier voltage is being controlled to maintain the desired current. In the event of a rectifier voltage drop (temporary fault) the rectifier controller attempts to increase the rectifier DC voltage to increase the DC current resulting in the line HI (maximum permissible rectifier voltage). Due to the lower rectifier voltage the DC current decreases until the DC current is in the range of the desired current minus the current margin. At this point the inverter voltage is then decreased by the inverter controller to maintain the DC current resulting in a new operating point at J.

This control is realized by the use of simple PI controllers with the filtered DC current completing the feedback loop.

3.3 Firing Control
The earlier HVDC firing methods utilized individual phase control by determining the firing instances for each valve individually from the actual AC voltage waveforms. This is done by detecting the phase voltage crossings which is the earliest possible firing instants and the delay implemented from these crossings [3]. This type of control has the advantage of being able to achieve the highest DC voltage possible under asymmetrical or distorted supply waveforms.

The disadvantage involved with this type of firing control occurs when a deviation from the ideal voltage waveform occurs. This has the effect of breaking the 120° symmetry of the current waveform which causes extra waveform distortion [4] due to the possibility of introducing triplen and even harmonics (absent in the Fourier analysis of an ideal 120° rectangular pulse). The introduction of these harmonics are avoided by the use of equi-distant firing schemes, of which in practice there are many different implementation methods [5].

The control scheme developed in this paper for the rectifier firing has to incorporate the varying AC supply frequency which depends on the speed of the generator. This control scheme utilizes a transformation from the

abc frame to the alpha-beta reference frame. The generator is directly connected to the converter with only one voltage transformation step, thus it is assumed that no faults should occur between the generator and the converter. The second assumption is that the abc voltages are balanced, thus making the alpha; beta calculation simpler and quicker. .

The abc voltages are measured at the generator terminals to include as much impedance as possible between the converters and the point of measuring, to attenuate as much of the harmonic distortion as possible. These voltages are filtered and transformed to obtain two rotating vectors (alpha and beta). These vectors are used to calculate the electrical angle eliminating the varying frequency problems. By knowing the electrical angle and the earliest firing point (diode operation), the firing delay can be implemented.

On the other hand the firing control scheme for the inverter does not have to incorporate a varying AC frequency since the inverter is connected to an infinite bus. For the purposes of these simulations it is assumed that the frequency of the infinite bus remains at fifty Herz. The inverter firing control.scheme is based on a digital format of a voltage controlled oscillator and the firing pulses is derived by calculating the inter-firing period (time between the last valve firing and the next valve firing) [6].

3.4 Current Controller Development
The rectifier system is modelled utilizing the standard [3] equation for the DC voltage of a rectifier below:

$$U_{dr} = U_{do}.\cos\alpha - \frac{3.X_c.I_d}{\pi}$$

where:

U_{dr} = DC Voltage

U_{do} = $\frac{2.\sqrt{3}}{\pi}.V_{peak}$

= Maximum DC Voltage

X_c = Commutating reactance

I_d = DC current

The above value of U_{dr} for a six pulse rectifier and must be doubled as there are two six pulse rectifier units in series on the DC side forming the twelve pulse rectifier.

The modelling of the system is treated as a continuous time system although the PI sampling and the rectifier firing is discrete with a finite sampling period (function of firing delay for the rectifier). This is due to the sampling period of the PI controller being much lower than the time constant of the rectifier (20ms/12s). In a similar manner the rectifier can be considered to be a continuous time system [7] with respect to the DC load as the time constant of the load is 200ms (L/R).

The equations used in the block diagram of Fig.4 are based on average values i.e. DC voltage and current. In practice the DC voltage and current contain a finite

ripple content. The design of the current controllers must therefore ensure that the controllers are sufficiently robust to handle the physical ripple.
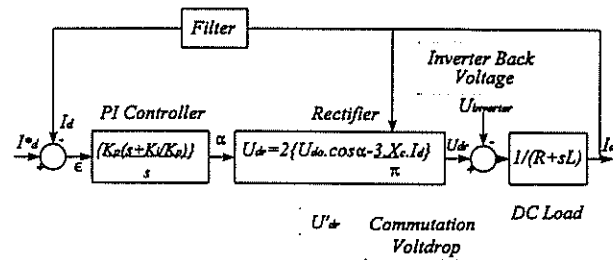
Fig.4. Complete system model

The first step is to linearize the system by inserting an inverse cos function ($\alpha = \cos^{-1}(U^*_d / U_{do})$), at the PI output, to cancel the non-linear DC voltage (U_{dr}), which is a function of cos. The PI controller outputs the required DC voltage ($U^*_d = U'_{dr}$) to overcome the inverter back voltage, the commutation voltdrop and the potential difference required to obtain the required DC current.

The inverter back voltage is a disturbance to the system and in order to cancel this effect a feedforward term equal to the inverter DC voltage is used to calculate U^*_d. The PI controller therefore solely handles the load dynamics (DC resistance and inductance) and thus outputs the potential difference necessary to apply to the DC load and overcome the commutation voltdrop to obtain the required DC current as shown in Fig.5
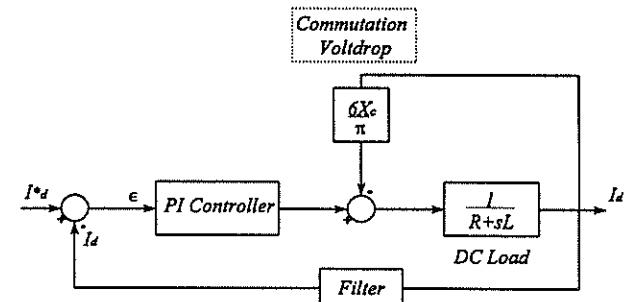
Fig.5. Simplified rectifier system

The resulting system equation becomes:

$$G = \frac{\frac{K_p}{L}.(s + \frac{K_i}{K_p})}{s.(s + \frac{R.\pi + 6.X_c}{\pi.L})} \qquad H = \frac{600}{(s + 600)}$$

The placement of the PI controller zero is difficult due to the exact value of the commutating reactance (X_c) not being properly defined. Without filters the commutations (brief phase to phase sort-circuits) are controlled by the generator emf behind the generator's subtransient reactance. The machine subtransient reactance needs to be averaged, due to the variation of the reactance around the air gap [8], to obtain an acceptable value, hence ($x"_d$ + $x"_q$)/2. The system pole is therefore not properly defined but rather an average value can be assumed.

The optimum position for the PI zero thus needs to be determined such that the effect of the uncertain value of the system pole is minimised. This becomes important with respect to the inverter controller design as the commutating reactance varies as the network (to which the inverter is connected) changes. The pole thus changes position, and a range of positions therefore need to be determined for the network changes, for which the controller must be designed to be robust to maintain control of the DC current.

4 HARMONIC ANALYSIS

A Matlab harmonic analysis program based on the fast Fourier transform (FFT) is utilized to determine the harmonic content of any waveform. This program is particularly useful in determining the harmonic content of the generator current for the Unit Connected scheme. This interest arises due to the lack of AC filters which means the converter-created harmonics being injected directly into the generator. The current waveform and the corresponding harmonic analysis is shown as Fig.6.
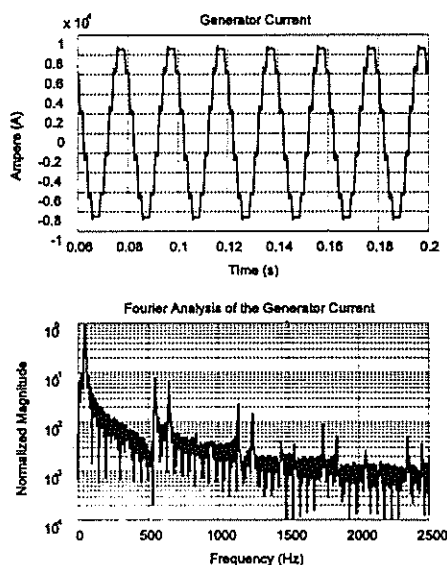
Fig.6. Harmonic analysis of the generator current

Apart from the fundamental 50 Hz, a number of the characteristic harmonics, scaled from the normalized fundamental, are also present (11th and 13th at 550 Hz and 650 Hz respectively e.t.c.). The generator design needs to incorporate the extra heating effects of these harmonics. The possibility of variable generator speed can be utilized to increase the fundamental frequency and therefore the frequency of the lower order harmonics. The higher harmonic frequency components will then be attenuated more by the large inductance of the machine thus lowering the harmonic content of the AC current. However the thermal capabilities of the generator needs to be assessed at higher rotor speeds.

5 CONCLUSION

The new concept of HVDC connection has been briefly described and a model used to investigate the Unit Connected scheme has been presented with the

associated control mechanisms for the converter firing and control. The results of a simple harmonic analysis on the generator indicate the detailed design required for the generator.·

The difficulty of controlling the **rectifier** side of the Unit Connected scheme lies in the increased commutation reactance on the AC side due to the lack of AC filters. The movement of the system pole of the inverter is universal to all HVDC schemes, however the uncertain pole of the **rectifier** is a characteristic problem of the Unit Connected scheme. Once a solution has been derived to this problem, the current controllers can be robustly designed to handle the pole movements (inverter) or pole uncertainty (rectifier).

APPENDIX.A.
Relevant Synchronous Machine Parameters:

Rated Output   281.5MVA
Rated Current   14775 A

x_d	1.33 p.u.	x_q	0.92 p.u.
x'_d	0.29 p.u.	x''_d	0.19 p.u.
x''_q	0.21 p.u.		

REFERENCES

[1] Rae, T.A., Harley, R.G., Jennings, G.D., Wishart, M.T.:"Unit Connected back-to-back Pump Storage Schemes" SAUPEC - 95, pp. 167-170, January 1995.

[2] Arrilaga, J., Bowles, J.P., Campos Barros, J.G., Kanngiesser, K.W. and Ingram, L.: "Direct Connection of Generators to HVDC Converters: Main Characteristics and Comparative Advantages" Electra, pp.19-39, August 1993.

[3] Arrilaga, J.:"High Voltage Direct Current Transmission" IEE Power Engineering Series 6, 1988.

[4] Krüger, K.H., Kulicke, B.:"Noncharacteristic Harmonics in a High Voltage Direct Current-Converter Station caused by System and Firing Angle Asymmetry", Siemens Forsch. -u. Entwickl.-Ber.Bd. 11,No 5, pp 241-244, 1982.

[5] Rumpf, E., Rande, S.:"Comparison of Suitable Control Systems for HVDC Stations connected to Weak Systems"IEEE Transactions on Power Apparatus and System, Vol PAS-91, No. 2, March/April 1972, pp 549-564.

[6] Alegria, C.M., Freris, L.L.:"Microcomputer Control of Power Converters", IEEE Transactions on Power Apparatus and Systems, Vol. PAS-103. No8, August 1984, pp2011-2017.

[7] Roland, J.H., Fang L.L.:"Stability Analysis of Thyristor Current Controllers", IEEE Transactions on Industry Applications, Vol IA-23, No. 1, January/Feburary 1987.

[8] Arrillaga, J., Macdonald, S.J., Watson, N.R., Watson, S.:"Direct Connection of Series Self-Excited Generators and HVDC Converters", IEEE Transactions on Power Delivery, Vol. 8, No. 4, October 1993.

'n Intydse Kragstelselsimulator vir Harmoniese Ondersoeke

A.P.J Rens, H.A. Jordaan
PU vir CHO

Samevatting *'n Laboratorium wat kragstelsel komponentmodelle fisies voorstel en waar spesifiek harmoniese penetrasie met analoogsimulasie ondersoek kan word, word by die PU vir CHO ontwikkel. Die ontwikkeling, regverdiging en toepassing van hierdie harmonieke laboratorium word bespreek.*

Inleiding

Die kwaliteit van die kragtoevoer het die afgelope dekade baie belangriker geraak, veral as gevolg van die toename in nie-lineêre laste. Die behoefte aan die verstaan van kragstelselharmonieke en golfvormversteuring [6] is nodig om die totale impak in die stelsel te kwantifiseer. Toerusting, beskerming, meetapparaat kan ernstige afwyking van die veronderstelde werkverrigting vertoon.

Alhoewel heelwat werk reeds in die veld van analoog kragstelselsimulasie gedoen is, is dit belangrik om die penetrasie van harmonieke in die kragstelsel beter te ondersoek want die vraag van wie tot wat in die interverbinde kragstelsel aanleiding gee, sal binnekort wetenskaplik en eenduidig gekwantifiseer moet word.

By die PU vir CHO word tans 'n laboratorium ontwikkel waar harmoniese ondersoeke op 'n analoog kragstelselsimulator gedoen kan word. Die omgewing en veranderlikes is gekontroleerd. Die verwarring van interpretasie van metings in die interverbinde kragnet word dus geminimaliseer.

Fisiese komponente bestaan in die stelsel en die simulasie word gekomplimenteer met 'n EMTP model. Die belang van toevoerkwaliteit word kortliks gemotiveer waarna 'n oorsig gegee sal word van beide kragstelselkwaliteit en kragstelselsimulators wêreldwyd. Daarna word die PU vir CHO se harmonieke laboratorium se ontwikkeling beskryf. 'n Belangrike bonus by die navorsingaspek is die opleidingsmoontlikhede en dit geniet ook aandag.

Kwaliteit van Toevoer

Toevoerkwaliteit het verskeie interpretasies, vir die doel hier word dit gedefinieer [3] as enige gestadigde- en oombliksafwyking van die nominale toevoer toestand wat die kragvoorsiener poog te waarborg. Dit dui dus op die voorkoms van ander frekwensiekomponente in die toevoer wat tot meetbare golfvormversteuring lei.

Effekte op Toerusting

Die effek van golfversteurings (harmonieke) op toerusting is wel bekend en beskryf [15], [16]. Die belangrikste hiervan kan as volg opgesom word:

1. GS en WS spoedbeheerders; teenstrydig daarmee dat vaste toestand ws en gs spoedbeheerders slegs gesien word as 'n bron van distorsie, word 'n reeds versteurde golfvorm as toevoer tot die beheerder gereken [14] as 'n faktor wat die betroubare werking van hierdie beheerders kan beinvloed.

2. Kapasitore; faling hiervan as gevolg van die [3] diëlektrikum se deurbreek, reaktiewe oorbelasting en moontlike resonansie met stelselinduktansie as harmonieke na aan natuurlike resonantpunt van die stelsel in die golf reeds voorkom.

3. Masjiene kan oormatige verhitting en draaimomentpulsasies ervaar.

4. Oorspannings a.g.v resonansie veroorsaak deur harmonieke by natuurlike resonantpunte.

5. Verhitting in geleiers is die gevolg van die verandering in stroomdigtheidverspreiding in die geleier en abnormale hoë strome in die neutraalgeleier kan tot 1.7 maal [16] die fasestroomgrootte wees. Die neutraalgeleier is gewoonlik dieselfde grootte as die fasegeleier.

7. Induktiewe interferensie met telefoonlyne wat naby is vind plaas. Die menslike oor se sensitiwiteit is 'n maksimum by 1 kHz en kragstelselharmonieke kan juis by die frekwensie voorkom.

8. Energiemeters kan die totale energie gelewer of geabsorbeer foutief intrepeteer ten koste van die verbuiker of die voorsiener, 20 % foute in versteurde golfvormmetings met induksie watt-uur metings is aangeteken [15].

9. Beskermingmeganismes se betroubare werking [1] word deur harmonieke in die golf beïnvloed.

10. Transformators ervaar ekstra stres wanneer versteurde golwe daardeur beweeg, nie net die addisionele hitte is 'n probleem nie, maar ook kan resonansie ontstaan as gevolg van die wisselwerking van transformatorinduktansie en stelselkapasitansie. Dit kan ook tot meganiese isolasiestres lei deurdat klein vibrasies in die kern ontstaan [17].

11. Verligtingtoestelle se lewensduur word negatief beïnvloed, gloeilampe se leeftyd volgens [16] kan afneem met soveel as 47 %.

Van hierdie effekte is reeds deeglik beskryf en nagevors. Ten einde die totale stelselimpak egter beter te verstaan is dit nodig om 'n geïsoleerde en dus gekontroleerde omgewing te skep waar karakterisering korrek vir harmoniese frekwensies gedoen kan word en dit is wat hierdie laboratorium sal fasiliteer.

Agtergrond

Steinmetz [3] het vroeg in die eeu die derde harmoniek van 'n transformator vasgevat met 'n deltawinding. Gedurende die 1940's het telefooninteferensie belangrik geraak met die in-

1

gebruik neem van boogoonde en groot gelykrigters. Die 1950's het egter halfgeleiertoestelle se geboorte aangekondig, deesdae is dit nie net die energieomsetters nie, ook transmissietegnologieë (bv. "FACTS- Flexible AC Transmission") maak deel uit van harmoniek-produserende tegnologie. Meer laste is aan die toevoer verbind wat sensitief is vir versteurde golwe en die verbruikers dring al hoe meer aan op gewaarborge kwaliteitstandaarde ekstra tot die probleme van die voorsiener hiermee. Daar word gereken dat 50 % van die totale elektriese energie in die VSA [6] deur halfgeleiermateriaal sal vloei teen die jaar 2000 en sou Suid Afrika Eerste Wêreldgewoontes in 'n stadium aanneem sal ons dit waarskynlik soortgelyk ervaar.

Kragstelselsimulators was aanvanklik groot en lomp waar van werklike swaar masjinerie gebruik gemaak is, die gevolglike omslagtigheid aan eksperimentering hiermee verbonde het gelei tot klein masjiene en toerusting [3] maar kon nie die karakteristieke gedrag van die stelsel altyd korrek voorstel nie. Die 1980's het vele hibriede simulators [4], [5] [6], [9], [10], [12], [13], [15], [17] beleef waar beide rekenaars en fisiese stelselkomponente gebruik is. Die sogenaamde "Transient Analyser" het, alhoewel kompleks in ontwerp, tog in terme van stelselstabiliteit baie insig gebied. Rekenaars het gemaak dat die entoesiasme hiervoor baie afgeneem het die afgelope twee dekades.

Die Puk laboratorium is nie uniek nie en soek nie regverdiging 'n dekade of wat uit fase nie. Domijan [3] beskryf 'n kwaliteit van toevoer laboratorium wat ontwikkel is by die Universiteit van Florida te Gainesville gedurende die vroeë negentigs. Die ondersteuning van EPRI as deel van hulle nasionale "Kragkwaliteit Toetsnetwerk" was deel van die ontwikkeling en soortgelyke navorsing en opleidingdoelwitte is geïmplementeer met hulle laboratorium. Die klem word egter meer gelê op stelselondersoeke as ondersoeke waar die individuele komponentgedrag aandag kry. Die grootste laboratorium gebaseer op fisiese modelle bestaan by die Waseda Universiteit in Japan [3], [13] maar die klem is ook op stelselondersoeke. Die Duitse model [10] is analoog. Die fisiese modelle se wiskundige beginsels word analoog voorgestel, maar dit is nie 'n geskaleerde voorstelling van die regte installasie nie, eerder 'n analoogrekenaar. Dit lewer wel akkurate resultate, maar die stelsel is nie baie plooibaar nie en baie doelgerig ontwerp.

'n Analoogsimulator in 1995 ?

Digitale modellering het laat in die tagtiger jare en tot op hede die algemene manier van kragstelselondersoeke geraak. Dit is as gevolg van die akkuraatheid van komponentmodelle en die beskibaarheid van EMTP gekombineer met kragtige persoonlike rekenaars. Dit bied vinnige betroubare resultate. Die waarde hiervan sal nooit onderskat kan word nie. Die kwaliteit van toevoer probleem se

kompleksiteit het egter sodanig toegeneem dat die penetrasie van harmonieke in die stelsel op 'n minder simplistiese en algemene wyse as met byvoorbeeld Harmflo moet ondersoek word. EMTP en basiese beginsels wat digitaal geïmplementeer word, bied vele insig, die fisiese analoogmodel bied egter 'n kontrole in harmoniese ondersoeke veral waar die klem gelê wil word op die antwoord van die vraag van wie gee aanleiding tot wat.

Op hierdie manier word dus gekontroleerde toestande geskep waar veranderlikes beheer kan word. Metodes, byvoorbeeld om die geografiese bron van 'n harmoniek te bepaal, kan geverifieër word onder verskillende beheerde kondisies.

Die analoogsimulator fasiliteer nie net genoemde navorsing nie, waarde word ook toegevoeg tot die huidige opleidings infrastruktuur aan die Puk deur die opleidingsmoontlikhede wat so 'n laboratorium bied.

Alhoewel 'n ondersoek in die VSA [2] harmonieke as die vierde gewildste veld van studie onder studente uitgewys het, bied die laboratorium egter 'n kombinasie van blootstelling in verskillende aspekte van Elektriese Ingenieurswese soos digitale elektronika (harmoniese generators), elektronika en seinverwerking (sensors en voorstelling van data) asook algemene kragstelselinsig en ervaring wat slegs met moeite en koste later in die werksomgewing opgedoen sou word deur die Elektriese Ingenieur. In Kragstelsels is opleiding slegs op rekenaarmodelle [3], [5] nie goed genoeg nie, 'n blootstelling aan die fisiese omgewing is belangrik. Die gewildheid van rekenaarsimulasies sal egter ongedemp bly, veral vanweë die min koste en gemak waarmee ondersoeke uitgevoer kan word.

Elektriese Ingenieurswese laboratoria se relevante leeftyd, beide in terme van opleiding en navorsing word in die VSA as slegs 5 jaar [10] gereken. Hierdie laboratorium se beplanning moet egter 'n langer nuttigheid verseker om in pas te wees met ekonomiese realiteite van Afrika. Dit is 'n verdere regverdiging van fisiese analoogmodelle wat basiese elektromagnetiese kragstelsel beginsels gebruik en bevestig.

Modellering en Konfigurasie

Aangesien die modellering van die totale stelsel [10] net so goed is as die mins akkuraat gemodelleerde komponent, moet die verskillende komponente se fisiese modellering baie aandag geniet. Aangesien die penetrasie van die harmonieke sentraal staan, geniet veral die voorstel van die transmissielyn (en transformator) baie aandag. Drie fase modellering [1] is nodig vir akkurate harmoniese penetrasie. In die literatuur [3], [9], [10], [11], [12], [13], [15] word behalwe vir die "Transient Analysers" verskeie transmissielynmodelle wat fisies geïmplementeer kan word, beskryf. Die ontwerp hiervan om na skalering realistiese werkverrigting ten opsigte van

die werklikheid te bied, is uiters omslagtig en kompleks [1], [10]. Hierdie proses is tans aan die gang.

Basiswaardes vir die stelsel is 5KVA; 380 V. Transmissielynmodules stel 10 km voor van die 88 kV stelsel waarop ondersoeke tans gerig is. Die nominale π kaskades wat gebruik word se frekwensiebereik is tot by die 25ste harmoniek. Verskillende lynlengtes kan voorgestel word deur die koppeling van die geskikte aantal modules. Verskillende werklike 88 kV toringstrukture soos deur Eskom gebruik, word in die modules gebruik. Werklike lyne waar toringstrukture verander, kan dus voorgestel word deur die regte kombinasie van modules.

'n Probleem met geskaleerde fisiese modelle is dat van die eienskappe van die werklike installasie tog verlore moet gaan, byvoorbeeld die per eenheid verliese is in 'n geskaleerde model is aansienlik groter [13].

Die modellering van 'n las om nie-lineêre gedrag deeglik voor te stel, is kompleks [10]. As die lastipe en grootte varieërbaar moet wees, word lasmodelle omslagtig. Weens die gekose basiswaardes is dit egter prakties om werklike laste te gebruik. Induksiemotors, sinkrone motors, beheerde en onbeheerde gelykrigters, verskillende verligtingapparaat asook wisselrigters word as laste gebruik. Verskillende tipe laste kan op die manier gekombineer word om 'n residensiële, industriële, kommersiële of landelike las voor te stel. Arbeidsfaktorverbeteringkapasitore is werklike kapasitore. Die opwekking van 'n gespesifiseerde versteurde golf word geïmplementeer deur die digitale opwekking en inkoppeling hiervan. Dit is soortgelyk aan die tegniek beskryf deur Girgis [5]. Die effek van boogoonde, ongebalanseerde driefase spanningsbronne met harmoniese distorsie asook siklorigters (wat nie-veelvoude van die grondkomponent kan opwek [1]) is moeilik fisies voorstelbaar. Dit kan deur die meting en hergenerering van werklik gemete gevalle in die kragstelsel voorgestel word.

Die Laboratoriummodel
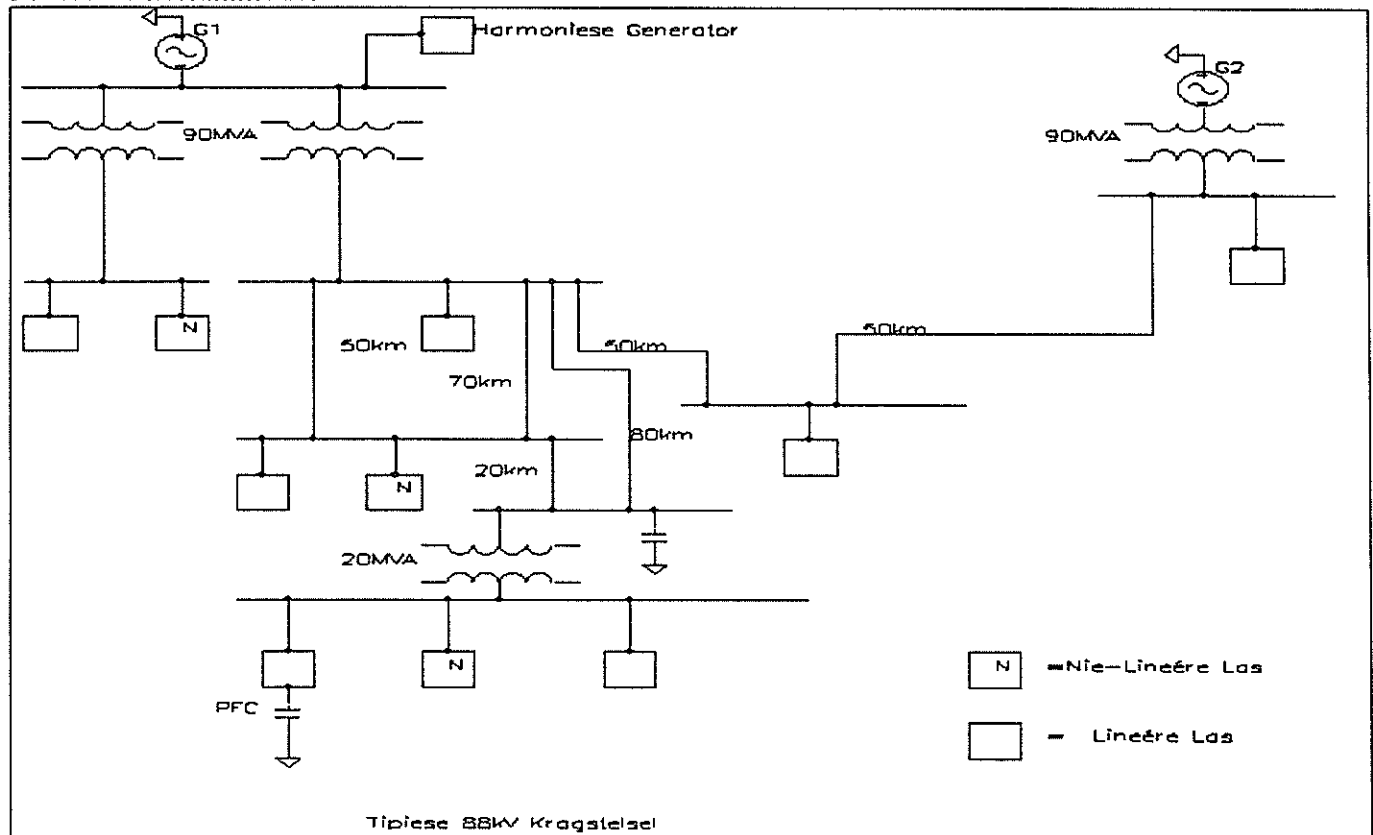
Figuur 1: Voorstelling van die 88kV Kragstelsel

Van die areas wat derhalwe onmiddellik met die analoogsimulator ondersoekbaar sal wees:

- Die meet van harmonieke en die interpretasie hiervan, dit sluit seinverwerkingprobleme in; verskaf die Fouriertransform genoeg golfinligting;

wat van die Gabortransform ?; en as nie-heelgetal veelvoude van die grondkomponent bydrae tot die distorsie ? Watter kwantifiseringtegniek is die geskikste ? Tydvlak ? Frekwensievlak ?

- Die penetrasie van harmonieke in die kragnet; hoe kan die geografiese oorsprong hiervan bepaal word ? Hoe en hoe akkuraat moet die

3

- kragnet gekarakteriseer word ? Met watter tipe metings en sensors, hoeveel en waar ?
- Wat is die invloed van 'n kapasitorbank met die aanwesigheid van harmonieke ?
- Hoe word die werkverrigting van onder andere relê's, watt-uur meters en ander instrumentasie beinvloed in versteurde golfvorme ?

Die beplanning met die laboratorium is om met stelselondersoeke te begin aan die einde van 1996, die onderskeie komponente word tans ontwikkel en geëvalueer vir frekwensiebereik.

Samevatting

Die toename in die gebruik van halfgeleiers gekoppel aan die nasionale kragnet bied duidelike elegansie aan die beheer en bedryf van kragverspreidingaspekte. Dit is egter golfversteurende tegnologie wat die interaksie met toerusting meer kompleks as slegs die waarneem en behandeling daarvan maak. Die penetrasie moet gekwantifiseer word op 'n eenduidige wyse sodat die bydrae van geografies wyd verspreide nie-lineêre laste aangetoon kan word. Navorsing in hierdie verband word dus gefasiliteer deur hierdie laboratorium. 'n Kombinasie van opleidingsmoontlikhede bestaan ook waarmee relevansie van voorgraadse opleiding by die PU vir CHO uitgebrei kan word.

Bibliografie

[1] Arrillaga, J.; Bradley, D.A. & Bodger, P.S. **Power System Harmonics**. New York: Wiley. 1985.

[2] Domijan, A. & Shoults, R.R. "Electric Power Engineering Resources of the United States of America and Canada", *IEEE Trans. on Power Systems*, Vol. 3, No 3, Augustus 1988, p1354-1360.

[3] Domijan, A. & Embriz-Santander, E. "A Novel Power Electric Laboratory for Power Quality and Energy Studies: Training Aspects". *IEEE Trans. on Power Systems*, Vol. 7, No 4, November 1992, p1571-1578.

[4] Foley, M.; Chen, y. & Bose, A., "A Real Tiem Power System Simulation Laboratory Environment", *IEEE Trans. on Power Systems*, Vol. 5, No 5, November 1990, p1401-1403.

[5] Girgis, A.A.; Makram, B.E. & Baldwin, T.L., "Computer Based Harmonic Generator Facilities to Study Harmonic Related Problems", *IEEE Trans. on Power Systems,_*Vol. 4, No 3, Augustus 1989, p1252-1257.

[6] Glover, D.J., Sarma, M. **Power System Analysis and Design**. Boston: PWS Publishing Company. 1994

[7] Joetten, R. et al., "A New Real Time Simulator for Power System Studies", *IEEE Trans. on Power Apparatus and Systems*, Vol. PAS-104, No 9, September 1985, p2604-2611.

[8] Makram, E. & Girgis, A.A., "A New Method in Teaching Power System Harmonics in the Undergraduate Power Curriculum", *IEEE Trans. on Power Systems*, Vol. 5, No. 4, November 1990, p1407-1413.

[9] Roitman, M., Watanabe, E.H. & Flavio, J.L., "Power System Analog Simulation Enhancement using a new Programmable Electronic Tool", *IEEE Trans. on Power Systems*, Vol 4, No. 1, Februarie 1989, p286-292.

[10]Shoults, R.R., Chen, M.S. & Domijan, J., "The Energy Ssytems Research Center Electric Power Systems Simulation Laboratory and Energy Management System Control Center", *IEEE Trans. on Power Systems*, Vol. 2, No. 1, Februarie 1987, p239-246.

[11] Shultz, R.D., Smith, R.A. & Hickey, G.L., "Calculation of Harmonic Currents and Voltages on Transmission Lines", *IEEE Trans. on Power Apparatus and Systems*, Vol. PAS-102, No.4, April 1983, p817-821.

[12] Swift, G.M., "A Comprehensive Generator-Line-Infinite-Bus Micromachine Model", *IEEE Trans. on Power Systems*, Vol. 8, No.4, November 1992, p1400-1405.

[13] Tamura, Y., et al., "Development of Power System Simulator for Research and Education", *IEEE Trans. on Power Systems*, Vol. 5, No. 2, Mei 1990, p492-499.

[14] Umans, S.D., Szajner, "A Model Power System-Part II - Design of System Elements and Test Results", *IEEE 1975 PES Winter Meeting*, NY, Paper No. C 75 173-0.

[15] Yacamini, R., "Power System Harmonics: Part 2, Meassurements and calculations", Februarie 1995, p51-56.

[16] IEEE Task Force Report on the Effects of Harmonics on Equipment, "Effects of Harmonics on Equipment", *IEEE Trans. on Power Systems*, Vol. 8, No. 2, April 1993, p672-680.

[17] IEEE Working Group on Power System Harmonics, "Power System Harmonics: An Overview", ", *IEEE Trans. on Power Apparatus and Systems*, Vol. PAS-102, No. 8, Augustus 1983, p2455-2460.

Adres van skrywer

J. Rens, Departement Elektroniese en Elektriese Ingenieurswese, PU vir CHO, Privaatsak X6001, Potchefstroom, 2520. Tel: 27-148-299 1979
eeiapjr@puknet.puk.ac.za

A supply friendly AC/DC converter for use in pulsed laser power supplies

N. Truter, J.H.C. Pretorius, P.H. Swart, J.D. van Wyk

Abstract : *In this paper an AC/DC force commutated controlled converter, designed for use in a pulsed laser power supply, is presented. The converter is controlled with a digital signal processor (DSP). The design of the controller is discussed, with emphasis on the DSP control. Some experimental results are also given.*

Introduction

CO_2 pulsed lasers require pulses of 35kV with peak current levels that typically extend to 12kA. When the optical outputs of several lasers are time-multiplexed into a common target at individual pulse repetition rates of 2kHz, very high collective pulse rates can be obtained. The nanosecond wide electrical pulses delivered to the lasers are furnished by multistage series pulse compressor circuits [1] that are, in turn, driven by thyristor-switched circuit topologies that generate the initial pulses by means of resonant transfer.

These initial half-sinusoidal current pulses of 800µs duration, are drawn from the rectified DC-voltage that is obtained from the 380V three-phase grid by a 6-pulse thyristor phase control bridge. This circuit is responsible for the injection of high-frequency components into the supply grid. All the harmonic components that are normally associated with 6-pulse conversion are present in the input. The 800µs half-sinusoidal current pulses that are drawn from the rectified DC-bridges by the pulse generation circuits, in addition, further aggravate the situation, because elaborate filtering is required to prevent their propagation into the supply grid. The pulsed power supplies presently operate at a power factor of 0.8 and at a total harmonic distortion level of 45% for the line currents.

Two approaches have been investigated for mitigation of the harmonics. The first approach is that of installing additional compensating equipment at the point of common coupling in the power supply network. Different topologies of passive, active and hybrid filters are being investigated and tested.

The second approach, which is presented here, is a supply friendly AC/DC force-commutated PWM controlled converter, designed for 380V, 80 kW operation. The converter draws sinusoidal currents from the supply at unity power factor. Control is done by means of a DSP. Both the design, as well as the experimental results, are presented in this paper.

Supply friendly AC/DC converter

This converter supplies a constant, adjustable DC-voltage to a variable non-linear load, while operating at approximately unity power factor, and

drawing approximately sinusoidal currents from the supply network.
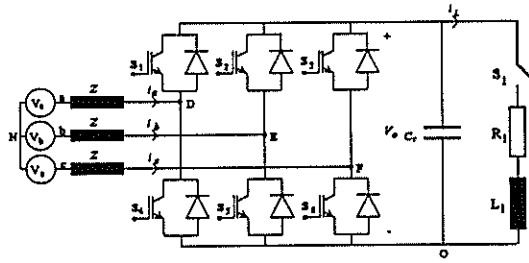
Figure 1 : Circuit diagram of the supply friendly converter with test load

Figure 1 shows the supply friendly converter with a test load. The converter uses standard PWM-techniques to force the reference currents (i_a^*, i_b^* and i_c^*) to flow in the supply lines [2][3]. The reference currents are determined as scaled in phase replicas of the line to neutral voltages (v_{aN}, v_{bN}, and v_{cN}). These currents are referred to in the literature [7] as Fryze currents. The DC-voltage (V_o) are kept constant and equal to the DC-voltage reference value (V_o^*), by adjusting the amplitude of the current reference values.

The control of this converter is carried out by a digital signal processor. The DSP is implemented on a PC-expansion board. The DSP card reads the analogue data via a 12-channel 12-bit A/D card. This A/D card is also a PC-expansion card. The A/D card implements 12 fast A/D converters operating in parallel. The system is thus able to sample 12 analogue channels simultaneously and then convert it to 12-bit digital format and read it into the DSP's memory, in less than 12μs. The DSP then calculates and generates the necessary control signals for the IGBT bridge (S_1 to S_6).

The block diagram of the control system is shown in figure 2 [3][4]. The DSP implements all the functions shown in figure 2.
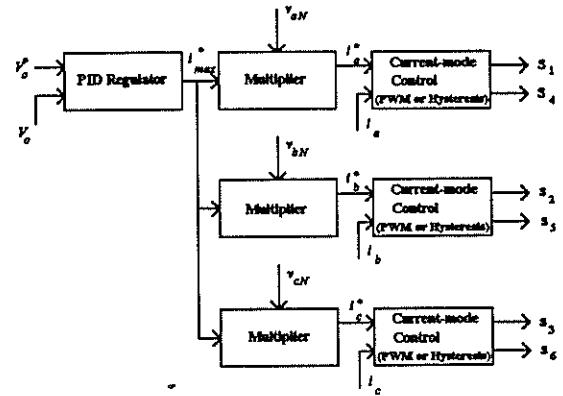
Figure 2 : Block diagram of control system

The difference between V_o and V_o^* is first put through a low pass filter with a cut-off frequency of less than the fundamental frequency of the supply line (50Hz). The output of the filter is referred to here as the error signal and is calculated as shown in (1).

$$error(s) = (V_o^* - V_o(s)) \cdot (\frac{1}{1 + D.s}) \quad (1)$$

D is the time constant of the filter and it is chosen so that the cut-off frequency (f_c) is lower than 50Hz.

$$f_c = \frac{1}{2.\pi.D} \quad (2)$$

The error signal is now put through a PID-regulator which calculates the amplitude (i_{max}^*) of the line current set values (i_a^*, i_b^* and i_c^*).

$$i_{max}^* = error(s).\frac{A}{s} - B.s \quad (3)$$

This PID regulator only implements an integral (A) and a differential (B)

component. i_{max}^{*} is now multiplied by the normalised instantaneous values of each of the voltages (v_{aN}, v_{bN}, and v_{cN}). This results in the current set values (i_{a}^{*}, i_{b}^{*} and i_{c}^{*}). This method does not provide for the possibility of a zero-order current. If this should prove to be be a problem, the DSP program could easily be changed. i_{a}^{*} and i_{b}^{*} will then be calculated as above, and i_{c}^{*} will be calculated by (4).

$$i_{c}^{*} = -(i_{a}^{*} + i_{b}^{*}) \qquad (4)$$

The value of i_{max}^{*} is calculated during each sample period. It is therefore necessary that f_c be low enough so that i_{max}^{*} can be regarded as constant during one fundamental cycle of the supply voltage (50Hz)

Equations (5) and (6) are obtained by performing z-transforms on (1) and (3), These are easily implemented in the DSP programme.

$$error(k) = T_s.2.\pi.f_c.(V_o^{*} - V_o(k)) + \qquad (5)$$
$$e^{-T_s.2\pi.f_c}.error(k-1)$$

$$i_{max}(k) = T_s.a.error(k) + i_{max}(k-1) + $$
$$b.(\frac{error(k) - error(k-1)}{T_s}) \qquad (6)$$

Here T_s is the sampling frequency, a and b are the parameters of the PID regulator (corresponding to A and B in (3)), and k is a counting index indicating the sample number.

The set value of the current is now determined by multiplying i_{max}^{*} with the normalised line to neutral voltage. Equation (7) shows the equation for

phase a. The same calculation is repeated for phases b and c.

$$i_a^{*}(k) = i_{max}^{*}(k).\frac{v_{aN}(k)}{v_{aN,max}} \qquad (7)$$

The current set value ($i_a^{*}(k)$) is now compared with the measured current ($i_a(k)$), and the state of the switches is determined to decrease the difference. This is done separately for all three phases. The only constraint is that the top three switches (S_1, S_2 and S_3) or the bottom three switches (S_4, S_5 and S_6) should not be closed simultaneously.

This switching strategy is called fixed frequency hysteresis or CRΔM (*Current regulated delta modulation*) [5][6]. After each sampling period a decision is taken if the state of the switches must be changed. The possible switching frequencies are given by (8).

$$f_s = \frac{1}{n.T_s} \ldots\ldots\ldots n = 1,2,3,\ldots \qquad (8)$$

The highest value of n was found to be lower than 4. For a sampling period of 50μs, switching frequencies of 20kHz, 10kHz and 5kHz are present. These harmonics can be removed by means of a high pass filter.

Experimental results

The system shown in figure 1 and described above was constructed and tested.

The following component values were apply:

Z : 10mH, C_r : 1.8mF, R_l : 12Ω, L_1 : 80nH, T_s : 50μs, and S_1 is switched at 1kHz. The duty cycle of S_1 is varied to

adjust the load. The system was tested on the 220V Eskom supply grid. The line currents drawn with a 30kW load is shown in figure 3. A current THD of 4% and a power factor 0.99 was obtained.
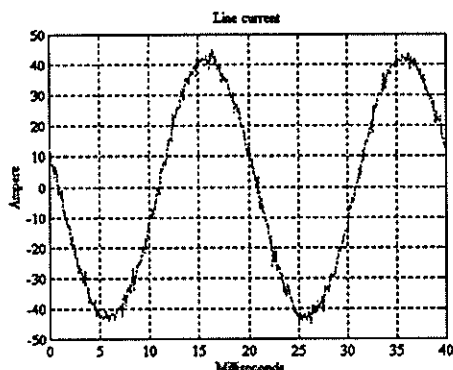
Figure 3 : Line current drawn by supply friendly converter

References

[1]   H. M. von Bergman, P.H. Swart, "Thyristor driven pulsers for multi-kilowatt average Power Lasers", IEEE Proceedings Part B, March 1992, Vol. 139, Num.2,p123

[2]   R. Wu, S.B. Dewan, R.G. Slemon, "A PWM AC to DC Converter with Fixed Switching Frequency", IEEE Transactions on Industry Applications, Vol. 26, No. 5, pp 880-885, Sept/Oct 1990

[3]   N. Mohan, T.M. Undeland, W.P. Robbins, "POWER ELECTRONICS : Converters, Applications and Design", John Wiley & Sons, 1989, Ch. 20-11-5, pp. 530-532

[4]   G. L. van Harmelen, J.H.R. Enslin, "Real-Time Dynamic Control of Dynamic Power Filters in Supplies with High Contamination", IEEE Transactions on Power Electronics, Vol.8, No.3, July 1993, pp.301-308

[5]   G . Venkataraman, D.M. Divan, T.H. Jahns, "Discrete Pulse Modulation Strategies for High-Frequency Inverter Systems", IEEE Transactions on Power Electronics, Vol.8, No.3, July 1993, pp.279-287

[6]   M. Kheraluwala, D.M. Divan, "Delta Modulation Strategies for Resonant Link Inverters", IEEE PESC 1987

[7]   S. Fryze, "Wirk-, Blind- und Scheinleistung in elektrischen Stromkreisen mit nichtsinus-formigen Verlauf von Strom und Spannung", Electrotechnische Zeitschrift, 1932, Heit 25, pp. 596-599, 625-627, 700-702

Address of author

Neill Truter, Atomic Energy Corporation of South Africa, P.O. Box 582, Pretoria, 0001

PREVENTION OF VOLTAGE INSTABILITY OR COLLAPSE BY STATIC VAR COMPENSATORS

V. Shikoana   S.I. Darie

Department of Electrical Engineering

University of Cape Town

Abstract

Static var compensator (SVC) is an established device for meeting reactive power requirements in transmission, distribution and industrial systems.

This paper analyses the application of SVC to prevent transient voltage instability that may lead to voltage collapse.

Analysis is supported by time simulations illustrating the effect of disturbances on the system with and without SVC. The results show that without SVC, voltage instability occurs and with SVC, transient voltage instabilities are eliminated and the load voltage is maintained near the rated value.

The possibility of replacing the SVC with breaker switched capacitor is also investigated.

Introduction

Recently, voltage collapse played a part in several major incidents throughout the world [1-3]. The latest major incidents occurred in January 1987 in France, and in Tokyo in July 1987. It was also the case in Florida in May 1985 and Utah(USA) in July 1985. This type of failures and many others justify the attention which must be paid to analysing this phenomena, studying methods and means which could be introduced to prevent risk of occurrence.

The static var compensator has established itself as the state of the art concept for high performance reactive power compensation in transmission networks[6-8]. The purpose of the SVC is to provide voltage support for abnormal regime in the system but other applications include damping of power oscillations, voltage balancing, steady state voltage support and stabilisation of voltage at fluctuating industrial loads.

This paper demonstrates the stabilisation effect of the SVC through transient time simulations of the industrial system. The dynamics of the loads, static var compensator, transmission lines, transformers and equivalent source network are represented by their respective transient models. Dynamic behavior of voltage is interpreted using transient trajectories of the combined voltage/power characteristics of the transmission line.

Studied system modelling

To define a representative power system that would exhibit the appearance of voltage collapse phenomenon in the absent of dynamic voltage support, the 132 kV system of Fig. 1 was used. The system represents a load with local generation to serve portion of the load. The load depends on the power imported over the transmission system. The system components are represented as follows : lumped π-equivalent circuit for each transmission line, fixed voltage source behind transient reactance for the source network, series R-L elements for transformers.

Modelling of the load was important for the simulation of voltage collapse phenomenon [5]. Typical industrial load was modelled. The load consisted of 75% induction motor load and the balance split evenly between constant current and constant impedance load. The induction motor was modelled in detail.
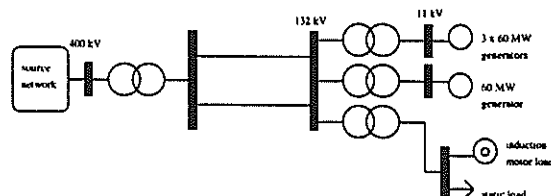
Fig. 1: 132 kV System Studied.

(a) Voltage

(b) Imported Power

(c) Net load P_L and Q_L
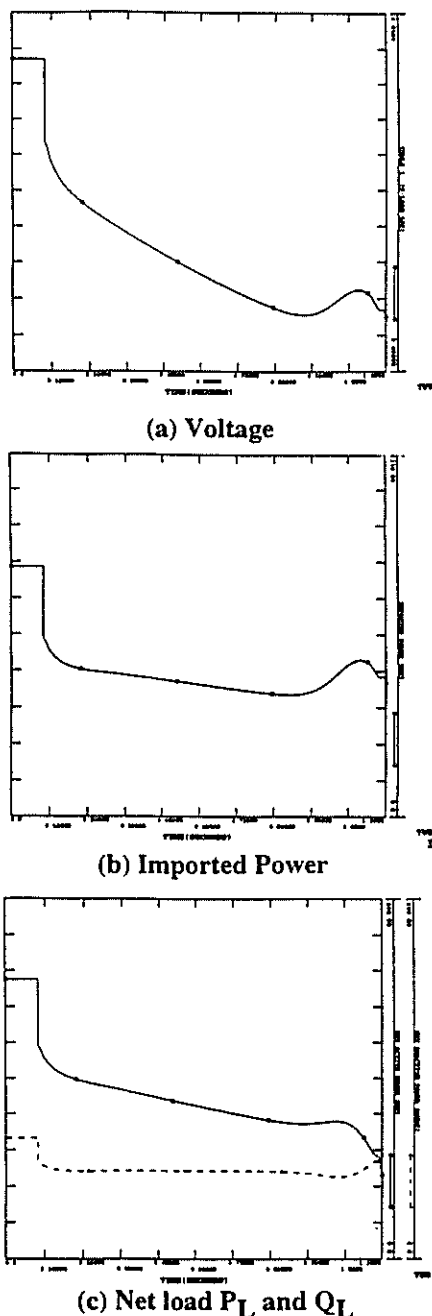
Fig. 2: System Response for Tripping One Generator(No SVC).

VOLTAGE INSTABILITY SIMULATIONS

For investigation, the disturbance chosen was to trip one of the generators. At the time of this disturbance, there was only a single 132 kV transmission line connected to the rest of the power system.

Fig. 2 illustrate the effect of tripping one of the local generators. The system is simulated without an SVC. These show that sudden voltage collapse occurs which leads to the stalling of induction motors.

SVC CHARACTERISTICS

Type

SVC with a combined thyristor switched capacitor and thyristor controlled reactor was chosen to generate fast variable capacitive reactive power at instant when voltage collapse appears.

The reason for choosing TSC/TCR is because of its capability to output zero reactive power during normal regime and have enough reactive power in the inductive range to limit any dynamic overvoltage following load rejection.

Rating

The capacitive rating is determined on steady state basis i.e it is the capacitive reactive power required to maintain the load voltage at the value which is marginally stable when one local generator is tripped out. This value is obtained from loadflow study of the system of fig. 1.

The inductive rating is determined by the capability of the compensator to limit the dynamic overvoltages to less than 10%. This was obtained by performing time simulations for cases of critical load rejections.

Voltage stabilisation

Fig. 3 shows the effect of tripping one generator with SVC. These show that the load voltage is stabilised and its magnitude recovers near its pre-disturbance value.

Fig. 4 shows the time response of the system when a breaker switched capacitor is considered instead of the SVC.

These show that after switching-in the capacitor, the voltage increases and then immediately falls followed by a progressive collapse similar to that original case of voltage instability without SVC.

SVC stabilisation effect is also illustrated by the transient voltage/power trajectory as shown in fig. 5. Fig. 6 shows the transient trajectory when no

(a) Voltage
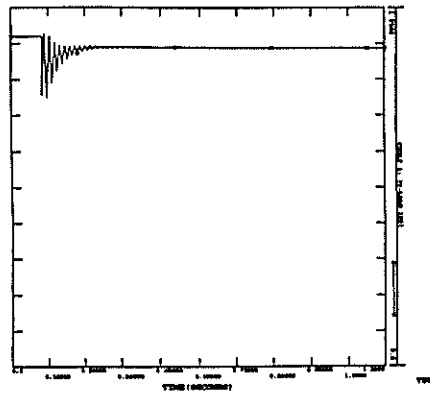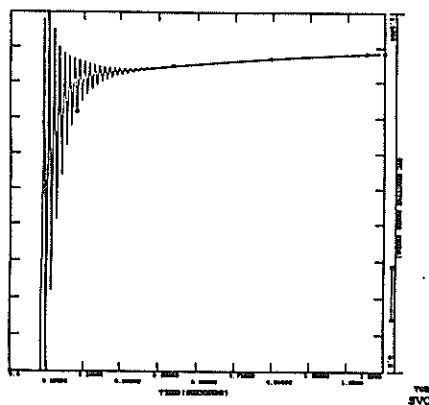
(a) Voltage

(b) Imported Power

(b) Imported Power

(c) SVC Net Output

(c) Net load P_L and Q_L

Fig. 3: System Response for Tripping One
Generator(with SVC).
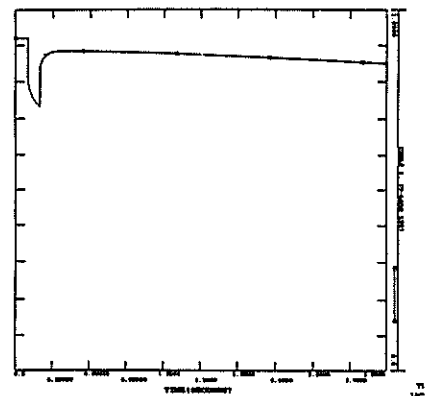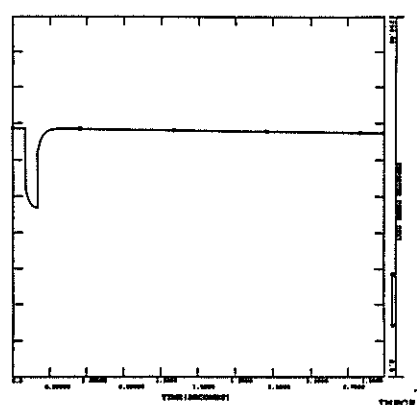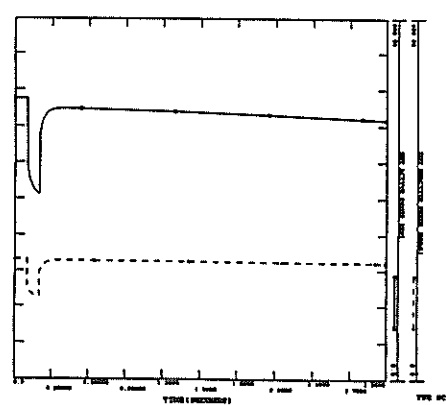
Fig. 4: System Response for Tripping One
Generator (with breaker switched capacitor).
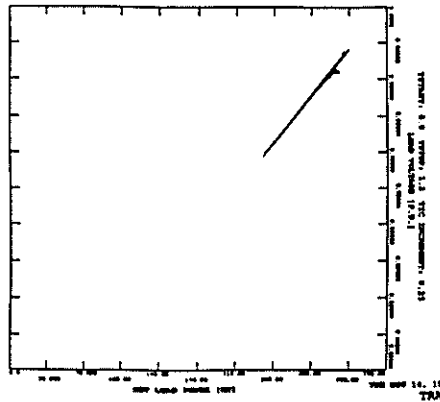
Fig. 5: Transient P/V trajectory of the system with SVC.

Fig. 7: Transient P/V trajectory of the system with breaker switched capacitor.

Fig. 6: Transient P/V trajectory of the system without SCV

SVC is connected, and Fig. 7 shows the trajectory when a breaker switched capacitor is used.

From these figures, it is shown that with the SVC. the voltage settles to a new stable level.

Conclusions

It has been shown that the SVC can prevent voltage instability. The SVC operate in the capacitive reactive power range.

It has also been shown that replacing the SVC with breaker switched capacitor does not guarantee voltage stability.

References

[1] C.W. Taylor," Power System Voltage Instability," EPRI. McGraw Hill, 1992.

[2] Y. Mansour et al," Voltage Stability Limit B.C Hydro's Practice," Proceedings: Bulk Power System Voltage Phenomenon -Voltage Stability and Security, 1989.

[3] M. Chau et al," Voltage Collapse in Bulk Transmission System," Proceedings: Bulk Power System Voltage Phenomenon -Voltage Stability and Security, 1989.

[4] A.E. Hammad, M.Z. El-Sadek," Prevention of Transient Voltage Instabilities due to Induction Motor Loads By Static Var Compensators," IEEE Trans. on PAS, Vol. 4, 1989.

[5] V. Shikoana, S.I. Darie," Effect of load Characteristics on Voltage Stability," SUPEES95, Nov 1995.

[6] B. Klerfors, T.Peterson," Balancing Asymmetries by Means of Thyristor - Controlled Static Var Compensators," CIGRE 38-05, Sep 1988.

[7] S. Torseng," Shunt Connected Reactors and Capacitors Controlled by Thyristors," Paper 1612C, IEE Technical Seminar on Control of Reactive Power, 1980.

[8] A. Petersson et al," Matching a Novel SVC Design to a Demanding Application from Specific Requirements to Actual Performance," CIGRE 14-05, Aug 1994.

Address: Victor Shikoana, Department of Electrical Engineering, University of Cape Town, Private Bag, Rondedosch, 7700.
E_mail :Shikoana @eleceng.uct.za.ac

A New Concept for the Control of Oscillations in Power Systems

Y. Bao   A. Petroianu

Department of Electrical Engineering, University of Cape Town,
Rondebosch 7700, South Africa

Abstract—A new idea of dealing with system stability is derived from the distribution of eigenvalues. The regular system is used to reveal the general understanding of oscillations in power systems. The fundamental characteristic of oscillations can be determined through the mathematical description, which is presented in detail. A real power system is taken as example to confirm the control strategy of using one machine model in multimachine power system.

Keywords:Power systems, regular system, oscillations, power system stabilizer.

1 Introduction

The rapid growth of electric power systems and the increase of interconnection between areas cause the power system oscillations to become a serious problem recently. The slow frquency oscillations are common in weakly connected large power systems and their fundamental characteristic is not clear.

The stability of synchronous machine with the case of one machine against an infinite bus is the basic phenomena[1]. The analysis for such phenomena develops insights into effects of excitation system and the requirement for power system control.

To improve the dynamic stability of power systems, power system stabilizer is widely used as a supplementary control device without reducing the high gain of excitation systems. The effective techniques for tuning the parameters of stabilizers are presented in many papers. However, the conventional one machine model for oscillation control is still studied and used in real power systems[2][3][4]. The efficiency and advantage of this model is obvious, but there is no proof in theory on its use in multimachine power systems.

The studies of multimachine system are presented in [5] [6] [7] with various system models for the analysis.

The fundamental study of inter-area oscillations in power systems is carried out by Ontario Hydro [8].

This paper is associated with the study of oscillations in power systems. The regular system is used to reveal the general understanding of oscillations. The mathematical description of oscillations in regular system and in non-regular system is presented in detail. The efficiency of using one machine model is explained through both mathematical and system structure aspects. A real power system is taken as example to confirm the control strategy of using one machine model in multimachine system.

2 The concept of regular system

Generally, the distribution of eigenvalues of a multimachine power system does not show any regularity in the complex plane. these eigenvalues form clusters or show dispersed forms. To reveal a more general understanding of oscillations, a new idea of dealing with system stability is derived from the distribution of eigenvalues. Considering a power system with identical machines connecting to symmetrcal network, it can be received that the eigenvalues of this system will form clusters in the complex plane. Such a system with identical machines and identical network is called regular system.

A regular system with three machines is shown in Figure 1. The eigenvalues of the regular system are given in table 1. These eigenvalues divide into several groups. To explain the reason of eigenvalues dividing into groups, two simple system with the same parameters as the regular system are considered. The first one shown in Figure 2(a) has one machine feeding a load. Figure 2(b) has one machine against an infinite bus. The eigenvalues of the two systems are given in table 2. By table 1 and table 2, it can be obviously seen that the eigenvalues of the regular system are composed of two classes. Class one corresponds to the unitary motion of the generators in the system and these eigenvalues are the same as that of one machine feeding a load; Class two corresponds to the relative motion of the machines with respect to each other and these eigenvalues are the same as that of one machine against an infinite bus. A real power system can be seen as disturbed case of the regular system. The disturbances cause a regular system to become such a real power system that its eigenvalues spread in the complex plane and do not exhibit any regularity.

The analysis for the regular system and the disturbed cases gives the following conclusions:

- The eigenvalues of a power system either with or without an infinite bus are composed of two classes;
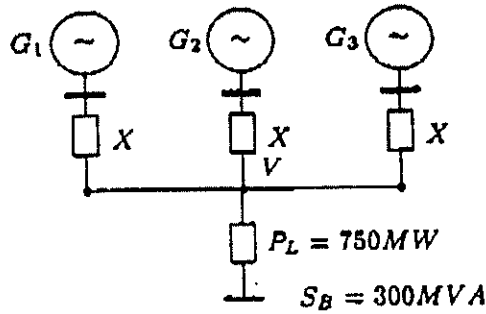
Figure 1: Three-machine regular system, X=0.3
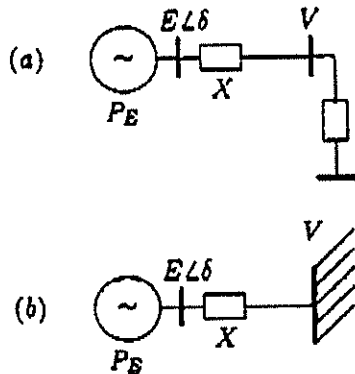
Figure 2: One machine system

- It is the eigenvalues that belonging to class two could cause oscillatory instability in power system.

Table 1: Eigenvalues
Regular system

-39.042+j0.000	-1.099±j2.081
-39.042+j0.000	-1.095±j0.203
-34.452+j0.000	-1.000+j0.000
-9.552+j0.000	-1.000+j0.000
-9.552+j0.000	-1.000+j0.000
-9.155+j0.000	-0.453±j1.147
-1.889+j0.000	-0.431±j8.229
-1.889+j0.000	-0.431±j8.229
-1.813±j0.583	-0.291±j0.510
-1.813±j0.538	-0.291±j0.510

3 The mathematical description of Oscillations

To further prove the conclusions above, the mathematical description of oscillations are prsented in this section. Since the eigenvalues belonging to class one represent unitary motion of the machines and will not cause oscillatory instability, the study of oscillations will pay attention to eigenvalues belonging to class two. It is accepted that the dominant poorly damped modes of concern are those related to machine inertias. In order to give analytical solution and deal with inertia swing modes, the classic machine model is used in the following and machine's X_d' is included in line reactance.

Table 2: Eigenvalues

Figure 2(a)	Figure 2(b)
-34.452+j0.000	-39.042+j0.000
-9.155+j0.000	-9.552+j0.000
-1.099+j2.081	-1.889+j0.000
-1.095+j0.203	-1.813±j0.583
-1.000+j0.000	-1.000+j0.000
-0.453±j1.147	-0.431±j8.229
	-0.291±j0.510

3.1 One machine against an infinite bus

Considering Figure 2(b) system of one machine against an infinite bus, the dynamic equations are given as:

$$P_E = \frac{EV \sin \delta}{X} \qquad (1)$$

$$\Delta P_E = \frac{EV \cos \delta}{X} \Delta \delta \qquad (2)$$

$$m \frac{d^2 \delta}{dt^2} = \omega_0 (P_M - P_E) \qquad (3)$$

Since the mechanical power P_M, infinite bus voltage V, sending end voltage E and inertia constant m are constant, the incremental form of equation (3) becomes:

$$m \frac{d^2 \Delta \delta}{dt^2} = \omega_0 (0 - \Delta P_E) = -\frac{\omega_0 EV \cos \delta}{X} \Delta \delta \qquad (4)$$

The eigenvalues of Figure 2(b) system are:

$$\lambda = \pm j \sqrt{\frac{\omega_0 EV \cos \delta}{mX}} \qquad (5)$$

3.2 Eigenvalues of two-machine regular system

A two-machine system is shown in Figure 3.
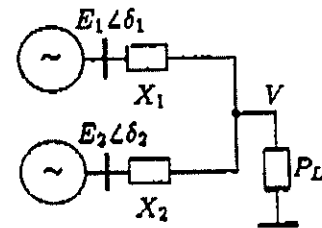
Figure 3: Two-machine system

If the parameters of Figure 3 system are set to be: $X_1 = X_2 = X$, $E_1 = E_2 = E$, $\delta_1 = \delta_2 = \delta$ and $m_1 = m_2 = m$, it will be a regular system and can be converted to a π-form system shown in figure 4. The parameters of Figure 4 system will be:

$$Y_{12} = \frac{R}{-X^2+j2RX} = \frac{R}{X\sqrt{X^2+4R^2}} e^{-j(90°-\alpha_{12})}$$
$$= y_{12} e^{-j(90°-\alpha_{12})} = \frac{\cos\alpha_{12}}{2X} e^{-j(90°-\alpha_{12})} \qquad (6)$$
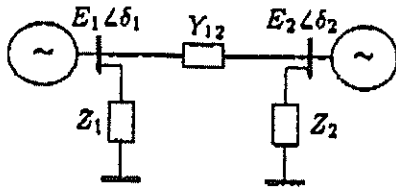
Figure 4: π-form two machine system

$$\alpha_{12} = \tan^{-1}(\frac{-X}{2R}) \tag{7}$$

$$\cos\alpha_{12} = \frac{2R}{\sqrt{X^2+4R^2}} = \frac{V^2}{\sqrt{P_E^2 X^2 + V^4}} \tag{8}$$

$$Z_1 = Z_2 = 2R + jX \tag{9}$$

$$R = V^2/P_L = V^2/2P_E \tag{10}$$

$$
\begin{aligned}
S_1 &= E_1\left[E_1 y_{11}e^{j(90°-\alpha_{11})} - E_2 e^{j\delta_{12}}y_{12}e^{j(90°-\alpha_{12})}\right]\\
&= E_1^2 y_{11}e^{j(90°-\alpha_{11})} - E_1 E_2 e^{j\delta_{12}}y_{12}e^{j(90°-\alpha_{12})}\\
&= E_1^2 y_{11}(\cos(90°-\alpha_{11}) + j\sin(90°-\alpha_{11}))\\
&\quad - E_1 E_2 y_{12}(\cos(90°+\delta_{12}-\alpha_{11})\\
&\quad + j\sin(90°+\delta_{12}-\alpha_{12}))\\
&= E_1^2 y_{11}(\sin\alpha_{11} + j\cos\alpha_{11})\\
&\quad + E_1 E_2 y_{12}(\sin(\delta_{12}-\alpha_{12}) - j\cos(\delta_{12}-\alpha_{12}))
\end{aligned}\tag{11}
$$

$$
\begin{aligned}
S_2 &= E_2^2 y_{22}(\sin\alpha_{22} + j\cos\alpha_{22})\\
&\quad - E_1 E_2 y_{12}(\sin(\delta_{12}+\alpha_{12}) + j\cos(\delta_{12}+\alpha_{12}))
\end{aligned}\tag{12}
$$

$$P_1 = E_1^2 y_{11}\sin\alpha_{11} + E_1 E_2 y_{12}\sin(\delta_{12}-\alpha_{12}) \tag{13}$$

$$P_2 = E_2^2 y_{22}\sin\alpha_{22} - E_1 E_2 y_{12}\sin(\delta_{12}+\alpha_{12}) \tag{14}$$

$$\Delta P_1 = E_1 E_2 y_{12}\cos(\delta_{12}-\alpha_{12})\Delta\delta_{12} \tag{15}$$

$$\Delta P_2 = -E_1 E_2 y_{12}\cos(\delta_{12}+\alpha_{12})\Delta\delta_{12} \tag{16}$$

$$\Delta\delta_{12} = \Delta\delta_1 - \Delta\delta_2 \tag{17}$$

Considering equation (15) and (16), the system dynamic equations are:

$$m_1\frac{d^2\Delta\delta_1}{dt^2} = -\omega_0 E_1 E_2 y_{12}\cos(\delta_{12}-\alpha_{12})\Delta\delta_{12} \tag{18}$$

$$m_2\frac{d^2\Delta\delta_2}{dt^2} = \omega_0 E_1 E_2 y_{12}\cos(\delta_{12}+\alpha_{12})\Delta\delta_{12} \tag{19}$$

In matrix form:

$$
\begin{bmatrix} \Delta\ddot{\delta}_1 \\ \Delta\ddot{\delta}_2 \end{bmatrix} = \begin{bmatrix} K_1 & -K_1 \\ K_2 & -K_2 \end{bmatrix}\begin{bmatrix} \Delta\delta_1 \\ \Delta\delta_2 \end{bmatrix}\tag{20}
$$

where:

$$K_1 = -\omega_0 E_1 E_2 y_{12}\cos(\delta_{12}-\alpha_{12})/m_1 \tag{21}$$

$$K_2 = \omega_0 E_1 E_2 y_{12}\cos(\delta_{12}+\alpha_{12})/m_2 \tag{22}$$

The system eigenvalues are obtained by:

$$
\begin{bmatrix} K_1 - \lambda^2 & -K_1 \\ K_2 & -K_2 - \lambda^2 \end{bmatrix} = \lambda^4 - (K_1 - K_2)\lambda^2 = 0 \tag{23}
$$

Taking account into $E_1 = E_2 = E$, $m_1 = m_2 = m$, $y_{12} = \frac{\cos\alpha_{12}}{2X}$ and $\delta_{12} = 0$, there are:

$$
\begin{aligned}
\lambda^2 &= (K_1 - K_2)\\
&= -\omega_0 E^2 y_{12}(\cos(\delta_{12}-\alpha_{12}) + \cos(\delta_{12}+\alpha_{12}))/m\\
&= -\omega_0 E^2 y_{12}(2\cos\delta_{12}\cos\alpha_{12})/m\\
&= -\frac{\omega_0 E^2\cos^2\alpha_{12}\cos\delta_{12}}{mX} = -\frac{\omega_0 E^2\cos^2\alpha_{12}}{mX}
\end{aligned}\tag{24}
$$

From equation (15) and (16), there is:

$$
\begin{aligned}
\Delta P_1 - \Delta P_2 &= E^2 y_{12}(\cos(\delta_{12}-\alpha_{12}) + \cos(\delta_{12}+\alpha_{12}))\Delta\delta_{12}\\
&= \frac{E^2\cos^2\alpha_{12}\cos\delta_{12}}{X}\Delta\delta_{12} = \frac{E^2\cos^2\alpha_{12}}{X}\Delta\delta_{12}
\end{aligned}\tag{25}
$$

From Figure 3, ΔP_1 and ΔP_2 can also be written as:

$$\Delta P_1 = \frac{E_1 V\cos\delta_1}{X}\Delta\delta_1 + \frac{E_1\sin\delta_1}{X}\Delta V \tag{26}$$

$$\Delta P_2 = \frac{E_2 V\cos\delta_2}{X}\Delta\delta_2 + \frac{E_2\sin\delta_2}{X}\Delta V \tag{27}$$

With $E_1 = E_2 = E$ and $\delta_1 = \delta_2 = \delta$, equation (26) and (27) give:

$$\Delta P_1 - \Delta P_2 = \frac{EV\cos\delta}{X}\Delta\delta_{12} \tag{28}$$

The comparision of equation (28) with equation (25) gives:

$$E\cos^2\alpha_{12} = V\cos\delta \tag{29}$$

Hence, equation (24) becomes:

$$\lambda = \pm j\sqrt{\frac{\omega_0 E^2\cos^2\alpha_{12}}{mX}} = \pm j\sqrt{\frac{\omega_0 EV\cos\delta}{mX}} \tag{30}$$

The eigenvalues obtained by equation (30) are obviously the same as that of equation (5) whereby the conclusion is given:

- The eigenvalues corresponding to the relative motion of the machines in a two-machine regular system are exactly the same as that of one machine against an infinite bus.

3.3 Eigenvelues of n-machine regular system

To deal with more common condition of multimachine system, a n-machine regular system is shown in Figure 5. The parameters of the system are: $P_i = P_E$, $E_i = E$, $P_L = nP_E$, $\delta_i = \delta$ and $m_i = m$.

Figure 5 system can also be converted to a two machine system shown in Figure 3, where machine 2 is a equivalent machine formed by (n-1) machines with $m_2 = (n-1)m$, $X_2 = X/(n-1)$. Then it can be converted to Figure 4 system.
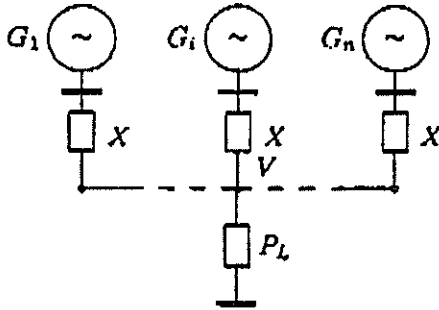
Figure 5: N-machine regular system

The parameters of Figure 4 system are:

$$Y_{12} = \frac{(n-1)R}{-X^2 + jnRX} = \frac{(n-1)Re^{-j(90^\circ - \alpha_{12})}}{X\sqrt{X^2 + n^2R^2}}$$

$$= y_{12}e^{-j(90^\circ - \alpha_{12})} \tag{31}$$

$$\alpha_{12} = \tan^{-1}(\frac{-X}{nR}) \tag{32}$$

$$Z_1 = nR/(n-1) + jX \tag{33}$$

$$Z_2 = nR + jX \tag{34}$$

$$R = V^2/P_L = V^2/nP_E \tag{35}$$

The dynamic equations are:

$$m\frac{d^2\Delta\delta_1}{dt^2} = -\omega_0 E^2 y_{12}\cos(\delta_{12} - \alpha_{12})\Delta\delta_{12} \tag{36}$$

$$(n-1)m\frac{d^2\Delta\delta_2}{dt^2} = \omega_0 E^2 y_{12}\cos(\delta_{12} + \alpha_{12})\Delta\delta_{12} \tag{37}$$

Let:

$$K_1 = \frac{-\omega_0 E^2 y_{12}}{m}\cos(\delta_{12} - \alpha_{12}) \tag{38}$$

$$K_2 = \frac{\omega_0 E^2 y_{12}}{(n-1)m}\cos(\delta_{12} + \alpha_{12}) \tag{39}$$

Considering $\delta_{12}=0$ and y_{12} of equation (31), the system eigenvalues are obtained by:

$$\lambda^2 = (K_1 - K_2) = -\frac{\omega_0 E^2 y_{12}}{m}(\cos(\delta_{12} - \alpha_{12})$$

$$+ \frac{1}{n-1}\cos(\delta_{12} + \alpha_{12})) = -\frac{\omega_0 E^2 y_{12}n}{m(n-1)}\cos\alpha_{12}$$

$$= -\frac{\omega_0 E^2 n}{m(n-1)}\frac{R(n-1)\cos\alpha_{12}}{X\sqrt{X^2 + n^2R^2}}$$

$$= -\frac{\omega_0 E^2}{m}\frac{nR\cos\alpha_{12}}{X\sqrt{X^2 + n^2R^2}} = -\frac{\omega_0 E^2\cos^2\alpha_{12}}{mX} \tag{40}$$

With $R = V^2/nP_E$, there is:

$$\cos\alpha_{12} = \frac{nR}{\sqrt{X^2 + n^2R^2}} = \frac{V^2}{\sqrt{P_E^2 X^2 + V^4}} \tag{41}$$

It is easy to know from equation (8) that $\cos\alpha_{12}$ of equation (41) is the same as that of equation (8). With equation (29), the eigenvalues of equation (40) are:

$$\lambda = \pm j\sqrt{\frac{\omega_0 E^2\cos^2\alpha_{12}}{mX}} = \pm j\sqrt{\frac{\omega_0 EV\cos\delta}{mX}} \tag{42}$$

The eigenvalues obtained by equation (42) are the same as that of equation (5). The above results lead the conclusion:

- The oscillation of one machine against all other machines in a regular system is exactly the same as that of one machine against an infinite bus.

3.4 Eigenvalues of two-machine non-regular system

A real power system is none regular any more. To get the description of oscillations in a non-regular system, the two-machine non-regular system in Figure 3 and its π-form system in Figure 4 are considered again:

$$Y_{12} = \frac{R}{-X_1X_2 + jR(X_1 + X_2)}$$

$$= \frac{Re^{-j(90^\circ - \alpha_{12})}}{\sqrt{X_1^2X_2^2 + R^2(X_1 + X_2)^2}} = y_{12}e^{-j(90^\circ - \alpha_{12})}$$

$$\tag{43}$$

$$\alpha_{12} = \tan^{-1}(\frac{-X_1X_2}{R(X_1 + X_2)}) \tag{44}$$

From equation (23), there will be:

$$\lambda^2 = -\omega_0 E_1 E_2 y_{12}(\frac{\cos(\delta_{12} - \alpha_{12})}{m_1} + \frac{\cos(\delta_{12} + \alpha_{12})}{m_2})$$

$$= \frac{-\omega_0 E_1 E_2 y_{12}}{\frac{m_1 m_2}{m_1 + m_2}}\frac{m_1\cos(\delta_{12} - \alpha_{12}) + m_2\cos(\delta_{12} + \alpha_{12})}{m_1 + m_2}$$

$$= \frac{-\omega_0 E_1 E_2}{M_t X_t}\cos\delta' \tag{45}$$

here:

$$M_s = \frac{m_1 m_2}{m_1 + m_2} \qquad (46)$$

$$X_s = 1/y_{12} \qquad (47)$$

$$\cos \delta' = \frac{m_1 \cos(\delta_{12} - \alpha_{12}) + m_2 \cos(\delta_{12} + \alpha_{12})}{m_1 + m_2} \qquad (48)$$

and there will be:

$$P_s = \frac{E_1 E_2 \sin \delta'}{M_s X_s} \qquad (49)$$

By equation (45), a equivalent system with one machine against an infinite bus can be used to represent the oscillatory characteristic of the two-machine non-regular system.

4 The control of oscillations

A real power system does not show regularity, but it can be seen as a disturbed case of the regular system. From mathematical point of view, equation (45) means that the oscillations in power system can be represented by a equivalent system of one machine against an infinite bus. From the structure point of view, a real power system is the projection of a regular system under disturbances. Figure 6 shows the relationship between a real power system and a disturbed regular system. The conversion between them can be seen as:

A real power system can be transformed to a netted-network by transfering or shifting loads with either constant impedance, constant power or constant current.

A netted-network corresponds to a star-network, i.e., there exactly exists a star-network, which can be transformed to the netted-network. This star-network is the disturbed regular system.

A multi-machine star-network can always be converted to a equivalent two-machine system. Using the conclusion about non-regular two-machine system, it can be known that the model of one machine against an infinite bus can be used to represent oscillations. The control of oscillations can be performed by using one machine model, since the oscillatory modes are corresponding to one machine against an infinite bus.

5 Example

To confirm the oscillation control using one machine model in multimachine power system, a real power system, Natal system of South Africa, is taken as example.

Natal system is a part of the ESKOM system in South Africa. Figure 7 shows the diagram of the system. This system has experienced undesirable oscillations during heavily stressed system conditions. To eliminate these undesirable oscillations, Power System Stabilizers(PSS) are planned to be equipped in generating stations. The stability studies for the Natal system show that under a heavy load condition there is a pair of dominant eigenvalues $0.0383 \pm j6.9574$ with positive real parts, which make the system oscillatory unstable. The eigenvector analysis shows that Drakensberg Generating Station
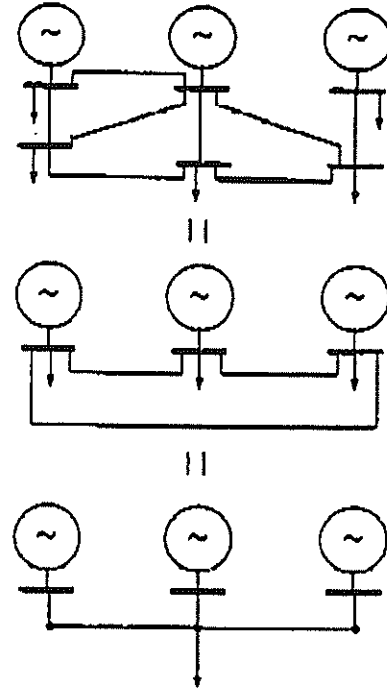
Figure 6: Network transformation

has the predominant effect on the unstable mode while other generating stations have slight effect on this mode. Drakensberg Generating Station has a rated capacity of 1000 MW consisting of four generating units. To eliminate the unstable mode, Power System Stabilizers shown in Figure 8 are considered to be applied on the generators of DGS.

The tuning of PSS parameters is based on phase compensation. The analysis of function $\Delta\omega(s)/\Delta V_r(s)$ of DGS considering the interaction of other genertors in the system indicates that PSS should provide around 70 degree phase advance at 6.9574 rad/s. The time constants of the lead-lag network are:

$$a = \frac{1 + \sin(35°)}{1 - \sin(35°)} = 3.69 \qquad (50)$$

$$T_2 = \frac{1}{\omega_d \sqrt{a}} = 0.075 \qquad (51)$$

$$T_1 = aT_2 = 0.276 \qquad (52)$$

The washout time constant $T_W = 3$ is specified to prevent steady changes in power from producing an output from PSS. The root locus plot shows that system stability is maintained for $0.05 < K_s < 5.0$. A value larger than 5.0 turns the exciter mode unstable while a value smaller than 0.05 turns unstable mode. The gain $K_s = 2.5$ is selected. The installation of PSS in DGS will shift the unstable eigenvalues to $-0.2654 \pm j7.187$ and the system can regain stability. The simulation results of $4^{\#}$ generator of DGS are shown in Figure 9.

6 Conclusions

A new idea of dealing with system stability is derived from the distribution of eigenvalues in the complex plane. The regular system as the idea cause of power
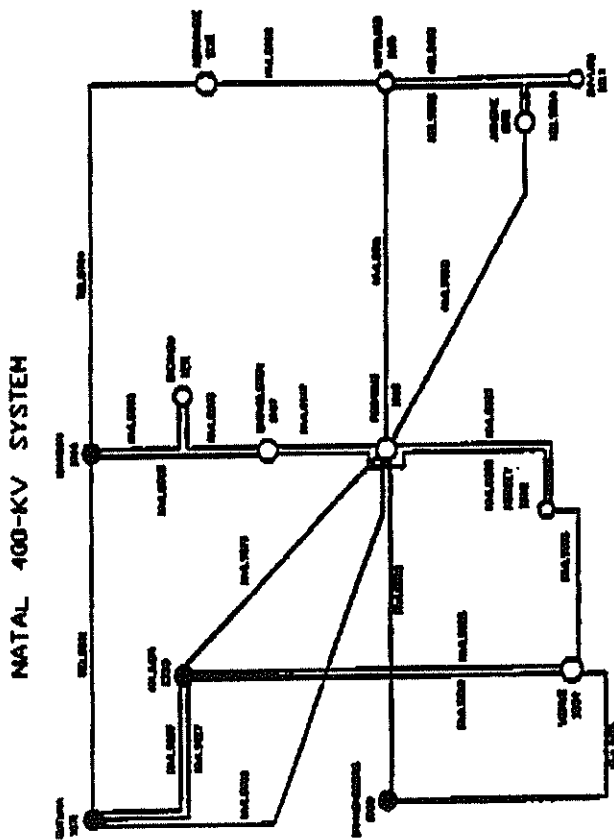
Figure 7: Natal system diagram
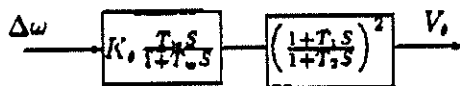
Figure 8: Power system Stabilizer
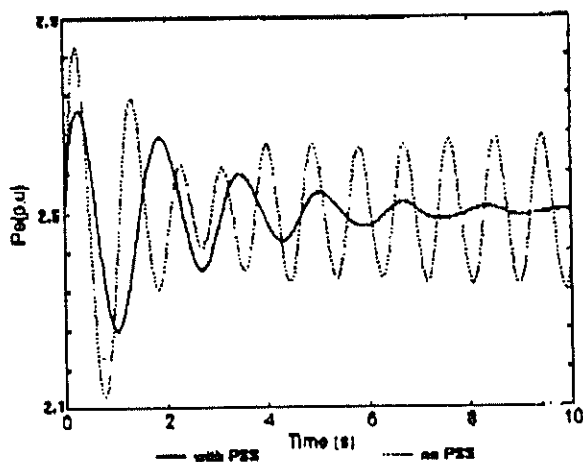
Figure 9: Oscillations of 4# generator in DGS

systems is used to reveal the general understanding of power system oscillations. A real power system can be seen as the disturbaned case of a regular system.

The mathematic description of oscillations In regular system and non-regular system is presented in detail. From these mathematic equations, it can be known that the basic oscillation composition is determined by one machine model. It is correct in theory to use one machine model to deal with the eigenvalues which are corresponding to the motion of one machine against an infinite bus.

Natal power system is taken as example to confirm the control of oscillations using one machine model.

References

[1] F.P.de Mello, C.Concordia, "Concepts of Synchronous Machine Stability as Affected by Excitation Control" IEEE Trans. PAS-88, 1969, pp.316.

[2] P.Kundur, D.C.Lee and H.M.Zein El-Din,"Power System Stabilizers for Thermal Units: Analytical Techniques and On-site Validation" IEEE Trans. PAS-100, 1981, pp.81.

[3] M.L.Crenshaw,J.M.Cutler,G.F.Wright,"Power System Stabilizer Application in A Two-Unit Plant Analytical Studies and Field Tests", IEEE Trans. PAS-102, 1983, pp.267.

[4] R.G.Farmer,B.L.Agrawal,"State-of-the-Art Technique for Power System Stabilizer Tuning" IEEE Trans. PAS-102, 1983,No.3, pp.699.

[5] R.J.Fleming, M.A.Mohan, K.Parvatisam, "Selection of Parameters of Stabilizers in Multimachine Power Systems" IEEE Trans. PAS-100, 1981, pp.2329.

[6] C. Liu, S.Zhou and Z. Feng, "Using Decoupled Characteristic in the Synthesis of Stabilizers in Multimachine Systems", IEEE Trans. on Power Systems, 1987, pp.31.

[7] D.R.Ostojic, "Stabilization of Multimodal Electromechanical Oscillations by Coordinated Application of Power System Stabilizers" IEEE Trans. on Power System, 1991, pp. 1439.

[8] M.Klein, G.J.Rogers, P.Kundur, "A Fundamental Study of Inter-Area Oscillations in Power Systems" IEEE Trans. on Power System, 1991, pp. 914.

[9] F.P. de Mello, P.J. Nolan, et al., "Coordinated Application of Stabilizers in Multimachine Power Systems", IEEE Trans. PAS-99, 1980, pp.892.

[10] M. Klein, L.X. Le, et al., "H_∞ Damping Controller Design in Large Power Systems" IEEE Trans. on Power Systems, 1995, pp.158.

OVERVIEW OF THE METHODS FOR THE DETERMINATION OF THE COST OF TRANSMISSION TRANSACTIONS

E. A. Gorodkova

Department of Electrical Engineering   University of Cape Town

Abstract

This paper presents an overview of the different approaches used for the determination of the cost of transmission transactions. Three methodologies are analysed, the Short-Run Marginal Cost methodology, the Long-Run Incremental Cost methodology, the Existing cost methodology. Since the latter is the most popular, it is explained in more detail. Advantages and disadvantages of the Postage Stamp method, the Contact Path method, the MW-mile method and the Usage method for calculating the cost of transmission transactions are discussed. This paper gives an overview of the procedure for evaluation of the cost of transmission transactions and demonstrates its estimation on a step by step basis.

1. Introduction

One of the suggested ways of creating an "efficient market" for electricity is by changing the nature of the relationship between the different segments of the industry. In this scheme the transmission business is seen as a separate service, which must be treated separately and funded independently. Therefore, it is necessary, to develop a procedure for the shared use of the transmission system by utilities and equitable mechanism for its compensation.

When the energy flow enters and leaves the transmission utility, the flows throughout the network change [8,9]. Transmission charges determine payments by a buyer (consumer), or a seller (supplier), or both to the transmission utility to compensate for the utility's network operating costs, that it incurs, as well as for the existing transmission investment costs. The actual cost of transmission transactions depends on two major factors

a) the type of transactions (firm *versus* non-firm)
b) the costs components considered [17].

- Firm transmission transactions: long-term transactions that are not subject to arbitrary interruptions.

- Non-firm transmission transactions: short-term transactions when transmission capacity becomes available at specific areas system at specific times.

Market based approaches for of the short-term transactions have been extensively described in the technical literature, for example, spot price methodology developed by F.C. Schweppe. [1,14].

The cost of transmission transactions consists of several major components:

1. *Operating cost*: production cost due to generation redispatch resulting from transmission transactions.

2. *Opportunity cost*: the cost that corresponds to benefits unrealised due to the operating constraints.

3. *Reinforcement cost*: capital cost of new transmission facilities, needed to accommodate the transmission transactions.

4. *Existing cost*: the cost of existing facilities used by the transmission transactions.

Generally, for a transmission transaction:

$$Cost_{Total} = Cost_{Oper.} + Cost_{Opport.} + Cost_{Reinf.} + Cost_{Exist.} \quad (1)$$

To various types of transmission transactions different cost components are applied. Present transmission charges follow a variety of different approaches with different combinations of cost components. Many of them are based on specific negotiations between involved parties and there is a lot of room for interpretation. There are several basic approaches, which are considered in the present paper.

2. Different approaches for evaluation of the cost of transmission transaction

2.1. Short-Run Marginal Cost (SRMC)

The marginal cost of transmission transactions is the cost of accommodating a marginal increase in the transmitted power. SRMC is the variable cost of production that the transmission utility incurs in order to accommodate the transaction [8-11]. The basic formula for this is:

$$SRMC = \frac{\partial OC}{\partial AET} \quad (2)$$

where: OC is the operating cost of transmission utility
      AET is the amount of energy being transmitted.

In the SRMC methodology the network is seen as an economic agent that "purchases" power from buses, corresponding to its generation pattern and "sells" this power at the buses, corresponding to its load pattern. The purchase and sale prices at each bus are the short-term marginal cost that measure the variation of system operating costs, as well as operating constraints. When a congestion occurs, the short-run cost contains the opportunity cost component. In practice however, opportunity cost is typically neglected.

In the long term, the transmission transactions may cause the installation of a new line to the network. It will reduce not only the opportunity costs on heavily loaded system but also the operating cost. In this case SRMC obviously fails to generate sufficient revenue to keep the transmission company financially viable. The percentage of total network cost recovery by SRMC on

average does not exceed 30 % [12]. To summarise, the prices based on short-run marginal costs encourage users of transmission system to make good short-run transfer decisions, but such prices can distort long-term decisions because they do not reflect reinforcement and existing cost components.

2.2. Long-Run Incremental Cost (LRIC)

Long-Run Incremental cost for transmission transactions accounts for the change in total costs incurred by the transmission utility in providing transmission service and incorporates both new installed capital and operating costs. [6,7]. There are two basic LRIC approaches.

The Standard approach seeks to determine the system reinforcements to accommodate the demand for transmission services over the term of a transmission transaction contract. System studies are performed with and without the transaction increment, using a long-term forecast to determine the changes in investment and other charges required over the entire contract period.

The Long Run Fully Incremental approach is more approximate and requires fewer studies and less data. This method assumes that excess transmission capability cannot be used for transactions and therefore assumes, that hypothetical system enhancements and corresponding investments have to be made to accommodate transmission transactions.

The other term, prevalently used in the industry is Long-Run Marginal Cost (LRMC) [1]. The LRIC and LRMC methodologies involve the solution of a transmission expansion planning model which is not covered by the present paper [5,17]. Thus one of the serious practical limitations of LRIC and LRMC methodologies is that the long term studies are extremely involved and time consuming due to the number of scenarios that require study.

Secondly, as can be seen from Figure 2.2.1 SRMC and LRIC approaches evaluate the direct costs of providing transmission service. In other words, the costs that are directly caused by the transaction.

existing cost   operating cost and reinforcement cost

the time when invest-   present time   time planning horizon
ments were made

Figure 2.2.1 The time horizon for a particular firm transaction.

The cost of the existing transmission system is the cost associated with the investments that have been already made until the present moment and represents "past " cost, which is not covered by LRIC approach. Because the cost of existing transmission system is generally large, the existing cost component of cost of a transmission transaction is usually the largest. For this and other historic reasons, this cost has received the most attention.

2.3. Embedded Cost methods

The starting point in determining the network charge based on existing costs is the valuation of fixed assets, which are used to transmit energy for particular transactions. The assets may be evaluated in a number of ways, for example, historic cost, historic cost less accumulated depreciation current cost at replacement value [4]. The decision is made according to the specific network configuration and transmission pricing objectives. For example, when the age of the network does not play a significant role in the pricing mechanism, the replacement cost of assets can be used.

Embedded cost approaches, as all long term approaches, require that a transmission utility's historic costs for the most current available year be collected and tabulated. These costs include annual transmission-related operating expenses and both the book cost (original cost) and depreciation for all transmission facilities. An annual fixed charge rate is a number between 0 and 1 which is calculated based on the following cost elements: the cost of capital (rate of return), taxes and depreciation expenses. The transmission revenue requirement is determined by multiplying the book cost of the transmission facilities by the fixed charge rate. If:

$$ATRR = AFCR \times CF \tag{3}$$

where: $ATRR$ - Annual Transmission Revenue Requirements
$AFCR$ - Annual Fixed Charge Rate
CF - Cost of Selected Facilities,

Annual per Unit Cost of used capacity (AUC) is

$$AUC \ (R/MW) = \frac{ATRR}{SDB} \tag{4}$$

where: SDB is selected demand basis either peak demand or peak demand plus firm transaction or designed system capacity or other appropriate load level.

Then the transmission utility for a particular transaction of MW would receive:

$$CTT = MW \times AUC \tag{5}$$

where: CTT is the cost of firm transmission transaction MW is the amount of the transaction.

If there are several users of the transmission system the important issue is how to allocate the embedded cost among them. There are several embedded methods of

---

[1] The difference between the marginal and incremental cost of wheeling is the size of the increment, with marginal costs estimated upon a unit change (1MW) and incremental costs measured by an increment equal to the size of the transaction. The LRMC is defined as the marginal cost of supplying an additional unit of energy when the installed capacity of the system is allowed to increase optimally in response to the marginal increase in demand. This methodology is quite similar to the LRIC approach.

allocating the existing cost of transmission system among firm users.

- the Contract Path method
- the Postage Stamp method
- the MW mile method
- the Usage method

The Contract Path method specifies an electrically continuous path from a point of receipt to a point of delivery. This approach assumes that the power flows along a specified electrically continues path through the transmission utility. The cost of selected facilities *CF* in (3) is the capital cost of those transmission facilities which lie along this assumed path and selected demand basis *SDB* in (4) is :

$$SDB = peak\ demand + the\ amount\ of\ transaction \qquad (6)$$

The Postage Stamp method assumes that the entire transmission system is used in transmission transaction. It results in the same cost of transactions irrespective to distance or location. The Postage Stamp method considers system-wide average transmission costs rather than the costs of specifically selected facilities. Thus for this method the cost of selected facilities *CF* in (3) is presented as a capital cost of the entire transmission system. *SDB* in (4) is usually the same as in the previous approach.

Despite the popularity of these two methods due to their simplicity, both methods have a serious limitation - neither of them require power flow execution, thus they ignore actual system operation. The following methods solve this shortcoming by applying Load Flow Algorithms.

The Boundary Flow method measures the overall net impact of a transaction on the transmission utility's lines at the utility's boundaries and allocates its embedded capital costs in proportion to the overall changes in inter-tie flows. A Boundary Flow analysis examines the impact of the transaction only on the transmission lines that tie one utility to another. For this method *CF* in (3) is the capital cost of all transmission facilities and *SDB* is the peak load. The Boundary Flow method is most useful when there are multiple transmission owners and it is easy to identify the ties between areas.

The MW-mile method calculates a R/MW-mile rate for the transmission utility instead of R/MW as in (3). This method examines the impact of a transaction on all individual line flows within a transmission network and allocates the embedded capital costs of the affected facilities in proportion to the changes in line flows. Presently there is a group of flow-mile methods (MW-mile method, extended MW-mile method, MVA-mile method), based on the following principle.

According to MW-mile methodology, real power flows on all network lines are calculated for every transaction t, using the DC power flow algorithm. The magnitude of MW flow on every line is then multiplied

by its length L_l and a predetermined MW-mile unit cost reflecting the cost per unit capacity of the line *AUC-mile* (7) and summed over all the network lines (8).

$$AUCmile(R\ /\ MW - mile) = \frac{ATRR}{\sum\limits_{lines} MW - mile} \qquad (7)$$

The MW-mile number is based either upon the line peak loading or line capacity.

The annual cost of transmission transaction according MW-mile methodology is:

$$CTT = \sum \Delta MW - mile \times AUC - mile \qquad (8)$$

where: $\sum \Delta MW$-mile represent the sum of the line MW-mile changes for the transaction.

The next method is *the Usage method* which has one important advantage in comparison with MW-mile approach. The extent of use of transformers or shunt transmission facilities, which do not have a physical mileage can not be determined by the MW-mile method. The Usage method solves this problem by accommodation of a measure of capacity used on a per facility base.

$$U_f = \frac{MW_{f,t}}{\sum\limits_t MW_{f,t}} \qquad (9)$$

where: U_f is the usage per facility,
$MW_{f,t}$ -the magnitude of MW flow on facility f due to transaction t,
$\sum MW_{f,t}$ -the total flow through facility f.

The usage method allocates transmission costs for each facility based on the ratio of MW flow of particular transactions to capacity or total flow through that facility.

All of the embedded cost methods have a few serious limitations. They consider only the costs of existing transmission facilities and do not recover the costs for any future investments until these facilities are placed in service. Secondly Figure 2.2.1 shows that existing cost is the cost which was incurred somehow in the past and does not reflect the present system conditions.

3.   Overview of stages for the evaluation of the cost of transmission transactions

The first step in the evaluation of the cost of transmission transactions is the investigation of the terms and conditions of the contract. The participating utilities will essentially need to provide all network data required by a power flow programme, including line and transformer parameters as well as bus load forecasts for each load level.

After all the necessary data is obtained, the suitable approach can be chosen according to the factors which were discussed in section 2. The combination of different methods as the embedded and marginal methods can also be utilised.

In the case of the Embedded cost approach, the capital cost of the existing system needs to be estimated. The annual revenue requirement is calculated according to equation (3).

The appropriate allocation mechanism is defined according to the pricing objectives. In the case of the Boundary Flow, MW-mile and Usage methods, load flow studies are performed. The per unit cost of capacity used is calculated according to equation (4).

The final step for evaluation of the cost of transmission transactions is the estimation of network charges by equation (5).
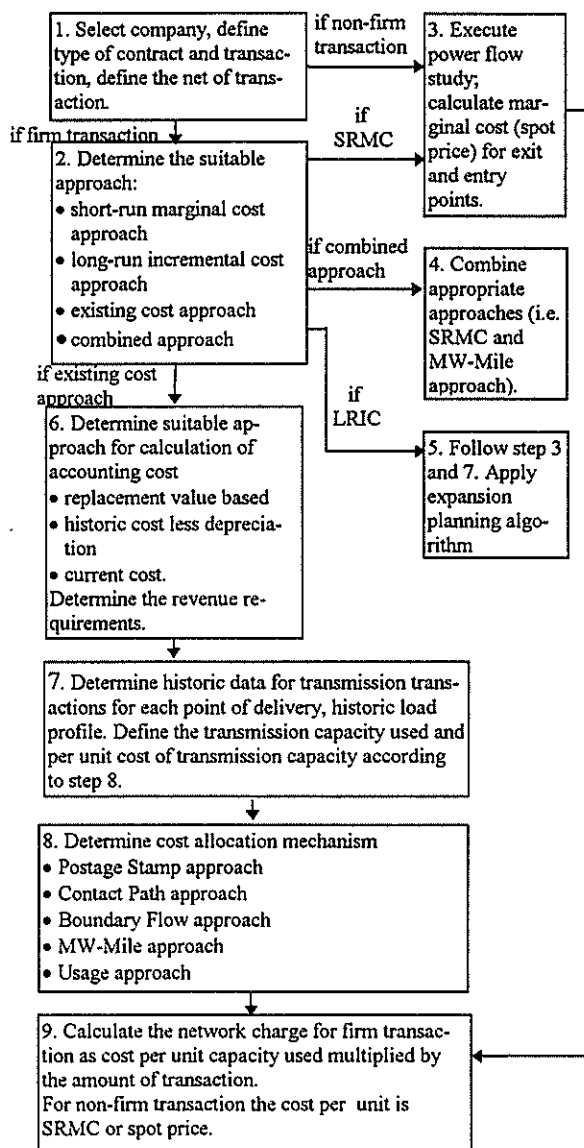
Figure 3.1   Summary of the stages the evaluation of the cost of transmission transactions

4. Conclusion

This paper has analysed and compared the different approaches for the evaluation of the cost of transmission transactions. This processes of selecting the strategy for

evaluation of the cost of transmission transactions has been summarised in Figure 3.1.

A further important conclusion is that each method alone actually is incapable to cover the total cost, while the combination of several approaches can give good results (for example the embedded cost plus marginal cost for firm service). International experience (Argentine, Norway, Peru and USA) clearly demonstrate broad opportunities of this approach [11,16].

5. References

[1] Caramanis M.C, Bohn R.E., Schweppe F.S., "The cost of wheeling and optimal wheeling rates", IEEE Transactions on Power Systems, vol.1, no.1, February 1986, p63-73.

[2] David A.K, Li Y.Z., "A rational approach for incorporating capital costs in the real-time pricing of electricity", Electrical Power and Energy Systems, vol.15, no.3, 1993, p179-184.

[3] Farmer E.D., Cory B.J., "Optimal pricing of transmission and distribution services in electricity supply", IEE Proc.-Generation, Transmission, Distribution , vol.142, no.1, January 1995

[4] Fleisher G.A., "Introduction To Engineering Economy", PWS Publishing Company, Boston, USA, 1994

[5] Goreinstin B.G., Campodonico N.M., "Power system expansion planning under uncertainty", IEEE Transactions on Power Systems, vol.8, no.1, February 1993, p129-135

[6] Happ H.H., "Cost of wheeling methodologies", IEEE Transactions on Power Systems, vol.9, no.1, February 1994, p147-156

[7] Kovacs R. Leverett L.L., "A load flow based method for calculating embedded, incremental and marginal cost of transmission capacity", IEEE Transaction on Power Systems, vol.9, no.1, February 1994, p272-278.

[8] Li Y.Z., David A.K., "Optimal multi-area wheeling", IEEE Transactions on Power Systems, vol.9, no.1, February 1994, p288-294.

[9] Lo K.L, Zhu S.P., "A theory for pricing wheeled power", Electric Power System Research, 28 (1994) 191-200

[10] Lo K.L, Zhu, S.P., "Wheeling and marginal wheeling rates: theory and case study results", Electric Power System Research, 27 (1993), p11-26

[11] Merrill H.M., Erickson B.W., "Wheeling rates based on marginal-cost theory", IEEE Transaction on Power Systems, vol.4, no.4, October 1989, p1445-1451

[12] Perez-Arriaga I.J., Rubio F.J., Puerta J.F., "Marginal pricing of transmission services: an analysis of cost recovery", IEEE Transactions on Power Systems, vol.10, no.1, February 1995, p546-553

[13] Perez-Arriaga I.J., RudnicK H., Stadlin W.O., "International power system transmission open access experience", IEEE Transactions on Power Systems, vol.10, no.1, February 1995, p554-564

[14] Schweppe F.C., Caramanis M.C., Tabors R.D., Bohn R.E., "Spot Pricing of Electricity", Kluwer, Deventer, Netherlands, 1988

[15] Schweppe F.C., Caramanis M.C., "Evaluation of spot price based electricity rates", IEEE Power Engineering Society Summer Meeting, 1984

[16] Shirmohammadi D., Gribik P.R., "Evaluation of transmission network capacity use for wheeling transactions", IEEE Transactions on Power Systems, vol.4, no.4, October 1989, p1405-1413

[17] Shirmohammadi D.C., Rajagopalan E.R, "Cost of transmission transaction: an introduction", IEEE Transactions on Power Systems, vol.6, no.3, August 1991, p1006-1016.

[18] Tabors R.,D., "Transmission system management and pricing: new paradigm and international comparisons", IEEE Transactions on Power Systems, vol.9, no.1, February 1994, p206-215

6. Address of author

E. A. Gorodkova, Department of Electrical Engineering, University of Cape Town, Private Bag, Rondebosh 7700, Cape Town. E-mail: elena@eleceng.uct.ac.za

TUNING OF A WLS STATE ESTIMATOR

R.Zivanovic

Pretoria Technikon

A.Petroianu

University of Cape Town

Abstract - In this paper the new method for bad data rejection is proposed. The method is based on tuning the weights in existing WLS state estimation programmes. It deals with measurement and parameter errors at the same time , what is the advantage comparing with the other available methods. Any rewriting of existing WLS programmes is not necessary; the method is completely external upgrade. Simulation of the case where mixed measurement and parameter errors corrupting the WLS estimator result has been done. The results are presented in the paper.

1. Introduction

Weighted Least Squares (WLS) is the method most commonly used in the commercially available power system state estimation programmes [1]. In this method the non-linear measurement equations are approximated with the linear equations. Then these linear equations are solved few times, each time correcting the result and approaching the final solution. For solving these overdetermined linear equations the efficient sparse matrix algorithms are used. The WLS method is statistically efficient and computation is very fast when outliers in measurements and parameters are not present [2]. In the situations when these outliers are present the solution of WLS estimator is biased. A number of methods for bad measurements detection and identification in WLS estimators are available [2]. Those methods are based on analysis of measurement residuals. The simplest method for suppressing the influence of the bad measurements on the solution is to use small weight for a measurement detected as bad, and solve the WLS equations again. Some commercial programs are using this technique. The more advanced technique is to correct bad measurements by using residuals [3]. Parameter (and topology) gross errors are treated separately from measurement gross errors, by again using measurement residuals [4]. A method for rejecting mix of bad parameter and bad measurement at the same time is not available and is still meter of academic research.

In this paper our intend is to present a simple method which can upgrade the existing commercially available WLS programmes. The novel method is capable to automatically determine the measurement weights in WLS algorithm, so that the influence of measurement and parameter gross errors (combination of both) on estimate is efficiently eliminated. In the first part of the paper short overview of WLS method is presented. In the second part, the method for weights tuning based on gradient search and Least Absolute Value criterion function is explained. The weights calculation method is tested on a simple 3-bus power system, and the results are presented in the last section of the paper.

2. An overview of WLS method

The first step in developing the WLS algorithm is to represent the link between measurements and state variables with appropriate mathematical model. In this paper we use linear model in the following form

$$z = Hx + v, \tag{1}$$

where
- z - (Mx1) measurement vector,
- x - (Nx1) state vector,
- H - (MxN) matrix relating measurements and states, and
- v - (Mx1) vector containing measurement small random errors modelled by using Gaussian distribution $N(0,R)$ with known covariance matrix $R = \text{diag}\{\sigma_i^2\}$.

It should be noted that if we consider the non-linear WLS algorithm, after linearization we have matrix equation in the same form as (1), where H is Jacobian matrix. All what is developed here for linear model (1) is applicable for linearized non-linear observation model.

By minimising the quadratic norm L_2 of weighted measurement residuals we find the optimal estimate in the least square sense

$$\hat{x} = (H^T W H)^{-1} H^T W z. \tag{2}$$

In the strict WLS method, the weighting matrix W is a diagonal matrix such that $W_{ii} = R_{ii}^{-1} = \sigma_i^{-2}$. In addition to

these Gaussian errors, calibration, scaling and quantization errors are present in every measurement. These errors are grouped together and are referred to as a fixed error. Sometimes the fixed error is large (due to serious failure in measuring system), and indicated as a bad data. The weighting matrix considering random and fixed errors is given by

$$W_{ii} = \frac{1}{(|\alpha_i z_i| + |\beta_i|)^2}, \qquad (3)$$

where α_i - the upper bound of the Gaussian percentage error, and

         β_i - the upper bound of the fixed error of the i-th measurement z_i.

To place proper confidence for each measurement, one must know the accuracy and the calibration errors of the various components of the data acquisition system. It is practically impossible to get all these information, and therefore this procedure is not followed by most of the utilities.

The weighting matrix used in utility programs is usually equal one over the expected upper bound of the measurement's fixed error. In order to estimate the upper bound of the fixed error some utilities use measurement residuals averaged over a number of measurements. Indicator that the quality of the estimate is improved with the new weights, is decreasing of the weighted least square criterion. Unfortunately, in some situations this technique does not solve the problem. In order to demonstrate why, let us write the measurement residuals for the linearized model (1)

$$\mathbf{r} = \overline{\mathbf{W}}\mathbf{v}, \qquad (4)$$

where $\overline{\mathbf{W}} = \mathbf{I} - \mathbf{H}(\mathbf{H}^T \mathbf{WH})^{-1}\mathbf{H}^T \mathbf{W}$ (5)

is the (MxM) residual sensitivity matrix. For instance, let us assume that two measurements have large fixed errors whereas the other errors are negligible. Using (5) we may write

$$\begin{aligned} r_1 &= \overline{W}_{11}v_1 + \overline{W}_{12}v_2 \\ r_2 &= \overline{W}_{21}v_1 + \overline{W}_{22}v_2 \end{aligned} \qquad (6)$$

If $|\overline{W}_{12}| > 0$ the residuals 1 and 2 are correlated. The corresponding measurements are situated in the vicinity of each other. It is evident that in (6) exist values of v_1 and v_2 that make the residuals small, and hence the fixed errors undetectable. We call these measurements multiple interacting bad measurements. The similar analysis can be done if we design the sensitivity matrix relating parameter errors and measurement residuals. As a conclusion we can say that the

method of weights calculation based on measurement residuals is not reliable in some likely to occur situations.

3. Tuning the weights using LAV criterion

As shown in the previous section, use of the measurement residuals in weights calculation is not always reliable method. The method can not deal with interacting fixed measurement errors, interacting parameter errors, and mixed measurement and parameter errors. In this section the novel method for weights calculation based on Least Absolute Value (LAV) criteria is proposed. The LAV criteria is chosen because it is more robust than WLS, and some of the problems should be overcome by using it.

The optimisation technique applied in minimisation of L_1 norm of the sum of measurement residuals is the kernel of the method. The objective function is formulated as

$$E(\mathbf{W}) = \frac{1}{2}\sum_{i=1}^{M} p_i r_i(\mathbf{W})^2, \qquad (7)$$

where $r_i(\mathbf{W}) = z_i - \mathbf{H}_i \hat{\mathbf{x}}(\mathbf{W})$ (8)

($\mathbf{H}_i$ is the i-th raw of $\mathbf{H}$), and p_i is the weighting parameter given by

$$p_i = \frac{1}{|r_i|}. \qquad (9)$$

On convergence the objective function (7) becomes

$$E = \frac{1}{2}\sum_{i=1}^{M}\frac{1}{|r_i|}r_i^2 = \frac{1}{2}\sum_{i=1}^{M}|r_i|, \qquad (10)$$

a minimum of the sum of absolute values of the residuals.

In this paper we use gradient search technique for minimisation of the objective function (7)

$$\widetilde{\mathbf{W}}_k = \left| \widetilde{\mathbf{W}}_{k-1} - \mu \nabla_{\widetilde{W}} E \right|, \qquad (11)$$

where $\widetilde{\mathbf{W}}_k = diag(\mathbf{W}_k)$ - (Mx1) weight vector,

       k - the iteration counter,

       μ - the gain parameter, and

       $\nabla_{\widetilde{W}} E$ - gradient of the objective function (7).

The gradient of the objective function can be found directly from (7) and (8)

$$\nabla_{\widetilde{W}} E = \mathbf{P}\frac{\partial \mathbf{r}}{\partial \widetilde{\mathbf{W}}}\mathbf{r} = -\mathbf{PH}\frac{\partial \hat{\mathbf{x}}}{\partial \widetilde{\mathbf{W}}}\mathbf{r}, \qquad (12)$$

where $\mathbf{P}$ is (MxM) matrix $\mathbf{P} = diag(p_i)$, and from (2)

$$\frac{\partial \hat{\mathbf{x}}}{\partial \widetilde{\mathbf{W}}_i} = (\mathbf{H}^T \mathbf{WH})^{-1}\mathbf{H}_i^T (z_i - \mathbf{H}_i \mathbf{x}) \quad i = 1...M. \qquad (13)$$

Finally, the iterative formula using (11), (12) and (13) is given by

$$\tilde{W}_k = \left| \tilde{W}_{k-1} + \mu PH(H^T W_{k-1} H)^{-1} H^T diag(r) r \right|, \quad (14)$$

where $diag(r)$ is (MxM) matrix with measurement residuals on a diagonal.

After the state estimate $\hat{x}$ is found using WLS, the new method (14) is used to further minimise the measurement residuals by changing the measurement weights, using LAV criterion. The method can be applied recursively on a number of estimates. It should be noted that the weights calculation method (14) does not make difference between measurement and parameter error. The method can deal with mixed errors if enough measurement redundancy is available. The iterative method (14) is computationally inefficient because it is based on gradient search. The number of iterations can be very large. However, second-order optimisation methods can be used to increase speed of computation.

4. Simulation results

The simulation study has been devised to demonstrate the performance of the new method for weights calculation. The test system with disposition of meters is shown in Figure 1.
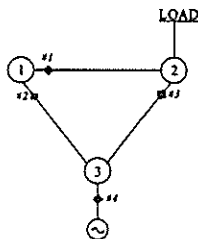
Figure 1: 3-bus test system

All measurements are active power measurements. It has been assumed that all voltages are equal to 1pu. Susceptances of the lines are: $B_{12}=B_{23}=1$pu and $B_{31}=1.5$pu. The constant matrix H from the observation model (1) is

$$H = \begin{bmatrix} 1 & -1.5 & 0 & -1.5 & 2.5 \\ -1 & 0 & 1 & -1 & -1 \end{bmatrix}^T . \quad (15)$$

The last row in (15) corresponds to zero injection measurement at node 1. There are two state values; phase angles x_1 and x_2. The phase angle at node 3 is considered as a reference. The initial values of the measurements and the corresponding states are given in Table 1.

Table 1: Initial data for 3-bus system

x_1	x_2	z_1	z_2	z_3	z_4
-0.25	-0.625	0.375	0.375	0.625	1

The most illustrative example is the simulation of mixed parameter error and measurement error. The parameter error is $B_{12}=0.1$pu instead of 1pu, yielding the observation matrix

$$H = \begin{bmatrix} 0.1 & -1.5 & 0 & -1.5 & 1.6 \\ -0.1 & 0 & 1 & -1 & -0.1 \end{bmatrix}^T . \quad (15)$$

The measurement error is $Z_3=-0.625$pu instead of 0.625pu. The small Gaussian errors are not simulated in this example. The gain parameter used in the iterative formula (14) is $\mu=0.5$, resulting in very slow iterative process. If we use $\mu=1$ the convergence speed will increase approximately 10 times for this example. The step-by-step correction of the state variables over the whole iterative process is presented in Figures 2 and 3. Weights calculation is shown in Figures 4 and 5.
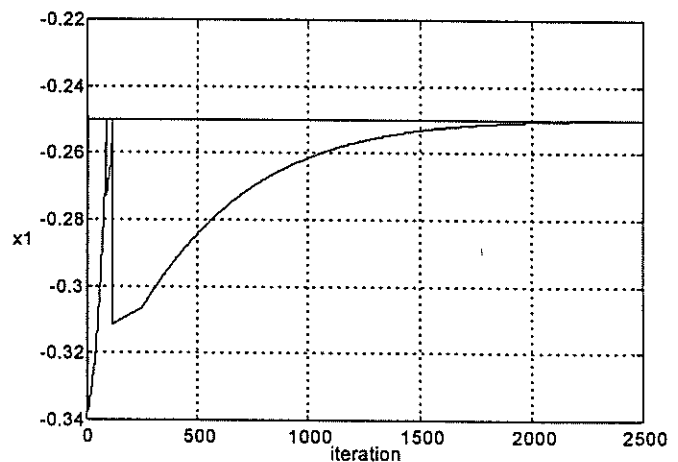
Figure 2: x_1 correction in the case of mixed measurement and parameter gross errors
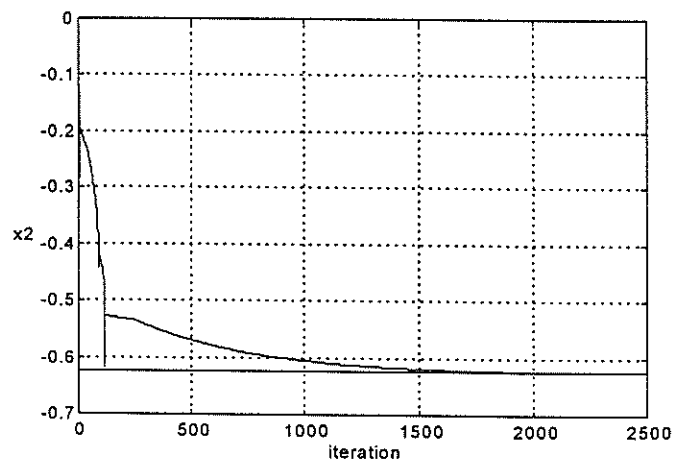
Figure 3: x_2 correction in the case of mixed measurement and parameter gross errors
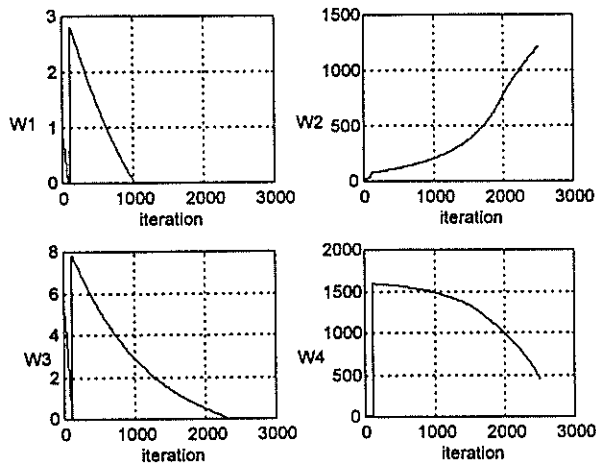
Figure 4: Iterative calculation of the measurement weights for the case of mixed measurement and parameter gross errors
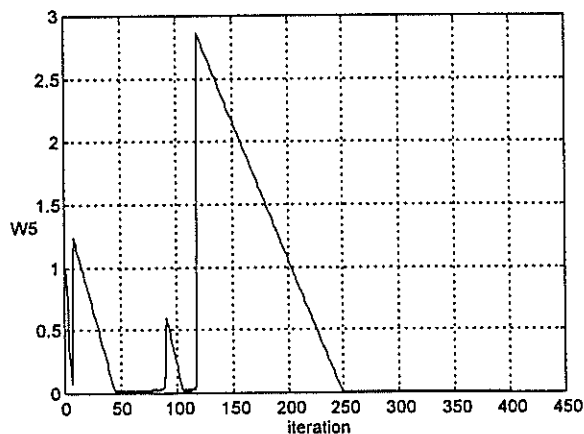
Figure 5: Iterative calculation of the pseudo measurement weight for the case of mixed measurement and parameter gross errors

It should be noted that the method set on 0 the weights for measurements 1, 3, and pseudo measurement 5 (weight 5 reach 0 faster then 1 and 3). The weights 2 and 4 reached the unnecessary large values; the fluctuation of the weights can be constrained. On that way three measurement equations are eliminated, and the state is find from the equations related to measurements 2 and 4. Just by tuning the weights the algorithm selects the most accurate two equations. The algorithm selects these equations by using LAV criteria, which always fit N measurements exactly, rejecting M-N measurements. The new feature is that the proposed method does not make any difference between measurement and parameter errors; it simply eliminates measurement equation containing either of these two errors (or both at the same time).

5. Conclusions

In this paper the new developments in upgrading the existing WLS estimation programmes used by utilities are reported. The main idea of making weights small for suspected bad data is well known. This idea is further developed, so that the automatic approach in weights calculation has been proposed. The method does not make difference between measurement and parameter errors, what is the advantage in comparing with other bad data rejection methods. The method is just external upgrade, so that the existing estimation programmes does not need to be replaced. The method controls the existing programmes only by tuning the weights. The potential of the method is demonstrated on the small linear system, using inefficient optimisation technique. In order to create complete algorithm the following issues have to be addressed: use of non-linear measurement equations; use of efficient optimisation method; possible errors because of not enough redundancy, numerical instability, interacting bad data and leverage points.

7. References

[1] F.C.Schweppe, at all, "Power system static state estimation", IEEE Trans. on PAS, Vol. PAS-89, Jan.1970, pp.120-135.
[2] L.Mili, at all., "Bad data identification methods in power system state estimation - a comparative study", IEEE Trans on PAS, Vol PAS-104, Nov.1985, pp.3037-3049
[3] L.Mili, at all, "Implementation of the hypothesis testing identification in power system state estimation", IEEE Trans on Power Systems, Vol. PWRS-3, Aug.1988, pp.887-893
[4] Th.Van Cutsem and V.Quintana, "Network parameter estimation using on-line data with application to transformer tap position estimation", IEE Proc.C, Vol.135, No.1, pp.31-40, 1988

AN APPLICATION OF THE PMU TECHNOLOGY IN FAULT LOCATION: PRELIMINARY STUDY

R.Zivanovic

Pretoria Technikon

C.Cairns

ESKOM TRI

Abstract - A novel method for transmission line fault location is presented in this paper. The method is based on measurements from both ends of the line, synchronised to the same reference. The measurements are obtained from Phasor Measurement Units, and they are in phasor format. A time-varying phasor concept is used in modelling the line. This concept is more accurate than steady-state phasors, taking the transients during the fault into account. The new method is not sensitive to varying operating conditions, fault infeed from the other end, or random value of fault resistance.

1. Introduction

The classical approach in determining fault location on high voltage transmission lines is based on voltage and current measurements taken only from one side of the line [1,2]. It is possible to classify these methods into three groups:

a) steady-state phasor approach in conjunction with filtering,

b) differential equation approach,

c) travelling-wave correlation methods utilising high frequency travelling waves.

It should be noted that the essence of the first group of methods is modelling measuring signals as phasors. In the majority of phasor methods only fundamental frequency steady-state phasors are considered and all other information generated by the fault are filtered out. The steady-state phasor approach is applicable only for short lines. The second group of methods is based on a mathematical model of the transmission line. The model can be either lumped parameter model for short lines, or a distributed parameter model for long lines. Noise filtering is achieved by averaging over a number of samples. These methods utilise more of the information generated by the fault than does the classical steady-state phasor approach. The last group of methods make use of the information in the post-fault electromagnetic travelling waves (forward wave from the source and backward wave

from the fault). The distance to the fault can be found by using a correlation technique to detect the time difference at the relay point between the arrival of the forward wave and its reflection from the fault point. These methods are applicable for long lines.

The first two approaches are computationally efficient but very sensitive to operating conditions, fault infeed from the other end and random value of the fault resistance. The travelling-wave approach offer some advantages in these meters, but the computational complexity is increased. Recently the new concept of utilising measurements from both ends of the line have been proposed to reinforce the phasor [3] and differential equation approaches [4]. When the samples obtained from two ends are synchronised and transformed into phasors the calculation is simple and fast. If they are not synchronised, a set of non-linear equations have to be solved and the resulting algorithm can be computationally very intensive [3]. The advantage of the differential equation approach [4] compared to the phasor approach [3] is the utilisation of all the information carried by fault induced signals. As long as the correct line model and synchronised samples from both ends are provided the method is insensitive to varying operating conditions, unbalances, fault type, variable fault resistance, and harmonics. The application for short lines is straightforward and very fast [4]. The application for long lines would use an approximation technique which leads to additional computation [4]. The disadvantage of the differential equation algorithm is a considerable increase in computation complexity required to achieve better filtering of noise and non-fundamental frequency signals. In order to filter noise a data averaging window is required, and for filtering non-fundamental frequency signals a model with more details (including shunt capacitance for example) is required [5].

In this paper a new fault location method utilising synchronised time-varying phasors [6] from both ends is presented. The method is based on recently developed Phasor Measurement Unit (PMU) technology [7]. It is presumed that

the method will retain the advantages of a differential equation approach, whilst employing the efficient filtering algorithm that is used by a PMU for estimating the fundamental frequency positive sequence phasor and its rate of change. In the first part of the paper a short review of PMU technology is presented. The time-varying phasor concept is explained in the second part, and then applied in designing the fault location algorithm. The utilisation of the time-varying phasor concept brings additional information into fault location algorithm which should give some advantages over the algorithms based on a steady-state phasor. The results from the simulation test of the new algorithm are presented in the last section.

2. Review of the PMU technology

The measurement technique for voltage and current phasors was first proposed as a part of Symmetrical Component Distance Relay [5]. Later it became apparent that it would be profitable to use phasor information in numerous protection and control applications [7]. The cost of synchronising measurements across a power system has been substantially reduced by the development of cheap Global Positioning System (GPS) [7].

The Phasor Measurement is based on a recursive Descrete Fourier Transform (DFT) algorithm [7]:

$$\underline{X}_{k+1} = \underline{X}_k + \frac{\sqrt{2}}{N}(x_{N+k} - x_k)e^{-jk\theta}, \qquad (1)$$

where $\underline{X}_k$ the fundamental frequency voltage or current phasor for sample k,

  x_k the sample k,

  N the number of samples per one cycle, and

  θ the sampling angle.

The phasor calculated by using (1) is stationary for 50Hz frequency. If the fundamental frequency deviates from 50Hz, the phasor will rotate with an angular velocity equal to the frequency deviation. It should be emphasised that the algorithm (1) will filter out all non-fundamental frequency signals.

A three phase version of this algorithm is directly derived from (1) using symmetrical component theory. The samples from all three phases are used and the positive sequence fundamental frequency phasor is estimated [7]. The algorithm is

capable of estimating positive sequence phasor from unbalanced three-phase signals.

3. Time-varying phasors

The traditional steady-state phasor concept is appropriate for use in the algorithms under quasi-stationary conditions. Here the transients are assumed to be sufficiently slow that the state of the system can be assumed stationary. It is evident that transients generated by a fault are not slow and that the steady-state concept is not valid for modelling a line under fault conditions. A time-varying phasor concept is introduced to model the transmission line without employing the quasi-stationary approximation [6].

A modulated signal of the form

$$x(t) = X(t)\cos(\omega_0 t + \delta(t)), \qquad (2)$$

where $X(t)$ the time-varying magnitude,

  $\delta(t)$ the time-varying phase angle, and

  ω_0 the carrier frequency of 50Hz,

can be used to represent voltage or current on a line during fault conditions. A time-varying phasor representation of the modulated signal (2) is by definition

$$\underline{X}(t) = X(t)e^{j\delta(t)}. \qquad (3)$$

The original signal x(t) is related to the time-varying phasor by

$$x(t) = \text{Re}\{\underline{X}(t)e^{j\omega_0 t}\}. \qquad (4)$$

By direct differentiation of the equation (4), we find

$$\frac{dx(t)}{dt} = \text{Re}\left\{\left(\frac{d\underline{X}(t)}{dt} + j\omega_0\underline{X}(t)\right)e^{j\omega_0 t}\right\}. \qquad (5)$$

The phasor of the derivative dx(t)/dt follows directly from equation (5), and definition (4)

$$P\left(\frac{dx(t)}{dt}\right) = \frac{d}{dt}P(x(t)) + j\omega_0 P(x(t)), \qquad (6)$$

where P is the phasor operator.

Now consider the differential equation relating voltage v(t) at inductor L terminals and current i(t) through inductor

$$v(t) = L\frac{di(t)}{dt}. \qquad (7)$$

Applying the differentiation rule (6), equation (7) can be represented by

$$\underline{V}(t) = L\frac{d\underline{I}(t)}{dt} + j\omega_0 L\underline{I}(t). \qquad (8)$$

It should be noted that for the steady-state assumption only the second term from the left side of equation (8) exists.

Similarly, the capacitor differential equation for time-varying phasors is represented by

$$\underline{I}(t) = C\frac{d\underline{V}(t)}{dt} + j\omega_0 C\underline{V}(t). \qquad (9)$$

The equation for resistance R is the same as under steady-state assumptions. The equations for R, L, and C together with Kirchoff's laws provide the relationships needed for writing a dynamical transmission line model a in time-varying phasor representation.

4. Fault location algorithm

In this preliminary study only the single-phase algorithm will be derived. This is enough to understand the new concept in fault location, the primary goal of the paper. The three-phase algorithm will be presented elsewhere.

The algorithm is uses voltage and current phasors from both ends of transmission line to compute the fault location. These phasors are obtained by using a recursive DFT algorithm (1) and they are synchronized to the same reference. The key point in the derivation of the algorithm is the observation that the point of fault is the unique location at which the voltage can be expressed in terms of both line ends' voltages and currents. By using a time-varying phasor representation for L (equation (8)) in the lumped parameter line model, the voltage at the fault point can be written as

$$\underline{V}_F = \underline{V}_S - (l-d)(R\underline{I}_S + L\frac{d\underline{I}s}{dt} + j\omega_0 L\underline{I}_S), \qquad (10)$$

and as

$$\underline{V}_F = \underline{V}_R - d(R\underline{I}_R + L\frac{d\underline{I}_R}{dt} + j\omega_0 L\underline{I}_R), \qquad (11)$$

where $\underline{V}_F$ the voltage phasor at the fault point,

$\underline{V}_S$ the voltage phasor at the sending point,

$\underline{V}_R$ the voltage phasor at the receiving point,

I_S the current phasor at the sending point,

I_R the current phasor at the receiving point,

R the resistance of the line per km,

L the inductance of the line per km,

l the total length of the line, and

d the length from the receiving point to the fault point

From (10) and (11)

$$\Delta\underline{V} + (\underline{Z}\Delta\underline{I} + L\Delta\underline{\dot{I}})d = 0, \qquad (12)$$

where $\Delta\underline{V} = \underline{V}_S - \underline{V}_R - l\underline{Z}\underline{I}_S - lL\underline{\dot{I}}_S$,

$\Delta\underline{I} = \underline{I}_S + \underline{I}_R$, and

$\underline{Z} = R + j\omega_0 L$.

The voltage and current at both ends are available in the sampled form. These values satisfy the equation (12) for each sample. For N samples we can write N equations (12) in the matrix form

$$\mathbf{A} + \mathbf{B}d = 0, \qquad (13)$$

where $\mathbf{A} = \begin{bmatrix} \Delta\underline{V}_1 & \cdots & \Delta\underline{V}_k & \cdots & \Delta\underline{V}_N \end{bmatrix}^T$,

$$\mathbf{B} = \begin{bmatrix} (\underline{Z}\Delta\underline{I}_1 + L\Delta\underline{\dot{I}}_1) \\ \vdots \\ (\underline{Z}\Delta\underline{I}_k + L\Delta\underline{\dot{I}}_k) \\ \vdots \\ (\underline{Z}\Delta\underline{I}_N + L\Delta\underline{\dot{I}}_N) \end{bmatrix}$$

Applying the least-squares technique to the system of equations (13) we can calculate the distance to the fault

$$d = (\mathbf{B}^+\mathbf{B})^{-1}\mathbf{B}^+\mathbf{A}, \qquad (14)$$

where + is conjugate transpose. The current derivatives used in (12) are approximated by using two point approximation; for the current $\underline{I}$

$$\underline{\dot{I}} = (\underline{I}_k - \underline{I}_{k-1})/\Delta t,$$

where Δt is the sampling rate.

5. Simulation test

In order to show some characteristics of the fault location algorithm presented in this paper, a simple single-phase transmission line model is used. The model consists of the line inductance $L=0.001$pu, sending-end voltage source $\underline{V}_S=1$pu, and receiving-end voltage source $\underline{V}_R = 1|\underline{\theta}$ pu. At the place of fault the fault resistance is equal 0.1pu for the first cycle, and 0pu for the second cycle, simulating the case when a variable arc resistance is established. The system was simulated over two cycles, and voltage and current phasors for each sample at both ends is estimated using the recursive DFT algorithm (1) and a sampling rate equal to 20 samples per cycle. It should be noted that full-cycle DFT (1) used here will efficiently filter-out the DC offset, so that the input to the fault location algorithm is only the modulated signals. The percentage error in fault location is assessed by using the

following formula:

$$e = \frac{|actual\ fault\ loc.-calculated\ fault\ loc.|}{total\ line\ length} x100.$$

The fault location algorithm based on time-varying phasors (14) is compared with the algorithm based on steady-state phasors [3]. The simulation results for the new algorithm (14) are presented in Table I. Three different fault locations (the total length of the line is 1), and the range of receiving-end voltage phase angles θ are simulated. The results for the algorithm based on steady-state phasors are presented in Table 2.

Table 1: Error *e* in %, for the algorithm based on time-varying phasors

θ \fault loc.	0.3	0.5	0.8
0°	0	0	0
5°	0.03	0.03	0.02
10°	0.05	0.06	0.04
15°	0.07	0.08	0.05
20°	0.08	0.09	0.06
25°	0.09	0.11	0.07
30°	0.1	0.11	0.07

Table 2: Error *e* in %, for the algorithm based on steady-state phasors

θ \fault loc.	0.3	0.5	0.8
0°	0	0	0
5°	0.04	0.04	0.03
10°	0.07	0.09	0.06
15°	0.11	0.13	0.09
20°	0.15	0.18	0.12
25°	0.19	0.22	0.15
30°	0.23	0.27	0.17

6. Conclusions

In this paper a time-varying phasor concept is used to develop a new fault location algorithm. The algorithm computes a fault location taking into account synchronised voltage and current phasor measurements from both ends of a line. These phasor measurements are available in real-time for each sample (in the paper we used 20 samples per cycle) from PMU. This makes possible tracking of phasor dynamic,

so that modelling of a line using time-varying phasors is necessary to fit measurements with a line model.

The simulation study results presented in the paper shows slightly better performance of the algorithm based on time-varying phasors compared to the algorithm based on steady-state phasors. The reason is that the algorithm based on steady-state phasors see the transients as a noise. That noise induce the additional error in fault location. Both algorithms are insensitive to variable arc resistance and fault infeed from both ends. Additional investigations should be done using EMTP to assess the performance of the new algorithm in more realistic situations; three-phase line, different types of faults, different incident angles, presence of harmonics and noise etc.

7. References

[1] T.Tagaki, et al.,"Development of new type fault locator using the one-terminal voltage and current data", IEEE Trans. on PAS, Vol. PAS-101, No.8, August 1982, pp.2892-2898

[2] B.Lian and M.M.A.Salama,"An overview of digital fault location algorithms for power transmission lines using transient waveforms",Electric Power Systems Research, 29 (1994), pp.17-25

[3] A.A.Girgis, et al.,"A new fault location technique for two and three-terminal lines", IEEE Trans. on Power Delivery, Vol.7, No.1, January 1992, pp.98-107

[4] M.Kezunovic, et al.,"An accurate fault location algorithm using synchronized sampling", Electric Power Systems Research, 29 (1994), pp.161-169

[5] A.G.Phadke and J.S.Thorp,"Computer Relaying for Power Systems", John Wiley & Sons 1988

[6] V.Venkatasubramanian,"Tools for dynamic analysis of the general large power system using time-varying phasors", International Journal of Electric Power & Energy Systems, Vol.16, No.6, 1994

[7] IEEE working group,"Synchronized sampling and phasor measurements for relaying and control", IEEE Trans on Power Delivery, Vol.9, No.1, January 1994, pp.442-452

THE USE OF ARTIFICIAL NEURAL NETWORKS IN SUBSTATION INTERLOCKING SYSTEMS.

F. Delport   **R. Zivanovic**

Technikon Pretoria

ABSTRACT

Protection systems had to be design for power devices like generators, transformers and transmission lines from the first time that these devices were used for power generation and distribution. Interlocks have been in use ever since the protective relaying schemes were implemented for these power devices. The Interlocking Philosophy has not changed much over time, but technology supporting it has made quantum leaps. The use of micro-computers stretched the technological leap even further. Progammable Logic Controllers (PLC's) have since been used in protection but proved that it can be limited due to a lack in memory space and/or tends to breakdown operation whenever loss of status input occurs. This paper looks at the use of Artificial Neural Networks(ANN) in Substation Interlocking Schemes, and accesses the advantages that it has over systems currently in use.

INTRODUCTION

Power system networks are becoming increasingly complex. Adding to this, the rise of production costs, are forcing generation companies, like ESCOM, to push their distribution networks to the limits

In recent years, ANN's have interested many researchers in various fields of science. It's application possibilities are gaining more momentum as experts utilizes it in more practical ways than one. The field of Power Engineering has also benefited from this utility.

In a power distribution network, decisions have to be taken quickly and safely. Control of switching operations in high voltage substations is necessary to maintain the quality of supply to consumers with maximum utilization of equipment. Interlocking schemes are part of the holistic approach to the management and maintenance of optimally utilized power distribution networks.

Interlocking schemes can be considered as basic and built-in protection mechanisms for power system equipment. It provides the means of safe switching for both operational and maintenance procedures. Care must be taken to avoid damage to equipment, hazardous working conditions to maintenance staff and unnecessary loss of supply to consumers. A good interlocking scheme should prevent all undesirable operations but allow all possible ones.[1]

Interlocking started of as conventional hardwire protection system. Problems arose when changes where made to substation topology.[4] Hardwire systems proved difficult to alter. In cases where substation had complex topologies, the same system proved to be impossible to modify. A complete redesign of the interlocking system had to be done to accommodate topology changes. PLC utilization took the technology supporting the interlocking principle a step further.[5] This added more flexibility to the philosophy. Software programs could be altered to suit any changes to the topology of a substation. The development or the storage of pre-planned sequences of switching operations did not pose any special problems, whereas, it was found to be very difficult to change conventional hardwire systems. In cases where the substation topology was complex, conventional systems could not be changed. A new system had to be designed from basics.

Time proved that PLC based interlocking systems tend to breakdown operation when input information becomes conflicting or when no

information is forthcoming from status censors. This can generally be attributed to faulty pilot cables or broken down switch status censors, etc..

ANN's offers machine intelligence to the interlocking principle.[1] The advantage thereof is that it can sift through conflicting and/or incorrect information and effect the correct operation commands to ensure the safe operation of all power devices involved. The basic hardware required to operate this system, is the same as that of any common PLC which is currently in use in an interlocking.

SYSTEM CONFIGURATION:

A mesh substation was modeled in which all possible states of operation was simulated for isolator 2. The model concerned can be viewed in fig. 1. These states formed a Substation Matrix(SM) which was used to train the ANN.
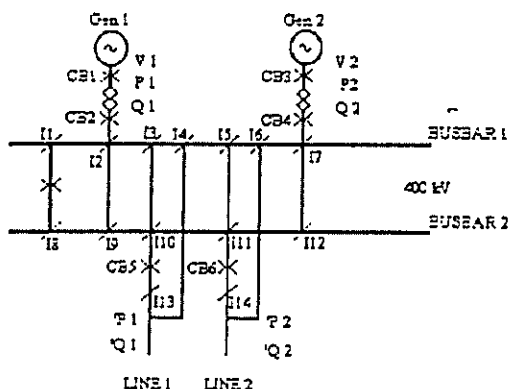
Fig. 1: Network Layout.

It is important to note that more input increases the reliability of the output. In the initial study, inputs were taken from all isolators[I(k)], circuit breakers[CB(k)], voltage-[V(k)], active-[P(k)], and reactive[Q(k)] power meters(k=1 - 14).

The ANN was then exposed to a specific test set were various operational states were modeled. These states included situations where operation

pertaining to Isolator 2 was possible and visa versa. Results were drawn at stages were the ANN had completed 100-, 500-, and 1000 epochs. The average error rate of the outputs from the ANN decreased steadily as can be seen from Fig. 2
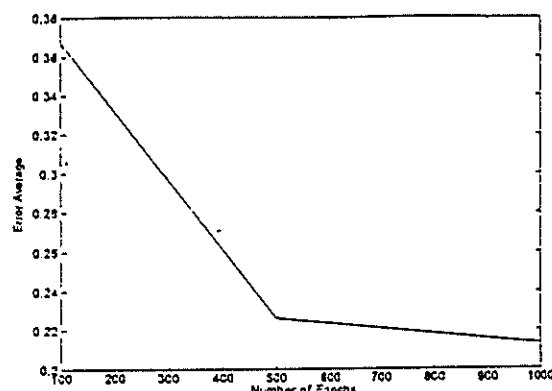
Fig. 2: Average Error Epoch Ratio.

For the purpose of this paper, the ANN was trained to 1000 epochs and a test set was drafted were it was attempted to push the ANN to a point were this package couldn't effect any output. This in turn was attempted by confronting the ANN with conflicting information to such an extent that it effected a zero output.

RESULTS

After training the ANN to the mentioned amount of 1000 epochs, and confronting the trained set with the test set which consisted of 20 different Input/Output Pairs (IO Pair), the following results, as shown in Fig. 3, were generated:
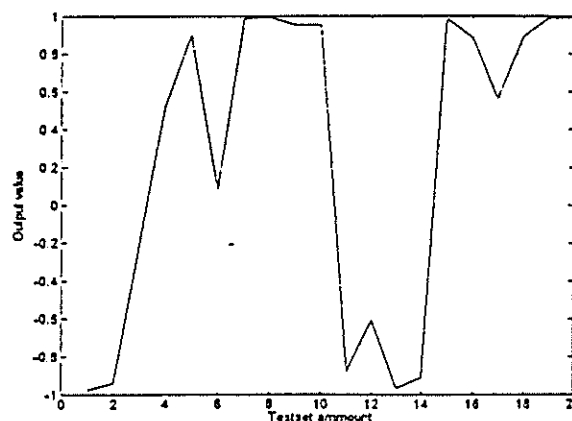
Fig. 3: Results of test set.

Above indicated results were modulated to draft average output values. The average values are reflected in Table 1.

Table 1: Table of Modulated Results:

Average:	0.8099
Std. Deviation:	0.2677
Maximum Value:	0.9950
Minimum Value:	0.0810

It must be noted that Table 1 reflects the modulus values of all results. The ANN indicated all results in the correct direction. This means that the ANN indicated which operations were possible and the ones that weren't. These attributes were consistent with the preconceived results of the test set.

It can be seen from the table above that the ANN managed to effect convincing outputs. The average is shown to be 0.8099. The minimum value reflects a IO Pair where virtually every aspect of the IO Pair is contradicting, e.g. active power is flowing at the transmission line point, but none of the generator meter readings are indicating any active power flow and reactive power flow is indicated at one of the generators, but none of the transmission line meters indicate any reactive power flow, etc. This conflicting pattern is carried through in this testing IO Pair.

DISCUSSION.

Conventional interlocking systems used relay/equipment contacts directly wired in series/parallel combinations in such a way as to realize the desired logical proposition(interlock) With the advent of high speed micro computers that had high reliability and low cost, PLC's found wide spread use in interlocking systems. These devises implement a logical switching function by continuously testing the validity of operation by means of running pre-programmed logic modules for the micro-computers.

The conventional relay/equipment contact based interlock logic worked well and was highly reliable. However, such a hard wired system left

very little room for quick or automatic alterations of the logical propositions arising due to switchyard change or due to system conditions. A contact based interlocking system was bulky which discouraged complex operations.

The PLC driven interlocking system had definite upper edge over the conventional contact based logic as these catered for a high degree of complexity, ease of logical function realization, and redefinition with virtually no change of wiring and offered compact size with low power consumption.

The conventional contact or PLC based interlocking system also could not handle incomplete or conflicting digital inputs. These kinds of inputs are quite frequent in practice. Situations were remedied by virtue of a "forced input" as effected by an operator on a keyboard or the physical changing of a switch.

Reasoning and logic can be attributed to man's intelligence.[3] It also could be viewed as a process created due to the particular connections and inter communication of neurons in the living brain. Neurons operate on a "All or None" principle. It is on this principle that ANN's are based. This principle can be employed in the interlock philosophy.

Incomplete or conflicting data is common in practice and most systems(contact or PLC based) fail to deal with this type of situation as was mentioned above. This results in a specific criteria that is not fulfilled(e.g. a specific CB, IS, etc. is not actioned). To demonstrate the use of ANN to solve this problem, the next discussion refers to Fig. 4.
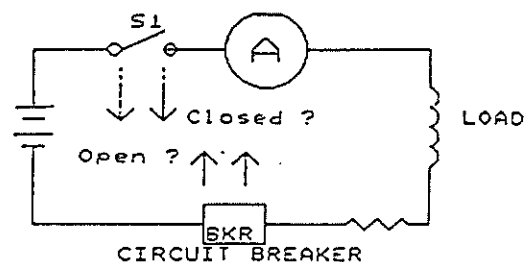
Fig. 4: A Circuit Having Possible Conflicting Status Signals.

A remote command is given to this circuit to open/close S1 by a operator or another interlock system. The operating condition is that it can neither make or break the circuit on load. The CB is meant to do so. S1 and the CB each have two status's(open or closed) and two command inputs(open or close).If both open and closed status's of S1 are active, it will be difficult to determine if S1 is in fact closed. Similarly, the same could be true for CB. The only way to determine this is to observe the supporting parameters such as the load current meter reading. This can effect a more worthy conclusion. A simple ANN can take care of such conflicting situation by deciding upon the current state of the S1 or CB by weighing the evidence of the current. This process can effect the desired output and improve the quality of operation in general.

CONCLUSION.

ANN's can be used for switching in high voltage substations. It has certain advantages over the conventional hardwire system such as:
- Flexibility to cope with the network configuration
- Decrease risk of wrong switching operation
- Speed of decision
- Ability to tackle complex problems

Future development and research can be done in respect of the incorporation of the 1st and 2nd laws of Kirchoff. It would also be possible to refine a interlocking system by including a system of threshold logic to each of the input neurons of the interlocking system. This affords an oppertunity to tune the ANN externally by assigning weights to each input. It will improve system reliability and reduce the risk of incorrect operation of Power System Devices.

Artificial Neural Networks have a much greater role to play in Power Engineering. Further research and development will have to indicate which roles that it has to fulfill.

REFERENCES:

[1] Agarwal, S. H., and Prabu, V. N.:"Application of Artificial Neural Networks in Adaptive Interlocking Systems", IEEE Conference Nr. 0-7803-1217-/-3. p453-458.(1993)

[2] Brand, K. P., Kopainsky, J., and Wimmer, B.: "Topology-based interlocking of Electrical Substations", IEEE Transactions on Power Delivery. Vol. PWRD-1, Nr. 3, p118-126. July.(1986)

[3] NeuroDynamX, Inc.:"Dyna Mind-User's Guide",(1992)

[4] Hoppe-Oehl, H.:"New methods and the procedure of application of the topology-based interlocking scheme LUISE", etzArchiv Bd. 12.(1990) H.7.

[5] Traca-ed-Almeida, A. :"Substation interlocking and sequence switching using a digital computer". IEEE Transactions on Power Apparatus and Systems. Vol. PAS-100, Nr. 6. July.(1981).

DETECTION OF BROKEN ROTOR BARS BY AXIAL VIBRATIONS PRODUCED IN SQUIRREL CAGE INDUCTION MOTORS HAVING INTERBAR CURRENTS

G.H. Müller   C.F. Landy

Department of Electrical Engineering, University of the Witwatersrand

ABSTRACT

Intuitively, a broken rotor bar in a squirrel cage induction motor implies an open circuit. Research[1] has shown that where the contact impedance between bar and core is sufficiently low, current still flows in the bar, by means of interbar currents. Not only do these interbar currents flow in the initial stages of the fault, but they dramatically damp the expected signature frequencies of the fault. Present vibration techniques for monitoring broken bars do not take cognisance of these interbar currents. This paper shows the origin of an axial force due to these interbar currents and also predicts the relevant frequency components. Experimental results substantiate the theory regarding the production of these axial force components.

LIST OF PRINCIPAL SYMBOLS

B	=	flux density along a conductor
B_{res}	=	stator flux density with respect to the stator
d	=	depth of rotor bar
f	=	supply frequency
I	=	current in a conductor
$I_b(x)$	=	bar current distribution along the length of the bar
I_c	=	total interbar current flowing into the core,
I_t	=	total current flowing in the 'broken' bar and the two adjacent bars
$J_c(x)$	=	current density of current flowing into the core along bar
l	=	net core length
l_{pu}	=	effective (per unit) length of the rotor
q_a	=	harmonic index for the stator flux density
q_b	=	harmonic index for the interbar current
R_c	=	contact resistance
s_q	=	per unit harmonic slip
$V_A(x),$ $V_B(x)$	=	differential voltage drops along the 'healthy' and 'broken' bars respectively
x	=	axial position along the rotor core from the 'healthy' side
Z_b	=	bar impedance
θ_{ref}	=	rotor reference angle
θ_s	=	angular slot pitch of the rotor
λ	=	ratio of bar impedance to core resistance
ω	=	angular rotation
φ_{bq}	=	phase angle of the impedance harmonic of the rotor bar

1. INTRODUCTION

The philosophy behind condition monitoring of electrical machines is to give an indication of the 'health' of any motor. Ideally any fault should be detected at an early stage so as to allow sufficient time to schedule 'shutdowns' or machine outages. Due to it's complexity, condition monitoring of broken rotor bars in squirrel cage induction motors has attracted the attention of many researchers in the past[2][3][4]. The need has arisen for a comprehensive understanding of the fault as well as improved diagnostic procedures.

When a bar breaks in a squirrel cage induction motor, the traditional approach is to assume that no current flows in the bar. The vibration frequencies produced by this phenomena are similar to that of dynamic eccentricity.

It is important to realise that when a bar initially breaks in a large squirrel cage induction motor, current still flows in the bar. Current flows in the broken rotor bar, until the core is severely burnt (often caused by repeated starting of the motor). Only at this stage of the fault does the broken bar form an open circuit in the secondary winding.

It has also been shown that interbar currents tend to mask the traditional signature frequencies[5]. The traditional signature frequencies are those frequencies particular to broken rotor bars, based on the assumption that the bar is an open circuit. In light of this, early diagnosis of broken rotor bars in large squirrel cage induction motors must include the effects of interbar currents.

In order to understand the presence and distribution of the interbar currents, the background theory regarding interbar currents and the interbar current model is discussed.

2. DESCRIPTION OF INTERBAR CURRENTS
(Kerszenbaum and Landy [1])

Kerszenbaum and Landy[1] established that interbar currents are present in large, copper cage, squirrel cage induction motors having broken bars. The simple model used to calculate the current distribution in the broken bar is given in figure 1.
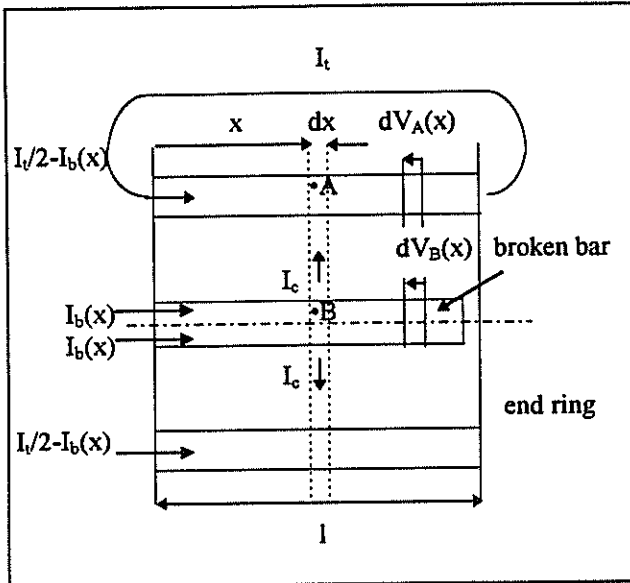
Figure 1: Diagram illustrating Kerszenbaum and Landy's model of the broken bar region.

This model assumes that the break occurs along the bar between the core and the endring. This is justified by realising that the most likely region of failure (weakest mechanical point) in the rotor is the joint between the bar and endring.

The current distribution along the bar length is given as:

$$I_b(x) = \frac{I_n}{2}[1 - \frac{\cosh(\lambda \cdot x)}{\cosh(\lambda \cdot l_{pu})}] \qquad (1)$$

The magnitude and distribution of current in the broken bar depends on lambda (λ). Lambda is the ratio of bar impedance to the interbar impedance of the iron and copper, where the interbar impedance comprises core and contact impedances. On comparing the magnitudes however, the contact resistance is by far the greater contributor to the interbar impedance. From this Lambda (λ) is given as:

$$\lambda = \sqrt{3\left|\frac{Z_b}{R_c}\right|} \qquad (2)$$

Kerszenbaum and Landy[1] found that for large motors, the contact resistance, at 50Hz, is $19\mu\Omega$ to $20\mu\Omega$ per one metre of effective core length. Christofides[6] measured the contact resistance for small die-cast aluminium motors as $600\mu\Omega$.

Christofides also states that the interbar impedance is purely resistive for frequencies up to several hundred hertz.

As the current in the broken bar approaches the break, it enters the core and flows tangentially to the adjacent 'healthy' bars. The current density distribution of the current entering the core is:

$$J_c(x) = \frac{1}{d}\frac{I_n}{2}\lambda\frac{\sinh(\lambda \cdot x)}{\cosh(\lambda \cdot l_{pu})} \qquad (3)$$

Again, it is evident that the core current density distribution is dependent on both the bar impedance and the bar contact resistance. An increase in λ would imply an increase in concentration of core current towards the broken end of the bar.

Modern practise in producing large squirrel cage induction motors requires that the rotor bars fit tightly into the laminated iron slots without insulating material. This results in a low contact resistance between the bar and the core, and thus large interbar currents when a bar breaks. As condition monitoring is applied more readily to large or 'critical' motors, it is important that the effect of interbar currents on the symptoms of the fault be considered.

The above theory only describes the magnitude and distribution of the interbar currents. It must be realised that the interbar currents are frequency dependant and that space and time harmonics are present.

3. AXIAL FORCE FREQUENCIES

If one considers a cross-section of the rotor taken in the plane of the laminations, figure 2 results.
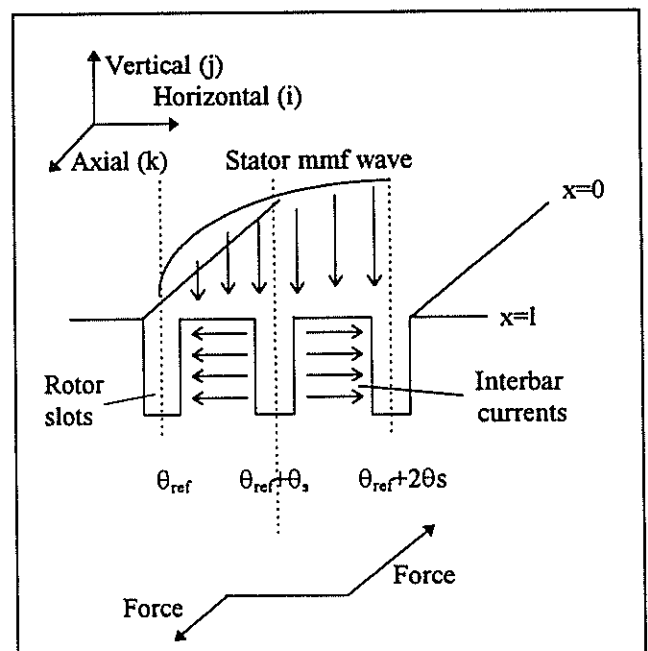
Figure 2: Production of Axial Force.

A force is present due to the interaction of the stator flux wave and the interbar currents. This is based on the fundamental equation [7];

$$F = (B \times I) \cdot 1 = \begin{vmatrix} i & j & k \\ B_i & B_j & B_k \\ I_i & I_j & I_k \end{vmatrix} = (I_i \cdot B_j)k \qquad (4)$$

The interaction of the stator flux (B_j) and the interbar currents (I_i) produces a force in the axial direction. The net axial force is dependant on the cross product of:

- the resultant stator flux density - (B_{res}) that is the difference in the average, stator flux density for a slot pitch on either side of the broken bar, and
- the total interbar current entering the core.(I_c)

It should be noted that the stator mmf wave consists of harmonics due to slotting of the stator. These stator mmf harmonics give rise to respective harmonic currents in the rotor. The mathematical cross product, of the stator mmf wave and the rotor currents, yields an array of axial force components having frequencies that are a combination of the different harmonics.

The axial force is obtained from the cross product and is given by:

$$F = [\sum_{q_a = 1, -5, 7, ...} B_{res} \cdot \cos(s_{qa}\omega t - q_a\theta_{ref} - q_a\theta s) \times$$

$$\sum_{q_b = 1, -5, 7, ...} \frac{I_c}{2} \cos(s_{qb}\omega t - \varphi_{bq})] \cdot 1 \qquad (5)$$

If one ignores the phase of the axial force, and only considers the frequency terms, the analytical equation for the force becomes,

$$F = \sum_{q_a = 1, -5, ...} \sum_{q_b = 1, -5, ...} B_{res} \cdot \frac{I_c}{2} \cdot [\cos(2\omega t - (q_a + q_b)\omega t +$$

$$(q_a + q_b)s\omega t) + \cos((-q_a + q_b)\omega t + (q_a - q_b)s\omega t)] \qquad (6)$$

4. EXPERIMENTAL VERIFICATION

Tests were performed on a 3 phase, inverted cage, experimental motor to verify the presence of these frequency components. The 220V, 4 pole machine has 24 stator slots and 36 rotor slots, with a rating of approximately 5kW. The tests were first performed on a 'healthy' cage and then on a broken cage. The inverted cage motor allows the measurement of the actual bar currents. A force transducer was placed between the machine frame and the rotor, where the rotor was allowed to move in the axial direction. It must be noted that only one bar in the cage was broken.

The components of the axial force are clearly multiples of the supply frequency, and are also slip related. The expected force components for a rotor with broken rotor bars, operating at 50Hz and a speed of 1444.5 RPM (slip of 0.037pu), are given in Table 1. The axial force component at 3.7Hz (2sf) is to be considered. This force is expected to be the largest because it is due to the interaction of the fundamental stator flux and the fundamental interbar current.

Table 1: Axial force components, frequencies and harmonic combinations

Compo-nent	Frequency	Harmonic combinations			
2sf	3.7 Hz	$B_1.I_1$ $B_{11}.I_{13}$	$B_7.I_5$ $B_{19}.I_{17}$	$B_5.I_7$ $B_{17}.I_{19}$	$B_{13}.I_{11}$
(6-8s)f	285.1 Hz	$B_7.I_1$ $B_5.I_{13}$	$B_{13}.I_5$ $B_{11}.I_{19}$	$B_1.I_7$	$B_{19}.I_{11}$
(6-6s)f	288.8 Hz	$B_1.I_5$ $B_5.I_{11}$ $B_{11}.I_{17}$	$B_1.I_7$ $B_{17}.I_{11}$ $B_{13}.I_{19}$	$B_5.I_1$ $B_7.I_{13}$	$B_7.I_1$ $B_{19}.I_{13}$	$B_{11}.I_5$
(6-4s)f	292.5 Hz	$B_5.I_1$ $B_{17}.I_{13}$	$B_1.I_5$ $B_{13}.I_{17}$	$B_{11}.I_7$	$B_7.I_{11}$

Healthy cage: As expected, only small axial force components of 0.31N occur at the 3.7Hz (2sf). See *Figure 3*
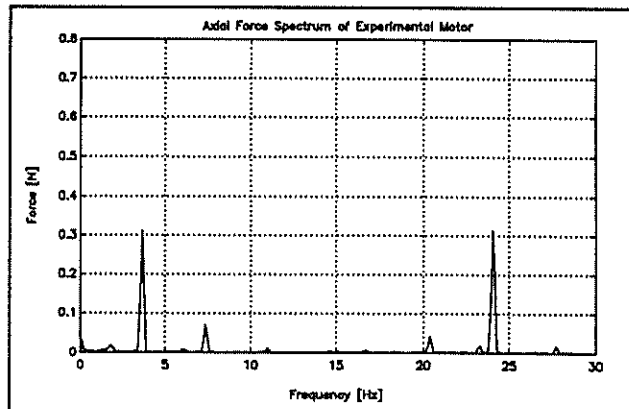
Figure 3: Axial force spectrum of experimental motor with 'healthy' cage at full load and full voltage.

It must be noted that the small 2sf component in the above spectrum for the 'healthy' motor is due to inherent interbar currents, as a result of high impedance endrings.

Broken bar cage:
- No Load: A small 2sf component occurs at 1.2Hz. *Figure 4*. This frequency component is expected, as the motor is inherently loaded by a flywheel.
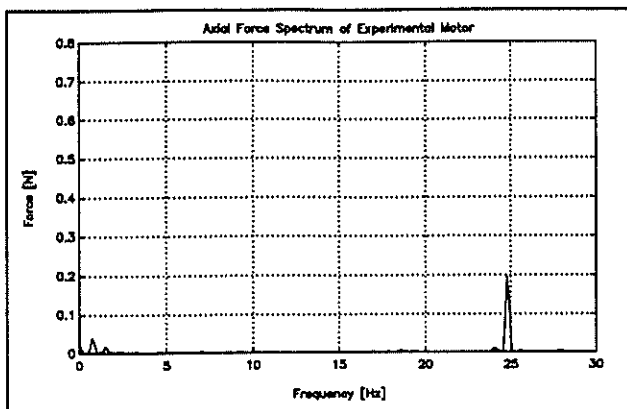
Figure 4: Axial force spectrum of experimental motor with broken bar at no load and full voltage.

- Full Load: A large, 7.8N component, occurring at 3.7Hz is present. *Figure 5*. Note that this peak has grown and shifted in frequency from no load. This illustrates that the axial force is slip dependant.
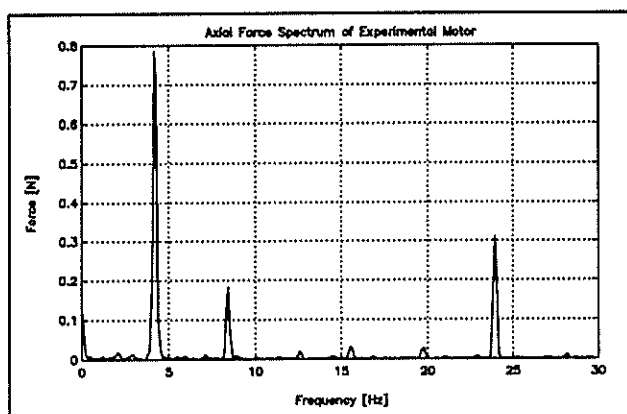
Figure 5: Axial force spectrum of experimental motor with a broken bar at full load and full voltage.

Despite the fact that the experimental motor is physically small (limited interbar currents), the 3.7Hz component grows from 0.31N to 0.78N, when one bar is broken.

5. CONCLUSION

The force components, postulated in the paper, were present in the axial force spectrum when a bar was broken. These axial force components are only expected when significant interbar currents are present in the motor. Despite the small physical size of the motor, the axial forces components are present and measurable. Significant interbar currents occur in large motors, when a bar is broken (or if there is rotor bar skewing) and when the motor is sufficiently loaded. The experimental results successfully substantiate the postulated theory.

This paper shows that cognisance of interbar currents when monitoring for broken rotor bars is essential as they occur in the initial stages of the fault. The paper also outlines a new vibration technique to monitor

squirrel cage induction motors with a broken rotor bar, taking into account the interbar current effect.

The axial force components are related to vibration of the motor by the transfer function of the frame. Further research into the relation between the axial force and the stator frame vibration is required.

6. ACKNOWLEDGEMENTS

7. REFERENCES

[1] Kerszenbaum and C.F. Landy , 'The existence of large interbar currents in three phase squirrel cage motors with rotor-bar and/or end-ring faults', IEEE Transactions on Power Apparatus and Systems, Vol. PAS-103, pp. 22-29, July 1984.

[2] Deleroi, 'Squirrel cage induction motors with broken bar in the rotor - physical phenomena and their experimental assessment', Proceedings of International Conference on Electrical Machines, 1982, pp. 767-771.

[3] Elkasby et. al., 'Detection of broken bars in the cage rotor on an induction machine', IEEE Transactions on Industry Applications, Vol. 28, January/February 1992, pp. 165-171.

[4] Hargis et. al., The detection of rotor defects in induction motors', Proceedings of International Conference on Electrical Machines - Design and Applications, 1982, pp. 216-220.

[5] Walliser and C.F. Landy, 'Determination of interbar current effects in the detection of broken rotor bars in squirrel cage induction motors', IEEE Transactions on Energy Conversion, October 1993.

[6] Christofides, 'Origins of no load losses in induction motors with cast aluminium rotors', Proceedings of IEE, 1965, pp. 2317-2332.

[7] Müller and C. F. Landy, 'Vibration produced in squirrel cage induction motors having broken rotor bars and interbar currents', Proceedings of International Conference on Electrical Machines, September 1994.

Principal author's details

G.H. Müller
Department of Electrical Engineering
University of Witwatersrand
Private Bag 3, WITS
Johannesburg
2050
Tel: +27 (11) 716 - 5497
Email: Muller@odie.ee.wits.ac.za

UNIVERSAL BRUSHLESS
PERMANENT MAGNET MOTOR DRIVE

JF Gieras M Wing

Department of Electrical Engineering, University of Cape Town

Abstract. A new high performance brushless permanent magnet (PM) motor operating both as a synchronous and d.c. shunt motor has been presented. For the load angle close to 90° the motor can be switched automatically from a.c. to d.c. mode. The complete integrated drive system consists of two parts: (1) motor with position sensors and (2) IGBT inverter together with control circuitry. The mode switching control strategy, operation, and performance have been discussed.

1. Introduction

Permanent magnet (PM) brushless motors fall into two principal categories: a.c. synchronous motors or *sinewave brushless PM motors* and d.c. electronically commutated motors or *square-wave controlled brushless PM motors* [1, 4, 6]. The electric and magnetic circuits of both two motors are, in principle, the same.

With the trend to energy conservation, fast dynamic response, high performance, stable speed, and integration of brushless motors with the electronic circuitry, there is a need for an universal kind of moving PM motor. Such a motor has a conventional three-phase stator and a rotor with rare earth PMs. This motor can run at synchronous speed with much improved efficiency and power factor compared to an induction motor. As soon as the load torque approaches the stability limit the motor starts to operate as a d.c. motor displaying a shunt characteristic.

2. AC – DC PM Motor Drive

In practice, the torque of a d.c. brushless motor is close to that of a synchronous brushless motor of identical construction. The speed–torque characteristic for an a.c. synchronous PM motor and a d.c. brushless PM motor with the same stator and rotor are shown in Fig. 1. For the PM synchronous motor the speed is constant. If the shaft torque does not exceed the stability limit the motor will run synchronously without any feedback. If for a certain shaft load the armature current is as high as to reach the point A (Fig. 1), the motor runs with maximum shaft torque permissible for synchronous operation. If a greater torque is applied the PM synchronous motor without position sensors will fall out of step. At the shaft torque corresponding to the point A the shaft position sensors should be activated in order to obtain a d.c. mode. With a high load torque and $V = constant$ the d.c. mode is more economical. Square-wave input waveforms are produced when the excitation is precisely synchronized with the rotor speed and instantaneous position. The basic elements of a synchronous — d.c. brushless motor drive (Fig. 2) are: PM motor, output stage (inverter), rectifier, shaft position sensor, gate signal generator, current detector, velocity encoder (if used), controller (microprocessor or personal computer with DSP board). For a synchronous operation the shaft position sensor is not needed.

A detailed circuital, finite element method (FEM) and experimental analysis of different constructions of PM motors has been made [2, 3]. Motors have been designed using a circuital approach with synchronous reactances being obtained from the FEM. A rotor with symmetrical buried NdFeB magnets has been finally selected. The design data are given in Table 1. The q-axis synchronous reactance X_{sq} is greater than the d-axis synchronous reactance X_{sd}.
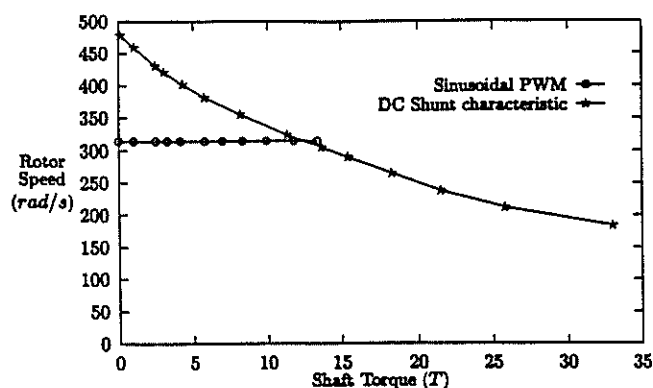
Figure 1: Speed—torque characteristics of a brushless PM motor in a.c. and d.c. modes.
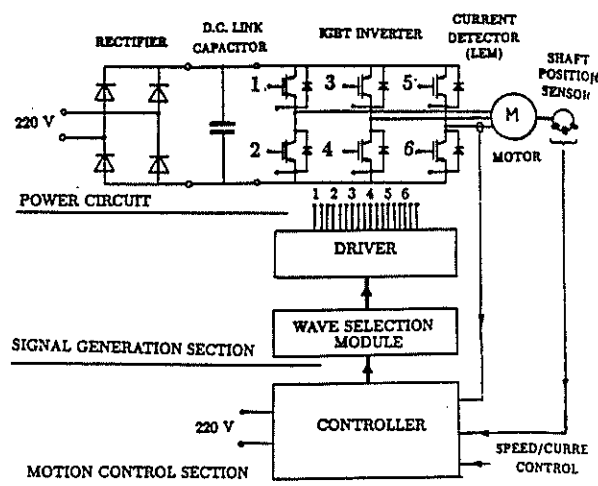
Figure 2: A three-phase a.c. — d.c. PM brushless motor drive.
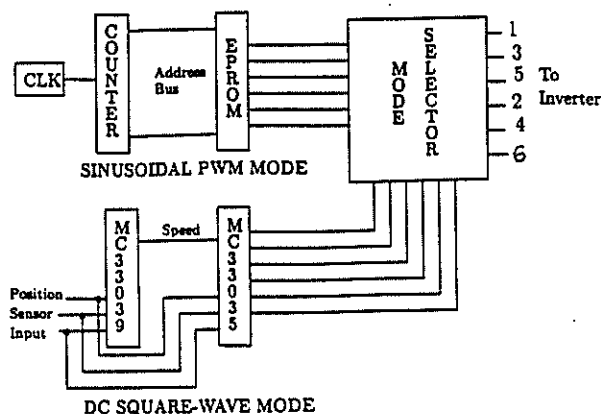
Figure 3: Block diagram showing the link between sinusoidal PWM and d.c. modes.

Table 1: Data of tested buried PM synchronous motor.

Quantity	Value
Input frequency, f	50 Hz
Input voltage (line-to-line)	380.0 V
Connection	Y
Inner diameter of the stator, D_{1in}	82.5 mm
Outer diameter of the stator, D_{1out}	136.0 mm
Airgap in d axis (clearance), g	0.55 mm
Effective length of the stator core, L_i	100.8 mm
Armature winding coil pitch, w_c	64.8 mm
Number of turns per phase, N_1	240
Number of parallel wires	2
Number of stator slots, z_1	36
Width of the stator slot opening, b_{14}	2.2 mm
Height of permament magnet, h_M	8.0 mm
Width of permanent magnet, w_M	20.0 mm
Length of permanent magnet, l_M	100.0 mm
Remanent magnetic flux density, B_r	1.05 T
Coercive force, H_c	764.0 kA

Table 2: RMS Voltages for Different Switching Modes

Switching mode	m_a	rms voltage
Square-wave		0.8159
Sinusoidal PWM	1	0.7071
	1.2	0.7831
	1.4	0.8234
	1.6	0.8502
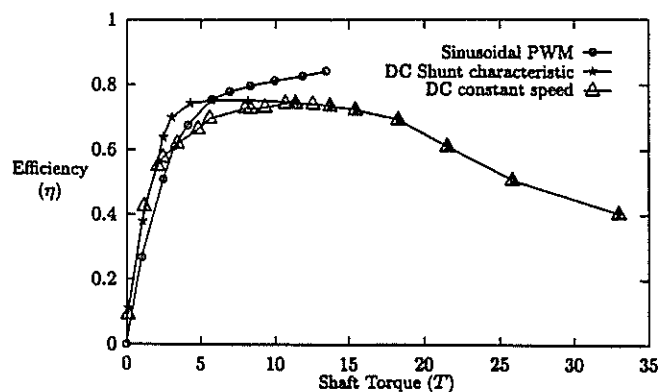
Figure 4: Efficiency against shaft torque of the tested universal PM brushless motor drive. Test results.

3. Operation

3.1. Sinusoidal PWM Switching

The synchronous operation of the motor is done using a sinusoidal PWM switching topology. A synchronous regular sampled PWM is used to ensure the maximum reduction in harmonics. The frequency modulation ratio m_f is an odd integer and a multiple of three, which also cancels out dominant harmonics.

The sinusoidal PWM switching consists of the constant frequency clock, a set of counters and an erasable programmable read-only memory (EPROM). A simplified block diagram is shown in Fig. 3. Six bits of each byte from the EPROM drive the six transistors of the inverter.

3.2. DC square wave switching

The square wave d.c. brushless motor controller can be designed around the monolithic integrated circuit MC33035 from *Motorola* [5]. The device consists of a rotor position decoder for proper commutation sequencing, temperature compensated reference capable of supplying sensor power, frequency programmable sawtooth oscillator, fully accessible error amplifier, PWM comparator, three open collector top drivers, three high current totem pole bottom drivers ideally suited for driving power MOSFETs, and protective features. The speed control function allows for a steady rise in speed from start-up with the added benefit of having current limiting at low speeds. The d.c. controller is used in three phase closed loop control using the rotor position and speed feedback. The speed signal is obtained from the feedback voltage generator integrated circuit MC33039 specifically designed for use with the MC33035 chip [5]. The MC33039 integrated circuit only uses the three position sensor outputs and is equivalent to a tachometer [5].

3.3. Mode Switching Control Circuit

The most frequently used mode of operation of an universal brushless motor is the synchronous mode. In industrial drives, a sudden increase in load is possible which would stall a normal synchronous motor. In this type of situation a reduced speed mode is better than no movement at all and thus the d.c. mode becomes essential until the load is reduced.

The aim of mode switching is to ensure that the motor operates continuously under all types of load conditions and switches between the two modes smoothly and automatically. The machine can start either as a synchronous or d.c. motor. In the d.c. mode the motor's speed is increased until the synchronous speed is reached, at which time it is switched to synchronous mode. If the load torque is high and motor is not able to reach synchronous speed the machine remains in d.c. mode indefinitely. When switching from d.c. mode to synchronous mode the sinusoidal PWM has to be synchronised to the rotor's position. This ensures that the phase angle between the inverter and motor is approximately zero at the time of synchronising. The switching from synchronous mode to d.c. mode is done when the load angle reaches 90^0. This load angle ensures that the motor is still in the synchronous stable region, since $X_{sd} < X_{sq}$.

4. Practical Integrated PM Motor Drive

The *integrated electric drive concept* is based on putting the electromagnetic, electrical and electronic components (Fig. 2) together in one or two cases.

A universal brushless motor with buried NdFeB PMs is recommended. The position sensor used by the authors is an electro-optical type, i.e. light-emiting diode and phototransistor. Position sensors are mounted on the end bell. Shaft rotation produces a shutter action. The controller has been based on *Motorola* MC33035 and MC33039 integrated circuits [5]. The MOSFET driver module has been replaced by IGBTs. The synchronous or d.c. mode can be selected automatically or manually after exceeding a selected maximum torque. The drive can be fed both from three-phase and single-phase mains.

The mode switching from synchronous to d.c. modes is done close to the synchronous stability limit. To ensure that this is possible the *rms* voltages of the two modes should be approximately equal.

The amplitude modulation ratio m_a, for the synchronous mode, is not kept in the linear region ($m_a \leq 1.0$), since the motor voltage has to be increased to match the d.c. mode. This increased voltage, due to overmodulation ($m_a > 1.0$), is to ensure that the synchronous motor can produce enough torque to match the d.c. mode's torque at synchronous speed. Table 2 shows the *rms* voltages for a 120^0 square-wave and sinusoidal PWMs with different m_a values. The amplitude modulation ratio is thus set to $m_a = 1.4$ to ensure

a stable transition from a.c. to d.c. modes and vice versa. There is no significant increase in harmonic content when m_a is increased from 1.0 to 1.4. The harmonic content of the current waveform for d.c. square-wave operation shows significantly more harmonics than the two PWM waves. The sinusoidal PWM mode with $m_a = 1.4$ is expected to be a more efficient mode of operation that the d.c. mode.

5. Performance

The steady state characteristics of the universal drive in different modes are shown in Figs 1 and 4. The sinusoidal PWM mode has $m_a = 1.4$. The d.c. mode is tested for constant speed operation and for maximum speed operation. The constant speed d.c. mode maintained a constant speed until it reached the shunt torque-speed characteristic of the d.c. mode. The constant speed d.c. mode uses PWM switching to reduce the average voltage and thus maintain a constant speed, but with increased switching losses over the maximum speed d.c. mode.

6. Conclusions

Recent achievements in power electronics and microelectronics allow for easy design of integrated universal brushless PM motor drives consisting of a high performance motor, sensors, converter, controller, and protections. The motor can operate either in synchronous or d.c. mode and can be fed from three-phase or single-phase mains. Both the electronic and electromechanical components are cheap except for the PM rotor. The output power range is from a few hundred Ws to several kWs although higher output powers are technically possible.

It has been found that the most efficient method of design of PM brushless motors is the combination of circuital methods with the FEM. The cicuital approach is simple and fast but the errors in calculating the synchronous reactances of PM motors cannot be accepted. The FEM gives much better results as compared with measurements.

The proposed universal PM brushless motor drive has distinct adventages when compared to the conventional cage induction motor-based drive and show signs to be the future choice for application in industry.

References

[1] Dote M and Kinoshita S, "Brushless servomotors — fundamentals and applications". Clarendon Press, Oxford, 1990.

[2] Gieras JF and Wing M, "Design of synchronous motors with rare-earth surface permanent magnets", Int. Conf. on Electr. Machines ICEM'94, Paris, France, vol. 1, 1994, pp. 159–164.

[3] Gieras JF and Wing M, "Integrated permanent magnet synchronous motor drive", 31th Symp. on Electrical Machines SME'95, Ustroń, Poland, 1995, pp. 266–271.

[4] Jahns TM, "Motion control with permanent magnet a.c. machines", Proceedings of the IEEE, vol. 82, No. 8, 1994, pp. 1241–1252.

[5] "Linear/interface ICs device data". Motorola Inc. vol.1, 1993.

[6] Miller TJE, "Brushless permanent-magnet and reluctance motor drives". Clarendon Press, Oxford, 1989.

Address of main author

Professor JF Gieras, Department of Electrical Engineering, University of Cape Town, Rondebosch 7700. E-mail: jgieras@eleceng.uct.ac.za

Aandrywing van 'n driefasige induksie motor vanaf 'n enkelfasige toevoer.

J.J. Strydom 9217290
G.M.L. Parsley

UITTREKSEL

Die onderwerp wat aangespreek gaan word, is die koppeling van 'n enkelfasige toevoer aan 'n driefasige induksie masjien met behulp van 'n statiese fase omsetter. Die fase omsetter word tussen twee terminale van die masjien gekoppel.
Die grootte van die fase omsetter sowel as die hoek benodig vir maksimum aansit draaimoment word bepaal. 'n Wiskundige analise word op bogenoemde uitgevoer.
Nullas en vollas bedryf van die stelsel en die ooreenkoms met die enkelfasige induksie masjien word beskou. Die invloed van las en toevoer spanning op die grootte van die fase omsetter word genoem. In die artikel word daar ook gewys op die verskil van die fase omsetter se impedansie grootte tussen aansit, vollas en nullas bedryf van die stelsel.

(1) INLEIDING

Eienskappe van die enkelfasige en driefasige induksie masjiene moet beskou word om 'n oplossing te implementeer.

'n Enkelfasige induksie motor sonder aansitwindings, kapasitor of enige rotasie van die rotor tydens aansit het geen aansit draaimoment nie. As die enkelfasige masjien eers begin draai sal daar aangehou word om te draai weens glip, of te wel verskil in rotasie snelhede van van rotor en magnetiese veld opgewek deur stator windings, dus word 'n hoekverskil veroorsaak tussen die magnetiese vloede van die stator en die rotor. Dit veroorsaak 'n krag en dus 'n draaimoment.

Die probleem is dus om 'n hoekverskil te verkry tussen die twee magnetiese motoriese kragte wat opgewek word. Dit word verkry deur 'n ekstra winding en 'n kapasitor toe te voeg.

Om 'n aansit draaimoment vir 'n driefasige induksie motor vanaf 'n enkelfasige toevoer te verkry kan die impedansie van die oorblywende windings aangepas word om 'n aansit draaimoment te veroorsaak.

Figuur 1 kom uit [1].

Indien die impedansie van die stator windings aangepas word verander die stelsel na 'n ongebalanseerde stelsel, en daar moet van die teorie van simmetriese komponente gebruik gemaak word om die impedansie benodig se grootte sowel as hoek te bepaal vir maksimum aansit draaimoment.

Volgens teorie van simmetriese komponente geld die volgende:

$$V_A = V_{AO} + V_{A1} + V_{A2} \qquad (1)$$

$$V_B = V_{A0} + a^2 V_{A1} + a V_{A2} \qquad (2)$$
$$V_C = V_{A0} + a V_{A1} + a^2 V_{A2} \qquad (3)$$

Waar:

V_A = Fase spanning en net so V_B en V_C [V].

V_{AO} = Nulvolgorde spanning [V].

V_{A1} = Positiewe volgorde (spannings roteer abc) [V].

V_{A2} = Negatiewe volgorde (spannings roteer acb) [V].

a = 'n Hoek van 120° [°].

Figuur 3 is afkomstig van Brown en Jha [1].

Vanaf figuur (3) :

Waar:

Admitansie van fase omsetter = Y [siemens].

Spanning oor fase A = V_A [V], dieselfde geld vir V_B en V_C.

Stroom in fase A = I_A [A], dieselfde geld vir I_B en I_C.

Deur gebruik te maak van Kirchhoff se wette en figuur (3). Kan die volgende vergelykings opgestel word:

$$I_A + I_B + I_C = 0 \qquad (4)$$
$$V - V_A + V_B = 0 \qquad (5)$$
$$V_C - V_A + I_C/Y = 0 \qquad (6)$$

Vergelykings (4), (5) en (6) is in die vorm wat Brown en Jha [1] gee. Deur vergelyking (4) en die teorie van onsimetriese komponente te gebruik volg die volgende:

$$V_0 = 0 \qquad (7)$$
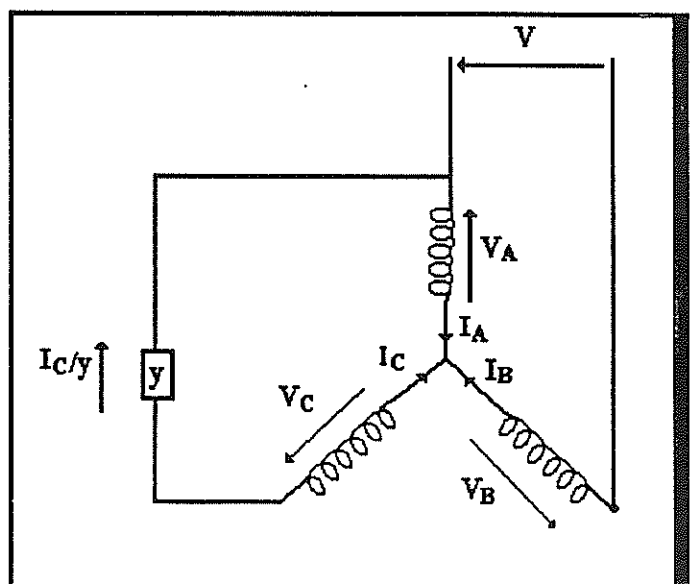
Figuur 1
Driefasige induksie motor aangedryf vanaf 'n enkelfasige toevoer, met 'n statiese fase omsetter in die stroombaan.

Waar:

Y_0, Y_1 en Y_2 = Die nulvolgorde, positiewevolgorde en negatiewevolgorde admitansie is [siemens].

V_0, V_1 en V_2 = Die nulvolgorde, positiewevolgorde en negatiewevolgorde spanning is [V].

Deur vervanging van vergelykings (1) en (2) in vergelyking (3) volg die volgende:

Uit vergelyking (5) en die toerie van simetriese komponente volg die volgende:

$T_{balanseerd}$ = Draaimoment van gewone driefasige omstandighede [N.m].

α = Hoekverskil tussen argumente van fase omsetter admitansie en argument van fase admitansie van die driefasige induksie motor [°].

y = | Y_s/Y |. Dit is dimensieloos.

Y_s = Admitansie per fase van die motor by stilstand onder gebalanseerde driefasige omstandighede

Figuur 2
Verhouding tussen draaimoment van die stelsel en draaimoment onder gebalanseerde driefasige omstandighede.
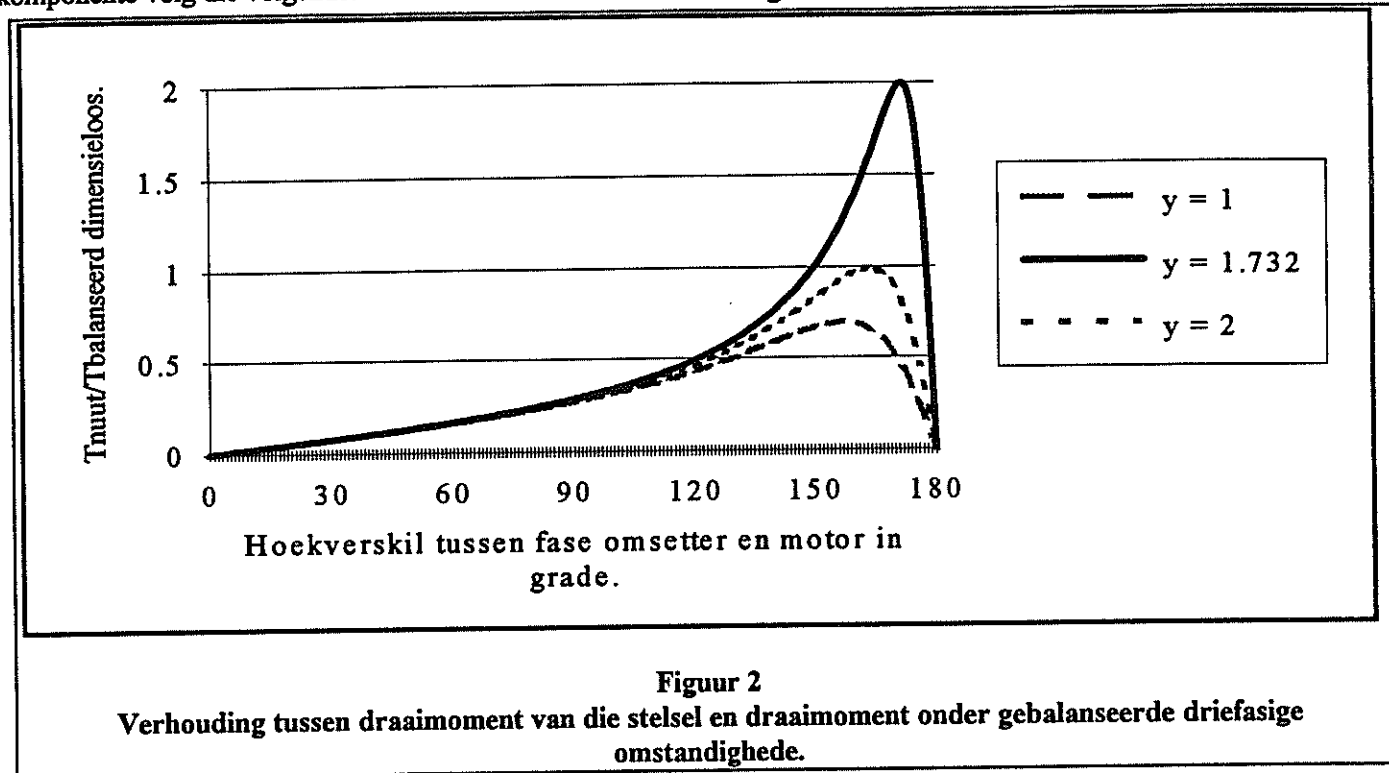
$V = -\sqrt{3} \angle -150° \; V_1 + \sqrt{3} \angle -30° \; V_2$

(8)

Uit vergelyking (12) volg:

$V_1 = (-V\angle 150°)/(\sqrt{3}) - V_2\angle 120°$ (9)

Vir die opstelling word die enkelfasige toevoer aan die oorblywende derde terminaal en een van die twee terminale wat reeds gebruik is, verbind. Die doel van die hele opstelling is om gebalanseerde toestande in die driefasige masjien na te boots met aansit sodat die gewone werkverrigting van die masjien vanaf 'n driefasige masjien nageboots kan word.

Vanuit bogenoemde vergelyking (9) en die toestande wat verkry wil word volg die volgende:

$T_{nuut} = T_{balanseerd}$

(10)

Uit vergelyking (10) gedeel deur vergelyking (9) volg die volgende:

$T_{nuut}/T_{balanseerd} = (|V1|^2 - |V2|^2)/V$

(11)

$T_{nuut} = (2*\sqrt{3}\,y*\sin(\alpha))*T_{balanseerd}/$
$(9 + 4y^2 + 12\cos(\alpha))$ (12)

Waar:

T_{nuut} = Draaimoment van die nuwe stelsel [N.m].

[siemens].

Y = Admitansie van die fase omsetter [siemens].

Vergelyking (16) is in die vorm wat Brown en Jha [1] gee.

Die vogende figure dui die noodsaaklikheid aan om 'n geskikte fase omsetter te kies vir maksimum aansit draaimoment: tussen die draaimoment onder gebalanseerde en ongebalanseerde toestande afhanklik is van die hoekverskil, α, sowel as y, die verhouding tussen Y en Ys. Tot en met 130° het die grootte van y 'n baie klein invloed. 'n Fase verskuiwing van 172° vir die geval waar y gelyk aan 1.732 is lewer die grootste draaimoment. Vir die geval waar y gelyk is aan 2 word 'n baie groter aansit draaimoment gelewer, dus sal daar gepoog word om y so groot as moontlik te maak. Daar sal egter in die praktyk 'n keerpunt wees weens koste verbonde sowel as die feit dat die windings net 'n sekere hoeveelheid stroom kan hanteer. Om 'n hoekverskil van 172° te verkry sonder die inherente fase verskuiwings vermoë van 'n gewende rotor te verkry is onmoontlik. Met stilstand van 'n gewende rotor kan die rotor fisies ten opsigte van die stator windings gedraai word om tydens stilstand die fase verskuiwing te veroorsaak.

'n Korotor kan nie 'n inherente fase verskuiwing veroorsaak deur die rotor te roteer nie. Die grootste fase verskuiwing wat plaas kan vind met die gebruik van 'n korotor is die gebruik van 'n kapasitor wat 'n verskuiwing van 90° veroorsaak. Vanaf figuur (2) duidelik dat 'n verskil in admitansie grootte van 1.5, dus die fase omsetter is 1.5 maal groter as die fase admitansie van die motor, die beste resultaat sal lewer.

Vanaf figuur (2) kan ook gesien word dat vanaf 'n admitansie verhouding tussen fase omsetter en motor van 1 tot baie groot is die wins in draaimoment vir 'n fase verskuiwing van 90° nie noemenswaardig is nie.

(2) Realisering en gevolgtrekking op resultate

Twee toetse, die geblokte rotor toets en die nullas toets is uitgevoer op die masjien, om die fase admitansie te bepaal.

'n Admitansie van die fase omsetter wat $\sqrt{3}$ maal groter as bogenoemde is lewer 'n redelike aansit draaimoment.Die kapasitansie benodig is dus:

$$| 2\pi fC| = | \text{Admitansie per fase by stilstand} |$$
$$* \sqrt{3} \quad [\text{siemens}] \tag{13}$$

Daar is gevind dat C ongeveer 'n millifarad per kilowatt is. Die aansit draaimoment is egter nie baie hoog nie, omdat die kapasitor slegs 'n fase verskuiwing van 90° veroorsaak. Indien 'n gewende rotor gebruik word en met stilstand 'n fase verskuiwing van 60° deur die gewende rotor verkry word sal die hoekverskil 150° wees. Dit lewer 'n veel groter draaimoment soos gesien kan word van figuur (2).

(3) Nullas en vollas omstandighede

Die fase omsetter is slegs bepaal vir aansit omstandighede. Die volgende stap is die bepaling vir 'n geskikte manier om onder nullas en vollas omstandighede die grootste moontlike draaimoment te verseker.

Daar word weer verwys na die enkelfasige induksie masjien, omdat die eienskappe van bogenoemde baie ooreenkom met die roterende masjien waarmee nou gewerk gaan word. Bogenoemde gedeelte verwys na [2].

Die probleem is dus om van die kapasitor vir aansit na 'n geskikte kapasitansie oor te skakel vir nullas en vollas omstandighede. Die kapasitor banke wat beskikbaar was, is gebruik om tussen kapasitansies te skakel en sodoende praksies die kapasitansie benodig vir nullas en vollas omstandighede te bepaal. Die kreteria wat gebruik is, is die kenwaardes van die masjien wat nie oorskry moet word nie. Dus daar is 'n

optimum waarde vir die kapasitansie van die fase omsetter gevind wat binne bogenoemde perke is en ook die minste drywing dissipeer.

Daar sal gepoog word om so na as moontlik aan gebalanseerde driefasige omstandighede te kom. Indien meer stroom aan masjien verskaf word as onder normale driefasige omstandhede sal die windings warm word. Die windings kan slegs vir 'n kort periode bo vollas werk. Dus sal dit beter wees om onder of by vollas omstandighede te werk. Vir normale driefasige omstandighede kan deur die spesifieke masjien 7.4 N.m gelewer word. In die bostaande geval, dus met die fase omsetter is die maksimum draaimoment wat gelewer kan word 4.9 N.m. Dus kan daar slegs 66% van die draaimoment verskaf word wat in gewone driefasige omstandighede verskaf kan word. Soos die las op die stelsel verander, verander die kapasitansie benodig vir die fase omsetter om die kleinste hoeveelheid drywing vanaf die toevoerbaan te verbruik. Figuur 3 dui die verwantskap tussen draaimoment en kapasitnsie aan.Spanning aangelê op die stelsel het ook 'n invloed op die kapasitansie benodig. Hoe hoër die aangelegde spanning hoe hoër die kapasitansie benodig.

Die rendement van die stelsel nie baie effektief is nie. By 'n draaimoment van 5 N.m sal die stelsel vollas omstandighede bereik en is die rendement ongeveer 70% wat nie baie hoog is nie.
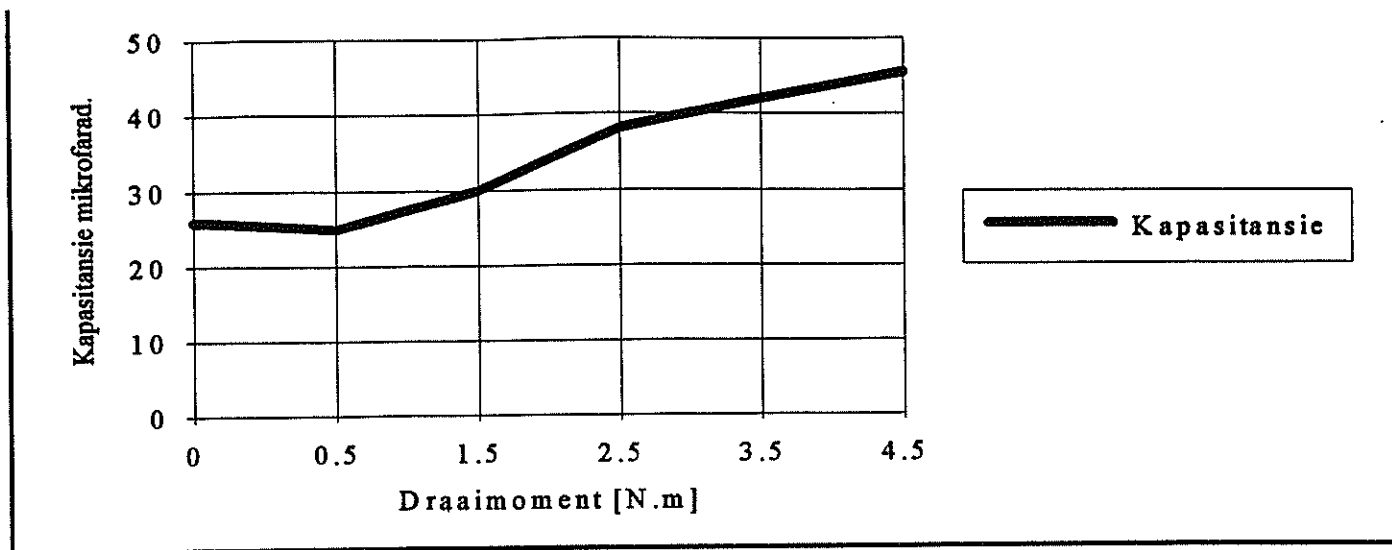
Figuur 3
Draaimoment teen kapasitansie van die fase omsetter.

(4) Gevolgtrekkings

Vir aansit word 'n redelike groot kapasitansie benodig soos gesien uit die gedeelte voorheen bespreek. Vir 'n korotor kan nie 'n baie goeie aansit draaimoment bereik word nie, ongeveer 40% van gebalanseerde driefasige omstandighede, aangesien die aansit draaimoment afhanklik is van die hoekverskil en slegs 'n hoekverskil van 90° kan bewerkstellig word met 'n kapasitor. Vir 'n gewende rotor kan egter 'n veel groter aansit draaimoment verkry word, selfs 'n paar maal die aansit draaimoment van normale omstandighede.

Die stelsel stem baie ooreen met 'n enkelfasige induksie motor, daarom kan van 'n kapasitor gebruik gemaak word wat aan sekere spesifikasies voldoen, om die beste resultate te lewer vir vollas en nullas omstandighede. Die kapasitansie benodig vir die fase omsetter is afhanklik van die las en die toevoerspanning. Die rendement van die stelsel is nie baie goed nie, ongeveer 70% by vollas. Die maksimum draaimoment wat gelewer kan word is slegs 66% van die maksimum draaimoment wat gelewer kan word deur gebalanseerde omstandighede indien die kapasitansie baie noukeurig bepaal is.

Indien daar slegs 'n enkelfasige toevoer beskikbaar is kan van die stelsel gebruik gemaak word.

(5) VERWYSINGS

(1) BROWN, J. E. en JHA, C. S.: 'The starting of a 3-Phase Induction Motor Connected to a Single-Phase Supply System', *Proceedings I.E.E.*, Paper No. 286 U, April 1959 (106 A, p. 183).

(2) SEN, P.C.:'Principles of Electric Machines and Power Electronics', 1989 (p 219).

1

Development of a cost efficient FEM system for the design of power apparatus

W.A. Cronje

Abstract

A FEM system for the two-dimensional analysis of power apparatus including busbars, transformers and electrical machines is developed in order to have acces to FEM source code that can be adapted to specific non-standard requirements.

I. INTRODUCTION

THE use of FEM has become generally accepted for the analysis and design of electromagnetic structures and components. Various commercial packages are available that enable the designer who don't want to write his own programs to also successfully perform FEM investigations.

The commercial FEM systems are very expensive however and often limited in their functionality. The cheaper systems are typically more constrained while the more expensive and powerful/flexible systems have extremely steep learning curves. Over and above these arguments the commercial packages are closed in nature with no source code available for adaptation to unusual problems. This last factor can be a serious stumbling block to application of commercial packages in academic or research environments.

This has formed the motivation for the development of a new FEM system.

II. CONSIDERATIONS

For use within the scientific/engineering/industrial community in South-Africa the computational requirements can not be as high as in Europe or the USA. One of the design constraints is therefore that the system should be suitable for the typical Intel PC-compatible platforms.

The chosen programming language is C/C++ due to its portability. It is currently possible to build and run the FEM system on SUN and HP workstations as well PC's running UNIX(Linux).

III. ARCHITECTURE

A number of decisions regarding the architecture of the system was taken. First of all it was decided to develop the system in a modular fashion similar to that employed for commercial systems. The conventional approach of pre-processor, solver and post-processor was employed because this allows the most flexibility.

In Fig.1 a schematic diagram of the architecture of a typical commercial FEM system is shown. In most cases the pre and post-processing capabilities are combined in the general purpose user interface as shown. This type of approach is excellent for field theoreticians who understand finite elements. Such a general purpose front-end requires the user to sepcify his problem in general electromagnetic terms and also perform any simplifications due to symmetry etc. These steps normally require some experience with the use of finite elements on the side of the system user which is often not the case and therefore present a hurdle to the wide and effective application of FEM in CAD/E systems.

In order to overcome the mentioned problems and provide a more suitable CAD/E system a front-end dedicated to a specific application type such as motor design is required which runs at a higher level than the FEM system with the general purpose interface. This situation is depicted in Fig.2. Work on such systems is already in progress based on commercial FEM software systems.

The approach described here is to flatten the hierarchical pyramid that results from the aforementioned approach and instead employ application oriented user-interfaces which directly communicate with the solver modules. This reduces the complexity of the overall system and also makes the system more cost efficient than the equivalent system employing a deep hierarchy.
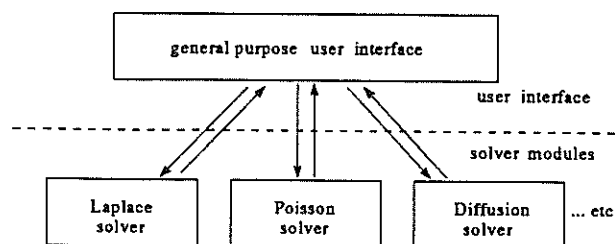
Fig. 1. The architecture of a general purpose FEM system
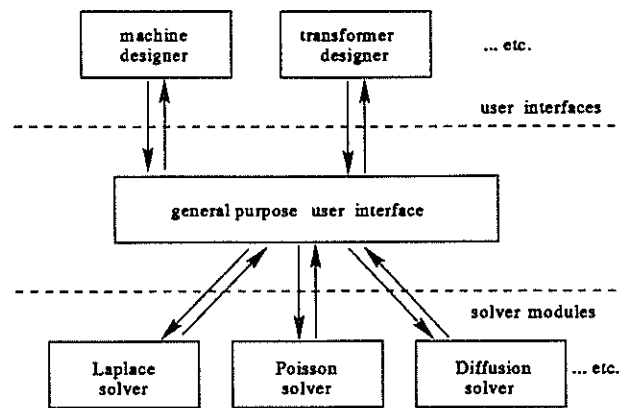
Fig. 2. The architecture of a general purpose FEM system provided with application specific fron-ends

No attempt is made to create general purpose pre and post-processor facilities of the same standard as encountered in commercial systems. Instead pre-processing can be done by hand or by a suitable user interface module which is specifically created for a restricted range of special applications as depicted in Fig.3. Post-processing can also be done by hand or by means of the dedicated user interface mentioned above which can be the same as or combined with the one for pre-processing. This is no severe restriction since most engineering applications require the calulation of lumped parameters such as losses, impedance, etc. Sophisticated graphical representation of fields is therefore not considered as essential in this approach but can be added at a later stage as an extension of a particular user interface if required.

Communication between the pre-processor and the solver/s occurs by means of ASCII files, which can be created and edited directly by the user of the system if required. The same approach is used for the communication between the solver/s and the post-processor.
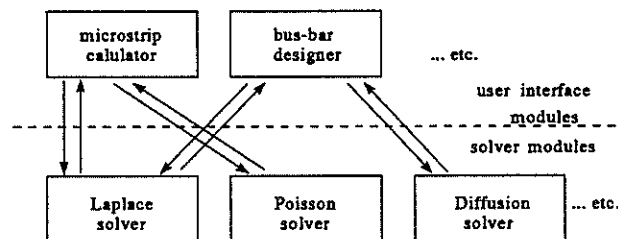
Fig. 3. The architecture of the new FEM system with provision for application specific fron-ends

The described approach makes it possible to concentrate on one module of the system at a time or even distribute development among different people if required. Up to now a suitable a meshing program has been adapted for use within the scheme set out here. Two solver modules have been completed to date, the one for solving Laplace's equation meant for application to mostly electrostatic problems and one for solving Poisson's equation meant for solving magnetic problems including different materials and current sources.

Examples of problems solved with the two solver modules are shown in the next section.

IV. EXAMPLES

An inportant part of using FEM is to verify that the solutions obtained are true solutions. This can be performed by comparison with analytical results or experimental measurements. For initial testing text-book examples can be used. These are the steps outlined here and the first example for testing the electrostatic solver module is the case of a parallel plate capacitor with two different dielectric materials sandwiched between the plates.

A. Multiple dielectric capacitor

The example examined here coresponds to the geometric situation depicted in Fig.4

The total capacitance for the situation depicted can be calculated from the following analytical equation

$$C = \frac{1}{\frac{d_1}{\epsilon_1 S} + \frac{d_2}{\epsilon_2 S}} \tag{1}$$

where S is the area of one of the plates given by $S = l \cdot w$.
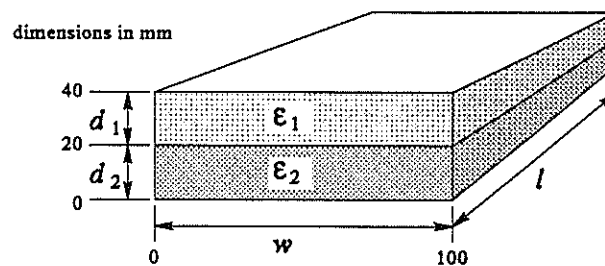
Fig. 4. The problem geometry for the case of a parallel plate capacitor filled with two different dielectrics.
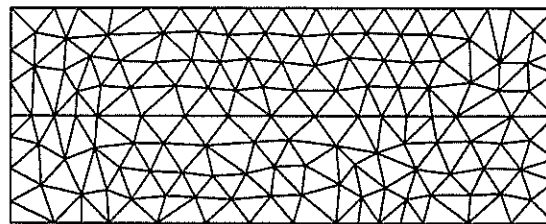
Fig. 5. The problem geometry for the case of a parallel plate capacitor filled with two different dielectrics.

The mesh created for this problem appears as in Fig.5. The results obtained from the analytical equation for the capacitance (1) and the capacitance determined by the FEM through integration of the stored field energy gave the following results:

$\varepsilon_1 : \varepsilon_2$	analytical	FEM
1:1	22.125pF	22.135pF
1:4	35.400pF	35.416pF
1:40	43.177pF	43.191pF

From the table it is clear that the results obtained by the different methods correspond very well. The advantage of the FEM method now lies in the fact that it can treat more complex geometries with various dielectric materials with ease. The correspondeing analytical approache would require a far bigger effort on the side of the designer.

B. Inductor with air-gap

To test the magnetic solver module an E-core based inductor configuration with an air-gap in the center leg is chosen. Due to symmetry only one quarter of the geometry need to be taken into account as depicted in Fig.7.
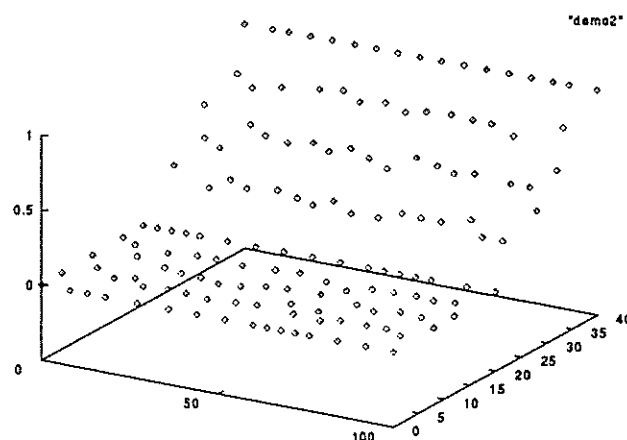
Fig. 6. The electric potential solution for the case of a parallel plate capacitor filled with two different dielectrics.
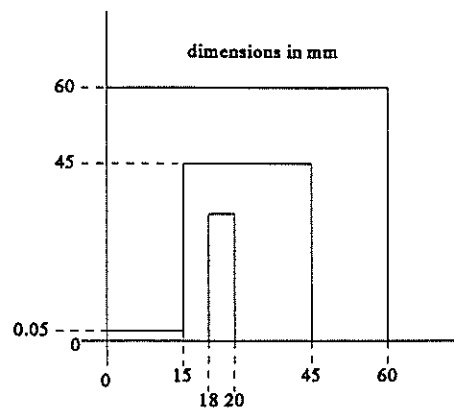
Fig. 7.   One quarter of the geometry of an E-core based inductor with an air-gap in the center leg.

The mesh generated for this problem is shown in Fig.8. An analytical solution is readily calculated by assuming that the core has infinite permeability. The inductance is then controlled by the air-gap and can be calculated by the simple relationship

$$L = \frac{\mu \cdot A}{g} \tag{2}$$

where A is the cross-sectional area with an aditional factor for the fringing taken into account and g is the length of the air-gap. The inductance calculate with the equation (2) is $38.956\mu H$ and the inductance calculated from the field energy by the FEM program is $39.208\mu H$
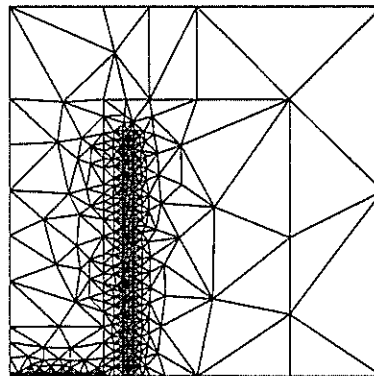
Fig. 8.   The mesh generated for one quarter of the geometry of an E-core based inductor with an air-gap in the center leg.

V. CONCLUSION

A 2D FEM system has been developed for analysing and designing power apparatus such as transformers, busbars and machines. The system has an open architecture allowing for future expansion and reusability of the various modules. Various application specific front-ends can be created according to the specific needs of users while retaining the basic solution modules in unchanged form.

Proposed future expansion include various user sepcific graphical front-ends as well as new solver modules for solving the diffusion equation in the time and frequency domain in order to treat eddy-current problems.

REFERENCES

[1]   P.P. Silvester, R.L. Ferrari, *Finite Elements for Electrical Engineers*, Cambridge University Press, 1990, 2nd Ed.
[2]   C. Johnson, *Numerical solution of partial differential equations by the finite element method*, Cambridge University Press, 1995.
[3]   R.C. Booton jr., *Computational Methods for Electromagnetics and Microwaves*, Wiley Interscience, 1992.

Dr. W.A. Cronje, Energy Laboratory, Rand Afrikaans University, PO Box 524, Aucklandpark, 2006.
e-mail: wac@ing1.rau.ac.za

THE USE OF FINITE ELEMENT ANALYSIS TO OPTIMISE INDUCTION MOTOR ROTOR PROFILES FOR SYNCHRONOUS RELUCTANCE OPERATION

M.A. ROHDE,   A.S. MEYER   C.F. LANDY

UNIVERSITY OF THE WITWATERSRAND

1 Abstract

Transforming a squirrel cage induction motor into a synchronous reluctance motor is not a new technique. Traditionally, the rotor was machined into a crucifix shape using adhoc calculations. By using finite element analysis, different rotor profiles may be examined to optimise the saliency ratio. The improved rotor geometry does not perform as well as the induction machine or modern axially laminated synchronous reluctance machine, but significantly improves on the traditional crucifix shape. The modified induction motor has application in the low cost synchronous reluctance market.

2 Introduction

The project involves modifying the rotor of a three phase squirrel cage induction machine so that it performs as a synchronous reluctance machine. The modified induction machine rotor was combined with the existing shell of the induction machine. The induction machine is mass manufactured and readily available and is hence inexpensive. The synchronous machine on the other hand is not mass manufactured in countries such as South Africa and is hence not as accessible or cheap as the induction machine. Modifying existing induction machine rotors will thus reduce the cost of a synchronous machine.

The emphasis of the design is low cost application. This also implies that the modifications to the rotor need to be simple. This allows any workshop to perform the modifications themselves and will keep the cost of the machine down. Attention must be paid to the way in which alterations are done to the rotor. The iron has to be cut away in such a way as to allow milling of the rotor. In other words, no fancy rotor geometries are possible as this would significantly increase the price of the machine. The implication of converting asynchronous machines for synchronous operations is that the stator has been developed for the induction machine and not for the synchronous machine. Although they are very similar, slight differences do exist and it needs to be noted that the performance will suffer (i.e. efficiency and power factor) (ref 7, Page 66). For this reason the research is targeting the smaller range of machines, where the bulk of the price is the purchase cost, and running cost is not as important as with larger machines.

Converting an induction machine into a synchronous reluctance machine is by no means a new technique. However, all the modifications on the induction machine rotor in the past have been empirical. The purpose of this project is to optimise the modification to obtain the best possible synchronous reluctance machine motor from the existing induction machine. The final product is to perform better than the conversions to date and is less expensive than modern synchronous reluctance machines.

The simulation is done on a commercial finite element package. Using finite element analysis as a basis to iteratively improve given geometries is extremely powerful because the effects of minor changes can be observed. It is very easy to change the shape of a rotor when modelled on software, rather than physically cutting away pieces of a rotor and then performing tests. Modelling by means of a computer hence saves time and money.

This is a great advantage for the local market due to the fact that synchronous reluctance machines are not readily available in South Africa. Existing induction machines can be converted into cheap synchronous reluctance motors as the application demands it.

3 Rotor Manipulation

The essence of the project involves the transformation of an asynchronous machine into a synchronous machine. This transformation will change the operating characteristics of the machine. The objective is to introduce saliency into the rotor. This is achieved by removing iron from the rotor to create this saliency. The cut away sections of iron constitute airgaps that will act as flux barriers. The artificially introduced flux barriers will enforce the natural flux pattern and fix it to the d- axis. Air has a much greater permeability than iron and is therefore an effective magnetic barrier.

In order to fix this natural flux pattern to the d- axis, it must be ensured that the d- axis is the preferred path for the flux. In other words, the reluctance in the q- axis must be maximised and the reluctance in the d- axis minimised. The flux will then flow along the path of 'least resistance', namely the d- axis. This requires iron to be removed in such a way as to limit the q- axis flux as much as possible. However, removing iron from the rotor will invariably also affect the d- axis

flux. Care has to be taken to introduce flux barriers that will influence the d- axis flux as little as possible and at the same time limit the q- axis flux.

Removing iron from the rotor implies that there is now less iron to contain the overall flux. Since most machines of this nature are designed to operate close to the saturation point, it is fair to assume that the machine will be saturated if run at the original rated values. Saturating the machine implies that the saliency ratio will decrease and the machine cannot operate efficiently. For this reason, it is necessary to de-rate the machine, and run it at a lower voltage. This obviously affects the output- per- kg for the machine.

The most important difference between synchronous and asynchronous operation, is the fact that at synchronous speed there are no currents induced in the rotor cage (neglecting harmonic effect). This implies that there will be no heating due to copper losses and iron losses, because the frequency of the magnetic flux is effectively zero in the rotor. Hence the overall losses of the machine have been reduced because all rotor losses have been eliminated.

The objective however, is to obtain the best possible ratio of output- per- kg. For this reason, the current density in the stator can be increased to try to get a better performance out of the machine. The losses in the stator will increase with this rise of current density in the stator windings, but since the rotor losses fall away, the overall losses will then be more or less constant. It needs to be noted that heating of the machine will now be different to that of the original induction machine because the losses have been redistributed. This actually simplifies the cooling process as it is easier to cool the stator than the rotor.

The fact that part of the rotor cage is still present in the rotor after the conversion gives rise to some interesting properties. The conventional synchronous machine cannot run up on its own. The modified induction motor is capable of starting on its own, just as the normal induction motor does. Even though the rotor cage is broken and incomplete, it allows sufficient current to flow to create enough torque at low speeds. The residual cage effectively performs the function of a damper bar winding.

If at any one time while in synchronous operation the load should exceed the maximum allowed limit, pole slipping will occur, but there will still be torque present. In this case, the load needs to be slightly reduced and the motor will once again synchronise. This property is desirable because the motor operation is not as load sensitive as conventional synchronous machines.

4 Measurements on the Testbed and Experimental Set-up

Modifications were made on an existing 5.5 kW, 380 V, 4-pole, 3 phase squirrel cage induction motor. The rotor has been remodelled into a simple salient pole or crucifix structure.
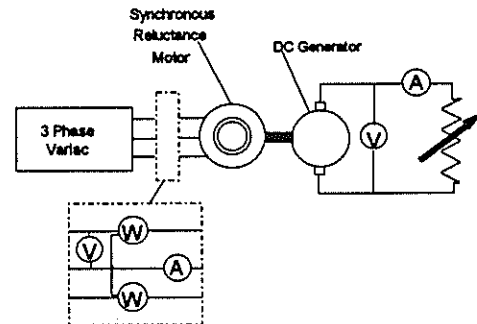
Figure 1. Experimental Set-up

From the torque measurements the difference of the relevant q- and d- axis inductance paths may be calculated. The d- axis flux can be measured by running the DC generator at synchronous speed and aligning the rotor exactly to the d- axis. Measuring this current and voltage, the inductance in that specific path can be calculated. Hence the saliency ratio can be calculated.

5 Modelling of the Motor

The major difference between the modelling and the actual measurements is the fact that the simulation can only depict the static case. This is in contrast to the dynamic nature of the measurements. This means, that the excitation of the simulation will only include the magnetising current and ignore the load current.

The motor was modelled in 2 dimensions, depicting a cross-sectional view of the motor. By default, Maxwell assumes the depth of the geometry to be 1 m into the plane of the screen (or drawing). A simple constant is used to scale the motor to the correct axial length. The d- and q-axes are modelled separately. The program calculates the respective maximum and minimum flux, and hence the inductances can be derived.

Particular care has to be taken with this approach not to operate the two individual cases at different saturation levels. Care needs to be taken to ensure constant flux linkages. In order to ensure this, the excitation was changed until the respective d- and q-axes cases yielded the same flux. The ratio of the excitation current then yields the saliency ratio. This implies that the two cases will be operating at the same level of saturation.

In an electric machine, the bulk of the energy is stored in the airgap and hence the accuracy of the solution in this area needs to be high. On advice from the simulation program manufacturers, the airgap requires at least 3 levels of triangles (i.e. the finite element mesh must be at least 3 triangles high) for the solution to be meaningful.

After the finite element solution process is complete, the post processor provides the facilities to interpolate the data. The quantity that is required is the flux per pole. In order to calculate this, a circular line is placed into the airgap, near the rotor. The line is situated at a radius of 63.2 mm, spanning exactly one pole (i.e. from 0 degrees to 90 degrees mechanical measure). The normal component of the B- vector along this line is integrated to yield the entire flux crossing the airgap over one pole. The result represents the net flux per pole that is transferred into the rotor.

6 Simulation Results

6.1 Crucifix Rotor

The existing crucifix rotor was simulated on the finite element package. A plot of the saliency ratio vs. the flux per pole was constructed and using the motor design package, the flux was related to voltages.
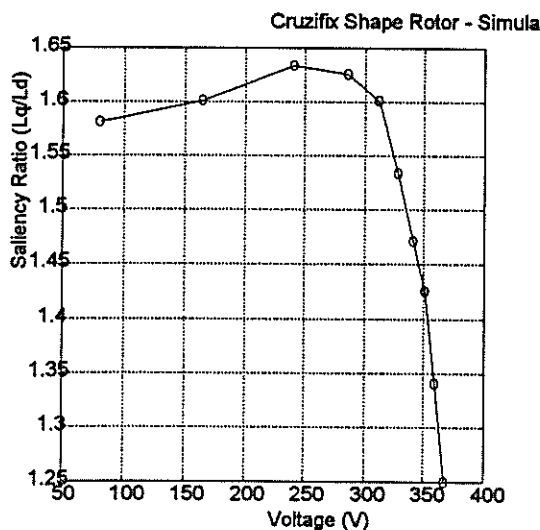
Figure 2. Crucifix Rotor Saliency Ratio

The plot (figure 2.) shows how the saliency ratio is dependant on the voltage. This specific shape of rotor has a maximum saliency ratio of 1.64 at 250 Volts. This means that this particular machine should be de-rated to 250 Volts for optimal performance. The plot clearly shows how saturation affects the saliency ratio. During this simulation, the magnetic properties of the shaft were defined as iron and did not limit the flux (i.e. defined as the same material as the rotor).

The material attributes of the shaft were altered in order to limit the flux within the shaft. The shaft was assumed to be air. This did not significantly affect the flux per pole in the crucifix rotor in either the d- or the q- axis case. There is sufficient iron left in the path for the flux to pass through. The flux per pole remained almost constant at 5.6 mWb at an excitation of 250 Volts.

In the insinc case, the rotor already carries a significant amount of flux and it would be difficult to increase this. Any improvements to the saliency ratio in this rotor profile would hence have to hamper the q-axis flux, rather than increasing the d- axis flux.
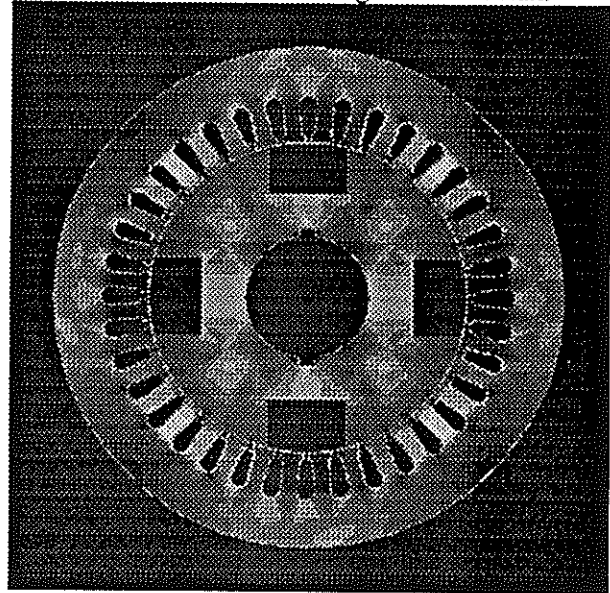
Figure 3. Crucifix Rotor Profile (non-magnetic Shaft) - d- Axis or Insinc Case

From the finite element results it can be seen that there is not significant saturation in the rotor itself. In order to hamper the flux in the outsinc plane, and so increase the saliency ratio, additional or different flux barriers have to be introduced.

6.2 Alternative Rotor Profiles

A variety of alternative rotor profiles were evaluated on the finite element package. While assigning the shaft as a magnetic material, it was found that altering the shape of the rotor did not significantly increase the saliency ratio as the flux retreated into the shaft (as seen in figure 4.). However, when the magnetic attributes of the shaft were changed to a non-magnetic material in order to limit the flux, the saliency ratio increased significantly from 1.63 to 2.6.

A typical shaft is made from high tensile steel. The relative permeability of mild steel is 2000, as compared to air that has a relative permeability of 1. The iron of the rotor has a far greater permeability

than mild steel. In real life, flux does penetrate into the shaft, but not to the extent that was depicted in the simulations (shaft of magnetic material).
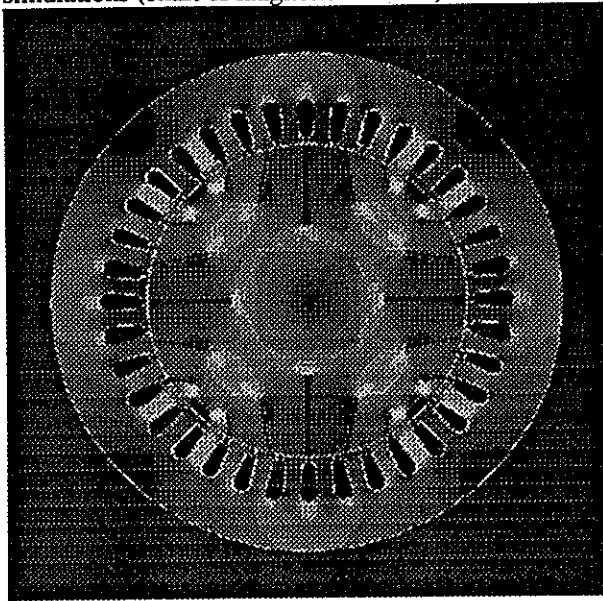
Figure 4. Improved Rotor Profile (Magnetic Shaft) - q-Axis or Outsinc Case

As different rotor shapes are evaluated, the amount of iron that is cut away from the rotor varies. It is important to keep in mind that if too much iron is removed, the motor will have to be de-rated further.

7 Further Work

The measurements on the testbed have to coincide with the simulation results in order for the project to be meaningful. The results of the simulations and from the testbed do not correlate closely enough. The discrepancy is introduced by the measurement of the torque angle. A small change in the angle brings about a significant change in the final saliency ratio. This 'confidence test' has to be made more accurate.

The centrifugal forces on the rotor are quite severe. Once the optimisation process has been completed, it has to be verified that the final geometry will not be too weak structurally. Once this has been determined, the final model will have to be built and tested to see if the finite element predictions hold true.

8 Conclusions

By altering the rotor profiles into patterns that roughly enforce the natural flux paths, the saliency ratio may significantly be increased. This however is subject to the amount of flux that is allowed to penetrate into the shaft, unlike with the conventional crucifix rotor profile shape. The best results would be achieved if the shaft was constructed by a non-magnetic material.

The nature of the design demands certain concessions regarding power factor and efficiency. For this reason the application of this project is limited to the smaller range of motor where a small loss of performance does not have severe financial penalties in regards to the power supplied. The final rotor profile also needs to be strong enough to withstand the centripetal forces without breaking.

9 References

1) P.C. Sen; Principles of Electric Machines and Power Electronics; Wiley; 1989; Canada

2) C.F. Landy; Space and Time Harmonics in Induction Motors (Course Notes); 1994; South Africa

3) D.A. Staton, T.J.E. Miller, S.E. Wood; Optimisation of the Synchronous Reluctance Motor Geometry; Electrical Machines and Drives Conference (IEEE); 11-13 September 1991; London, UK; No 341; Pages 156-160

4) D. Platt; Reluctance Motor with strong Rotor Anisotropy; Industry Application Society Annual Meeting; 7-12 October; 1990; Seattle, USA; Vol 1; Pages 224-229

5) X. Feng, R. Belmans, D. Verdyck, W. Geysen, K.U. Leuven; Reluctance Motor with a Radially Laminated Rotor using Anisiotropic Materials; Electrical Machines and Drives Conference (IEEE); 8-10 September; 1993; Oxford, UK; Vol 376; Pages 79-84

6) N. Balbo; R. D'Andrea; L. Malesani; P.Tomasin; Synchronous Reluctance Motors for Low cost Medium Performance Drives; 5th European Conference on Power Electronics and Applications (IEEE); Brighton, UK; 13-16 September; 1993; Vol 6; No 377; Pages 77-81

7) A. Vagati; G. Franceschini; I. Marongiu; G.P. Traglia; Design Criteria for High Performance Synchronous Reluctance Motors;

8) EPE Journal; European Power Electronics and Drives; Vol 4; NO 3; Brussels; September 1994

10 Address of Main Author

Mark Andreas Rohde, Department of Electrical Engineering, University of the Witwatersrand, Private Bag 3, 2050, South Africa, E-mail: rohde@odie.ee.wits.ac.za

FACILITY LOCATION OPTIMIZATION IN ELECTRICAL DISTRIBUTION DESIGN

J Apostolellis   B Dwolatzky   A S Meyer

University of the Witwatersrand, Johannesburg, South Africa

ABSTRACT

The development of a computer implemented optimization algorithm that is intended to aid the electrical distribution designer is discussed. The purpose of this algorithm is to find the optimal location of a single junction in an electrical distribution network. This optimality is defined in terms of the minimum cost of network components corresponding to the junction location. It applies the 'Hill Descent' optimization algorithm to search for the optimal junction position in a narrowed down search space. This approach is well suited to the highly non-linear nature of the problem at hand.

1. INTRODUCTION

A large percentage of South African households are currently without electricity. This is especially the situation in rural areas. Fortunately major electrification efforts are being carried out. One of the tasks in bringing electricity to a community is the design of the distribution network for connecting actual stands to a source of electricity. It is in the interest of all parties concerned that such networks are implemented in a cost-effective manner. The cost of a distribution network is made up of two significant components. The most obvious is that of the actual physical network which depends on the locations, types and quantities of the facilities that comprise it coupled with the cost of installing these facilities. The other component is the cost of producing the distribution network design which depends on the amount of human and other resources allocated towards it.

This implies that although a cheapest network configuration in terms of its physical configuration could be found, the process of finding and verifying this solution would be too expensive. This is because a thorough search for it would consume excessive amounts of resources in the design phase. This is especially true in the sense that this design phase has typically been carried out manually by a designer who would have to tediously calculate cable lengths, costs, voltage drops, etc. while exploring various network configurations.

Hence there is a need for optimisation tools that aid distribution design. This paper discusses one such tool, which utilises the algorithm to find optimal junction locations.

The development of this tool is part of a larger ongoing research effort that has been carried out at the University of the Witwatersrand under the supervision of Dr B. Dwolatzky and Mr A.S Meyer [2]. This research group has focused on the development of software tools that are intended to automate and facilitate various aspects of the electrical distribution network design process. The algorithm presented in this paper uses the functionality of some of the software tools that have already been developed by this research group. These include an algorithm that automatically finds an optimal cable configuration by selecting cables from a fixed set of available cables [4] as well as an automated routing tool that finds the cheapest route between two points over an area that is composed of various cost regions [5]. The algorithm uses a 'Hill Descent' optimization method [1].

The background to how this algorithm fits into the electrical distribution design process is discussed in the next section. This is followed by a description of how the actual algorithm has been implemented and in what ways the algorithm can be extended.

2. BACKGROUND TO ELECTRICAL DISTRIBUTION

In an electrical distribution network there are normally a large number of stands that must be connected to a source of electricity by a particular hierarchy of facilities. From a MV/LV distribution transformer a number of low voltage junctions are fed by feeder cables. Service cables are connected between junctions or distribution transformers and load points (consumer termination points) at stands. Each junction can supply a number of load points. This hierarchy of facilities is illustrated by figure 2.1

It is the electrical distribution designer's task to arrange these facilities into a suitable distribution network. The ultimate design of the network should be of the cheapest possible configuration in terms of the cost of equipment and installation of components. It should also satisfy various constraints such as not exceeding the allowable

voltage drop in cables and not having facilities placed over regions in which their placement is not allowed.
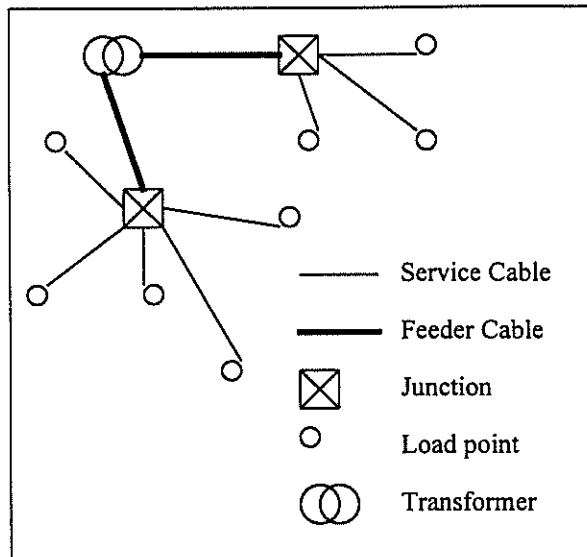
FIGURE 2.1 Hierarchy of network components

Considering the spatial nature of distribution networks, it is impossible for a designer to calculate the network cost for all possible network configurations, because the number of conceivable configurations is infinite. Therefore it is impossible to find the cheapest possible configuration. However with the application of common sense and a few rules of thumb, a designer could quite successfully narrow down the search space in which to look for a solution.

One suggestion is to handle the position of one junction at a time. This is the impetus behind the algorithm presented in this paper. Consider the simple situation in which a single junction feeds a fixed number of designated stands. The designer has the freedom to reposition that junction amongst the stands until an optimal position for that junction has been found. The optimal position will typically be related to the minimum of the sum of the feeder cable distances while still obeying other constraints such as not violating the maximum volt drop allowed in the feeder cables. If done manually this would be extremely tedious, making it difficult to find the optimal location. However with the computer implemented algorithm presented in this paper the technique of optimally positioning junctions is made feasible.

3. POSITIONAL OPTIMIZATION OF A SINGLE JUNCTION

The purpose of the algorithm is to find the optimum position of the hypothetical junction mentioned above. This junction is connected to another single junction

(or a transformer) via a feeder cable and to a number of load points(stands) via service cables. Therefore the routes of these feeder cables and service cables will also have to be found, because they will dictate the feasibility of the junction's location. These routes will influence the lengths of these cable segments. The lengths of cable segments determine what type of cables are to be used so as to not violate voltage drop constraints and therefore determine the overall cable costs of this simple network.

The algorithm is presented here as a number of steps, each specifying a particular action that the computer implementation of the algorithm has been designed to perform. The framework of the software with which the algorithm has been linked has a suitable means of intelligently representing a map of the area for which the reticulation network is to be produced. This has been done by representing map elements such as roads, stands and other features by well designed data structures.

STEP A : Find an initial junction position

The first step of the algorithm is to find a suitable initial position for the junction from which further iterations in the search loop can proceed. It is recommended that this initial position is calculated as the load centroid of all the intended load points. When reticulation is performed for a particular township, a value for the township's After Diversity Maximum Demand (ADMD) [3] must be attained before hand and used for cable rating selection. This implies that all stands will have equal load demand and therefore in calculating the load centriod it is assumed that all load points are equal. Calculation of the coordinates of the load centroid are made by simply averaging the load point coordinates. An example of the load centroid is shown in figure 3.1, in which the rectangles surrounding load points represent stands.
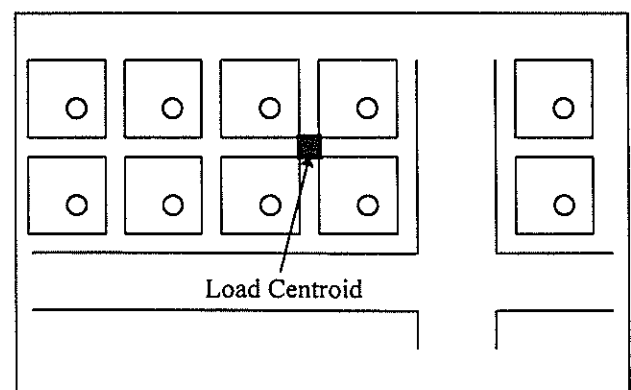
FIGURE 3.1 Location of centroid amongst load points

If the load centroid found in the manner suggested above is not in a suitable position as dictated by the geography of the area for which the reticulation design is being made, then its coordinates are adjusted until it is. This is done by searching for the closest suitable position from the initial

position by using an outwardly spiralling search path from this position. Favour is given to locations that are closest to the other fixed junction.

STEP B : Find routes for feeder and service cables

The next step is to use the automated routing algorithm [5] mentioned above to find routes for the feeder cable and all the service cables. The inputs to this algorithm are made so that cable routes will not cross stands and other unsuitable regions by assigning the geometric regions defining them with very high cost factors. 'Midblock' routes, which is the term given to cable routes placed between adjacent stands, can also be either encouraged or discouraged in a similar way by either defining thin strips of low cost regions between adjacent stands or not. Figure 3.2 shows feeder and service cable routes.
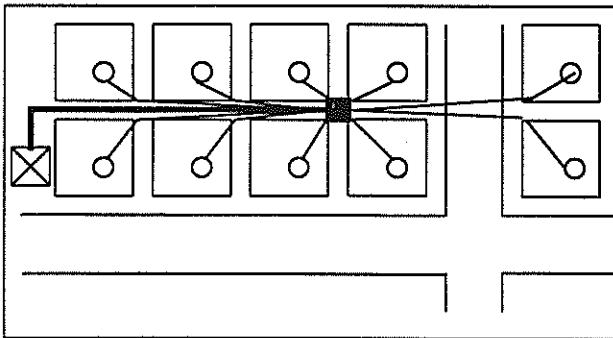
FIGURE 3.2 Feeder and service cable routes corresponding to initial junction position

STEP C : Select cable types for feeder and service cables

The automatic cable selection algorithm is used to find an optimal cable selection for the current network configuration by using the feeder and service cable lengths, the maximum voltage drop allowed from the fixed junction to any of the load points, the ADMD, Diversity Factor (DF) and Unbalanced Correction Factor (UCF) curves [3], and the database of available cable types which includes their resistivity and cost per unit length. Using the output of the cable selection algorithm, the cost of cabling is calculated by summing all the individual cable costs and their corresponding installation costs. This value is the physical cost of the current network configuration.

STEP D: Iteratively search for best junction position

This part of the algorithm has a repetitive nature in which the junction position is iteratively repositioned while searching for its optimal position. The assumption is made that a close enough to optimal position for the junction can be found along the feeder cable route corresponding to the initial junction position. This assumption is a key simplification used by the algorithm to narrow down the search space, and hence making the search for an optimal junction position a feasible task. Therefore the data representing this initial feeder cable route is stored and used as a locus along which other trial junction positions are explored. This locus will be termed the 'search locus'.

A new position for the junction is investigated by changing its coordinates to the position at about one twentieth of the total length of the search locus back along the search locus from the previous junction position (i.e. in the direction towards the fixed junction). This fraction of the total length of the search locus should be set at the desired resolution which will be determined by the desired accuracy and available processing time.

This is where the 'Hill Descent' optimization method [1] is applied to the algorithm. The method entails incrementally changing the attributes of an operating point until a minimum value associated with this point is found. This minimum point indicates optimality. In this algorithm the junction is the operating point and its attributes which are changed are the coordinates of its location. The value associated with this location is the corresponding cost of the network.
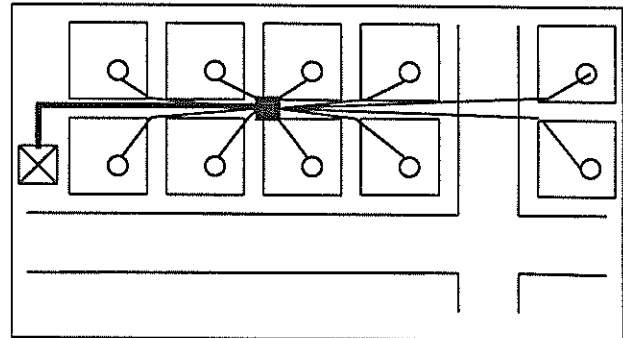
FIGURE 3.3 Junction position has been move along feeder cable

Figure 3.3 illustrates the incremental change in the junction's coordinates. Steps B and C are repeated at the new junction position and the new network cost is evaluated at this location. This whole process is repeated until further movements of the junction along the search locus cause an increase in the network cost from the previous position. The ultimate optimal junction position is assumed to be at this point along the search locus.

4. EXTENSION OF THE ALGORITHM

This algorithm has the capacity to be extended for use in finding optimal configurations of networks having multiple junctions and for finding optimal transformer positions. It can also be made more robust by having the search loop carried out along the entire search locus and then selecting the optimal junction position where the cost profile is the cheapest along the search locus. This is superior to the method mentioned in section 3 because it can detect subsequent mimima in the cost profile if any exist. However it would require additional processing.

4.1 MULTIPLE JUNCTIONS

In a typical reticulation network, the output of a junction could either be connected to just load points via service cables or it could be connected to other junctions via feeder cables as well or even just other junctions. This means that the algorithm discussed in this paper would have to be modified to handle these other situations. This could be done by treating the other junctions as load points and applying a similar approach as mentioned above.

The typical situation is one in which there is only one feeder cable and multiple service cables coming out of the junction. This should be treated by finding a search locus between the two fixed junctions that passes through the centroid of the load points associated with the service cables. This centroid will serve as the initial position of the junction from which movement of the junction along the search locus will occur. The search locus should be the route of the incoming feeder cable concatenated with the route of the outgoing feeder cable.

4.2 TRANSFORMER LOCATION
     OPTIMIZATION

In the same way that a single junction acts as the link between another junction and a number of load points, a transformer acts as the link between a Medium Voltage Tee-off and a number of low voltage junctions. Therefore the algorithm discussed in this paper could be applied to the problem of finding an optimal location for a transformer, given fixed tee-off (medium voltage substation) and junction positions. In this case the voltage drop in the medium voltage cable run between the tee-off and the transformer would be very small and possibly insignificant for the problem at hand.

5. CONCLUSIONS

In the past electrical distribution design has generally been carried out manually, making it extremely difficult and tedious for a network designer to improve on a design. Thus making it almost impossible to ultimately produce an optimal network configuration.

Various software tools have been developed by a research group at the University of the Witwatersrand [2] to help automate this design process, thus enabling the designer to focus on improving the design instead of wasting resources on the tedious work inherent in distribution design.

The design of an algorithm that finds the optimal position of a single junction is discussed in this paper. It uses previously developed tools, namely an automated routing algorithm [5] and an automatic cable selection algorithm [4]. It is designed to search for this position along a locus thus simplifying the search process into one that is feasible in terms of required processing. It uses a 'Hill Descent' optimization algorithm [1] which is suitable for this extremely non-linear application.

The algorithm can be extended for use in finding optimal junction locationss for multiple junctions as well as finding optimal transformer locations.

REFERENCES

[1] Dixon L "Non-Linear Optimization" Bell and Bain, 1972.

[2] Dwolatzky B and Meyer A S "The development of an integrated set of software tools for use in the design of an electrical reticulation network" South African Universities Power Engineering Conference (SAUPEC) 95, Pretoria, January 1995.

[3] Meyer A S, Van Coller J M, Nortje F "The Design of Low Voltage Reticulation Systems with Emphasis on Low Voltage Electrification Systems" Winter School '94, University of the Witwatersrand, Johannesburg 1994.

[4] Nicolson J M "Object oriented design of cable selection software for low voltage networks" Master's Thesis, University of the Witwatersrand, Johannesburg, April 1993.

[5] West N A, Dwolatzky B and Meyer A S "Software which automatically Routes Cables in a Power Reticulation Design System" The Transactions of the South African Institute of Electrical Engineers" September 1994.

AERIAL PHOTOGRAPH INTERPRETATION FOR ELECTRICAL RETICULATION

S. P. Levitt   B. Dwolatzky   A. S. Meyer

University of the Witwatersrand, Johannesburg, South Africa

This project involves the interpretation of black and white aerial photographs of rural areas, for the purposes of electrical reticulation. The emphasis of the interpretation process is on the identification of houses, buildings and other man-made structures. Once such structures have been recognised it is possible to generate a stand hypothesis for each house or building. These stand hypotheses can then be used as a starting point for planning the reticulation of the rural area. The methods being used in the interpretation process are both pixel-based and structural. The interpretation or vision system is being implemented in the C++ programming language, and particular care has been taken in designing a class hierarchy which is capable of supporting both data-driven and goal-driven processing.

1. INTRODUCTION

A significant amount of the research which is being conducted by the Wits SED (Software for Electrical Distribution) group, lies in the area of reticulation optimisation. This document discusses one particular aspect of the research which is being conducted by the SED team, namely computer vision or computational image interpretation for the purposes of electrical reticulation.

In order to produce an optimised electrical reticulation plan, certain information about the area which is to be electrified needs to be known. More specifically, information concerning existing houses, roads and other significant land features is required. Usually, for well developed urban areas, a fairly large body of information has *already* been captured. The scenario is however dramatically different if one considers the more rural and underdeveloped areas of our country. In such areas, like parts of Kwazulu/Natal, almost no cadastral information of any sort is available [Quick, 1995].

One manner of gathering the required information, involves making use of aerial surveys. Skilled photo-interpreters are able to identify houses, transport systems, crop types, drainage patterns and even structure height from high resolution aerial photographs. Once a land feature has been identified it has to be manually delineated either by tracing the feature on vellum paper overlaying the photograph or by using a digitised version of the photograph and graphical software specifically designed for outlining features. The final outcome, no matter which method is used, is a map which consists of the particular extracted feature and is capable of being utilised by the SED team, in automatic optimisation exercises.

The project at hand involves the development of a system which will have the capability of semi-automating the identification, delineation and mapping of certain land features which are visible from aerial photographs. The system is not intended to completely automate the recognition process, rather a user will be required to work in conjunction with the system, in order to achieve adequate interpretation of images.

The following section presents the background to the project by reviewing certain fundamental image interpretation techniques and concepts. The approach which has been taken is then discussed. Finally some implementation issues are considered.

2. REVIEW OF IMAGE INTERPRETATION TECHNIQUES AND CONCEPTS

According to Argialas and Harlow [1990], image interpretation techniques have evolved from general methods for image-processing and classification which could be used in many spheres, to techniques which require extensive and specific knowledge about a narrow domain and are used to create very specialised applications. This paradigm shift is reflected in the history of image interpretation through the different interpretation models which have been developed over the last few decades.

2.1 STATISTICAL MODELS

Statistical models use a statistical or decision theoretic approach to image interpretation and are ideal for applications in which each of the pattern classes can be described by a set of distinct features [Argialas and Harlow, 1990]. The classification of the feature vectors of unknown patterns takes place by statistical decision rules.

Such models typically deal with the image at a pixel level and no abstractions are made. Usually individual pixels are classified according to their multispectral characteristics. This leads to several severe limitations as spatial context is completely ignored.

2.2 STRUCTURAL MODELS

Structural models have been developed in order to try an overcome the weakness which is inherent in statistical models. A structural description of a pattern or object involves describing the pattern or object as an organisation of subpatterns, objects or elements [Argialas and Harlow, 1990]. The relationships between each of the subpatterns has to be specified. Structural descriptions are recursive in that each subpattern or object once again has its own structure which can be described.

Recognition of objects in structural interpretation systems involves searching for a particular configuration of subpatterns or objects. The ground level objects or patterns from which more complicated structures will be formed have to be defined. These basic elements are known as primitives. Furthermore, a syntax or grammar has to be drawn up. The syntax of a system is a set of rules specifying which aggregations of primitives are allowed.

Structural image interpretation models have been proven to be more robust than per-pixel feature vector classification techniques [Argialas and Harlow, 1990].

2.3 HYBRID MODELS

A hybrid system is one which incorporates both statistical and qualitative techniques (structural). The statistical and syntactical approaches can be mixed in number of fashions and these have been identified in the literature. Argialas and Harlow [1990] state that an *efficient pattern recognition system for aerial images requires integration of statistical and structural tools in various stages of the design.*

2.4 HIGH, MEDIUM AND LOW LEVELS OF REPRESENTATION

As has been shown it is possible to classify an image interpretation system by the pattern recognition methodology employed. There is also a conceptual classification that can be made with regard to the manner in which the information contained in an image is represented. Information about a scene can be represented at different levels of abstraction. Three such levels are recognised - low, medium and high.

High-level representations describe the image in terms of highly semantic constructs. A high level representation of a scene allows the scene to be interpreted in terms of the final goals of the analysis [Argialas and Harlow, 1990]. Although high-level objects are the ultimate goal of a vision system, these objects have to be synthesised from medium level objects, which in turn are constructed from the aggregation of primitives or low-level objects.

Naturally different image analysis techniques/ segmentation methods are employed depending on the level of representation that is being dealt with. Examples of low-level image analysis processes include edge and arc detection, thresholding, and spatial and statistical classification. Medium-level processes include region growing, boundary detection, curve linking and relaxation labelling, amongst others. A large number of low- and medium- level algorithms have been developed and these are documented in the literature [Ballard and Brown, 1982; Rosenfeld and Kak, 1982; Pavlidis, 1982]. High-level segmentation methods utilise domain specific knowledge concerning the class of scenes that are to be understood [Argialas and Harlow, 1990]. They are therefore more sensitive to the context of the scene, and they are more responsive to the specific recognition needs. Examples of such techniques include semantic nets [Ballard and Brown, 1982], predicate logic and production rules.

2.5 GOAL-DRIVEN VERSUS DATA-DRIVEN ANALYSIS

Goal-driven image analysis is typically used when the image to be interpreted has a definite predefined structure. A example of a goal-driven vision system would be a system responsible for finding ribs in a chest x-ray [Ballard and Brown, 1982] . In such a case a great deal of knowledge is known *a priori* - such as the approximate location and shape of the ribs, as well as, the number of ribs likely to be found. The details concerning the high-level objects (the ribs) which need to be found in the scene can be quite accurately specified before the image is even processed. The high level objects are then decomposed into constituent medium-level objects, which are further subdivided into a configuration of primitives. The image can then be interpreted by trying to find the appropriate primitive configuration. The goals pertaining to the lowest level of the hierarchy first have to be achieved before moving on to the next level.

Top-down processing or goal-driven processing as described above is *not* suitable for the analysis of aerial images which have a highly variable structure that does not allow for stringent goal definitions. Most aerial image interpretation systems use a data-driven or bottom-up analysis strategy [Argialas and Harlow, 1990]. This involves starting at the bottom of the hierarchy and identifying primitives. These primitives are then combined into more general and meaningful entities. Rejection of candidate objects or patterns may occur frequently at points fairly deep within the hierarchy, as domain specific knowledge is brought to bear on the interpretation process.

The bottom-up analysis process is subject to several deficiencies, which are detailed in Argialas and Harlow, [1990]. These deficiencies arise from the fact that higher level knowledge is excluded from the low- and middle-level segmentation processes, which results in

these processes being less effective and more prone to error than they should be.

To conclude, a vision system should be both goal- and data-driven, in order to be able to take advantage of knowledge from any level at any stage of the analysis [Argialas and Harlow, 1990] . This has important ramifications for the design of the C++ class hierarchy, as the proposed classes must try to model this interdependence.

3. THE APPROACH TAKEN

The project is currently in the development phase, and several different methods of solution are being investigated. This section describes one of the possible avenues that is being explored and discusses the relevant issues that need to be considered.

It has been decided that the emphasis of the interpretation process should be placed on the identification of houses. Once such structures have been recognised it will be possible to generate a stand hypothesis for each house or building. These stand hypotheses will then be used as a starting point for planning the reticulation of the particular area.

Grey level orthophotographs at a scale of 1:10000 of rural areas are being used for initial testing. If the system cannot perform sufficiently well (see 3.1.1) with photographs at this scale then the scale will be reduced, or the resolution increased. The photographs are being scanned in, in a bitmap (BMP) format. The analysis algorithms mentioned in sections 3.2 and 3.3 will deal directly with the pixel intensities as they are contained in the BMP format.

3.1 OVERVIEW OF THE DESIGN

The system which has been designed is in essence a hybrid system (section 2.3), incorporating both per-pixel classification methods and structural methods of interpretation. Two low level methods are being used in the interpretation process, namely edge detection, and the use of a fractal error metric to detect man-made objects. Medium-level analysis will then be applied to the edge detected version of the image in order to remove spurious edges, link curves and ultimately find boundaries. Finally the processed edge-detected image will be combined with the results of the fractal error metric algorithm in order to generate building hypotheses.

The two different low-level approaches are co-relative in that an edge detection algorithm will find the *edges* of (for instance) a house, while the use of the fractal error metric will identify the *interior* of the house. Combining the two distinct methods should offer superior results as the methods complement one another.

3.1.1 Measuring Performance

As with the design of any system it is important to consider how one is to grade the performance of the system. The approach taken here is similar to that which has been taken in other vision systems. A human photo-interpretation of a particular scene will be viewed as the "ground truth" or the ideal for that scene. If one considers the domain of buildings and houses, then if the vision system is able to recognise 80% of the structures that a human photo-interpreter is able to recognise - it will be deemed to have performed successfully.

3.2 EDGE DETECTION

Simple edge detection algorithms are being investigated in order to determine how effective they are within the context of finding edges within aerial images. The two algorithms being considered are the Sobel edge operator [Ballard and Brown, 1982] and the Canny operator [Canny, 1986].

The medium-level analysis of the edge-detected image is more challenging. The aim of this analysis is to attempt to significantly reduce the number of edges, leaving behind only edges which form part of buildings. Venkateswar and Chellapa [1992] have made significant progress in this regard. They have developed a process for extracting straight lines from an edge-detected image. This involves scanning the edge image and labelling each edge pixel. Each of the edge pixels are then linked to form edges and collinear edges are merged. Edges of insignificant length, and isolated edges are removed. The medium-level techniques to be used in this system will be based on the concepts which form part of the work mentioned above.

3.3 FRACTAL ERROR

The fractal error metric has been shown to be a successful in discriminating man-made features from natural ones [Cooper, Chenoweth and Selvage, 1994]. This is because the metric is based on a fractional Brownian motion model and natural features tend to fit this model well, while man-made features do not and consequently have a much greater fractal error [Cooper et al, 1994].

Fractal error is calculated locally for each pixel in the original image. If one chooses an appropriate threshold it is possible to fairly successfully separate the pixels of the original image into two classes - one representing man-made features and representing natural features.

3.4 GENERATING A STAND HYPOTHESIS

In order to generate a stand/building hypothesis with a high degree of accuracy it is necessary to combine the above two processes. A well defined edge boundary which contains a large number of pixels having a high fractal error is a good candidate for a building. It will be necessary to find all such candidates in the image and

then to generate a vector map containing polygons approximating each of the stand/building hypotheses. Finally a user will be required to correct any incorrect hypotheses and to add to any buildings which have been excluded by the interpretation process. The vector map will then be suitable for input to the optimisation and routing routines that are currently being developed by other SED members (see section 4.1).

3.5 FUTURE ISSUES

The system which has been described does not perform any sort of high-level interpretation and it is felt that the incorporation of such techniques will improve the system's performance. Such a technique could be employed once all the building hypotheses for a scene have been generated. The interpretation system could then look for rows of houses and if a row appears to have a gap where a house should be, then the 'gap area' in the scene could be re-examined either with a different algorithm or with the algorithms already mentioned, but using slightly different thresholds and parameters. This requires a combination of both goal-driven and data-driven processing.

A high level interpretation technique could also be employed to relate a road finding subsystem to this building finding subsystem.

4. THE SOFTWARE IMPLEMENTATION

The software is being implemented in the C++ programming language using the object-oriented paradigm. The class hierarchy of the system has been designed and partially implemented. The design tries to reflect the conceptual ideas and relationships mentioned in section 2. These are namely the encapsulation and compartmentalisation of low-, medium- and high-level analysis techniques. However, as mentioned, communication needs to occur between the different levels involved in order to allow for both top-down and bottom-up analysis. There also has to some sort of entity which will have overall control of the interpretation process. This may or may not be the user - whatever the case it needs consideration and has been catered for in the design. It is extremely important that a design of this sort is modular because it allows for experimentation with different image analysis and interpretation techniques, and it allows the existing work to be easily extended in the future.

4.1 INTEGRATION INTO THE SED TESTBED

The software being developed for this project will be integrated into the SED testbed. The testbed is a collaborative effort by the SED team and it is being used for the testing of all the optimisation and routing software being developed by individual team members. The software developed for this project will integrate seamlessly with the testbed and in doing so, a complete reticulation solution will be achieved - starting with a scanned-in aerial photograph and ending with a reticulation design for the area represented by the photograph.

5. CONCLUSION

This paper has briefly presented the concepts behind and the design of an aerial image interpretation system. The system presented is a hybrid system, using both pixel-based classification techniques as well as structural techniques. The system has been designed in this manner in order to overcome the difficulties inherent to each technique alone. The implementation details of the design have also been addressed. The class hierarchy has been constructed in a modular and open-ended fashion, allowing for methods to be easily interchanged and for extensions to be added. In order to fully harness the benefits of the system, the system will be incorporated into a framework of tools which allow for planning the reticulation of electrical townships.

6. REFERENCES

Argialas D.P. and Harlow C.A. [1990], Computational Image Interpretation Models: An Overview and Perspective, *Photogrammetric Engineering and Remote Sensing*, vol. 56, no. 6, pp. 871-886

Ballard D. and Brown C. [1982], *Computer Vision*, Prentice-Hall

Canny J.F. [1986], A Computational Approach to Edge Detection, *IEEE Transactions on Pattern Analysis and Machine Intelligence*, vol. PAMI-8, pp. 679-698

Cooper B.E., Chenoweth D.L. and Selvage J.E. [1994], Fractal Error for Detecting Man-made Features in Aerial Images, *Electronics Letters*, vol. 30, no. 7, pp. 554-555

Pavlidis T. [1977], *Structural Pattern Recognition*, Springer-Verlag, Berlin

Quick P. [1995], Eskom Employee, E-mail correspondence and personal communication

Rosenfeld A. and Kak A. [1982], *Digital Picture Processing*, Academic Press, New York

Venkateswar V. and Chellapa R. [1992], Extraction of Straight Lines in Aerial Images, *IEEE Transactions on Pattern Analysis and Machine Intelligence*, vol. 14, no. 11, pp. 1111-1114

7. ADDRESS OF AUTHOR

Mr S. P. Levitt,
Department of Electrical Engineering,
University of the Witwatersrand,
Private Bag 3,
P.O Wits, 2050

A Technique for Automating Stands to Junction Allocation in Electrification Design using Heuristics

S.C.J Tumazos   B Dwolatzky   A.S Meyer
University of the Witwatersrand South Africa

This paper discusses an application that uses an Expert System Shell to automatically allocate stands to junctions in an effort to further enhance cost minimisation in a computer aided electric reticulation design system. This involves the incorporation of heuristic rules (a knowledge base) into an otherwise solely algorithmically driven optimisation process. The expert shell with its accompanying fuzzy logic ability is found to be suited to solving this problem, which is conventionally solved manually (artificial intelligence instead of human intelligence). The rule base and the incorporation of this application into the larger software system are also discussed.

1. Introduction

South Africa is at present faced with the huge task of providing electricity to about two thirds of the population who still do not have this facility. The cost of installation and maintenance of an electrical distribution system is known to comprise a larger cost than the actual production and distribution of the electricity to the consumer households. Therefore, the creation of an optimising reticulation system is being undertaken by the Software Engineering department at the University of the Witwatersrand. This system is currently named CART (Computer Aided Reticulation of Townships).

At present, CART is a system for designing reticulation networks and has the ability of aiding the user with his/her design. Most help comes in the form of 'cable type' optimisation. However, an Expert System Shell has been developed for CART to give it 'artificial intelligence'. An application named Automated Stand-to-Junction Allocation (ASJA) uses this new mechanism to enhance the automating ability of CART. Given an 'intelligent' township map, ASJA allocates each stand to a junction (load point), thereby grouping stands (which are allocated to the same junction) together. This is useful as it produces a region for each junction where the junction point is most likely to be positioned. Refer to [1] for more information on the underlying ideas and abilities of CART.

This paper examines the ability and viability of expert systems in power problems and notes the

capability of fuzzy logic which enhances expert systems. The rules (rule base) which are used to do the allocating is explored and exactly how ASJA fits into CART is explained.

2. Background to Heuristics

A heuristic is a rule of thumb, a principle that can prove useful in the solution of a problem, but does not guarantee a solution [6]. This is how heuristics differ from algorithms which are solution-guaranteeing procedures. This is not an entirely accurate description when it comes to solving problems using expert systems or fuzzy logic. The method which the expert system applies to reach its conclusions is precise, it will always produce a solution (although the validity is not definite) and the expert shell can display exactly which rules it utilised to come to a conclusion. However , the actual rules involved are not always rigorous. Such rules include 'rules-of-thumb' and various other rules which work without obvious reason. They work to steer the expert system in the right direction as opposed to presenting a solution. It is important to note that the bulk of the rules are not of that nature, but have logical and spatial reasons for working.

2.1 Expert Systems in General

The main components of an expert system are the knowledge base (comprised of a rule base and a data base) and the inference mechanism. The idea behind an expert system is to imitate the reasoning a human expert would go through to find a solution to a particular problem. Expert systems typically store information borrowed from these human experts in it's rule base. The data base stores the data that the rules will use in solving the problem, while the data defines the problem domain. The inference mechanism is the method whereby the rule base act on the knowledge base. The two basic methods are backward chaining and forward chaining.

Forward chaining involves making use of existing information to make inferences from rules to deduce new information until this engine finds (or doesn't find) a suitable solution to a query. On the other hand backward chaining starts with a goal which it

assumes to be true and attempts to prove or disprove it. Both methods use the rules to give simple 'true or false' answers. It is important to note that the rules are separate from the data which makes changing either a simple task. This attributes expert systems with high maintainability.

2.2 Fuzzy Logic in General

Fuzzy logic is a useful extension to the power of expert systems. Instead of the conventional binary nature of rules (true or false, 0 or 1), the rules can yield answers between 0 and 1. This adds a new dimension to the decision making ability of the expert system. In this fashion answers closer to, say, 1 would be 'more' correct to answers closer to 0. This gives a 'best' solution as opposed to a definite solution.

2.3 Heuristics in Power Reticulation

Expert systems in Power reticulation is not a new idea. Hsu et. al. [2] have used expert systems to facilitate in the location of substations and the determination of the feeder configuration. The power of the expert system is that one can get information from experienced reticulation designers and planners and then convert them into tangible rules that will be use in the rule base. Other papers on the application of expert systems in power include [3], [4], [5].

3. Design of the Stand Allocation System

The design of an expert system application begins with building a knowledge base which is made up of the data base and the rule base [2]. Another important issue is how the inference engine has access to the rule and data base. The rule base is the 'given' in the problem domain (i.e. the 'intelligent' map), while the rule base is a list of rules which is established by gathering the knowledge from experts in the given field (i.e. stand to junction allocation).

3.1 Problem Definition

The problem can be defined by what is given and what is required. The solution process is the expert rule base that is driven by the inference mechanism.

Given: A graphical map combined with a data base that defines graphical items.

Required: Regions, defined by groups of stands, which each define the feasible location of a low voltage junction.

3.2 Data Base

In this application the data base generally consists of the graphical information that is supplied by the 'intelligent' map (a graphical map combined with an informational data base - GIS system). Information in the data base include the stand positions, relationships between the stands (i.e. which stand is next to which other stands and along which borders), relationships between stands and roads and also the type of reticulation required (mid-block or no mid-block, underground, overhead, etc.). All this graphical and electrical information is converted into assertions which the inference engine can use when firing up the rule base.

3.3 Rule Base

The rule base consists of a series of rules that are used by the inference engine. ASJA asks the expert system repeatedly for suitable stands and each time the same rules are used in finding a new stand. The only difference between iterations is that the previously selected stand is no longer available for selection, but is now part of a junction region. This information is added to the data base as new assertions.

The rules deal with geographical information and other electrical considerations. Many rules are required in generating feasible regions. The basic rule that is used is: if a stand is next to a region then consider it for inclusion. Other factors are then taken into account, such as number of junctions already located, or whether mid-block routing is being used. Other elements of cable routing must also be considered. Depending on the type of routing, an example rule could be, say, not to group a stand to a junction region if there is a primary road between them.

An important feature of having the rule base separate from the data base is that either can be easily updated. The data base is updated continually when new stands are allocated to regions. However; the rule base is not changed on a regular basis. Better rules or new governmental rules can be entered into the rule base by the programmer or user without changing the C++ code. This makes the system very maintainable

3.4 How ASJA fits into CART

CART has a combination of reticulation optimisation tools. CART is programmed in C++ and is object

oriented, which makes it very maintainable. CART has the necessary design and infrastructure to make communication between its evolving GIS (Graphical Information System) and expert system seamless. ASJA is an object that can be called by other processes to specifically allocate stand regions to junctions. It has a method which repeatedly asks the expert system for new stands which it can join to the current junction region. After a stand is allocated the 'intelligent' map is updated with the new information i.e. the data base containing map information and the 'stand object' are updated for future iterations. A graphical representation is also displayed on the Graphical User Interface (GUI) which makes it easy for the user to note the junction regions. When the junction has enough stands allocated to it, the expert system informs ASJA, so that the next junction region can then be defined.

ASJA has access to the GIS data through object communication, while the rule base is simply read in from an ASCII rule base file. Any process can call ASJA, but only one process needs ASJA at the moment. This process involves the placement of a junction within a given junction region (i.e. ASJA's output is a required input). The process (Facility Location Optimisation) is being developed for CART by Justin Apostolellis.

4. Conclusion

Expert systems with the ability of using fuzzy logic are well suited to the problem of allocating stands to junctions. The main reason for this is that there are no mathematical algorithms as such that can solve this problem directly. Instead, 'rules-of-thumb' and other rules involving graphical and electrical logic are used. These rules could have been hard coded, but that would have severely impeded the high maintainability aspect of this solution and would have excluded other useful properties inherent in expert systems. Due to this successful application of expert systems within CART, other applications will be examined.

5. References

[1] Dwolatzky B, Meyer A.S, "The Development of an Integrated Set of Software Tools for the use in the Design of an electrical Reticulation Network", South African Universities Power Engineering Conference (SAUPEC) 95, Pretoria, January 1995.

[2] Hsu Yuan-Yih, Chen Jiann-Liang, "Distribution Planning using a Knowledge-Based Expert System",

IEEE Transactions on Power Delivery, Vol. 5, No. 3, July 1990.

[3] Shao Jinqiu, Rao N.D, Zhang Yimin, "An Expert System for Secondary Distribution System Design", IEEE Transactions on Power Delivery, Vol. 6, No. 4, October 1991.

[4] Sumic Z, Vankata S.S, Pistorese Todd, "Automated Underground Residential Distribution Design Part 1: Conceptual Design", IEEE Transactions on Power Delivery, Vol. 8, No. 2, April 1993.

[5] Sumic Z, Vankata S.S, Pistorese Todd, Helena Males-Sumic, "Automated Underground Residential Distribution Design Part 2: Prototype implementation and results", IEEE Transactions on Power Delivery, Vol. 8, No. 2, April 1993.

[6] Heil J, "First Order logic", Jones and Bartlett Publishers, England,1994, pp.99.

6. Address of Authors

Stavros Tumazos, Department of Electrical Engineering, University of the Witwatersrand, Private Bag 3, WITS, 2050

Dr Barry Dwolatzky, Department of Electrical Engineering, University of the Witwatersrand, Private Bag 3, WITS, 2050

Alan Meyer, Department of Electrical Engineering, University of the Witwatersrand, Private Bag 3, WITS, 2050

UTILISATION OF A RULE BASED EXPERT SYSTEM TO AID

IN POWER RETICULATION DESIGN

M.P Patricios   B Dwolatzky   A.S Meyer

University of the Witwatersrand, Johannesburg, South Africa

This paper presents a project in progress which, by means of rules in a custom rule-based expert system shell, aims to aid in the design of power reticulation systems. The advantage of this "expert" assistance over standard context-sensitive help is discussed with reference to a particular application in the domain; namely that of modeling non-domestic loads found in predominantly domestic areas.

1. INTRODUCTION

The drive to electrify the large percentage of South Africa which is without this facility will be taking place over the next twenty years. The need to develop power-reticulation designs as economically as possible is of major importance to these electrification programs.

The shortfall of technical skills and experience in this area have prompted the development of this project, in which a rule-based expert system is used as an integral part of an existing power-reticulation CAD system, Computer Aided Reticulation of Townships[1] (CART), to provide "expert" assistance to the user. This differs from standard context-sensitive help in that it may involve a certain amount of user-interaction as well as conditions and calculations, so that suggestions may be given to the user regarding various aspects of the reticulation design.

The system, as an integral part of the CAD system aims to provide an "artificially intelligent" help system, which will make up for the lack of skill in an inexperienced designer, and which will aid a more experienced designer to reach an end-design more quickly. This is achieved in the system by either attempting to come to some conclusion on an issue which the user is unclear on, or interactively checking the design to see if it contradicts any of the rules that have been provided to it, in which case the user can be warned that there is a problem with the design.

The expert system shell was developed utilising object-oriented design techniques and implemented using C++. The shell is general purpose and could easily be utilised for other applications. The functionality of the shell is discussed to emphasize the power that it wields within the CART system, and, given suitable rule-bases to work with, what it is capable of.

2. EXPERT SYSTEMS

An expert system is a software system which mimics the reasoning of a human expert in some particular field to provide solutions to real-world problems. A brief explanation of the functioning of expert systems in general follows, with particular emphasis on the system developed for this project (referred to as Cart Expert System, or CES, for the remainder of this paper).

2.1 Expert Systems in General

An expert system typically poses and answers questions relating to information which has been borrowed from human experts in the field and stored in the system's knowledge-base (or rule-base). Answers are automatically extracted from the data by an inference process which is invisible to the user. For a system to be useful, however, it should always be able to explain the steps it has taken in reaching the answers which it gives to the user.

The data in a rule-base is presented in a high-level, human-oriented manner. This data may often be vague and not be totally certain; thus facilitating the need for some sort of computational ability to represent the certainty of facts and evidence transmission [1]. In other words, a certain degree of *uncertainty* and *fuzziness* exists in most real world problems and should be representable in an expert system for it to be useful.

2.2 Components of an Expert System

An expert system consists of two basic components: the *knowledge-base* and the *inference mechanism*. A

---

[1] CART is an ongoing project at the University of the Witwatersrand. It provides an integrated set of software tools to aid in the design of reticulation systems, particularly for rural townships.

distinct separation between these two elements should exist and this characterises expert systems in contrast to conventional programming systems.

An expert system should have an interchangeable system for user-supplied rules and the assertions which would apply to them, with a separate inference-engine and parser. Most expert system shells work in this manner, including CES.

2.3 Functioning of an Expert System

Knowledge is represented in an expert system by *assertions* and *rules*. Assertions represent knowledge which is true at a particular time, such as *'Voltage is high'*; whereas rules contain a set of conditions (usually referred to as the left-hand side, or LHS, of the rule), as well as actions that should be taken upon the satisfaction of these conditions (usually referred to as the right-hand side, or RHS, of the rule). When the LHS of a rule is satisfied, the rule is said to be *triggered*. When the actions on the RHS are performed, the rule is said to be *fired*.

The LHS of a rule usually consists of a list of assertions which must all be true in order for the rule to fire. More complex systems may allow rules which include assertions related by logical operators other than AND (such as OR, NAND and NOR). CES provides this facility.

The RHS of the rules in the system characterise the system type. Two distinct types may be identified [2]. *Deduction systems* have rules whose RHS may only specify assertions to be placed in memory when the rule is fired. *Reaction systems* have rules whose RHS may specify any actions to be performed (rather than just assertions); these actions may include adding assertions, as well as retracting existing assertions, or executing some other procedure which may have nothing to do with assertions at all. Rules defined in the CES system may be of either type, or a mixture of the two - this is facilitated by splitting the RHS into distinct reactive and deductive parts.

In CES, incomplete assertions may be used in rules. These incomplete expressions contain markers indicating that there is a symbol (or symbols) missing from the expression. At run-time, pattern-matching techniques are used to instantiate valid symbols in these positions. At different times during the processing of the rule-base, several different symbols may be instantiated in these positions, depending on what is being sought by the expert system at that time.

CES also allows assumption-overrides on the LHS of rules. These are expressions which specify an assumption that may be made if the expression in question is not (or cannot be) solved. This assumption

may in turn be another expression containing an assumption and so forth.

This "assumption" feature of CES together with the symbolic pattern-matching facility give CES its real power.

2.4 Templates

CES supports the definition of *legal values* for assertions, which are templates which specify what assertions are valid. They allow strict control over the rule-base, particularly in the development phase.

CES also supports the definition of *questions*, which are templates which specify how the user should be prompted if a particular unknown cannot be resolved with rules alone, and user interaction is required. This allows CES to ask meaningful questions to the user.

2.5 Inference

Expert systems generally operate in one of two ways. The system can make use of existing assertions to make inferences from rules and deduce new information (*data-driven*), or the system may start with a goal, assume this goal to be true and then attempt to prove or disprove the validity of this assumption using rules (*goal-driven*).

As rules in the knowledge-base are processed by the engine, other rules -- which may not have initially been relevant -- become relevant; hence as inference starts, many rules may be processed in succession in a procedure referred to as rule-chaining. Rule-chaining occurs in either a forward or backward manner; forward-chaining is data-driven and backward-chaining is goal driven. CES performs both forward and backward chaining.

2.6 Certainty

In the real world, not all facts can be said to be one hundred percent definite. Some assertions may represent absolute certainty, whereas others may be less certain. Rule-based deduction systems usually associate a certainty factor with each assertion in working memory. This certainty factor is a value representing the degree of confidence in the certainty of that assertion. The certainty factor varies from 0 to 1, where 0 indicates that the assertion is definitely *false* and 1 that the assertion is definitely *true*. An assertion with a certainty factor of 0.5 thus has as much chance of being false as it has of being true. Assertions which have not been asserted at all (or were asserted and then retracted) have an unknown certainty. This unknown state is referred to as *nil* in CES.

The basic logical operators NOT, AND and OR (and all the others, which can be derived from these three) can still be used with this range of values $\{0..1\}$, which is actually a superset of the traditional Boolean set $\{0,1\}$. These definitions are as follows (with $x \; \varepsilon \; \{0..1\}$ and $y \; \varepsilon \; \{0..1\}$):

> $not \; x = 1 - x$
> $x \; and \; y = minimum(x,y)$
> $x \; or \; y = maximum(x,y)$

These definitions yield the same truth-tables as conventional Boolean logic when only the limits of the range (0 and 1) are used. This is called the *extension principle* [3], which states that the classical results of Boolean logic are recovered from these operations when all the members of the operand set are restricted to the traditional set $\{0,1\}$.

In order to trigger a rule, the certainty of the entire LHS of the rule must be determined. If this is not *nil*, the rule is triggered. If this certainty is less than one, it means that the conditions for firing the rule are not 100% definite; thus, the certainty of all the assertions made as a result of firing this rule should be scaled by this certainty factor.

2.7 Fuzzy Logic

Several expert systems, including CES, facilitate the definition of fuzzy subsets to represent ranges of values. Fuzzy subsets differ from traditional sets in that elements may have a degree of membership to the set, as opposed to either being a member or a non-member. This degree of membership is usually a value from 0 to 1 (much like certainty factors associated with assertions), a value of 1 indicates definite membership to the set and a value of 0 indicates non-membership.

Fuzzy subsets are useful for representing non-discrete concepts, such as "*tall*", "*medium*" and "*short*"

3. INTEGRATION OF CES WITH CART

At the stage of writing this paper, CES has been integrated into a "testbed" form of CART called the Software for Electrical Distribution (SED) Testbed. This program is a C++ implementation of CART, but lacks the CAD front-end. It was developed specifically to test modules which are being developed for future versions of CART (such as CES).

All the functionality of CES required for public access is encapsulated in one C++ class. Integration of CES with the SED Testbed involved linking this class (and its underlying supporting classes) into the testbed architecture. The CES class was also provided with references to some of the testbed classes; this gives

CES the ability to glean whatever data is required from the SED Testbed databases. This data includes network data (which junctions are connected to each other and what cables join them), graphical or spatial information (where all the various items on the map are positioned in space) and miscellaneous project data (information pertaining to the network and the area such as ADMD etc.)

The ability to use values from the SED Testbed databases greatly adds to the functionality of CES. It allows for future work which has rules relating to spatial information or network data; where the expert can fire off rules and check aspects of the design without superfluous user-interaction.

4. MODELING NON-DOMESTIC LOADS WITH THE EXPERT SYSTEM

When a network is being designed using the CART system, each consumer on the grid is considered to be a domestic load. The usual way of dealing with non-domestic loads (such as schools, shops, etc.) is to account for the larger power requirement by placing more than one domestic load on the stand point so that the non-standard load is seen as an integer multiple of a domestic load.

This practice implies that all non-standard loads have the same load-profile and diversity factor curve as domestic loads. This assumption is incorrect and can lead to the over-design of feeder-cables and distribution transformers when these loads are integrated into a system with domestic loads. The more the load-profile valleys overlap with domestic peaks (and vice-versa), the greater the error will be.

4.1 Representation of Non-Domestic Loads

CART calculates the current in a three-phase feeder cable supplying N consumers with the following equation:

$$I_F = NI_s \times CF(N) = \frac{NI_s}{DF(N)}$$

Where DF is the diversity factor, which is a function of N. DF accounts for the loss of diversity to be expected when a small batch of consumers are supplied with a particular cable. CF is the inverse of this, $1/DF(N)$, and is referred to as the co-incidence factor.

I_S is the current in the service cable. The worst-case for this current is $I_S = I_{max}$ (which, in CART, is defined as a constant value for a particular area).

Each domestic load contributes I towards the value of

N. A non-domestic load connected to the same cable might contribute a value other than I to this value. The amount it does contribute depends not only on its size, but also its load profile, whether it is a single-phase or three-phase load, and the value of N for the cable servicing it (before its contribution is added).

A non-domestic load in a domestic area is thus still modeled as a multiple of a domestic load, but this multiplier is determined taking into account more factors than just the size of the load. This multiplier is also not limited to only integer values. It should be noted that DF (or CF) is often read off a table representing the factor for discreet (integer) values of N. Thus, to calculate DF (or CF) for a non-domestic load with a non-integer multiplier, interpolation of a value from the table by considering the values at discreet points, is necessary.

4.2 The Rule-Base

The parameters of the load which affect the selection of the load multiplier are size (amount of power required), load-profile, whether the load will be supplied with single-phase or three-phase power, and the number of loads connected to the same junction as the non-domestic load.

The rule-base contains rules pertaining to all these factors. Some knowledge is gained from the SED Testbed databases, whilst other knowledge can be inferred from stored knowledge. Most of the knowledge however, can be inferred from information which is provided by the user as responses to questions posed by the expert system.

Inference of knowledge from other knowledge is the essence of an expert system. For example, the load-profiles for particular load types can be inferred by the expert system simply by knowing what sort of load it is (for example a school has a predictable profile). Uncertain facts, which may cause problems with an algorithmic approach, may be handled better by an expert system.

The data used in this rule-base (such as typical load profiles for different non-domestic loads) were taken from an undergraduate study done in a rural village in Lebowa [4]. This data is by no means accurate for all situations, but serves to illustrate the functionality of the system. A more detailed survey would be necessary for the final implementation of the system in CART.

4.3 User's View

This expert system application is always user-invoked. When using the SED Testbed and a non-domestic load is placed, the user may manually enter a multiplier, or request expert assistance by clicking a button. The

CES system is invoked and the non-domestic load modeling rule-base loaded into it. As the expert system works through the rules, questions are posed to the user to determine the nature of the load. Once the expert system has determined a multiplier for the load, the value is passed back to the SED Testbed to be inserted into the database. This value is always visible to the user who can manually adjust it if he strongly disagrees with the value determined by the expert system.

5. CONCLUSION

Expert systems hold much potential as part of the solution to make up for the shortfall of technical skills and experience of designers, not only in the field of power reticulation, but in all fields, particularly where computer-aided design plays an important role. This paper has presented rule-based expert systems and discussed the utilisation of one such system as an integral part of a CAD reticulation design program. The system, though still in its infancy, has proved to be a useful facility for a designer to have and with continued work, could grow to become an invaluable tool.

6. REFERENCES

[1]   Negotia, Constantin Virgil, "Expert Systems and Fuzzy Systems", Hunter College, City University of New York. Benjamin Cummings Publishing Co. Inc. 1985. pp.viii

[2]   Winston, Patrick Henry, "Artificial Intelligence", Massachusetts Institute of Technology. Addison-Wesley Publishing Co. 1992. pp. 120.

[3]   Horstkotte E, Joslyn C, Kantrowitz M, "Answers to Questions About Fuzzy Logic and Fuzzy Expert Systems", FAQ File fuzzy.faq version 1.8, April 7 1994. Section 2. Available via anon. FTP from ftp.cs.cmu.edu /user/ai/pubs/faqs/fuzzy/

[4]   Mascher A, "Research and Evaluating End Use Load Profiles of Typical Rural Commercial Users and their Integration into a Domestic Reticulation Design to Optimise its Cost-Effectiveness", Final Year Project Report, Department of Electrical Engineering, University of the Witwatersrand, November 1992.

7. ADDRESS OF AUTHOR

M.P Patricios
Department of Electrical Engineering
University of the Witwatersrand
Private Bag 3, PO Wits
2050

The Sensitivity of Calculated Voltage Drop to Changes in Load Sample Averaging Interval

RL Sellick[1], CT Gaunt[2], R Herman[3], CE Dingley[1]

[1] *Department of Electrical Engineering, University of Cape Town*
[2] *HKS Law Gibb, P O Box 3965, Cape Town, 8000*
[3] *Department of Electrical and Electronic Engineering, University of Stellenbosch*

ABSTRACT

This paper addresses the calculation of voltage drop on low-voltage feeders in residential areas, and is based on a final-year thesis by RL Sellick. The sensitivity of the Herman Beta algorithm for voltage drop calculation to the sample averaging interval used to derive the load model is investigated. The work is based on the use of one-minute sampled data taken by R Herman. The results of this paper include curves relating the sample averaging interval and the ADMD, some measure of the degree of sensitivity of the calculated voltage drop to a change in the sample averaging interval used for the load model, and information about the existence of a transfer function between different sample averaging intervals.

1. INTRODUCTION

In voltage drop calculations, the after-diversity maximum demand load current (ADMD) and the load current distribution are important factors. These parameters are derived from a load modelling process which has an attached sample averaging interval. It is important that the design engineer has a correct perception of the consumer load.. More specifically, an understanding of the limitations and capabilities of the calculation algorithm and representation is desirable.

This paper deals with the assumptions made by the voltage drop calculation process. Then, a network and calculation algorithm which form the basis of the comparison are presented. Next, the dependence of the ADMD on the sample averaging interval is given. Then, theory relating to a load model transfer function is proposed, and the dependence of the calculated voltage drop on the sample averaging interval is demonstrated. Finally, conclusions are drawn.

2. ASSUMPTIONS

Certain assumptions are made by the designer in order to simplify the calculation process. The following assumptions are made with respect to voltage drop calculations.
- the power factor is always at or close to unity.
- the system performance at any other instant throughout the year is no worse than during the instant of peak demand.
- the consumer load distribution fits a β-distribution. The appropriateness of modelling the load with a β-distribution, and the associated inaccuracies introduced, have been discussed [1,2]. The parameters describing a β-distribution are α and β, with a scaling factor, c_b.

3.   STANDARD TESTS

For the tests performed, a network and calculation algorithm are required, which will form the basis of the comparison. Using this algorithm, each combination of derived α and β values is passed through the network, and the results compared.

3.1 Benchmark network

The network given in Figure 1 has been chosen from work on benchmark studies [3]. It is a relatively balanced network, with 24 consumers distributed along the length of the feeder.
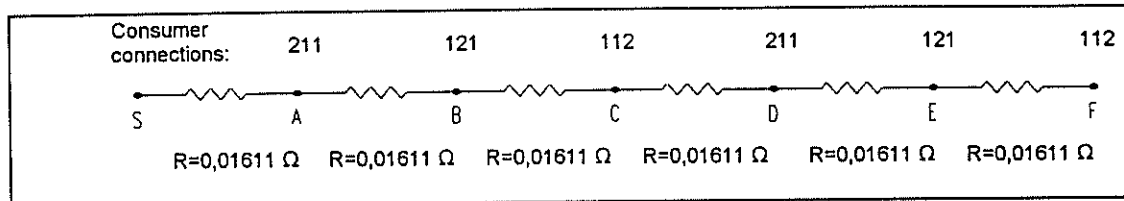
Figure 1: Benchmark network chosen for tests

The consumer connections apply to the red, white and blue phases respectively. All resistances quoted in ohms are the actual phase resistances of the conductors between successive kiosks. All neutral-to-line impedance ratios are taken as unity.

3.2 Calculation algorithm

The Herman Beta algorithm for voltage drop calculation has been chosen. All voltage drops will be calculated with this algorithm. Inaccuracies arise in this algorithm when the network is highly unbalanced, or has a most heavily loaded phase which "rotates" down the feeder. However, for a more typical network which is less extreme, such as that shown in Figure 1, the Herman Beta algorithm is consistently sufficiently accurate [3]. All calculated values are referenced against a Monte Carlo simulation, to test the calculation accuracy.

4.   DEPENDENCE OF THE ADMD ON THE SAMPLE AVERAGING INTERVAL

For each specific sample averaging interval, there are changes in the ADMD and the specific load current distribution. The magnitude of the peak demand on the system varies with the degree of smoothing, or sample averaging interval. Further, the instant of occurrence of the system maximum changes as the sample averaging interval is changed.

If the global average maxima for each sample averaging interval are plotted, ignoring the
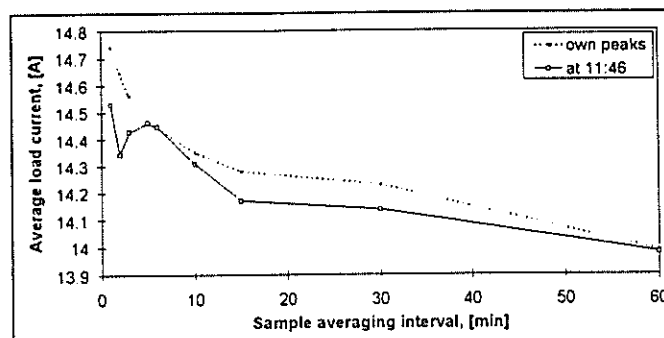
Figure 2:   Dependence of ADMD on sample averaging interval.

instants at which those maxima occur, the dotted line in Figure 2 results. However, the load distributions change with time. Thus, a reference instant is required for this investigation. The 5-minute peak, which occurs at 11:46 was chosen. Taking the average loads at 11:46, the solid line in Figure 2 results.

5. TRANSFER FUNCTION FOR THE PARAMETRIC LOAD DESCRIPTION

As the sample averaging interval is increased, the degree of smoothing on the load curves increases. This has an effect on the consumer load current distribution. This in turn affects the parameters which describe the β-distribution , namely α and β. The scaling factor, c_b, is taken as the circuit-breaker size.

A transfer function will allow the transformation of data describing one specific sample averaging interval to that describing another. Two theoretical transfer functions are a transform of the input load curve, or a transform of the parametric description of the input load curve.

Load curve transformation is impractical, due to the large amount of data to be considered. Further, there is a large amount of wasted calculation effort. The demand placed on the system for most of the day does not need to be taken into consideration by the designer. The sections requiring attention are when the demand is at, or close to, its peak. Thus, a function to transfer the parametric description of the load from one sample averaging interval to another is preferred.

Instead, consider the peak portions of the load curve only. The assumption is made that the parametric description of the peak demand on the system represents these portions. Further, assume that there is a relationship between the parameters describing the load distribution and the average currents used to obtain that load distribution. It is theoretically possible to obtain an n-th order transfer function to convert the description of one sample averaging interval to that of another.

The principles which should be observed in a generalised transfer function are that the values for α and β may never go below unity, and that the gradient of any transfer function will depend on the height of the value above unity. As a practical implementation of this transfer function, a ratio of the height of the points above unity is suggested. This ratio will be according to the heights of the values for α and β, as a function of the sample averaging interval. The hard boundary at unity is imposed by using the ratios of values above unity, and adding one. To generalise this transfer function, tests need to be performed on other data sets.

6. DEPENDENCE OF THE CALCULATED VOLTAGE DROP ON THE SAMPLE AVERAGING INTERVAL

Calculations were performed using the network and algorithm described in Section 3. These were done using the derived values for α and β for various sample averaging intervals. The calculated percentile voltage drops shown in Figure 3 result.

The calculated voltage drop increases with a decrease in the sample averaging interval. For a sample averaging interval of 5 minutes, the voltage drop calculated by the Herman Beta algorithm is 2.8% lower than that for a sample averaging interval of 1 minute. For a sample averaging interval of 30 minutes, the calculated value is 10.0% lower than that for 1
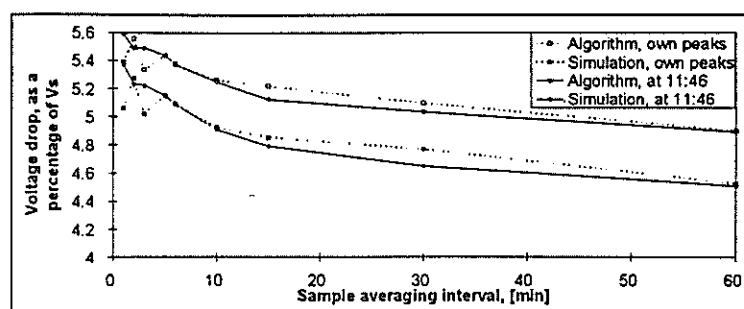
Figure 3: Dependence of the calculated voltage drop on the sample averaging interval.

minute. There is no significant change in the output of the Herman Beta algorithm with a change in the sample averaging interval.

7.   CONCLUSIONS

A change in the sample averaging interval causes a change in the instant of occurrence of the system ADMD, and thus also the magnitude of the ADMD. This is an important scaling factor in voltage drop calculations, and will thus impact the calculated voltage drop.

A transfer function which transforms the parametric description of the load for one sample averaging interval to that of another has been proposed. This incorporates practical limits on the domain of the describing parameters. However, for a generalised transfer function to be proposed, further data sets need to be examined.

A change in the sample averaging interval has an effect on the calculated voltage drop. Specifically, an increase in the sample averaging interval will result in a decrease in the calculated voltage drop.

The consideration of the sample averaging interval is important when voltage drop calculations are performed. This paper has demonstrated certain areas which are affected by the choice of sample averaging interval.

8.   ACKNOWLEDGEMENTS

REFERENCES

[1]   Herman R., "Voltage Regulation Analysis for the Design of Low Voltage Networks Feeding Stochastic Domestic Electrical Loads", University of Stellenbosch, 1993.

[2]   Sellick R.L., "The Sensitivity of the Calculated Voltage Drop to the Load Sample Averaging Interval", University of Cape Town, 1995.

[3]   Sellick R.L., Gaunt C.T., "Comparing Methods of Calculating Voltage Drop in Low Voltage Feeders", SAIEE Transactions, accepted for publication, September 1995.

Using the Bootstrap method for evaluating variations due to sampling in Voltage Regulation Calculations

R. Herman,
Dept. of Electrical and Electronic Engineering
University of Stellenbosch
STELLENBOSCH 7600

Abstract - This paper shows how the statistical technique called "bootstrapping" may be applied to an electrical distribution engineering problem to evaluate the effects of data sampling. In this case it is used to determine the effects of load current sampling variations on voltage drop calculations in low voltage residential feeders supplying stochastic domestic loads.

I. INTRODUCTION

The two basic procedures involved in the design of low voltage distribution feeders are their thermal sizing and the calculation of voltage regulation in the feeder. The voltage drop calculations used by designers are often based on empirical formulations. These empirical derivations attempt to compensate for the stochastic properties of the residential load currents. When the consumers are considered in groups, their aggregated load currents posses statistical properties. However, the exact description of the load current statistics have generally been misunderstood in the past.

In recent years inexpensive, micro-processor based data loggers have made it possible to collect load data for design purposes. Even with these sophisticated data acquisition systems there will always be some uncertainty about the validity and accuracy of the observed data. A statistical technique known as the bootstrap method has been applied to examine uncertainty in daily load model parameters by Belzer and Kellogg [1]. In this paper the bootstrap method is used to gauge the uncertainty resulting from the specific case of voltage regulation calculations that are based on a statistical load model derived from observed load current data.

II. TYPICAL RESIDENTIAL DISTRIBUTION NETWORK

In the typical South African method of distribution, the single-phase residential customers are connected between a phase and a neutral conductor of a three-phase, four-conductor, low-voltage feeder. The typical line-voltage would be 380 volts and the phase-to-neutral voltage would be 220 volts. The basic distribution network considered in this paper is shown in fig. 1.
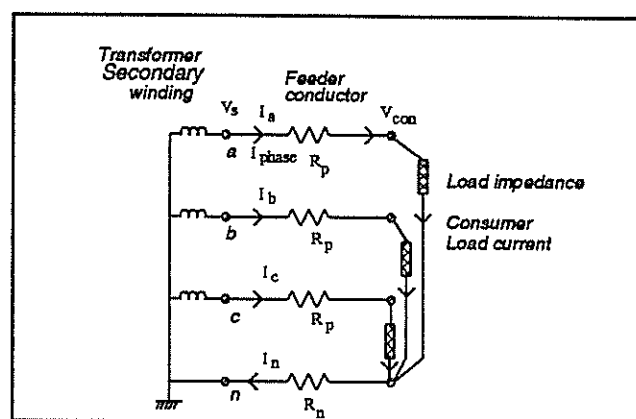
Fig. 1 Basic distribution network

III LOAD CHARACTERISTICS

Accurate cable and over-head line parameters are freely available. However, customer loads have to be modelled from sampled observations of customer load currents for expected load conditions. A variety of issues can affect the accuracy and validity of these data. These include the size of the sample, accuracy of the data loggers, accuracy of the load transducers and the homogeneity of the sample. It is therefore imperative to account for these variations in the design procedure. The effect of load current sampling variations will be investigated using the bootstrap method.

Research has been done locally for some years into the characteristics of grouped residential electrical load currents. Individual load currents were monitored concurrently at predetermined averaging intervals using locally developed data loggers.
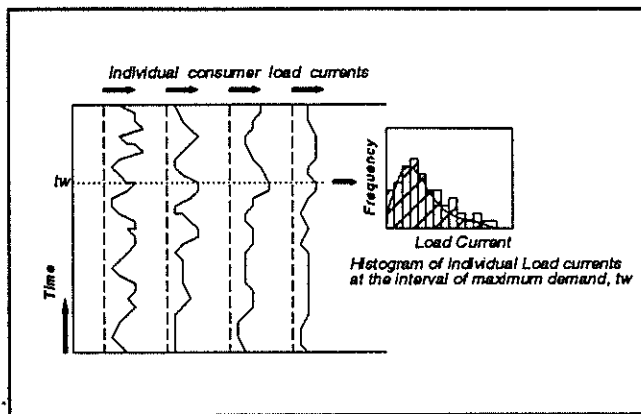
Fig. 2 Diagrammatic representation of the variation of individual customer load currents with time

Fig. 2 illustrates the typical behaviour of such loads. The design of the low voltage distribution network must be based on the maximum collective loading conditions expected. Note in fig. 2 that this maximum demand occurs at the time interval indicated as tw. At this time-slot the individual load currents may be represented in the form of a load current histogram - shown in the inset. These sampled load currents may now be used to calculate voltage drops in the low voltage feeders. We note that by considering the loading at the time interval of the system maximum demand, tw, we no longer have a time-dependent load signal but a **load current statistic**. Since the load currents are statistically distributed, the feeder voltage drop will also be statistically distributed. A single design quantile must be extracted from this distribution of voltages, for a specified level of risk for design purposes.

It has been found that an appropriate statistical model for these sampled currents was the Beta distribution function [2]. This departs from previous work that assumed that the Gaussian, or normal distribution was adequate for the purpose [3]. Essentially, the arguments in favour of the beta model are:

(a) Observed distributions can be asymmetrical. The Beta distribution can be skewed either to the right or the left. Both conditions have been found to exist in residential load current distributions.

(b) It is supported on a finite base - it has a lower and an upper limit. This corresponds to zero load current and a maximum value, usually determined by a circuit breaker size.

The individual load currents in the basic network are sampled at random from the population probability distribution of individual load currents. The magnitudes of the feeder voltage drops will be a function of the feeder resistance and the load current distribution resulting from the

number of customers connected to each of the phase conductors. .

Suppose that the actual population distribution function, F of load currents is given. Then there are basically two methods of deriving the distribution of the customer voltage, V_{con}, from F. One is to simulate the voltage drops by successively drawing random sample currents from the observed load data, combining them according to the customer connections and then calculating the resultant voltages. For this purpose the raw load data may be used or the currents may be randomly generated from a statistical parametric description of the observed load data. The other method would be to estimate the statistical parameters of the load current probability distribution function and then to develop an analytical procedure, using a knowledge of the characteristics of the distribution function. Such an analytical method has been developed for calculating the voltage drops in the feeders carrying stochastic load currents, using the beta model [4]. The resulting formulation is simple to apply and may be incorporated into a standard spread-sheet program.

Whatever method is used (simulation or analytical), the distribution of V_{con}, and any characteristics thereof, such as a "design quantile", Q_v, is a function of F. Call it $Q_v(F)$. In practice F is never exactly known. It has to be estimated by sampled observations from the population of customers. The histogram in fig.2 depicts an estimate of the probability density function corresponding to F. The empirical cumulative distribution function derived from the same data is an estimate F_n, of F. The actual quantile Q_v (F) is in practice estimated by, say, $Q_v(F_n)$ and a fundamental issue is the uncertainty (error) associated with this estimate owing to F_n being used instead of F. Further uncertainties may be encountered when the simulation method is used. These include inaccuracies resulting from too few samples being drawn and/or errors in the random number generators. A cumulative distribution of the probable customer terminal voltage is shown in fig.3, illustrating these uncertainties.

There are two ways of considering the uncertainties depicted in fig. 3. It is observed that there is a range of likely customer voltages for a given level of risk. These probable values would form part of a distribution with the greatest likelihood somewhere between the two extremes shown. Alternatively, for a given value of customer voltage there is a range of percentiles, or risk levels. In this paper we investigate a method for evaluating the variational effects that the load current sampling has on the estimated value of the customer voltage.
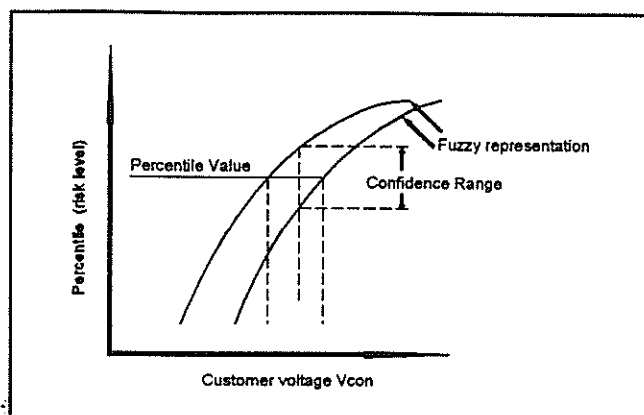
Fig. 3 Uncertainty associated with voltage drop calculations

IV. THE BOOTSTRAP METHOD FOR EVALUATING UNCERTAINTY

In general terms $Q_v(F)$ and its estimation by $Q_v(F_n)$ is considered. Owing to the complexity of the dependence of Q_v on F it is not generally possible to give a simple expression of, for example, the standard error of the estimate $Q_v(F_n)$. If F were known it would be possible to generate repeated samples of size n from the population and from the resulting sequence of Q_v values to evaluate the uncertainty associated with the estimate $Q_v(F_n)$, in particular its standard error. However, F is not known and in the algorithm for finding the standard error F itself has to be replaced by the observed empirical F_n.

This procedure, which is generally applicable to a variety of engineering problems, is known as the "bootstrap method" [5]. Random resampling, with replacement, is done from F_n to produce exactly n "bootstrap samples" and their corresponding estimates $F_{n,1}, F_{n,2} \ldots F_{n,B}$. Each of these is then used to calculate the quantile values $Q_v(F_{n,1})$, $Q_v(F_{n,2}) \ldots Q(F_{n,B})$. The statistical distribution of these values gives an indication of the variability of the estimates of $Q_v(F)$ derived from n sampled observations taken from the population, F. The number B is referred to as the "bootstrap sample size". For the purpose of obtaining the standard error of $Q_v(F_n)$ the bootstrap sample size need not be very large.

V. APPLICATION OF THE BOOTSTRAP METHOD TO VOLTAGE CALCULATIONS

The load data in this investigation were collected concurrently from 71 individual customer connections in what was regarded as an acceptably homogeneous residential area. The analogue-to-digital resolution is 8-bits and the over-all accuracy of the system (including the current-to-voltage transducers) is approximately 2.5% of full-scale

value. An analogue low-pass filter with a 2-second time constant is used to convert the rectified and scaled input signal into current measurements. These sampled measurements are then averaged over a sampling interval of 1-minute. The set of load currents at the time of annual maximum demand (tw) is used for calculating the expected worst case voltage drops.

The bootstrap method is illustrated by applying it to the simulation method of calculating voltage regulation for a simple case. Here the phase and neutral conductor resistances (R_p and R_n) are equal to 0.1 ohm each and one customer is connected to each phase, i.e. m = 3 (ma = mb = mc = 1). Phase-to-neutral supply voltage is taken as 220 volts. It is convenient to use standard computer packages such as Matlab® and Statgraphics® for these calculations. The algorithms developed in reference [4] may be performed on a standard spread-sheet, without recourse to simulation.

The Matlab® program of the simulation procedure is shown in fig 4. In the first block the load current data from the 71 observations are read in. Next, Bootstrap resampling is done to give a new set of 71 currents - "Fn(i)". This random resampling must be done with replacement. Selection of values are next assigned to R_p, R_n and to the number of customers on each phase ma, mb and mc. Random selection of load currents from the bootstrap load data array is performed in the next block. A total of m, (ma + mb + mc), random samples are drawn. In the case analysed m = 3. In the next block the quadrature components of the voltage drop, ΔV_{re} and ΔV_{im}, due to the m=3 randomly selected currents are calculated. The customer voltage is then:

$$V_{con} = V_s - (\Delta V_{re} + j\Delta V_{im}) \qquad (1)$$

The simulation count, ns, is now updated and the process repeated. A suitably large number of simulations must be done, say 1 000. An array of (1000) "Qv1", simulations is thus obtained for the first bootstrap sample. For the purposes of the analysis, 90- and 95-percentile values were determined from this array of voltages. Alternatively, the analytical method referred to earlier [4] may be used at this stage, where new statistical distribution parameters for the beta distribution model are determined after each "bootstrap sample". The whole process is repeated (ensuring that a reliable random number generator is used) a significant number of times. 40 bootstrap samples (bootstrap sample size, B = 40) were done in the investigation. These 40 sets of results yielded the statistics shown in Table 1.

The voltage regulation is usually given as the scalar difference between the supply voltage, V_s = 220 volts, and the quantile customer voltage, V_{con}.

```
Load Currents;
for i = 1:71;
        Boot(i) = round(rand*70)+1; {Bootstrap sampling}
        Fn(i) = Currents(Boot(i));
end;

rp = 0.1; {Voltage drop simulations}
rn = 0.1;
m = 3:
for ns = 1:1000;
        for i = 1:m;
                user(i) = round(rand*70)+1);
        end;
        ia = 0; {Balance customers among phases}
        ib = 0;
        ic = 0;
        count = 1;
        while count<=m;
                iuser(count) = Fn(user(count));
                ia = ia+iuser(count);
                count = count + 1;
                if count <= m;
                        iuser(count) = Fn(user(count));
                        ib = ib+iuser(count);
                        count = count+1;
                end;
                if count<=m;
                        iuser(count) = Fn(user(count));
                        ic = ic+iuser(count);
                        count = count+1;
                end;
        end;
        q = sqrt(3)/2;
        j = sqrt(-1);
        real = (rp+rn)*ia - rn*(ib+ic)/2;
        imag = J*q*rn(ib - ic);
        dv(int) = 220 - abs(220 - (real+imag));
        vint(ns,:) = dv(int);
        dvv(ns) = vint(ns,:);
        dvr = (dvv)';
end;
save Qvl dvr /ascii;
end.
```

Fig. 4 Matlab® Program for Bootstrap calculations

	V_{con} - 90%-tile	V_{con} - 95%-tile
Mean	216.73	216.17
Std Deviation	0.20	0.31

Table 1. Bootstrap analysis statistics

Assuming that the distribution of the estimates of the voltages are Gaussian at a given quantile, then the results of the analysis may be described as follows:

"There is a 95% probability that the 90-percentile customer voltage is 216.73 ± 0.388 volts and for the 95-percentile it is 216.17 ± 0.615 volts."

The results thus show that the variation in voltage

regulation calculation expressed as a percentage of the mean, for a 95% probability, is ± 11.87% for the 90-percentile value and ± 16.06% for the 95-percentile value. This is a surprising result and exceeds the expected accuracy of the measuring equipment by a large margin, even though every care was taken to ensure correct measurement. It accentuates the necessity for accurate and representative load data acquisition for the purposes of distribution network design.

VI. CONCLUSION

The bootstrap technique has been shown to be effective in determining uncertainty in voltage regulation calculations in low voltage distribution networks that are based on sampled load current data. The method is a general one and may have further application in other areas of uncertainty.

VII. REFERENCES

[1]   D.B. Belzer and M.A. Kellogg, "Incorporating sources of uncertainty in forecasting peak power loads - a Monte Carlo analysis using the extreme value distribution," *IEEE Transactions on Power Systems*, vol. 8, no. 2, pp 730 - 736, May 1993.

[2]   R. Herman and J.J. Kritzinger, "The statistical description of grouped domestic electrical load currents," *Electric Power Systems Research*, vol. 27, no. 1, pp 43 - 48, May 1993.

[3]   M. Davies and R.G. Paterson, "Phase unbalance in low voltage distribution systems," *Proc. IEE*, Part 109A, pp. 535 - 542, 1962.

[4]   R. Herman, J.S. Maritz and J.H.R. Enslin, "The analysis of voltage regulation in residential distribution networks using the beta distribution model", *Electric Power Systems Research*, vol. 29, no. 3, pp 213 - 216, 1994.

[5]   *An introduction to the Bootstrap*, B. Efron and R.J. Tibshirani, Chapman and Hall, 1993.

MODELLING OF A WRITTEN-POLE SYNCHRONOUS MOTOR

BY H.G. ACAR & C.F. LANDY

UNIVERSITY OF THE WITWATERSRAND, JOHANNESBURG, SOUTH AFRICA

1.ABSTRACT:

The mathematical and computer modelling of rotating electrical machines is aided by the use of generalized electrical machine theory which is based on the linear functions of the electrical quantities [2]. This paper presents an introduction to the principle and the d-q axis modelling of a new structure of synchronous machine using the generalized electrical machine theory as appliedto the analysis of a conventional synchronous machine.

2.INTRODUCTION:

In recent years work in the field of magnetic materials has significantly improved the performance of synchronous motors [1]. The written-pole synchronous machine has a continous ferrite-magnetic layer on the surface of the rotor which substitutes for the field system. The main windings of the stator are similiar to those of conventional machines [3]. A single exciter winding is located on the stator for writing salient poles continously and instantaneously on the ferrite-magnetic layer with any desired pole pattern, while the machine is running. Starting torque is provided by designing the motor magnetic circuit to allow for hysterisis torque and via the squirrel cage [3]. In a conventional synchronous motor the position of the field m.m.f is stationary with respect to the winding of origin.The technique applied here provides an effective way for controlling the position of the field flux vector with respect to the ferrite-magnetic layer which acts as the rotor field winding of a conventional synchronous motor. By controlling the position of the flux vector the motor can be operated at unity power factor. This feature provides torque control over a wide range. The principle applied here is to energize the exciter winding with DC at about 80 % of the mechanical synchronous speed [3] . By writing poles in this way the field flux vector can be surpassed according to the three phase winding flux vector. By creating this artifical misalignment repeatedly the motor will accelerate with the maximum synchronous torque to a predetermined mechanical synchronous speed. After reaching the synchronous speed the exciter can be turned off and the motor will continue to operate as a permanent magnet synchronous motor [3].
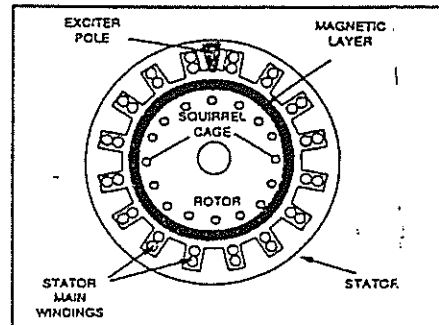
Fig 1: Construction of "Written-Pole" motor

3. THEORY OF MODELLING A WRITTEN-POLE SYNCHRONOUS MACHINE :

In machine analysis it is often convenient to interchange the rotor and stator windings.[4]. The modelling of the Written-Pole machine will comprise a salient pole stator. The stator is provided with two orthogonal axes of symmetry ; a d-axis coincident with the pole axis and a q-axis situated midway between poles. Since the field flux vector can be repositioned according to the winding, the field winding is represented as two windings; F_D and F_Q. The strength of the field produced by the ferrite magnetic material is constant. Since the squirrel cage supplies starting torque, the analysis will assume the presence of damper windings as s and t.
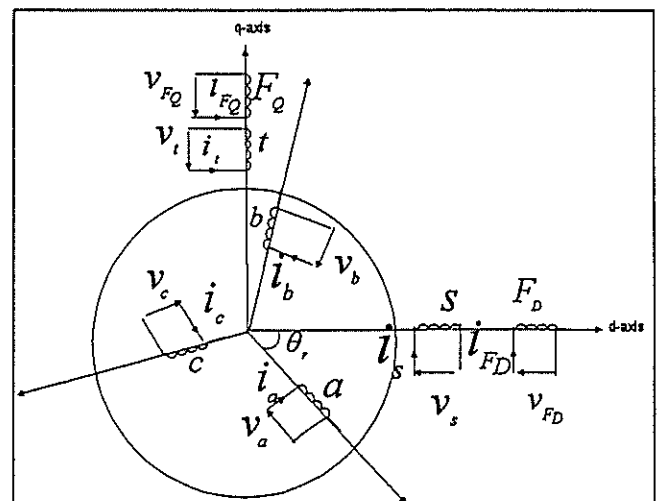
fig 2: Three phase winding represantation of a Written-Pole synchronous machine

3.1 Machine analysis and inductances:

In fig. 3 the Written-Pole machine is represented as an equivalent d-q axis machine comprising a stationary array of stator coils and pseudo- stationary rotor coils. To determine the primitive machine inductances the windings are transformed to $dq\gamma$ axis quantities using abc to $dq\gamma$ transformations.
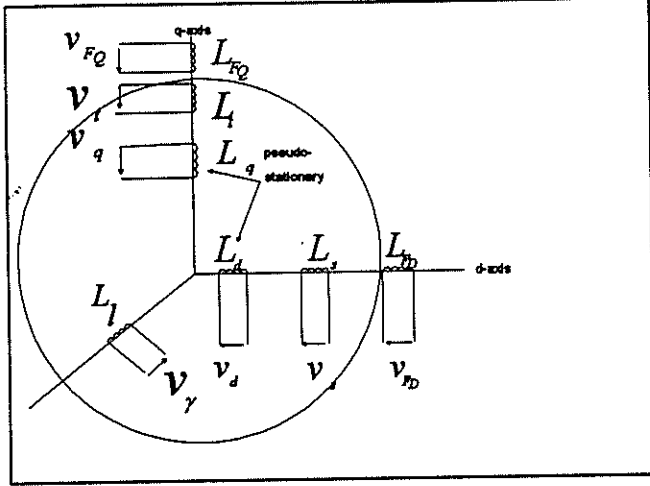
fig 3: d-q axis coil inductances

4.THREE PHASE WINDING TRANSFORMATIONS

Stationary and rotating three-phase windings can be represented as an equal part of the d-q axis machine coil structure. The method adopted here is first to establish a transformation between a three phase (abc) and two phase $(\alpha\beta)$ winding. Then a second transformation is performed between the rotating two-phase $(\alpha\beta)$ and stationary two - phase (dq) windings.

4.1Transformation between three-phase (abc) and two-phase ($\alpha\beta\gamma$) winding:

Referring to figure 4 the three-phase winding, supported by a cylindrical magnetic structure is represented.Resolving instantaneous m.m.f.s along the ($\alpha\beta$)axes and arranging them to give an inverse relationships, three-phase m.m.f.s and two-phase m.m.f.s are given as:
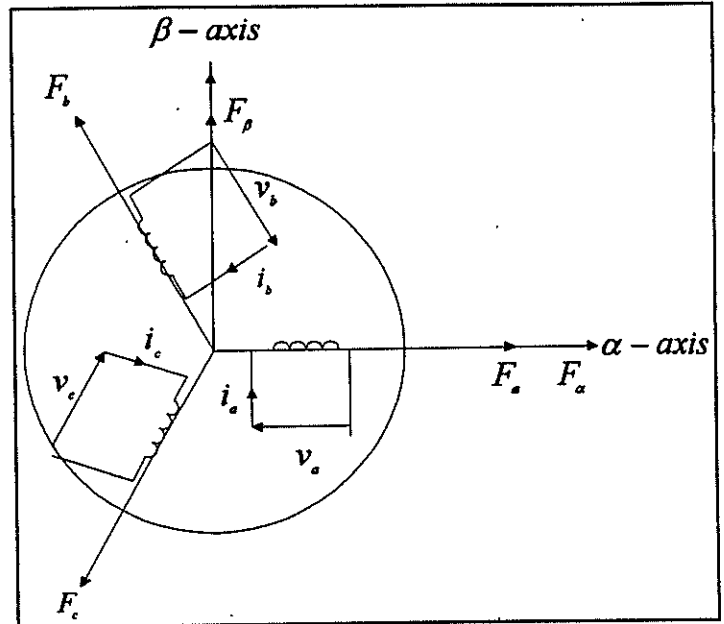
fig4: Three-phasecylindrical rotor winding

$$\begin{bmatrix} F\alpha \\ F\beta \\ F\gamma \end{bmatrix} = \begin{bmatrix} 1 & -\frac{1}{2} & -\frac{1}{2} \\ 0 & \frac{\sqrt{3}}{2} & -\frac{\sqrt{3}}{2} \\ m & m & m \end{bmatrix} \begin{bmatrix} F_a \\ F_b \\ F_c \end{bmatrix}$$

inverting this matrix gives,

$$\begin{bmatrix} F_a \\ F_b \\ F_c \end{bmatrix} = \frac{2}{3}\begin{bmatrix} 1 & 0 & \frac{1}{2m} \\ -\frac{1}{2} & \frac{\sqrt{3}}{2} & \frac{1}{2m} \\ -\frac{1}{2} & -\frac{\sqrt{3}}{2} & \frac{1}{2m} \end{bmatrix} \begin{bmatrix} F\alpha \\ F\beta \\ F\gamma \end{bmatrix}$$

These two equations can be written as:

$$\left[F_{\alpha\beta\gamma}\right]=[A]\left[F_{abc}\right] ; \left[F_{abc}\right]=\left[A^{-1}\right]\left[F_{\alpha\beta\gamma}\right]$$

where $m=\frac{1}{\sqrt{2}}$

$$[A]=\sqrt{\frac{3}{2}}[B] \quad \text{and} \quad \left[A^{-1}\right]=\sqrt{\frac{2}{3}}[B_t]$$

where $[B]=\sqrt{\frac{2}{3}}\begin{bmatrix} 1 & -\frac{1}{2} & -\frac{1}{2} \\ 0 & \frac{\sqrt{3}}{2} & -\frac{\sqrt{3}}{2} \\ \frac{1}{2} & \frac{1}{2} & \frac{1}{2} \end{bmatrix}$ thus $\left[F_{\alpha\beta\gamma}\right]=\sqrt{\frac{3}{2}}[B][F_{abc}]$

and $\left[F_{abc}\right]= \frac{2}{3}[B_t]\left[F_{\alpha\beta\gamma}\right]$.   For balanced conditions

$F_a+F_b+F_{c=0}$ and $F_\gamma =0$

Voltage and current transformations:

$$\left[V_{\alpha\beta\gamma}\right]=[B][V_{abc}] ; \left[i_{\alpha\beta\gamma}\right]=[B][i_{abc}]$$

$$\left[V_{abc}\right]=[B_t]\left[V_{\alpha\beta\gamma}\right] ; \left[i_{abc}\right]=[B_t]\left[i_{\alpha\beta\gamma}\right]$$

impedance, inductance and flux-linkage transformations are of the same order as the current and voltage transformations.

4.2 Transformation between three-phase (abc) and two phase ($dq\gamma$) windings.

In figure 5 the three phase abc winding and its supporting cylindrical structure is now assumed to rotate clockwise with angular velocity ω_r electrical rad/sec. Resolving F_α and F_β along the d-q axes and writing these equations in matrix form to obtain direct transformation between a rotating three-phase (abc) and stationary ($dq\gamma$) windings
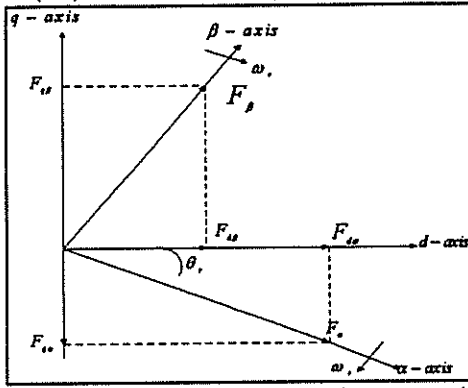
fig5: Transformations from $(\alpha\beta)$ to fixed (dq) axes

$$\begin{bmatrix} F_d \\ F_q \\ F_\gamma \end{bmatrix} = \begin{bmatrix} \cos\theta_r & \sin\theta_r & 0 \\ -\sin\theta_r & \cos\theta_r & 0 \\ 0 & 0 & 1 \end{bmatrix} \begin{bmatrix} F\alpha \\ F\beta \\ F\gamma \end{bmatrix}$$

where $\left[F_{dq\gamma} \right] = \left[S \right]\left[F_{\alpha\beta\gamma} \right]$

inverse relationship ;

$$\begin{bmatrix} F_\alpha \\ F_\beta \\ F_\gamma \end{bmatrix} = \begin{bmatrix} \cos\theta_r & -\sin\theta_r & 0 \\ \sin\theta_r & \cos\theta_r & 0 \\ 0 & 0 & 1 \end{bmatrix} \begin{bmatrix} F_d \\ F_q \\ F_\gamma \end{bmatrix}$$ where $\left[F_{\alpha\beta\gamma} \right] = \left[S_t \right]\left[F_{dq\gamma} \right]$

combining these results with the previous transformations, the inductance matrix becomes as:

$$\left[L_{dq\gamma FDstFQ} \right] = \begin{bmatrix} L_d & 0 & 0 & M_{dFD} & M_{ds} & 0 & 0 \\ 0 & L_q & 0 & 0 & 0 & M_{qt} & M_{qFQ} \\ 0 & 0 & L_l & 0 & 0 & 0 & 0 \\ M_{dFD} & 0 & 0 & L_{FD} & M_{FDs} & 0 & 0 \\ M_{ds} & 0 & 0 & M_{sFD} & L_s & 0 & 0 \\ 0 & M_{qt} & 0 & 0 & 0 & L_t & M_{tFQ} \\ 0 & M_{qFQ} & 0 & 0 & 0 & M_{FQt} & L_{FQ} \end{bmatrix}$$

and defining mutual inductance coefficients

$$M_{dFD} = M_{FD} = \sqrt{\tfrac{3}{2}} M_{rFD}$$

$$M_{ds} = M_{sd} = \sqrt{\tfrac{3}{2}} M_{rs}$$

$$M_{qt} = M_{tq} = \sqrt{\tfrac{3}{2}} M_{rt}$$

$$M_{qFQ} = M_{FQ} = \sqrt{\tfrac{3}{2}} M_{rFQ}$$

Forming the rotational coefficient matrix $[G]$ in terms of inductance coefficients :

$$\left[G_{dq\gamma FDstFQ} \right] = \begin{bmatrix} 0 & -L_q & 0 & 0 & 0 & -M_{qt} & -M_{qFQ} \\ L_d & 0 & 0 & M_{dFD} & M_{ds} & 0 & 0 \\ 0 & 0 & 0 & 0 & 0 & 0 & 0 \\ 0 & 0 & 0 & 0 & 0 & 0 & 0 \\ 0 & 0 & 0 & 0 & 0 & 0 & 0 \\ 0 & 0 & 0 & 0 & 0 & 0 & 0 \\ 0 & 0 & 0 & 0 & 0 & 0 & 0 \end{bmatrix}$$

5.VOLTAGE AND TORQUE EQUATIONS:

Substituting the $[G],[L]$ and $[R]$ matrices in the general voltage equation and writing $v_s = v_t = 0$ as coils s and t represent closed damper winding

$$\left[V_{dq\gamma FDstFQ} \right] = \left\{ \left[R_{dq\gamma FDstFQ} \right] + \left[L_{dq\gamma FDstFQ} \right] p + \omega_r \left[G_{dq\gamma FDstFQ} \right] \right\} \left[I_{dq\gamma FDstFQ} \right]$$

$$\begin{bmatrix} v_d \\ v_q \\ v_\gamma \\ v_{FD} \\ v_s = 0 \\ v_t = 0 \\ v_{FQ} \end{bmatrix} =$$

$$\begin{bmatrix} (R+pL_d) & -\omega_r L_q & 0 & M_{dFD}p & M_{ds}p & -\omega_r M_{qt} & -\omega_r M_{qFQ} \\ \omega_r L_d & (R+pL_q) & 0 & \omega_r M_{dFD} & \omega_r M_{ds} & M_{qt}p & M_{qFQ}p \\ 0 & 0 & (R+pL_l) & 0 & 0 & 0 & 0 \\ M_{dFD}p & 0 & 0 & (R_{FD}+pL_{FD}) & M_{FDs}p & 0 & 0 \\ M_{ds}p & 0 & 0 & M_{sFD}p & (R_s+pL_s) & 0 & 0 \\ 0 & M_{qt}p & 0 & 0 & 0 & (R_t+pL_t) & M_{tFQ} \\ 0 & M_{qFQ}p & 0 & 0 & 0 & M_{FQt}p & (R_{FQ}+pL_{FQ}) \end{bmatrix} \begin{bmatrix} i_d \\ i_q \\ i_\gamma \\ i_{FD} \\ i_s \\ i_t \\ i_{FQ} \end{bmatrix}$$

expanding this equation

$$V_d = Ri_d + p(L_d i_d + M_{dFD} i_{FD} + M_{ds} i_s) - \omega_r \left(L_q i_q + M_{qt} i_t + M_{qFQ} i_{FQ} \right)$$

$$V_q = Ri_q + p(L_q i_q + M_{qt} i_t + M_{qFQ} i_{FQ}) + \omega_r (L_d i_d + M_{dFD} i_{FD} + M_{ds} i_s)$$

$$V_\gamma = Ri_\gamma + p(L_l i_\gamma)$$

$$V_{FD} = R_{FD} i_{FD} + p(M_{dFD} i_D + L_{FD} i_{FD} + M_{FDs} i_s)$$

$$V_s = 0 = R_s i_s + p(M_{ds} i_d + M_{sFD} i_{FD} + L_s i_s)$$

$$V_t = 0 = R_t i_t + p(M_{qt} i_q + L_t i_t + M_{tFQ} i_{FQ})$$

$$V_{FQ} = i_{FQ} R_{FQ} + p(M_{qFQ} i_q + M_{FQt} i_t + L_{FQ} i_{FQ})$$

where $p = \dfrac{d}{dt}$

torque equation;

$$T_e = (pole - pairs) \times \left[i_d i_q i_\gamma i_{F_D} i_s i_t i_{F_Q} \right] \left[G_{dqrF_D sF_Q} \right] \left[i_d i_q i_\gamma i_{F_D} i_s i_t i_{F_Q} \right]$$

substituting the matrices in torque equation;

$$T_e = (pole - pairs) \times \left[i_d i_q i_\gamma i_{F_D} i_s i_t i_{F_Q} \right]$$

$$\begin{bmatrix} 0 & -L_q & 0 & 0 & 0 & -M_{qt} & -M_{qF_D} \\ L_d & 0 & 0 & M_{dF_D} & M_{ds} & 0 & 0 \\ 0 & 0 & 0 & 0 & 0 & 0 & 0 \\ 0 & 0 & 0 & 0 & 0 & 0 & 0 \\ 0 & 0 & 0 & 0 & 0 & 0 & 0 \\ 0 & 0 & 0 & 0 & 0 & 0 & 0 \\ 0 & 0 & 0 & 0 & 0 & 0 & 0 \end{bmatrix} \begin{bmatrix} i_d \\ i_q \\ i_\gamma \\ i_{F_D} \\ i_s \\ i_t \\ i_{F_Q} \end{bmatrix}$$

expanding this matrix for total electromagnetic torque;

$$T_e = (pole - pairs) \times$$

$$\left[(L_d - L_q) i_d i_q + i_q i_{F_D} M_{dF_D} + i_q i_s M_{ds} - i_t i_d M_{qt} - i_d i_{F_Q} M_{qF_Q} \right]$$

The torque components are;

Cylindrical torque $= \left(i_q i_{F_D} M_{dF_D} - i_d i_{F_Q} M_{qF_Q} \right) \times (pole - pairs)$

Saliency torque $= \left(L_d - L_q \right) i_q i_d \times (pole - pairs)$

Damping torque $= \left(i_q i_s M_{ds} - i_t i_d M_{qt} \right) \times (pole - pairs)$

2-) D. Karnopp " State Functions and Band Graph Dynamic Models for Rotary , Multi Winding Electrical Machines " Journal of the Franklin Institute ,vol. 328 No:1 pp. 45-54 1991.

3-) M.Hippner, A.R. Perkin "Electrical Motor For Low Cost Reticulation Scheme" South African Universities Power Engineering Conference Proceedings pp.57-60 Pretoria, January 1995.

4-) D.O'Kelly, S.Simmons " Introduction to Generalized Electrical Machine Theory " Maidenhead Berkshire, England 1968.

Address of authors: Department of Electrical Engineering University of the Witwatersrand
2050 WITS

6.FURTHER WORK:

Future work will include the modelling of the machine on the computer by using the CASED programme. Afterwards the model will be tested and the results will be verified.

7.CONCLUSION :

A procedure has been developed a model of the "Written-Pole" machine..The procedure is based on converting the topology of the machine to look like that of a synchronous machine with two field windings.The circuit equations describing this model have been developed in d-q form.

REFERENCES

1-) F. Parasiliti , P.Paffet "A model for Saturation Effects in High- Field Permanent Magnet Synchronous Motors " IEEE Transactions on Energy Conversion , vol : 4 No:3 pp. 487-494 Sept 1989.

Position Control of a Ropeless Elevator

BT le Roux, N El-Hage, RJ Cruise and CF Landy

The University of the Witwatersrand, Johannesburg.

ABSTRACT: *This paper is an extension of some of the issues raised at the First Symposium on Linear Drives for Industry Applications (LDIA '95) held in Nagasaki, Japan. At LDIA '95 there was great interest shown in using linear synchronous motors (LSM's) to propel ropeless elevators in tall buildings. This idea is extended to the South African mining industry and a small prototype is designed and constructed to test the feasibility of such a system. A position and speed control algorithm is also implemented to show that accurate control of the lift cage (or mover) can be achieved. Stringent safety requirements have to be met, particularly in the event of a power failure. Thus, the model is used to demonstrate the fact that if an interruption occurs in the electrical supply, the dynamic braking characteristics of the system can control the falling mover. The vertical thrust force is calculated using the Finite Element Method (FEM) and compared to measured values. The results of this study show that a linear synchronous motor propelled hoist is both a feasible and safe option for ultra-deep level mining applications.*

1. Introduction

As the mining resources of the Witwatersrand and other regions become less attainable, new technologies have to be developed to ensure that the remaining ore rich deposits can be extracted as efficiently and economically as possible. Up to now, the typical hoisting system consisted of a cable and winding motor. Unfortunately, this type of hoisting system is not viable over depths of 2500m due to limits placed on the hoisting cables. For greater depths, sub-vertical shafts have to be sunk. This not only results in increased capital outlay, but also increases the general operating costs due to the bottleneck which occurs for both human and rock transport. Investigation has therefore shown that mining at depths greater than 4000m is only viable under single shaft hoisting conditions[1].

As is evident from the above, a new system of vertical transport is required to ensure continued revenue from South Africa's most valued natural resource. Thus the development of linear motors has been investigated to test the validity of utilizing a cable free system to supersede the currently employed system.

2. LSM Construction

A linear synchronous motor (LSM) has been constructed and a basic position control system developed to test the feasibility of the proposed vertical transport system. The LSM constructed is that of a

4-pole double-sided, long stator design with permanent magnet excitation on the mover.

Figure 1: Stator Construction

The stator (primary windings) consists of a total of 10 individual cores, five along either side of the motor, giving the mover a total travel of 2.5m. To ensure minimal energy consumption, only those stators which are in close proximity to the mover are excited. The mover (or secondary), as shown in *Figure 2*, consists of 10 buried permanent magnets (Nd-Fe-B) which excites the four mild-steel shoes on either side. The guide system consists of 4 flanged nylon wheels on either side of the mover which run on a central rail mounted along the length of the support frame.

Figure 2: Mover Construction

3. Control System

The control system was implemented on a personal computer interfaced to the motor via a digital-to-analogue converter driving a constant-flux inverter and a position encoder. The control algorithm that was used is best described as time optimal control.

Figure 3: Basic control loop

The maximum velocity and final destination are passed to the algorithm which then determines the maximum possible acceleration according to the load, the thrust produced by the motor and the points of maximum acceleration and deceleration (refer to *Figure 4* **Pos1** and **Pos2** respectively).

Figure 4: Position transfer control signal

The output signal is then mapped to the current position of the mover, hence utilizing the encoder signal as an output signal reference. The above method of control is only applicable to the synchronous machine due to its natural frequency tracking characteristic[2]. Upon

reaching its destination, the motor is held in position by ensuring that the mmf wave produced by the stators is stationary. This is achievable in systems with minimal output frequencies (0.1 Hz in this case) by rapidly toggling the direction of voltage output.

4. Results

Initial design performance was tested using finite element method (FEM). The determined thrust produced by the motor was in the region of 450N indicating sufficient thrust to overcome the mass of the mover ($\approx$20kg). Final testing of the motor produced forces of up to 400N. The main discrepancy in results were due to errors in mechanical construction, an expected error of 10% from using FEM as well as possible effects of armature reaction and other electromagnetic phenomena not accounted for in FEM.

The effects of Detent forces[3] were also evident in the oscillatory motion of the mover. Although the forces produced by the motor ensured accurate position control (within 5mm), the Detent forces resulted in a slight jerky motion at low speeds. Future designs should therefore incorporate either semi-closed slots or magnetic slot wedges to reduce the Detent effect.

A final observation was that of the regenerative breaking characteristic of the permanent magnet LSM. Under power failure conditions, the mover drops at a controlled rate. This is due to the opposing forces produced during generation. Under such conditions, the coils of the stator are short-circuited, ensuring a current path. As the mover falls, the alternately energised pole shoes produce a changing flux in the coils which induces an emf which results in current flow. The mmf wave produced by the induced current opposes the original change in flux, hence producing a negative thrust[4,5]. When the supply is interrupted and the coils are short-circuited, the mover drops at a rate of 0.24m.s^{-1} and takes 9 seconds to reach the bottom. During the free fall (open-circuited) case over the same distance (2.2 m) the cage reaches the bottom within 0.7 seconds, obtaining a velocity of over 6m.s^{-1}. The vast difference in velocity of the mover under open- and short-circuited conditions demonstrates the considerable braking force ($\approx$190N) experienced by the falling mover.

5. Application in the Mining Industry

As mentioned above, the primary advantage in using linear motors in hoisting applications is that of the lack of requirement for a hoisting cable. This implies unlimited depth of operation, limited only by economical constraints. Further advantages of using a linear motor propelled hoist is the multi-direction and multi-vehicle capabilities of the system.

As the direction of travel is determined solely by the construction of the guide system, both horizontal and vertical

transport is possible (*Figure 5b*). This ensures minimized transport time as workers can be transported directly from hostel to rock face without interruption. Similarly, the gold-bearing ore can be taken from the stope directly to the crusher. At the same time, as no direct link is required between the mover and the surface, more than one vehicle can travel down the same shaft at any time. Thus, in a dual shaft operation, an endless number of vehicles may be utilized in a cyclic motion to ensure a constant mode of transportation (*Figure 5a*). This results in both a decrease in transit rate as well as a reduction in vehicle size, reducing the overall diameter of the shaft sunk.
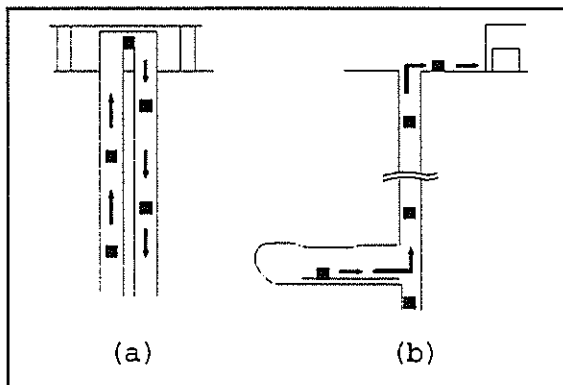
Figure 5: LSM operation in mines

The main advantage of the permanent magnet LSM propelled hoist is that of the regenerative breaking. No other hoisting system exhibits such a characteristic which ensures a controlled drop rate under power loss conditions. Although the regenerative braking feature will not bring the lift cage to a complete standstill, it will reduce the speed significantly, reducing the requirements placed on any mechanical braking system.

6. Conclusion

The design, construction and performance of a small-scale linear synchronous motor hoist have been presented. The advantages of using such a system in the mining industry have also been highlighted, indicating the feasibility of using linear motors, permanent magnet LSM's in particular, as an economically viable and safer alternative to the current methods of hoisting.

References

1. Stewart, A.T. **Hoisting systems for ultra-deep vertical shafts**, *XVth CMMI Congress*, Johannesburg, SAIMM, 1994 vol. 1, pp. 39-44.

2. Sen, P.C. *Principles of Electric Machines and Power Electronics*, John Wiley & Sons, 1989, pp 370,307,335,336.

3. Yoshimura, T. Watada, M. Torii, S. Ebihara, D. **Study on the reduction of Detent force of permanent magnet linear synchronous motor**, *The First International Symposium on Linear Drives for Industrial Applications*, Nagasaki, 1995.

4. Yamaguchi, H. and Watanabe, T. **Dynamic braking characteristic of linear synchronous motor with permanent magnet secondary and long stators for elevator**, *The First International Symposium on Linear Drives for Industrial Applications*, Nagasaki, 1995.

5. Giancoli, D.C. *Physics for Scientists and Engineers*, 2nd Edition, Prentice-Hall International Inc.,1988, pp 676.

NEURAL NETWORKS FOR FAULT DETECTION IN VIBRATING STRUCTURES.

JFG de Freitas   A Gaylard   AL Stevens   JN Ridley   CF Landy

Department of Electrical Engineering, University of the Witwatersrand

Abstract

Multivariate network-based nonparametric regression is proposed for the identification of vibrating structures and fault detection. A network that makes use of the theory of autoregressive models and functional approximation is employed to generate a structural model for a 3 kW induction motor. A feature of this network is the use of different basis functions in each hidden layer. Observation of the network weights shows which basis functions dominate, thereby revealing information about the physical system. The network exhibits a 100% success rate in the detection of 1.8 A armature current variations.

1   Introduction

System identification deals with the problem of determining a model for a dynamic system based on a finite record of noisy input-output data. The model can be used to detect any changes in the physical dynamic system. By mapping a vibration signal obtained in one part of an induction motor case to a vibration signal obtained in another part of the case, it is possible to obtain a structural model of the motor. This model may be used to automatically detect any changes in the vibration signatures of the motor.

The lack of knowledge about the structural configuration of this nonlinear dynamic system motivates the use of nonparametric regression. In this case, identification becomes a search for a class of basis functions that can approximate the required nonlinear multivariate transfer function. This problem can be solved using some kind of network, often referred to as neural network. Networks constitute a graphical notation for a considerable number of function approximation algorithms [1].

2   Proposed Networks

Various attempts have been made to solve the nonlinear identification problem using an extension of the theory of linear autoregressive models (ARX) combined with network based nonparametric regression [2, 3, 4, 5, 6, 7, 8]. In these attempts, however, the basis functions used in each network layer are identical and its relation to the physical system is not studied. This article introduces a network which uses different basis functions in the same layer as shown in Figure 1. In doing so, it is possible to determine which basis functions dominate by observing the network weights, thereby revealing information about the physical system being modelled. Furthermore, by using only the dominant basis functions fewer parameters are required. Consequently, it is possible to reduce error variance (overfitting) and improve generalisation.
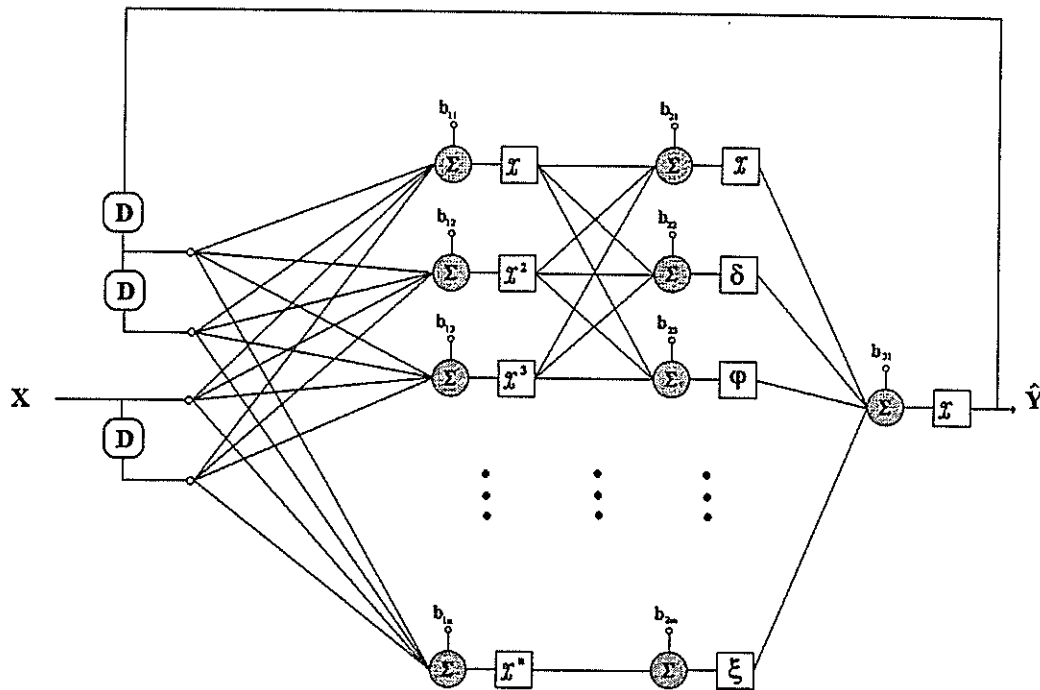
Figure 1: Network structure proposed for system identification

Using more than one hidden layer, allows estimators of higher order to be obtained using fewer parameters. For example, in the case of polynomial basis functions, a single hidden layer network can achieve polynomial orders equal to the number of basis functions n. On the other hand, a two layer network can achieve polynomial orders of $\frac{n^2}{2}$ if n is even and $\frac{(n-1)(n+1)}{4}$ if n is odd. If the basis functions are differentiable, the network can easily be trained with a gradient descent technique, preferably back-propagation with the Levenberg-Marquardt Optimisation [9, 7].

3 Structural Identification of an Induction Motor

Knowledge of the dynamic characteristics of a structure involves cognisance of the functional relations between the excitations and responses at various parts of the structure. Various techniques for obtaining structural models, by mapping a vibration signal obtained in one part of a structure to a vibration signal obtained in another part of the same structure, have been developed in the past. Udwadia and Marmarelis [10, 11] used Wiener techniques of nonparametric identification for the identification of building structural systems. They realised that vibration signals can be segmented to ensure stationarity and that they have a strong linear component and an unknown nonlinear component. Unfortunately, powerful techniques for nonparametric regression were not available to them.

Popescu [12, 13] used ARMA models for pseudolinear identification of structures subject to earthquake ground motions. Finally, Uhrig [14] used neural networks for the identification of check valves in nuclear plants. However, instead of approximating a dynamic system by

an autoregressive nonparametric model, he tried to map the Fourier transform of the input signal to the Fourier transform of the output signal. Considering that the system modelled was nonlinear, the use of Fourier transforms was not appropriate. Furthermore, the network was used simply as a black box tool and no insight was gained into the problem. In the present paper, a technique based on the network structure of Figure 1 is proposed for the structural identification of a 3 KW induction motor. After trying various basis functions, the authors have arrived at the preliminary conclusion that the studied vibration signals exhibit linear and quadratic components. The results obtained in predicting a segment of the validation record are illustrated in Figure 1. The model obtained was used to detect
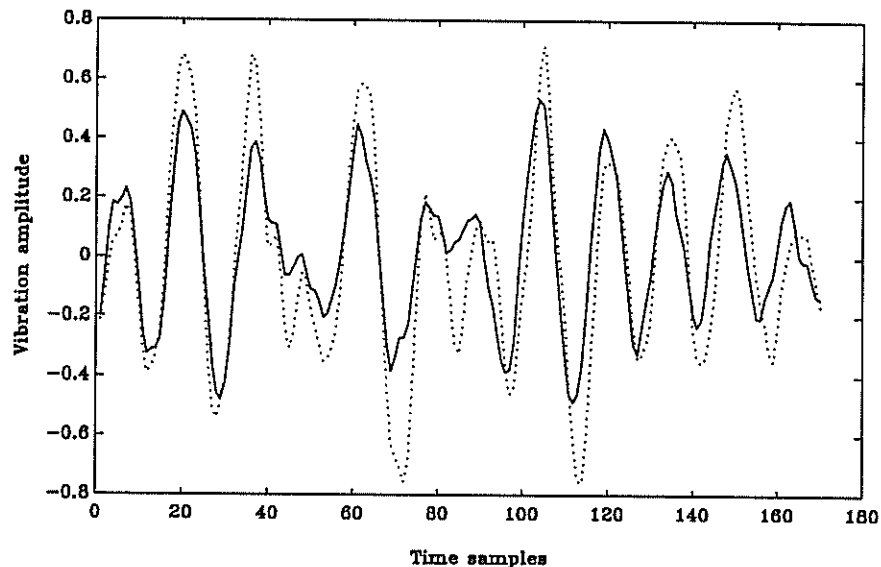
Figure 2: Vibration signals. [···] Actual output [—] Predicted output.

simulated faults in the induction motor. The success rate for detecting a change of 1.8 A in the armature current was 100%.

4 Conclusions

The network based nonparametric technique presented in this paper was successfully employed in the detection of incipient faults and in the modelling of the structural dynamics of an induction motor. The ideas of using different basis functions and observing the network parameters to identify which basis functions dominate, sets the ground for a joint combination of nonlinear systems theory and network theory in order to improve our understanding of nonlinear dynamical systems.

References

[1] T. Poggio and F. Girosi, "Networks for approximation and learning," *Proceedings of the IEEE*, vol. 78, pp. 1481–1497, September 1990.

[2] B. R. Pramod and S. C. Bose, "System identification using ARMA modeling and neural networks," *Journal of Engineering for Industry*, vol. 115, pp. 487–491, November 1993.

[3] J. Sjöberg, H. Hjalmarsson, and L. Ljung, "Neural networks in system identification," in *10Th IFAC Symposium on System Identification*, (Copenhagen), pp. 187–190, 1994.

[4] O. Nerrand, L. Personnaz, and G. Dreyfus, "Non-linear recursive identification and control by neural networks: A general framework," in *Proceedings of the Second European Control Conference*, (Groningen, Netherlands), pp. 93–98, 1993.

[5] H. J. M. Telkamp and A. A. H. Damen, "Neural network learning in nonlinear system identification and controller design," in *Proceedings of the Second European Control Conference*, (Groningen, Netherlands), pp. 798–804, 1993.

[6] K. Narendra and K. Parthasarathy, "Identification and control of dynamical systems using neural networks," *IEEE Transactions on Neural Networks*, vol. 1, pp. 4–27, 1990.

[7] J. Sjöberg, Q. Zhang, L. Ljung, A. Benveniste, B. Deylon, P. Glorenec, H. Hjalmarsson, and A. Juditsky, "Non-linear black-box modelling in system identification: A unified overview," tech. rep., Linköping University, Sweden, 1995.

[8] A. Juditsky, H. Hjalmarsson, A. Benveniste, B. Deylon, L. Ljung, J. Sjöberg, and Q. Zhang, "Non-linear black-box models in system identification: Mathematical foundations," tech. rep., Linköping University, Sweden, 1995.

[9] A. Cichocki and R. Unbehauen, *Neural Networks for Optimization and Signal Processing*, ch. 1, pp. 23–29. John Wiley & Sons, 1993.

[10] F. E. Udwadia and P. Z. Marmarelis, "The identification of building structural systems i. the linear case," *Bulletin of the Seismological Society of America*, vol. 66, pp. 125–151, February 1976.

[11] P. Z. Marmarelis and F. E. Udwadia, "The identification of building structural systems ii. the nonlinear case," *Bulletin of the Seismological Society of America*, vol. 66, pp. 153–171, February 1976.

[12] T. D. Popescu and S. Demetriu, "Analysis and simulation of strong earthquake ground motions using arma models," *Automatica*, vol. 26, no. 4, pp. 721–737, 1990.

[13] T. D. Popescu, "Identification of a vibrating structure subject to a transient natural excitation," in *Proceedings of the Second European Control Conference*, (Groningen, Netherlands), pp. 627–632, 1993.

[14] R. Uhrig, L. H. Tsoukalas, A. Ikonomopoulos, M. Essawy, C. Black, and S. Yancy, "Using neural networks to monitor the operability of check valves," in *Proceedings of the Conference on Expert System Applications for the Electric Power Industry*, (Arizona), 1993.

Address of Main Author

JFG de Freitas. Department of Electrical Engineering. University of the Witwatersrand. Private bag 3. WITS 2050. South Africa. E-mail: gomes@odie.ee.wits.ac.za

IDENTIFICATION AND CONTROL OF INDUCTION MOTORS USING ARTIFICIAL NEURAL NETWORKS WITH RANDOM WEIGHT CHANGE TRAINING

Bruce Burton and Ronald G. Harley

Department of Electrical Engineering, University of Natal, King George V Ave, Durban, 4001, South Africa
email: bburto@elaine.ee.und.ac.za

Abstract. This paper highlights some of the latest developments in ongoing work on the practical implementation of a continually online trained neural network induction motor controller. In particular, it considers the potential use of a proposed *analogue* VLSI sigmoidal feedforward neural network, with *on-chip* random weight change training, for rapid control of induction motor stator currents. The random weight change training algorithm is described and its convergence mechanism explained by comparison with that of backpropagation training. Simulation results also demonstrate the potential induction motor current control performance achievable with random weight change in comparison with that of backpropagation training.

1. INTRODUCTION

Adaptive identification and control of the currents *and* the shaft speed of induction motors using continually online trained (COT) artificial neural networks (ANNs) was first proposed in [1], where simulation results demonstrated the self commissioning ability and adaptive performance of the ANN method as potential advantages over standard field oriented control (FOC).

A subsequent paper [2] reported on initial investigations on the practical implementation of the ANN controllers. In particular, [2] considered the use of alternative ANN types and training algorithms and concluded that the sigmoidal feedforward ANN trained by the backpropagation algorithm, as originally proposed in [1], was most suitable for *microprocessor* implementation.

A further paper [3] summarised subsequent progress made on the practical implementation of the ANN controllers. In particular, [3] described a prototype implementation of the *current* control loop of the method on a single *transputer* based high speed *digital* controller. Comparison of simulated and measured current responses demonstrated the practical success of the COT ANN current loop within the bandwidth limitations of the single transputer. The computational burden of COT ANNs was analysed and two novel methods of *parallelising* the massively connected ANN structure and COT algorithm were introduced. The potential success of each of these methods was demonstrated by means of simulation and it was shown how they could be combined to achieve a potential parallelisation speed up factor of at least four times with the use of four *microprocessors* or *DSPs*.

This paper considers the potential use of a proposed [4] *analogue* VLSI sigmoidal feedforward ANN ASIC, with on-chip random weight change (RWC) training, as a low cost alternative to software implementation of the

backpropagation algorithm for COT of microprocessor or DSP based ANNs. The paper begins by illustrating the mechanisms by which the structure of three layer sigmoidal feedforward ANNs accommodate the learning of any desired function. The basis of the backpropagation training algorithm is then described and used to explain the convergence mechanism of the RWC algorithm. Finally, the application of COT ANNs to identify and control induction motor stator currents is reviewed and the current control performance produced by RWC is compared with that of backpropagation training by means of simulation.

2. ANN LEARNING OF DESIRED FUNCTIONS

This section describes the *feedforward function* of the three layer sigmoidal ANN illustrated in fig. 1, the *mechanisms of function approximation* of this type of ANN, the basis of *backpropagation training*, and the convergence mechanism of the *RWC training* algorithm.
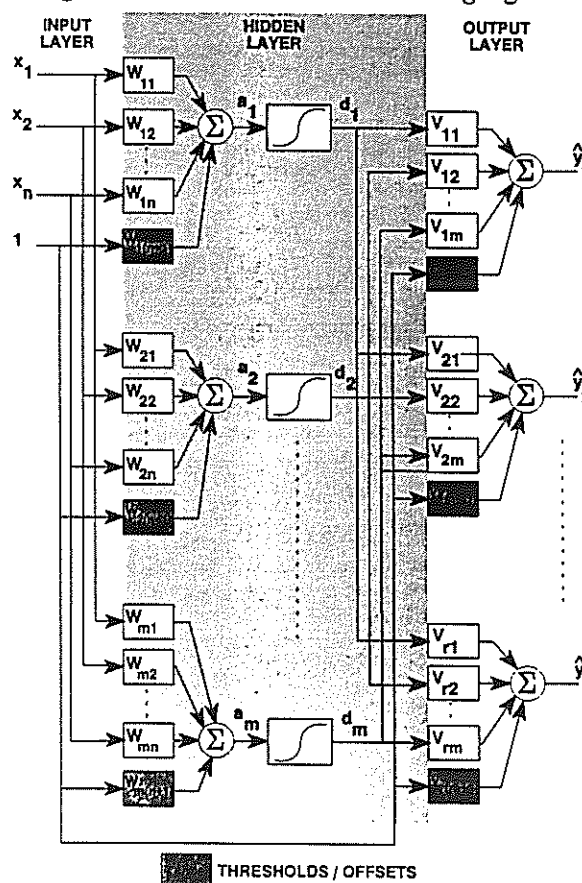

THRESHOLDS / OFFSETS

Fig. 1. Structure of a 3 layer sigmoidal feedforward ANN

(a) Feedforward Function. The input/output mapping function $g(\cdot)$ of an $n \times m \times r$ (n-input, m-hidden neuron, r-output) ANN is defined as:

$$\hat{y} \cdot g(\underline{x}, W, V) \qquad (1)$$

where *input vector* $\underline{x} \in \mathbf{R}^n$, *input weight matrix* $W \in \mathbf{R}^{m \times (n \cdot 1)}$, *output weight matrix* $V \in \mathbf{R}^{r \times (m \cdot 1)}$ and *output vector* $\hat{y} \in \mathbf{R}^r$. The ANN function $g(\cdot)$ is normally evaluated in several steps. First, the *activation vector* $\underline{a} \in \mathbf{R}^m$ is determined as the sum of *input thresholds* and weighted inputs:

$$a_i \cdot W_{i,(n \cdot 1)} \cdot \sum_{j \cdot 1}^{n} x_j W_{i,j} \qquad (2)$$

The *decision vector* $\underline{d} \in \mathbf{R}^m$ is then determined by passing each element of the activation vector through a sigmoid function:

$$d_i \cdot sig(a_i) \qquad (3)$$

where:

$$sig(\cdot) \cdot \frac{1}{1 \cdot e^{-(\cdot)}} \qquad (4)$$

Finally, the output vector is determined as the sum of *output thresholds* and weighted decision vector elements:

$$\hat{y}_i \cdot V_{i,(m \cdot 1)} \cdot \sum_{j \cdot 1}^{r} d_j V_{i,j} \qquad (5)$$

(b) Mechanisms of Function Approximation. It has been proved [5] that, by an appropriate choice of weights, the feedforward function $g(\cdot)$ of a three layer sigmoidal ANN, with a sufficient number of hidden neurons, can be made to approximate any continuous function $f(\cdot)$ to an arbitrary degree of accuracy over some predefined range

In mathematical terms, [5] proves the existence of weight matrices $W^* \in \mathbf{R}^{m \times (n \cdot 1)}$ and $V^* \in \mathbf{R}^{r \times (m \cdot 1)}$ such that:

$$|f(\underline{x}) \cdot g(\underline{x}, W^*, V^*)| < \epsilon \qquad (6)$$

for *any* $\epsilon > 0$ and for *all* $\underline{x}$ in some bounded region of $\mathbf{R}^n$, where n and r are determined by the dimensions of the domain and range of $f(\cdot)$ respectively. Rather than repeating the proof of [5], however, this section illustrates the basic mechanisms through which the structure of the ANN accommodates this function approximation capability via appropriate choice of the **number of hidden neurons** m and **weight values** respectively.

Each output of the ANN is a linear combination of *weighted sigmoids* and a constant *offset* or threshold. The **number of hidden neurons**, or the *number of weighted sigmoids* required to approximate the desired mapping $f(\cdot)$ between the input vector and each of the outputs depends on:

1. the *complexity* or *form* of $f(\cdot)$ over the desired *range* of approximation, and
2. the desired *accuracy* of approximation.

Even if $f(\cdot)$ is known, however, the number of hidden neurons is usually determined heuristically due to the present lack of analytical tools for this complex task.

The *form* of each *weighted sigmoid*, and thus the *form* of the *approximating function* $g(\cdot)$ is determined by the **weight values**. Fig. 2 shows a $1 \times 1 \times 1$ ANN, whose output consists of the sum of *one* weighted sigmoid and an offset. The individual effects of each of the ANN weights on the *form* of $g(\cdot)$ is illustrated in fig. 3. Fig. 4 illustrates how the function $f(x) \cdot 2x^2 \cdot 1$ can be approximated for $x \in [-1, 1]$ with *two* weighted sigmoids and an offset (ie. with a $1 \times 2 \times 1$ ANN).
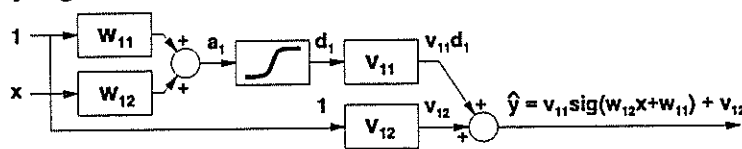

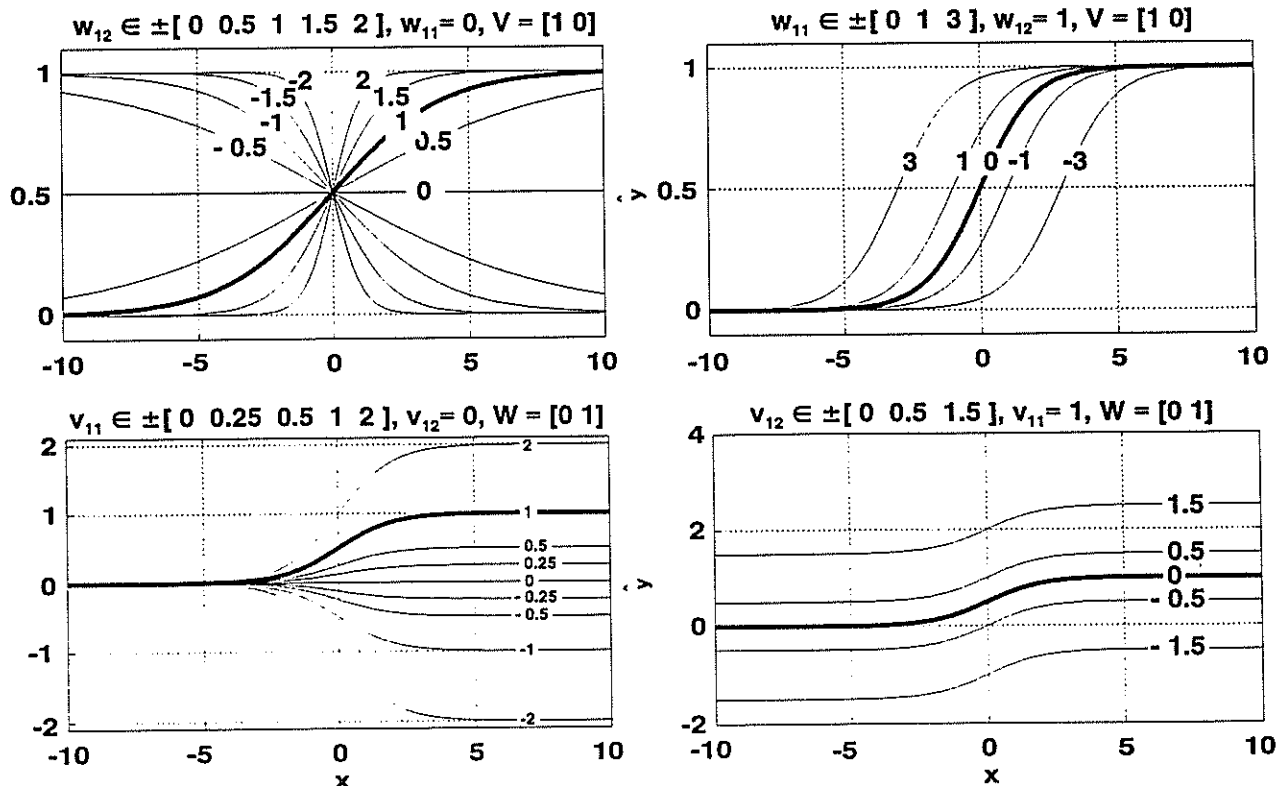Fig. 2.   A $1 \times 1 \times 1$ three layer ANN

Fig. 3.   The effects of each weight of a $1 \times 1 \times 1$ ANN on the form of $g(.)$
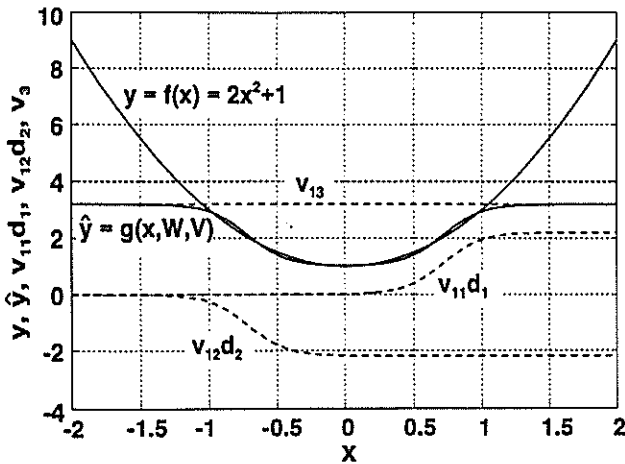
Fig. 4. Approximation of $2x^2+1$ with $m = 2$.

Fig. 5. Recursive training to minimise $f(.) - g(.)$

The objective of **training** is to recursively adjust the weights in order to minimise the difference between $g(\cdot)$ and the desired function $f(\cdot)$ over the desired range, as shown in fig. 5.

(c) Backpropagation Training. In its simplest form, the backpropagation training algorithm is merely a set of equations which are a closed form solution to the *gradient descent* rule as applied to each of the input and output weights of the ANN, ie.

$$\Delta w_{i,j} = -k\frac{\partial E(\cdot)}{\partial w_{i,j}} \text{ and } \Delta v_{i,j} = -k\frac{\partial E(\cdot)}{\partial v_{i,j}} \quad (7)$$

where $k > 0$ is known as the *learning rate* (and is heuristically determined for optimal convergence) and $E(\cdot)$ is the scalar function:

$$E(\cdot) = \frac{1}{2}|f(\underline{x}) - g(\underline{x}, W, V)|^2 \quad (8)$$

In other words, *the backpropagation algorithm calculates the exact gradient* of $E(\cdot)$ with respect to each of the weights and changes them in the *negative* direction of this gradient so as to reduce the value of $E(\cdot)$, which corresponds to improving the approximation of the desired function $f(\cdot)$ by the ANN function $g(\cdot)$. Unfortunately, these calculations require *high precision arithmetic* in order for training to converge and thus the backpropagation training algorithm is not suitable for *analogue* VLSI implementation. The RWC algorithm was thus specifically developed for analogue VLSI implementation

· **(d) Random Weight Change Training.** Instead of *calculating* the exact gradient of $E(\cdot)$, the RWC algorithm *randomly searches* for the gradient in the following way:

1. The value of $E(\cdot)$ is stored as E_{best} and the stored matrices ΔW_{best} and ΔV_{best} are initialised to zero.
2. Each of the ANN weights are changed by a fixed amount, ie.

$$\Delta w_{i,j} = \rho\delta \text{ and } \Delta v_{i,j} = \rho\delta \quad (9)$$

where δ is some *small positive* constant (roughly analogous to the learning rate in backpropagation training) which is heuristically determined for optimal convergence, and ρ is a random variable which may assume either the value of +1 or -1 with equal probability.

2. The new value of $E(\cdot)$ is compared with E_{best}.

3. If $E(\cdot) < E_{best}$, $E(\cdot)$ is stored as E_{best} and all of the weight changes stored in ΔW_{best} and ΔV_{best}.
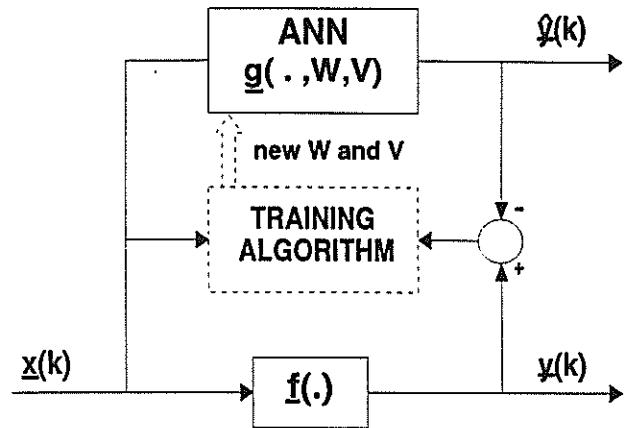
4. Each of the ANN weights are restored to their original values (the values they possessed at step 1).
5. Steps 2, 3 and 4 (collectively known as *1 random trial*) are repeated *N-1* times.
6. Each of the ANN weights are changed by the corresponding values stored in matrices ΔW_{best} and ΔV_{best}.

The total *number of trials N* is determined beforehand by the time T within which each training cycle (one evaluation of steps 1 to 6) is required to be completed. For adaptive identification and control of induction motor currents, T corresponds to the portion of each sampling period which may be devoted to training. It is predicted that an analogue VLSI implementation of RWC will allow $N=20$ for $T=50$ μs, which will correspond to a sampling rate of approximately 10 kHz. Under these circumstances, in each training cycle, the RWC algorithm will choose a direction in which to change the ANN weights from a set of twenty different random directions. The direction which is chosen will be that which will produce the greatest decrease in the value of $E(\cdot)$. Thus the direction which is chosen will be that which is *closest* to the exact negative gradient of $E(\cdot)$. Since backpropagation always changes the weights in the exact direction of the negative gradient (the steepest descent) it is reasonable to expect that backpropagation may converge faster than RWC. Nevertheless, RWC will eventually converge since there is always a finite probability that a direction will be found in which the weights can be changed so as to reduce the value of $E(\cdot)$. The question of whether or not the convergence of RWC is sufficient to produce rapid and reliable adaptive induction motor current control is investigated by simulation in section 4.

3. ANN STATOR CURRENT ID AND CONTROL

The NARMAX (Nonlinear AutoRegressive Moving Average with eXogenous inputs) discrete time model of the electrodynamics of the induction motor was introduced in [1]. It gives the one step ahead stator current vector in the stationary $\alpha\beta$ reference frame as a function of the present and delayed current vector values $\underline{i}(k)$ and $\underline{i}(k-1)$, the present and delayed shaft speed values $\omega(k)$ and $\omega(k-1)$ and the present and delayed voltage vector values $\underline{v}(k)$ and $\underline{v}(k-1)$, as:

$$\underline{i}(k-1) = f(\cdot) = c_v\underline{v}(k) \quad (10)$$

where $f(.)$ is some continuous nonlinear function . The linearity of $i(k+1)$ with respect to the controlled variable, the present voltage vector value $\underline{v}(k)$, is the key to the ANN current control method. An ANN is used to identify $f(.)$ and c_v by feeding it with the values of the arguments of equation (1) captured from the motor, as shown in fig. 1. The ANN then estimates the one step ahead current vector as:

$$\hat{\underline{i}}(k+1) \, \cdot \, \underline{g}(\cdot) \, \cdot \, \hat{c}_v \underline{v}(k) \qquad (11)$$

and the accuracy of the estimate is determined by the closeness of $g(.)$ and $\hat{c}_v$ to $f(.)$ and c_v. The one step ahead current vector estimate is delayed by one sampling period and compared with the actual current vector at that time to obtain the error for backpropagation training of the ANN and update of its weights. This online training takes place continuously to ensure that the ANN identifies changes in the motor as they occur. An exact control law is derived from equation (2) by substituting the desired value of the one step ahead current vector $\underline{i}^*(k+1)$ for the estimated value and solving for $\underline{v}(k)$ to get

$$\underline{v}(k) \, \cdot \, \frac{\underline{i}^{*(k+1)} \, - \, \underline{g}(\cdot)}{\hat{c}_v} \qquad (12)$$

This means that the desired current vector may be made to flow in the machine by applying the voltage calculated by equation (3). The accuracy with which the actual current vector tracks the desired value simply depends on how accurately the ANN has identified equation (1), as equation (2), and adaptive control is ensured by continuous online training.

4. SIMULATED RESULTS

Figs 6(a) and 6(b) show the simulated induction motor current control performance produced by COT of a 8×12×2 ANN (with random initial weights) using the backpropagation and RWC algorithms respectively. Both results show the rapid self commissioning and good adaptive tracking of the ANN controller. Furthermore, the rapid and reliable current control performance produced by RWC demonstrates its potential to replace the backpropagation algorithm in practice.

5. CONCLUSION

This paper has demonstrated the potential feasibility of practical implementation of an ANN induction motor current controller using a proposed analogue VLSI ASIC with on-chip random weight change training. Future theoretical work will include the investigation of (sensorless) ANN induction motor speed control and more detailed simulations of the actual VLSI components of the proposed ASIC in collaboration with the manufacturers, prior to eventual fabrication and practical tests. Practical work is also to be done on ANN induction motor speed control and the parallel implementation of COT ANNs on multiple microprocessors/ASICs (as proposed in [3]).

ACKNOWLEDGEMENT

REFERENCES

[1] Wishart MT and Harley RG, "Identification and Control of Induction machines Using Artificial Neural Networks", *Conf. Rec. of SAUPEC'94*, Cape Town, South Africa, Jan. 1994, pp 200 - 206.

[2] Burton B, Harley RG et al, "Implementation of a Neural Network Induction Machine Control Strategy", *Conf. Rec. of SAUPEC'94*, Cape Town, South Africa, Jan. 1994, pp 195 - 199.

[3] Burton B, Harley RG, Rodgerson JL and Levy DC, "The Practical Development of a Neural Network Induction Motor Drive", *Record of the Fourth Southern African Universities Power Engineering Conference SAUPEC'95*, Pretoria, Jan. 1995.

[4] Hirotsu K, Brooke MA, "An Analog Neural Network Chip With Random Weight Change Learning Algorithm", *Conf. Rec. of IJCNN*, Nagoya, Japan, Oct. 1993.

[5] Cybenko G, "Approximations by Superpositions of a Sigmoidal Function", *Mathematics of Control, Signals and Systems*, Vol. 2, 1989, pp. 303-314.

Fig. 6(a). Backpropagation current control
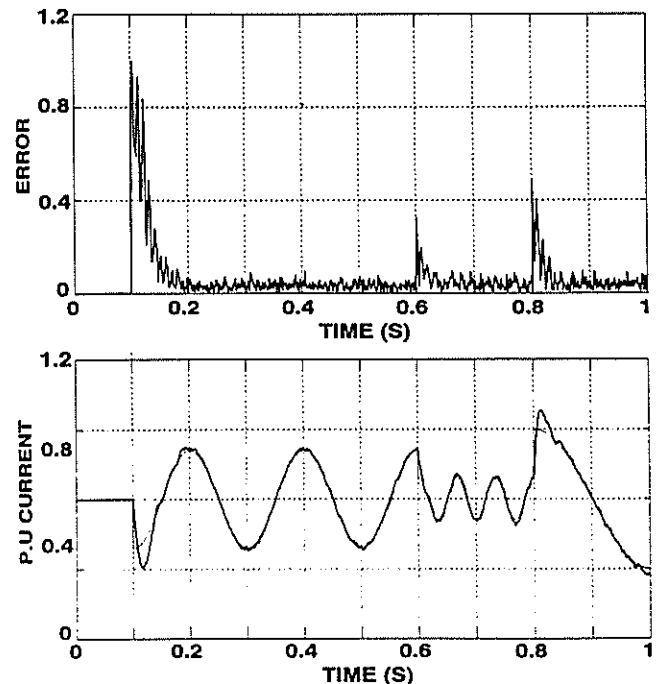
Fig. 6(b). Random wieght change current control

AN INVESTIGATION INTO THE FEASIBILITY OF USING NEURAL NETWORKS TO CONTROL TURBOGENERATORS

NM Shepstone   RG Harley   G Jennings   J Rodgerson

Department of Electrical Engineering, University of Natal

ABSTRACT: This paper reports on the feasibility of using an online learning neural network as an adaptive turbogenerator controller to replace the automatic voltage regulator and the turbine governor. Results are presented which show that the neural network can control the turbogenerator at least as well as the conventional controller, but more importantly, its performance does not degrade when system conditions change.

1 INTRODUCTION

Turbogenerators are central to the security and stability of modern power systems, and therefore effective control of these devices is very important. A turbogenerator is a fast acting, nonlinear, multiple input multiple output device, with a wide range of possible operating points. Furthermore its dynamic characteristics depend on the power system to which it is connected, for example, the transmission line impedance. Conventional automatic voltage regulators and turbine governors are designed to control, in some optimal fashion, the turbogenerator around one operating point; at any other point the generator's performance is degraded. Attempts have been made to design adaptive controllers using various techniques such as parameter lookup tables [Limebeer] and adaptive autoregressive moving average reference models [Wu] with varying degrees of success. This paper reports on the feasibility of using an online learning neural network as an adaptive turbogenerator controller.

2 SIMULATION MODEL DEVELOPMENT

2.1 Turbogenerator Modelling

The generator is described by the two axis dq-equations with the machine currents taken as the model's states; one damper winding is used on each axis giving a seventh order model. The automatic voltage regulator (AVR) and exciter are modelled as a second order device. The exciter is assumed to be a high speed solid state exciter with limits on its output voltage levels. The turbine and governor are modelled as a fourth order device so that reheating between the high pressure and intermediate pressure stages may be included in the model. The output of the turbine is limited between zero and 110%.

The mathematical implementation of the turbogenerator model and the neural networks were carried out in SIMULINK. SIMULINK proved to be a simple and flexible way of modelling the thirteenth order nonlinear differential equations for a turbogenerator and for implementing the neural networks.

2.2 Turbogenerator Identification

In order to design a neural network controller it is necessary to ascertain whether a neural network is able to identify the model of the turbogenerator. To do this a neural network was built which consisted of twelve inputs, one hidden layer with fourteen neurons in the hidden layer, and two outputs. The inputs to the neural network consisted of the inputs to the turbine, the inputs to the exciter, the output voltage of the generator, and the output speed of the generator. Each of these four inputs was time delayed by one, by two, and by three 20 ms sample periods giving a total of twelve inputs. The outputs of the neural network were required to be the speed and the terminal voltage of the turbogenerator.

The number of neurons in the hidden layer of the neural network was determined empirically. Because the network is small various numbers of neurons could be tried until the performance of the overall network was acceptable.

The neural network weights were initially set to small random values and they were updated using the standard backpropagation algorithm. The learning rate parameter in the network is determined empirically by running the network and setting the learning rate parameter so that a compromise between the training time and the accuracy of the network is achieved.

In order to train the neural network pseudorandom binary signals were fed into the exciter and the turbine to excite the full range of the dynamic response of the turbogenerator. The results of the turbogenerator identification simulations are illustrated in figure 1 in which it is shown that the neural network was able to learn the speed deviation of the turbogenerator model in about 5 to 10 seconds of training. Similar results are obtained for the neural network's ability to learn the output terminal voltage of the turbogenerator.

Since the results of the turbogenerator identification simulations indicated that a neural network is able to identify a turbogenerator it was decided to investigate the feasibility of designing a neural network controller for the turbogenerator.

2.3 Controller Design

The first step in the design of a controller is to select the architecture of the controller. An inverse model [Hunt] is unlikely to be successful due to the high gain loops around a turbogenerator, and a reference model [Narendra] is also unlikely to be successful because of the difficulty in developing a reliable reference model for a turbogenerator. In this study a three layer neural network was designed using a similar approach to the truck-backer problem of Nguyen and Widrow. Figure 2 is a schematic diagram of the controller that was designed.

For the controller a neural network was built which consisted of six inputs, a hidden layer with ten neurons, and two outputs. The inputs were the turbogenerator's speed and terminal voltage deviations. Each of these inputs was time delayed for one, two and three sample periods. The outputs of the controller formed the inputs to the turbogenerator's exciter and turbine. As in the turbogenerator identification stage the number of neurons in the hidden layer and the learning rate parameter were determined empirically.

The controller illustrated in figure 2 operates with online learning, however, it is necessary to train the controller initially before the online operation is undertaken. As with the turbogenerator identification neural network training was done using pseudorandom input signals to the exciter and turbine. Training is continued for 30 seconds to ensure that the controller had learnt the turbogenerator sufficiently accurately for online control to be undertaken.

Once the controller has been trained for a particular operating point of the turbogenerator the neural network controller is put into the online training mode and it then proceeds to control the generator's operation. The basic steps used by the controller are as follows:

    a)   Sample the output of the turbogenerator and the neural network modeller (see figure 2). Using the square of the difference between these two outputs and the backpropagation algorithm update the weights in the neural network modeller. Fix these weights.

    b)   Using the same input signals as in step (a) again sample the output of the neural network modeller and compare the output of the modeller with the desired response for the turbogenerator. Using the square of the difference of these two signals and the backpropagation algorithm backpropagate the error signal back through the neural network modeller to the output of the neural network controller.

    c)   Using the error signal at the output of the controller obtained in step (b), and the backpropagation algorithm, update the weights in the controller. Apply the output of the controller obtained with these new weights to the exciter and turbine of the turbogenerator.

    d)   Repeat steps (a) to (d).

The signals used by the controller were deviations from set points rather than actual values. This approach meant that when the turbogenerator was operating at the desired set point, without any deviation, the inputs to the neural network controller were zero giving zero output signal deviation even if the network learning had not placed the controller and modeller in global minimums but only in local minimums. Furthermore, when the turbogenerator

is operating without any deviation from its set points and the input signals to the controller are zero no online learning is taking place. Whereas, if actual signals values had been used, rather than deviations, online learning would be taking place all the time and it is possible that, due to the controller not being in a global minimum, controller drift could take place.

3 SIMULATION RESULTS

In order to evaluate the dynamic and transient operation of the above controller two types of conditions were simulated: a three phase short circuit, and positive and negative 5% steps in the set point of the terminal voltage. Each of these conditions is investigated with the turbogenerator running at a leading and at a lagging powerfactor, and with different transmission line impedances.

The parameters for the conventional controllers were obtained from Anderson and Fouad and modified to obtain the best overall response for the tests undertaken.

A sample of the results obtained is shown in figures 3 to 6. Figure 3 shows the performance of the controller for 5% step changes in terminal voltage with the turbogenerator operating at 1 pu power and 0,85 lagging power factor. (In all the result graphs the conventional controller is shown with a solid line and the neural network controller with dotted lines.) Figure 4 shows the turbogenerator operating under the same conditions and experiencing a 100 ms three phase short circuit. Figure 5 shows the results of a 50 ms short circuit with double the transmission line impedance used in figure 4 (50 ms is used because the turbogenerator is unstable for longer time periods). Figure 6 shows the results of a 100 ms short circuit, the same line impedance as in figure 4 but an output power of 0,4 - j0,1 pu. In each of these graphs it is apparent that the neural network controller has a performance at least comparable to that of a conventional controller and in each case the neural controller has similar response times with better damping.

Tests at other values of real and reactive power, and line impedances confirmed the above results, and showed that the controller was able to adapt its performance to these different operating points.

4 CONCLUSIONS

These initial simulation studies show that a neural network controller has the potential to control a turbogenerator and that it would be worth while extending this work into a hardware implementation of a neural controller for a turbogenerator.

5 REFERENCES

[1]   Anderson PM and Fouad AA, "Power System Control and Stability", IEEE Press, 1993, p442-443

[2]   Hunt KJ and Sbarbaro D, "Neural Networks for Control Systems", Peter Peregrins Ltd, 1992, p94-122

[3]   Limebeer DJN, "Discrete-time Optimal Control of a Synchronous Turbogenerator under Transient Conditions", MSc Thesis, University of Natal, Durban, 1977

[4]   Narendra KS and Parthasarathy K, "Identification and Control of Dynamical Systems Using Neural Networks", IEEE Transactions on Neural Networks, Vol 1, No 1, Mar 1990, p4-27

[5]   Nguyen DH and Widrow B, "Neural Networks for Self-Learning Control Systems", IEEE Control System Magazine, Apr 1990, p18-23

[6]   Wu QH and Hogg BW, "Adaptive Controller for a Turbogenerator System", IEE Proceedings, Vol 135, Pt D, No 1, Jan 1988, p35-42

6 ADDRESS OF MAIN AUTHOR

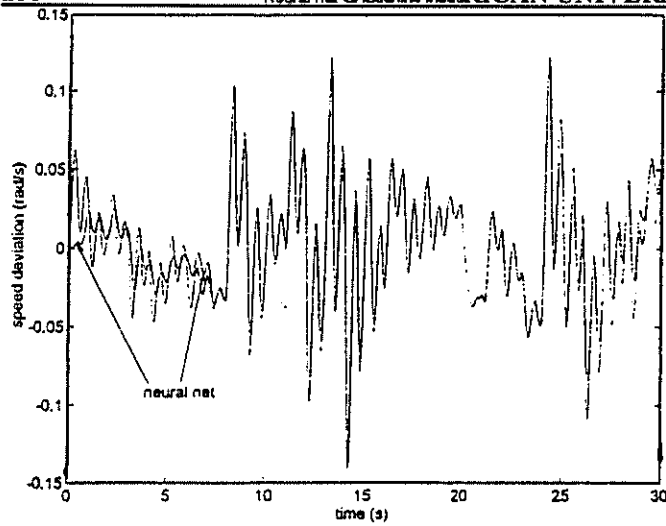NM Shepstone, Department of Electrical Engineering, University of Natal, P Bag X10, Dalbridge, 4014, email: shepston@elaine.ee.und.ac.za
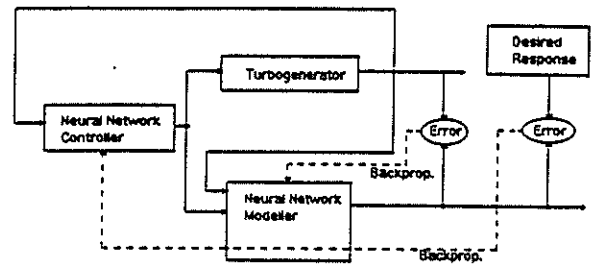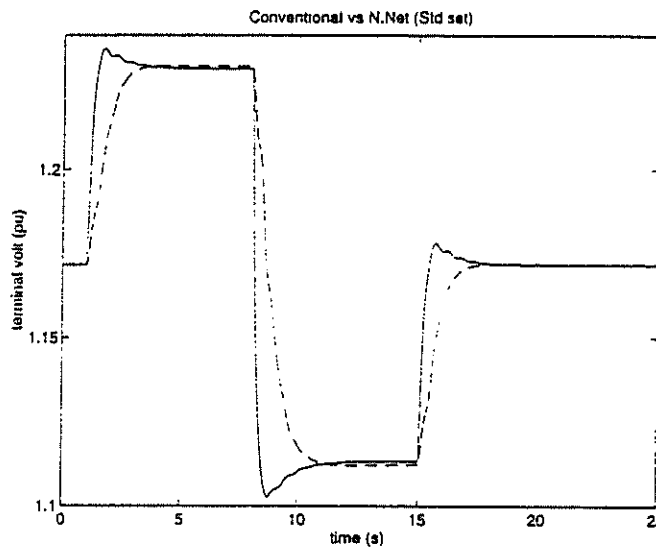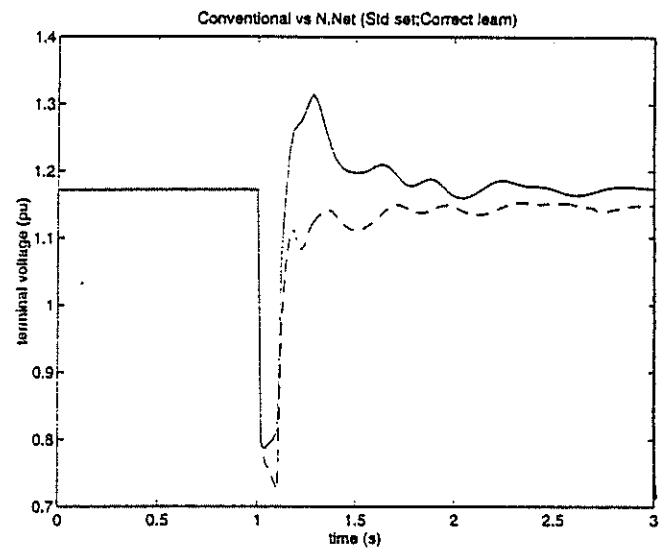
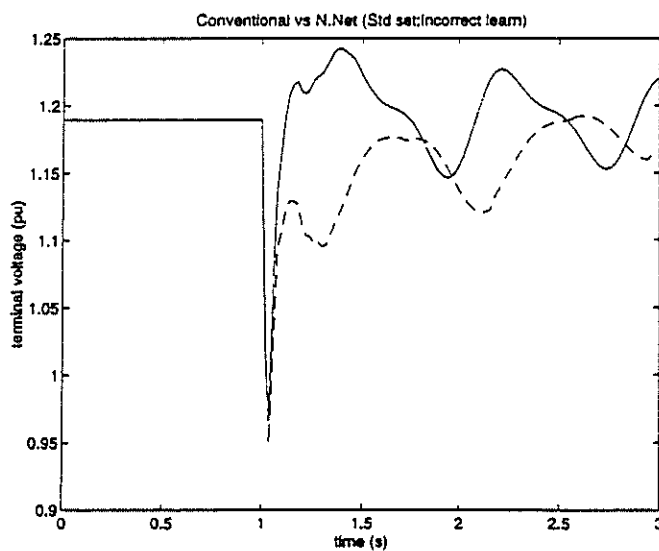Figure 1

Figure 2

Figure 3
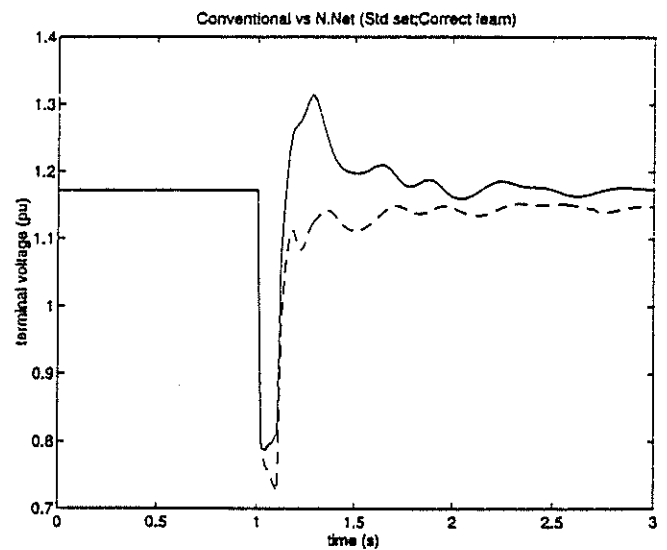

Figure 4

Figure 5

Figure 6

A PROGRAMMABLE I/O SYSTEM FOR REAL-TIME AC DRIVE CONTROL APPLICATIONS

D.R. Woodward, D.C. Levy *, R.G. Harley

Department of Electrical Engineering, University of Natal.
* Department of Electrical Engineering, University of Sydney, Australia.

Abstract. *This paper describes a programmable hardware structure capable of interfacing a conventional microprocessor to various sensors / actuators in a real-time AC drive control environment. The objective of the interface structure is to handle the low level data manipulation and supervisory control operations of the sensors / actuators and consequently free the resources of the host microprocessor for higher level tasks such as the real-time control algorithm of the application. The paper*

1 Introduction

Electrical drive systems have in the past been dominated by DC machines as a consequence of the simple requirements of their control structures. The mechanical commutator employed by a DC machine, however limits the speed and torque capability of the machine and requires periodic maintenance. More recently, due to advances in microprocessor technology, AC machines coupled with sophisticated control algorithms are capable of matching the dynamic performance of DC machines. The implementation of the control algorithms for the AC machine requires fast and complex signal processing which must be provided by the microprocessor based programmable controller[1].

A programmable controller capable of implementing complex AC drive control algorithms such as Field Oriented Control [2] with digital current control loops achieving sampling rates of approximately 5 - 10 kHz has several requirements. These requirements include high computational performance coupled to an efficient I/O system to enable the controller to sample the AC machine phase currents, shaft speed and position variables, and control the AC machine by generating pulse width modulation (PWM) inverter control signals to modify the magnitude, phase and frequency of the AC supply to the machine. Figure 1 shows the components of a typical Voltage

Fig. 1 A Typical AC Drive Configuration.

Source Inverter (VSI) based AC drive system and clearly identifies the interfaces required to connect the various sensors and actuators in the AC drive environment to the microprocessor based controller. The example application shown in Fig. 1 cites only VSI based AC drive controllers; however, in practice many variations exist not only with regard to the type of inverter employed (eg. Current Source Inverter CSI, resonant link inverter) but also in the combination of other interfaces required for various applications.

Commercial AC drive control systems employ high performance embedded microprocessors coupled to interfaces based on Application Specific Integrated Circuits (ASICs), to provide the computational power required to execute the machine control algorithms and to interface to the numerous sensors and actuators within the AC machine environment. The use of a combination of microprocessor and ASIC devices in AC drive control systems, whilst providing acceptable performance, remains limited to high volume AC drive applications due to the high cost of development and limited user configurability of the ASIC devices. Lower volume and less general AC drive control systems thus have to rely on the facilities offered by standard embedded microprocessors, to handle the low level requirements of the sensor and actuator interfaces as well as the execution of the control algorithm, and consequently the performance of these control systems is limited.

To overcome these problems this paper describes a programmable interface architecture based on Field Programmable Gate Array (FPGA) technology, that is capable of interfacing a conventional microprocessor to the various sensors / actuators in a real-time AC drive control environment. The objective of the interface structure is to handle the low level data manipulation and supervisory control operations of the sensors/actuators and consequently free the resources of the host microprocessor for higher level tasks such as the real-time control algorithm of the application, whilst at the same time providing user programmability and configurability to the interface.

The recent availability of large Field Programmable Gate Arrays (FPGAs) containing tens of thousands of logic gates with the ability to be configured and reconfigured in a matter
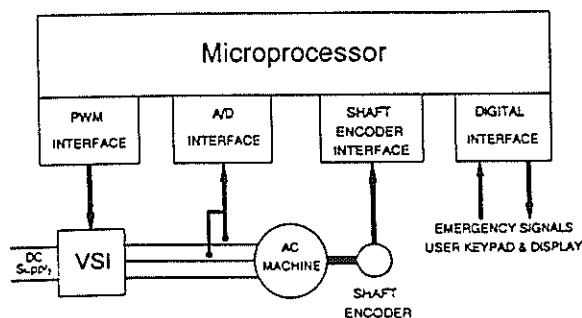
of milliseconds without the use of costly programming hardware, provides an excellent platform upon which the user configurability requirements of the interface can be implemented. To further address the requirements of user configurability the interface design adopts a slightly unconventional approach to generating the configuration data necessary to program the FPGA devices. Conventional methods of FPGA device configuration rely on the use of CAD software to layout gate level circuit diagrams or alternatively, Hardware Description Languages (such as VHDL) to define the required circuit configuration. This level of design entry is, however, complex and requires extensive knowledge of digital logic and its timing requirements to enable a successful design to be implemented, and is thus likely to be beyond the capabilities of the average AC drives engineer.

The I/O Coprocessor design adopts the use of the high level algorithmic description method of design entry to describe and realise the architecture of the coprocessor. This level of design entry enables the user to describe the behaviour of a hardware circuit without actually having to define low level entities such as gates, registers and their interconnections. Typically the hardware algorithm is described using a special description language and then CAD software is utilised to convert the description into a netlist of gates and registers based on a fundamental structure and timing paradigm. The resulting netlist is then processed via placement and routing software to generate the FPGA configuration information. A number of researchers [3],[4],[5] have developed algorithmic description languages and their associated compilers, and demonstrated that functional hardware circuits can be reliably constructed using these methods whilst requiring significantly less effort on the part of the user. Of particular interest is the work conducted by Page et al [3], [6] of Oxford University who have defined an algorithmic description language Handel and implemented CAD software capable of directly compiling the Handel language into a netlist form suitable for the configuration of Xilinx FPGA devices.

The Handel language is based on the concepts of Communicating Sequential Processes (CSP) [7] and consequently has a rich set of constructs that enable the simple description of several concurrently executing processes and a secure communication mechanism between them. Furthermore, the Handel language has a well defined set of formal semantics that allows the user to check a description based on the language for errors and treat the description as an "executable specification" which can be compiled like a conventional software language and used to simulate the behaviour of the intended hardware circuit. The Handel language and its associated compiler therefore provide an excellent algorithmic design entry platform through which to design and implement the I/O Coprocessor. The remaining sections of the paper describe the overall structure of the I/O Coprocesor and then concentrate on the design of a shaft encoder interface based on the coprocessor
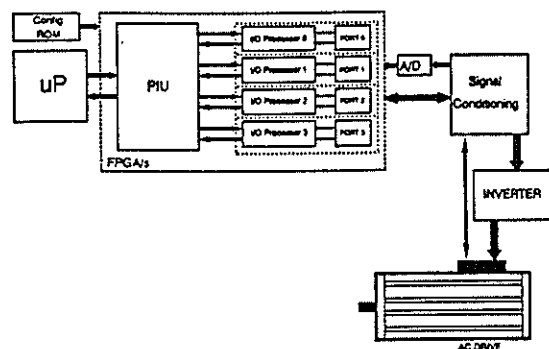
Fig. 2 The I/O Coprocessor Architecture.

structure and implemented using the techniques discussed in the preceding paragraphs.

2 The I/O Coprocessor Architecture

A general interface structure that is compatible with a wide range of I/O functions commonly found in AC drive applications has been developed. The interface structure takes the form of an I/O Coprocessor (see Fig. 2) which operates in conjunction with the host processor and communicates directly with it. The I/O Coprocessor is in turn composed of a number of concurrently operating subcomponents which implement the overall I/O task of the interface. The subcomponents of the coprocessor comprise a processor interface unit (PIU) and four independent I/O channel structures each containing an "I/O Processor" and an associated "I/O Port".

The structure of the I/O channels adopts the idea that the operations required to implement most I/O interface functions can be divided into two basic groups; word level operations and bit level operations. At the word level, complex operations such as scaling, offset, transformation, packaging etc. take place, whilst at the bit level simple operations such as Boolean manipulation, latching, counting, shifting etc. take place. Based on these observations each of the I/O channel subcomponents employ random logic circuit structures to perform the bit level operations of the I/O functions where speed is of the essence (I/O Port Units), and utilise microprocessor like structures to perform the word level operations that can tolerate lower response times (I/O Processor Units). This approach attempts to benefit from the speed advantages offered by random logic circuit structures whilst at the same time optimising the use of FPGA silicon resources by enabling "circuit structure reuse" where speed is not required.

The following paragraphs describe the details of the coprocessor subcomponents and the configurability of the overall I/O Coprocessor structure.

The Processor Interface Unit (PIU):- The PIU combines the functions of a host processor interface and a command

interpreter. The command interpreter function is responsible for receiving and interpreting high level commands and data from the host microprocessor and distributing them to the relevant I/O channels. The algorithm executing within the host microprocessor may use these high level commands to pass data to or receive data/status from the I/O Coprocessor. *The I/O Processor Units* :-The I/O Processor Units are based on conventional microprocessor architecture with built in memory structures and a highly optimised and restricted instruction set to handle the word level operations required by the I/O functions of each I/O channel. The architecture of the I/O Processor and the instruction word format is designed to facilitate the simple addition or removal of instructions from the overall instruction set to enable the instruction set to be optimised for particular applications without grossly affecting the basic structure of the processor.

The I/O Port Units :- The I/O Port Units of the I/O Coprocessor are based on random logic circuits and implement the high speed, time critical, bit level operations required by the I/O functions of each channel. A simple interface links the I/O Port to the corresponding I/O Processor of each channel. The I/O Port Unit structures are responsible for ensuring that bit level operations occur in the correct sequence and at the correct instant in time and consequently require careful design and implementation to match the requirements of the sensors and actuators to which they are connected.

The basic subcomponents of the I/O Coprocessor are self contained and communicate with each other via unidirectional, synchronous point-to-point data channels. Consequently this modular structure is readily expandable to cater for multiple I/O functions and is partitionable over several FPGA devices to accommodate complex I/O functions requiring logic configurations which exceed the gate densities currently available in single FPGA devices.

To address the requirements of user configurability, the structure of the I/O Coprocessor provides three levels of programmable capability to the user. At the lowest level where the FPGA configuration information is generated, sufficiently skilled users may generate different versions of the PIU to support alternative host processor types, the I/O Processors can be optimised to perform certain functions, and the bit level operations performed by the I/O Port Units can be modified to suit particular sensor / actuator requirements. The next level of programmable capability involves the generation of programs for each of the I/O Processors. Programs may be written and downloaded to each of the I/O Processors to suit a particular application without requiring the reconfiguration of the basic structure of the I/O Coprocessor. The third and final level of programmable capability possible with the I/O Coprocessor architecture is the execution of high level commands issued by application code executing on the host microprocessor and forming part of the overall control algorithm of the controller. These commands enable data to be passed to and from the I/O Coprocessor and the I/O Processors to be reset and booted with programs.

3 The Implementation of a Shaft Encoder Interface

This section describes the implementation of a shaft encoder interface for an AC drive application based on the I/O Coprocessor architecture. The diagram illustrated in Fig. 3 shows the overall process structure of an interface to connect a transputer processor to an incremental shaft encoder of the type commonly found in machine and robotics control applications. The interface decodes the quadrature squarewave signals produced by the shaft encoder sensor to generate angle and speed information which is then made available to higher level tasks executing as software processes on the host transputer processor. The I/O Coprocessor structure in this application only requires the use of a single I/O channel (I/O Processor + I/O Port) and thus consists of five interconnected parallel processes co-operating to achieve the required interface function. The details of each of these processes is explained in the following paragraphs.
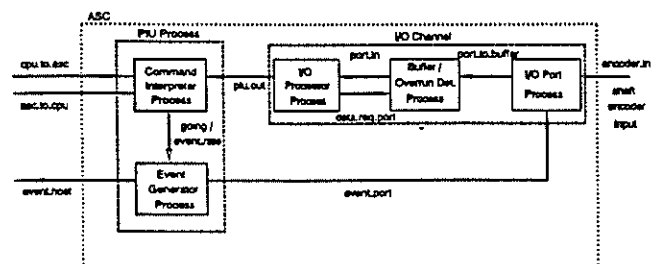
Fig. 3 The Shaft Encoder Interface Structure.

I/O Port Process :- The I/O Port process accesses the two single bit shaft encoder signals via the "encoder.in" channel. Each squarewave signal is captured and passed through a simple digital filter to remove noise glitches before being passed onto a quadrature decoder. The decoder treats the shaft encoder as a simple four state finite state machine (FSM) with the states arranged as a loop (see Fig. 4) and determines the current state of the FSM by interpreting the filtered quadrature signals generated by the encoder. Using current state information and noting the previous transition from either the left or the right adjacent states, the decoder can determine the direction of rotation of the shaft encoder and increment or decrement a 16 bit position counter accordingly. The I/O Port Process thus generates a continually updated count value corresponding to the shaft
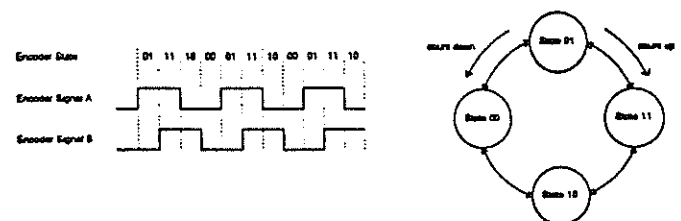
Fig. 4 Shaft Encoder State Diagram.

position which is then available to be passed to the Buffer / Overrun Detection Process for onward transmission to the I/O Processor Process. The transfer of data between the I/O Port Process and the Buffer/Overrun Det. Process occurs at the sampling instants determined by the event signals generated by the Event Generator Process. Appendix A shows the Handel code listing for the I/O Port Process.

The Buffer / Overrun Detection Process :- The Buffer / Overrun Detection Process provides the interface with the means of detecting and informing the user of the occurrence of sampling overrun. Sampling overrun occurs when the event signal frequency is too high compared to the execution rates of the tasks within the I/O Processor or the host transputer based S/W.

The I/O Processor Process :- The I/O Processor process receives count data from the I/O Port process (via the Buffer /Overrun Det.Process) and manipulates this data to generate angle and speed estimates that are made available to the host transputer via the Processor Interface Unit (PIU) process. The I/O Processor Process implements a custom microprocessor with two general purpose 16 bit registers, a 4 bit instruction register, a 16 bit operand register, a 5 bit instruction pointer register, a single 16 bit temporary register, and a set of 18 instructions.

The PIU Process :- The PIU process contains the interface to the host transputer processor and as can be seen from Fig. 3 consists of the Command Interpreter Process and the Event Generator Process. The Command Interpreter Process is linked to the host transputer via two channels "cpu.to.asc" and "asc.to.cpu", the former is used to pass high level commands to the I/O Coprocessor and the latter channel is used to return speed and angle data to the host transputer. The commands recognised by the Command Interpreter process are as follows; En / Dis-able event generation, Set event generator parameters, Get speed and angle data. The Event Generator Process generates a regular event signal which is passed to the I/O Port Process via the "event.port" channel and to the host transputer via the "event.host" channel.

The entire I/O Coprocessor structure for the shaft encoder interface has been described as a set of parallel processes using the Handel language and successfully simulated to verify correct operation (due to space constraints only the I/O Port section of the description is shown in Appendix A).

4 Conclusion

A programmable interface structure based on Field Programmable Gate Arrays that is capable of interfacing a conventional microprocessor to the various sensors / actuators in a real-time AC drive control environment has been developed. The interface structure is based on a coprocessor like structure and was developed using the Handel algorithmic description language and its associated hardware compilation techniques.

5 References

[1] W Leonhard, "20 Years Field Orientation, 10 Years Digital Signal Processing with Controlled AC Drives", invited paper, 6th conference on Power Electronics and Motion Control (PEMC), Budapest, Hungary, Oct 1990.

[2] F Blaschke, "The principle of field orientation as applied to the new TRANSVECTOR closed loop control systems for rotating field machines", Siemens Review, 1972.

[3] I Page, W Luk, "Compiling Occam into Field Programmable Gate Arrays", Research Report, Programming Research Group, Oxford University Computing Laboratory, Oxford, England.

[4] G De Micheli, D Ku, F Mailhot, T Truong, "The Olympus Synthesis System", IEEE Design & Test of Computers, Vol 7, No. 5, Oct 1990.

[5] A.S. Weban, J.W. O'Leary, G.M. Brown, "Codesign of Communications Protocols", IEEE Computer, vol 26, No. 12, Dec 1993.

[6] Many references to the Oxford work are available via the World Wide Web home page at URL http://www.comlab.ox.ac.uk/oucl/hwcomp.html.

[7] C A R Hoare, "Communicating Sequential Processes", Prentice-Hall International, London, 1988.

Appendix A - I/O Port Process Handel Listing

```
WHILE TRUE
   PAR
      encoder_in ? encoder_data
      {{{ filter encoder signal a
      SIMUL
         t_minus_1_a := (encoder_data \\ 0) 1
         t_minus_2_a := t_minus_1_a
         t_minus_3_a := t_minus_2_a
      IF
         (t_minus_1_a AND t_minus_2_a) AND t_minus_3_a
            ch_a_fil := TRUE
         TRUE
            IF
               ((NOT t_minus_1_a) AND (NOT t_minus_2_a))
               AND (NOT t_minus_3_a)
                  ch_a_fil := FALSE
               TRUE
                  ch_a_fil := ch_a_fil
      }}}
      ... filter encoder signal b -- this is a repeat of the filter
                           process above
      {{{ quadrature decoder
      IF
         (complex Boolean expression1 involving ch_a/b_fil,
                           ch_a/b_fil_old)
            count := count + 1
         TRUE
            IF
               (complex Boolean expression2 involving
                           ch_a/b_fil, ch_a/b_fil_old)
                  count := count - 1
               TRUE
                  DELAY
      ch_a_fil_old, ch_b_fil_old := ch_a_fil, ch_b_fil
      }}}
      {{{ output to buffer
      PRIALT
         event_0 ? event_any
            port_to_buffer ! count
         SKIP
            DELAY
      }}}
```

Address of main Author

D.R. Woodward, Department of Electrical Engineering, University of Natal, Private Bag X10, Dalbridge, Durban 4014, South Africa, Email: dwoodw@elaine.ee.und.ac.za.

A KNOWLEDGE-BASED END-USER DEMAND RESPONSE MODELLING TOOL FOR CUSTOMISED ELECTRICITY PRICING AGREEMENTS

JG Roos   IE Lane*

Centre for New Electricity Studies (CNES),
Department of Electrical and Electronic Engineering, University of Pretoria.
* Energy Efficiency Enterprises CC.

Abstract: Customised electricity pricing agreements are usually arranged between an Electricity Supply Industry (ESI) and its key customers, who are energy-intensive end-users of electricity. These special agreements will provide on the one side enough financial incentives for the key customers to participate in the utility's demand-side management (DSM) programs, while on the other side will provide the utility with sufficient revenue as well as a way to reach some of their DSM objectives. However, the design of these customised pricing agreements can be sub-optimal unless a well formulated methodology is followed. Such a methodology will be proposed in this paper, and a knowledge-based end-user demand response modelling approach to assist in this customised design will also be discussed. The concept is illustrated with an industrial case study.

1. INTRODUCTION

Few of mankind's endeavours have had the same impact on the world as energy production and consumption do. Electricity is often the most visible energy form because it has the most complex production, delivery and utilisation system. It is therefore natural that electricity is the focus of much of today's debate on energy efficiency and conservation. In the view of this, and because the industrial sector exhibits a great potential for DSM actions, this study concentrates on industrial load management (ILM) which can be defined as follows [1]:

"any action taken by industrial customers and/or the electric utility to change the customer's present load curve shape in order to gain from reduced total system peak loads, increased load factors and improved utilisation of scarce and expensive resources, i.e. fuels or transmission capacity".

In order for the utility to achieve the wanted load changes on a voluntary basis, it is very important that the incentives for the customers are sufficient. The main incentive for customers to implement these ILM alternatives is <u>more money in their pockets</u>. Electric energy tariff designs and incentive programs constitute a powerful class of DSM tools. The next section will cover a proposed methodology to design customised electricity

tariffs, while the structure of an end-user demand response modelling tool will be discussed in the ensuing section, which will be illustrated with an industrial case study.

2. CUSTOMISED ELECTRICITY PRICING DESIGN METHODOLOGY

An illustrative schematic presentation of the proposed methodology is shown in Figure 1. A customised pricing agreement may be initiated by anyone of the two parties involved. For instance, the supply utility may propose such an agreement to its key customer when the utility beliefs that there exists a load management opportunity at that customer's plant from which the utility can benefit. On the other hand, the end-user may initiate such an agreement when he beliefs that he qualifies for a better electricity pricing deal because of his intense use of electrical energy.

The main objective in developing a customised pricing agreement, is to design an electricity tariff structure in such a way that both parties will reap maximum benefit when implementing it. By means
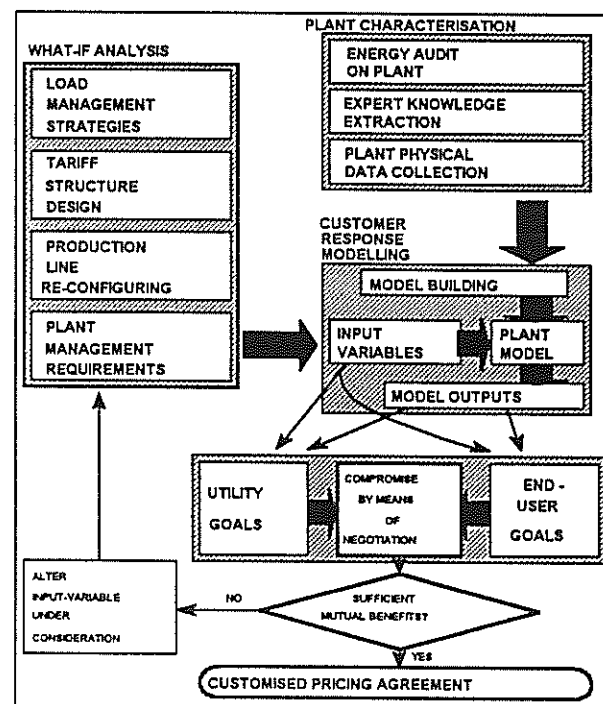

Figure 1: Customised Electricity Pricing Methodology

of negotiations the two parties will try to make a compromise on their respective performance criteria (or goals), after which each party must be satisfied with the benefits which it can expect from:

- The proposed electricity tariff structure and levels;
- The type and extent of load management strategies to apply;
- Possible production line re-configuration, e.g. smaller or larger buffer sizes;
- Fulfilment of plant management requirements, e.g. production targets.

Should one or both of the parties not be completely satisfied with the expected benefits after the compromising effort, one or more of these listed variables should be altered in a feedback process in an effort to increase the mutual interest of the parties.

As can be seen from Figure 1, these variables are part of a 'what-if' analysis and serve as inputs to a customer response model, which forms an imperative building block in this methodology. Typical outputs of the customer response model will include total production costs, electricity costs, production figures, production costs per unit produced, load profiles, load factors, production schedules, and production line configurations.

3. END-USER DEMAND RESPONSE MODELLING

3.1 The Knowledge-based Approach

As the structure of dynamic prices becomes more and more complex due to innovative customised pricing agreements, it is not only the metering and communication technology that will have to adapt to the need of technological advance, but innovation must also occur on the demand control and energy management side of an industrial load management scheme.

End-user demand response modelling can be accomplished by building a dynamic model of the end-user's plant from physical and economical properties of the plant. This quantitative approach has been followed by others [2,3]. However, a knowledge-based modelling approach can provide a further advantage in the sense that heuristic rules of the plant can be extracted from human experts (operators) at the plant and included as qualitative (descriptive) modelling in the dynamic model. This will support the quantitative modelling of the plant.

Knowledge about the plant are stored in a knowledge-base, while some of the physical properties of the plant can be modelled qualitatively (in the form of rules) rather than quantitatively, thereby taking advantage of the inference capabilities of the expert system. Due to

its artificial intelligence, the knowledge-base can 'reason' about input data from the plant or user of the expert system, and is able to assist the user in decision-making.

3.2 The Hierarchical Structure of the Model

One of the main objectives in developing the infrastructure of end-user demand response models, is to make the model-structure as general as possible. The idea is to build a model of almost any energy-intensive industrial plant without starting from square one each time. Therefore an object-oriented approach is followed in building a dynamic model of an industrial plant. This approach provides an unprecedented level of generality.

Figure 2 displays the hierarchical structure of the plant model which is used in this study. Due to space limitations this figure contains of the more important information only. At top level any industrial plant consists of objects like process-items, materials, flow-lines and management-items.
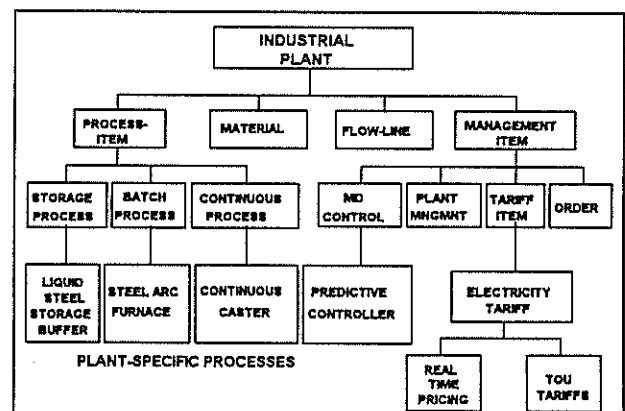
Figure 2: The Model Hierarchical Structure

Each of these objects can be broken down to the next hierarchical level. General types of process-items are storage processes, batch processes, continuous processes, etc. General types of materials are minerals, add-inns, etc. Flow-lines can be pipes, conveyer belts, etc. General types of management-items can be maximum demand (MD) controllers, a plant-management object, tariff-items, orders, order lists, etc. At this level general qualitative (rules) and quantitative properties surrounding each of these general objects are programmed. These rules should comply to any type of industrial plant, and once these rules are included in the knowledge-base, they can be used in the modelling of almost any type of industry.

At the next level in the hierarchical structure, **plant-specific** rules about the plant under investigation are included in the knowledge-base. For example, if a steel manufacturing plant must be modelled, the steel arc furnace in the plant will have its own set of production rules which will be

programmed in the knowledge-base. Apart from these knowledge, it also inherits all the attributes and rules from the batch type process at the higher hierarchical level, which already are contained in the knowledge-base. This object-oriented approach therefore will speed up the modelling of any type of industry.

3.3 Response Simulation

As soon as the model of the plant is built, the response of the plant (end-user) to various input variables should be evaluated. One of the more important 'what-if'scenarios to be analysed, is the demand response of the plant to tariff structures. Attributes and rules about various tariff structures, e.g. real-time pricing, TOU tariffs, etc., are included in the knowledge-base at a low hierarchical level, as is shown in Figure 2.

The simulation is started by giving plant-management an order to produce an end-product within a certain time period. The simulation is then run as fast as possible. Due to an event-driven approach that is followed, the simulation-time will at the end of each simulation-step increment with a non-fixed step size to the time when a next event is expected. This speeds up the whole simulation procedure when compared with the case when the step size of the time increments is fixed. The production costs of the plant are then calculated for the given tariff structure, as well as revenue to the electricity supplier.

An 'optimisation'procedure can then be run to re-schedule the plant production levels during the production period in order to take advantage of the tariff structure and thereby decreasing production costs. This is in fact a load-shifting procedure.

This process can be repeated until both parties in the customised tariff design process are satisfied with the outcome of the results.

4. IMPLEMENTATION AND AN INDUSTRIAL CASE STUDY

4.1 The G2® Real-time Expert System

G2® is a real-time expert system and a product of Gensym in the USA. It is a complete application development environment for building and deploying intelligent applications. Unlike other programming environments, G2® supports the entire application life cycle with object-oriented tools, graphical tools and a structured natural language that support rapid prototyping and enable close communication between developers and end-users. G2® enables both quantitative and qualitative modelling and simulation of dynamic systems and processes by using objects, rules, procedures and formulas. It is therefore an ideal

tool for implementing the end-user demand response models as proposed in this paper.

4.2 Case Study: Description of the Plant

The new plant under investigation will produce ceramic materials for refractory applications. It has one 4 MW electric arc furnace to melt the mix of raw input materials at 2000 °C. The minimum power level is 2.1 MW, which means the process should never be switched off. The plant has a base load of 600 kW, while the power losses of the arc furnace are ± 600 kW. It inherits attributes and rules from a continuous-in type process, because the material inflow to the furnace is continuous, while the outflow to the ingots is discrete. Specific production rules about this process, e.g. the electrical energy consumption calculation as a function of the input materials' chemical properties, were included in the G2® knowledge-base.

4.3 Tariff Structure "What-if" Scenarios and Results

During the tariff customisation process the most important performance criterion of the end-user was that the tariff should result in relatively low production costs. The electricity supplier, on the other hand, was looking for a tariff that will give the end-user enough incentives to shift its load away from peak periods, but which will still guarantee enough revenue to the supplier.

Two tariff structures were investigated. Eskom's Maxiflex time-of-use (TOU) tariff, and a new two-part real-time pricing (RTP) tariff. The latter consists of a customer base load (CBL) at a fixed energy tariff, and the difference between the actual power consumption and the CBL, at the hourly marginal rate (see Figure 4 as an example). The CBL, of which an example is shown in Figure 3 for two days, is based on a historical load profile of an existing customer, or on an agreed upon load profile for a new customer. The customer agrees to consume at least the amount of energy beneath the CBL in one month, at a fixed hourly energy tariff for the whole month. This will ensure
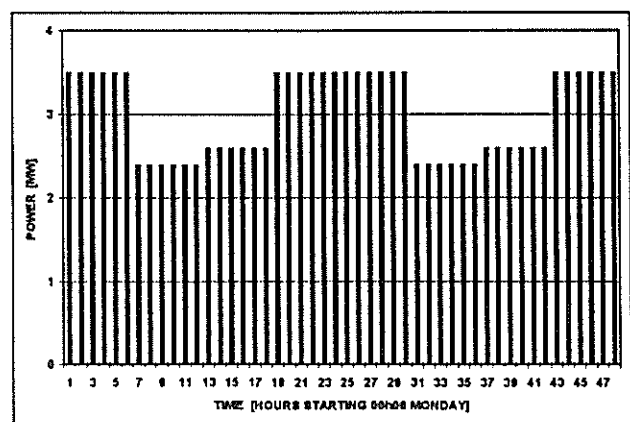
Figure 3: Customer Base Load (CBL)

a minimum revenue to the supplier.

Various scenarios were analysed with the aid of the developed plant model in G2®. For a production target of 350 tons of end-product within 48 hours, the influence of the CBL structure were investigated on the production costs. The first structure that was investigated, was a flat profile at 3 MW, resulting in electricity costs of R38260. When changing the profile to the one that is shown in Figure 3, with the same area underneath (same energy) as for the previous case, the electricity costs were 3.5% higher. Using the last profile, but shifting it 6 hours on, resulted in roughly the same electricity costs as for the flat case. It is thus clear that the CBL profile will not influence the production costs of the end-user dramatically, but it will definitely determine if the load shifting DSM goal of the supplier will be met or not.

With the CBL chosen as the one shown in Figure 3, the plant was given a production target of 600 tons in 168 hours. The electricity costs obtained from the Maxiflex TOU tariff and from the two part RTP tariff were compared, and were R104998 and R67760 respectively. Although the TOU tariff would mean a higher income to the supplier, this type of tariff will not have the same indirect savings to the supplier as the RTP will have, due

to the timeous load shifting actions that will result from the latter one.

Another scenario that was investigated, is the possible incremental cost savings of the end-user if he can control his load intelligently. The concept here is to decrease his load during hours when the hourly marginal rate is high, and vice-versa. An 'optimum" solution is to either run at minimum power level or maximum power level, but never in between. The prove of this statement will not be covered in this paper.

The 'optimisation" procedure determines the 'ideal" production schedule during the production period. With the given CBL and the production target of 160 tons in 48 hours, the electricity costs can be decreased from R17215 to R15485 (-10%). In this case the arc furnace was run at minimum power level (2.1 MW) when the hourly marginal rate is above 10.05 c/kWh. The hourly marginal rates in Figure 4 apply, and Figure 5 shows the scheduled power consumption profile. For higher production rates the possible cost savings will decrease.

5. CONCLUDING REMARKS

A methodology to design customised electricity tariff agreements between an electricity supplier and a key customer is proposed in the paper. It is suggested that this methodology should be supported by using an end-user demand response model. An industrial case study is given and from the results it is clear that the knowledge-based modelling approach possesses certain advantages which will be to the benefit of the electricity supplier and the end-user in incrementing their cost savings.

Figure 4: Hourly Marginal Rates

6. REFERENCES

[1]   Björk, C.O :'Industrial Load Management : Theory, Practice and Simulations", Elsevier Science Publishers, Amsterdam, 1989.

[2]   David, A.K. :'Optimal consumer response for electricity spot pricing", IEE Proceedings, Vol. 135, Part C, No. 5, Sep. 88, pp. 378-384.

[3]   Manichaikul, Y., Schweppe, F.C.: 'Physically based industrial electric load", IEEE Transactions on Power Apparatus and Systems, Vol. 98, No. 4, Jul. 79, pp. 1439-1445.

Figure 5: Scheduled Power Consumption

7. ADDRESS OF MAIN AUTHOR

Mr JG Roos, Department of Electrical and Electronic Engineering, University of Pretoria, Pretoria, 0002.   E-mail: johan.roos@ee.up.ac.za

SAUPEC - An integrated electricity tariff system for the North East Rand TMC

C.M. Schoonbee[1]   B.R.A. Mountain[2]   C.E. Dingley[1]

[1] Dept of Electrical Engineering, UCT

[2] Kennedy and Donkin Africa (Pty) Ltd.

ABSTRACT

This paper discusses the development of rationalised tariffs within the North East Rand TMC. A cost-of-supply methodology was developed to analyse the structure and level of costs. This was used to determine more cost-reflective tariffs within the constraints indentified. Such an approach promises a better compromise between the conflicting objectives of a tariff system.

1. INTRODUCTION

This paper arose out of an investigation into the restructuring of the municipal electricity distribution undertakings within the North East (NE) Rand Transitional Metropolitan Council (TMC). Tariff rationalisation is a key element of this restructuring and is the specific focus of this paper. Quantification aspects of the investigation are yet to be completed and so firm figures are not given. These will be available in an undergraduate thesis based on this investigation.

The paper begins by describing the current situation in the NE Rand and sets out the objectives of the tariff investigation. It then discusses cost-of-supply as a basis for the tariff study. This leads on to an explanation of how the investigation was carried out. The proposed tariffs are then outlined and their impact discussed. Finally conclusions are drawn, emphasising the key issues.

2. BACKGROUND TO THE INVESTIGATION

The NE Rand TMC is situated to the north-east of the Witwatersrand and consists of three substructures :Kempton Park / Tembisa; Midrand / Ivory Park / Rabie Ridge and Edenvale / Modderfontein.

It contains industrial areas (including some very large users of electricity), established and electrified residential areas as well as low-income and under-developed residential areas. Total bulk electricity purchases for the TMC exceed R 280 million p.a.. A single licence has been granted to the TMC for the distribution of electricity within its region. An integrated tariff must therefore be implemented no later than the start of the next financial year i.e. July 1996.

The 'black' local authorities, which are experiencing almost total non-payment for services, have been amalgamated with their 'white' counterparts, where electricity sales generated considerable surpluses. This has placed a severe burden on the combined resources (financial and human) of electricity undertakings within the TMC.

Furthermore, electricity pricing in the NE Rand is sub-optimal. Firstly, the average prices paid by comparable consumers differ widely within the TMC as shown by Table 1. There are also significant cross-subsidies from commercial and industrial to residential consumers. The extent can be estimated from a comparison of tariff ratios with countries where cost-reflective tariffs have been an entrenched policy[1]. This is shown in Table 2.

Type of consumer	Domestic (800 kWh p.m.)	Small non-residential (25 kVA, 40% load factor)	Large (1 MVA, 70% load factor)
Highest average price [c/kWh]	21.2 (Midrand)	31.5 (Edenvale)	18.6 (Edenvale)
Lowest average price [c/kWh]	13.0 (Modder-fontein)	21.4 (Midrand)	12.4 (Modder-fontein)
Highest/Lowest price	163 %	147 %	150 %

Table 1. Price variation within the NE Rand TMC

	Range of ratios within TMC	Ratios established from international study [1]
Residential / Industrial	126 - 133 %	201 %
Residential/ Small non-residential	47 - 87 %	124 %

Table 2. Comparison with international cost-reflective tariffs

3. PURPOSE AND OBJECTIVES OF THE TARIFF INVESTIGATION

The objectives of the tariff investigation were as follows:
1. To investigate the current state of electricity pricing within the TMC.
2. To develop an approach to the determination of tariffs.
3. To develop a system of tariffs which will address the problems outlined above as well as comply with the requirements of the National Electricity Regulator.

The requirements to be met by the actual tariffs are that they
- should be cost-reflective in terms of their structure and levels,
- should ensure the financial viability of the electricity distribution industry within the TMC,
- should ensure access to electricity by the poor and
- should take account of implementation constraints and the need for stability and understandability.

It was clear at the outset that these requirements conflict and that some compromise would be unavoidable.

4. TARIFF DETERMINATION

Given the similar tariff structures of the different electricity undertakings, an obvious and simple approach to the development of integrated tariffs would be to use an average of the tariff levels weighted by the size of electricity sales. Instead, the tariff development was based on a cost-of-supply methodology. The reasons for this decision are :
- Cost-reflective tariffs based on long-run marginal costs aid economic efficiency by promoting effective resource allocation. The development of tariffs that are cost reflective in their structure and level necessitates a cost of supply methodology.
- The use of a cost of supply methodology also provides a rational basis for consistency and equity in the prices charged to consumers by different undertakings.
- As mentioned earlier, the objectives of a tariff system may conflict to some extent. A rigorous and sound costing methodology helps to make the implications of trade-offs between the objectives explicit.

The tariff investigation was performed in the following stages.

1. The current tariffs were investigated to obtain a picture of the *status quo*.
2. A cost of supply model was then used to analyse the structure and level of supply cost components such as energy and distribution capacity in terms of cost determinants such as time of use, supply voltage and load factor.
3. Cost-reflective tariffs were then developed to reflect both the structure and level of these costs.
4. The revenue from the proposed tariffs was then forecast.
5. Adjustments were made to the tariffs to ensure that revenue requirements were met and to meet other objectives such as subsidising poorer consumers while distorting the information on costs, conveyed by the tariffs, as little as possible.

5. PROPOSED TARIFF SYSTEM

Although final figures are not yet available, the form of the proposed tariffs are known. Because of the time and metering constraints, the initial tariffs will be based on the current tariff structures. This precludes truly cost-reflective tariffs, which the cost of supply study shows, would have to be based on time-of-use (TOU). However, it is important for such tariffs to be developed and work will continue on this. The TMC is implementing a sophisticated, remote metering system over the next few years. It is envisioned that TOU tariffs, using the new metering system, will be available after two years to those customers for whom the benefits are worthwhile.

The proposed tariff structures for various consumers are summarised in Table 3 below.

	Fixed monthly charge	kWh charge	Maximum Demand Charge
Residential (Option 1)	✓	✓	✗
Residential (Option 2)	✗	✓	✗
Small non-residential	✓	✓	✗
Large non-residential	✓	✓	✓

Table 3. Proposed Tariff Structures

The tariffs will be made more cost-reflective in their levels and in in their structure through the use of options which allow more accurate categorisation of consumers into cost groupings.

Residential users
Two tariff options are proposed for residential users. The first consists of a fixed monthly charge of about R30 together with a single kWh charge. The second option has no fixed charge but has a higher kWh charge than in the first option. The second option will therefore be cheaper for consumers using less than a certain 'break-even' amount while the first option will be cheaper for consumption above that amount. The first option reflects the structure of supply costs, which is shown by the costing study to be represented by a fixed charge and a variable charge. The second option provides a subsidy to low consumption (and generally low-income) consumers. It is proposed to set the break-even amount at 400 kWh p.m. This is above what can be considered a basic level of consumption (about 150 kWh p.m.) but a break-even at this level will allow an increased subsidy at low consumption levels while phasing out the subsidy more gradually.

This approach of offering options is in contrast to the often proposed alternative of a single kWh rate for all residential consumers with no fixed charge. However, such a scheme cross-subsidises low consumption users through entrenching a non-cost-reflective structure. This is not a satisfactory compromise. Perhaps the reason why it is popular is that a fixed charge is considered difficult to implement on pre-payment meters. As mentioned earlier, the N-E Rand is moving to a

remote metering system with a centralised database. This allows prepayment as well as the easy implementation of more complicated (and cost-reflective) tariff structures where appropriate.

Small non-residential consumers
An analysis of supply costs does not provide evidence that such users' supply costs differ substantially from those of residential consumers. It is therefore proposed to extend the residential tariffs to this category.

Large consumers
As discussed above, the proposed tariff structure will be based on the current structure. However, the levels will be adjusted and the tariffs will be made more cost-reflective in their structure by offering options. These options will allow consumers to be categorised by their load factor ('high' or 'low') and supply voltage (above 400 V or not) which were shown to be important cost determinants by the costing study. This allows four cost categories (2 x 2), each with different demand and energy charges, while still using the same metering technology.

6. IMPACT OF THE PROPOSED TARIFF SYSTEM

This section discusses some political and social implications of implementing the proposed tariffs. Firstly, the average prices to be paid by residential consumers will increase by about 50 %. For reasons of affordability, political acceptability and tariff stability, such a large increase cannot be immediately implemented. A way of dealing with this is to phase in the final tariffs over a period of say three to four years. This should also alleviate the problem of significant differences between residential tariffs in the NE Rand and neighbouring areas where residential users are still cross-subsidised. The next few years should see cost-reflective tariffs being developed in these areas as well and this problem will then disappear.
Poorer consumers may not be able to afford cost-reflective prices. The issue of their cross - subsidisation will have to be addressed. Given the already substantial increase proposed for residential tariffs, this burden will probably have to be spread across all consumer groupings. Solving the non-payment problem really requires political and national solutions. Until then, the losses will probably have to be made up by paying consumers in all consumer categories.
The prices for commercial and industrial consumers will generally be significantly lower. This should improve their competitiveness and attract further industrial development.

7. CONCLUSIONS

This paper has outlined the rationale for, and the execution of, an investigation into the development of rationalised tariffs for the NE Rand. It has outlined the proposed tariffs and discussed the possible impact of their implementation. The emphasis has been on the use of a cost-of-supply methodology to develop tariffs which meet their objectives in an optimal compromise given the constraints of the real world.

REFERENCES

1. Mountain, B.R.A. '*The current state of electricity pricing in the South African Electricity Supply and Distribution Industry*' ,National Electricity Regulator : September 1995

Acknowledgements

A COMPARISON OF ABC AND UNDERGROUND CABLE FOR LV MAINS IN URBAN ELECTRIFICATION PROJECTS

Conrad G. Blignaut   Charles Dingley

Department of Electrical Engineering, University of Cape Town

ABSTRACT

Aerial Bundled Conductor (ABC) is compared to underground cable for LV reticulation in urban electrification projects. Two existing townships that were electrified with ABC are redesigned using three alternative types of underground cable. The capital installation costs of the respective systems are then calculated. A theoretical township layout is developed to investigate the installation cost variation for the variation of input design parameters. It is concluded that, depending on conditions, an ABC installation costs between R1220 to R1760 per erf, while an underground installation costs between R1840 to R3630 per erf.

1. INTRODUCTION

Current urban electrification projects of informal residential areas almost exclusively utilise Aerial Bundled Conductor (ABC) for the low voltage installation. The main consideration in this choice appears to be the cheap installation cost of ABC systems as opposed to conventional underground systems. The question arises however as to whether the saving in initial installation cost is not outweighed by the long-term benefits of an underground system. This paper attempts to give a broad answer to that question, based on a 4-month BSc final-year thesis project [1].

R E Zietsman [2] compares five different distribution network types, with results based on cost estimates prepared for a real township layout of averaged sized stands in an area of 1630 erven. The ABC and underground system installation costs are found to be R1345 and R1775 respectively, a difference of 32%. Irving and Chesterton [3] do not differentiate between the LV and MV reticulation and conclude that a fully ABC system leads to a 20% saving on a fully underground system. A report by the Port Elizabeth Municipality [4] points out that, under certain conditions, the availability of low interest financing is subject to the use of ABC, and that in low-income areas, the capital investment is barely recovered in the case of an ABC installation.

This paper proceeds with a general description of the hardware requirements for ABC and underground LV systems respectively, a discussion of two case studies and a description of the theoretical model developed. Finally, the results are analysed and discussed.

2. HARDWARE REQUIREMENTS FOR LV SYSTEMS

In both the underground and ABC design, standard installation practices were followed, e.g. underground cable is laid in trenches, using bedding sand for protection, and PVC cable

ducts at road crossings, while ABC is mounted on 9m poles with standard mounting hardware.

2.1 Transformer Installation

The transformer specified for both designs is of the pole-mounted type commonly used in current urban electrification projects. Conventional underground designs use either brick-built or miniature substations for housing the transformer, but this is thought to be too expensive (an equivalent minisubstation costs about 97% more) for the purpose of a comparison of alternative cable types. Discussions with design engineers indicate that this is a viable system, particularly where the MV side is overhead cable.

2.2 Service Connections

For an ABC system, pole-mounted service protection boxes (SPB's) are used, with either one or two ABC phases per box feeding single phase consumers. Airdac cable is run from inside the SPB to the consumer premises, mounted with airdac strain clamps on either side of the connection. For the underground system, underground service connections are used with terminations similar to those for the LV cable (at the CDU), and split-concentric service cables laid in trenches to the consumer premises. Both systems used service cable sizes of $16mm^2$ and $10mm^2$ with ReadyBoard and Prepayment metering at the consumer premises.

2.3 Earthing

For the ABC system, ESKOM's Electrification Standard specifies as the preferred practice for the earthing of the LV distributor [5], a multiple earthed neutral (MEN) system, where the supply distributor is combined neutral and earth (CNE) and the arrangement of the service connection is separate neutral and earth (SNE). It is common practice for an underground LV distributor to be earthed at the transformer star point and at all remote ends.

3. CASE STUDIES

Scenery Park, a township outside East London, and Khayelitsha, in the Western Cape, are two layouts originally designed using ABC.
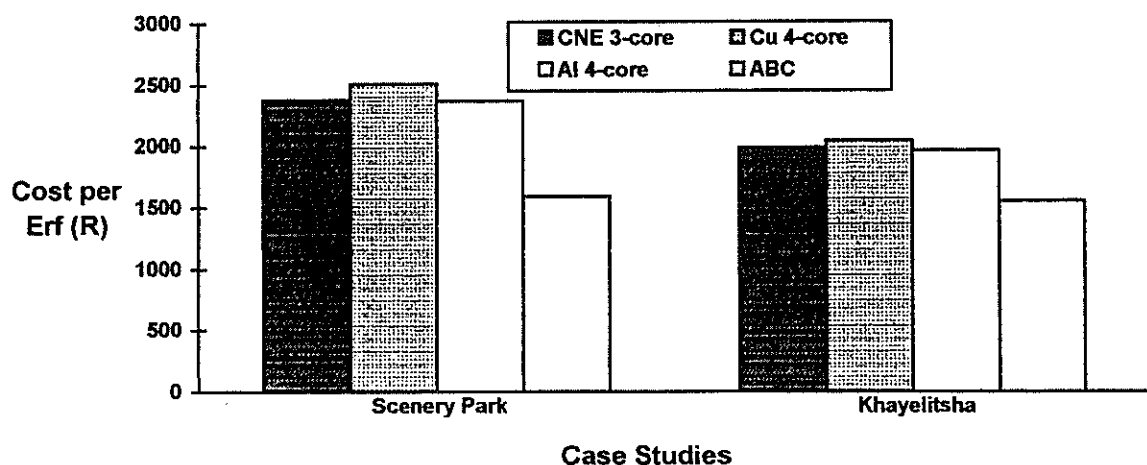

Figure 1: Cost per erf for case studies, using different cable options

By compiling a Bill of Materials, and applying current contractor rates, the cost of the ABC system is calculated. The underground system is then designed, using a software package known as CARD ("Computer Aided Reticulation Design") for optimal sizing of the LV cables within the 6% volt drop constraint. For each layout, this process is repeated for three different types of underground cable, namely four-core copper PVC-insulated cable, four-core aluminium PVC-insulated cable, three-core XLPE-insulated aluminium CNE cable. Figure 1 shows the costs per erf for ABC and three alternative underground cable types.

4. A THEORETICAL MODEL

A theoretical township layout was implemented as a computer program, with the intention of determining the effect on the cost per erf as various input design parameters are varied. The user is required to enter the feeder structure for a transformer area, specifying cable sizes, cable lengths and the number of consumers at a particular node. It is assumed that a transformer area is sufficiently representative of the entire area, and the program calculates all branch currents, power losses, the annual cost of losses and the cost per erf for the area.
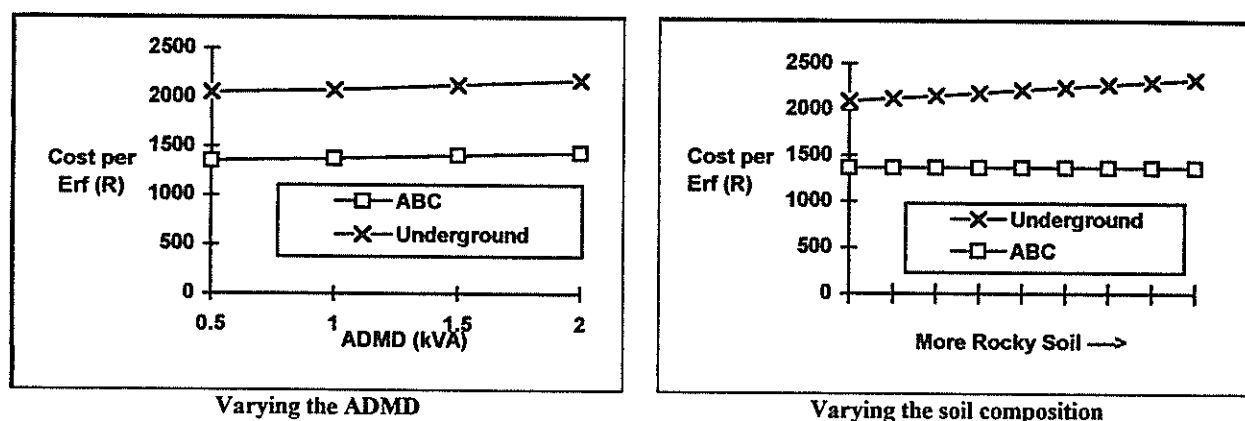
Figure 2: The effect on the cost per erf as various parameters are varied

Figure 2 shows the results for two parameters that are varied, as determined for a transformer area of Khayelitsha, using the computer program. The theoretical model can be used to determine the range of the cost per erf for an underground and ABC system respectively, as the various parameters are varied between their maximum and minimum values. For all the parameters set at their minimum values, it is determined that an ABC system costs R1353 per erf, while an underground system costs R2051 per erf. At the maximum values of parameters, an ABC and underground system cost R1595 and R3302 respectively. If a 10% margin is added at each limit, it is determined that the cost of an underground system varies between R1840 and R3630 per erf, and that of an ABC system between R1220 and R1760 per erf.

5. CONCLUSIONS

5.1 Case Studies

For the two case studies, it is concluded that if Scenery Park had been designed using an underground LV system with pole-mounted transformers, it would have cost between 47% to 58% more, depending on the choice of underground cable, while the corresponding figure for Khayelitsha is 26% to 32%. The difference for the case studies may be because Khayelitsha

was designed using underground service connections, and because soil conditions are highly favourable for trenching (giving a lower cost for the underground system).

5.3 Studies of the Theoretical Layout

Studies with the theoretical model suggest an increase of around 6% in the cost difference of the two systems for an increase of 1.5kVA in the design ADMD. Soil conditions, the level of development and the average width of roads have a negligible effect on the cost of an ABC system but are shown to have a significant effect on an underground system, suggesting that an underground system is far more sensitive to the prevailing conditions. The results further indicate that the cost difference between the two systems is minimum where a low level of development exists in the township, hardly any rocky soil is encountered, narrow, untarred roads are found, and the consumption level is low. Ironically, these are exactly the conditions in which an ABC system is favoured from the point of view of recovery of the initial capital investment. In considering the results from the model, it must be kept in mind that the input factors do not vary independently, for example, a higher level of development is likely to mean a higher design ADMD. The model does however give a good indication of the approximate effects of varying these parameters.

5.4 The Capital Cost Difference: Underground vs ABC

From the results obtained above it is concluded that as a worst case scenario, an underground system may cost up to 198% more than an ABC system, while at best it would be 4.5% more expensive. These figures suggest that the question of underground versus ABC is not an absolute, but is highly dependent on the conditions in the area. There may be conditions where an underground system can be installed at a capital installation cost of only 5% higher than that for an equivalent ABC system.

REFERENCES

1. Blignaut C G, *A Cost Comparison of ABC vs Underground Cable for Urban Low Voltage Distribution Networks*, BSc thesis in partial fulfilment of a degree in Electrical Engineering, University of Cape Town, November 1995.
2. Zietsman R E, *A Comparison of Alternative Distribution Networks for the Supply of Electricity to Urban Domestic Consumers*, presented at the Conference on Appropriate Technology for Developing Communities, Windhoek, June 1992.
3. Irving D J and Chesterton W, *Appropriate Township Distribution*, paper at the Workshop on Electrification of Developing Communities: Innovation and Standardisation, November 1991.
4. Port Elizabeth Municipality, *Report to Traffic and Engineering Services Committee*, August 1994.
5. Eskom, *Electrification Standard*, Section 2 : Earthing, pp 2.30 REV 1.

Acknowledgements

Investigation into the feasibility of implementing a 132-kV network in the eastern suburbs of Pretoria.

CJ Scherman, GJ Delport, JLM Pretorius

Centre for New Electricity Studies,
Department of Electrical and Electronic Engineering, University of Pretoria.

ABSTRACT:

A great deal of risk is involved in forecasting future load capacities of newly planned areas. Due to the uncertainty of the development in urban areas this risk involves the correct selection of equipment to meet the electricity needs of the newly planned area. Today this risk is greatly reduced thanks to modern technological aids, such as computer simulation and load forecasting software.

I. INTRODUCTION

Pretoria has one of the biggest municipal areas in South Africa. Engineers of the City Council of Pretoria were given the utmost challenge to design and construct a distribution network for the developing city in the early years of this century. This task was not the easiest due to insufficient data being available for the planning of the future load of certain developing suburbs. Another problem, the lack of communication and co-ordination of data, also became a big factor when the planning of some of these areas was done. The outcome was that some of the regions today are stranded on islands in the distribution network with insufficient capacity available for a growing load.

II. DESCRIPTION OF THE CURRENT NETWORK

Pretoria's distribution network consists of a 132 kV network, where each 132 kV substation is supplying its own 11 kV network. These 11 kV networks consist of secondary substations that are fed by 11 kV feeders from the 132 kV substation. Each 132 kV substation has its own theoretically supplying radius ranging from 1 and 3 km, depending on the load density of the region, from where the next primary substation must supply. Faerie Glen and Garsfontein make out one of the so-called "dead regions" that is located between the geographical supply areas of four surrounding 132 kV substations.
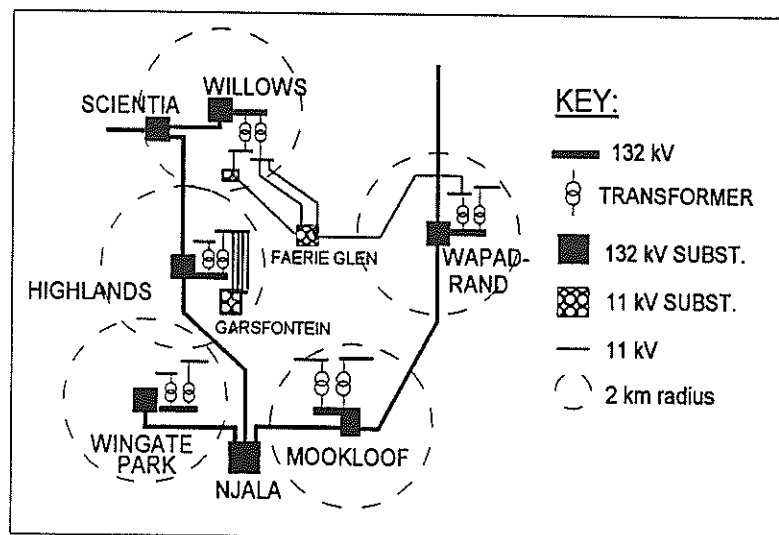

Figure 1 (Schematic drawing of study region)

Figure 1 shows the layout of the situation schematically. The "dead region" lies between the inner and outer 132 kV ring, covering Faerie Glen and Garsfontein.

III. FURTHER COMMENTS ON THE PROBLEM

Winter reports show that the study area's load is growing quite rapidly, and that the current operation of the network will not be suitable within a few years. This means that a solution has to be found urgently to avoid consumer dissatisfaction due to power failures because of overloaded equipment.

IV. DESCRIPTION OF THE CURRENT OPERATION

Faerie Glen is fed from Willows II, by ways of three 11 kV cable feeders, and from Wapadrand, by ways of one 11 kV cable feeder. Due to the loadgrowth around Willows, this way of operation can no longer be sustained. Willows does not have the capacity, nor the expandability due to physical limitations, to supply Faerie Glen and the local consumers around Willows anymore [1]. Thus a new solution must be found.

Wapadrand does have the capacity and the expandibilty for supplying in the local consumerload as well as Faerie Glen's, for the time being. This situation will not be able to continue for much longer, due to the residential and commercial growth around Wapadrand and in Faerie Glen.

Garsfontein is fed from Highlands by ways of four 11 kV cable feeders. An increase in the load of Highlands substation, due to much commercialisation around Menlyn, also arised concern in the future supplying of this mainly residential load.

It is because of this network limitations that this study had to be made, to find a way to supply Faerie Glen and Garsfontein for the next 25 years. This study must find a practical cheap solution that will satisfy the City Council of Pretoria, as well as the consumers in Faerie Glen and Garsfontein.

V. CRITERIA USED TO FIND A SOLUTION

By studying the load growth of the consumers and the future development in the region, a solution must be built to supply the load in the region. Each possible solution must be judged and compared by way of certain pre-determined criteria, which will result in a most economic and acceptable solution for both the consumer and the City Council of Pretoria. The following questions must be asked to enable us to make a decision on which solution will be the best for this region, they are in order of importance;

1.   What is the cost involved for the solution?
2.   Will the reliability of the system be improved by the solution?
3.   Will the solution be able to supply in the future load of the region?
4.   Are there the necessary servitutes and sites available for the solution?
5.   Can we make use of the current equipment to save costs?
6.   Can we improve the solution by importing new technology?
7.   Will the solution be able to satisfy the future customers in the region? (Who are the future customers?)
8.   Is the solution integratable with the current network?
9.   Will there be any voltage drop over long distances, which will affect the consumers negatively?
10. Is the solution aesthetically acceptable for the average consumer in the region?
11. What will the ecological impact of the solution be on the environment, and how will it affect the consumers?

The above mentioned questions make out the criteria that will be best satisfied by the winning solution. Due to the extent of the problem, many solutions can be explored. This means that criteria such as reliability, cost and environmental acceptability must be analysed and weighed against each other. We have decided to give each of the criteria a weighing factor to make the decision for finding the best solution easier. For example cost and reliability will weigh much heavier than the ecological impact on the environment. Other physical obstructions must be taken into account, such as the availability of servitutes and building sites for new substations. Because Faerie Glen is situated in a high income area, and most of the terrain has already been bought up and developed, the aforementioned criteria could extend in magnitude.

VI. STUDIED SOLUTIONS

A) Build a new 132 kV substation in Faerie Glen.

This solution will solve the loadgrowth of Faerie Glen and Garsfontein, and might also be used to help supply in the electrisity need of the surrounding substation areas. It will also solve the problem of voltage drop, because no 11 kV feeder will be longer than 3 km, due to the overlapping of supply areas between adjacent substations. This solution will also be able to integrate with the current network, and might increase the electricity reliability for the average consumer, if correctly implemented.

Unfortunately this solution is very expensive. A further problem, easthetics, arises. No consumer, especially in this rich income area, will allow the reduction of property value, due to an unsightly 132 kV transmission line through their suburb. This will escalate the cost, because 132 kV cable will have to be used, which is approximately five times more expensive than a transmission line.

This solution can work, if the consumer is taken into account, and if the customer is able to help capitalize the cost for such a big project.

B) Maximize the capacity of the surrounding substations.

This means that the surrounding substations is used by ways of 11 kV sattelite substations, to feed into the problem area. This means that a few smaller and cheaper 11 kV substations must be build, to function as sattelite substations. This will be much more acceptable to consumers, because there will be made use of 11 kV cable feeders.

Although it is cheaper than solution 1, this solution will not be able to cope with the growing load in and around the study area for very long. Another disadvantage of this system, is that more consumers will be affected by a 132 kV substation power-failure if such an event happens.

Servitutes and sites may also be a big obstacle to overcome, because of the fast development going on in the area.

C) Upgrade Highlands substation to supply in the study area's need:

This solutions is much more realistic than solution 1 and 2. Highlands consist of two stages. It was designed to be able to function as a three stage substation. This means that it can be upgraded with 35 MVA more capacity to supply the growing load of Faerie Glen, which is situated nearby Highlands. The solution will be suffucient for at least 25 years, and will improve the reliability of the network.

The disadvantage of this solution is the problem that arises with the integration with the existing 11 kV network. New 11 kV feeders will have to be laid to the existing 11 kV substations. The solution will still have a problem with voltage drop due to the long supply radius from Highlands. It is also not certain how much development will take place around Highlands, seeing that there are so much commercialisation taking place in this area, this solution might take some of the capacity needed for future consumers.

D) Upgrade Wapadrand substation to supply in the study area's need:

After a lot of consideration this solution was found to be ideal. Wapadrand is also situated near Faerie Glen and does have the possibility of expansion. This substation was designed to function as a ABC+R substation in the future, this means that three transformers supply in the load, while the other one acts as a reserve for the three in operation. The substation yard has sufficient space for upgrading to a ABCDE+R substation. Currently it is operated as a A+R, which gives us the oppertunity to utilize this substation as a source of power for the "dead area". The cost involved for upgrading the substation to a AB+R substation is mainly the purchasing of a transformer with it's switchgear. This solution will also please the consumer, because noo serious alterations will be made to their surrounding environment, and no new unsightly power lines will have to be build. This solution will be able to supply the region for more than 25 years, due to the large expansion

possibilities of the substation yard. Development around Wapadrand is slow, because of the large number of agricultural holdings, which is more difficult to develope than farms. This solutions also increase the capacity of Wapadrand, for when development starts to increase rapidly, to give the council a safety time buffer to supply the future load of this region. The integration with the existing 11 kV network, will also be much easier in cheaper, seeing that most of the 11 kV cables is laid from Wapadrand to supply some of the sattelite substations in Faerie Glen.

This is propably the only acceptable solution for both the City Council and the consumers, for this specific region.

A factor which have not be discussed so far is the future load, which could have an effect on the solution.

It can happen that the growth shown from the City Council's winter reports, can be misleading. The current consumers is on average age, still young and thus quite hungry in using domestic appliances. This might change over ten years, with a reduction in electricity demand due to the more mature average consumer. Less appliances, and less unnecessary wasting of electricity. The region might be in the last stages of development that will mean a much smaller target demand in ten years time. This aspects might mean that there are no need for concern for the next 25 years, which means all solutions are invalid. On the other hand, recent figures obtained of applications for subdivision of stands, and building of more than one house on one stand in the study region and surrounding areas, show that the future electricity demand for this region could double in a few years time. This can mean that the upgrading of Wapadrand must be ABC+R rather than AB+R, to supply in the need.

VII. CONCLUSIONS

After each solution was judged by the pre- determined criteria, a point was awarded for the solution in as much the solution satisfied that specific critaria. Afterwards, all the marks was added up and the solution with the least marks won. This study showed conclusively that the best solution for this region at this time, is to upgrade Wapadrand to a ABC+R substation.

Although the solutions mentioned in this article covers a broad spectrum of solutions, there are still other solutions that can be studied. These solutions however will mainly be permutations of the mentioned solutions due to the restrictions set by the pre-mentioned criteria.

It must be stated that the solutions discussed in this study is unique, and the conditions hold exclusively for this region. The solutions may differ quite dramatically for a region situated in another demographic area.

REFERENCES

[1] - PM Erasmus: CCP intern winter report for 1994.

ADDRESS OF MAIN AUTHOR

CJ Scherman, Department of Electrical and Electronic Engineering, University of Pretoria, Pretoria. 0002.

A Mathematical Algorithm
for Investigating
Soil Resistivity

DAVIDSON, Innocent E
Department of Electrical and Electronic Engineering,
University of CapeTown,
Rondebosch 7700, SOUTH AFRICA
Phone: 27 (21) 650 4093, Fax.: 27 (21) 650 3465
E-Mail: innocent@emf1.ee.uct.ac.za

Abstract

Grounding systems are designed to ensure continuity of power supply, safety of equipment and personnel in electrical power operations, and to confine ground voltage elevations within limits tolerable to the human body. This is achieved using protection schemes such as earthing devices. This paper presents a mathematical model for estimating earth resistance values at different depths using the Linear Regression Technique and thus investigate soil resistivity. Results from experimental tests are presented and discussed.
Key words: Grounding systems, soil resistivity, earthing practices.

1   Introduction

The Nigerian economy like that of many other developing nations, is becoming more dependent on electricity as a major resource for its energy needs. The level of economic growth presently enjoyed in the country, has been brought about by the availability and efficient distribution of electrical power as well as its safe application[1]. Irrespective of the security and safety of supply, electric power could be hazardous to personel and property. This could be due to stray currents arising from defects in energised apparatus.

In electrical power operations, the safety of the equipment and personel cannot be over-emphasized. It is considered equally as important as the continuity of power supply[2]. The use of inadequate protection schemes in the operation of distribution networks has contributed to the disruption of electrical service, especially during the rainy season. The purpose of designing adequate grounding system is to ensure continuity of supply, safety of equipment and personel in electrical power operations, and to confine ground voltage elevation within limits tolerable to the human body. To ensure equipment and personel safety in industries as well as in residential and commercial sectors, various protection schemes including earthing devices have been exploited.

The method of earthing as well as the value of the earth resistance are important factors to be considered in system grounding or equipment earthing. Earthing resistance values vary with time[3] depending on the prevailing soil conditions of the local environment under consideration. Soil resistivity studies and investigations provide adequate data and information for the design of an appropriate grounding system.

An accurate and adequate grounding system is defined by the direct contact to earth of such system and a low earth resistance value. This can be achieved if the resistivity of the earth/soil at the desired location can be investigated and obtained. The factors which affect soil resistivity value include soil moisture content, temperature, soil depth, and soil type. Typical earth resistance values can be obtained from experimental tests. Subsequently, average values of soil resistivity can be deduced using the established relationship between earth resistance and soil resistivity.

2   Measurement of Earth Resistance

There are several methods of measuring earth resistance values as fully discussed in [3]. The fall of potential method used in obtaining these data and the various sites chosen are fully discussed in [1]. Since we are interested in the variation of resistivity (and thus resistance) with depth, suitable statistical methods can be employed to obtain a relationship between resistivity ρ and depth of measurement D. According to [3], earth resistance R is related to resistivity ρ by the expression:

$$R = \frac{\rho}{4\pi D_i}[In\frac{4D_i}{A} - 1] + \frac{\rho}{4\pi S}[1 - \frac{D_i^2}{3S^8} + \frac{2D_i^4}{5S^4}] \quad (1)$$

Empirical methods for correlation and regression can be applied for two parameters possessing a joint normal distribution[4].

2.1   Linear Regression

Empirical correlation methods are often used in studying how two variables are related, so that

any relationship that is discovered can be used to assist in predicting (estimating) one of the variables. Considering two variables X and Y that are jointly normally distributed, the regression curve of Y on X is a straight line whose equation is given by:

$$\bigcup_{Y/X} = \bigcup_Y + \rho\frac{\delta Y}{\delta X}[X - \bigcup_X] \qquad (2)$$

The value of one variable, Y, corresponding to $X = x$ will be predicted from $\bigcup_{Y/X}$. If X and Y do not possess a joint normal distribution, this technique cannot be applied. The application of linear regression technique for the data analysis depends on the resistivity ρ being jointly normally distributed with depth, D. The measure of their relationship is determined by, τ, the sample correlation coefficient.

Since the value of Y corresponding to $X = x$ can be predicted by $\bigcup_{Y/X}$, the empirical problem of prediction involves estimating the regression function (2). The parameters in this function are readily estimated from sampled data. The desired sample estimate of Y_X is given by:

$$\bigcup_{Y/X} = \overline{Y} + \tau\frac{S_Y}{S_X}[x - \overline{X}] \qquad (3)$$

2.2   Correlation Coefficient (r)

The sample correlation coefficient is given by;

$$\tau = \frac{\sum_{i=1}^{n}[x_i - \overline{X}][Y_i - \overline{Y}]}{nS_X S_Y} \qquad (4)$$

This can be reduced to:

$$\tau = \frac{n\sum XY - \sum X\sum Y}{\sqrt{[(n\sum x^2 - (\sum X)^2)(n\sum Y^2 - (\sum Y)^2)]}} \qquad (5)$$

The value will be equal to $\pm$, if and only if, the points of the scattergram lie on a straight line.

2.3   Computation of r

Using the equation (5), values of τ were obtained for the sampled data. From the results,

$$-0.975 < \tau < -0.886$$

Considering the confidence interval, degrees of freedom and other statistical parameters obtained in the analysis, we can deduce according to [4], that resistivity ρ and depth D are jointly normally distributed.

2.4   Constants

From the data and results, the following constants can be obtained: A, S, $\overline{p}, \overline{D}$, S_ρ, S_D, τ

3   Estimating Earth Resistance for Varying Depth

The linear regression technique can be used to analyze ρ and D, since resistivity and depth have a joint normal distribution.
From equation (3),

$$\bigcup_{\rho/D} = \rho + \tau\frac{S_\rho}{S_D}(D - \overline{D}) \qquad (6)$$

where $\bigcup_{\rho/D}$ is the predicted value of ρ at depth $D_i = D$. S_ρ, S_D are the sample standard deviations.

From the data, the constants are known for each temperature and site. Substituting equation (6) in (1),

$$R = \rho(G_D) \dots\dots\dots\dots\dots\dots\dots\dots\dots\dots\dots(1)$$

Now, for a depth D_i,

$$G_D = \frac{1}{4\pi D_i}[In(\frac{4D_i}{A}) - 1] + \frac{1}{4\pi S}[1 - \frac{D_i^2}{3S^8} + \frac{2D_i^4}{5S^4}] \qquad (7)$$

Since the new value $\bigcup_{\rho/D_i} = \rho$ at depth D_i,

$$\rho = \overline{p} + \tau\frac{S_\rho}{S_D}(D_i - \overline{D}) \qquad (8)$$

Substituting (7) and (8) in (1); we have the estimated value of earth resistance at depth D_i; and this is given by:

$$R_i = [\overline{p} + \tau\frac{S_\rho}{S_D}(D_i - \overline{D})][\frac{In(\frac{4D_i}{A}) - 1}{4\pi D_i} + \frac{1 - \frac{D_i^2}{3S^8} + \frac{2D_i^4}{5S^4}}{4\pi S}] \qquad (9)$$

Equation (9) relates R to D. For any chosen value of D_i, the earth resistance R_i can be obtained. Using the same depths to estimate the earth resistance, results were obtained for the estimated resistance values.

3.1   Results of Resistance Estimation

The results obtained for the various depths at the same temperature for each location are shown in Fig.1 to 3. The initial results (ic) were improved upon using a logarithmic function to improve the linearity. The results from this technique (fc) were far better as shown in fig 1 to 3. The deviations are high because of the small set of data used.

3.2   Mean Correlation Coefficient

From the results obtained, the mean correlation coefficient is: $\tau_m = 0.9484$. Using τ_m to test the sampled data, the results obtained are also shown in fig.1 to 3.

Figure 1. Earth Resistance Variation with Depth: 1 - Measurement, 2 - Initial Estimated, 3 - Final Estimated, 4 - Mean Estimated

Figure 3. Earth Resistance Variation with Depth: 1 - Measurement, 2 - Initial Estimated, 3 - Final Estimated, 4 - Mean Estimated

Figure 2. Earth Resistance Variation with Depth: 1 - Measurement, 2 - Initial Estimated, 3 - Final Estimated, 4 - Mean Estimated

Figure 4. Earth Resistance Variation with Depth: 1 - Measurement, 2 - Estimated

4 Discussion

A methodology for estimating earth resistance at various depths has been developed using an empirical correlation method - linear regression. However, more accurate algorithms can be developed for better results.

4.1 Earth Resistance Estimation for Varying Depth

The earth resistance value can be estimated for varying depth using empirical correlation methods based on the linear regression technique. The results obtained using the sampled field data are shown in fig 4. A comparism of the results show that the estimated value of earth resistance shows a good agreement.

Therefore, this estimation technique is reliable and suitable in predicting earth resistance values at various depths and can be improved upon. Using a sampled set of readings, the results obtained are as shown in fig 4.

At a depth of 285cm, the estimated resistance is 1.01Ω. Thus, in grounding systems design and earthing practices, a suitable depth for the grounding rod to be embedded can be reasonably estimated depending on the resistance required for such standard installations. If a resistance R_i is to be obtained, varying values of depth, D_i are substituted into expression (9), until the desired resistance R_i is obtained as well as the practicable depth for use. The depth so obtained is that required to drive in the earthing rod for an efficient grounding system.

5   Conclusion

The development of more efficient and accurate algorithms for computing earth resistance (and thus soil resistivity) at various depths for different types of soils, and the evaluation of the constants and coefficients used, are areas for further consideration.

References

[1] I. E. Davidson, *Soil Resistivity Determination Using Statistical Analysis*, M.Eng Thesis, University of Ilorin, Nigeria, Sept., 1987.

[2] A. A. Esan, *Soil Resistivity Determination on Unilorin Main Campus*, Proceedings of ESSAN, Vol 5, 1985.

[3] I. E. E. E Industry, *I.E.E.E. Recommended Practice for Applications Society: Grounding of Industrial and Commercial Power Systems*, I E E E Std, 1972.

[4] P. G. Hoel, *Introduction to Mathematical Statistics*, 4th Edition, Wiley International, New York, 1971.

A DSP program with hardware configuration

J. Zhao, M J Kamper and F S van der Merwe
Electrical and Electronic Engineering, University of Stellenbosch

1 Abstract

In the paper an example is given of how to program a DSP (Digital Signal Processor) for the control of electrical machines and how to communicate between the DSP (TMS320C31) card, a 32 channel A/D card and an interface board (Fig. 1). The latter includes D/D (input and output) and D/A functions. From this example it is a straightforward matter to realize different control methods using the DSP technique.

2 Introduction

The DSP technology is being used more and more in electrical machine control systems because of its high speed processing and 32 bit floating-point capability. In R. Lagerquist et al. [1], several torque control methods are researched using the DSP technique with ANSI-C programming language (control interval is presently 576 μs). In [2-4], several kinds of DSP cards are used to do research on the different control systems (the control programs are written in assembly langauge). In the papers [1-4] mentioned above, it is shown that DSP technology is capable of being used for complex control systems.

The DSP programme can be written using two kinds of languages, one is the ANSI-C language, the other is assembly language. Using ANSI-C language to write a programme is easier than using assembly language, but the control interval of the DSP programme written in assembly langauge is much smaller than with the ANSI-C language. In order to reduce the control interval speed of the DSP programme as low as possible, it is recommended that assembly language be used to write the control programme, especially for a complex control system.

The DSP technology is not easy to learn for a first time user, especially to know how to write the DSP programme, how to communicate between the DSP interface board and DSP card and how to check the programme and hardware design for correctness. In this paper the technique of designing a DSP interface board is explained, an example programme written in assembly language is given to show the first time user of the DSP technology how to write the programme and how to communicate between the DSP card and the hardware. Using " Debug" to check the DSP programme is also described. This method can check that the logical functions of the programme are correct or not. This method also can indirectly check that the time sequence circuit of the hardware design is correct or not.

In the control system of this paper, the DSP TMS320C31 has been used, Its main characteristics are:(1) Clock frequency is 40 MHz, (2) Speed is 20.0 MIPS integer and (3) is 40 MFLOPS floating point. The PC/C31 board is a real time application platform based around the TMS320C31 which is a 32 bit floating-point Digital Signal Processor (DSP) from Texas Instruments.

3 Hardware

In order to receive digital signals from the position sensor, phase current sensors etc. a DSP interface board and a 32 channel A/D card are used. Also to send digital signals to the inverter for switching and to sense the waveforms of the signals, the DSP interface board is used. The block diagram of the hardware is shown in Fig. 1. From Fig. 1 the following can be seen: The D/A channels output analogue current,voltage, speed and torque signals. The D/D-input channel receives a digital shaft position signal while the D/D-output outputs digital control signals through fibre optics to control the power electronic inverter. The 32 channel A/D card receives the analogue current and torque signals.

4 Description of the DSP interface board design

One of the most important factors concerning the design of the DSP interface board is to understand the relation between the /IOE and R/W signals. The /IOE waveform enables input or output signals, and R/W indicates whether data is read from, or written to the bus. The /IOE and R/W are control signals set by the DSP card. Unfortunately, it is difficult for the first time user to understand the relation

between /IEO and R/W from DSP manuals. In this section the relation between /IOE and R/W signals and how to design address decoding logic are introduced as follows:

4.1 The timing relationship of /IEO and R/W signals

The timing relationship of the /IEO and R/W signals of the DSP board is shown in Fig. 2. The /IEO and R/W signals were used to control the buffer to read or write signals on the data bus lines. From Fig. 2 it can be seen that when R/W and /IOE signals are both low, the digital signals on the Data bus of the DSP card can be sent out (write). When the R/W signal is high and the /IOE signal is low, the signals from the outside can be received by the DSP card (read). It is very important to know and understand the timing of the DSP card so as to correctly design the DSP interface card.

Figure 1: The block diagram of the DSP interface card and 32 channel A/D card.

4.2 Address lines

In this design , address lines, A1, A2 and A3 from the DSPLink2 connector of the DSP board are the address lines for the DSP interface card. According to Fig. 2 the address decoding circuit is designed as shown in Fig. 3. It is important to know that the data lines of the DSP interface board is connected with the data lines (from D16-D31) of the DSP card. So when this data is received, it must be shifted to the right by 16 bits before it is used in the DSP programme.

Figure 2: Time sequence between R/W, /IOE and DATA

5 Programme

In order to demonstrate the DSP technology easily a example programme written in assembly language is given (see appendix). The command structure of the assembly language supports the TMS320C31 DSP card. (Note: Different types of DSP chips use different assembly languages.)

Some functions of the programme are to obtain the data from the 32 channel A/D card. In this programme, the 3 channels of the 32 channel A/D card are used. Changing timings in DSPlink2 space can change pulse width of /IEO. Note: because the clock frequency of the DSP card in this project is 40 MHz, the DSPlink2 space is set up to Space-2 so that /IOE has enough pulse width when data is read from the A/D card(detail in part 2 of the DSP example programme). The programme can also obtain digital position signals from the DSP interface card and send an analogue position signal to the oscilloscope and digital control signals to the inverter through the interface board.

Figure 3: Address selected circuit in the DSP interface board

The DSP program includes two parts: one is *.asm file (It is the assembly language file and an example is shown in the appendix), the other is *.cmd file (*.cmd is a command file and in the example it is not used). After the required programs are written, a source file is assembled using the command: asm30 -1 - s name.asm. The assembler produces an object file with the same name but with a .obj extension. Then the linker is invoked by the command: lnk30 name.cmd. This produces an executable object code file with a map file. The symbolic information embedded in the object must be sorted using the command: c31sort name.out and then use the command:mon31 name.out to load this file. Then the RUN command is used
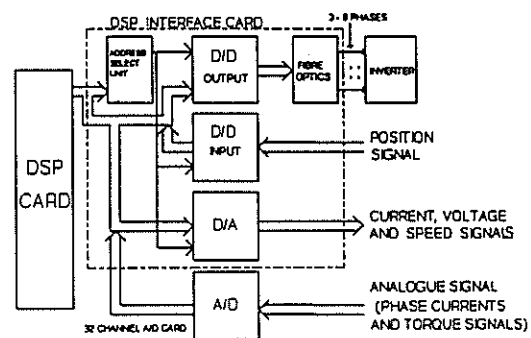
to run this file.

6 Checking the programme by using "Debug"

In this section it is explained how to use "Debug" to test a program that is written in assembly language. Before using this file to control the inverter etc., the logical functions of the programme must be checked. For this programme, the method called "Debug" is used to check the programme. A sample is given below to show how to use the Debug monitor to check the logical functions of this programme. First set a breakpoint at a point at which one wants to cause the programme to pause, after using the command "mon31 name.out". Modifying a breakpoint to a new value is achieved by entering mbrk, this produces a prompt for a breakpoint number (type 0 or 1 or ...15). The second prompt then requests for an address. For this sample programme, the breakpoint is 0 and the address is 478430h. Use "go" to run the programme. Then use "ssi" to single step the programme and use "dreg" to display all register values. Using this method the data in the registers can be checked as well as the logical functions of the programme. More detailed information can be read in [8].

7 Conclusion

The method called "Debug" is a very useful tool to check the programme. It helps the user to find a problem that may be in the programme or hardware. It is essential to understand the relation between the /IEO and R/W signals in designing the DSP interface board. It is important to choose the correct timing in DSPlink2 space to make the programme work. The DSP example programme written in assembly language has the function to initialize the programme, communicate with the DSP card and the hardware. On the basis of this work, it is straightforward to develop different control programmes.

8 References

[1]   R. Lagerquist, R. B. Betz and T. J. E. Miller, "DSP96002 Based High Performance Digital Vector Controller for Synchronous Reluctance Motors," ICEM92, vol. 3, Lanchester, pp903-907, Sept. 1992.
[2]   N. Matsui, and H. Ohashi, "DSP-Based Adoptive Control of a Brushless Motor," IEEE Trans. Industry Applications, vol. 28, no. 2, pp. 448-454, March/April 1992.
[3]   T. G. Habetler, and D. M. Divan, "Control Strategies for Direct Torque Control Using Discrete Pulse Modulation," IEEE Trans. Industry Applications, vol. 27, No. 5, pp. 893-898, September/October 1991.
[4]   D. C. Lee, S.K. Sul, and M. H. Park, " High Performance Current Regulator for a Field-Oriented Controlled Induction Motor Drive," IEEE Trans. Industry Applications, vol. 30, no. 5, pp. 1247-1257, September/October 1994.
[5]   H Kubota, K. Matsuse, and T. Nakano, "DSP-Based Speed Adaptive Flux Observer of Induction Motor," IEEE Trans. Industry Applications, vol. 29, no. 2, pp 344-348, March/April 1993.
[6]   "The DSP Catalogue," Loughbotough Sound Images Ltd, The Technology centre, Epinal way, Loughbotough, Leics LE11 0QE, England, 1993/94.
[7]   "32 Channel Analogue Data Acquisition Card User Manual" Version 1.02, Loughbotough Sound Images Ltd,March 1992.
[8]   "PC/C31 Board Technical Reference Manual," Version 1.02 May 1993, Loughbotough Sound Images Ltd.
[9]   "TMS320C3x User' s Guide," 2558539-9721 revision F, July 1992, Texas Instruments Incorporated.
[10]   "TMS320 Floating-Point DSP Assembly Language Tools User's Guide," 2676328-9721 revision A, September 1991, Texas Instruments Incorporated.

9 ACKNOWLEDGEMENTS

10 Address of main author

Mr J. Zhao, Department of Electrical Engineering, University of Stellenbosch, Private Bag X1, 7602 Matieland, South Africa. E_mail: Zhao@firga.sun.ac.za

10 Appendix

```
;*** Interrupt Vectors starting at address 809FC1h on the
;Note:The part2 and part3 of this programme are deleted
;because paper pages are limited.
;TMS320C31 ***(Part1)
;Part1 is for initializing inerrupt vectors. When the DSP card
;receives a interrupt signal (INT2) from 32 channel A/D card
;(ADC), it will response interrupt procedure to complete
;EOC branch.

            .sect ".vecs"

INTO     BR      MAIN     ;General purpose external
                         ;interrupts
INT1     BR      MAIN     ;"          "
INT2     BR      EOC      ;This interupt is used by the
                         ;ADC
INT3     BR      MAIN     ;General purpose external
                         ;interrupts
XINTO    BR      MAIN     ;Serial-port TX buffer empty
RINTO    BR      MAIN     ;Serial-port RX buffer empty
         .space  2                 ;Reserved for XINT1 &
                         ;RINT1 on the C30
TINTO    BR      MAIN     ;Timer0:no using
TINT1    BR      MAIN     ;Timer1:no using
DINT     BR      MAIN     ;DMA interrupt


;*** Constant Declarations *** (Part2)
;In this section, the DSPlink2 is mapped to space 2. The
;necessary constants of the ADC and parameters of ADC's
;registers as well as the addresses of the DSP interface board
;are set.( This section is ignored)

;*** Data Section *** (Part 3)
;The ADC' s channel numbers are set. The constants are
;decided in detail in [7] ( This section is ignored.).

;*** Program Section *** (Part4)
;This is the main procedure. In this section, all necessary
;registers in this programme are run. The initialization work
;of the programme is finished.

            .text to see P.4-57 [10]
            .def   MAIN
MAIN:
         LDP     RAMBLK2      ; Set up Data Page
                             ;Pointer
         LDI     @PRIMCTRL, AR ; Set up Primary
                             ;Bus
         LDI     @PRIMMASK, R0 ; Zero Wait States
         STI     R0, *AR0      ; & 32K Block size
         LDI     @RAMBLK2, SP  ; Set up Stack
                             ;Pointer
CALIBRATE:
         LDI     @CH32CTRL,AR0 ;The 32 Channel
                             ;ADC's S/H needs
         LDI     @ZEROMASK,R0  ; to be calibrated.
         STI     R0, *AR0      ; by writing to bit 5
                             ;of the ADC's
         LDI     @CALMASK,R1   ; Control Reg.
         STI     R1, *AR0      ;
         STI     R0, *AR0      ;
POLL:
         LDI     @CALMASK,R0   ; Keeps polling the
                             ;Calibration
         AND     *AR0,R0       ; Complete Bit of
                             ;the ADCs Status
         BZ      POLL          ;Reg. until it is set.
```

```
ADDRESS_REG:
         LDI     @CH32CTRL,AR0 ;Loads ADC control
                             ;register
         LDI     @CH32DATA,AR1     ;Loads ADC
                             ;result register
         LDI     @LOC_CTRL,AR2  ;Loads ADC
                          ;controle table
         LDI     @LOC_DPRAM, AR6  ;Setup
                          ;reference signal location
         LDI     @DINPUT, AR7  ;
LDI      @TNV_CTRL, AR4
         LDI     *AR1, R0      ;Clear EOC status
                             ;flag
         LDI     l_shift, R0   ;The timer value
                          ;must be left
         LDI     @ADCTIMER, R1 ; shifted by 16 bits
         ASH     R0, R1        ;
         STI     R1, *AR1      ;
         LDI     *AR2++%, R1   ; Selects the first
                             ;channel
         STI     R1, *AR0      ; from the ADC's
                             ;controle table.
         OR      @EOCSET, IE   ; Enable INT2
         OR      @STSET, ST    ; Set global
                          ;interrupt enable
WAIT:
         BR      WAIT          ; Endless loop...


;**Interrupt Procedure for End Of Conversion (EOC)
;**(Part 5)
;This is the interrupt procedure programme. In this section,
ADC' ;results and position signals can be received. The D/A
and ;control signals can sent out.

EOC:
         LDI     *AR0, R0 ; Get ADC Status value
         LDI     @EOCFLAG, R1 ;Get EOC Flag Mask
         TSTB    R0, R1   ;See if interrupt is valid
         BZD     EOC_EN   ;Branch to END if not
                          ;valid.
         LDI     chans, BK     ;
         LDI     r_shift, R0 ; The ADC result must be
                          ;right
         ASH     R0, *AR1, R1  ; shifted by 20 bits
         FLOAT   R1            ; Convert integer
                             ;result => float
         LDF     R1, R6   ; Save the result to be used
                          ;later
         LDI     *AR2++%, R2   ; Selects the next
                             ;channel in the
         STI     R2, *AR0      ;Control Register
         STF     R1, *AR6++%   ;
         LDI     *AR7, R5      ;input digital signal
         LDI     @D_AOUTPUT, AR5
         STI     R5, *AR5      ;send out analogue
                             ;signal
         LDI     *AR4++%, R3   ;obtain    inverter
                             ;control signal
         LDI     @FIRBEROUT, AR5 ;send the control
                             ;signal
         STI     R3, *AR5

EOC_END:
         RETI
```

NOTES:

NOTES:

NOTES:

NOTES:

NOTES:

NOTES: